frontiers | Research Topics

Women in cardiovascular genetics and systems medicine

Edited by
Laura Arbour, Anindita Das and Elisa Anamaria Liehn

Published in
Frontiers in Cardiovascular Medicine

ISSN 1664-8714
ISBN 978-2-8325-4796-0
DOI 10.3389/978-2-8325-4796-0

About Frontiers

Frontiers is more than just an open access publisher of scholarly articles: it is a pioneering approach to the world of academia, radically improving the way scholarly research is managed. The grand vision of Frontiers is a world where all people have an equal opportunity to seek, share and generate knowledge. Frontiers provides immediate and permanent online open access to all its publications, but this alone is not enough to realize our grand goals.

Frontiers journal series

The Frontiers journal series is a multi-tier and interdisciplinary set of open-access, online journals, promising a paradigm shift from the current review, selection and dissemination processes in academic publishing. All Frontiers journals are driven by researchers for researchers; therefore, they constitute a service to the scholarly community. At the same time, the *Frontiers journal series* operates on a revolutionary invention, the tiered publishing system, initially addressing specific communities of scholars, and gradually climbing up to broader public understanding, thus serving the interests of the lay society, too.

Dedication to quality

Each Frontiers article is a landmark of the highest quality, thanks to genuinely collaborative interactions between authors and review editors, who include some of the world's best academicians. Research must be certified by peers before entering a stream of knowledge that may eventually reach the public - and shape society; therefore, Frontiers only applies the most rigorous and unbiased reviews. Frontiers revolutionizes research publishing by freely delivering the most outstanding research, evaluated with no bias from both the academic and social point of view. By applying the most advanced information technologies, Frontiers is catapulting scholarly publishing into a new generation.

What are Frontiers Research Topics?

Frontiers Research Topics are very popular trademarks of the *Frontiers journals series*: they are collections of at least ten articles, all centered on a particular subject. With their unique mix of varied contributions from Original Research to Review Articles, Frontiers Research Topics unify the most influential researchers, the latest key findings and historical advances in a hot research area.

Find out more on how to host your own Frontiers Research Topic or contribute to one as an author by contacting the Frontiers editorial office: frontiersin.org/about/contact

Women in cardiovascular genetics and systems medicine

Topic editors

Laura Arbour — University of British Columbia, Canada

Anindita Das — Virginia Commonwealth University, United States

Elisa Anamaria Liehn — University of South Denmark, Denmark

Citation

Arbour, L., Das, A., Liehn, E. A., eds. (2024). *Women in cardiovascular genetics and systems medicine*. Lausanne: Frontiers Media SA. doi: 10.3389/978-2-8325-4796-0

Table of contents

frontiers in Cardiovascular Medicine

ORIGINAL RESEARCH
published: 16 August 2021
doi: 10.3389/fcvm.2021.704175

MicroRNAs hsa-miR-618 and hsa-miR-297 Might Modulate the Pleiotropic Effects Exerted by Statins in Endothelial Cells Through the Inhibition of ROCK2 Kinase: *in-silico* Approach

*Karla Leal, Kathleen Saavedra, Camilo Rebolledo and Luis A. Salazar**

Center of Molecular Biology and Pharmacogenetics, Scientific and Technological Bioresource Nucleus, Department of Basic Sciences, Faculty of Medicine, Universidad de La Frontera, Temuco, Chile

OPEN ACCESS

Edited by:
Fadi N. Salloum, Virginia Commonwealth University, United States

Reviewed by:
Lazaros Lataniotis, University of California, San Francisco, United States
Raj Sewduth, VIB KU Leuven Center for Cancer Biology, Belgium
Tobias Jakobi, University of Arizona, United States

***Correspondence:**
Luis A. Salazar
luis.salazar@ufrontera.cl

Specialty section:
This article was submitted to Cardiovascular Genetics and Systems Medicine, a section of the journal Frontiers in Cardiovascular Medicine

Received: *04 May 2021*
Accepted: *20 July 2021*
Published: *16 August 2021*

Citation:
Leal K, Saavedra K, Rebolledo C and Salazar LA (2021) MicroRNAs hsa-miR-618 and hsa-miR-297 Might Modulate the Pleiotropic Effects Exerted by Statins in Endothelial Cells Through the Inhibition of ROCK2 Kinase: in-silico Approach. Front. Cardiovasc. Med. 8:704175. doi: 10.3389/fcvm.2021.704175

Several studies show that statin therapy improves endothelial function by cholesterol-independent mechanisms called "pleiotropic effects." These are due to the inhibition of the RhoA/ROCK kinase pathway, its inhibition being an attractive atheroprotective treatment. In addition, recent work has shown that microRNAs, posttranscriptional regulators of gene expression, can affect the response of statins and their efficacy. For this reason, the objective of this study was to identify by bioinformatic analysis possible new microRNAs that could modulate the pleiotropic effects exerted by statins through the inhibition of ROCK kinases. A bioinformatic study was performed in which the differential expression of miRNAs in endothelial cells was compared under two conditions: Control and treated with simvastatin at 10 μM for 24 h, using a microarray. Seven miRNAs were differentially expressed, three up and four down. Within the up group, the miRNAs hsa-miR-618 and hsa-miR-297 present as a predicted target to ROCK2 kinase. Also, functional and enriched pathway analysis showed an association with mechanisms associated with atheroprotective effects. This work shows an *in-silico* approach of how posttranscriptional regulation mediated by miRNAs could modulate the pleiotropic effects exerted by statins on endothelial cells, through the inhibition of ROCK2 kinase and its effects.

Keywords: statins, pleiotropic effects, microRNAs, atheroprotective effects, kinases

INTRODUCTION

Cardiovascular diseases (CVDs) are the leading cause of death worldwide. An estimated 17.9 million people died from CVDs in 2016, representing 31% of all global deaths. Of these deaths, 85% are due to heart attack and ischemic stroke (1). Most CVDs can be prevented by addressing lifestyle-related risk factors: tobacco use, physical inactivity, hypertension, diabetes, and hyperlipidemia (2). The treatment of choice for hypercholesterolemia is the use of statins, which inhibit the enzyme 3-hydroxy-methylglutaryl coenzyme A (HMG-CoA) reductase, which limits the biosynthesis of liver cholesterol (3). Experimental and clinical studies suggest that statins may exert

cardiovascular protective effects by mechanisms independent of cholesterol lowering called "pleiotropic effects" (4, 5). It has been described that the mechanism by which statins produce their pleiotropic effects is through inhibition of the mevalonate pathway. Mevalonate is a precursor not only of cholesterol but also of several other isopropenoids (6). These include farnesylpyrophosphate (FPP) and geranylgeranylpyrophosphate (GGP), which are lipids needed for posttranslational prenylation of Rho GTPase proteins, which act as biological switches through signal transduction (6, 7). The inhibition of mevalonate synthesis prevents the activation of Rho and the subsequent activation of Rho-associated protein kinase (ROCK) (8, 9). Several studies have reported the importance of the RhoA/ROCK pathway in endothelial function affecting vascular tone, platelet aggregation, smooth-muscle cell proliferation, leukocyte adhesion, production of nitric oxide synthase (eNOS), and bioavailability of nitric oxide (NO). The mechanisms associated with eNOS are of great importance, since the decrease of NO corresponds to one of the first manifestations of atherosclerosis (10, 11). Therefore, inhibition of the RhoA/ROCK pathway by statins influences NO signaling in endothelial cells (12). This has been demonstrated by two mechanisms: stability of eNOS messenger RNA (mRNA) and an increase in its activity through activation of phosphatidylinositol 3-kinase (PI3K)/AKT (13, 14). For this reason, inhibition of the RhoA/ROCK kinase pathway might be an attractive atheroprotective treatment for the development of CVD.

MicroRNAs (miRNAs) are important regulators of gene expression that bind complementary target mRNAs and repress their expression. The miRNAs are small non-coding RNA molecules, evolutionarily conserved. They have approximately 22 nucleotides, and their functions are gene regulation through posttranscriptional mechanisms. The miRNAs are involved in a variety of biological processes (15). Over the past few years, a total of 2,300 miRNAs have been reported in humans and it is estimated that human mRNA information exceeds 25,000 (16, 17). For this reason, current laboratory technologies do not allow to test globally every possible interaction between gene and miRNAs. However, the use of bioinformatics approaches for miRNA target prediction is used as a guide for laboratory validation experiments to more quickly elucidate gene regulation networks (18). The bioinformatics development combined with diverse experiments has allowed them to be used as potential biomarkers for diagnosis, prognosis, and personalized treatment (19).

Several studies in the area of cancer have demonstrated the regulation of transcriptional expression by miRNAs of the ROCK1 and ROCK2 isoforms of the RhoA/ROCK kinase pathway, reporting beneficial effects such as decreased proliferation and migration by modulating the expression of these miRNAs (20, 21). Zambrano et al. (22) showed that treatment with atorvastatin and simvastatin at 10 micromolar (μM) in HepG2 cells for 24 h deregulated the expression of 13 miRNAs by atorvastatin and 2 miRNAs by simvastatin. Other studies also show that atorvastatin can lower miR-221 and miR-222 levels in cell endothelial parents of patients with coronary disease (23). In particular, the effects observed by statins are heterogeneous, appearing to be independent of their chemical composition (lipophilic vs. hydrophilic) (24). It has also been reported that miRNAs would have the ability to influence endothelium atheroprotective effects, such as increasing nitric NO. Cerda et al. (25) described that these miRNAs increase the levels of NO and the expression of eNOS3 in endothelial cells. This background reveals that statin-modulated miRNAs influence their response and effectiveness. For this reason, the objective of this study was to identify by bioinformatic analysis possible new miRNAs that could modulate the pleiotropic effects exerted by statins through the inhibition of ROCK1 and ROCK2 kinases, and also to explore the pathways associated with the atheroprotective capacity of endothelial cells through an *in-silico* approach. Therefore, a bioinformatics study was performed comparing the differential expression of miRNAs in human umbilical vein endothelial cells (HUVEC) under two conditions: control and treated with simvastatin at 10 (μM) for 24 h.

MATERIALS AND METHODS

Identification of Differential Expression miRNAs

The gene expression profile data (GSE126290, file GSE126290_RAW.tar) was downloaded from the NCBI Gene Expression Omnibus (GEO) database. The dataset contained the miRNA profile of HUVEC cells treated with simvastatin 10 μM and HUVEC cells without treatment as control. The analysis was performed using the Gene Expression Analysis Platform version 0.3.2 (GEAP), which uses R program packages for gene expression data processing and statistical analysis (26–30). In this analysis, the statistical package used was "Linear models and differential expression for microarray data" (Limma), making the comparison between groups considering as criteria the "false discovery rate" (FDR) p-value < 0.05 and logFC > 1 (31). From GEAP software, volcano plot, scatter plot, and heat map of the distances between arrays were generated. For principal component analysis (PCA), Ggfortify (32) and ggbiplot (33) of R Program were used. For the hierarchical clustering heat maps, Morpheus was used.

Gene Ontology and Pathway Enrichment Analysis

To predict the target genes of the prognostic miRNAs, we used the mirDIP 4.1 online software that provides 152 million predictions using 30 different resources and obtained the score of each interaction between miRNAs and the target (34). In addition, gene ontology (GO) and pathway enrichment analyses of Kyoto Encyclopedia of Genes and Genomes (KEGG) were performed with target genes of the differential miRNAs expressed through the ShinyGO v0.61 (35) program, FDR p-value < 0.05.

Target Predictions of Upregulated miRNAs for ROCK1 and ROCK2 Kinases

The upregulated miRNAs were evaluated for their ability to bind to the 3′UTR of the ROCK1 and/or ROCK2 kinases using three miRNA target predictor softwares to increase specificity

and precision: TargetScan version 7.2, which considered as criteria the type of seed region and the weighted context++ score (WCS) that uses 16 important characteristics for miRNA target recognition (36); miRDB which considered as criteria the location of the seed region in the 3′UTR and the score assigned by the computational algorithm for target prediction, showing that a score above 80 presents a higher probability of union (37); and mirDIP 4.1.

RESULTS

Identification of Differentially Expressed miRNAs Between Simvastatin-Treated 10 μM HUVEC Cells (24 h Treatment) and Control HUVEC Cells

To determine the quality control of our analysis, two PCA plots and a false-color heat map were generated. PCA shows

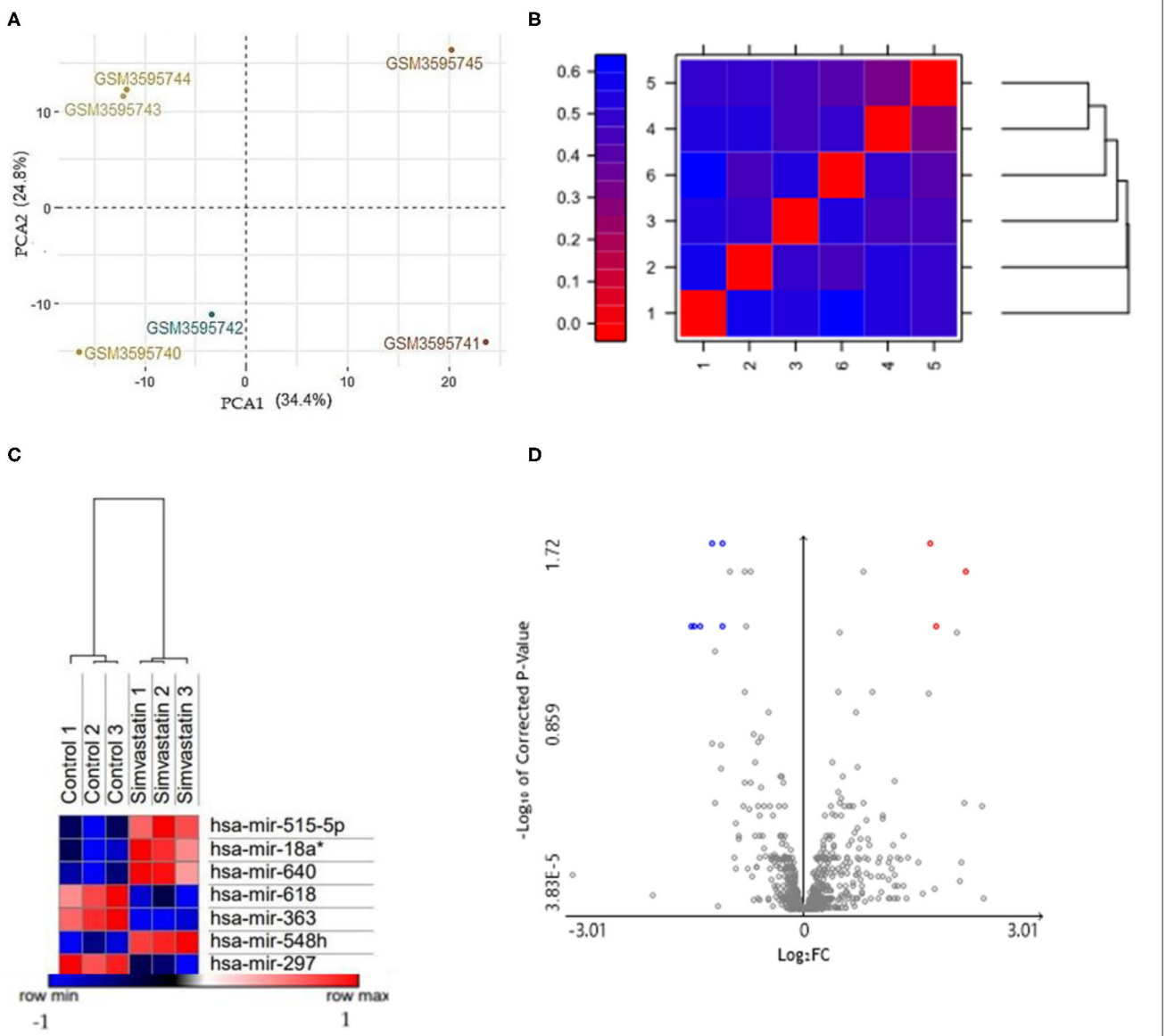

FIGURE 1 | (A) PCA based on microarrays showed that samples were grouped. The HUVEC control (GSM3595740; GSM3595741; GSM3595742) and HUVEC cells treated with 10 μM simvastatin (GSM3595743; GSM3595744; GSM3595745) were separated by PC2. **(B)** False color heat maps indicating distances between matrices. 1 (Control 1); 2 (Control 2); 3 (Control 3); 4 (Simvastatin 1); 5 (Simvastatin 2); 6 (Simvastatin 3). **(C)** Hierarchical clustering heat maps with differentially expressed miRNAs in both conditions: control and simvastatin treated. In the graph, the red samples represent the highly expressed values while the blue ones show the low expressed values. The values are expressed in Log2. **(D)** Volcano plot of the differentially expressed miRNAs. The gray points represent genes with no significant difference. The red points represent upregulated genes screened based on the fold change > 1.0 and a corrected *p*-value of < 0.05. The green points represent downregulated genes screened based on the fold change > 1.0 and a corrected *p*-value of < 0.05.

TABLE 1 | Differentially expressed miRNAs in HUVEC cells treated with 10 μM simvastatin for 24 h.

miRNA_ID	logFC	AveExpr	T	p value	adj. p val	B	Expression
hsa-miR-515-5p	−1.07	10.1	−6.94	0.000662	0.0471	0.255	Downregulated
hsa-miR-18a*	−1.43	9.06	−7.18	0.000559	0.0471	0.43	Downregulated
hsa-miR-640	−1.35	9.31	−7.06	0.00061	0.0471	0.34	Downregulated
hsa-miR-618	1.72	5.82	6.81	0.00073	0.0471	0.155	Upregulated
hsa-miR-363	1.64	10.7	13.4	2.2E-05	0.0191	3.48	Upregulated
hsa-miR-548h	−1.19	12.9	−10.9	6.43E-05	0.0191	2.55	Downregulated
hsa-miR-297	2.1	11.7	8.53	0.000233	0.026	1.32	Upregulated

logFC, log2 fold change; AveExpr, average log2 expression; T, moderated t-statistic; p-value, raw p-value; adj. p-value, adjusted p-value; B, log-odds.

the separation of the groups in the two conditions evaluated, simvastatin-treated HUVEC cells, and control (untreated) HUVEC cells (**Figure 1A**). Along with this, the false heat map indicates the distances between the matrices, calculated between the mean distances between the data (**Figure 1B**). Subsequently, the differential expression of miRNAs from the GSM126290 database is shown. The criteria used were $p < 0.05$ and logFC > 1 (**Table 1**). A total of seven miRNAs were identified as differentially expressed, three miRNAs upregulated and four miRNAs downregulated, between the conditions: 10-μM simvastatin-treated and control cells. This was represented in a hierarchical clustering heat map (**Figure 1C**). Along with this, the volcano plot showing the dataset and the differentially expressed samples is shown (**Figure 1D**).

Functional and Pathway Enrichment Analysis of Differentially Expressed miRNAs

Gene Ontology and Pathway Enrichment analysis were made to explore the biological pathways in which deregulated miRNAs would be implicated. The first step was to determine the target genes for differentially expressed miRNAs, using the mirDIP 4.1 program. This program brings together 30 different resources. A total of 4,756 target genes were found with extremely high score. Later, the 4,756 genes were used for ontological genes and enrichment pathways. Gene Ontology enrichment analysis classified them into three groups, a biological process group, a cellular component group, and a molecular function group, which are shown in **Table 2**. The biological processes that showed the highest number of genes were regulation of biosynthetic processes (1,055 genes), regulation of macromolecule biosynthetic processes (1,010 genes), and positive regulation of nitrogen compound metabolic processes (819 genes). The cellular components genes are mostly associated with nuclear part (1,060 genes), nucleoplasm (869 genes), and nuclear lumen (976 genes). The most presented molecular functions were transcription regulator activity (543 genes), regulatory region nucleic acid binding (301 genes), and transcription regulatory region DNA binding (299 genes). Pathway enrichment analysis shows miRNAs in cancer, axon guidance, and pathways in cancer, in higher probability, which are shown in **Table 3** and **Figure 2**.

miRNA Target Prediction for ROCK1 and ROCK2 Kinases

To determine the interaction between the upregulated miRNAs hsa-miR-618, hsa-miR-363, and hsa-miR-297, with the 3′UTR sequence of ROCK1 and ROCK2 kinases, three online platforms were combined, TargetScan, miRDB, and mirDIP 4.1, considering the most important metrics of each program (**Figure 3** and **Table 4**). The strategy was to specifically target ROCK1 and ROCK2 kinases, due to the major role these proteins play in atherosclerotic pathology and also in the pleiotropic effects exerted by statins. However, genes associated with cholesterol metabolism (*ABCA1*, *APOE*, *LDLR*, *SCAP*, *SREP2*, *PCSK9*, and *VLDLR*), as well as genes related to eNOS pathways (*ROCK2*, *PI3K,* and *AKT*), were also evaluated. These genes are not presented as predicted targets of miRNAs.

DISCUSSION

In the present *in-silico* study, we analyzed data collected from the GEO database (GSE126290) in which the differential expression of miRNAs between two conditions was evaluated: HUVEC cells treated with simvastatin at 10 μM and control cells (without treatment) for 24 h. The bioinformatic analysis on differential expression analysis of miRNAs showed the deregulation of a group of seven miRNAs (hsa-miR-515-5p, hsa-miR-18a*, hsa-miR-640, hsa-miR-618, hsa-miR-363, hsa-miR-548h, and hsa-miR-297) considering as cutoff criteria a logFC > 1 and FDR p-value < 0.05. Among the group of seven miRNAs, four are downregulated (hsa-miR-515-5p, hsa-miR-18a*, hsa-miR-640, and hsa-miR-548h) and three are upregulated (hsa-miR-618, hsa-miR-297, and hsa-miR-363). Liang et al. (38) performed a differential expression analysis from the same data set presented in this paper. Their results showed that miRNA hsa-miR-652-3p inhibits ISL1, a protein involved in the decrease of NO bioavailability in endothelial cells. However, this miRNA is not upregulated in our analysis. One of these differences is due to their cutoff values considered: p-value of 0.1 and fold change ± 0.2. This would also establish a difference in the amount of deregulated miRNAs, since they present a total of 167, in relation to our analysis which were 7.

Our work supports previous reports on the effect of statins on the dysregulation of miRNA expression and also proposes the way in which statins can exert pleiotropic effects associated with

TABLE 2 | Gene ontology enrichment analysis of differentially expressed miRNAs was divided into three groups: biological processes, cellular components, and molecular functions.

Functional category	E. FDR	N. G. S	N. G. T
BIOLOGICAL PROCESS			
Nervous system development	4.6E-72	696	2,474
Positive regulation of metabolic process	2.4E-60	911	3,789
Positive regulation of macromolecule metabolic process	2.4E-60	858	3,498
Regulation of biosynthetic process	2.2E-56	1,055	4,687
Regulation of macromolecule biosynthetic process	2.2E-56	1,010	4,426
Positive regulation of nitrogen compound metabolic process	2.2E-56	819	3,351
Regulation of cellular biosynthetic process	6.4E-56	1,040	4,610
Neurogenesis	7.9E-56	495	1,683
Cell development	1.8E-55	604	2,230
Regulation of nucleobase-containing compound metabolic process	6.7E-55	1,014	4,482
CELLULAR COMPONENT			
Nuclear part	1.9E-44	1,060	4,966
Nucleoplasm	3.1E-44	869	3,861
Nuclear lumen	1.7E-41	976	4,545
Neuron part	2.1E-27	440	1,808
Synapse	5.5E-24	326	1,268
Axon	7.7E-21	190	639
Neuron projection	3.5E-20	333	1,371
Plasma membrane bounded cell projection	5.8E-19	481	2,214
Cell projection	8.0E-19	493	2,287
Synapse part	1.5E-18	257	1,004
MOLECULAR FUNCTIONS			
Transcription regulator activity	7.5E-37	543	2,183
Regulatory region nucleic acid binding	3.1E-34	301	1,002
Transcription regulatory region DNA binding	9.6E-34	299	1,000
Sequence-specific DNA binding	1.1E-33	338	1,189
RNA polymerase II regulatory region DNA binding	1.3E-33	260	823
DNA-binding transcription factor activity	4.9E-33	455	1,793
RNA polymerase II regulatory region sequence-specific DNA binding	1.2E-32	256	816
Sequence-specific double-stranded DNA binding	1.2E-31	276	920
Transcription regulatory region sequence-specific DNA binding	1.4E-31	266	875
DNA-binding transcription factor activity, RNA polymerase II-specific	1.4E-31	427	1,673

E. FDR, enrichment FDR; N. G. S, number of genes selected; N. G. T, number of genes total.

TABLE 3 | Pathway enrichment analysis of differentially expressed miRNAs.

Functional category	E. FDR	N. G. S	N. T. G.
ENRICHMENT PATHWAYS			
MicroRNAs in cancer	5.5E-13	62	150
Axon guidance	1.5E-10	65	181
Pathways in cancer	5.4E-09	134	528
MAPK signaling pathway	8.4E-09	86	295
Proteoglycans in cancer	1.6E-08	64	198
Transcriptional misregulation in cancer	5.2E-08	60	186
Endocytosis	8.6E-08	72	244
PI3K-Akt signaling pathway	1.1E-07	94	353
Ubiquitin-mediated proteolysis	1.3E-07	47	135
Signaling pathways regulating pluripotency of stem cells	1.3E-07	48	139

E. FDR, enrichment FDR; N. G. S, number of genes selected; N. G. T, number of genes total.

the RhoA/ROCK kinase pathway. These miRNAs are modulating various processes associated with CVDs (39, 40). We observed that simvastatin can modulate seven miRNAs in endothelial cells, and two that are upregulated could modify their expression through binding to the 3′UTR region of the ROCK2 kinases. Nowadays, there are several tools available to predict miRNA targets based mainly on detecting the complementarity of the miRNA sequence with the 3′UTR region of the target gene (41). However, many of these predictions show false negatives in the experimental validation. One strategy to maximize performance and minimize false results *in vitro* and *in vivo* functional experiments is the union of bioinformatics tools for miRNA-target prediction that will allow increasing the specificity and precision of the analysis (42). For this reason, three prediction programs were used together: TargetScan, miRDB, and mirDIP 4.1. All three tools showed that hsa-miR-618 and hsa-mir-297 had ROCK2 as a target. The hsa-miR-618 miRNA shows complementarity in three regions of the 3′UTR of ROCK2. Studies have shown that the more seed bonds it has in the 3′UTR, the stronger the miRNA-induced regulation (43). On average, the change in Log2 was linearly correlated with the number of seed regions, suggesting that the effect of seeds is independent and multiplicative (44). For this reason, we can suggest that hsa-miR-618 would have a greater effect on the 3′UTR.

Considering that many of the pathologies associated with the vasculature are related to morphological changes that can be regulated by the interaction of hemodynamic forces, one of the limitations of our work is that the database used contains data from an *in vitro* model and not from an *in vivo* model. Also, in the vasculature there is presence of different cell types that contribute to the physiopathology. An example of this, in the adhesion of leukocytes, is the production of inflammatory cytokines by macrophages, etc. However, many authors agree that HUVEC is a model of representative study of the vasculature and also it has allowed the study of physiological and pathological effects in isolation as in coculture with leukocytes and smooth-muscle cells (45, 46). For this reason, it is important to consider validating these results *in vitro* and *in vivo* models.

ROCK2 is a 160-kDa serine/threonine kinase protein, and its functions are the regulation of smooth-muscle contraction, organization of the actin cytoskeleton and stress fibers, formation of focal adhesions, and retraction of neurons and cellular adhesions (47). Therefore, its function in different cells and how it contributes to different pathologies through mechanisms

TABLE 4 | Software and metrics used to determine the binding of miRNAs with ROCK2.

miRNAs	Fold change		Gene target	TargetScan		miRDB		mirDIP 4.1
	LogFC	Expression		S. T	C++S	S. L	T. S	
hsa-miR-618	1.75	Up	ROCK2	7mer-A1	−0.15	306	83	X
				7mer-m8	−0.04	2,139		
				8mer	−0.01	3,066		
hsa-miR-297	2.1	Up	ROCK2	7mer-m8	−0.06	117	88	X
				7mer-m8	−0.01	2,600		

S.T, site type; C++S, context score; S.L, seed location; T.S, target score.

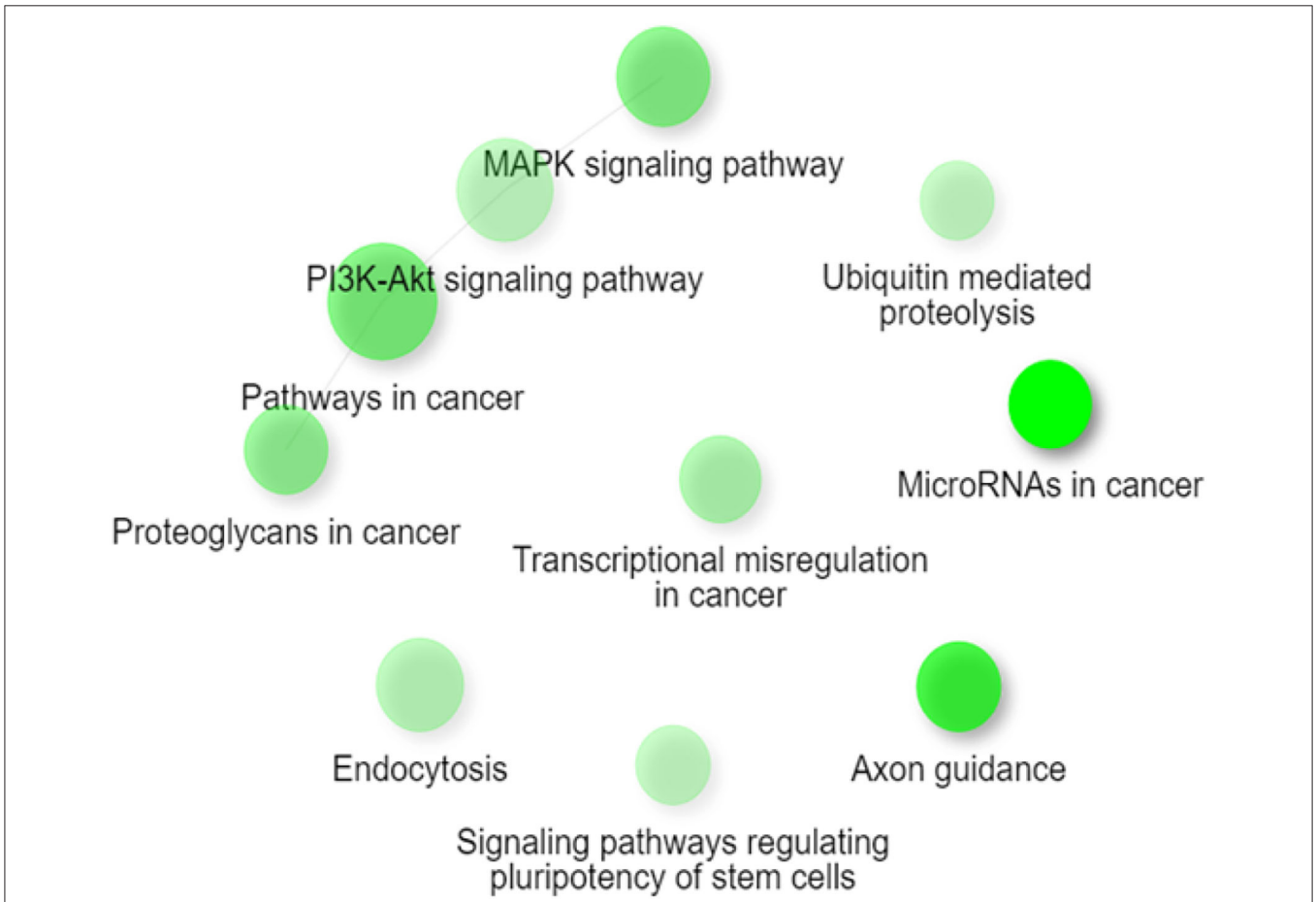

FIGURE 2 | Network figure showing the relationship between the enriched pathways obtained from the classification from KEGG. The nodes in green correspond to an enriched pathway, and their size is related to a set of larger genes. MAPK signaling, PI3K-Akt signaling pathway, pathways in cancer, and proteoglycans in cancer are connected as they share ≥ 20% of genes. Figure extracted from ShinyGO v0.61.

mediated by miRNAs have been studied. Liu et al. (48) demonstrated that hsa-miR-122 can inhibit the proliferation of prostate carcinoma cells due to the negative regulation of ROCK2 expression. Furthermore, the hsa-mir-185/ROCK2 pathway was shown to have potential to improve therapies in hepatocellular carcinoma, through metastasis inhibition (49). However, miRNAs hsa-miR-618 and hsa-miR-297 have not been experimentally validated as ROCK2 targets. The hsa-miR-618 has been reported to be unregulated in pathologies as epilepsy (50) and squamous cells from head and neck carcinomas (51). The case of hsa-miR-297 has been associated with prostate cancer (52) and with colorectal carcinoma, specifically with drug resistance (53).

The set of differentially expressed miRNAs and their gene ontological analysis showed the following biological processes: regulation of biosynthesis processes, regulation of biosynthetic

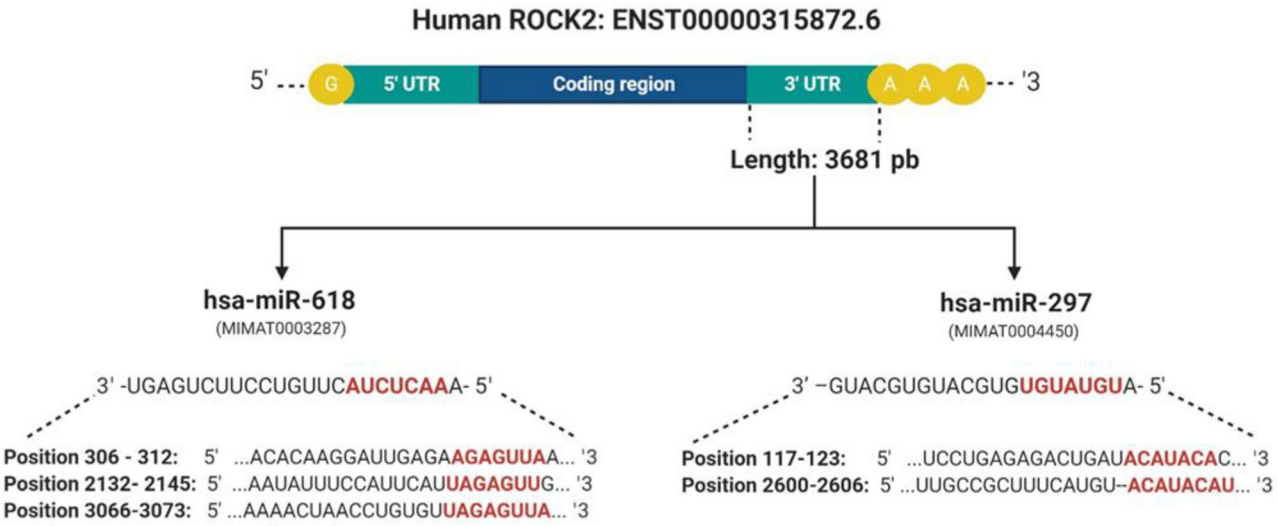

FIGURE 3 | Presentation of complementary sites and base pairs of the miRNAs hsa-miR-618 and hsa-miR-279 with the 3′UTR sequence of the ROCK2 kinase. These were predicted by software: TargetScan, miRDB, and mirDIP 4.1. Created with BioRender.com.

macromolecule processes, and positive regulation of nitrogen compound metabolic processes; this last process could be related to the gene's enrichment involved in the mechanisms associated with the ability of statins to increase the bioavailability of NO, through the inhibition of ROCKs (9). The increased expression of ROCKs reduces the expression of eNOS, and the inhibitors (Y-27632 and fasudil) have been shown to increase eNOS (54). In the case of the statins, the increased expression of eNOS was not due to FPP and LDL-C; it was due to inhibition of GGP involved with RhoA and ROCK signaling (6).

Other biological processes and cellular components highlighted in the analysis are neurogenesis, development of the nervous system, and cellular development. Several studies in animal models of spontaneous intracerebral hemorrhage that have been treated with statins have improved neurological function, reduced cerebral edema effects, increasing angiogenesis, and neurogenesis, and have decreased the infiltration of inflammatory cells. This supports the possible neuroprotective effects of statins (55–57).

Statins may also exert their pleiotropic effects through Kruppel-like factor-2 (KLF2). Statins induced the increase in mRNA expression of KLF2 in endothelial cells, which is necessary for eNOS expression (58). This could be associated with the results of molecular functions obtained like the transcription regulator activity in ontological gene analysis.

Inside the analysis associated with the biological pathways, the following ones might be highlighted: signaling pathways regulating pluripotency of stem cells, axon guidance, PI3K-AKT signaling pathways, and miRNAs in cancer. The signaling pathways regulating pluripotency of stem cells has been associated with the transforming growth factor (TGF-B) superfamily, performing important functions during the differentiation of vascular progenitor cells derived from mouse embryonic stem cells (59). Statins can exert pleiotropic effects by increasing the mobilization of endothelial progenitor cells. Damaged endothelial progenitor cells are associated with impaired endothelial function and reduced NO levels. Studies show that prehypertension and hypertension in patients are related to early senescence of progenitor cells and impaired endothelial function (60). Another route mentioned is the axon guidance, which could represent a key stage in the formation of the neural network. This mechanism has been associated with the Rho GTPase pathway through the reorganization of the cytoskeleton that determines the direction that will guide the growth cone (61). A study conducted on brain slices of oxygen-glucose-deprived cells that were exposed to fasudil (ROCK inhibitor) showed an improvement in neuronal viability (62, 63). These findings could be linked to the neuroprotective effects that statins would have on the neurovascular system. Furthermore, the PI3K-AKT signaling pathway corresponds to one of those affected by ROCK inhibition by statins as mentioned above. ROCK is a negative regulator of AKT, possibly through activation of phosphatase and the homolog of tensin (64). Also, the regulation of AKT is known to influence the expression of eNOS and thus an increase in the bioavailability of NO. This effect has been shown to contribute to a decrease in the proliferation of smooth-muscle cells, a key mechanism in the development of atherosclerosis (65). Studies have revealed that statins modulate miRNAs associated with influence the change from senescent contractile phenotype to proliferative phenotype. This could be associated with the enrichment of the miRNA pathway in cancer (66).

Finally, *in-silico* analysis has shown that statins might exert pleiotropic effects through the modulation of miRNAs that would inhibit ROCK2 kinase and also generate atheroprotective effects in endothelial cells (**Figure 4**). Although our work proposes new miRNAs that regulate the RhoA/Rock kinase pathway through an *in-silico* approach, it is necessary to

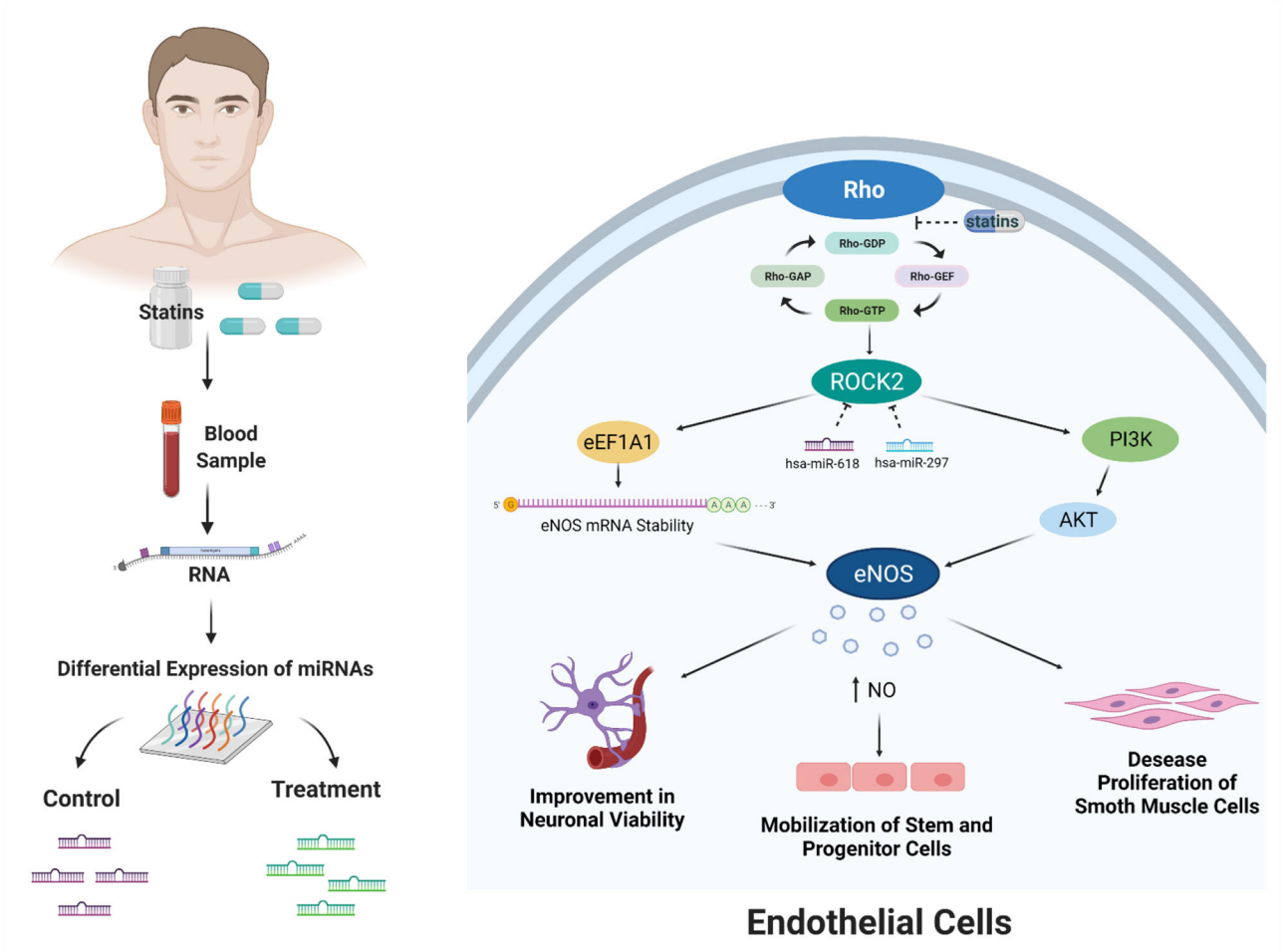

FIGURE 4 | Bioinformatic analysis showed that miRNAs modulated by statin treatment could exert the pleiotropic effects. These effects would occur due to the posttranscriptional inhibition of ROCK2 kinase by the miRNAs hsa-miR-618 and hsa-miR-297. ROCK2 kinase expression has been described by two mechanisms: stability of eNOS messenger RNA and increased activity by activation of phosphatidylinositol 3-kinase (PI3K)/AKT. The increased activity and expression of eNOS produce an increase in the bioavailability of NO. This effect of increasing NO affects improvement in neuronal viability, mobilization of stem and progenitor cells, and decreased proliferation of smooth muscle cells. Created with BioRender.com.

continue with the experimental validation of the miRNAs expressed differentially in endothelial cells through *in vitro* and *in vivo* study models. In addition, the functional role of hsa-miR-618 and hsa-miR-297 miRNAs as inhibitors of ROCK2 gene expression and in the mediation of pleiotropic effects should be evaluated.

CONCLUSION

In this work, we report that simvastatin treatment deregulates the expression of seven miRNAs (hsa-miR-515-5p, hsa-miR-18a*, hsa-miR-640, hsa-miR-618, hsa-miR-363, hsa-miR-548h, and hsa-miR-297) in HUVEC cell culture. *In-silico* analysis shows that the miRNAs hsa-miR-618 and hsa-miR-297 are upregulated, and the 3′UTR region of ROCK2, an important protein of the RhoA/Rock kinase pathway involved in modulation of pleiotropic effects exerted by statins, is predicted as a potential target for both miRNAs. In addition, functional analysis and enriched pathways revealed an important association with the pleiotropic effects produced by statins and with the inhibition of RhoA/ROCKs. These results open a new way to understand how statins, through the deregulation of the miRNA expression, might cause an atheroprotective effect through the inhibition of ROCK2 kinase.

In summary, our work through the use of bioinformatics tools contributes with new potential candidates that could regulate the pleiotropic effects in response to statin treatment. However, the functional role of hsa-miR-618 and hsa-miR-297 miRNAs and their mediation of pleiotropic effects must be evaluated by validating *in vitro* and *in vivo* models.

DATA AVAILABILITY STATEMENT

Publicly available datasets were analyzed in this study. This data can be found here: Accession number GSE126290.

AUTHOR CONTRIBUTIONS

KL and CR performed the bioinformatics analysis. KL wrote the manuscript. KS and LS contributed in writing—review and editing. All authors read and approved the final manuscript.

FUNDING

This study was supported by the Chilean National Fund for Scientific and Technological Development (FONDECYT, Grant numbers 1171765 and 3160567) and Dirección de Investigación of the Universidad de La Frontera (Grant numbers DI19-2018 and DI19-0094). KL is the recipient of ANID scholarship (21181008).

REFERENCES

1. World Health Organization (2020). Available online at: www.who.int (accessed July 27, 2020)
2. Berry JD, Dyer A, Cai X, Garside DB, Ning H, Thomas A, et al. Lifetime risks of cardiovascular disease. *N Engl J Med.* (2012) 366:321–9. doi: 10.1056/NEJMoa1012848
3. Maron DJ, Fazio S, Linton MF. Current perspectives on statins. *Circulation.* (2000) 101:207–13. doi: 10.1161/01.cir.101.2.207
4. Liao JK, Laufs U. Pleiotropic effects of statins. *Annu Rev Pharmacol Toxicol.* (2005) 45:89–118. doi: 10.1146/annurev.pharmtox.45.120403.095748
5. Davignon J. Beneficial cardiovascular pleiotropic effects of statins. *Circulation.* (2004). 109: III39–43. doi: 10.1161/01.CIR.0000131517.20177.5a
6. Hall A. Rho GTPases and the actin cytoskeleton. *Science.* (1998) 279:509–14. doi: 10.1126/science.279.5350.509
7. Van Aelst L, D'Souza-Schorey C. Rho GTPases and signaling networks. *Genes Dev.* (1997) 11:2295–322. doi: 10.1101/gad.11.18.2295
8. Riento K, Ridley AJ. ROCKs: multifunctional kinases in cell behaviour. *Nat Rev Mol Cell Biol.* (2003) 4:446–56. doi: 10.1038/nrm1128
9. Rikitake Y, Kim HH, Huang Z, Seto M, Yano K, Asano T, et al. Inhibition of Rho kinase (ROCK) leads to increased cerebral blood flow and stroke protection. *Stroke.* (2005) 36:2251–7. doi: 10.1161/01.STR.0000181077.84981.11
10. Oesterle A, Laufs U, Liao JK. Pleiotropic effects of statins on the cardiovascular system. *Circ Res.* (2017) 120:229–43. doi: 10.1161/CIRCRESAHA.116.308537
11. Takemoto M, Liao JK. Pleiotropic effects of 3-hydroxy-3-methylglutaryl coenzyme a reductase inhibitors. *Arterioscler Thromb Vasc Biol.* (2001) 21:1712–9. doi: 10.1161/hq1101.098486
12. De Caterina R, Libby P, Peng HB, Thannickal VJ, Rajavashisth TB, Gimbrone MA, et al. Nitric oxide selectively reduces endothelial expression of adhesion molecules and proinflammatory cytokines. *J Clin Invest.* (1995) 96:60–8. doi: 10.1172/JCI118074
13. Laufs U, Liao JK. Post-transcriptional regulation of endothelial nitric oxide synthase mRNA stability by Rho GTPase. *J Biol Chem.* (1998) 273:24266–71. doi: 10.1074/jbc.273.37.24266
14. Wang J, Xu Z, Kitajima I, Wang Z. Effects of different statins on endothelial nitric oxide synthase and AKT phosphorylation in endothelial cells. *Int J Cardiol.* (2008) 127:33–9. doi: 10.1016/j.ijcard.2007.10.034
15. Krol J, Loedige I, Filipowicz W. The widespread regulation of microRNA biogenesis, function and decay. *Nat Rev Genet.* (2010) 11:597–610. doi: 10.1038/nrg2843
16. Alles J, Fehlmann T, Fischer U, Backes C, Galata V, Minet M, et al. An estimate of the total number of true human miRNAs. *Nucleic Acids Res.* (2019) 47:3353–64. doi: 10.1093/nar/gkz097
17. Pertea M, Salzberg SL. Between a chicken and a grape: estimating the number of human genes. *Genome Biol.* (2010) 11:206. doi: 10.1186/gb-2010-11-5-206
18. Kyrollos DG, Reid B, Dick K, Green JR. RPmirDIP: reciprocal perspective improves miRNA and targeting prediction. *Sci Rep.* (2020) 10:1–13. doi: 10.5683/SP2/LD8JKJ
19. Wang J, Chen J, Sen S. MicroRNA as biomarkers and diagnostics. *J Cell Physiol.* (2016) 231:25–30. doi: 10.1002/jcp.25056
20. Wong CM, Wei L, Au SLK, Fan DNY, Zhou Y, Tsang FHC, et al. MiR-200b/200c/429 subfamily negatively regulates Rho/ROCK signaling pathway to suppress hepatocellular carcinoma metastasis. *Oncotarget.* (2015) 6:13658. doi: 10.18632/oncotarget.3700
21. Zhou L, Xu Z, Ren X, Chen K, Xin S. MicroRNA-124 (MiR-124) inhibits cell proliferation, metastasis and invasion in colorectal cancer by downregulating Rho-associated protein kinase 1 (ROCK1). *Cell Physiol Biochem.* (2016) 38:1785–95. doi: 10.1159/000443117
22. Zambrano T, Hirata RD, Hirata MH, Cerda Á, Salazar LA. Altered microRNome profiling in statin-induced HepG2 cells: a pilot study identifying potential new biomarkers involved in lipid-lowering treatment. *Cardiovasc Drugs Ther.* (2015) 29:509–18. doi: 10.1007/s10557-015-6627-0
23. Minami Y, Satoh M, Maesawa C, Takahashi Y, Tabuchi T, Itoh T, et al. Effect of atorvastatin on microRNA 221/222 expression in endothelial progenitor cells obtained from patients with coronary artery disease. *Eur J Clin Invest.* (2009) 39:359–67. doi: 10.1111/j.1365-2362.2009.02110.x
24. Mohammadzadeh N, Montecucco F, Carbone F, Xu S, Al-Rasadi K, Sahebkar A. Statins:Epidrugs with effects on endothelial health? *Eur J Clin Invest.* (2020). 50:e13388. doi: 10.1111/eci.13388
25. Cerda A, Fajardo CM, Basso RG, Hirata MH, Hirata RDC. Role of microRNAs 221/222 on statin induced nitric oxide release in human endothelial cells. *Arq Bras Cardiol.* (2015) 104:195–201. doi: 10.5935/abc.20140192
26. Dunning MJ, Smith ML, Ritchie ME, Tavaré, S. beadarray: R classes and methods for Illumina bead-based data. *Bioinformatics.* (2007) 23:2183–4. doi: 10.1093/bioinformatics/btm311
27. Kauffmann A, Gentleman R, Huber W. arrayQualityMetrics-a bioconductor package for quality assessment of microarray data. *Bioinformatics.* (2009) 25:415–6. doi: 10.1093/bioinformatics/btn647
28. Smith ML, Baggerly KA, Bengtsson H, Ritchie ME, Hansen KD. illuminaio: an open source IDAT parsing tool for Illumina microarrays. (2013). *F1000Res.* 2:264. doi: 10.12688/f1000research.2-264.v1
29. Huber W, Carey VJ, Gentleman R, Anders S, Carlson M, Carvalho BS, et al. Orchestrating high-throughput genomic analysis with Bioconductor. *Nat Methods.* (2015) 12:115–21. doi: 10.1038/nmeth.3252
30. R Core Team. *R: A Language and Environment for Statistical Computing.* Vienna: R Foundation for Statistical Computing (2020). Available online at: https://www.R-project.org/ (accessed July 15, 2020).
31. Ritchie ME, Phipson B, Wu DI, Hu Y, Law CW, Shi W, et al. limma powers differential expression analyses for RNA-sequencing and microarray studies. *Nucleic Acids Res.* (2015) 43:e47. doi: 10.1093/nar/gkv.007
32. Tang Y, Horikoshi M, Li W. ggfortify: unified interface to visualize statistical results of popular R packages. *R J.* (2016) 8:474–85. doi: 10.32614/RJ-2016-060
33. Vu VQ. *ggbiplot: A ggplot2 Based Biplot. R package version 0.55.* (2011). Available online at: http://github.com/vqv/ggbiplot (accessed July 15, 2020).
34. Tokar T, Pastrello C, Rossos AE, Abovsky M, Hauschild AC, Tsay M, et al. mirDIP 4.1—integrative database of human microRNA target predictions. *Nucleic Acids Res.* (2018). 46:D360–70. doi: 10.1093/nar/gkx1144
35. Ge SX, Jung D, Yao R. ShinyGO: a graphical gene-set enrichment tool for animals and plants. *Bioinformatics.* (2020) 36:2628–9. doi: 10.1093/bioinformatics/btz931
36. Agarwal V, Bell GW, Nam JW, Bartel DP. Predicting effective microRNA target sites in mammalian mRNAs. *Elife.* (2015) 4:e05005. doi: 10.7554/eLife.05005

37. Chen Y, Wang X. miRDB: an online database for prediction of functional microRNA targets. *Nucleic Acids Res.* (2020) 48:D127–31. doi: 10.1093/nar/gkz757
38. Liang L, Su W, Zhou L, Cao Y, Zhou X, Liu S, et al. Statin downregulation of miR-652-3p protects endothelium from dyslipidemia by promoting ISL1 expression. *Metabolism.* (2020) 107:154226. doi: 10.1016/j.metabol.2020.154226
39. Zhang C. MicroRNAs: role in cardiovascular biology and disease. *Clin Sci.* (2008) 114:699–706. doi: 10.1042/CS20070211
40. Ono K, Kuwabara Y, Han J. MicroRNAs and cardiovascular diseases. *FEBS J.* (2011) 278:1619–33. doi: 10.1111/j.1742-4658.2011.08090.x
41. Rajewsky N. microRNA target predictions in animals. *Nat Genet.* (2006) 38:S8–S13. doi: 10.1038/ng1798
42. Oliveira AC, Bovolenta LA, Nachtigall PG, Herkenhoff ME, Lemke N, Pinhal D. Combining results from distinct MicroRNA target prediction tools enhances the performance of analyses. *Front Genet.* (2017) 8:59. doi: 10.3389/fgene.2017.00059
43. Fang Z, Rajewsky N. The impact of miRNA target sites in coding sequences and in 3′ UTRs. *PLoS ONE.* (2011) 6:e18067. doi: 10.1371/journal.pone.0018067
44. Selbach M, Schwanhäusser B, Thierfelder N, Fang Z, Khanin R, Rajewsky N. Widespread changes in protein synthesis induced by microRNAs. *Nature.* (2008) 455:58–63. doi: 10.1038/nature07228
45. Garbern JC, Mummery CL, Lee RT. Model systems for cardiovascular regenerative biology. *Cold Spring Harb Perspect Med.* (2013) 3:a014019. doi: 10.1101/cshperspect.a014019
46. Medina-Leyte DJ, Domínguez-Pérez M, Mercado I, Villarreal-Molina MT, Jacobo-Albavera L. Use of human umbilical vein endothelial cells (HUVEC) as a model to study cardiovascular disease: a review. *Appl Sci.* (2020) 10:938. doi: 10.3390/app10030938
47. Fukata Y, Kaibuchi K, Amano M. Rho–Rho-kinase pathway in smooth muscle contraction and cytoskeletal reorganization of non-muscle cells. *Trends Pharmacol Sci.* (2001) 22:32–9. doi: 10.1016/s0165-6147(00)01596-0
48. Liu H, Hou T, Ju W, Xing Y, Zhang X, Yang J. MicroRNA-122 downregulates Rho-associated protein kinase 2 expression and inhibits the proliferation of prostate carcinoma cells. *Mol Med Rep.* (2019) 19:3882–8. doi: 10.3892/mmr.2019.9995
49. Niu Y, Tang G. miR-185-5p targets ROCK2 and inhibits cell migration and invasion of hepatocellular carcinoma. *Oncol Lett.* (2019) 17:5087–93. doi: 10.3892/ol.2019.10144
50. Miller-Delaney SF, Bryan K, Das S, McKiernan RC, Bray IM, Reynolds JP, et al. Differential DNA methylation profiles of coding and non-coding genes define hippocampal sclerosis in human temporal lobe epilepsy. *Brain.* (2015) 138:616–31. doi: 10.1093/brain/awu373
51. Hui L, Wu H, Yang N, Guo X, Jang X. Identification of prognostic microRNA candidates for head and neck squamous cell carcinoma. *Oncol Rep.* (2016) 35:3321–30. doi: 10.3892/or.2016.4698
52. Osip'Yants AI, Knyazev EN, Galatenko AV, Nyushko KM, Galatenko VV, Shkurnikov MY, et al. Changes in the level of circulating hsa-miR-297 and hsa-miR-19b-3p miRNA are associated with generalization of prostate cancer. *Bull Exp Biol Med.* (2017) 162:379–82. doi: 10.1007/s10517-017-3620-6
53. Xu K, Liang X, Shen K, Cui D, Zheng Y, Xu J, et al. miR-297 modulates multidrug resistance in human colorectal carcinoma by down-regulating MRP-2. *Biochem J.* (2012) 446:291–300. doi: 10.1042/BJ20120386
54. Goldstein JL, Brown MS. Regulation of the mevalonate pathway. *Nature.* (1990) 343:425–30. doi: 10.1038/343425a0
55. Yang D, Knight RA, Han Y, Karki K, Zhang J, Chopp M, et al. Statins protect the blood brain barrier acutely after experimental intracerebral hemorrhage. *J Behav Brain Sci.* (2013) 3:100. doi: 10.4236/jbbs.2013.31010
56. Yang D, Zhang J, Han Y, James E, Chopp M, Seyfried DM. Acute statin treatment improves recovery after experimental intracerebral hemorrhage. *World J Neurosci.* (2013) 3:69. doi: 10.4236/wjns.2013.32010
57. Chen CJ, Ding D, Ironside N, Buell TJ, Elder LJ, Warren A, et al. Statins for neuroprotection in spontaneous intracerebral hemorrhage. *Neurology.* (2019) 93:1056–66. doi: 10.1212/WNL.0000000000008627
58. Sen-Banerjee S, Mir S, Lin Z, Hamik A, Atkins GB, Das H, et al. Kruppel-like factor 2 as a novel mediator of statin effects in endothelial cells. *Circ Hagertown.* (2005) 112:720–6. doi: 10.1161/CIRCULATIONAHA
59. Watabe T, Nishihara A, Mishima K, Yamashita J, Shimizu K, Miyazawa K, et al. TGF-β receptor kinase inhibitor enhances growth and integrity of embryonic stem cell–derived endothelial cells. *J Cell Biol.* (2003) 163:1303–11. doi: 10.1083/jcb.20030514
60. Giannotti G, Doerries C, Mocharla PS, Mueller MF, Bahlmann FH, Horvàth T, et al. Impaired endothelial repair capacity of early endothelial progenitor cells in prehypertension: relation to endothelial dysfunction. *Hypertension.* (2010). 55:1389–97. doi: 10.1161/hypertensionaha.109.141614
61. Govek EE, Newey SE, Van Aelst L. The role of the Rho GTPases in neuronal development. *Genes Dev.* (2005) 19:1–49. doi: 10.1101/gad.125640
62. Yamashita K, Kotani Y, Nakajima Y, Shimazawa M, Yoshimura SI, Nakashima S, et al. Fasudil, a Rho kinase (ROCK) inhibitor, protects against ischemic neuronal damage *in vitro* and *in vivo* by acting directly on neurons. *Brain Res.* (2007) 1154:215–24. doi: 10.1016/j.brainres.2007.04.013
63. Li Q, Huang XJ, He W, Ding J, Jia JT, Fu G, et al. Neuroprotective potential of fasudil mesylate in brain ischemia-reperfusion injury of rats. *Cell Mol Neurobiol.* (2009) 29:169–80. doi: 10.1007/s10571-008-9308-8
64. Van der Heijden M, Versteilen AM, Sipkema P, van Nieuw Amerongen GP, Musters RJ, Groeneveld AJ. Rho-kinase-dependent F-actin rearrangement is involved in the inhibition of PI3-kinase/Akt during ischemia–reperfusion-induced endothelial cell apoptosis. *Apoptosis.* (2008) 13:404–12. doi: 10.1007/s10495-007-0173
65. Torella D, Iaconetti C, Catalucci D, Ellison GM, Leone A, Waring CD, et al. MicroRNA-133 controls vascular smooth muscle cell phenotypic switch *in vitro* and vascular remodeling *in vivo*. *Circ Res.* (2011) 109:880–93. doi: 10.1161/CIRCRESAHA.111.240150
66. Mohajeri M, Banach M, Atkin SL, Butler AE, Ruscica M, Watts GF, et al. MicroRNAs: novel molecular targets and response modulators of statin therapy. *Trends Pharmacol Sci.* (2018) 39:967–81. doi: 10.1016/j.tips.2018.09

Conflict of Interest: The authors declare that the research was conducted in the absence of any commercial or financial relationships that could be construed as a potential conflict of interest.

frontiers in Cardiovascular Medicine

REVIEW
published: 15 October 2021
doi: 10.3389/fcvm.2021.771349

Brugada Syndrome: Warning of a Systemic Condition?

Sara D'Imperio[1†], *Michelle M. Monasky*[1†], *Emanuele Micaglio*[1], *Giuseppe Ciconte*[1], *Luigi Anastasia*[2] *and Carlo Pappone*[1,2*]

[1] *Arrhythmology Department, Istituto di Ricovero e Cura a Carattere Scientifico (IRCCS) Policlinico San Donato, Milan, Italy,*
[2] *Faculty of Medicine and Surgery, University of Vita-Salute San Raffaele, Milan, Italy*

Brugada syndrome (BrS) is a hereditary disorder, characterized by a specific electrocardiogram pattern and highly related to an increased risk of sudden cardiac death. BrS has been associated with other cardiac and non-cardiac pathologies, probably because of protein expression shared by the heart and other tissue types. In fact, the most commonly found mutated gene in BrS, *SCN5A*, is expressed throughout nearly the entire body. Consistent with this, large meals and alcohol consumption can trigger arrhythmic events in patients with BrS, suggesting a role for organs involved in the digestive and metabolic pathways. Ajmaline, a drug used to diagnose BrS, can have side effects on non-cardiac tissues, such as the liver, further supporting the idea of a role for organs involved in the digestive and metabolic pathways in BrS. The BrS electrocardiogram (ECG) sign has been associated with neural, digestive, and metabolic pathways, and potential biomarkers for BrS have been found in the serum or plasma. Here, we review the known associations between BrS and various organ systems, and demonstrate support for the hypothesis that BrS is not only a cardiac disorder, but rather a systemic one that affects virtually the whole body. Any time that the BrS ECG sign is found, it should be considered not a single disease, but rather the final step in any number of pathways that ultimately threaten the patient's life. A multi-omics approach would be appropriate to study this syndrome, including genetics, epigenomics, transcriptomics, proteomics, metabolomics, lipidomics, and glycomics, resulting eventually in a biomarker for BrS and the ability to diagnose this syndrome using a minimally invasive blood test, avoiding the risk associated with ajmaline testing.

Keywords: Brugada syndrome (BrS), sudden cardiac death (SCD), arrhythmia, genetics, epilepsy, ajmaline, thyroid, cancer

OPEN ACCESS

Edited by:
George W. Booz,
University of Mississippi Medical Center School of Dentistry, United States

Reviewed by:
Hariharan Raju,
Macquarie University, Australia
Oscar Campuzano,
University of Girona, Spain

***Correspondence:**
Carlo Pappone
carlo.pappone@af-ablation.org

[†] These authors have contributed equally to this work

Specialty section:
This article was submitted to Cardiovascular Genetics and Systems Medicine, a section of the journal Frontiers in Cardiovascular Medicine

Received: *06 September 2021*
Accepted: *23 September 2021*
Published: *15 October 2021*

Citation:
D'Imperio S, Monasky MM, Micaglio E, Ciconte G, Anastasia L and Pappone C (2021) Brugada Syndrome: Warning of a Systemic Condition? Front. Cardiovasc. Med. 8:771349. doi: 10.3389/fcvm.2021.771349

INTRODUCTION

Brugada syndrome (BrS) is a hereditary disorder, highly related to an increased risk of sudden cardiac death (1), characterized by a type 1 (coved type) ST-segment elevation ≥2 mm followed by a negative T-wave in ≥1 of the right precordial leads V1 to V2 on the electrocardiogram (ECG) (2), which can occur spontaneously or after pharmacologically induced. The typical symptoms of BrS are syncope and cardiac arrest due to ventricular fibrillation (VF) or ventricular tachycardia (VT), in the absence of overt cardiac structural changes, typically between 30 and 50 years of age (3, 4). BrS has been associated with several other cardiac disorders, such as early repolarization syndrome (5), arrhythmogenic right ventricular cardiomyopathy/dysplasia (ARVC/D) (6–9), progressive cardiac conduction defect (Lenègre syndrome) (10, 11), LQTS (12–14), Wolff-Parkinson-White (15, 16),

hypertrophic cardiomyopathy (17, 18), atrial flutter (19), and atrial fibrillation (20–23). In addition, BrS has also been associated with non-cardiac pathologies, such as epilepsy, thyroid disorders, cancer, skeletal muscle sodium channelopathies, laminopathies, and diabetes. One reason for this may be due to similar ion channel expression shared by the heart and other tissue types (24–27). In fact, the most commonly found mutated gene in BrS, *SCN5A* (28), is expressed throughout the entire body, with the largest protein expression levels found in the plasma, heart, and pancreatic juice (29). Consistent with this, large meals, alcohol, specific drugs, and fever can trigger arrhythmic events in patients with BrS, suggesting a role for organs involved in the digestive and metabolic (including mitochondrial) pathways (28, 30).

Drugs used to induced the type 1 BrS ECG pattern include Ajmaline, Flecainide, and Procainamide, which are often thought of as sodium channel blockers (4, 31, 32). Many centers prefer the use of Ajmaline because of its lower false-negative rate (33). However, several studies have highlighted the complex mechanism of Ajmaline, which does not act solely as a sodium channel blocker, but rather acts additionally on potassium and calcium channels (34, 35). Ajmaline can have side effects on non-cardiac tissues, such as the liver and mitochondria (36), further supporting the idea of a role for organs involved in the digestive and metabolic pathways in BrS.

In addition to cardiac, neural, digestive, and metabolic involvement, BrS may also affect other areas of the body. Potential biomarkers for BrS have been reportedly found in the serum or plasma of BrS patients (37, 38), although the conclusions are disputed (39). Indeed, a multi-omics approach would be appropriate to study this syndrome, including not only genetics, but also epigenomics, transcriptomics, proteomics, metabolomics, lipidomics, and glycomics (28). Here, we review the known associations between BrS and various systems and demonstrate support for the hypothesis that BrS is not only a cardiac disorder, but rather a systemic one that affects virtually the whole body.

BRS GENE CANDIDATES AND AJMALINE MOLECULAR TARGETS EXPRESSED IN MULTIPLE ORGAN SYSTEMS

BrS was once viewed as a pure monogenic Mendelian disorder, caused by a single variant in a single gene. In some families, this may in fact still be the case. However, the view of BrS genetics has more recently evolved to recognize, in most cases, that BrS is an oligogenic syndrome, which can result from the combined effect of multiple variants, even in multiple genes, that occur in the same person (28, 40, 41). Much research is underway to determine what genes may be involved. Candidate genes (2, 28) commonly involve those encoding for sodium, potassium, and calcium channels (42–46), as well as, less commonly, sarcomeric and structural proteins (17, 18, 45, 47, 48) and mitochondrial genes (49) (**Table 1**).

There are several candidate genes currently under investigation, reviewed elsewhere (2, 28, 40). Here, we do not seek to exhaustively list every single candidate gene that exists, but rather, we focus on a selected number of them to highlight the concept that these genes are expressed not only in the heart, but throughout the body, and thus mutations in any of these genes could have pathogenic effects not only on the heart, but also on other organ systems. The most widely screened BrS candidate genes encoding for sodium channels include *SCN5A*, *SCN10A*, *SCN1B*, *SCN2B*, and *SCN3B*, while genes encoding for potassium channels include *HCN4*, *KCND2*, *KCND3*, *KCNE3*, *KCNE5*, *KCNH2*, and *KCNJ8*, and genes encoding for calcium channels include *CACNA1C*, *CACNA2D1*, *CACNB2*, *PLN,* and *TRPM4* (2, 28, 40). These genes are expressed not only in the heart, but also throughout the rest of the body. **Figure 1** shows the organs in which the protein level encoded by certain sodium, potassium, and calcium genes described in BrS is highly expressed. However, many of these genes encode for proteins that are expressed to a lesser extent in several other organs. Despite being expressed to a lesser extent, the low expression of these proteins in other cell types can influence disease expression and contribute to overlap pathologies. For more details on the organs and cell types in which these genes are expressed to a lower extent, see GeneCards (29).

Calcium is the connection between excitation and contraction, and in fact, arrhythmias and sudden death can occur as a result of calcium mishandling, including altered calcium signaling resulting from sarcomeric mutations (50). Recent studies have suggested a possible involvement of sarcomeric mutations in BrS (17, 45, 51) that alter calcium signaling (18, 42). BrS sarcomeric gene candidates include *TPM1*, *MYBPC3*, *DSG2*, *PKP2*, *LMNA*, *MYH7*, *TTN*, and *GATA4* (17, 45, 47, 48, 52). In BrS, it has been proposed that loss of the action potential, and consequent reduced calcium channel current and cardiomyocyte calcium depletion, could result in wall motion abnormalities, dilation of

TABLE 1 | BrS candidate genes.

BRUGADA SYNDROME CANDIDATE GENES		
ABCC9	KCNE2	SCN2B
ACTC1	KCNE3	SCN3B
AKAP9	KCNE5/KCNE1L	SCN4B
ANK2	KCNH2	SCN5A
CACNA1C	KCNJ2	SCN10A
CACNA2D1	KCNJ5	SEMA3A
CACNB2	KCNJ8	SNTA1
CASQ2	KCNQ1	TMEM43
CAV3	RANGFR / MOG1	TNNI3
DSC2	MYBPC3	TNNT2
DSG2	MYH7	TPM1
DSP	MYL2	TRPM4
FLNC	MYL3	LMNA
GPD1L	PKP2	PLN
HCN4	PLN	CBL
JUP	NOS1AP	tRNA-Ala
KCND3	RYR2	tRNA-Gln
KCNE1	SCN1B	tRNA-Met

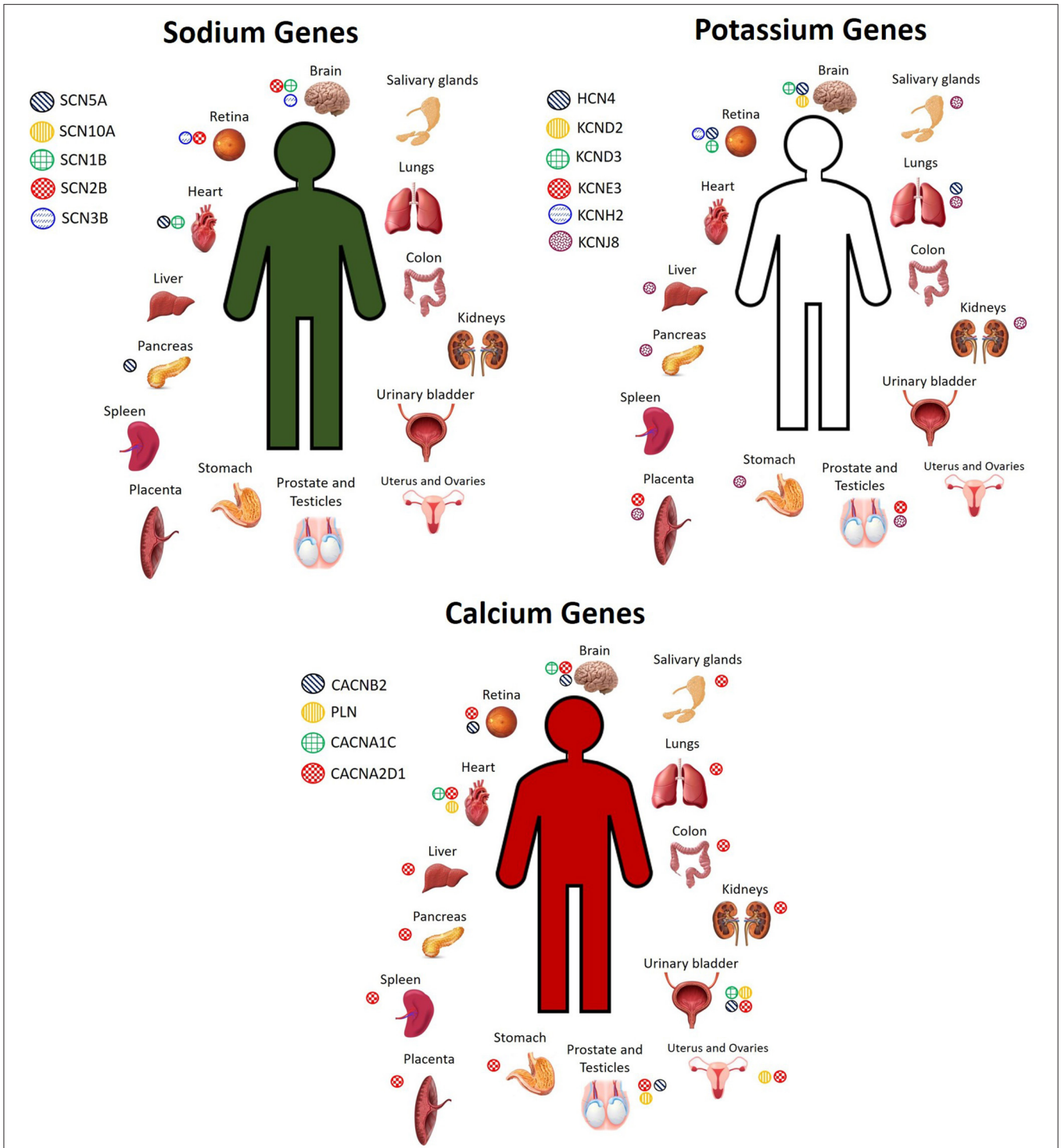

FIGURE 1 | Cell and tissue types in which sodium, potassium, and calcium channel BrS candidate genes encode for high levels of protein expression. Not pictured: Sodium genes: *SCN5A*: plasma, pancreas juice. *SCN10A*: monocytes, neutrophil, B cells, T cells, skin. *SCN2B*: spinal cord, fetal heart, fetal brain. *SCN3B*: fetal brain. Potassium genes: *HCN4*: plasma, PBMCs, fetal heart. *KCND2*: fetal brain. *KCND3*: fetal brain, bones. *KCNJ8*: lymph node, bone marrow, stromal cells, nasopharynx, rectum, thyroid, adrenal, breast, gallbladder, skin, cervix, seminal vesicles Calcium genes: *CACNA2D1*: serum, plasma, PBMCs, lymph nodes, tonsil, bones, skin, bone marrow, esophagus, adipocytes, fetal brain, frontal cortex, cerebral cortex, cerebral spinal fluid, spinal cord, fetal heart, oral epithelial, cardia, fetal gut, rectum, thyroid, adrenal, gallbladder, urine, fetal ovary, fetal testis, seminal vesicles. *PLN*: tonsil, fetal heart, esophagus, urinary bladder, seminal vesicles. *CACNB2*: fetal brain. *CACNA1C*: frontal cortex, fetal heart, urinary bladder. *TRPM4:* Spinal cord, nasal respiratory epithelium, rectum, breast (29).

the right ventricular outflow tract (RVOT) region, and reduced ejection fraction (EF) (31, 42, 53, 54), which have, in fact, been recently observed clinically in patients affected by BrS (55). BrS candidate genes encoding for proteins important in cell signaling include *AKAP9*, *ABCC9*, and *CBL* (40, 45, 56), and these, like the other BrS gene candidates, are expressed not only in the heart, but additionally throughout the rest of the body. The cell or tissue types in which these genes are highly expressed are shown in **Figure 2**. For a more comprehensive assessment of all the tissue types in which they are expressed even to a lesser extent, please see GeneCards (29).

Genes identified in BrS genetics research as candidate genes related to the mechanism of BrS are expressed throughout the human body (**Figures 1**, **2**), and variants identified in any one of them could modify not only heart function, but the function of any tissue type in which they are expressed. To what extent is uncertain, and we summarize below studies which support the idea that we are only seeing the tip of the iceberg in what can be learned from BrS research, namely, the molecular connections between multiple pathologies throughout the body.

BRUGADA SYNDROME AND THE NEURAL SYSTEM

An overlap between cardiac arrhythmia and epilepsy has been described, possibly because of common mutations in genes encoding for ion channels. Several studies point toward the possibility of co-expression of ion channels in both the heart and brain, leading to the manifestation of both cardiac arrhythmia and epilepsy (57–59). Many of these studies have identified gene mutations known to cause cardiac arrhythmia syndromes such as LQTS and BrS. For example, idiopathic epilepsy and LQTS may be linked by mutations in the potassium channel gene, *KCNQ1* (58). Also the sodium channel gene, *SCN5A*, usually associated with SCD and BrS (60–62), has been of particular interest to understand the effects of specific mutations (63–68) or even polymorphisms (69–73) in this gene, and their relation with BrS, and this gene has been linked to sudden unexplained death in epilepsy (SUDEP) (74). In fact, this gene has already been implicated in an overlap syndrome involving both epilepsy and BrS (24). Indeed, up to 18% of patients affected by epilepsy

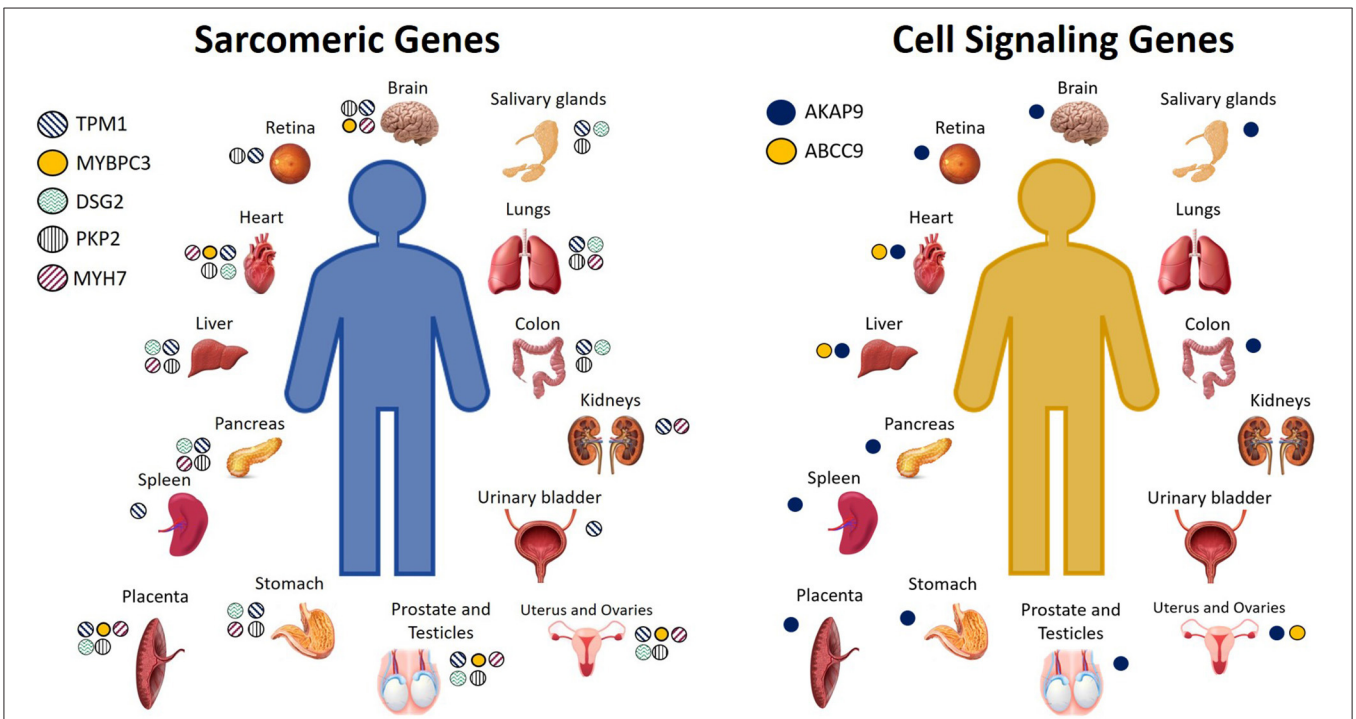

FIGURE 2 | Cell and tissue types in which sarcomeric and cell signaling BrS candidate genes encode for high levels of protein expression. Not pictured: Sarcomeric genes: *TPM1*: Serum, plasma, monocytes, neutrophil, B lymphocytes, CD8 T cells, NK cells, PBMCs, platelets, lymph nodes, tonsils, bone marrow, fetal brain, spinal cord, fetal heart, bone, oral epithelial, nasopharynx, esophagus, cardia, gut fetal, rectum, fetal liver, adipocytes, amniocytes, thyroid, adrenal, breast, milk, gallbladder, urine, skin, fetal ovary, fetal testis, seminal vesicles. *MYBPC3*: fetal brain, fetal heart, oral epithelium, fetal liver, adrenal, fetal testis. *DSG2*: serum, plasma, platelets, tonsils, fetal heart, oral epithelia, esophagus, cardia, fetal gut, rectum, fetal liver, adipocytes, synovial fluid, amniocytes, thyroid, breast, gallbladder, urine, urinary bladder, skin, fetal ovary. *PKP2*: platelets, spinal cord, fetal heart, fetal gut, rectum, amniocytes, adrenal, breast, gallbladder, skin, fetal ovary, fetal testis. *MYH7*: platelets, tonsil, fetal brain, spinal cord, fetal heart, esophagus, rectum, fetal liver, adipocytes, fetal ovaries, fetal testis. Cell signaling genes: *AKAP9*: monocytes, PBMCs, platlets, lymph node, brain fetal, esophagus, cardia, rectum, fetal liver, adipocytes, amniocytes, adrenal, pancreatic juice, islet of Langherans, gallbladder, ovary fetal, testis fetal. *ABCC9*: plasma, bone marrow, heart fetal, fetal liver (29).

die of SUDEP (59). Unfortunately, autopsy performed on SUDEP patients does not reveal the cause of death nor any evidence related to pulmonary or cardiac pathology (75); however, SUDEP and sudden cardiac death due to cardiac arrhythmia share a few risk factors: age and sex (76). Furthermore, it has also been shown through EEG/ECG combined studies that patients with true epileptic seizures have a high prevalence (33–44%) of cardiac arrhythmias (58, 77–81), including, at least, LQTS, BrS, QT dispersion, sinus tachycardia, T-wave alternans, bradyarrhythmia, or asystole, sometimes through common genetic mutations (25–27, 82–88). Potential gene candidates for SUDEP include *FBN1*, *HCN1*, *SCN4A*, *EFHC1*, *CACNA1A*, *SCN11A*, and *SCN10A* (89). *SCN10A* is also a gene candidate for BrS (70, 90, 91), and patients with this syndrome and variants in this gene have been shown to have similar clinical presentations to patients with variants in the gene *SCN5A* (43).

Episodes of cardiac arrhythmia in patients affected by epilepsy may also be induced by antiepileptic drugs, such as carbamazepine and lamotrigine, which are known to target sodium voltage-gated channels (92–94). Carbamazepine, an anti-epileptic drug used also to treat schizophrenia, induced the BrS ECG pattern in a patient with schizophrenia (95). In a patient with epilepsy and intellectual disability, the drug Lamotrigine induced the BrS ECG pattern, possibly in conjunction with a genetic predisposition for cardiac arrhythmia due to a variant in the *SCN9A* gene, also possibly in association with a genetic variant in the gene *AKAP9* (96). The overlap between epilepsy and cardiac arrhythmias demonstrated in several studies suggest that patients with either of these conditions should be checked for the other. Many of the variants thought to be responsible for cardiac arrhythmias occur in genes that have a low expression in the brain. However, their expression is nevertheless present, and, as can be seen from the literature, very relevant. Thus, future studies certainly should investigate these associations.

BRUGADA SYNDROME AND CIRCULATING ELECTROLYTES, POISONS, AND BLOOD

An elevated ST segment, which looks identical to the ECG pattern used to diagnose BrS, has been described as a result of potassium or calcium imbalances in the blood. Often, this type of ECG pattern discovered as a result of electrolyte imbalances is described as a BrS "phenocopy." However, so much is not known about the mechanism of BrS, and given the fact that BrS has historically been defined more for what it is *not* than for what it *is*, it may actually be premature to discount ST segment elevations occurring in the presence of electrolyte imbalances in the quest to unveil the mechanism of BrS (41). Several studies have described hypokalemia (97–99), hyperkalemia (100–104), or hypercalcemia (105–107) in association with the BrS ECG pattern, or in association with an elevated ST segment that appears identical to the BrS pattern. Diseases related to these conditions, such as Gitelman syndrome, which results in potassium depletion, usually attributed to the *SLC12A3* gene, can lend new candidate genes to the field of BrS (108). In patients with severe hyperkalemia, the ST segment elevation, even if described at the time as a "phenocopy," was described in association with malignant arrhythmias secondary to resting potential depolarization, reduced sodium current availability, and fibrosis at the right ventricular outflow tract (102), signs which are now typically described also in association with "true BrS," whatever that is. Hypercalcaemia can be responsible for the ST segment elevation, resembling the BrS ECG pattern, and ventricular fibrillation, secondary to calcium-dependent loss of sodium channel function (106). This mechanism too is consistent with current theories about the possible mechanisms of "true BrS." Furthermore, hypercalcaemia is associated with hyperthyroidism (109), which is additionally implicated in the development of an ST segment elevation resembling the BrS ECG pattern.

In addition to electrolyte imbalances, abnormalities of the blood occurring even from blood transfusion can result in the BrS ECG pattern. The type 1 BrS ECG pattern appeared after cardiac iron overload after blood transfusion (110). Another patient developed the BrS ECG pattern during febrile neutropenia after undergoing high dose chemotherapy followed by autologous peripheral blood cell transplantation (ABSCT) for acute myeloid leukemia (111). These cases of apparent transmission of the BrS could provide further insight into the mechanisms of the development of the BrS ECG pattern.

Plasmic proteomic changes have been observed in patients with BrS, including increased levels of apolipoprotein E, prothrombin, vitronectin, complement-factor H, vitamin-D-binding protein, voltage-dependent anion-selective channel protein 3, and clusterin (37). Similarly, decreased protein levels were observed for alpha-1-antitrypsin, fibrinogen, and angiotensinogen, and post-translational modifications of antithrombin-III were observed (37).

An elevated ST segment identical to the BrS ECG pattern can also be elicited by environmental factors, which ultimately act on the heart. It has been established that metals could induce this pattern. Several studies reported the manifestation of the BrS ECG pattern after the consumption of metal phosphides, which are mainly found in rodenticide, insecticide, and fumigant, and they are used as suicidal agents. These substances, such as aluminum phosphide (ALP), zinc phosphide (ZnP), calcium phosphide, and magnesium phosphide, are very toxic because they release phosphine gas as soon as they interact with hydrochloric acid in the stomach. The phosphine gas is a non-competitive inhibitor of cytochrome c oxidase in the mitochondria, and the mechanism of toxicity includes the formation of highly reactive free hydroxyl radicals (112). It can result in myocardial toxicity and cardia arrhythmia, which eventually can lead to death (113). Moreover, the intoxication from metal phosphides can result in several ECG abnormalities, including ST segment elevation in leads V1-V3, like the BrS ECG pattern. For example, three different cases of patients who ingested rat poison containing aluminum phosphide manifested significant abnormalities, including the ST segment elevation in leads V1-V3 (114–116). Moreover, another case reported a patient who intoxicated himself with rodenticide, which contained ZnP. The ECG of the patient showed a type 1 BrS

pattern, which then normalized after 24 h (117). Finally, a male patient, after the ingestion of 7.5 g of Ratol paste, which is another rodenticide, showed prolonged PR interval, prolonged QRS duration, and the BrS ECG pattern (118). The manifestation of the BrS ECG pattern was related to the yellow phosphorous (YP), which is a protoplasmic poison contained in the paste, and it can cause damage to the liver, kidney, pancreas, brain, and heart (119). These reports about metal poisoning eliciting a BrS ECG pattern are also consistent with the fact that metals, such as zinc and copper, can act as endogenous regulators of sodium, potassium, and calcium channels, including $Na_V1.5$, the sodium channel most implicated in BrS, through mechanisms that could be important not only for the heart, but also for diseases such as Alzheimer's disease and epilepsy (120). Thus, metals could play an important clue in understanding the various ways in which the BrS ECG pattern can be developed.

Whether through genetics, electrolyte imbalance, blood transfusion, poisoning, or other factors, the ECG pattern exhibiting an elevated ST segment can be developed in a number of different ways. However, regardless of the many initiating factors, all these pathways ultimately converge into one: the BrS ECG pattern, and we must not lose sight of the fact that, whatever we want to call it—"true BrS" or "phenocopy"—all of these initiating factors have converged into the same life-threatening arrhythmogenesis pathway, manifesting as the BrS ECG pattern, and the patient is at increased risk of ventricular fibrillation and SCD.

BRUGADA SYNDROME AND THYROID DYSFUNCTION

Several studies have identified and described the relationship between thyroid hormone imbalances and cardiovascular diseases (121). It is known that thyroid hormone receptors are expressed in many different cell types, including heart (122), and, therefore, systemic vascular resistance, cardiac contractility, blood pressure, myocardial oxygen consumption, and heart rhythm can be disrupted by both hypothyroidism and hyperthyroidism (123, 124). Indeed, both of these thyroid dysfunctions can lead to cardiovascular disorders, including atrial fibrillation and ventricular arrhythmia (121). These correlations were also confirmed by cardiac electrophysiological studies focused on the activity of multiple ion channel subunits, transporters, and exchangers (121, 125). Moreover, a possible overlap of hypothyroidism and BrS has been reported in three case reports. All cases showed three men affected by hypothyroidism with a BrS ECG pattern in leads V1-V3. The BrS ECG pattern disappeared in all patients when the thyroid function was normalized (126–128). Therefore, the normalization of the ECG was considered directly related with the restoration of thyroid hormone balance. Moreover, one of the three patients with hypothyroidism was also affected by liver dysfunction, which returned to normal after thyroid function went back to normal (128). Only one of the patients underwent genetic testing. This patient resulted positive for three common variants in the *SCN5A* gene (127). Furthermore, a possible overlap between hyperthyroidism and BrS has been reported. A male patient suffered a cardiac arrest, and after his resuscitation, his ECG showed a type 1 BrS pattern. The laboratory tests showed also low K^+ levels, low TSH levels, and high FT4 levels. However, the BrS ECG pattern was only transient, it normalized after carbimazole administration, and the patient resulted negative to ajmaline and flecainide tests. Genetic testing was not performed (129). Moreover, another patient with Graves' hyperthyroidism developed ventricular fibrillation, and she was implanted with an ICD. An ECG that was performed after she was re-admitted for fever and pleural effusion exhibited the type 2 BrS ECG pattern, although the report is unclear whether she performed ECG at the time of the actual fever. Genetic testing revealed a likely pathogenic mutation in the *SCN5A* gene (130). Therefore, genetic studies could be helpful to better understand the link between the manifestation of the BrS ECG pattern and thyroid dysfunction.

BRUGADA SYNDROME AND CANCERS

The overexpression of voltage-gated sodium channels has been shown to be associated with metastatic behavior in a variety of human cancers, including breast cancer, prostate cancer, lung cancer, colorectal cancer, cervical cancer, lymphoma, and neuroblastoma (131, 132). Overexpression of the neonatal isoform of the voltage-gated sodium channel, Nav1.5 (nNav1.5), is associated with aggressive human breast cancer metastasis and patient death (131, 133, 134). Nav1.5 overexpression increases metastasis and invasiveness of breast cancer cells by altering H+ efflux and promoting epithelial-to-mesenchymal transition and the expression of cysteine cathepsin (132), possibly due to reduced expression of salt-inducible kinase 1 (SIK1) (135). Both neonatal and adult (aNav1.5) forms of Nav1.5 are expressed at the messenger RNA level in colorectal cancer (136) and the *SCN5A* gene encoding for the Nav1.5 channel protein is an important regulator of the colon cancer invasion network, involving genes that encompass Wnt signaling, cell migration, ectoderm development, response to biotic stimulus, steroid metabolic process, and cell cycle control (137). Therefore, in the field of cancer, drug treatments that aim to block Nav1.5-dependent inward currents are of interest. However, sodium channel blockers used to treat patients with cancer may exacerbate underlying predispositions for cardiac arrhythmias, as sodium channel blockers, especially those targeting the Nav1.5 channel, may provoke arrhythmias such as the BrS ECG pattern. In fact, drugs studied for possible use in cancer therapy, such as Ranolazine (138) or Tetrodotoxin (136), are known to act not only on cancer cells, but on other cells in the body. Ranolazine acts on cardiac sodium channels and sarcomeric proteins (139). Recent studies have implicated cardiomyocyte sarcomeric alterations as possible mechanisms of BrS (28). Tetrodotoxin, believed to be one of the most selective inhibitors of voltage-gated fast sodium channels, actually acts additionally on other channels, including cardiac L-type calcium channels (140). Calcium channels and their related proteins have been implicated in a number of cardiac pathologies, including catecholaminergic polymorphic ventricular tachycardia, congenital long QT

syndrome, idiopathic ventricular fibrillation, hypertrophic cardiomyopathy, arrhythmogenic cardiomyopathy, dilated cardiomyopathy, heart failure, atrial fibrillation (141), and BrS (28, 42). Thus, the possible development of cardiac arrhythmias should be considered for any drugs used for cancer treatment.

BRUGADA SYNDROME, TESTOSTERONE, AND PROSTATE CANCER

Although equally transmitted to both genders (142), BrS seems to be more predominant in males (143), possibly due to hormonal action, among other factors (42). Specifically, males with BrS have been described to have higher testosterone, serum sodium, potassium, and chloride levels compared to controls, after adjusting for age, exercise, stress, smoking, and medication for hypertension, diabetes, and hyperlipidemia (144). In the same study, males with BrS had significantly lower body-mass index and body fat percentage than controls (144). Thus, a link between high levels of plasma testosterone, BrS, and prostate cancer was suggested (145). Men with Brugada-like electrocardiogram patterns have a higher risk of prostate cancer independent of age, smoking habit, and radiation exposure, and thus, men with either a Brugada-like ECG or prostate cancer should be checked for the other (145). The BrS ECG pattern can disappear after surgical castration for prostate cancer (146). The hypothesis for hormonal involvement in the development of BrS is further supported by cases in which BrS signs and symptoms manifest only in adulthood in patients who tested ajmaline negative in childhood (147). Moreover, healthy men are known to have differences in the ECG, compared to healthy women, for example, shorter and faster repolarization and a shorter duration of QTc and JTc intervals (148), supporting the idea that ventricular repolarization can be disrupted by androgens. Furthermore, no sex-differences in repolarization are observed in neonates or in children before puberty, probably due to low levels of testosterone (149). Cases in which BrS is found in pre-adolescent children, including also infants or when it is expected to be the cause of spontaneous abortions, may be due to certain genetic factors found in those families. For example, certain *SCN5A* mutations are known to be so detrimental that they can lead to sudden infant death (150), or they have been suspected as the cause of spontaneous abortions (151). In these cases, testosterone may play less (if any) of a role. However, testosterone is certainly one of the many factors that may contribute to the development of the BrS ECG pattern in many patients. Thus, future studies should investigate further the relationship between testosterone levels and the development of both BrS and prostate cancer.

MITOCHONDRIA AND BRUGADA SYNDROME

Mitochondria influence cellular physiology in a variety of ways (41), and are involved in many pathologies, including epilepsy (152, 153), thyroid function (154), cancer (155–158), diabetes (159, 160), and BrS (41), among others. Mitochondria produce adenosine triphosphate (ATP), which is required for protein phosphorylation, a process that is required for normal protein function (161). Protein phosphorylation is a normal regulatory process used by the cell to control the force-frequency relationship (the heart beats harder and relaxes faster to accommodate the need for higher heart rates) (162), the length-dependent relationship (Frank-Starling relationship, the heart beats harder when the muscle is stretched) (163), and other necessary intracellular communications (164–168). Proteins that are normally phosphorylated under certain conditions include several of those known to be important for arrhythmia development, including the sodium channel Nav1.5 (encoded by the *SCN5A* gene; important for BrS) (41), L-type calcium channels (encoded by the *CACNA1C* gene; important for BrS) (28), ryanodine receptors [encoded by the *RYR2* gene; important for catecholaminergic polymorphic ventricular tachycardia (169)], phospholamban [encoded by the *PLN* gene; important for arrhythmogenic cardiomyopathy and dilated cardiomyopathy (170)], cardiac myosin-binding protein-C (encoded by the *MYBPC3* gene; BrS candidate gene) (48), tropomyosin (encoded by the *TPM1* gene; BrS candidate gene) (28), and other sarcomeric proteins that regulate cardiac function (50, 163–166, 171), such as troponin I (encoded by the *TNNI3* gene), myosin light chain-2 (encoded by the *MLC2* gene), and troponin T (encoded by the *TNNT2* gene). Therefore, mitochondrial dysfunction that results in ATP depletion would alter the function of these proteins, possibly resulting in cardiac arrhythmias (50, 172–174). Furthermore, mitochondria are additionally responsible for the production of reactive oxygen species (ROS), and a mutation in the GPD1-L protein, encoded by an important BrS candidate gene (175), has been shown to promote ROS production, which could be detrimental to the sodium current (176). BrS has been associated with mutations in mitochondrial transfer RNA (tRNA) genes (49) and a specific mitochondrial DNA (mtDNA) allelic combination and a high number of mtDNA single nucleotide polymorphisms (SNPs) (177, 178). Thus, mitochondrial genes and function are important for BrS. Mitochondrial products that can lead to arrhythmias are shown in **Figure 3**.

BRUGADA SYNDROME AND DIABETES

Ion channel dysfunction has been associated with diabetes mellitus (DM), leading to the development of a heart disorder called diabetic cardiomyopathy (179, 180), characterized by contractile dysfunction, abnormal cardiac electrical activity, mitochondrial dysfunction, arrhythmia, and sudden cardiac death (159, 160). Several patients affected by DM have been reported to exhibit the BrS ECG pattern, whether it was considered "true BrS" or a "BrS phenocopy" (104, 181–184), although a difference between "true BrS" and "BrS phenocopy" may not actually exist (41). A case report described a 16-year-old boy affected by DM and a mutation in the *GPD1L* gene who died suddenly during the night (185). The autopsy examination excluded hypoglycemia as the cause of death due to a full stomach and normal glucose levels in the vitreous humor. Indeed, the

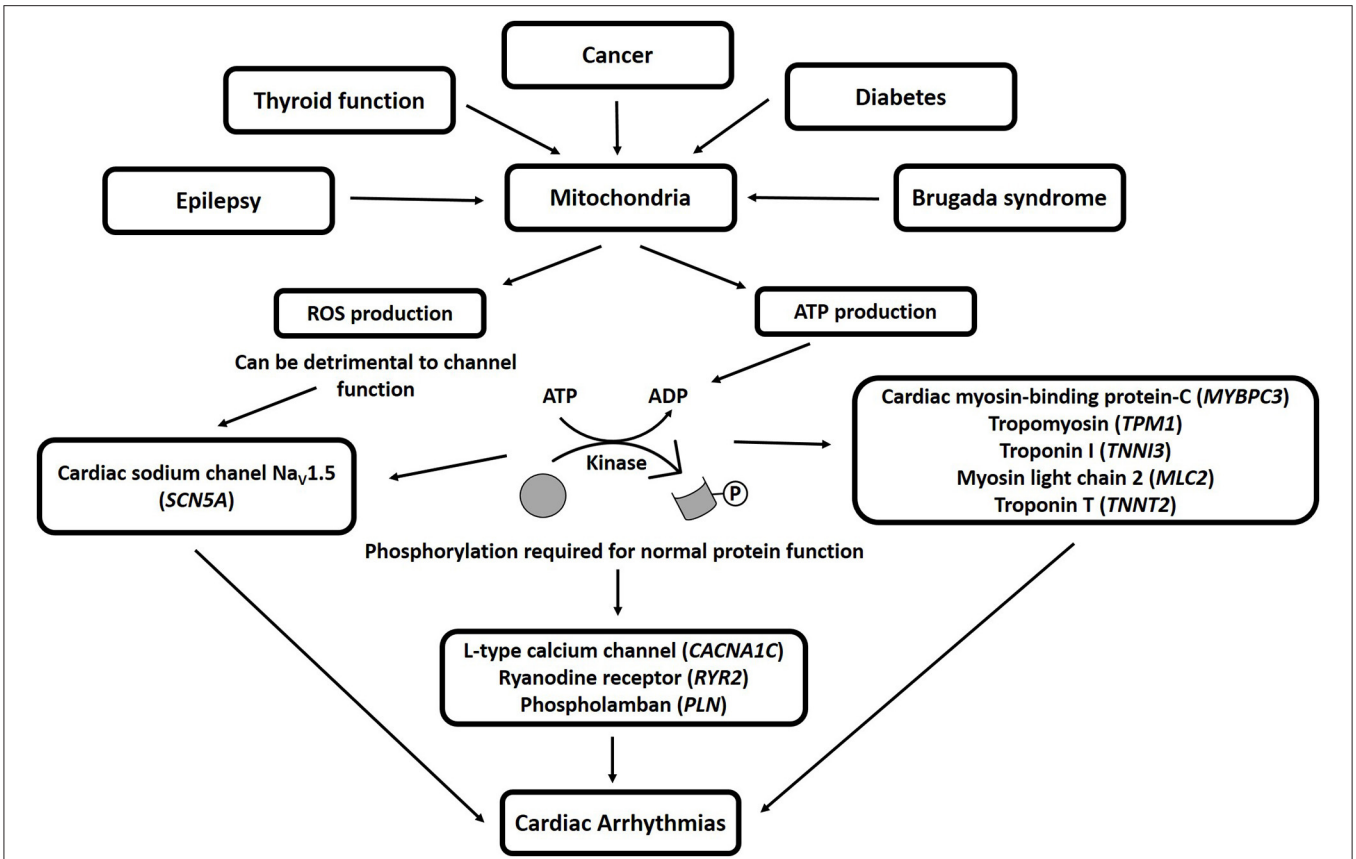

FIGURE 3 | Mitochondrial products that can lead to arrhythmias**.** ROS, reactive oxygen species; ATP, adenosine triphosphate; ADP, adenosine diphosphate.

GPD1L gene is important for BrS, and may have been the cause of death (186). Variants in this gene have also been linked to sudden infant death syndrome (SIDS) (187). Therefore, a genetic link may exist between diabetes and BrS that could result in a phenotypic overlap. However, diabetes can also be caused by non-genetic factors, such as life style, food, persistent organic pollutants, and the gut ecosystem (188), and diabetes can cause fibrosis leading to diastolic heart failure with preserved ejection fraction, which may deteriorate into the development of arrhythmias and sudden death (189). Therefore, we cannot rule out that disease overlap is always caused by genetic factors, but instead the situation may be the evolution of one disease eventually resulting in the other, or there may be no mechanistic overlap at all in some patients (two different mutations, or a mutation and an environmental influence). In any case, an overlap exists between diabetes, cardiac arrhythmias, and sudden death that will be the subject of future investigations.

BRUGADA SYNDROME, SKELETAL MUSCLE SODIUM CHANNELOPATHIES, AND LAMINOPATHIES

The *SCN4A* gene encodes for the voltage-gated sodium channel Na$_V$1.4, and its mutations are usually related to non-dystrophic myotonia, periodic paralysis, and myasthenic syndrome (190). This gene has also been implicated in overlap between BrS and skeletal muscle sodium channelopathies (122). Indeed, several patients with pathogenic mutations in the *SCN4A* gene and cardiac electrophysiological abnormalities have been described (191, 192). For example, a patient affected by non-dystrophic myotonia with a mutation in the *SCN4A* gene resulted positive to BrS with both flecainide and ajmaline challenges (192). Additionally, in a different study, the authors investigated whether BrS can be part of the clinical phenotype associated with *SCN4A* variants, and whether patients with BrS present with non-dystrophic myotonia or periodic paralysis and related gene mutations. Three patients from families with an *SCN4A*-associated non-dystrophic myotonia had also BrS. Also, the authors found a high prevalence of myotonic features in the families with BrS, involving other genes (191). Na$_V$1.4 and Na$_V$1.5 are both expressed in the skeletal muscle during embryogenesis (193), and they have 65% sequence identity (194). However, during the development, the relative Na$_V$1.5 expression decreases, making Na$_V$1.4 the most abundantly expressed sodium channel in skeletal muscle (193, 195). Taken together, patients with BrS or skeletal muscles channelopathies should be evaluated for the other.

Lamin A and C are intermediate filament proteins of the nuclear protein, and they are encoded by the *LMNA* gene. Diseases associated with the *LMNA* gene include

Hutchinson-Gilford Progeria Syndrome, Emery-Dreifuss Muscular Dystrophy 2, Autosomal Dominant (29), and inherited cardiomyopathies, such as arrhythmogenic cardiomyopathy and dilated cardiomyopathy (125). A patient who experienced a cardiac arrest and manifested a BrS ECG pattern resulted positive for a variant in the *LMNA* gene, suggesting an overlap between BrS and laminopathies (125). Thus, this gene could be investigated in patients with BrS in future studies.

BRUGADA SYNDROME AND CARDIAC DISORDERS OVERLAP

There have been several excellent studies regarding the overlap between BrS and other cardiac pathologies, including early repolarization syndrome (5), arrhythmogenic right ventricular cardiomyopathy/dysplasia (ARVC/D) (6–9), progressive cardiac conduction defect (Lenègre syndrome) (10, 11), LQTS (12–14), Wolff-Parkinson-White (15, 16), hypertrophic cardiomyopathy (17, 18), atrial flutter (19), and atrial fibrillation (20–23). Therefore, whatever mechanisms that ultimately lead to the development of the BrS ECG pattern may also be involved in other pathways that result in other cardiac pathologies. These mechanisms may include genetic variants, fibrosis, altered calcium signaling, and anatomical substrate overlap.

BrS has been hypothesized to be like focal epicardial arrhythmogenic cardiomyopathy, and the final common pathway "reduced RVOT conduction reserve," regardless of the genetics or non-genetic factors that may have been responsible. In that study, the patient's intrinsic RVOT conduction reserve was hypothesized to be age- and sex-dependent, with marginal reserves able to be exposed by the use of certain drugs or altered vagal tone (196).

Genetic Overlap

The genetics of BrS remain elusive, as the most commonly found mutated gene, *SCN5A*, is only found to be mutated in a minority of patients. However, this gene is widely studied, and is the only one considered by some groups to have definitive evidence to be involved in BrS, while the involvement of the other genes is disputed (197). Since then, several other studies have been published supporting the role of other genes, although research is still underway to understand fully the genetic background of patients with BrS (44). The discovery of genes involved in BrS may be complicated by the possibility of BrS to be transmitted as a polygenic or oligogenic disease, making the data more complicated to interpret, and thus impeding the ability to reclassify these variants (40).

There is already a lot of evidence for genetic overlap between BrS and other cardiac pathologies. Overlap between BrS and LQTS type 3 has been described (198), even sharing the same mutation in the *SCN5A* gene as the likely molecular cause (13, 199). In fact, variants in the *SCN5A* gene have been described as causative for a number of other cardiac pathologies, such as ARVC/D, atrial standstill, atrial fibrillation, left ventricular non-compaction, dilated cardiomyopathy, LQTS, sick sinus syndrome, idiopathic ventricular fibrillation, and heart block (200, 201). In addition, several other genes associated with BrS are also associated with other cardiac pathologies, as previously reviewed elsewhere (202), such as *PKP2*, *DSC2*, *JUP*, *DSG2*, and *RYR2* in ARVC (108, 202), *SCN1B* and *CACNA1C* in LQTS, *CACNA1C*, *CACNA2D1*, and *CACNB2* in short QT syndrome, and *CACNA1C*, *CACNA2D1*, *CACNB2*, *HCN4*, and *KCNJ8* in early repolarization syndrome (202). Atrial fibrillation is associated with a number of genes that have been suspected in BrS, including SCN5A, SCN1B, SCN2B, SCN3B, SCN4B, SCN10A, ABCC9, HCN4, KCNQ1, KCNJ2, KCNJ5, KCNJ8, KCNE1, KCNE2, KCNE3, KCNE5, KCNH2, KCND3, RYR2, and CACNB2 (203). Therefore, genetics may play more of a role in the overlap of these pathologies than currently understood.

Disturbances of the connexome, the complex of structures of the intercalated disc that connect cardiomyocytes, could be involved in the mechanism of overlap between BrS and both arrhythmogenic cardiomyopathy and ARVC (9, 41). In addition to the overlap of several causative genes, the extracellular matrix and fibrosis may play a role in the overlap of several of these pathologies, as it is found to be present in BrS (204, 205), early repolarization syndrome (5), ARVC/D (206), Lenègre syndrome (207), LQTS (208–210), Wolff-Parkinson-White (211, 212), hypertrophic cardiomyopathy (213), atrial flutter and atrial fibrillation (214, 215). Thus, disturbances of the connexome and fibrosis can be important elements in the overlap of BrS with other cardiac pathologies.

Arrhythmogenic Substrate and Anatomical Overlap

There may be an effect of anatomical overlap between BrS and other cardiac pathologies. For example, sarcomeric alterations, which are known to cause hypertrophic or dilated cardiomyopathy, are able to cause calcium mishandling that can lead to sudden death (216, 217), and so, over time, overlap may occur as the pathology progresses and affects other areas of the cell.

An arrhythmogenic substrate (AS) is consistently identified in all patients with BrS. This AS is commonly found in the RVOT of the right ventricle (RV) epicardium. Ajmaline administration reveals the full extent of the AS, which is useful for radiofrequency ablation, which results in ECG normalization and the patients are no longer inducible for VT/VF during electrophysiological study (EPS) (4, 218). The size of the AS has been independently associated with arrhythmia inducibility, with a substrate area of greater than 4 cm^2 predicting patient inducibility to VT/VF during the EPS (219). The size of the AS can be altered not only by ajmaline, but by also a number of other factors, including genetics, temperature, anesthetics (220), and other factors known to trigger syncopic episodes or the BrS ECG sign. A larger AS is associated with reduced contractility and mechanical dysfunction (51). Patients harboring *SCN5A* variants exhibit more pronounced epicardial electrical abnormalities (60, 62), and the AS is comparable in patients with *SCN10A* variants (43). The procedure of epicardial mapping together with ajmaline challenge can be used to identify and ablate the AS in patients

with other cardiomyopathies, thus preventing the recurrence of VT/VF in those patients as well (48).

FUTURE DIRECTIONS

While BrS was described for decades as a simple monogenic disease originating only as a channelopathy, more recent studies have begun to recognize that actually BrS is an oligogenic disease with altered metabolics (28, 40). BrS has traditionally been described more for what it is *not* than for what it *is*, being described as a particular ECG pattern in the absence of certain criteria, but we believe that whenever the BrS ECG pattern is present, the sign should be taken for what it really is: a warning of increased risk of sudden death of the patient (41). It does not matter how the sign arose—from a channelopathy, a cardiomyopathy, an electrolyte imbalance, heavy meals, alcohol intake, or even poisoning—the BrS mechanism is a particular ECG warning of the increased risk of sudden death. Rather than being thought of as a single disease, it should be thought of as the final step in many pathways in many diseases or after exposure to certain environmental situations, that ultimately manifests as the BrS ECG pattern—a mechanism that can cause sudden death.

The BrS ECG sign does not always indicate solely cardiac dysfunction, but, in fact, this ECG sign could be the result of a larger systemic problem. Genetic mutations that are expressed in multiple cell types may contribute to overlap pathologies. We hypothesize that, with time, more overlap phenotypes will emerge in a host of other cell types, especially since many of the genes suspected to be involved in BrS are expressed throughout the body. Thus, future studies may focus on the effects of these genetic mutations in various cell and tissue types, identifying other problems for which the patients must be treated, as well as possible mechanisms for doing so. This could connect a whole magnitude of other pathologies to BrS, lending further evidence to the mechanism of BrS, arriving finally at better therapeutic options.

Ideally, where available, whole genome sequencing should be performed for the identification of new candidate genes. The effects of these specific genetic mutations in specific patients should then be assessed on a case-by-case basis to try to understand the effects of these mutations on other tissue types, in a move toward personalized medicine. Additionally, a multi-omics approach would be appropriate to study this syndrome, including not only genetics, but also epigenomics, transcriptomics, proteomics, metabolomics, lipidomics, and glycomics, resulting eventually in a biomarker for BrS and the ability to diagnose this syndrome using a minimally invasive blood test, avoiding the risk associated with ajmaline testing.

AUTHOR CONTRIBUTIONS

SD'I and MM: conceptualization, literature search, and writing—original draft preparation. CP: funding acquisition. SD'I, MM, and CP: writing—draft revision. SD'I, MM, EM, GC, LA, and CP: reviewed and provided comments. All authors have read and agreed to the published version of the manuscript.

FUNDING

This study was partially supported by Ricerca Corrente funding from Italian Ministry of Health to IRCCS Policlinico San Donato.

REFERENCES

1. Fernandez-Falgueras A, Sarquella-Brugada G, Brugada J, Brugada R, Campuzano O. Cardiac channelopathies and sudden death: recent clinical and genetic advances. *Biology.* (2017) 6:7. doi: 10.3390/biology6010007
2. Brugada J, Campuzano O, Arbelo E, Sarquella-Brugada G, Brugada R. Present status of brugada syndrome: JACC state-of-the-art review. *J Am Coll Cardiol.* (2018) 72:1046–59. doi: 10.1016/j.jacc.2018.06.037
3. Antzelevitch C, Brugada P, Borggrefe M, Brugada J, Brugada R, Corrado D, et al. Brugada syndrome: report of the second consensus conference: endorsed by the Heart Rhythm Society and the European Heart Rhythm Association. *Circulation.* (2005) 111:659–70. doi: 10.1161/01.CIR.0000152479.54298.51
4. Pappone C, Santinelli V. Brugada syndrome: progress in diagnosis and management. *Arrhythm Electrophysiol Rev.* (2019) 8:13–8. doi: 10.15420/aer.2018.73.2
5. Boukens BJ, Potse M, Coronel R. Fibrosis and conduction abnormalities as basis for overlap of brugada syndrome and early repolarization syndrome. *Int J Mol Sci.* (2021) 22:1570. doi: 10.3390/ijms22041570
6. Perez Riera AR, Antzelevitch C, Schapacknik E, Dubner S, Ferreira C. Is there an overlap between Brugada syndrome and arrhythmogenic right ventricular cardiomyopathy/dysplasia? *J Electrocardiol.* (2005) 38:260–3. doi: 10.1016/j.jelectrocard.2005.03.009
7. Corrado D, Zorzi A, Cerrone M, Rigato I, Mongillo M, Bauce B, et al. Relationship between arrhythmogenic right ventricular cardiomyopathy and brugada syndrome: new insights from molecular biology and clinical implications. *Circ Arrhythm Electrophysiol.* (2016) 9:e003631. doi: 10.1161/CIRCEP.115.003631
8. Kataoka S, Serizawa N, Kitamura K, Suzuki A, Suzuki T, Shiga T, et al. An overlap of Brugada syndrome and arrhythmogenic right ventricular cardiomyopathy/dysplasia. *J Arrhythm.* (2016) 32:70–3. doi: 10.1016/j.joa.2015.10.007
9. Moncayo-Arlandi J, Brugada R. Unmasking the molecular link between arrhythmogenic cardiomyopathy and Brugada syndrome. *Nat Rev Cardiol.* (2017) 14:744–56. doi: 10.1038/nrcardio.2017.103
10. Probst V, Allouis M, Sacher F, Pattier S, Babuty D, Mabo P, et al. Progressive cardiac conduction defect is the prevailing phenotype in carriers of a Brugada syndrome SCN5A mutation. *J Cardiovasc Electrophysiol.* (2006) 17:270–5. doi: 10.1111/j.1540-8167.2006.00349.x
11. Shimizu W. Does an overlap syndrome really exist between Brugada syndrome and progressive cardiac conduction defect (Lenegre syndrome)? *J Cardiovasc Electrophysiol.* (2006) 17:276–8. doi: 10.1111/j.1540-8167.2006.00406.x
12. Kotta CM, Anastasakis A, Stefanadis C. Effects of mutations and genetic overlap in inherited long-QT and Brugada arrhythmia syndromes. *Hellenic J Cardiol.* (2012) 53:439–46.
13. Kanters JK, Yuan L, Hedley PL, Stoevring B, Jons C, Bloch Thomsen PE, et al. Flecainide provocation reveals concealed brugada syndrome in a long QT syndrome family with a novel L1786Q mutation in SCN5A. *Circ J.* (2014) 78:1136–43. doi: 10.1253/circj.CJ-13-1167
14. Nakaya H. SCN5A mutations associated with overlap phenotype of long QT syndrome type 3 and Brugada syndrome. *Circ J.* (2014) 78:1061–2. doi: 10.1253/circj.CJ-14-0319

15. Jaiswal A, Heretis K, Goldbarg S. Coexistent Brugada Syndrome and Wolff-Parkinson-White syndrome: what is the optimal management? *Indian Pacing Electrophysiol J.* (2013) 13:173–7. doi: 10.1016/S0972-6292(16)30669-6
16. Erdogan O. Coexistence of Wolff-Parkinson-White and Brugada ECG. *Turk Kardiyol Dern Ars.* (2018) 46:433–4. doi: 10.5543/tkda.2018.75271
17. Mango R, Luchetti A, Sangiuolo R, Ferradini V, Briglia N, Giardina E, et al. Next generation sequencing and linkage analysis for the molecular diagnosis of a novel overlapping syndrome characterized by hypertrophic cardiomyopathy and typical electrical instability of Brugada syndrome. *Circ J.* (2016) 80:938–49. doi: 10.1253/circj.CJ-15-0685
18. Monasky MM, Ciconte G, Anastasia L, Pappone C. Commentary: next generation sequencing and linkage analysis for the molecular diagnosis of a novel overlapping syndrome characterized by hypertrophic cardiomyopathy and typical electrical instability of Brugada syndrome. *Front Physiol.* (2017) 8:1056. doi: 10.3389/fphys.2017.01056
19. Hothi SS, Ara F, Timperley J. p.Y1449C SCN5A mutation associated with overlap disorder comprising conduction disease. Brugada syndrome, and atrial flutter. *J Cardiovasc Electrophysiol.* (2015) 26:93–7. doi: 10.1111/jce.12470
20. Francis J, Antzelevitch C. Atrial fibrillation and Brugada syndrome. *J Am Coll Cardiol.* (2008) 51:1149–53. doi: 10.1016/j.jacc.2007.10.062
21. Kewcharoen J, Rattanawong P, Kanitsoraphan C, Mekritthikrai R, Prasitlumkum N, Putthapiban P, et al. Atrial fibrillation and risk of major arrhythmic events in Brugada syndrome: a meta-analysis. *Ann Noninvasive Electrocardiol.* (2019) 24:e12676. doi: 10.1111/anec.12676
22. Tse G, Lee S, Mok NS, Liu T, Chang D. Incidence and predictors of atrial fibrillation in a Chinese cohort of Brugada syndrome. *Int J Cardiol.* (2020) 314:54–7. doi: 10.1016/j.ijcard.2020.05.007
23. Vlachos K, Mascia G, Martin CA, Bazoukis G, Frontera A, Cheniti G, et al. Atrial fibrillation in Brugada syndrome: current perspectives. *J Cardiovasc Electrophysiol.* (2020) 31:975–84. doi: 10.1111/jce.14361
24. Parisi P, Oliva A, Coll Vidal M, Partemi S, Campuzano O, Iglesias A, et al. Coexistence of epilepsy and Brugada syndrome in a family with SCN5A mutation. *Epilepsy Res.* (2013) 105:415–8. doi: 10.1016/j.eplepsyres.2013.02.024
25. Sandorfi G, Clemens B, Csanadi Z. Electrical storm in the brain and in the heart: epilepsy and Brugada syndrome. *Mayo Clin Proc.* (2013) 88:1167–73. doi: 10.1016/j.mayocp.2013.06.019
26. Camacho Velasquez JL, Rivero Sanz E, Velazquez Benito A, Mauri Llerda JA. Epilepsy and Brugada syndrome. *Neurologia.* (2017) 32:58–60. doi: 10.1016/j.nrl.2015.03.010
27. Abdelghani MS, Chapra A, Asaad N, Hayat SA. Epilepsy and Brugada Syndrome: association or uncommon presentation? *Heart Views.* (2020) 21:114–7. doi: 10.4103/HEARTVIEWS.HEARTVIEWS_34_20
28. Monasky MM, Micaglio E, Ciconte G, Pappone C. Brugada Syndrome: OLIGOGENIC OR MENDELIAN DISEASe? *Int J Mol Sci.* (2020) 21:1687. doi: 10.3390/ijms21051687
29. *GeneCards: The Human Gene Database* [Online] (2021). Available online at: https://www.genecards.org/ (accessed July 22, 2021).
30. D'Imperio S, Monasky MM, Micaglio E, Negro G, Pappone C. Impact of dietary factors on Brugada syndrome and long QT syndrome. *Nutrients.* (2021) 13:2482. doi: 10.3390/nu13082482
31. Antzelevitch C. Brugada syndrome. *Pacing Clin Electrophysiol.* (2006) 29:1130–59. doi: 10.1111/j.1540-8159.2006.00507.x
32. Obeyesekere MN, Klein GJ, Modi S, Leong-Sit P, Gula LJ, Yee R, et al. How to perform and interpret provocative testing for the diagnosis of Brugada syndrome, long-QT syndrome, and catecholaminergic polymorphic ventricular tachycardia. *Circ Arrhythm Electrophysiol.* (2011) 4:958–64. doi: 10.1161/CIRCEP.111.965947
33. McMillan MR, Day TG, Bartsota M, Mead-Regan S, Bryant R, Mangat J, et al. Feasibility and outcomes of ajmaline provocation testing for Brugada syndrome in children in a specialist paediatric inherited cardiovascular diseases centre. *Open Heart.* (2014) 1:e000023. doi: 10.1136/openhrt-2013-000023
34. Fish JM, Antzelevitch C. Role of sodium and calcium channel block in unmasking the Brugada syndrome. *Heart Rhythm.* (2004) 1:210–7. doi: 10.1016/j.hrthm.2004.03.061
35. Kiesecker C, Zitron E, Lück S, Bloehs R, Scholz EP, Kathöfer S, et al. Class Ia anti-arrhythmic drug ajmaline blocks HERG potassium channels: mode of action. *Naunyn Schmiedebergs Arch Pharmacol.* (2004) 370:423–35. doi: 10.1007/s00210-004-0976-8
36. Chukhlova EA, Sadykov I, Kholmukhamedov EL, Grenader AK. [Effect of trimecaine, ajmaline, stenopril and chloracizine on fluctuations in K+ currents in rat liver mitochondria]. *Ukr Biokhim Zh.* (1984) 56:207–10.
37. Di Domenico M, Scumaci D, Grasso S, Gaspari M, Curcio A, Oliva A, et al. Biomarker discovery by plasma proteomics in familial Brugada Syndrome. *Front Biosci.* (2013) 18:564–71. doi: 10.2741/4120
38. Chatterjee D, Pieroni M, Fatah M, Charpentier F, Cunningham KS, Spears DA, et al. An autoantibody profile detects Brugada syndrome and identifies abnormally expressed myocardial proteins. *Eur Heart J.* (2020) 41:2878–90. doi: 10.1093/eurheartj/ehaa383
39. Wilde AM, Lodder EM. A highly specific biomarker for Brugada syndrome. Also too good to be true? *Eur Heart J.* (2020) 41:2891–3. doi: 10.1093/eurheartj/ehaa468
40. Campuzano O, Sarquella-Brugada G, Cesar S, Arbelo E, Brugada J, Brugada R. Update on genetic basis of Brugada syndrome: monogenic, polygenic or oligogenic? *Int J Mol Sci.* (2020) 21:7155. doi: 10.3390/ijms21197155
41. Monasky MM, Micaglio E, Locati ET, Pappone C. Evaluating the use of genetics in Brugada syndrome risk stratification. *Front Cardiovasc Med.* (2021) 8:652027. doi: 10.3389/fcvm.2021.652027
42. Monasky MM, Pappone C, Piccoli M, Ghiroldi A, Micaglio E, Anastasia L. Calcium in Brugada syndrome: questions for future research. *Front Physiol.* (2018) 9:1088. doi: 10.3389/fphys.2018.01088
43. Monasky MM, Micaglio E, Vicedomini G, Locati ET, Ciconte G, Giannelli L, et al. Comparable clinical characteristics in Brugada syndrome patients harboring SCN5A or novel SCN10A variants. *Europace.* (2019) 21:1550–8. doi: 10.1093/europace/euz186
44. Di Mauro V, Ceriotti P, Lodola F, Salvarani N, Modica J, Bang ML, et al. Peptide-based targeting of the L-type calcium channel corrects the loss-of-function phenotype of two novel mutations of the CACNA1 gene associated with Brugada syndrome. *Front Physiol.* (2020) 11:616819. doi: 10.3389/fphys.2020.616819
45. Pappone C, Micaglio E, Locati ET, Monasky MM. The omics of channelopathies and cardiomyopathies: what we know and how they are useful. *Eur Heart J Suppl.* (2020) 22:L105–9. doi: 10.1093/eurheartj/suaa146
46. Monasky MM, Rutigliani C, Micaglio E, Pappone C. Commentary: Peptide-based targeting of the L-type calcium channel corrects the loss-of-function phenotype of two novel mutations of the CACNA1 gene associated with Brugada syndrome. *Front Physiol.* (2021) 12:682567. doi: 10.3389/fphys.2021.682567
47. Di Resta C, Pietrelli A, Sala S, Della Bella P, De Bellis G, Ferrari M, et al. High-throughput genetic characterization of a cohort of Brugada syndrome patients. *Hum Mol Genet.* (2015) 24:5828–35. doi: 10.1093/hmg/ddv302
48. Pappone C, Monasky M, Ciconte G. Epicardial ablation in genetic cardiomyopathies: a new frontier. *Eur Heart J Suppl.* (2019) 21:B61–6. doi: 10.1093/eurheartj/suz028
49. Tafti MF, Khatami M, Rezaei S, Heidari MM, Hadadzadeh M. Novel and heteroplasmic mutations in mitochondrial tRNA genes in Brugada syndrome. *Cardiol J.* (2018) 25:113–9. doi: 10.5603/CJ.a2017.0104
50. Yar S, Monasky MM, Solaro RJ. Maladaptive modifications in myofilament proteins and triggers in the progression to heart failure and sudden death. *Pflugers Arch.* (2014) 466:1189–97. doi: 10.1007/s00424-014-1457-7
51. Pappone C, Monasky MM, Micaglio E, Ciconte G. Right ventricular electromechanical abnormalities in Brugada syndrome: is this a cardiomyopathy? *Eur Heart J Suppl.* (2020) 22:E101–4. doi: 10.1093/eurheartj/suaa071
52. Han H, Wang Y, Zhou F, Chen X. [Analysis of DSG2, TTN and GATA4 gene variants in patients with Brugada syndrome from Henan]. *Zhonghua Yi Xue Yi Chuan Xue Za Zhi.* (2021) 38:488–91. doi: 10.3760/cma.j.cn511374-20200416-00275
53. Antzelevitch C. Brugada syndrome: historical perspectives and observations. *Eur Heart J.* (2002) 23:676–8. doi: 10.1053/euhj.2001.3145
54. Antzelevitch C, Yan GX, Ackerman MJ, Borggrefe M, Corrado D, Guo J, et al. J-Wave syndromes expert consensus conference report: emerging concepts and gaps in knowledge.

J Arrhythm. (2016) 32:315–39. doi: 10.1016/j.joa.2016.07.002
55. Pappone C, Mecarocci V, Manguso F, Ciconte G, Vicedomini G, Sturla F, et al. New electromechanical substrate abnormalities in high-risk patients with Brugada syndrome. *Heart Rhythm.* (2020) 17:637–45. doi: 10.1016/j.hrthm.2019.11.019
56. Allegue C, Coll M, Mates J, Campuzano O, Iglesias A, Sobrino B, et al. Genetic analysis of arrhythmogenic diseases in the era of NGS: the complexity of clinical decision-making in Brugada syndrome. *PLoS ONE.* (2015) 10:e0133037. doi: 10.1371/journal.pone.0133037
57. Aurlien D, Leren TP, Tauboll E, Gjerstad L. New SCN5A mutation in a SUDEP victim with idiopathic epilepsy. *Seizure.* (2009) 18:158–60. doi: 10.1016/j.seizure.2008.07.008
58. Goldman AM, Glasscock E, Yoo J, Chen TT, Klassen TL, Noebels JL. Arrhythmia in heart and brain: KCNQ1 mutations link epilepsy and sudden unexplained death. *Sci Transl Med.* (2009) 1:2ra6. doi: 10.1126/scitranslmed.3000289
59. Chahal CA, Salloum MN, Alahdab F, Gottwald JA, Tester DJ, et al. Systematic review of the genetics of sudden unexpected death in epilepsy: potential overlap with sudden cardiac death and arrhythmia-related genes. *J Am Heart Assoc.* (2020) 9:e012264. doi: 10.1161/JAHA.119.012264
60. Ciconte G, Monasky MM, Santinelli V, Micaglio E, Vicedomini G, Anastasia L, et al. Brugada syndrome genetics is associated with phenotype severity. *Eur Heart J.* (2021) 42:1082–90. doi: 10.1093/eurheartj/ehaa942
61. Monasky MM, Micaglio E, Ciconte G, Rivolta I, Borrelli V, Ghiroldi A, et al. Novel SCN5A p.Val1667Asp missense variant segregation and characterization in a family with severe Brugada syndrome and multiple sudden deaths. *Int J Mol Sci.* (2021) 22:4700. doi: 10.3390/ijms22094700
62. Pappone C, Ciconte G, Micaglio E, Monasky MM. Common modulators of Brugada syndrome phenotype do not affect SCN5A prognostic value. *Eur Heart J.* (2021) 42:1273–4. doi: 10.1093/eurheartj/ehab071
63. Micaglio E, Monasky MM, Ciconte G, Vicedomini G, Conti M, Mecarocci V, et al. SCN5A Nonsense mutation and NF1 frameshift mutation in a family with Brugada Syndrome and neurofibromatosis. *Front Genet.* (2019) 10:50. doi: 10.3389/fgene.2019.00050
64. Micaglio E, Monasky MM, Ciconte G, Vicedomini G, Conti M, Mecarocci V, et al. Novel SCN5A frameshift mutation in brugada syndrome associated with complex arrhythmic phenotype. *Front Genet.* (2019) 10:547. doi: 10.3389/fgene.2019.00547
65. Micaglio E, Monasky MM, Resta N, Bagnulo R, Ciconte G, Gianelli L, et al. Novel SCN5A p.W697X Nonsense mutation segregation in a family with Brugada syndrome. *Int J Mol Sci.* (2019) 20:4920. doi: 10.3390/ijms20194920
66. Monasky MM, Micaglio E, Ciconte G, Benedetti S, Di Resta C, Vicedomini G, et al. Genotype/phenotype relationship in a consanguineal family with Brugada syndrome harboring the R1632C missense variant in the SCN5A gene. *Front Physiol.* (2019) 10:666. doi: 10.3389/fphys.2019.00666
67. Monasky MM, Micaglio E, Giachino D, Ciconte G, Giannelli L, Locati ET, et al. Genotype-phenotype correlation in a family with brugada syndrome harboring the novel p.Gln371* nonsense variant in the SCN5A gene. *Int J Mol Sci.* (2019) 20:5522. doi: 10.3390/ijms20225522
68. Monasky MM, Micaglio E, Ciconte G, Borrelli V, Giannelli L, Vicedomini G, et al. Novel SCN5A p.V1429M variant segregation in a family with Brugada syndrome. *Int J Mol Sci.* (2020) 21:5902. doi: 10.3390/ijms21165902
69. Lizotte E, Junttila MJ, Dube MP, Hong K, Benito B, Zutter MDE, et al. Genetic modulation of Brugada syndrome by a common polymorphism. *J Cardiovasc Electrophysiol.* (2009) 20:1137–41. doi: 10.1111/j.1540-8167.2009.01508.x
70. Bezzina CR, Barc J, Mizusawa Y, Remme CA, Gourraud JB, Simonet F, et al. Common variants at SCN5A-SCN10A and HEY2 are associated with Brugada syndrome, a rare disease with high risk of sudden cardiac death. *Nat Genet.* (2013) 45:1044–9. doi: 10.1038/ng.2712
71. Makarawate P, Chaosuwannakit N, Vannaprasaht S, Sahasthas D, Koo SH, Lee EJD, et al. SCN5A genetic polymorphisms associated with increased defibrillator shocks in Brugada syndrome. *J Am Heart Assoc.* (2017) 6:e005009. doi: 10.1161/JAHA.116.005009
72. Matsumura H, Nakano Y, Ochi H, Onohara Y, Sairaku A, Tokuyama T, et al. H558R, a common SCN5A polymorphism, modifies the clinical phenotype of Brugada syndrome by modulating DNA methylation of SCN5A promoters. *J Biomed Sci.* (2017) 24:91. doi: 10.1186/s12929-017-0397-x
73. Wijeyeratne YD, Tanck MW, Mizusawa Y, Batchvarov V, Barc J, Crotti L, et al. SCN5A Mutation type and a genetic risk score associate variably with Brugada Syndrome phenotype in SCN5A families. *Circ Genom Precis Med.* (2020) 13:e002911. doi: 10.1161/CIRCGEN.120.002911
74. Ravindran K, Powell KL, Todaro M, O'Brien TJ. The pathophysiology of cardiac dysfunction in epilepsy. *Epilepsy Res.* (2016) 127:19–29. doi: 10.1016/j.eplepsyres.2016.08.007
75. Cihan E, Devinsky O, Hesdorffer DC, Brandsoy M, Li L, Fowler DR, et al. Temporal trends and autopsy findings of SUDEP based on medico-legal investigations in the United States. *Neurology.* (2020) 95:e867–77. doi: 10.1212/WNL.0000000000009996
76. Sveinsson O, Andersson T, Carlsson S, Tomson T. The incidence of SUDEP: A nationwide population-based cohort study. *Neurology.* (2017) 89:170–7. doi: 10.1212/WNL.0000000000004094
77. Nei M, Ho RT, Sperling MR. EKG abnormalities during partial seizures in refractory epilepsy. *Epilepsia.* (2000) 41:542–8. doi: 10.1111/j.1528-1157.2000.tb00207.x
78. Opherk C, Coromilas J, Hirsch LJ. Heart rate and EKG changes in 102 seizures: analysis of influencing factors. *Epilepsy Res.* (2002) 52:117–27. doi: 10.1016/S0920-1211(02)00215-2
79. Zijlmans M, Flanagan D, Gotman J. Heart rate changes and ECG abnormalities during epileptic seizures: prevalence and definition of an objective clinical sign. *Epilepsia.* (2002) 43:847–54. doi: 10.1046/j.1528-1157.2002.37801.x
80. Britton JW, Ghearing GR, Benarroch EE, Cascino GD. The ictal bradycardia syndrome: localization and lateralization. *Epilepsia.* (2006) 47:737–44. doi: 10.1111/j.1528-1167.2006.00509.x
81. McKeon A, Vaughan C, Delanty N. Seizure versus syncope. *Lancet Neurol.* (2006) 5:171–80. doi: 10.1016/S1474-4422(06)70350-7
82. Fauchier L, Babuty D, Cosnay P. Epilepsy, Brugada syndrome and the risk of sudden unexpected death. *J Neurol.* (2000) 247:643–4. doi: 10.1007/s004150070135
83. Girard S, Cadena A, Acharya Y. Woman with Brugada syndrome and epilepsy: a unifying diagnosis? *South Med J.* (2008) 101:1150–3. doi: 10.1097/SMJ.0b013e318182095b
84. Surges R, Sander JW. Sudden unexpected death in epilepsy: mechanisms, prevalence, and prevention. *Curr Opin Neurol.* (2012) 25:201–7. doi: 10.1097/WCO.0b013e3283506714
85. Zimmer T, Haufe V, Blechschmidt S. Voltage-gated sodium channels in the mammalian heart. *Glob Cardiol Sci Pract.* (2014) 2014:449–63. doi: 10.5339/gcsp.2014.58
86. Tiron C, Campuzano O, Perez-Serra A, Mademont I, Coll M, Allegue C, et al. Further evidence of the association between LQT syndrome and epilepsy in a family with KCNQ1 pathogenic variant. *Seizure.* (2015) 25:65–7. doi: 10.1016/j.seizure.2015.01.003
87. Gigli L, Bertero G, Vidal MC, Iglesias A, Campuzano O, Striano P, et al. Juvenile myoclonic epilepsy and Brugada type 1 ECG pattern associated with (a novel) plakophillin 2 mutation. *J Neurol.* (2017) 264:792–5. doi: 10.1007/s00415-017-8414-2
88. García Gozalo M, Bermejo Arnedo I, de Vera McMullan P. KCNQ1 gene mutation and epilepsy in patient with long QT syndrome. *Med Clin.* (2020). doi: 10.1016/j.medcli.2020.09.008. [Epub ahead of print].
89. Coll M, Allegue C, Partemi S, Mates J, Del Olmo B, Campuzano O, et al. Genetic investigation of sudden unexpected death in epilepsy cohort by panel target resequencing. *Int J Legal Med.* (2016) 130:331–9. doi: 10.1007/s00414-015-1269-0
90. Hu D, Barajas-Martinez H, Pfeiffer R, Dezi F, Pfeiffer J, Buch T, et al. Mutations in SCN10A are responsible for a large fraction of cases of Brugada syndrome. *J Am Coll Cardiol.* (2014) 64:66–79. doi: 10.1016/j.jacc.2014.04.032
91. Behr ER, Savio-Galimberti E, Barc J, Holst AG, Petropoulou E, Prins BP, et al. Role of common and rare variants in SCN10A: results from the Brugada syndrome QRS locus gene discovery collaborative study. *Cardiovasc Res.* (2015) 106:520–9. doi: 10.1093/cvr/cvv042
92. Farber NB, Jiang XP, Heinkel C, Nemmers B. Antiepileptic drugs and agents that inhibit voltage-gated sodium channels prevent NMDA antagonist neurotoxicity. *Mol Psychiatry.* (2002) 7:726–33. doi: 10.1038/sj.mp.4001087

93. Cronin NB, O'Reilly A, Duclohier H, Wallace BA. Binding of the anticonvulsant drug lamotrigine and the neurotoxin batrachotoxin to voltage-gated sodium channels induces conformational changes associated with block and steady-state activation. *J Biol Chem.* (2003) 278:10675–82. doi: 10.1074/jbc.M208356200
94. Nakatani Y, Masuko H, Amano T. Effect of lamotrigine on Na(v)1.4 voltage-gated sodium channels. *J Pharmacol Sci.* (2013) 123:203–6. doi: 10.1254/jphs.13116SC
95. Ota H, Kawamura Y, Sato N, Hasebe N. A Carbamazepine-induced Brugada-type electrocardiographic pattern in a patient with schizophrenia. *Intern Med.* (2017) 56:3047–50. doi: 10.2169/internalmedicine.8875-17
96. Banfi P, Coll M, Oliva A, Alcalde M, Striano P, Mauri M, et al. Lamotrigine induced Brugada-pattern in a patient with genetic epilepsy associated with a novel variant in SCN9A. *Gene.* (2020) 754:144847. doi: 10.1016/j.gene.2020.144847
97. Araki T, Konno T, Itoh H, Ino H, Shimizu M. Brugada syndrome with ventricular tachycardia and fibrillation related to hypokalemia. *Circ J.* (2003) 67:93–5. doi: 10.1253/circj.67.93
98. Swe T, Dogar MH. Type 1 Brugada pattern electrocardiogram induced by hypokalemia. *J Family Med Prim Care.* (2016) 5:709–11. doi: 10.4103/2249-4863.197295
99. Baranchuk A, Antiperovitch P, Gottschalk BH. Brugada phenocopy due to hypokalemia. *J Family Med Prim Care.* (2018) 7:1141–2. doi: 10.4103/jfmpc.jfmpc_64_17
100. Maheshwari A, Von Wald L, Krishnan B, Benditt DG. Hyperkalemia-induced Brugada phenocopy. *JACC Clin Electrophysiol.* (2017) 3:1058–9. doi: 10.1016/j.jacep.2016.12.012
101. Tomcsanyi K, Tomcsanyi J. Brugada sign in a patient with hyperkalemia due to rhabdomyolysis in hypothermia. *J Electrocardiol.* (2017) 50:375–7. doi: 10.1016/j.jelectrocard.2016.12.006
102. Rivera-Juarez A, Hernandez-Romero I, Puertas C, Zhang-Wang S, Sanchez-Alamo B, Martins R, et al. Clinical characteristics and electrophysiological mechanisms underlying Brugada ECG in patients with severe hyperkalemia. *J Am Heart Assoc.* (2019) 8:e010115. doi: 10.1161/JAHA.118.010115
103. Zhuo M, Li J, Lecker SH. Brugada phenocopy induced by hyperkalemia. *Kidney Int.* (2019) 95:471. doi: 10.1016/j.kint.2018.07.014
104. Pfirman KS, Donley CJ, Fryman EB, Champaneria SU, Gatewood WT. Brugada pattern manifesting during hyperkalemia, diabetic ketoacidosis, and acute alcohol intoxication. *Am J Case Rep.* (2021) 22:e932048. doi: 10.12659/AJCR.932048
105. Mehta S, Parameswaran AC, Greenspan A, Figueredo VM. Hypercalcemia due to rhabdomyolysis mimicking Brugada syndrome. *Pacing Clin Electrophysiol.* (2009) 32:e14–5. doi: 10.1111/j.1540-8159.2009.02520.x
106. Zeb M, McKenzie DB, Naheed B, Gazis T, Morgan JM, Staniforth AD. Hypercalcaemia and a Brugada-like ECG: an independent risk factor for fatal arrhythmias. *Resuscitation.* (2010) 81:1048–50. doi: 10.1016/j.resuscitation.2010.04.025
107. Sonoda K, Watanabe H, Hisamatsu T, Ashihara T, Ohno S, Hayashi H, et al. High frequency of early repolarization and Brugada-type electrocardiograms in hypercalcemia. *Ann Noninvasive Electrocardiol.* (2016) 21:30–40. doi: 10.1111/anec.12303
108. *Online Mendelian Inheritance in Man* [Online] (2021). Available online at: https://www.omim.org/ (accessed August 5, 2021).
109. Chen K, Xie Y, Zhao L, Mo Z. Hyperthyroidism-associated hypercalcemic crisis: a case report and review of the literature. *Medicine.* (2017) 96:e6017. doi: 10.1097/MD.0000000000006017
110. Sun XR, Liu T, Liu XP. Type 1 Brugada phenotype induced by cardiac iron overload after blood transfusion. *HeartRhythm Case Rep.* (2020) 6:187–90. doi: 10.1016/j.hrcr.2019.12.011
111. Matsubara E, Fujisaki T, Minamoto Y, Aoki K, Yokota E. [Brugada syndrome occurring after autologous peripheral blood stem cell transplantation for acute myeloid leukemia]. *Rinsho Ketsueki.* (2004) 45:481–3.
112. Nath NS, Bhattacharya I, Tuck AG, Schlipalius DI, Ebert PR. Mechanisms of phosphine toxicity. *J Toxicol.* (2011) 2011:494168. doi: 10.1155/2011/494168
113. Bumbrah GS, Krishan K, Kanchan T, Sharma M, Sodhi GS. Phosphide poisoning: a review of literature. *Forensic Sci Int.* (2012) 214:1–6. doi: 10.1016/j.forsciint.2011.06.018
114. Nayyar S, Nair M. Brugada pattern in toxic myocarditis due to severe aluminum phosphide poisoning. *Pacing Clin Electrophysiol.* (2009) 32:e16–7. doi: 10.1111/j.1540-8159.2009.02522.x
115. Udriste AS, Dumitriu S, Ceausu M, Radu D, Capatina CO. Aluminium phosphide fatal poisoning associated with a Brugada-like ECG pattern. *Rom J Leg Med.* (2013) 21:249–52. doi: 10.4323/rjlm.2013.249
116. Guru S, Kumar R, Behera A, Patra S, Kumar P Jr. Aluminium phosphide-induced expression of covertly present Brugada pattern in electrocardiogram: a rare case report. *Cureus.* (2020) 12:e10552. doi: 10.7759/cureus.10552
117. Prabhu MA, Agustinus R, Shenthar J. Suicidal Zinc Phosphide poisoning unmasking Brugada Syndrome and triggering near fatal ventricular arrhythmia. *Pacing Clin Electrophysiol.* (2016) 39:198–201. doi: 10.1111/pace.12749
118. Dharanipradab M, Viswanathan S, Kumar GR, Krishnamurthy V, Stanley DD. Yellow phosphorus-induced Brugada phenocopy. *J Electrocardiol.* (2018) 51:129–31. doi: 10.1016/j.jelectrocard.2017.08.033
119. Mohideen SK, Kumar KS. Should ratol paste be banned? *Indian J Crit Care Med.* (2015) 19:128–9. doi: 10.4103/0972-5229.151026
120. Mathie A, Sutton GL, Clarke CE, Veale EL. Zinc and copper: pharmacological probes and endogenous modulators of neuronal excitability. *Pharmacol Ther.* (2006) 111:567–83. doi: 10.1016/j.pharmthera.2005.11.004
121. Cappola AR, Desai AS, Medici M, Cooper LS, Egan D, Sopko G, et al. Thyroid and cardiovascular disease research agenda for enhancing knowledge, prevention, and treatment. *Circulation.* (2019) 139:2892–909. doi: 10.1161/CIRCULATIONAHA.118.036859
122. Flamant F, Gauthier K. Thyroid hormone receptors: the challenge of elucidating isotype-specific functions and cell-specific response. *Biochim Biophys Acta.* (2013) 1830:3900–7. doi: 10.1016/j.bbagen.2012.06.003
123. Udovcic M, Pena RH, Patham B, Tabatabai L, Kansara A. Hypothyroidism and the heart. Methodist Debakey. *Cardiovasc J.* (2017) 13:55–9. doi: 10.14797/mdcj-13-2-55
124. Razvi S, Jabbar A, Pingitore A, Danzi S, Biondi B, Klein I, et al. Thyroid hormones and cardiovascular function and diseases. *J Am Coll Cardiol.* (2018) 71:1781–96. doi: 10.1016/j.jacc.2018.02.045
125. Tribulova N, Knezl V, Shainberg A, Seki S, Soukup T. Thyroid hormones and cardiac arrhythmias. *Vascul Pharmacol.* (2010) 52:102–12. doi: 10.1016/j.vph.2009.10.001
126. Kitahara A, Hirai R, Matsui Y, Ikeda Y, Nakamura H. A case of hypothyroidism with brugada electrocardiographic waveforms. *Endocr J.* (2008) 55:589–94. doi: 10.1507/endocrj.K07E-024
127. Taira K, Fujino A, Watanabe T, Ogyu A, Ashikawa K, Shimizu W. Brugada-type electrocardiogram in a patient with hypothyroidism. *J Cardiol Cases.* (2010) 2:e147–50. doi: 10.1016/j.jccase.2010.05.011
128. Zhao YH, Zhang JY, Xu Y, Zhang XY. Hypothyroid patient with Brugada electrocardiographic waveforms: case report. *Pacing Clin Electrophysiol.* (2012) 35:e222–5. doi: 10.1111/j.1540-8159.2010.02960.x
129. Elgara M, Khalil MO, Raza T. Hyperthyroidism precipitating cardiac arrest in a patient with Brugada pattern. *BMJ Case Rep.* (2021) 14:e240038. doi: 10.1136/bcr-2020-240038
130. Stawiarski K, Clarke JD, Pollack A, Winslow R, Majumdar S. Ventricular fibrillation in Graves disease reveals a rare SCN5A mutation with W1191X variant associated with Brugada syndrome. *HeartRhythm Case Rep.* (2021) 7:95–9. doi: 10.1016/j.hrcr.2020.11.010
131. Dutta S, Lopez Charcas O, Tanner S, Gradek F, Driffort V, Roger S, et al. Discovery and evaluation of nNav1.5 sodium channel blockers with potent cell invasion inhibitory activity in breast cancer cells. *Bioorg Med Chem.* (2018) 26:2428–36. doi: 10.1016/j.bmc.2018.04.003
132. Luo Q, Wu T, Wu W, Chen G, Luo X, Jiang L, et al. The functional role of voltage-gated sodium channel Nav15 in metastatic breast cancer. *Front Pharmacol.* (2020) 11:1111. doi: 10.3389/fphar.2020.01111
133. Yamaci RF, Fraser SP, Battaloglu E, Kaya H, Erguler K, Foster CS, et al. Neonatal Nav1.5 protein expression in normal adult

human tissues and breast cancer. *Pathol Res Pract.* (2017) 213:900–7. doi: 10.1016/j.prp.2017.06.003
134. Murtadha AH, Azahar MII, Sharudin NA, Che Has AT, Mokhtar NF. Influence of nNav1.5 on MHC class I expression in breast cancer. *J Biosci.* (2021) 46:70. doi: 10.1007/s12038-021-00196-w
135. Gradek F, Lopez-Charcas O, Chadet S, Poisson L, Ouldamer L, Goupille C, et al. Sodium channel Nav15 controls epithelial-to-mesenchymal transition and invasiveness in breast cancer cells through its regulation by the salt-inducible kinase-1. *Sci Rep.* (2019) 9:18652. doi: 10.1038/s41598-019-55197-5
136. Guzel RM, Ogmen K, Ilieva KM, Fraser SP, Djamgoz MBA. Colorectal cancer invasiveness *in vitro*: predominant contribution of neonatal Nav1.5 under normoxia and hypoxia. *J Cell Physiol.* (2019) 234:6582–93. doi: 10.1002/jcp.27399
137. House CD, Vaske CJ, Schwartz AM, Obias V, Frank B, Luu T, et al. Voltage-gated Na+ channel SCN5A is a key regulator of a gene transcriptional network that controls colon cancer invasion. *Cancer Res.* (2010) 70:6957–67. doi: 10.1158/0008-5472.CAN-10-1169
138. Driffort V, Gillet L, Bon E, Marionneau-Lambot S, Oullier T, Joulin V, et al. Ranolazine inhibits NaV1.5-mediated breast cancer cell invasiveness and lung colonization. *Mol Cancer.* (2014) 13:264. doi: 10.1186/1476-4598-13-264
139. Lovelock JD, Monasky MM, Jeong EM, Lardin HA, Liu H, Patel BG, et al. Ranolazine improves cardiac diastolic dysfunction through modulation of myofilament calcium sensitivity. *Circ Res.* (2012) 110:841–50. doi: 10.1161/CIRCRESAHA.111.258251
140. Hegyi B, Komaromi I, Kistamas K, Ruzsnavszky F, Vaczi K, Horvath B, et al. Tetrodotoxin blockade on canine cardiac L-type Ca(2)(+) channels depends on pH and redox potential. *Mar Drugs.* (2013) 11:2140–53. doi: 10.3390/md11062140
141. Landstrom AP, Dobrev D, Wehrens XHT. Calcium Signaling and Cardiac Arrhythmias. *Circ Res.* (2017) 120:1969–93. doi: 10.1161/CIRCRESAHA.117.310083
142. Meregalli PG, Wilde AA, Tan HL. Pathophysiological mechanisms of Brugada syndrome: depolarization disorder, repolarization disorder, or more? *Cardiovasc Res.* (2005) 67:367–78. doi: 10.1016/j.cardiores.2005.03.005
143. Nademanee K, Veerakul G, Nimmannit S, Chaowakul V, Bhuripanyo K, Likittanasombat K, et al. Arrhythmogenic marker for the sudden unexplained death syndrome in Thai men. *Circulation.* (1997) 96:2595–600. doi: 10.1161/01.CIR.96.8.2595
144. Shimizu W, Matsuo K, Kokubo Y, Satomi K, Kurita T, Noda T, et al. Sex hormone and gender difference–role of testosterone on male predominance in Brugada syndrome. *J Cardiovasc Electrophysiol.* (2007) 18:415–21. doi: 10.1111/j.1540-8167.2006.00743.x
145. Haruta D, Matsuo K, Ichimaru S, Soda M, Hida A, Sera N, et al. Men with Brugada-like electrocardiogram have higher risk of prostate cancer. *Circ J.* (2009) 73:63–8. doi: 10.1253/circj.CJ-08-0680
146. Matsuo K, Akahoshi M, Seto S, Yano K. Disappearance of the Brugada-type electrocardiogram after surgical castration: a role for testosterone and an explanation for the male preponderance. *Pacing Clin Electrophysiol.* (2003) 26:1551–3. doi: 10.1046/j.1460-9592.2003.t01-1-00227.x
147. Conte G, De Asmundis C, Ciconte G, Julia J, Sieira J, Chierchia GB, et al. Follow-up from childhood to adulthood of individuals with family history of Brugada syndrome and normal electrocardiograms. *JAMA.* (2014) 312:2039–41. doi: 10.1001/jama.2014.13752
148. Bidoggia H, Maciel JP, Capalozza N, Mosca S, Blaksley EJ, Valverde E, et al. Sex differences on the electrocardiographic pattern of cardiac repolarization: possible role of testosterone. *Am Heart J.* (2000) 140:678–83. doi: 10.1067/mhj.2000.109918
149. Stramba-Badiale M, Spagnolo D, Bosi G, Schwartz PJ. Are gender differences in QTc present at birth? MISNES Investigators. Multicenter Italian Study on Neonatal Electrocardiography and Sudden Infant Death Syndrome. *Am J Cardiol.* (1995) 75:1277–8. doi: 10.1016/S0002-9149(99)80781-4
150. Wedekind H, Smits JPP, Schulze-Bahr E, Arnold R, Veldkamp MW, Bajanowski T, et al. *De novo* mutation in the SCN5A gene associated with early onset of sudden infant death. *Circulation.* (2001) 104:1158–64. doi: 10.1161/hc3501.095361
151. Najafi K, Mehrjoo Z, Ardalani F, Ghaderi-Sohi S, Kariminejad A, Kariminejad R, et al. Identifying the causes of recurrent pregnancy loss in consanguineous couples using whole exome sequencing on the products of miscarriage with no chromosomal abnormalities. *Sci Rep.* (2021) 11:6952. doi: 10.1038/s41598-021-86309-9
152. Waldbaum S, Patel M. Mitochondria, oxidative stress, and temporal lobe epilepsy. *Epilepsy Res.* (2010) 88:23–45. doi: 10.1016/j.eplepsyres.2009.09.020
153. Kovac S, Dinkova Kostova AT, Herrmann AM, Melzer N, Meuth SG, Gorji A. Metabolic and homeostatic changes in seizures and acquired epilepsy-mitochondria, calcium dynamics and reactive oxygen species. *Int J Mol Sci.* (2017) 18:1935. doi: 10.3390/ijms18091935
154. Cioffi F, Senese R, Lanni A, Goglia F. Thyroid hormones and mitochondria: with a brief look at derivatives and analogues. *Mol Cell Endocrinol.* (2013) 379:51–61. doi: 10.1016/j.mce.2013.06.006
155. Wallace DC. Mitochondria and cancer. *Nat Rev Cancer.* (2012) 12:685–98. doi: 10.1038/nrc3365
156. Yang Y, Karakhanova S, Hartwig W, D'Haese JG, Philippov PP, Werner J, et al. Mitochondria and mitochondrial ROS in cancer: novel targets for anticancer therapy. *J Cell Physiol.* (2016) 231:2570–81. doi: 10.1002/jcp.25349
157. Zong WX, Rabinowitz JD, White E. Mitochondria and cancer. *Mol Cell.* (2016) 61:667–76. doi: 10.1016/j.molcel.2016.02.011
158. Burke PJ. Mitochondria, bioenergetics and apoptosis in cancer. *Trends Cancer.* (2017) 3:857–70. doi: 10.1016/j.trecan.2017.10.006
159. Shen GX. Oxidative stress and diabetic cardiovascular disorders: roles of mitochondria and NADPH oxidase. *Can J Physiol Pharmacol.* (2010) 88:241–8. doi: 10.1139/Y10-018
160. Song J, Yang R, Yang J, Zhou L. Mitochondrial dysfunction-associated arrhythmogenic substrates in diabetes mellitus. *Front Physiol.* (2018) 9:1670. doi: 10.3389/fphys.2018.01670
161. Doenst T, Nguyen TD, Abel ED. Cardiac metabolism in heart failure: implications beyond ATP production. *Circ Res.* (2013) 113:709–24. doi: 10.1161/CIRCRESAHA.113.300376
162. Varian KD, Janssen PM. Frequency-dependent acceleration of relaxation involves decreased myofilament calcium sensitivity. *Am J Physiol Heart Circ Physiol.* (2007) 292:H2212–9. doi: 10.1152/ajpheart.00778.2006
163. Monasky MM, Biesiadecki BJ, Janssen PM. Increased phosphorylation of tropomyosin, troponin I, and myosin light chain-2 after stretch in rabbit ventricular myocardium under physiological conditions. *J Mol Cell Cardiol.* (2010) 48:1023–8. doi: 10.1016/j.yjmcc.2010.03.004
164. Bers DM, Despa S. Cardiac myocytes Ca2+ and Na+ regulation in normal and failing hearts. *J Pharmacol Sci.* (2006) 100:315–22. doi: 10.1254/jphs.CPJ06001X
165. Solaro RJ, Kobayashi T. Protein phosphorylation and signal transduction in cardiac thin filaments. *J Biol Chem.* (2011) 286:9935–40. doi: 10.1074/jbc.R110.197731
166. Monasky MM, Taglieri DM, Patel BG, Chernoff J, Wolska BM, Ke Y, et al. p21-activated kinase improves cardiac contractility during ischemia-reperfusion concomitant with changes in troponin-T and myosin light chain 2 phosphorylation. *Am J Physiol Heart Circ Physiol.* (2012) 302:H224–30. doi: 10.1152/ajpheart.00612.2011
167. Herren AW, Bers DM, Grandi E. Post-translational modifications of the cardiac Na channel: contribution of CaMKII-dependent phosphorylation to acquired arrhythmias. *Am J Physiol Heart Circ Physiol.* (2013) 305:H431–445. doi: 10.1152/ajpheart.00306.2013
168. Monasky MM, Taglieri DM, Jacobson AK, Haizlip KM, Solaro RJ, Janssen PM. Post-translational modifications of myofilament proteins involved in length-dependent prolongation of relaxation in rabbit right ventricular myocardium. *Arch Biochem Biophys.* (2013) 535:22–9. doi: 10.1016/j.abb.2012.10.005
169. Venetucci L, Denegri M, Napolitano C, Priori SG. Inherited calcium channelopathies in the pathophysiology of arrhythmias. *Nat Rev Cardiol.* (2012) 9:561–75. doi: 10.1038/nrcardio.2012.93
170. Hof IE, Van Der Heijden JF, Kranias EG, Sanoudou D, De Boer RA, Van Tintelen JP, et al. Prevalence and cardiac phenotype of patients with a phospholamban mutation. *Neth Heart J.* (2019) 27:64–9. doi: 10.1007/s12471-018-1211-4

171. Heijman J, Dewenter M, El-Armouche A, Dobrev D. Function and regulation of serine/threonine phosphatases in the healthy and diseased heart. *J Mol Cell Cardiol.* (2013) 64:90–8. doi: 10.1016/j.yjmcc.2013.09.006
172. Anderson ME. Ca2+-dependent regulation of cardiac L-type Ca2+ channels: is a unifying mechanism at hand? *J Mol Cell Cardiol.* (2001) 33:639–50. doi: 10.1006/jmcc.2000.1354
173. Eisner DA, Kashimura T, Venetucci LA, Trafford AW. From the ryanodine receptor to cardiac arrhythmias. *Circ J.* (2009) 73:1561–7. doi: 10.1253/circj.CJ-09-0478
174. Kumar M, Haghighi K, Kranias EG, Sadayappan S. Phosphorylation of cardiac myosin-binding protein-C contributes to calcium homeostasis. *J Biol Chem.* (2020) 295:11275–91. doi: 10.1074/jbc.RA120.013296
175. Brugada R, Campuzano O, Sarquella-Brugada G, Brugada P, Brugada J, Hong K. Brugada Syndrome In: *GeneReviews(R)*. Pagon RA, Adam MP, Ardinger HH, Wallace SE, Amemiya A, Bean LJH, Bird TD, Ledbetter N, Mefford HC, Smith RJH, Stephens K, editors. Seattle, WA (1993).
176. Liu M, Sanyal S, Gao G, Gurung IS, Zhu X, Gaconnet G, et al. Cardiac Na+ current regulation by pyridine nucleotides. *Circ Res.* (2009) 105:737–45. doi: 10.1161/CIRCRESAHA.109.197277
177. Stocchi L, Polidori E, Potenza L, Rocchi MB, Calcabrini C, Busacca P, et al. Mutational analysis of mitochondrial DNA in Brugada syndrome. *Cardiovasc Pathol.* (2016) 25:47–54. doi: 10.1016/j.carpath.2015.10.001
178. Polidori E, Stocchi L, Potenza D, Cucchiarini L, Stocchi V, Potenza L. A high number of 'natural' mitochondrial DNA polymorphisms in a symptomatic Brugada syndrome type 1 patient. *J Genet.* (2020) 99:66.. doi: 10.1007/s12041-020-01228-4
179. Jia G, Hill MA, Sowers JR. Diabetic cardiomyopathy: an update of mechanisms contributing to this clinical entity. *Circ Res.* (2018) 122:624–38. doi: 10.1161/CIRCRESAHA.117.311586
180. Hegyi B, Ko CY, Bossuyt J, Bers DM. Two-hit mechanism of cardiac arrhythmias in diabetic hyperglycemia: reduced repolarization reserve, neurohormonal stimulation and heart failure exacerbate susceptibility. *Cardiovasc Res.* (2021) cvab006. doi: 10.1093/cvr/cvab006
181. Postema PG, Vlaar AP, Devries JH, Tan HL. Familial Brugada syndrome uncovered by hyperkalaemic diabetic ketoacidosis. *Europace.* (2011) 13:1509–10. doi: 10.1093/europace/eur151
182. Alanzalon RE, Burris JR, Vinocur JM. Brugada phenocopy associated with diabetic ketoacidosis in two pediatric patients. *J Electrocardiol.* (2018) 51:323–6. doi: 10.1016/j.jelectrocard.2017.10.017
183. Haseeb S, Kariyanna PT, Jayarangaiah A, Thirunavukkarasu G, Hegde S, Marmur JD, et al. Brugada pattern in diabetic ketoacidosis: a case report and scoping study. *Am J Med Case Rep.* (2018) 6:173–9. doi: 10.12691/ajmcr-6-9-2
184. Kalkan S, Guner A, Kalcik M, Gecmen C, Ozkan M. Type I Brugada pattern associated with diabetic ketoacidosis in a patient with type II diabetes mellitus. *Anatol J Cardiol.* (2019) 21:E1. doi: 10.14744/AnatolJCardiol.2018.43789
185. Skinner JR, Marquis-Nicholson R, Luangpraseuth A, Cutfield R, Crawford J, Love DR. Diabetic dead-in-bed syndrome: a possible link to a cardiac ion channelopathy. *Case Rep Med.* (2014) 2014:647252. doi: 10.1155/2014/647252
186. London B, Michalec M, Mehdi H, Zhu X, Kerchner L, Sanyal S, et al. Mutation in glycerol-3-phosphate dehydrogenase 1 like gene (GPD1-L) decreases cardiac Na+ current and causes inherited arrhythmias. *Circulation.* (2007) 116:2260–8. doi: 10.1161/CIRCULATIONAHA.107.703330
187. Van Norstrand DW, Valdivia CR, Tester DJ, Ueda K, London B, Makielski JC, et al. Molecular and functional characterization of novel glycerol-3-phosphate dehydrogenase 1 like gene (GPD1-L) mutations in sudden infant death syndrome. *Circulation.* (2007) 116:2253–9. doi: 10.1161/CIRCULATIONAHA.107.704627
188. Mambiya M, Shang M, Wang Y, Li Q, Liu S, Yang L, et al. The play of genes and non-genetic factors on type 2 diabetes. *Front Public Health.* (2019) 7:349. doi: 10.3389/fpubh.2019.00349
189. Russo I, Frangogiannis NG. Diabetes-associated cardiac fibrosis: cellular effectors, molecular mechanisms and therapeutic opportunities. *J Mol Cell Cardiol.* (2016) 90:84–93. doi: 10.1016/j.yjmcc.2015.12.011
190. Nicole S, Fontaine B. Skeletal muscle sodium channelopathies. *Curr Opin Neurol.* (2015) 28:508–14. doi: 10.1097/WCO.0000000000000238
191. Bissay V, Van Malderen SC, Keymolen K, Lissens W, Peeters U, Daneels D, et al. SCN4A variants and Brugada syndrome: phenotypic and genotypic overlap between cardiac and skeletal muscle sodium channelopathies. *Eur J Hum Genet.* (2016) 24:400–7. doi: 10.1038/ejhg.2015.125
192. Cavalli M, Fossati B, Vitale R, Brigonzi E, Ricigliano VAG, Saraceno L, et al. Flecainide-induced Brugada syndrome in a patient with skeletal muscle sodium channelopathy: a case report with critical therapeutical implications and review of the literature. *Front Neurol.* (2018) 9:385. doi: 10.3389/fneur.2018.00385
193. Mannikko R, Wong L, Tester DJ, Thor MG, Sud R, Kullmann DM, et al. Dysfunction of NaV1.4. A skeletal muscle voltage-gated sodium channel, in sudden infant death syndrome: a case-control study. *Lancet.* (2018) 391:1483–92. doi: 10.1016/S0140-6736(18)30021-7
194. Loussouarn G, Sternberg D, Nicole S, Marionneau C, Le Bouffant F, Toumaniantz G, et al. Physiological and pathophysiological insights of Nav1.4 and Nav1.5 comparison. *Front Pharmacol.* (2015) 6:314. doi: 10.3389/fphar.2015.00314
195. Cannon SC. Sodium channelopathies of skeletal muscle. *Handb Exp Pharmacol.* (2018) 246:309–30. doi: 10.1007/164_2017_52
196. Behr ER, Ben-Haim Y, Ackerman MJ, Krahn AD, Wilde AAM. Brugada syndrome and reduced right ventricular outflow tract conduction reserve: a final common pathway?. *Eur Heart J.* (2001) 42:1073–81. doi: 10.1093/eurheartj/ehaa1051
197. Hosseini SM, Kim R, Udupa S, Costain G, Jobling R, Liston E, et al. Reappraisal of reported genes for sudden arrhythmic death: evidence-based evaluation of gene validity for Brugada syndrome. *Circulation.* (2018) 138:1195–205. doi: 10.1161/CIRCULATIONAHA.118.035070
198. D'Imperio S, Monasky MM, Micaglio E, Negro G, Pappone C. Early morning QT prolongation during hypoglycemia: only a matter of glucose? *Front Cardiovasc Med.* (2021) 8:688875. doi: 10.3389/fcvm.2021.688875
199. Bezzina C, Veldkamp MW, Van Den Berg MP, Postma AV, Rook MB, Viersma JW, et al. A single Na(+) channel mutation causing both long-QT and Brugada syndromes. *Circ Res.* (1999) 85:1206–13. doi: 10.1161/01.RES.85.12.1206
200. Gosselin-Badaroudine P, Moreau A, Chahine M. Nav 1.5 mutations linked to dilated cardiomyopathy phenotypes: is the gating pore current the missing link? *Channels.* (2014) 8:90–4. doi: 10.4161/chan.27179
201. Zaklyazminskaya E, Dzemeshkevich S. The role of mutations in the SCN5A gene in cardiomyopathies. *Biochim Biophys Acta.* (2016) 1863:1799–805. doi: 10.1016/j.bbamcr.2016.02.014
202. Sarquella-Brugada G, Campuzano O, Arbelo E, Brugada J, Brugada R. Brugada syndrome: clinical and genetic findings. *Genet Med.* (2016) 18:3–12. doi: 10.1038/gim.2015.35
203. Campuzano O, Perez-Serra A, Iglesias A, Brugada R. Genetic basis of atrial fibrillation. *Genes Dis.* (2016) 3:257–62. doi: 10.1016/j.gendis.2016.09.003
204. Campuzano O, Brugada R. Age, genetics, and fibrosis in the Brugada syndrome. *J Am Coll Cardiol.* (2015) 66:1987–9. doi: 10.1016/j.jacc.2015.09.006
205. Nademanee K, Raju H, De Noronha SV, Papadakis M, Robinson L, Rothery S, et al. Fibrosis, connexin-43, and conduction abnormalities in the Brugada syndrome. *J Am Coll Cardiol.* (2015) 66:1976–86. doi: 10.1016/j.jacc.2015.08.862
206. Cipriani A, Bauce B, De Lazzari M, Rigato I, Bariani R, Meneghin S, et al. Arrhythmogenic right ventricular cardiomyopathy: characterization of left ventricular phenotype and differential diagnosis with dilated cardiomyopathy. *J Am Heart Assoc.* (2020) 9:e014628. doi: 10.1161/JAHA.119.014628
207. King JH, Huang CL, Fraser JA. Determinants of myocardial conduction velocity: implications for arrhythmogenesis. *Front Physiol.* (2013) 4:154. doi: 10.3389/fphys.2013.00154
208. Pietrasik G, Zareba W. QRS fragmentation: diagnostic and prognostic significance. *Cardiol J.* (2012) 19:114–21. doi: 10.5603/CJ.2012.0022

209. Foo B, Williamson B, Young JC, Lukacs G, Shrier A. hERG quality control and the long QT syndrome. *J Physiol.* (2016) 594:2469–81. doi: 10.1113/JP270531
210. Chadda KR, Ahmad S, Valli H, Den Uijl I, Al-Hadithi AB, Salvage SC, et al. The effects of ageing and adrenergic challenge on electrocardiographic phenotypes in a murine model of long QT syndrome type 3. *Sci Rep.* (2017) 7:11070. doi: 10.1038/s41598-017-11210-3
211. Bartlett TG, Friedman PL. Current management of the Wolff-Parkinson-White syndrome. *J Card Surg.* (1993) 8:503–15. doi: 10.1111/j.1540-8191.1993.tb00401.x
212. Lee HJ, Uhm JS, Hong YJ, Hur J, Choi BW, Joung B, et al. Altered myocardial characteristics of the preexcited segment in Wolff-Parkinson-White syndrome: a pilot study with cardiac magnetic resonance imaging. *PLoS ONE.* (2018) 13:e0198218. doi: 10.1371/journal.pone.0198218
213. Raman B, Ariga R, Spartera M, Sivalokanathan S, Chan K, Dass S, et al. Progression of myocardial fibrosis in hypertrophic cardiomyopathy: mechanisms and clinical implications. *Eur Heart J Cardiovasc Imaging.* (2019) 20:157–67. doi: 10.1093/ehjci/jey135
214. Everett THT, Olgin JE. Atrial fibrosis and the mechanisms of atrial fibrillation. *Heart Rhythm.* (2007) 4:S24–7. doi: 10.1016/j.hrthm.2006.12.040
215. Sohns C, Marrouche NF. Atrial fibrillation and cardiac fibrosis. *Eur Heart J.* (2020) 41:1123–31. doi: 10.1093/eurheartj/ehz786
216. Marian AJ, Braunwald E. Hypertrophic cardiomyopathy: genetics, pathogenesis, clinical manifestations, diagnosis, and therapy. *Circ Res.* (2017) 121:749–70. doi: 10.1161/CIRCRESAHA.117.311059
217. Geske JB, Ommen SR, Gersh BJ. Hypertrophic cardiomyopathy: clinical update. *JACC Heart Fail.* (2018) 6:364–75. doi: 10.1016/j.jchf.2018.02.010
218. Pappone C, Brugada J, Vicedomini G, Ciconte G, Manguso F, Saviano M, et al. Electrical substrate elimination in 135 consecutive patients with Brugada syndrome. *Circ Arrhythm Electrophysiol.* (2017) 10:e005053. doi: 10.1161/CIRCEP.117.005053
219. Pappone C, Ciconte G, Manguso F, Vicedomini G, Mecarocci V, Conti M, et al. Assessing the malignant ventricular arrhythmic substrate in patients with Brugada syndrome. *J Am Coll Cardiol.* (2018) 71:1631–46. doi: 10.1016/j.jacc.2018.02.022
220. Ciconte G, Santinelli V, Brugada J, Vicedomini G, Conti M, Monasky MM, et al. General anesthesia attenuates brugada syndrome phenotype expression: clinical implications from a prospective clinical trial. *JACC Clin Electrophysiol.* (2018) 4:518–30. doi: 10.1016/j.jacep.2017.11.013

Conflict of Interest: The authors declare that the research was conducted in the absence of any commercial or financial relationships that could be construed as a potential conflict of interest.

Publisher's Note: All claims expressed in this article are solely those of the authors and do not necessarily represent those of their affiliated organizations, or those of the publisher, the editors and the reviewers. Any product that may be evaluated in this article, or claim that may be made by its manufacturer, is not guaranteed or endorsed by the publisher.

frontiers in Cardiovascular Medicine

MINI REVIEW
published: 23 December 2021
doi: 10.3389/fcvm.2021.782596

The Mechanism of Ajmaline and Thus Brugada Syndrome: Not Only the Sodium Channel!

Michelle M. Monasky[1], *Emanuele Micaglio*[1], *Sara D'Imperio*[1] *and Carlo Pappone*[1,2]*

[1] Arrhythmology Department, IRCCS Policlinico San Donato, San Donato Milanese, Milan, Italy, [2] Vita-Salute San Raffaele University, Milan, Italy

Ajmaline is an anti-arrhythmic drug that is used to unmask the type-1 Brugada syndrome (BrS) electrocardiogram pattern to diagnose the syndrome. Thus, the disease is defined at its core as a particular response to this or other drugs. Ajmaline is usually described as a sodium-channel blocker, and most research into the mechanism of BrS has centered around this idea that the sodium channel is somehow impaired in BrS, and thus the genetics research has placed much emphasis on sodium channel gene mutations, especially the gene *SCN5A*, to the point that it has even been suggested that only the *SCN5A* gene should be screened in BrS patients. However, pathogenic rare variants in *SCN5A* are identified in only 20–30% of cases, and recent data indicates that *SCN5A* variants are actually, in many cases, prognostic rather than diagnostic, resulting in a more severe phenotype. Furthermore, the misconception by some that ajmaline only influences the sodium current is flawed, in that ajmaline actually acts additionally on potassium and calcium currents, as well as mitochondria and metabolic pathways. Clinical studies have implicated several candidate genes in BrS, encoding not only for sodium, potassium, and calcium channel proteins, but also for signaling-related, scaffolding-related, sarcomeric, and mitochondrial proteins. Thus, these proteins, as well as any proteins that act upon them, could prove absolutely relevant in the mechanism of BrS.

Keywords: Brugada syndrome (BrS), ajmaline, arrhythmias, sudden cardiac death (SCD), sodium channel, potassium channel, calcium channel, mitochondria

OPEN ACCESS

Edited by:
Alexander Pott, Ulm University Medical Center, Germany

Reviewed by:
Ranjan K. Dash, Medical College of Wisconsin, United States
Gerrit Frommeyer, University Hospital Münster, Germany

***Correspondence:**
Carlo Pappone
carlo.pappone@af-ablation.org

Specialty section:
This article was submitted to Cardiovascular Genetics and Systems Medicine, a section of the journal Frontiers in Cardiovascular Medicine

Received: *24 September 2021*
Accepted: *29 November 2021*
Published: *23 December 2021*

Citation:
Monasky MM, Micaglio E, D'Imperio S and Pappone C (2021) The Mechanism of Ajmaline and Thus Brugada Syndrome: Not Only the Sodium Channel! Front. Cardiovasc. Med. 8:782596. doi: 10.3389/fcvm.2021.782596

INTRODUCTION

Ajmaline is used as a pharmacologic test to diagnose Brugada syndrome (BrS) and identify people who are at higher risk of developing life-threatening arrhythmias and sudden cardiac death. Many patients are ultimately implanted with an implantable cardioverter-defibrillator that can save their lives. The BrS is an inherited disease characterized by a coved-type ST-segment elevation in the right precordial leads (V_1-V_3) on the electrocardiogram (ECG). The true prevalence of BrS is unknown, since many people are asymptomatic. In fact, the syndrome may not even be suspected until an incidence of cardiac arrest. Certain "trigger situations," such as fever, drug use, or consumption of alcohol or large meals can elicit the BrS ECG pattern (1). Since the systematic introduction of sodium-channel blockers to screen for the syndrome, the diagnosis, and thus the perceived incidence, of BrS has increased (2).

Sodium channel blockers, such as ajmaline, flecainide, or procainamide can be used to provoke the type-1 BrS ECG pattern, which is said to affirmatively diagnose the syndrome (3, 4). Thus, the disease is defined at its core as a particular response to these drugs. Some clinicians prefer the use of ajmaline, which appears to have a lower false negative rate, due to its higher sensitivity (5, 6). This higher sensitivity of ajmaline, compared to flecainide, may be due to flecainide's greater inhibition of I_{to}, which then renders it less effective (5). Whole-cell patch clamp experiments demonstrated a reduced I_{to} total charge with an IC_{50} of 216 and 15.2 μM for ajmaline and flecainide, respectively, while sodium channel current was affected similarly by both drugs, as suggested by equivalent changes in QRS and PQ intervals (5). However, reports have cautioned about ajmaline's false positive rate, stating that a positive ajmaline test does not always mean that a patient has BrS (7–10). In fact, ajmaline metabolism is very complex (11) for several reasons relating to the liver metabolism, kidney metabolism, plasma proteins binding, and variability in the expression of ajmaline-metabolizing enzymes (12). Ajmaline undergoes some major metabolic pathways: mono- and di-hydroxylation of the benzene ring with subsequent O-methylation, reduction of the C-21, oxidation of both C-17 and C-21-hydroxyl function and N-oxidation (13). Consequently, one of the major genes controlling ajmaline metabolism is *CYP2D6*, encoding for a cytochrome C component. Thus, it is not surprising that patients harboring variants or even polymorphisms in the *CYP2D6* gene might display a different capability to metabolize ajmaline (14). To date, more than 70 allelic variants of the *CYP2D6* gene have been reported, and altered *CYP2D6* function has been associated with both adverse drug reactions and reduced drug efficacy (15). This is the main reason why poor metabolizer alleles can be important as a possible cause of false positivity during ajmaline challenge test.

Ajmaline challenges must be conducted in specialized centers due to the potential development of life-threatening ventricular arrhythmias, such as polymorphic ventricular tachycardia (VT) or ventricular fibrillation (VF) (16–18). Ajmaline infusion should be done carefully, stopping as soon as the result is positive or when QRS broadens to ≥130% of baseline or frequent pre-mature ventricular complexes occur (17, 19, 20).

Ajmaline is usually described as a sodium-channel blocker (3), and most research into the mechanism of BrS has centered around this idea that the sodium channel is somehow impaired in BrS (21, 22), and thus the genetics research has placed much emphasis on sodium channel gene mutations, especially the gene *SCN5A*, whereas systematic studies on other genes are lacking (23). The research up until this point has focused so much on the *SCN5A* gene that it has even been suggested that only the *SCN5A* gene should be screened in BrS patients (23), something that has been hotly debated (24–26), as many argue that research is needed to understand the possible role of several other genes in this disease (27–32). However, pathogenic rare variants in *SCN5A* are identified in only 20–30% of ajmaline-positive cases (33–36), and recent data indicates that mutations in *SCN5A* are actually, in many cases, prognostic rather than diagnostic, resulting in a more severe phenotype (26, 35, 37–39). Furthermore, the misconception by some that ajmaline only influences the sodium current, and thus sodium channels should be the only channels of interest in BrS, is flawed, in that ajmaline actually acts additionally on potassium and calcium currents, as well as mitochondria and metabolic pathways. Thus, potassium channels, calcium channels, mitochondrial proteins, and metabolic pathway proteins, or factors that act upon these proteins, could prove absolutely relevant, as their function is directly influenced by the very drug that is used to diagnose the disease in the first place.

MULTIPLE BINDING SITES OF AJMALINE ON Na^+, K^+, AND Ca^{2+} CHANNELS

Ajmaline has multiple sites of action, including sodium, potassium, and calcium channels. Plant alkaloids, including ajmaline, act on at least six receptor sites on voltage-gated Na^+ channels (40). In single intact amphibian skeletal muscle fibers, it appeared that ajmaline has multiple sites of action, including the positively charged S4 voltage-sensing segment of Na^+ and K^+ channels (40). However, ajmaline also blocks channels that do not have a voltage sensor (e.g., K_{ATP}) (40).

In human embryonic kidney (HEK) cells, ajmaline has an inhibitory effect on human ether a-go-go related gene (HERG) potassium channels in the open, but not in the closed states, and probably binds at aromatic residues Tyr-652 and Phe-656 in the channel pore cavity (41). The inhibitory effect was stronger at higher frequencies (41). Ajmaline is an open channel inhibitor at therapeutic concentrations of cardiac potassium $K_V1.5$ and $K_V4.3$ channels, responsible for cardiac I_{Kur} and I_{to} current, respectively (42). Ajmaline potently blocks glibenclamide-sensitive K^+ channels in *Xenopus* oocytes in a concentration-dependent manner (43). There is an effect of ajmaline on the inhibition of K^+ outflow from rat liver mitochondria (44). In rat right ventricular myocytes, the decreased amplitude and time integral of I_{to} by ajmaline is dependent on concentration, but not frequency or use (45). In rat right ventricular myocytes, ajmaline blocks the transient outward potassium current (I_{to}) when the channel is in the open state and there is fast recovery from the block at resting voltage (45).

Whole cell patch clamp technique used to determine the effect of ajmaline on action potential (AP) and ionic current components in rat right ventricular myocytes demonstrated an inhibitory effect on sodium current (I_{Na}), L-type calcium current (I_{Ca-L}), transient outward potassium current (I_{to}), the current measured at the end of 300 ms depolarizing pulse ($I_{K,end}$), and ATP-sensitive potassium current [$I_{K(ATP)}$] (46). The inhibition

Abbreviations: AP, action potential; BrS, Brugada syndrome; Ca^{2+}, calcium; ECG, electrocardiogram; HEK, human embryonic kidney; HERG, human ether a-go-go related gene; I_{Ca-L}, L-type calcium current; I_K, delayed rectifier potassium current; I_{K1}, inwardly rectifying potassium current; $I_{K(ATP)}$, ATP-sensitive potassium current; $I_{K,end}$, the current measured at the end of 300 ms depolarizing pulse; I_{Kur}, ultrarapid outward potassium current; I_{Na}, sodium current; I_{to}, transient outward potassium current; K^+, potassium; K_{ATP}, ATP-sensitive potassium channel; Na^+, sodium; NCX, sodium-calcium exchanger; NPA, N-propyl ajmaline, a quaternary derivative of ajmaline; PVCs, pre-mature ventricular complexes; RV, right ventricle; Vas, ventricular arrhythmias; VF, ventricular fibrillation; VT, ventricular tachycardia.

of I_{Na} causes both the decreased rate of rise of depolarizing phase and the lowered amplitude of AP (46). Additionally, I_{to} inhibition was responsible for AP prolongation after ajmaline administration (46). In isolated guinea pig ventricular cardiomyocytes, ajmaline suppressed calcium currents (I_{Ca}) in a dose-dependent manner without affecting the steady-state inactivation kinetics and the voltage dependency of the current-voltage relationship, inhibited inwardly rectifying potassium current (I_{K1}), and decreased the delayed rectifier potassium current (I_K) without altering the activation or deactivation time courses (47). A study recording intracellular action potentials and transmural ECG in canine RV wedge preparations suggested that combined sodium and calcium channel block may be more effective than sodium channel block alone in unmasking the BrS pattern (48). The study used terfenadine to block both sodium and calcium current, which resulted in the loss of the epicardial AP dome, ST segment elevation, phase 2 reentry, and spontaneous polymorphic VT/VF (48). This effect of terfenadine was normalized with 4-aminopyridine, which inhibits I_{to} (48). The drugs flecainide, ajmaline, and procainamide alone did not generate polymorphic VT, but they did so together with the calcium channel blocker verapamil (48).

N-propyl ajmaline (NPA) is the quaternary derivative of ajmaline. The permanently charged NPA and protonated ajmaline both act mainly with open channels, while unprotonated ajmaline acts mainly on inactivated Na^+ channels in frog myelinated fibers (49). In frog myelinated fibers, sodium and potassium currents are inhibited by ajmaline and NPA, for sodium in both directions, but for potassium, only the outward potassium current, not the inward potassium current (49). The location of the binding sites have been suggested to be in the inner mouths of Na^+ and K^+ channels (49). In voltage clamp experiments using frog nodes of Ranvier, the binding site for NPA has been described to be located in the inner mouth of the Na^+ channels, and it becomes available to the charged blocker (NPA) only after opening of the activation gate (50). NPA in enzymatically isolated cells of adult rats inhibits I_{Na} due to a voltage-dependent interaction with open Na^+ channels, and NPA has similar blocking effects on Na^+ channels in myocardial cells and nerve fibers (51).

GENETICS OF CHANNELS IMPLICATED BY FUNCTIONAL STUDIES

Functional studies have identified several molecular targets of ajmaline. Many of these molecular targets are encoded for by genes that have been associated with BrS in clinical studies. **Table 1** lists the known molecular targets of ajmaline and their related genes. **Figure 1** shows a schematic of ajmaline targets in the cell, as demonstrated by functional studies.

A Unique Role for Calcium: Excitation-Contraction Coupling in Brugada Syndrome

Calcium signaling is responsible for connecting the electrical signaling of the cell to the mechanical force of contraction and relaxation of the sarcomeric proteins. Thus, calcium imbalances in the cell could result in alterations to the force production. In porcine epicardial shavings, excitation failure by current-to-load mismatch was shown to cause ST segment elevation modulated by I_{to} and I_{CaL} (54). A study by Biamino et al. demonstrated a relaxing effect of ajmaline on vascular smooth muscle using aortic helical strips, attributing the effect possibly to a reduction in Ca^{2+} and probably Na^+ conductance (55). In BrS patients, ajmaline administration results in a decrease of right ventricular ejection fraction and minimum principal strain in the right ventricular outflow tract and right ventricular anterior wall (56, 57). In fact, it has been previously suggested that the electromechanical coupling in BrS, including calcium handling and sarcomeric alterations, should be investigated (28, 57). Reduced intracellular calcium, which may result in a reduction of force production, has been proposed as a possible mechanism in BrS (8, 28, 58, 59). Additionally, administration of pharmaceuticals that act on outer cell membrane receptors can result in signaling changes within the cell (60, 61). It would be interesting to see in future studies whether ajmaline affects intracellular processes, such as signaling pathways that lead to post-translational modifications, affecting various proteins, such as those located in the sarcoplasmic reticulum or the myofilaments.

GENETICS OF CHANNELS IMPLICATED BY CLINICAL STUDIES

The genetics of BrS remains a hotly debated subject. More than 20 genes are currently included in diagnostic genetic testing panels, previously reviewed in detail elsewhere (32), although the significance of variants in all but the *SCN5A* gene are disputed, since most studies to-date have focused on understanding better variants in the *SCN5A* gene, while studies on the other genes are generally lacking (23). However, pathogenic rare variants in *SCN5A* are identified in only 20–30% of ajmaline-positive cases (33–36), and recent data indicates that mutations in *SCN5A* are actually, in many cases, prognostic rather than diagnostic, resulting in a more severe phenotype (26, 35, 37–39). Several important studies of other genes are now available, and more are needed to better understand the mechanism of ajmaline in provoking the type-1 BrS ECG pattern.

Sodium channel-related genes other than *SCN5A* that have been previously implicated in BrS, and they include *SCN10A*, *SCN1B*, *SCN2B*, *SCN3B*, *SCN4B*, *RANGRF* (*MOG1*), and *GPD1L*. Potassium-related genes previously associated in BrS include *KCND2*, *KCND3*, *KCNE1*, *KCNE2*, *KCNE3*, *KCNE5*, *KCNH2*, *KCNJ2*, *KCNJ5*, *KCNJ8*, *KCNQ1*, *ABCC9*, and *HCN4*, while calcium-related genes previously described in BrS include *CACNA1C*, *CACNA2D1*, *CACNB2*, *RYR2*, and *TRPM4* (32, 62). In addition, the gene *PKP2* has been associated with BrS, and studies have shown a relationship between *PKP2* and both sodium and potassium channels. For example, in a study by Cerrone et al., loss of PKP2 caused decreased I_{Na} and $Na_V1.5$ (63). Hong et al. demonstrated an interaction between PKP2 and K_{ATP} channels in rat heart (64).

Sarcomeric properties have been directly linked to arrythmogenic sudden death (61, 65), and variants in myofilament genes, including *TPM1* and *MYBPC3*, have

TABLE 1 | Known molecular targets of ajmaline and potential genes that they implicate.

Protein or current described in functional studies targeted by ajmaline	Examples of genes that these targets implicate (52)
Sodium channel current (I_{Na}) (40, 46)	*SCN5A, SCN10A, SCN1B, SCN2B, SCN3B, SCN4A*
Potassium channel current (I_K) (46)	*KCNA4*, *KCNE4*
ATP-sensitive potassium channel (K_{ATP}) (40, 46)	*ABCC8, ABCC9, KCNJ1, KCNJ5, KCNJ8, KCNJ11*
human ether a-go-go related gene (HERG) potassium channels (41)	*hERG (KCNH2)*
K_V1.5 channels, responsible for cardiac I_{Kur} (42)	*KCNA5*
K^+ outflow from mitochondria (mitoK_{ATP}) (44)	Formed by 5 components (53): • Mitochondrial ATP-binding cassette protein 1 (mABC1): *ABCB8* • Phosphate carrier: *MPCD, SLC34A1, SLC17A1, SLC17A7, SLC17A6, SLC25A26, SLC25A3, SLC25A25, SLC37A4, SLC25A23* • Adenine nucleotide translocator: *SLC25A4, SLC25A5, SLC25A6, SLC25A31, SLC25A6* • ATP synthase: *ATP5PF, ATP5F1C, ATP5F1B, ATP5F1D, ATP5F1A, ATP5ME, MC5DN2, ATP5PO, ATP5G1, ATP5G2* • Succinate Dehydrogenase: *SDHC, SDHB, SDHA, SDHD, SDHAF2, SDHAF4, SDHAF1* (2021)
K_V4.3 channels and outward potassium current (I_{to}) (42, 45)	*KCND3*
L-type calcium current (I_{Ca-L}) (46)	*CACNA1C, CACNB2*
inwardly rectifying potassium current (I_{K1}) (47)	*KCNJ2*, *KCNJ5*, *KCNJ8*
delayed rectifier potassium current (I_K) (47)	*KCNS3, KCNS1, KCNS2*

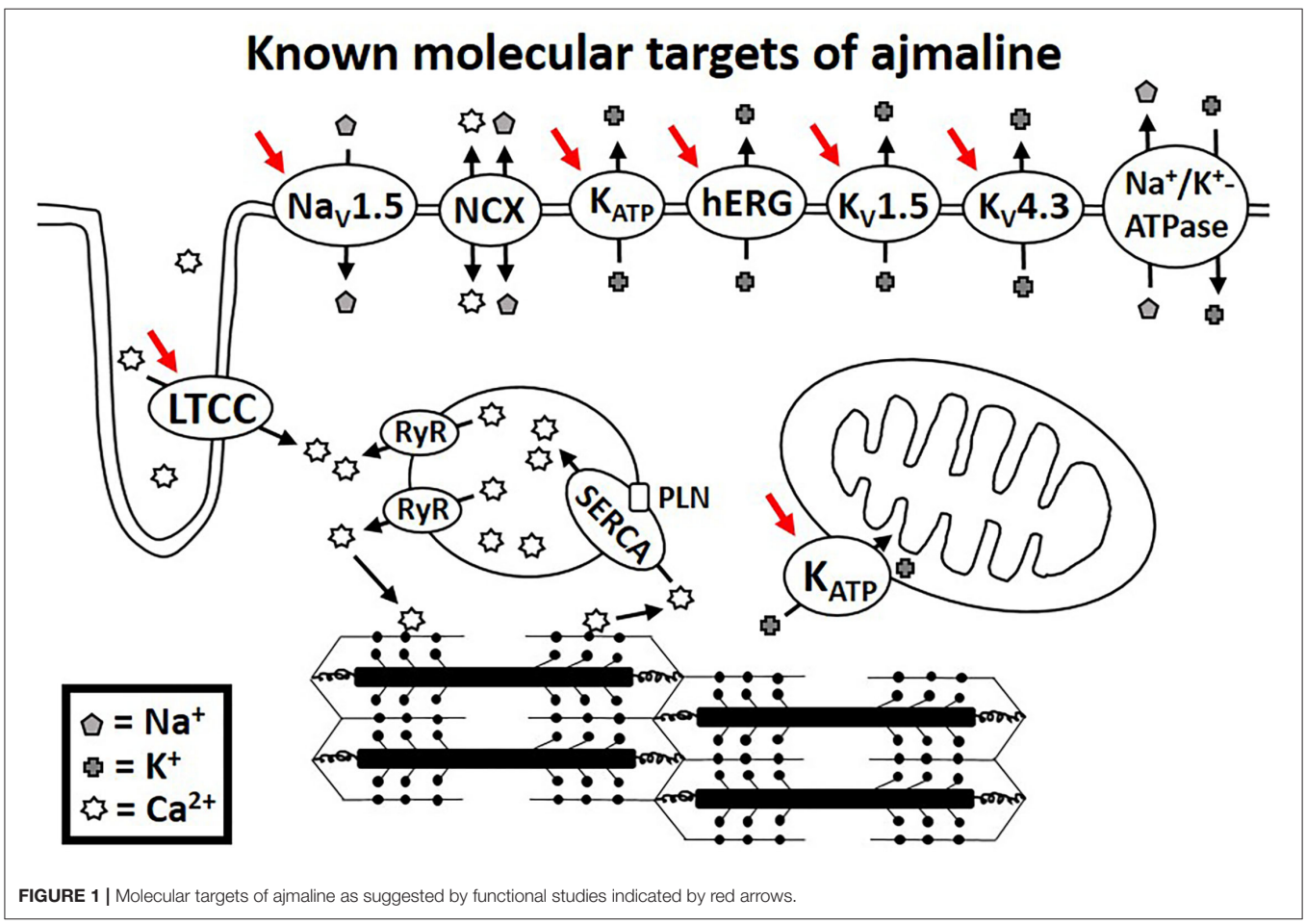

FIGURE 1 | Molecular targets of ajmaline as suggested by functional studies indicated by red arrows.

been found in BrS patients (27, 66, 67). Several other genes, encoding signaling and scaffolding proteins, including *AKAP9*, *ANK2*, *CASQ2*, *CAV3*, *CBL*, *DSC2*, *DSG2*, *DSP*, *FGF12*, *HEY2*, *JUP*, *LMNA*, *LRRC10*, *NOS1AP*, *SEMA3A*, *SLMAP*, *SNTA1*, and

TMEM43, have been suggested as candidate genes (32, 62, 68). The function of proteins that are affected by protein kinase A or reactive oxygen species (ROS), such as the protein products of many of the genes listed above, may be altered by changes in mitochondrial function, which is responsible for ATP and ROS production (26). In fact, studies have implicated a direct role for mitochondria in BrS, specifically, severe cases have been associated with a particular mitochondrial DNA (mtDNA) allelic combination and a high number of mtDNA single nucleotide polymorphisms (69, 70), and a role for mitochondrial transfer RNA genes has been suggested (71). Thus, in addition to *SCN5A*, various other genes have been suggested to have a role in BrS, including other sodium channel-related genes, as well as several potassium-related, calcium-related, signaling-related, scaffolding-related, sarcomeric, and mitochondrial genes, consistent with the identified molecular targets of the ajmaline drug used to unmask and diagnosis the syndrome.

Although it is generally agreed that variants in the *SCN5A* gene are involved in BrS, it is important to think of variants even within this gene as individual variants with specific effects, rather than thinking of all *SCN5A* variants collectively, as some may be benign, while others pathogenic (26). Along these lines, several studies have sought to understand the effect of specific *SCN5A* variants (37, 72–80). It has been recently suggested that variants in the *SCN5A* gene may actually be prognostic, rather than diagnostic (35, 38, 39).

Studies to better understand the role of variants in each of the above-mentioned genes will be an important area of future research. A recent study by Di Mauro et al. demonstrated an important role for *CACNA1C* (31), highlighting the importance of functional studies of genes that may be involved in BrS, but for which we currently lack the proof (81). Recent studies have also focused on the roles of the genes *SCN10A* and *HEY2* in BrS (29, 82). However, much work remains to be done before we can understand the role of each of the protein products of these genes, as well as the role of the proteins that signal to them and alter their function. Currently, the understanding of genetics in BrS is in its infancy, and genetic testing alone should not be used for diagnostic purposes, but rather, diagnosis of BrS should be based upon an arrhythmological examination by a specialized cardiologist (26). The presence of a variant in the *SCN5A* gene, however, may be relevant for prognostic purposes (35, 38).

LIMITATIONS AND FUTURE STUDIES

Most of the studies to better understand the mechanism of ajmaline have been performed in cellular models using non-cardiomyocyte cell types or in animal models that are sometimes not even mammalian. While these models give us some insight, each model comes with its own set of advantages and limitations (83). The functional studies performed to-date indicate that ajmaline does not act solely on sodium channels and suggests that clinical genetic testing could be expanded for research purposes to include, for example, genes that encode for potassium and calcium channels. Thus, the mechanism of BrS could be researched from also this clinical direction. Regarding future functional studies, it would be interesting to quantify ajmaline signaling to, and effects on, particular sodium, potassium, and calcium channels and the resulting effect of sodium, potassium, and calcium handling, to ultimately understand the mechanism behind the altered ECG.

CONCLUSION

The misconception by some that ajmaline only influences the sodium current, and thus sodium channels should be the only channels of interest in BrS, is flawed, in that ajmaline actually acts additionally on potassium and calcium currents, as well as mitochondria and metabolic pathways. Clinical studies have implicated several candidate genes in BrS, encoding not only for sodium, potassium, and calcium channel proteins, but also for signaling-related, scaffolding-related, sarcomeric, and mitochondrial proteins. Thus, these proteins, as well as any proteins that act upon them, could prove absolutely relevant in the mechanism of BrS.

AUTHOR CONTRIBUTIONS

MM: conceptualization and writing—original draft preparation. MM, EM, and SD'I: literature search and writing—draft revision. CP: funding acquisition. MM, EM, SD'I, and CP: reviewed and provided comments. All authors have read and agreed to the published version of the manuscript.

FUNDING

This study was partially supported by Ricerca Corrente funding from Italian Ministry of Health to IRCCS Policlinico San Donato. The funders had no role in the design of the study; in the collection, analyses, or interpretation of data; in the writing of the manuscript, or in the decision to publish the results.

REFERENCES

1. D'imperio S, Monasky MM, Micaglio E, Negro G, Pappone C. Impact of dietary factors on Brugada syndrome and long QT syndrome. *Nutrients.* (2021) 13:2482. doi: 10.3390/nu13082482
2. Priori SG, Blomstrom-Lundqvist C, Mazzanti A, Blom N, Borggrefe M, Camm J, et al. 2015 ESC Guidelines for the management of patients with ventricular arrhythmias and the prevention of sudden cardiac death: the task force for the management of patients with ventricular arrhythmias and the prevention of sudden cardiac death of the European Society of Cardiology (ESC). Endorsed by: Association for European Paediatric and Congenital Cardiology (AEPC). *Eur Heart J.* (2015) 36:2793–867. doi: 10.1093/eurheartj/ehv316
3. Brugada R, Brugada J, Antzelevitch C, Kirsch GE, Potenza D, Towbin JA, et al. Sodium channel blockers identify risk for sudden death in patients with ST-segment elevation and right bundle branch block but structurally normal hearts. *Circulation.* (2000) 101:510–5. doi: 10.1161/01.CIR.101.5.510

4. Therasse D, Sacher F, Petit B, Babuty D, Mabo P, Martins R, et al. Sodium-channel blocker challenge in the familial screening of Brugada syndrome: safety and predictors of positivity. *Heart Rhythm.* (2017) 14:1442–8. doi: 10.1016/j.hrthm.2017.06.031
5. Wolpert C, Echternach C, Veltmann C, Antzelevitch C, Thomas GP, Spehl S, et al. Intravenous drug challenge using flecainide and ajmaline in patients with Brugada syndrome. *Heart Rhythm.* (2005) 2:254–60. doi: 10.1016/j.hrthm.2004.11.025
6. Cheung CC, Mellor G, Deyell MW, Ensam B, Batchvarov V, Papadakis M, et al. Comparison of ajmaline and procainamide provocation tests in the diagnosis of brugada syndrome. *JACC Clin Electrophysiol.* (2019) 5:504–12. doi: 10.1016/j.jacep.2019.01.026
7. Viskin S, Rosso R, Friedensohn L, Havakuk O, Wilde AA. Everybody has Brugada syndrome until proven otherwise? *Heart Rhythm.* (2015) 12:1595–8. doi: 10.1016/j.hrthm.2015.04.017
8. Antzelevitch C, Yan GX, Ackerman MJ, Borggrefe M, Corrado D, Guo J, et al. J-Wave syndromes expert consensus conference report: emerging concepts and gaps in knowledge. *Heart Rhythm.* (2016) 13:e295–324. doi: 10.1016/j.hrthm.2016.05.024
9. Tadros R, Nannenberg EA, Lieve KV, Skoric-Milosavljevic D, Lahrouchi N, Lekanne Deprez RH, et al. Yield and pitfalls of ajmaline testing in the evaluation of unexplained cardiac arrest and sudden unexplained death: single-center experience with 482 families. *JACC Clin Electrophysiol.* (2017) 3:1400–8. doi: 10.1016/j.jacep.2017.04.005
10. Viskin S, Rosso R. Read my lips: a positive ajmaline test does not always mean you have brugada syndrome. *JACC Clin Electrophysiol.* (2017) 3:1409–11. doi: 10.1016/j.jacep.2017.05.016
11. Yasuhara M, Hashimoto Y, Okumura K, Hori R, Sakurai T, Kawai C. Kinetics of ajmaline disposition and pharmacologic response in beagle dogs. *J Pharmacokinet Biopharm.* (1987) 15:39–55. doi: 10.1007/BF01062938
12. Padrini R, Piovan D, Javarnaro A, Cucchini F, Ferrari M. Pharmacokinetics and electrophysiological effects of intravenous ajmaline. *Clin Pharmacokinet.* (1993) 25:408–14. doi: 10.2165/00003088-199325050-00006
13. Koppel C, Tenczer J, Arndt I. Metabolic disposition of ajmaline. *Eur J Drug Metab Pharmacokinet.* (1989) 14:309–16. doi: 10.1007/BF03190117
14. Zhou SF. Polymorphism of human cytochrome P450 2D6 and its clinical significance: part I. *Clin Pharmacokinet.* (2009) 48:689–723. doi: 10.2165/11318030-000000000-00000
15. Taylor C, Crosby I, Yip V, Maguire P, Pirmohamed M, Turner RM. A Review of the important role of CYP2D6 in Pharmacogenomics. *Genes (Basel).* (2020) 11:1295. doi: 10.3390/genes11111295
16. Conte G, Sieira J, Sarkozy A, De Asmundis C, Di Giovanni G, Chierchia GB, et al. Life-threatening ventricular arrhythmias during ajmaline challenge in patients with Brugada syndrome: incidence, clinical features, and prognosis. *Heart Rhythm.* (2013) 10:1869–74. doi: 10.1016/j.hrthm.2013.09.060
17. Poli S, Toniolo M, Maiani M, Zanuttini D, Rebellato L, Vendramin I, et al. Management of untreatable ventricular arrhythmias during pharmacologic challenges with sodium channel blockers for suspected Brugada syndrome. *Europace.* (2018) 20:234–42. doi: 10.1093/europace/eux092
18. Ciconte G, Monasky MM, Vicedomini G, Borrelli V, Giannelli L, Pappone C. Unusual response to ajmaline test in Brugada syndrome patient leads to extracorporeal membrane oxygenator support. *Europace.* (2019) 21:1574. doi: 10.1093/europace/euz139
19. Antzelevitch C, Brugada P, Borggrefe M, Brugada J, Brugada R, Corrado D, et al. Brugada syndrome: report of the second consensus conference: endorsed by the Heart Rhythm Society and the European Heart Rhythm Association. *Circulation.* (2005) 111:659–70. doi: 10.1161/01.CIR.0000152479.54298.51
20. Nault I, Champagne J. How safe is ajmaline challenge in patients with suspected Brugada syndrome? *Heart Rhythm.* (2013) 10:1875–6. doi: 10.1016/j.hrthm.2013.10.047
21. Bebarova M, O'hara T, Geelen JL, Jongbloed RJ, Timmermans C, Arens YH, et al. Subepicardial phase 0 block and discontinuous transmural conduction underlie right precordial ST-segment elevation by a SCN5A loss-of-function mutation. *Am J Physiol Heart Circ Physiol.* (2008) 295:H48–58. doi: 10.1152/ajpheart.91495.2007
22. Petitprez S, Jespersen T, Pruvot E, Keller DI, Corbaz C, Schlapfer J, et al. Analyses of a novel SCN5A mutation (C1850S): conduction vs. repolarization disorder hypotheses in the Brugada syndrome. *Cardiovasc Res.* (2008) 78:494–504. doi: 10.1093/cvr/cvn023
23. Hosseini SM, Kim R, Udupa S, Costain G, Jobling R, Liston E, et al. Reappraisal of reported genes for sudden arrhythmic death. *Circulation.* (2018) 138:1195–205. doi: 10.1161/CIRCULATIONAHA.118.035070
24. London B. Reappraisal of reported genes for sudden arrhythmic death: evidence-based evaluation of gene validity for brugada syndrome*Circulation.* (2019) 139:1758–9. doi: 10.1161/CIRCULATIONAHA.118.036889
25. Wilde AM, Gollob MH. Reappraisal of Reported Genes for Sudden Arrhythmic Death: Evidence-Based Evaluation of Gene Validity for Brugada Syndrome". *Circulation.* (2019) 139:1760–1. doi: 10.1161/CIRCULATIONAHA.119.039065
26. Monasky MM, Micaglio E, Locati ET, Pappone C. Evaluating the use of genetics in brugada syndrome risk stratification. *Front Cardiovasc Med.* (2021) 8:652027. doi: 10.3389/fcvm.2021.652027
27. Monasky MM, Ciconte G, Anastasia L, Pappone C. Commentary: next generation sequencing and linkage analysis for the molecular diagnosis of a novel overlapping syndrome characterized by hypertrophic cardiomyopathy and typical electrical instability of Brugada syndrome. *Front Physiol.* (2017) 8:1056. doi: 10.3389/fphys.2017.01056
28. Monasky MM, Pappone C, Piccoli M, Ghiroldi A, Micaglio E, Anastasia L. Calcium in Brugada syndrome: questions for future research. *Front Physiol.* (2018) 9:1088. doi: 10.3389/fphys.2018.01088
29. Monasky MM, Micaglio E, Vicedomini G, Locati ET, Ciconte G, Giannelli L, et al. Comparable clinical characteristics in Brugada syndrome patients harboring SCN5A or novel SCN10A variants. *Europace.* (2019) 21:1550–8. doi: 10.1093/europace/euz186
30. Campuzano O, Sarquella-Brugada G, Cesar S, Arbelo E, Brugada J, Brugada R. Update on genetic basis of brugada syndrome: monogenic, polygenic or oligogenic? *Int J Mol Sci.* (2020) 21:7155. doi: 10.3390/ijms21197155
31. Di Mauro V, Ceriotti P, Lodola F, Salvarani N, Modica J, Bang ML, et al. Peptide-based targeting of the L-type calcium channel corrects the loss-of-function phenotype of two novel mutations of the CACNA1 gene associated with brugada syndrome. *Front Physiol.* (2020) 11:616819. doi: 10.3389/fphys.2020.616819
32. Monasky MM, Micaglio E, Ciconte G, Pappone C. Brugada syndrome: oligogenic or mendelian disease? *Int J Mol Sci.* (2020) 21:1687. doi: 10.3390/ijms21051687
33. Probst V, Wilde AA, Barc J, Sacher F, Babuty D, Mabo P, et al. SCN5A mutations and the role of genetic background in the pathophysiology of Brugada syndrome. *Circ Cardiovasc Genet.* (2009) 2:552–7. doi: 10.1161/CIRCGENETICS.109.853374
34. Kapplinger JD, Tester DJ, Alders M, Benito B, Berthet M, Brugada J, et al. An international compendium of mutations in the SCN5A-encoded cardiac sodium channel in patients referred for Brugada syndrome genetic testing. *Heart Rhythm.* (2010) 7:33–46. doi: 10.1016/j.hrthm.2009.09.069
35. Ciconte G, Monasky MM, Santinelli V, Micaglio E, Vicedomini G, Anastasia L, et al. Brugada syndrome genetics is associated with phenotype severity. *Eur Heart J.* (2021) 42:1082–92. doi: 10.1093/eurheartj/ehaa942
36. Wijeyeratne YD, Tanck MW, Mizusawa Y, Batchvarov V, Barc J, Crotti L, et al. SCN5A mutation type and a genetic risk score associate variably with brugada syndrome phenotype in SCN5A families. *Circ Genom Precis Med.* (2020) 13:e002911. doi: 10.1161/CIRCGEN.120.002911
37. Denham NC, Pearman CM, Ding WY, Waktare J, Gupta D, Snowdon R, et al. Systematic re-evaluation of SCN5A variants associated with Brugada syndrome. *J Cardiovasc Electrophysiol.* (2019) 30:118–27. doi: 10.1111/jce.13740
38. Pappone C, Ciconte G, Micaglio E, Monasky MM. Common modulators of Brugada syndrome phenotype do not affect SCN5A prognostic value. *Eur Heart J.* (2021) 42:1273–4. doi: 10.1093/eurheartj/ehab071
39. Postema PG, Walsh R, Bezzina CR. Illuminating the path from genetics to clinical outcome in Brugada syndrome. *Eur Heart J.* (2021) 42:1091–3. doi: 10.1093/eurheartj/ehaa994
40. Friedrich OF, VW, Wink M, Fink RH. NA+- and K+-channels as molecular targets of the alkaloid ajmaline in skeletal muscle fibres. *Br J Pharmacol.* (2007) 151:82–93. doi: 10.1038/sj.bjp.0707194
41. Kiesecker C, Zitron E, Luck S, Bloehs R, Scholz EP, Kathofer S, et al. Class Ia anti-arrhythmic drug ajmaline blocks HERG potassium channels:

mode of action. *Naunyn Schmiedebergs Arch Pharmacol.* (2004) 370:423–35. doi: 10.1007/s00210-004-0976-8
42. Fischer F, Vonderlin N, Zitron E, Seyler C, Scherer D, Becker R, et al. Inhibition of cardiac Kv1.5 and Kv4.3 potassium channels by the class Ia anti-arrhythmic ajmaline: mode of action. *Naunyn Schmiedebergs Arch Pharmacol.* (2013) 386:991–9. doi: 10.1007/s00210-013-0901-0
43. Sakuta H, Okamoto K, Watanabe Y. Blockade by antiarrhythmic drugs of glibenclamide-sensitive K+ channels in Xenopus oocytes. *Br J Pharmacol.* (1992) 107:1061–7. doi: 10.1111/j.1476-5381.1992.tb13407.x
44. Chukhlova EA, Sadykov I, Kholmukhamedov EL, Grenader AK. Effect of trimecaine, ajmaline, stenopril and chloracizine on fluctuations in K+ currents in rat liver mitochondria. *Ukr Biokhim Zh (1978).* (1984) 56:207–10.
45. Bebarova M, Matejovic P, Pasek M, Simurdova M, Simurda J. Effect of ajmaline on transient outward current in rat ventricular myocytes. *Gen Physiol Biophys.* (2005) 24:27–45.
46. Bebarova M, Matejovic P, Pasek M, Simurdova M, Simurda J. Effect of ajmaline on action potential and ionic currents in rat ventricular myocytes. *Gen Physiol Biophys.* (2005) 24:311–25.
47. Enomoto K, Imoto M, Nagashima R, Kaneko T, Maruyama T, Kaji Y, et al. Effects of ajmaline on non-sodium ionic currents in guinea pig ventricular myocytes. *Jpn Heart J.* (1995) 36:465–76. doi: 10.1536/ihj.36.465
48. Fish JM, Antzelevitch C. Role of sodium and calcium channel block in unmasking the Brugada syndrome. *Heart Rhythm.* (2004) 1:210–7. doi: 10.1016/j.hrthm.2004.03.061
49. Khodorov BI, Zaborovskaya LD. Blockade of sodium and potassium channels in the node of Ranvier by ajmaline and N-propyl ajmaline. *Gen Physiol Biophys.* (1983) 2:233–68.
50. Zaborovskaia LD, Khodorov BI. Localization of the binding site for quaternary derivatives of ajmaline in the Na channel of an excitable membrane. *Biull Eksp Biol Med.* (1985) 100:297–9. doi: 10.1007/BF00839409
51. Zil'berter Iu I, Khodorov BI, Shubert B. Stimulus-dependent blockade of the Na channels of isolated myocardial cells in the rat by the anti-arrhythmia agent N-propyl ajmaline (neogiluritmal). *Biull Eksp Biol Med.* (1983) 95:55–8. doi: 10.1007/BF00838861
52. Online Mendelian Inheritance in Man (2021). Available online at: https://www.omim.org/ (accessed August 5, 2021).
53. Ardehali H, Chen Z, Ko Y, Mejia-Alvarez R, Marban E. Multiprotein complex containing succinate dehydrogenase confers mitochondrial ATP-sensitive K+ channel activity. *Proc Natl Acad Sci USA.* (2004) 101:11880–5. doi: 10.1073/pnas.0401703101
54. Hoogendijk MG, Potse M, Vinet A, De Bakker JM, Coronel R. ST segment elevation by current-to-load mismatch: an experimental and computational study. *Heart Rhythm.* (2011) 8:111–8. doi: 10.1016/j.hrthm.2010.09.066
55. Biamino G, Wessel HJ, Noring J. Ajamline-induced changes in mechanical and electrical activity of vascular smooth muscle. *Blood Vessels.* (1975) 12:68–80. doi: 10.1159/000158039
56. Pappone C, Mecarocci V, Manguso F, Ciconte G, Vicedomini G, Sturla F, et al. New electromechanical substrate abnormalities in high-risk patients with Brugada syndrome. *Heart Rhythm.* (2020) 17:637–45. doi: 10.1016/j.hrthm.2019.11.019
57. Pappone C, Monasky MM, Micaglio E, Ciconte G. Right ventricular electromechanical abnormalities in Brugada syndrome: is this a cardiomyopathy? *Eur Heart J Suppl.* (2020) 22:E101–4. doi: 10.1093/eurheartj/suaa071
58. Antzelevitch C. Brugada syndrome: historical perspectives and observations. *Eur Heart J.* (2002) 23:676–8. doi: 10.1053/euhj.2001.3145
59. Antzelevitch C. Brugada syndrome. *Pacing Clin Electrophysiol.* (2006) 29:1130–59. doi: 10.1111/j.1540-8159.2006.00507.x
60. Monasky MM, Taglieri DM, Henze M, Warren CM, Utter MS, Soergel DG, et al. The beta-arrestin-biased ligand TRV120023 inhibits angiotensin II-induced cardiac hypertrophy while preserving enhanced myofilament response to calcium. *Am J Physiol Heart Circ Physiol.* (2013) 305:H856–866. doi: 10.1152/ajpheart.00327.2013
61. Yar S, Monasky MM, Solaro RJ. Maladaptive modifications in myofilament proteins and triggers in the progression to heart failure and sudden death. *Pflugers Arch.* (2014) 466:1189–97. doi: 10.1007/s00424-014-1457-7
62. Allegue C, Coll M, Mates J, Campuzano O, Iglesias A, Sobrino B, et al. Genetic analysis of arrhythmogenic diseases in the era of NGS: the complexity of clinical decision-making in Brugada syndrome. *PLoS ONE.* (2015) 10:e0133037. doi: 10.1371/journal.pone.0133037
63. Cerrone M, Lin X, Zhang M, Agullo-Pascual E, Pfenniger A, Chkourko Gusky H, et al. Missense mutations in plakophilin-2 cause sodium current deficit and associate with a Brugada syndrome phenotype. *Circulation.* (2014) 129:1092–103. doi: 10.1161/CIRCULATIONAHA.113.003077
64. Hong M, Bao L, Kefaloyianni E, Agullo-Pascual E, Chkourko H, Foster M, et al. Heterogeneity of ATP-sensitive K+ channels in cardiac myocytes: enrichment at the intercalated disk. *J Biol Chem.* (2012) 287:41258–67. doi: 10.1074/jbc.M112.412122
65. Baudenbacher F, Schober T, Pinto JR, Sidorov VY, Hilliard F, Solaro RJ, et al. Myofilament Ca2+ sensitization causes susceptibility to cardiac arrhythmia in mice. *J Clin Invest.* (2008) 118:3893–903. doi: 10.1172/JCI36642
66. Mango R, Luchetti A, Sangiuolo R, Ferradini V, Briglia N, Giardina E, et al. Next generation sequencing and linkage analysis for the molecular diagnosis of a novel overlapping syndrome characterized by hypertrophic cardiomyopathy and typical electrical instability of brugada syndrome. *Circ J.* (2016) 80:938–49. doi: 10.1253/circj.CJ-15-0685
67. Pappone C, Monasky M, Ciconte G. Epicardial ablation in genetic cardiomyopathies: a new frontier. *Eur Heart J Suppl.* (2019) 21:B61–6. doi: 10.1093/eurheartj/suz028
68. Pappone C, Micaglio E, Locati ET, Monasky MM. The omics of channelopathies and cardiomyopathies: what we know and how they are useful. *Eur Heart J Suppl.* (2020) 22:L105–9. doi: 10.1093/eurheartj/suaa146
69. Stocchi L, Polidori E, Potenza L, Rocchi MB, Calcabrini C, Busacca P, et al. Mutational analysis of mitochondrial DNA in Brugada syndrome. *Cardiovasc Pathol.* (2016) 25:47–54. doi: 10.1016/j.carpath.2015.10.001
70. Polidori E, Stocchi L, Potenza D, Cucchiarini L, Stocchi V, Potenza L. A high number of 'natural' mitochondrial DNA polymorphisms in a symptomatic Brugada syndrome type 1 patient. *J Genet.* (2020) 99:66. doi: 10.1007/s12041-020-01228-4
71. Tafti MF, Khatami M, Rezaei S, Heidari MM, Hadadzadeh M. Novel and heteroplasmic mutations in mitochondrial tRNA genes in Brugada syndrome. *Cardiol J.* (2018) 25:113–9. doi: 10.5603/CJ.a2017.0104
72. Samani K, Ai T, Towbin JA, Brugada R, Shuraih M, Xi Y, et al. A nonsense SCN5A mutation associated with Brugada-type electrocardiogram and intraventricular conduction defects. *Pacing Clin Electrophysiol.* (2009) 32:1231–6. doi: 10.1111/j.1540-8159.2009.02470.x
73. Kapplinger JD, Giudicessi JR, Ye D, Tester DJ, Callis TE, Valdivia CR, et al. Enhanced classification of Brugada syndrome-associated and long-QT syndrome-associated genetic variants in the SCN5A-encoded Na(v)1.5 cardiac sodium channel. *Circ Cardiovasc Genet.* (2015) 8:582–95. doi: 10.1161/CIRCGENETICS.114.000831
74. Micaglio E, Monasky MM, Ciconte G, Vicedomini G, Conti M, Mecarocci V, et al. SCN5A Nonsense mutation and NF1 frameshift mutation in a family with Brugada syndrome and neurofibromatosis. *Front Genet.* (2019) 10:50. doi: 10.3389/fgene.2019.00050
75. Micaglio E, Monasky MM, Ciconte G, Vicedomini G, Conti M, Mecarocci V, et al. Novel SCN5A frameshift mutation in Brugada syndrome associated with complex arrhythmic phenotype. *Front Genet.* (2019) 10:547. doi: 10.3389/fgene.2019.00547
76. Micaglio E, Monasky MM, Resta N, Bagnulo R, Ciconte G, Gianelli L, et al. Novel SCN5A p.W697X nonsense mutation segregation in a family with Brugada syndrome. *Int J Mol Sci.* (2019) 20:4920. doi: 10.3390/ijms20194920
77. Monasky MM, Micaglio E, Ciconte G, Benedetti S, Di Resta C, Vicedomini G, et al. Genotype/phenotype relationship in a consanguineal family with Brugada syndrome harboring the R1632C missense variant in the SCN5A gene. *Front Physiol.* (2019) 10:666. doi: 10.3389/fphys.2019.00666
78. Monasky MM, Micaglio E, Giachino D, Ciconte G, Giannelli L, Locati ET, et al. Genotype-phenotype correlation in a family with Brugada syndrome harboring the novel p.Gln371* nonsense variant in the SCN5A gene. *Int J Mol Sci.* (2019) 20:5522. doi: 10.3390/ijms20225522
79. Monasky MM, Micaglio E, Ciconte G, Borrelli V, Giannelli L, Vicedomini G, et al. Novel SCN5A p.V1429M variant segregation in a family with brugada syndrome. *Int J Mol Sci.* (2020) 21:5902. doi: 10.3390/ijms21165902
80. Monasky MM, Micaglio E, Ciconte G, Rivolta I, Borrelli V, Ghiroldi A, et al. Novel SCN5A p.Val1667Asp missense variant segregation and characterization in a family with severe Brugada syndrome and multiple sudden deaths. *Int J Mol Sci.* (2021) 22:4700. doi: 10.3390/ijms22094700
81. Monasky MM, Rutigliani C, Micaglio E, Pappone C. Commentary: peptide-based targeting of the L-type calcium channel corrects the loss-of-function phenotype of two novel mutations of the CACNA1

gene associated with Brugada syndrome. *Front Physiol.* (2021) 12:682567. doi: 10.3389/fphys.2021.682567
82. Bezzina CR, Barc J, Mizusawa Y, Remme CA, Gourraud JB, Simonet F, et al. Common variants at SCN5A-SCN10A and HEY2 are associated with Brugada syndrome, a rare disease with high risk of sudden cardiac death. *Nat Genet.* (2013) 45:1044–9. doi: 10.1038/ng.2712
83. Milani-Nejad N, Janssen PM. Small and large animal models in cardiac contraction research: advantages and disadvantages. *Pharmacol Ther.* (2014) 141:235–49. doi: 10.1016/j.pharmthera.2013.10.007

Conflict of Interest: The authors declare that the research was conducted in the absence of any commercial or financial relationships that could be construed as a potential conflict of interest.

Publisher's Note: All claims expressed in this article are solely those of the authors and do not necessarily represent those of their affiliated organizations, or those of the publisher, the editors and the reviewers. Any product that may be evaluated in this article, or claim that may be made by its manufacturer, is not guaranteed or endorsed by the publisher.

frontiers in Cardiovascular Medicine

ORIGINAL RESEARCH
published: 23 December 2021
doi: 10.3389/fcvm.2021.766339

South Asian-Specific *MYBPC3*$^{\Delta 25bp}$ Deletion Carriers Display Hypercontraction and Impaired Diastolic Function Under Exercise Stress

Sholeh Bazrafshan[1]*, *Robert Sibilia*[1], *Saavia Girgla*[1], *Shiv Kumar Viswanathan*[1], *Megan J. Puckelwartz*[2], *Kiranpal S. Sangha*[1], *Rohit R. Singh*[1], *Mashhood Kakroo*[1], *Roman Jandarov*[1], *David M. Harris*[1], *Jack Rubinstein*[1], *Richard C. Becker*[1], *Elizabeth M. McNally*[2] *and Sakthivel Sadayappan*[1]*

[1] Division of Cardiovascular Health and Disease, Department of Internal Medicine, Heart, Lung and Vascular Institute, College of Medicine, University of Cincinnati, Cincinnati, OH, United States, [2] Center for Genetic Medicine, Feinberg School of Medicine, Northwestern University, Chicago, IL, United States

OPEN ACCESS

Edited by:
George W. Booz,
University of Mississippi Medical Center School of Dentistry, United States

Reviewed by:
Christopher N. Toepfer,
University of Oxford, United Kingdom
Patrick G. Burgon,
Qatar University, Qatar

***Correspondence:**
Sholeh Bazrafshan
sh.bazrafshan.k@gmail.com
Sakthivel Sadayappan
sadayasl@ucmail.uc.edu

Specialty section:
This article was submitted to Cardiovascular Genetics and Systems Medicine, a section of the journal Frontiers in Cardiovascular Medicine

Received: 28 August 2021
Accepted: 22 November 2021
Published: 23 December 2021

Citation:
Bazrafshan S, Sibilia R, Girgla S, Viswanathan SK, Puckelwartz MJ, Sangha KS, Singh RR, Kakroo M, Jandarov R, Harris DM, Rubinstein J, Becker RC, McNally EM and Sadayappan S (2021) South Asian-Specific MYBPC3$^{\Delta 25bp}$ Deletion Carriers Display Hypercontraction and Impaired Diastolic Function Under Exercise Stress. Front. Cardiovasc. Med. 8:766339. doi: 10.3389/fcvm.2021.766339

Background: A 25-base pair (25bp) intronic deletion in the *MYBPC3* gene enriched in South Asians (SAs) is a risk allele for late-onset left ventricular (LV) dysfunction, hypertrophy, and heart failure (HF) with several forms of cardiomyopathy. However, the effect of this variant on exercise parameters has not been evaluated.

Methods: As a pilot study, 10 asymptomatic SA carriers of the *MYBPC3*$^{\Delta 25bp}$ variant (52.9 ± 2.14 years) and 10 age- and gender-matched non-carriers (NCs) (50.1 ± 2.7 years) were evaluated at baseline and under exercise stress conditions using bicycle exercise echocardiography and continuous cardiac monitoring.

Results: Baseline echocardiography parameters were not different between the two groups. However, in response to exercise stress, the carriers of Δ25bp had significantly higher LV ejection fraction (%) (CI: 4.57 ± 1.93; $p < 0.0001$), LV outflow tract peak velocity (m/s) (CI: 0.19 ± 0.07; $p < 0.0001$), and higher aortic valve (AV) peak velocity (m/s) (CI: 0.103 ± 0.08; $p = 0.01$) in comparison to NCs, and E/A ratio, a marker of diastolic compliance, was significantly lower in Δ25bp carriers (CI: 0.107 ± 0.102; $p = 0.038$). Interestingly, LV end-diastolic diameter ($LVID_{dia}$) was augmented in NCs in response to stress, while it did not increase in Δ25bp carriers (CI: 0.239 ± 0.125; $p = 0.0002$). Further, stress-induced right ventricular systolic excursion velocity s' (m/s), as a marker of right ventricle function, increased similarly in both groups, but tricuspid annular plane systolic excursion increased more in carriers (slope: 0.008; $p = 0.0001$), suggesting right ventricle functional differences between the two groups.

Conclusions: These data support that *MYBPC3*$^{\Delta 25bp}$ is associated with LV hypercontraction under stress conditions with evidence of diastolic impairment.

Keywords: *MYBPC3*, South Asians, hypertrophic cardiomyopathy, ventricular diastolic dysfunction, stress echocardiography, 25bp deletion, DOSA study, myosin binding protein-C

INTRODUCTION

Mutations in sarcomere genes are a common cause of familial hypertrophic cardiomyopathy (HCM), a prevalent cardiovascular genetic disorder that affects ∼1 in 200–500 asymptomatic young adults in the United States (1–11). Mutations in *MYBPC3*, which encodes cardiac myosin-binding protein-C (cMyBP-C), a thick-filament cardiac muscle protein that regulates cardiac contractility (6, 7, 12–14), are associated with ∼40% of all HCM cases (9, 15), many of which present late in life (16–22). HCM is characterized by asymmetric left ventricular (LV) thickening, diastolic dysfunction, heart failure (HF), and sudden cardiac death (SCD) (4, 23, 24). Affected individuals can remain asymptomatic or present with symptoms, such as dyspnea, angina, or palpitation (9), in early or late adulthood (11, 22). Heterogeneity in the phenotypic expression of disease from *MYBPC3* genetic variation requires an understanding of early features, optimal care, and longitudinal follow-up.

The prevalence of HCM may be affected by ancestry (4, 25), but the contribution of ancestry-based genetic variants in the pathogenesis of the disease is not yet well-established. Of the South Asian (SA)-specific variants, a polymorphic 25-base pair (bp) deletion in intron 32 (Δ25bp) of *MYBPC3* is present in 4–6% (26–28) of SA individuals and a risk allele for late-onset LV dysfunction, hypertrophy, and HF with multiple forms of cardiomyopathy, such as HCM with an odds ratio of ∼7 (26, 29) (**Figures 1A,B**). Data have shown that asymptomatic *MYBPC3*$^{\Delta 25bp}$ carriers are at risk of late-onset disease progression (16, 22, 26). This variant was defined as a risk allele based on a large case-control study from 6,273 individuals belonging to 107 ethnic populations across 35 Indian states and 2,085 individuals of 63 ethnic/racial groups from 26 countries, including all five continents (26, 30). Nonetheless, in recent studies, *MYBPC3*$^{\Delta 25bp}$ was reported with incomplete penetrance, and the presence of additional genetic or non-genetic risk factors may predispose carriers to cardiomyopathies (26, 27, 31). Our recent investigation has revealed no significant difference in cardiac features between the carrier and non-carrier (NC) cohorts at baseline (27). However, several individual *MYBPC3*$^{\Delta 25bp}$ carriers showed increased fractional shortening at baseline, and this hyperdynamic state is often seen as an early pathological finding in HCM (27). Harper et al. identified an enriched haplotype in SAs with HCM with both *MYBPC3*$^{\Delta 25bp}$ and an associated variant, *MYBPC3* c.1224-52G>A (31). However, in Harper's study, only 134 subjects out of 5,394 HCM cases were defined as SAs, and only 17 carried the *MYBPC3*$^{\Delta 25bp}$ variant. We also recently identified a co-segregating novel variant, D389V (*MYBPC3*^{D389V}). It was observed in ∼10% of *MYBPC3*$^{\Delta 25bp}$ carriers and associated with hyperdynamic cardiac features on baseline echocardiography (27). These data have led to the hypothesis that the risk of HCM is not caused by the *MYBPC3*$^{\Delta 25bp}$ allele alone, but rather conferred by additional rare, pathogenic variants present on the *MYBPC3*$^{\Delta 25bp}$ haplotype. This possible coinheritance of additional risk alleles changes the interpretation of the role of the *MYBPC3*$^{\Delta 25bp}$ in the development of LV dysfunction and HCM. It also means that the pathogenicity of the *MYBPC3*$^{\Delta 25bp}$ variant alone and in the presence of additional modifying risk factors needs further investigation and correlation, considering the growing number of SA carriers with the *MYBPC3*$^{\Delta 25bp}$ variant, predisposing them to severe adverse events, such as SCD, even with the occult clinical phenotype (23).

MYBPC3 gene variants, such as the *MYBPC3*$^{\Delta 25bp}$, are generally associated with late-disease onset (16, 22, 26). Herein, we continued genetic screening of the United States (US) SA general population for the presence of *MYBPC3*$^{\Delta 25bp}$ and additional rare risk alleles using next-generation sequencing (NGS) technology. To determine the pathogenicity of the *MYBPC3*$^{\Delta 25bp}$ variant, we conducted an exploratory pilot study and prospectively evaluated 10 asymptomatic male carriers of the *MYBPC3*$^{\Delta 25bp}$ variant and 10 age-matched NCs for the changes in cardiac function under exercise stress using submaximal bicycle stress exercise echocardiography (BSE) and continuous cardiac monitoring. We hypothesized that asymptomatic *MYBPC3*$^{\Delta 25bp}$ SA carriers have detectable subclinical risk factors under exercise stress conditions that predispose this group to develop LV hypercontractility and impaired relaxation. Our results suggest that *MYBPC3*$^{\Delta 25bp}$ is consistent with its role as a risk allele for LV dysfunction and cardiomyopathy in SAs.

METHODS

Enrollment of Study Subjects: Prevalence and Genotype-Phenotype

This research study was reviewed and approved by the Institutional Review Board (IRB) of Loyola University Chicago and University of Cincinnati and was conducted in accordance with the Declaration of Helsinki. Subjects 18 years of age and older from US SA descendants from 9 countries, namely, India, Pakistan, Bangladesh, Sri Lanka, Nepal, Bhutan, Maldives, Afghanistan, and Myanmar, participated in the prevalence study (Loyola University Chicago IRB# LU207815 and 207359, Chicago, Illinois and University of Cincinnati IRB# 2016-7580, Cincinnati, OH, USA) and provided either blood or saliva samples through sample collection outreach events for detection of *MYBPC3*$^{\Delta 25bp}$ variants. Additionally, carriers of *MYBPC3*$^{\Delta 25bp}$ variants and age- and gender-matched NCs were recruited in the follow-up genotype-phenotype study (University of Cincinnati IRB# 2016-4948, Cincinnati, OH, USA) to perform ECG tracing and baseline transthoracic echocardiography (TTE) and BSE.

Sample Collection and Genetic Screening of the Human *MYBPC3*$^{\Delta 25bp}$ Variant

After giving written consent, blood or saliva samples of the US SA subjects were collected in community outreach events and initially screened for the detection of *MYBPC3*$^{\Delta 25bp}$ variants. Blood samples (10 ml) were collected in ethylenediaminetetraacetic acid (EDTA) vacutainers (Catalog No. 367862; BD Bioscience, Woburn, MA, USA), and saliva samples (1–2 ml) were collected in sterile screw-cap transport 5-ml tubes. Saliva samples were transported in ice and stored at

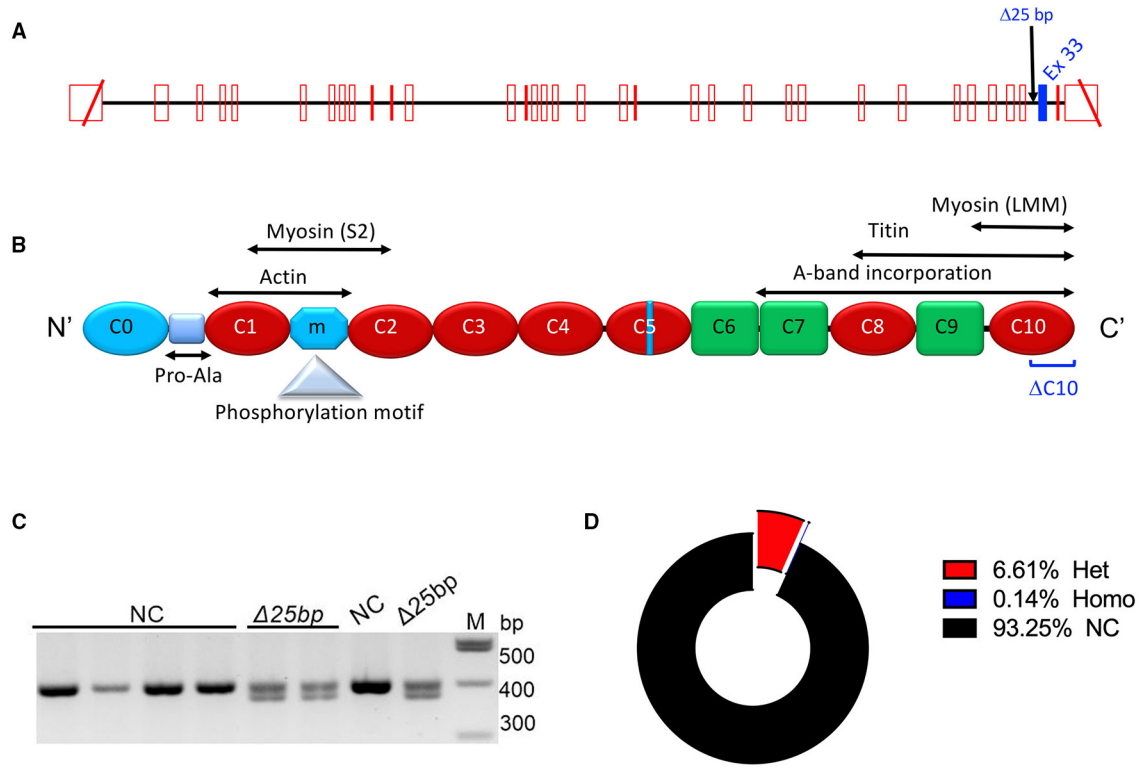

FIGURE 1 | *MYBPC3*$^{\Delta 25bp}$ genotyping and prevalence. **(A)** Schematic diagram of the MYBPC3 gene that includes the location of *MYBPC3*$^{\Delta 25bp}$ variant in Intron 32. Exon 33 is highlighted in blue as a potential skipped exon and altered splicing exon when the *MYBPC3*$^{\Delta 25bp}$ variant is pathogenic. **(B)** cMyBP-C domains are drawn with interacting partners, proline-alanine (Pro-Ala)-rich region, phosphorylation motif, and potential C10 domain that could be modified if exon 33 is altered (DC10). **(C)** Agarose gel electrophoresis of PCR-based genotyping of the *MYBPC3*$^{\Delta 25bp}$ variant. **(D)** *MYBPC3*$^{\Delta 25bp}$ distribution of 3,432 South Asian participants. Among carriers of the *MYBPC3*$^{\Delta 25bp}$ variant, 6.61% of carriers (227, red color sector) were heterozygous (Het), and 0.14% of carriers (5, blue color sector) were homozygous (Homo). NCs, non-carriers.

−20°C. Blood and saliva samples were used for human genomic DNA isolation using the QIAmp DNA Blood Mini Kit (Catalog No. 51106; Qiagen, Germantown, MD, USA). The polymerase chain reaction was used for genotyping of the *MYBPC3*$^{\Delta 25bp}$ (rs36212066) variant with the forward 5′-GTT TCC AGC CTT GGG CAT AGT C-3′ and reverse 5′-GAG GAC AAC GGA GCA AAG CCC-3′ primer sequences on 2.5% agarose gel (27). After initial genotyping, we recruited carriers and NCs of the *MYBPC3*$^{\Delta 25bp}$ variant for the follow-up genotype-phenotype study (27). After giving written consent, the recruited subjects provided an additional 10-ml blood sample for genotype confirmation and NGS analysis (27).

Clinical and Cardiac Function Evaluation at Baseline and Under Exercise Stress

Carriers of the *MYBPC3*$^{\Delta 25bp}$ variant and age- and gender-matched NCs 18 years of age and older of US SA descendants were invited to participate in the follow-up genotype-phenotype study to undergo ECG and baseline TTE and BSE, as monitored by a team cardiologist (**Figure 2**). Recruited subjects for the follow-up study had no uncontrolled comorbidities and no significant differences in the frequency of hypertension, diabetes mellitus, dyslipidemia, and obesity between the two groups. The subjects were instructed to abstain from alcoholic, caffeinated, tobacco products, and drugs, such as β-blockers (if applicable), for 24 h prior to stress testing. Echocardiographic images were captured by two cardiac sonographers of similar level and length of experience. Both subjects and observers, i.e., sonographers and team cardiologists, were blinded to *MYBPC3*$^{\Delta 25bp}$ genotype results. Medical, medication, social, habit, and family history information of all participants were collected using a comorbidity questionnaire after giving written consent on the test day. Two additional forms, a prerecruitment questionnaire (PRQ) and a pre-procedural questionnaire (PPQ), were used for subjects who were scheduled for BSE. Before scheduling subjects for BSE testing, past medical and medication history was collected using the PRQ. Completed PRQs were then reviewed by a team cardiologist for any possible contraindications or medication modification. On the test day, subjects' compliance with BSE test instructions was evaluated using the PPQ.

Cardiac electrical activity was recorded using a standard 12-lead ECG with rhythm strips, and a Vivid E9 GE Healthcare instrument was used for TTE and BSE imaging using the 2-dimensional method in conjunction with color Doppler flow examination. Exclusion criteria for performing BSE included (1) acute myocardial infarction in the last 3 months; (2) ongoing

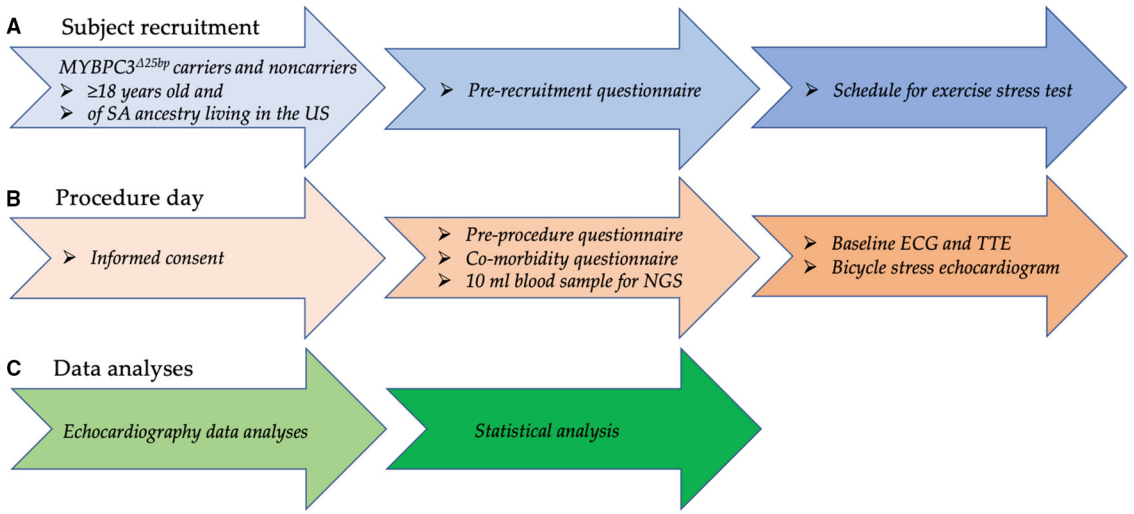

FIGURE 2 | Flow chart depicting the recruitment process, employed questionnaires, and echocardiography and clinical data analyses for the genotype-phenotype study. **(A)** Carriers of *MYBPC3*$^{\Delta 25bp}$ variant and age- and gender-matched non-carriers 18 years of age and older of US SA ancestry were recruited. Then, past medical and medication history was collected using a prerecruitment questionnaire, and, if no contraindication, subjects were scheduled to perform an exercise stress test using a bicycle ergometer. **(B)** On the test day, informed consent was obtained; then, a comorbidity questionnaire was used to collect comprehensive medical, medication, social, habit, and family history information from all participants. To look for other genetic modifiers via NGS testing, a 10-ml blood sample was collected. Compliance with exercise stress test instructions was evaluated via a pre-procedure questionnaire. Cardiac function was evaluated by ECG and TTE at rest and by bicycle ergometer during exercise stress testing for any detectable underlying risk factor. **(C)** While blinded, two observers independently measured echocardiography variables. Statistical significance ($p < 0.05$) was calculated using two-way ANOVA and simple linear regression, and the results were reported as mean ± SEM. SA = South Asian, NGS = next-generation sequencing. TTE, transthoracic echocardiography.

unstable angina; (3) known obstructive left main coronary artery stenosis; (4) recent stroke or transient ischemic attack in the last 3 months; (5) acute pulmonary embolism, pulmonary infarction, or deep vein thrombosis in the last 3 months; (6) moderate-to-severe aortic stenosis with velocity over 3 m/s; (7) hypertrophic obstructive cardiomyopathy with severe resting gradient of over 3 m/s; (8) uncontrolled cardiac arrhythmia with hemodynamic compromise; (9) advanced heart block; (10) decompensated HF; (11) active endocarditis; (12) acute myocarditis or pericarditis; (13) physical disability that would preclude safe and adequate testing; (14) pregnancy; (15) mental impairment with limited ability to cooperate; (16) history of severe hypertension (resting systolic blood pressures >200 or diastolic blood pressures 110 mm Hg) or uncontrolled diabetes mellitus; and (17) uncorrected anemia, electrolyte imbalance or hyperthyroidism. Subjects were provided with the instructions for BSE preparation prior to the test that included (1) fasting for 4 h, (2) refraining from caffeinated and decaffeinated coffee and tea, colas, soft drinks, and chocolate for 24 h, and (3) refraining from smoking and other nicotine-containing products for 12 h.

Moreover, target heart rate (THR) was calculated for BSE as 220 – (0.85 × subject's age). Then, the subjects began cycling at a resistance of 15 Watts (W), increasing every 3 min by additional resistance of 15 W until the endpoint. Heart rate (HR), blood pressure, and oxygen saturation were monitored and documented at each minute of exercise. Endpoints of the test were one of the following: (1) achievement of THR; (2) significant angina; (3) significant shortness of breath; (4) significant ischemic changes, such as ST-segment elevations in ECG; (5) hypertension (>240 mmHg systolic blood pressure/ 120 mmHg diastolic blood pressure); (6) hypotension >15 mmHg decline in systolic blood pressure from baseline; (7) significant arrhythmia/aortic valve (AV) block; (8) new or worsening wall-motion abnormalities; (9) drop of oxygen saturation below 90%; (10) intolerable symptoms; (11) upon subject's request to stop; or (12) development of dynamic LV outflow tract (LVOT) gradient of >4.5 m/s.

Finally, two observers independently measured echocardiography variables under the guidance of team cardiologists. The measurements of one observer were used for the analysis in this study, except LV ejection fraction (LVEF) for which the average value measured by two observers was used. The Biplane Simpson method was used to measure LVEF and LV fractional shortening.

Next-Generation Sequencing

A panel of 174 genes related to cardiovascular diseases was DNA sequenced to identify the presence of any genetic variants using the TruSight Cardio Kit (Catalog No. FC-141-1011; Illumina, San Diego, CA, USA) on an Illumina MiSeq with 150-base pair paired-end reads, as described previously (27). Burrows-Wheeler alignment (BWA) and Genome Analysis Toolkit haplotype caller were applied as described in MegaSeq generate variant call files (VCFs) (32). Variants were excluded if they met any of the following criteria: biallelic balance >0.75; quality score <30; depth of coverage >360; strand bias more than −0.01, and mapping quality zero reads ≥10. Variant ranking and prioritization: variants were annotated using SnpEFF. HIGH and MODERATE variants were scored using Polyphen, Genomic Evolutionary Rate Profiling, and Sorting Intolerant

From Tolerant, to predict pathogenicity. All variants were ranked by minor allele frequency (MAF) based on data from public databases (ExAc). All variants were crosschecked against ClinVAR. The American College of Medical Genetics guidelines (ACMG) were used for determining pathogenicity (33). Sanger sequencing was applied for validation using individual primers.

Statistical Analyses

The prevalence of genotype results was reported as a percentage. Descriptive statistics were reported in frequency tables to compare cardiac phenotype outcomes by genetic variants and by demographics. The chi-square statistics and unpaired *t*-test were used for categorical parameters and numerical variables at baseline, respectively. Regression analysis was used to compare differences in slopes between the groups, and a two-way ANOVA was performed to estimate the effect of exercise stress and genotype on cardiac phenotype continuous outcomes. All analyses were reported as mean ± SEM at a significance level of 0.05, and 95% CIs and *p*-values were reported using GraphPad Prism (version 8.4.3).

RESULTS

Increased Prevalence of *MYBPC3*$^{\Delta 25bp}$ Variant Among US SAs

We previously reported the frequency of *MYBPC3*$^{\Delta 25bp}$ variant carriers to be 6% among the US SA population (27). Cumulative screening to date, which could be subject to ascertainment bias, estimated a slightly higher prevalence of *MYBPC3*$^{\Delta 25bp}$ at 6.75%. Of 3,432 participants, 232 (6.75%) were carriers of the *MYBPC3*$^{\Delta 25bp}$ variant, i.e., 227 (6.61%) heterozygous and 5 (0.14%) homozygous (**Figures 1C,D**).

Absence of Second Genetic Variants by NGS

To assess the presence of any additional pathogenic variants, apart from the *MYBPC3*$^{\Delta 25bp}$ variant, NGS was performed on a 172 gene cardiovascular panel (TruSight Cardio Sequencing Kit, Illumina), and no pathogenic, or likely pathogenic, variants were identified in the present cohort (27). None of the 20 subjects included in the current study was found to carry the previously reported, potentially pathogenic *MYBPC3*$^{-52}$ allele (c.1224-52G>A) (31) or the novel *MYBPC3*^{D389V} variant (27). We also did not identify any additional modifying loci in *MYBPC3* as no other rare variants were identified in the coding region that occurred in more than one cohort subject. Lastly, among the 172 genes of the TruSight Panel, we only identified one pathogenic variant in one subject who carried an APOA4 variant in one of the 10 variant carriers.

MYBPC3$^{\Delta 25bp}$ Was Associated With Hypercontraction Under Exercise

To test the hypothesis that asymptomatic *MYBPC3*$^{\Delta 25bp}$ US SA carriers have detectable subclinical risk factors under exercise stress conditions, we conducted an exploratory pilot study to evaluate asymptomatic *MYBPC3*$^{\Delta 25bp}$ US SA carriers compared to controls for subclinical cardiac changes under exercise stress conditions (**Figure 2**). We prospectively studied 20 male subjects of US SA ancestry, including 10 carriers of the *MYBPC3*$^{\Delta 25bp}$ variant (52.9 ± 2.14 years) and 10 age- and gender-matched NCs (50.1 ± 2.7 years), for any changes in cardiac function at baseline prior to exercise and under exercise stress using bicycle exercise echocardiography and continuous cardiac monitoring (**Tables 1**, **2**). The two groups (*MYBPC3*$^{\Delta 25bp}$ carriers and NCs) showed no significant difference in body surface area, body mass index, and baseline mean arterial pressure (MAP) and HR, and no difference in the frequency of comorbidities, such as hypertension, diabetes mellitus, and dyslipidemia (**Table 1**). Similarly, monitored exercise MAP and HR were similar in both groups (**Table 2**). All 20 subjects were able to complete at least 15 min of exercise at 75 W equivalent to 4.9 METs, while 4 subjects completed 30 min of exercise at 150 W equivalent to 8.5 METs.

While baseline echocardiography parameters were not different between the two groups (*MYBPC3*$^{\Delta 25bp}$ carriers and NCs) (**Table 1**), significant differences came to light under exercise stress condition in the following parameters: LV end-diastolic diameter ($LVID_{dia}$), LVEF, LVOT and AV peak velocities (pv), and the ratio of early to late ventricular filling velocity (E/A ratio) (**Table 2**, **Figures 3**, **4**). Stress-induced $LVID_{dia}$ augmented in NCs, while it did not increase in *MYBPC3*$^{\Delta 25bp}$ carriers with a significant difference between the two groups (CI: 0.239 ± 0.125; $p = 0.0002$), indicative of impaired relaxation and diastolic impairment. Strikingly, the estimated effect of exercise stress and genotype showed that *MYBPC3*$^{\Delta 25bp}$ carriers had significantly higher LVEF (%) (CI: 4.57 ± 1.93; $p < 0.0001$), higher LVOT pv (m/s) (CI: 0.197 ± 0.069; $p < 0.0001$), and higher AV pv (m/s) (CI: 0.103 ± 0.081; $p = 0.01$) in comparison to NCs. This was consistent with the findings that stress-induced $LVID_{dia}$ increase was significantly muted in carriers during exercise, as compared to NCs (CI: 0.239 ± 0.125; $p = 0.0002$). Further, E/A ratio, a marker of ventricular diastolic compliance, was significantly lower in carriers as compared to NCs (CI: 0.107 ± 0.102; $p = 0.038$) and the ratio of early transmitral peak velocity flow to early diastolic mitral annulus velocity (E/e' ratio), which showed a non-significant difference between the groups (CI: 0.738 ± 0.795; $p = 0.068$). Although stress-induced right ventricular systolic excursion velocity (s') was increased similarly in both groups, tricuspid annular plane systolic excursion (cm) increased more in carriers (slope: 0.008; $p = 0.0001$) from the baseline, consistent with right ventricle functional differences. These findings are indicative of LV hypercontractility among asymptomatic carriers of the *MYBPC3*$^{\Delta 25bp}$ variant under exercise stress conditions and evidence of diastolic impaired relaxation at high workloads, suggesting that *MYBPC3*$^{\Delta 25bp}$ is an independent risk allele with subclinical pathology prior to late-onset LV dysfunction (16, 22) in the US SA population.

DISCUSSION

The present study evaluated the exercise response in asymptomatic *MYBPC3*$^{\Delta 25bp}$ SA carriers to determine the presence of any subclinical features. Overall, our findings

TABLE 1 | Demographics, baseline echocardiography parameters, and clinical characteristics of 20 South Asian subjects who participated in a bicycle exercise study.

Variable	Total	*n*	NC	*n*	*MYBPC3*$^{\Delta 25bp}$	*n*	*P*-value
	n (%), mean ± SEM		*n* (%), mean ± SEM		*n* (%), mean ± SEM		
Male (%)	20(100)	20	10(100)	10	10(100)	10	-
Age (years)	51.50 ± 1.71	20	50.1 ± 2.70	10	52.90 ± 2.14	10	0.427
BMI (kg/m^2)	26.15 ± 0.611	20	26.23 ± 0.58	10	26.06 ± 1.11	10	0.893
BSA (m^2)	1.95 ± 0.037	20	1.98 ± 0.04	10	1.91 ± 0.06	10	0.301
MAP (mmHg)	101.1 ± 2.00	20	98.70 ± 2.78	10	103.5 ± 2.82	10	0.244
HR (bpm)	74.65 ± 1.96	20	76.90 ± 2.42	10	72.40 ± 3.03	10	0.262
Echocardiographic parameters							
$LVID_{dia}$ (cm)	4.06 ± 0.10	20	3.97 ± 0.15	10	4.16 ± 0.13	10	0.376
$LVID_s$ (cm)	2.78 ± 0.08	20	2.69 ± 0.10	10	2.87 ± 0.14	10	0.331
LVEF (%)	53.65 ± 1.38	20	53.59 ± 1.81	10	53.70 ± 2.17	10	0.969
LVFS (%)	31.38 ± 0.99	20	31.55 ± 0.91	10	31.21 ± 1.82	10	0.867
IVS (cm)	0.94 ± 0.04	20	0.96 ± 0.07	10	0.93 ± 0.03	10	0.71
LVPW (cm)	0.88 ± 0.03	20	0.93 ± 0.03	10	0.83 ± 0.04	10	0.111
IVS/LVPW ratio	1.09 ± 0.05	20	1.04 ± 0.08	10	1.14 ± 0.05	10	0.351
LAV 4C Mod	31.75 ± 2.95	18	30.25 ± 4.69	8	32.95 ± 3.94	10	0.663
LVOT peak velocity (m/s)	0.79 ± 0.03	19	0.76 ± 0.05	9	0.82 ± 0.03	10	0.424
AV peak velocity (m/s)	0.98 ± 0.03	19	0.96 ± 0.06	9	1.01 ± 0.04	10	0.551
E/A ratio	1.15 ± 0.08	20	1.10 ± 0.13	10	1.20 ± 0.11	10	0.596
Average E/e' ratio	7.18 ± 0.46	20	7.20 ± 0.49	10	7.16 ± 0.82	10	0.973
Average e'/a' ratio	1.01 ± 0.08	20	0.90 ± 0.10	10	1.13 ± 0.13	10	0.204
RV s' (m/s)	0.097 ± 0.003	20	0.094 ± 0.004	10	0.09 ± 0.004	10	0.458
LV s' average (m/s)	0.07 ± 0.002	20	0.07 ± 0.003	10	0.07 ± 0.003	10	0.437
TAPSE (cm)	2.21 ± 0.12	19	2.40 ± 0.23	9	2.04 ± 0.10	10	0.166
Clinical characteristics							
HTN (%)	5(25)	20	2(20)	10	3(30)	10	>0.999
DM (%)	5(25)	20	3(30)	10	2(20)	10	>0.999
DLP (%)	8(40)	20	4(40)	10	4(40)	10	>0.999

Statistical significance ($p < 0.05$) was calculated using unpaired t-test for numerical variables and Fisher's exact test for categorical variables.
The results were reported as mean ± SEM. NCs, non-carriers; MYBPC3$^{\Delta 2bp}$, A 25-base pair deletion in cardiac myosin-binding protein C3; SEM, standard error of mean; BMI, body mass index; BSA, body surface area; MAP, mean arterial pressure; HR, heart rate; $LVID_{dia}$, left ventricular internal diameter in diastole; $LVID_s$, left ventricular internal diameter in systole; LVEF, left ventricular ejection fracture; LVFS, left ventricular fractional shortening; IVS, interventricular septum; LVPW, left ventricular posterior wall; LAV 4C Mod, left atrial volume four-chamber method of disc; LVOT, left ventricular outflow tract; AV, aortic valve; E/A ratio, ratio of early diastole transmitral peak velocity flow to late diastole peak velocity flow; E/e' ratio, ratio of early transmitral peak velocity flow to early diastolic mitral annulus velocity; e'/a' ratio, ratio of early diastolic mitral annulus velocity to late diastolic mitral annulus velocity; RV, right ventricle; s', peak systolic annular velocity; LV, left ventricle; TAPSE, tricuspid annular plane systolic excursion; HTN, hypertension; DM, diabetes mellitus; DLP, dyslipidemia.

determined the presence of hyperdynamic manifestations under exercise conditions in asymptomatic *MYBPC3*$^{\Delta 25bp}$ variant carriers of US SA ancestry as compared to NCs who were presented with significantly higher EF, LVOT, and AV peak velocities, and impaired relaxation presented with a significant difference in the $LVID_{dia}$ and E/A ratio, but the non-significant difference in the average E/e' ratio. Hyperdynamic features and evidence of cardiac dysfunction were detected by echocardiography in *MYBPC3*$^{\Delta 25bp}$ carriers. These findings are also in line with the phenotype of genotype-positive individuals at stage 1 or those with non-hypertrophic HCM. These individuals can remain asymptomatic or present with subtle echocardiographic phenotype, such as diastolic dysfunction (34–36). In stage 2, however, individuals present with hypertrophy and LV hyperdynamic status (36), whereas *MYBPC3*$^{\Delta 25bp}$ variant carriers in the current study were non-hypertrophic, but did show hyperdynamic phenotype under exercise conditions. As shown in the regression lines, NCs and carriers responded differently to the stress stage, the independent variable, as resistance increased. Starting at 75 W equiv. 4.9 METs, the regression line showed no increase in EF% in NCs after 15 min of exercise. This finding can be explained by the Frank-Starling law, which holds that an increase in workload and venous returns stretches myocardial muscle fibers and increases preload (end-diastolic volume), stroke volume, and, ultimately, cardiac output until maximum capacity is reached. However, the weak increase in $LVID_{dia}$ from the baseline, as indicated in the regression line for carriers (**Figure 4A**), could be a contributing factor in maintaining an upward trend in EF% in carriers after 75 w since lower $LVID_{dia}$ can contribute to lower LV diastolic volume (LVEDV) as resistance augments. However, further studies with an adequate number of subjects are needed to decisively explain this observed phenotypic feature. Collectively, then, these data suggest that exercise stress itself, as a secondary

TABLE 2 | Clinical and bicycle exercise echocardiography parameters of 20 South Asian subjects.

Stress stage (W)		0		15		30		45		60		75		90		105		120		
Variables		**Mean ± SEM**	***n***	**Mean ± SEM**	***n***	**Mean ± SEM**	***n***	**Mean ± SEM**	***n***	**Mean ± SEM**	***n***	**Mean ± SEM**	***n***	**Mean ± SEM**	***n***	**Mean ± SEM**	***n***	**Mean ± SEM**	***n***	***P*-value**
MAP (mmHg)	NC	98.70 ± 2.78	10	107.93 ± 2.37	10	110.1 ± 3.55	10	110.03 ± 3.73	10	109.2 ± 3.74	10	114.43 ± 2.94	10	114.75 ± 3.56	8	119.62 ± 4.96	8	117.33 ± 7.19	6	0.412
	MYBPC3$^{\Delta 25bp}$	103.46 ± 2.82	10	109.92 ± 3.44	9	108.77 ± 2.74	9	112.53 ± 3.40	10	111.66 ± 4.34	10	112.76 ± 5.89	10	113.14 ± 6.31	9	123.44 ± 5.89	6	121.13 ± 4.57	5	
HR (bpm)	NC	76.90 ± 2.42	10	92.5 ± 1.8	10	98 ± 2.04	10	105.2 ± 2.4	10	112.5 ± 2.6	10	118 ± 2.02	10	125.75 ± 3.39	8	137.12 ± 4	8	146.83 ± 5.38	6	0.21
	MYBPC3$^{\Delta 25bp}$	72.40 ± 3.03	10	91.2 ± 2.56	10	96.7 ± 2.92	10	103.5 ± 2.60	10	111.3 ± 3.34	10	119.5 ± 3.25	10	125.11 ± 3.63	9	132.83 ± 4.93	6	143.66 ± 4.69	6	
$LVID_{dia}$ (cm)	NC	3.97 ± 0.15	10	4.4 ± 0.08	9	4.52 ± 0.11	9	4.56 ± 0.11	9	4.29 ± 0.12	9	4.59 ± 0.15	7	4.57 ± 0.1	6	4.59 ± 0.12	5	4.44 ± 0.13	4	0.0002
	MYBPC3$^{\Delta 25bp}$	4.16 ± 0.13	10	4.14 ± 0.13	10	4.17 ± 0.09	10	4.15 ± 0.08	9	4.18 ± 0.12	9	4.34 ± 0.15	7	4.32 ± 0.07	7	4.31 ± 0.16	6	4.01 ± 0.21	4	
$LVID_s$ (cm)	NC	2.69 ± 0.1	10	2.81 ± 0.07	9	2.77 ± 0.1	9	2.65 ± 0.09	9	2.47 ± 0.08	9	2.67 ± 0.05	7	2.53 ± 0.09	6	2.45 ± 0.09	5	2.36 ± 0.07	4	0.06
	MYBPC3$^{\Delta 25bp}$	2.87 ± 0.14	10	2.68 ± 0.1	10	2.63 ± 0.07	10	2.48 ± 0.05	9	2.37 ± 0.1	9	2.54 ± 0.07	7	2.39 ± 0.07	7	2.39 ± 0.07	6	2.24 ± 0.12	4	
LVEF (%)	NC	53.59 ± 1.81	10	55.26 ± 1.60	10	58.14 ± 2.09	10	59.99 ± 2.17	10	61.53 ± 2.12	10	64.03 ± 2.27	10	62.86 ± 2.83	7	61.83 ± 3.05	7	61.37 ± 3.39	5	<0.0001
	MYBPC3$^{\Delta 25bp}$	53.7 ± 2.17	10	58.26 ± 1.62	10	60.76 ± 1.69	10	63.07 ± 1.63	10	65.91 ± 1.71	10	67.65 ± 1.09	9	68.82 ± 1.48	8	70.19 ± 0.75	7	71.43 ± 0.58	4	
LVFS (%)	NC	31.55 ± 0.91	10	35.75 ± 0.95	9	38.79 ± 1.13	9	42.02 ± 1.03	9	42.19 ± 1.55	9	42.9 ± 1.81	7	44.62 ± 1.29	6	45.83 ± 2.33	5	46.39 ± 2.66	4	0.218
	MYBPC3$^{\Delta 25bp}$	31.2 ± 1.82	10	35.98 ± 1.68	10	36.98 ± 1.41	10	40.15 ± 1.39	9	43.44 ± 2.14	9	41.24 ± 1.71	7	44.51 ± 1.9	7	43.72 ± 2.03	6	43.93 ± 1.53	4	
LVOT peak velocity (m/s)	NC	0.76 ± 0.05	9	0.94 ± 0.06	9	0.91 ± 0.04	9	0.97 ± 0.06	10	1.00 ± 0.07	10	1.06 ± 0.04	8	1.13 ± 0.03	6	1.18 ± 0.04	5	1.33 ± 0.11	4	<0.0001
	MYBPC3$^{\Delta 25bp}$	0.82 ± 0.03	10	1.12 ± 0.06	10	1.08 ± 0.06	9	1.17 ± 0.06	10	1.34 ± 0.08	10	1.29 ± 0.07	10	1.36 ± 0.08	9	1.39 ± 0.07	7	1.49 ± 0.14	4	
AV peak velocity (m/s)	NC	0.96 ± 0.06	9	1.15 ± 0.06	9	1.09 ± 0.08	10	1.23 ± 0.09	9	1.30 ± 0.09	9	1.35 ± 0.07	8	1.43 ± 0.07	6	1.41 ± 0.13	4	1.61 ± 0.14	3	0.012
	MYBPC3$^{\Delta 25bp}$	1.01 ± 0.04	10	1.2 ± 0.06	10	1.25 ± 0.08	8	1.31 ± 0.07	10	1.38 ± 0.07	10	1.45 ± 0.07	10	1.49 ± 0.08	8	1.6 ± 0.06	8	1.75 ± 0.07	4	
E/A	NC	1.10 ± 0.13	10	1.16 ± 0.06	10	1.15 ± 0.08	10	0.97 ± 0.06	9	1.10 ± 0.06	10	0.96 ± 0.09	9	1.05 ± 0.03	6	1.10 ± 0.04	6	1.15 ± 0.20	3	0.03
	MYBPC3$^{\Delta 25bp}$	1.2 ± 0.11	10	0.9 ± 0.05	9	1.00 ± 0.09	9	1.01 ± 0.07	10	1.00 ± 0.1	9	0.96 ± 0.07	7	0.89 ± 0.09	5	0.77 ± 0.05	3	1.03 ± 0.27	2	
E/e' average	NC	7.20 ± 0.49	10	7.01 ± 0.50	9	7.31 ± 0.56	10	6.86 ± 0.63	8	7.25 ± 0.31	10	7.84 ± 0.63	7	8.38 ± 0.72	5	7.52 ± 0.40	6	8.81 ± 0.53	2	0.068
	MYBPC3$^{\Delta 25bp}$	7.16 ± 0.82	10	7.44 ± 0.98	9	6.27 ± 0.74	7	7.32 ± 0.80	9	7.58 ± 0.87	7	6.84 ± 0.92	6	6.19 ± 0.89	4	6.62 ± 0.47	3	6.11 ± 0.84	2	
RV s' (m/s)	NC	0.095 ± 0.004	10	0.107 ± 0.007	10	0.109 ± 0.007	10	0.121 ± 0.006	8	0.130 ± 0.01	10	0.139 ± 0.009	9	0.16 ± 0.009	7	0.158 ± 0.01	7	0.172 ± 0.009	6	0.35
	MYBPC3$^{\Delta 25bp}$	0.1 ± 0.005	10	0.12 ± 0.004	8	0.117 ± 0.005	8	0.131 ± 0.005	8	0.132 ± 0.008	8	0.139 ± 0.009	8	0.152 ± 0.009	6	0.157 ± 0.01	5	0.175 ± 0.014	3	
LV s' average (m/s)	NC	0.07 ± 0.004	10	0.08 ± 0.003	10	0.08 ± 0.004	10	0.08 ± 0.003	9	0.09 ± 0.003	10	0.101 ± 0.004	9	0.101 ± 0.006	8	0.114 ± 0.009	5	0.118 ± 0.014	3	0.557
	MYBPC3$^{\Delta 25bp}$	0.07 ± 0.003	10	0.08 ± 0.002	9	0.08 ± 0.003	9	0.09 ± 0.004	9	0.09 ± 0.003	8	0.103 ± 0.005	9	0.106 ± 0.005	7	0.107 ± 0.004	6	0.112 ± 0.006	4	
TAPSE (cm)	NC	2.40 ± 0.23	9	2.34 ± 0.19	9	2.31 ± 0.13	9	2.42 ± 0.14	9	2.47 ± 0.16	9	2.53 ± 0.22	7	2.63 ± 0.13	6	2.44 ± 0.15	5	2.53 ± 0.13	4	0.065
	MYBPC3$^{\Delta 25bp}$	2.04 ± 0.1	10	2.27 ± 0.13	10	2.38 ± 0.16	9	2.55 ± 0.13	10	2.68 ± 0.21	9	2.81 ± 0.1	7	2.52 ± 0.18	3	2.81 ± 0.23	6	3.71 ± 0.00	1	

Statistical significance ($p < 0.05$) was calculated using two-way ANOVA. The results were reported as mean ± SEM. NCs, non-carriers; MYBPC3$^{\Delta 25bp}$*, A 25-base pair deletion in cardiac myosin binding protein C3; SEM, standard error of mean; MAP, mean arterial pressure; HR, heart rate;* $LVID_{dia}$*, left ventricular internal diameter in diastole;* $LVID_s$*, left ventricular internal diameter in systole; LVEF, left ventricular ejection fracture; LVFS, left ventricular fractional shortening; LVOT, left ventricular outflow tract; AV, aortic valve; E/A ratio, ratio of early diastole transmitral peak velocity flow to late diastole peak velocity flow; E/e' ratio, ratio of early transmitral peak velocity flow to early diastolic mitral annulus velocity; RV, right ventricle; s', peak systolic annular velocity; LV, left ventricle; TAPSE, tricuspid annular plane systolic excursion.*

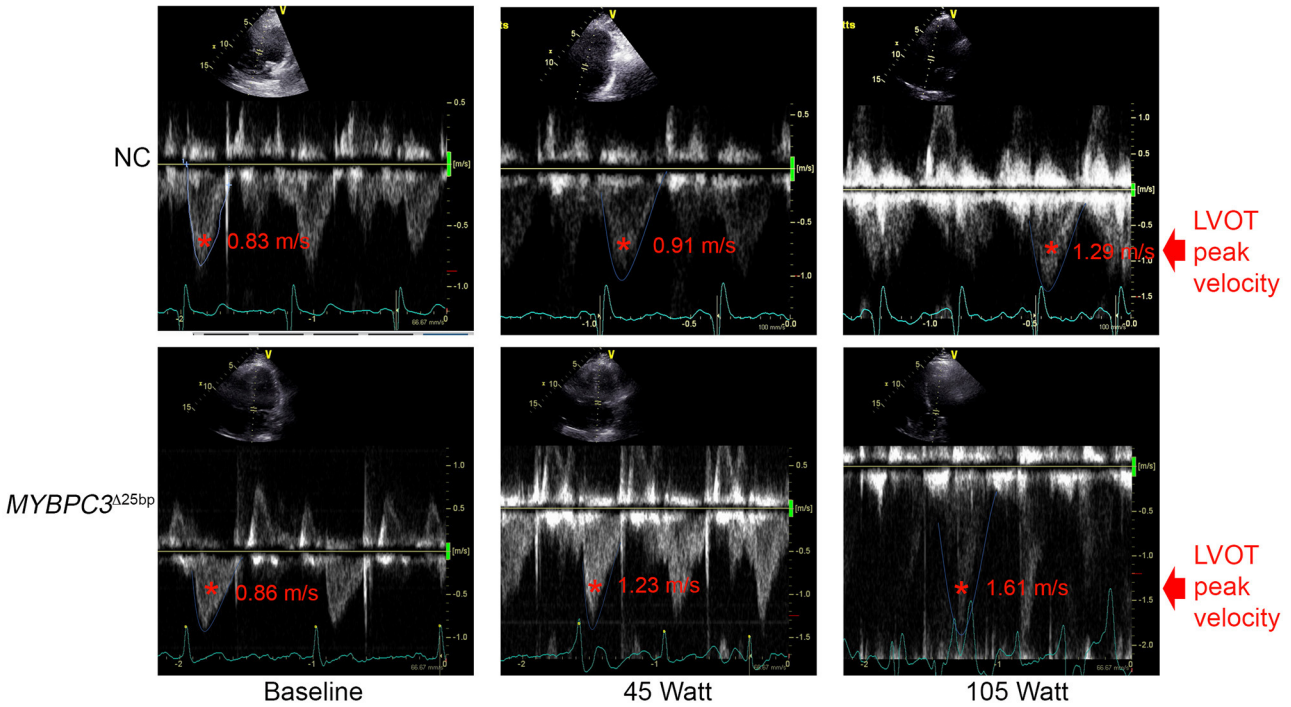

FIGURE 3 | Spectral Doppler data depict LVOT peak velocity. Representative apical five-chamber view at baseline, 45 (W), and 105 (W) in a NC (upper panel) subject and a *MYBPC3*$^{\Delta 25bp}$ variant carrier (lower panel). NC, non-carriers.

risk factor, potentially triggered hyperdynamic phenotype in asymptomatic *MYBPC3*$^{\Delta 25bp}$ carriers, as compared to NCs, considering that the hemodynamic parameters of MAP and HR did not differ between the two groups (*MYBPC3*$^{\Delta 25bp}$ variant carriers and NCs).

Previous studies have examined the distribution (26, 27, 37, 38) and clinical correlations (26, 27, 31, 39) of the *MYBPC3*$^{\Delta 25bp}$ variant, noting, importantly, that most of these studies were conducted in individuals of SA ancestry. In the first report (2003), the *MYBPC3*$^{\Delta 25bp}$ variant was initially detected in two affected Indian families. Then, it was reported in 16 of 229 unrelated healthy SA individuals and present in 3.8% of the general population, confirming variability in disease penetrance (29). In the next case-control study with a multi-ethnic population of 6,273 individuals in the SA Diaspora, the carrier frequency of the *MYBPC3*$^{\Delta 25bp}$ variant was reported to be 4% (26). Simonson et al. (38) and Bashyam et al. (37) reported 8 and 6%, respectively, in their studies. In 2018, we determined 6% prevalence in a sample taken from individuals of SA ancestry living in the United States (27). However, *MYBPC3*$^{\Delta 25bp}$ is largely associated with incomplete penetrance and delayed onset (26, 27, 29). In the current study, we identified a slightly higher prevalence at 6.75%, but given the nature of our study, this result may have been influenced by ascertainment. Collectively, these data support that *MYBPC3*$^{\Delta 25bp}$ is a common variant and that its distribution is associated with ethnicity (4, 25). Furthermore, our interpolation indicates that a prevalent SA-specific *MYBPC3*$^{\Delta 25bp}$ variant predisposes an estimated ∼100 million people of SA ancestry worldwide (26) to such adverse cardiac events as cardiomyopathies, arrhythmias, HF, and SCD.

Previously, we reported no significant difference in clinical characteristics, ECG, or echocardiographic parameters between US SA carriers of the *MYBPC3*$^{\Delta 25bp}$ variant and NCs at rest, except for LV fractional shortening (27), which was slightly higher in carriers as compared to NCs ($p = 0.04$), suggesting a minimal effect of the *MYBPC3*$^{\Delta 25bp}$ variant on the development of HCM phenotype. Compared to the current study, prior analyses included more individuals (n = 47 carriers) who were younger (47.6 years) and, importantly, included both men and women (27). Both sex inclusion and age may have reduced the ability to detect a hyperdynamic state, which we discovered upon exercise stress. Many affected individuals could also remain asymptomatic until late adulthood (16, 22). Therefore, early detection of any subtle clinical phenotype and/or secondary contributing risk factors triggering symptoms in the carrier population, as we have suggested in our findings, is potentially relevant clinically. In the prior study, we also identified a second co-segregating novel variant (D389V) identified in ∼10% of *MYBPC3*$^{\Delta 25bp}$ carriers associated with hyperdynamic cardiac features on echocardiogram as a potential secondary modifying factor for HCM (27). In this current investigation, however, no *MYBPC3*$^{\Delta 25bp}$ subjects with the D389V variant were included, meaning that the findings herein cannot be attributed to D398V. As previously noted, Harper et al. separately identified a haplotype in SAs with HCM with both the *MYBPC3*$^{\Delta 25bp}$ variant and a potentially pathogenic variant, *MYBPC3* c.1224-52G>A

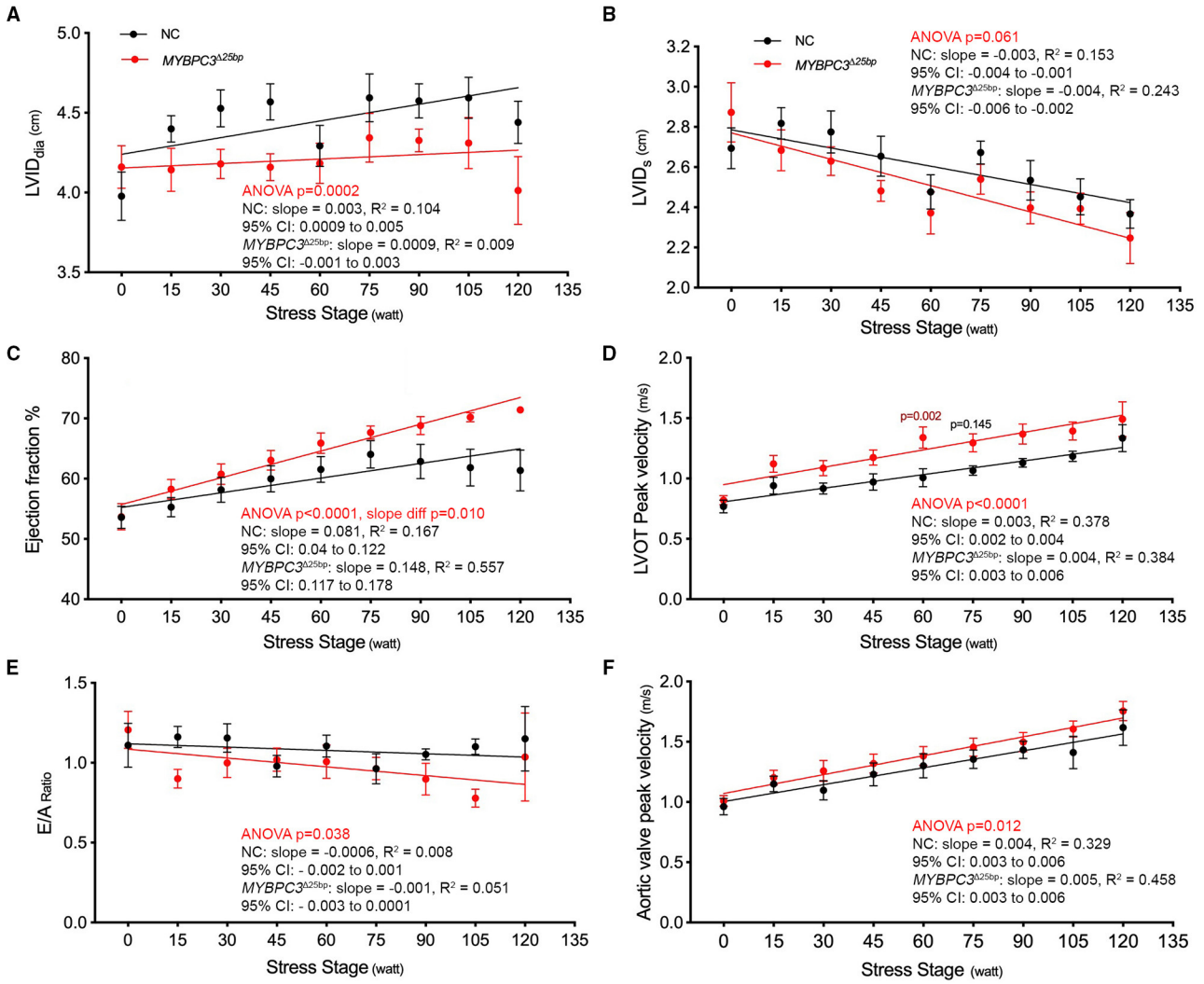

FIGURE 4 | Prevalent South Asian-specific *MYBPC3*$^{\Delta 25bp}$ variant is associated with hypercontraction and impaired relaxation under exercise stress (10 NCs vs. 10 *MYBPC3*$^{\Delta 25bp}$ carriers). **(A)** A significant difference in $LVID_{dia}$ is observed between carriers of the *MYBPC3*$^{\Delta 25bp}$ variant and NCs (Two-way ANOVA, $p = 0.0002$; CI: 0.239 ± 0.125). In response to stress, $LVID_{dia}$ increases significantly from baseline in NCs, whereas it does not significantly change in *MYBPC3*$^{\Delta 25bp}$ carriers. **(B)** The graph depicts a non-significant difference between *MYBPC3*$^{\Delta 25bp}$ variant carriers and NCs in $LVID_s$ in response to stress (Two-way ANOVA, $p = 0.061$; CI: 0.09 ± 0.09). In addition, carriers of the *MYBPC3*$^{\Delta 25bp}$ variant show significantly higher **(C)** ejection fraction (CI: 4.57 ± 1.93) and **(D)** LVOT peak velocity (CI: 0.197 ± 0.069) compared to NCs (Two-way ANOVA, $p < 0.0001$, both). **(E)** With exercise, the average E/A ratio shows a significant difference between *MYBPC3*$^{\Delta 25bp}$ carriers and NCs (Two-way ANOVA, $p < 0.038$; CI: 0.107 ± 0.102). **(F)** The graph depicts significantly higher aortic valve peak velocity in *MYBPC3*$^{\Delta 25bp}$ variant carriers compared to NCs (Two-way ANOVA, $p < 0.012$; CI: 0.103 ± 0.081). $LVID_{dia}$, left ventricular internal diameter in diastole; $LVID_s$, left ventricular internal diameter in systole; LVOT, left ventricular outflow tract; NC, non-carriers.

(31). None of the members of our *MYBPC3*$^{\Delta 25bp}$ cohort were, in fact, found to carry the variant identified by Harper et al. Altogether, we propose that *MYBPC3*$^{\Delta 25bp}$ is still a valid risk variant in the etiology of HCM and that it arises from a secondary risk factor, namely, exercise stress, and manifests as hypercontraction and impaired relaxation associated with late-onset LV dysfunction.

Exercise stress echocardiography is a standard clinical assessment and diagnostic armamentarium of HCM to assess exercise-induced LVOT obstruction in patients with resting LVOT gradient <50 mm Hg (40). The only limitation is that not all patients with HCM and controls are able to perform stress exercises. Patients with HCM usually present with dynamic LVOT gradient, arrhythmias, and mitral regurgitation. However, for asymptomatic carriers with pathogenic sarcomere mutations, the exercise stress test is potentially an advantageous method for unmasking subclinical diseases, such as impairment in diastolic function and dynamic outflow tract obstruction in the absence

of a pathologically hypertrophied LV. The exercise stress test results presented here seem to have to accurately detect early changes in cardiac function, and the testing procedure was shown to be safe for enhancing and visualizing mid-range changes in cardiac function in variant carriers (41). Based on the results, asymptomatic *MYBPC3*$^{\Delta 25bp}$ carriers do have sublevel phenotype during exercise, which is masked under baseline conditions. These data further indicate that exercise testing may assist in risk stratification for the presence of any cardiac events as previously described (41–43).

Hypertension, diabetes mellitus, coronary artery disease, and other comorbid conditions were known to confound the phenotypic effects of cardiomyopathy and cardiac dysfunction. Initial studies have shown that the *MYBPC3*$^{\Delta 25bp}$ variant is associated with HCM (29), but then it was also determined to be associated with dilated and restrictive cardiomyopathies and HF (26). Later, it was determined that *MYBPC3*$^{\Delta 25bp}$ is significantly associated with LV dysfunction secondary to coronary artery disease (39, 44). After myocardial infarction, results from these studies have suggested that patients with *MYBPC3*$^{\Delta 25bp}$ show poor cardiac remodeling and recovery from the damage. This could be explained in several ways. First, cMyBP-C is sensitive to proteolysis during myocardial infarction and could be a potential earlier biomarker for heart attack (45–47). Thus, patients with *MYBPC3*$^{\Delta 25bp}$ may not have enough wild-type cMyBP-C turnover, resulting in haploinsufficiency (48). The failure to compensate for the loss of wild-type during myocardial infarction finally results in poor cardiac remodeling. Second, when *MYBPC3*$^{\Delta 25bp}$ carriers undergo myocardial infarction, it is possible that initial damage hinders quick recovery by the poison polypeptide effect (49). In the present study, we provided subjects with a questionnaire asking for information pertaining to their demographics, family history, medical history, and current and past medications. Using this as our guide, we then excluded any *MYBPC3*$^{\Delta 25bp}$ carriers who were presented with such secondary risk factors, thus eliminating them from participation in the stress echo study. This means that the outcome of the stress echo was based solely on the presence of *MYBPC3*$^{\Delta 25bp}$ and its effects on cardiac function. Collectively, results from the present study suggest LV hypercontractility under exercise stress conditions with evidence of diastolic stiffening and impairment among male asymptomatic *MYBPC3*$^{\Delta 25bp}$ carriers. As such, these results also suggest the presence of some subclinical pathology in *MYBPC3*$^{\Delta 25bp}$ carriers under exercise stress conditions. Based on the presence of HCM in transgenic mice expressing *MYBPC3*$^{\Delta 25bp}$ mRNA (49) and subclinical cardiomyopathy phenotype in carriers (26), *MYBPC3*$^{\Delta 25bp}$ can, therefore, be considered a potential risk allele for abnormal diastolic function and cardiomyopathy.

Complementary DNA sequencing of mRNA isolated from the biopsy of an *MYBPC3*$^{\Delta 25bp}$-positive patient confirmed the presence of exon 33 skipping *in vivo* (26, 29). Exon 33 skipping results in the loss of 62 amino acids, resulting in a modified C10 domain of cMyBP-C (13). Exon 33 skipping also moves the stop codon to the 3′ untranslated region (UTR), adding a novel 55 amino acids in this newly modified C10 domain at the carboxyl terminus (cMyBP-C$^{\Delta C10}$) (49). However, if the C10 domain is modified, or truncated, then cMyBP-C will not properly localize in the sarcomere (50–52). The repercussions of this event can involve pathogenicity with the onset of HCM.

In fact, we have previously demonstrated that the presence of the *MYBPC3*$^{\Delta 25bp}$ variant could lead to exon 33 skipping during transcription (26, 29). We next determined that the *MYBPC3*$^{\Delta 25bp}$ variant in the presence of exon 33 skipping is pathogenic, both *in vitro* (46) and *in vivo* (49). Using a transgenic mouse model, we demonstrated that the expression of cMyBP-C$^{\Delta C10}$ is sufficient to cause HCM. Based on this observation, we propose that haploinsufficiency increases the disordered relaxed state (DRX) and decreases the super relaxed state (SRX) of myosin, leading to hypercontraction and HCM (53, 54). However, the molecular mechanism underlying these phenomena is yet to be validated in a humanized knock-in *MYBPC3*$^{\Delta 25bp}$ mouse model that shows normal cardiac function under baseline conditions (55). Thus, future studies will involve defining the pathogenicity of *MYBPC3*$^{\Delta 25bp}$ in a humanized knock-in mouse model in the presence of a comorbidity or acute insult.

Study Limitation

This study is limited by its single-center nature, small cohort size, and inclusion of only men. Although HCM has equal distribution in both sexes (4, 56), women are more likely to remain undiagnosed (4); therefore, including female carriers and evaluating gender-specific manifestations under exercise stress conditions are strongly recommended. However, among those contacted for this study, male subjects were more willing to perform TTE and/or BSE, accounting for the disparity. We were also limited by the coronavirus disease-2019 (COVID-19), which resulted in a delay in recruitment and the need to follow health and safety protocols, such as wearing a mask during stress exercise. While the present study is valuable for its novel outcome, it is, by design, only a pilot study, so further, larger studies are needed.

AUTHOR'S NOTE

We presented the current data at the American Heart Association Scientific Sessions on November 12, 2020 (abstract # 13481) entitled "South Asian-specific *MYBPC3*$^{\Delta 25bp}$ Intronic Deletion Carriers Demonstrate Hypercontractility and Impaired Diastolic Function Under Exercise Stress" (Circulation. 2020; 142:A13481; https://doi.org/10.1161/circ.142.suppl_3.13481).

DATA AVAILABILITY STATEMENT

The original contributions presented in the study are included in the article/supplementary material, further inquiries can be directed to the corresponding author/s.

ETHICS STATEMENT

The studies involving human participants were reviewed and approved by Prevalence study: Loyola University Chicago IRB# LU207815 and 207359, Chicago, Illinois and University

of Cincinnati IRB# 2016-7580, Cincinnati, Ohio. Genotype-phenotype study: University of Cincinnati IRB# 2016-4948, Cincinnati, Ohio. The patients/participants provided their written informed consent to participate in this study.

AUTHOR CONTRIBUTIONS

SB, SV, EM, and SS: conceptualization. SB, RS, SG, MP, KS, RRS, MK, DH, JR, and EM: data curation. SB, RS, SG, KS, MK, RJ, DH, JR, and EM: formal analysis. RB and SS: funding acquisition. SB, RS, SG, MP, MK, DH, JR, EM, and SS: investigation. SB, SV, MP, RJ, DH, JR, EM, and SS: methodology. DH, EM, and SS: project administration. RS, KS, RRS, RJ, DH, JR, RB, EM, and SS: resources. DH, EM, and SS: supervision. RJ, JR, and RB: validation. SB, MP, and SS: writing the original draft. SB, SS, MP, RJ, DH, JR, RB, EM, and SS: writing, reviewing, and editing. All authors contributed to the article and approved the submitted version.

FUNDING

This research was supported by Heart, Lung, and Vascular Institute startup funding at the College of Medicine, University of Cincinnati. The investigators were further supported by the National Institutes of Health grants R01 AR078001 (SS), R01 HL130356 (SS), R01 HL105826 (SS), R38 HL155775 (SS), R01 HL143490 (SS), U01 HL131914 (EM), and R01 HL128075 (EM), and the American Heart Association 2019 Institutional Undergraduate Student (19UFEL34380251, SS), Cardiovascular Genome-Phenome Study (15CVGPSD27020012, SS, MP, and EM), Catalyst (17CCRG33671128, SS, MP, and EM), Transformation (19TPA34830084, SS), Career Development (189CDA34110460, MP), and Postdoctoral Training Fellowship (17POST33630157, SV) awards, and the PLN Foundation (PLN crazy idea, SS). RRS was supported by an Amgen Postdoctoral Fellowship.

ACKNOWLEDGMENTS

We thank Karen Moore and Kim Labowsky, echocardiography sonographers, for all their support and advice in conducting this study, and all staff at the Human Research Protection Service and University of Cincinnati College of Medicine. We also thank our research subjects and volunteers who kindly supported our investigation.

REFERENCES

1. Maron BJ, Gardin JM, Flack JM, Gidding SS, Kurosaki TT, Bild DE. Prevalence of hypertrophic cardiomyopathy in a general population of young adults. Echocardiographic analysis of 4111 subjects in the CARDIA Study Coronary Artery Risk Development in (Young) Adults. *Circulation.* (1995) 92:785–9. doi: 10.1161/01.CIR.92.4.785
2. Maron BJ, Peterson EE, Maron MS, Peterson JE. Prevalence of hypertrophic cardiomyopathy in an outpatient population referred for echocardiographic study. *Am J Cardiol.* (1994) 73:577–80. doi: 10.1016/0002-9149(94)90337-9
3. Semsarian C, Ingles J, Maron MS, Maron BJ. New perspectives on the prevalence of hypertrophic cardiomyopathy. *J Am Coll Cardiol.* (2015) 65:1249–54. doi: 10.1016/j.jacc.2015.01.019
4. Ommen SR, Mital S, Burke MA, Day SM, Deswal A, Elliott P, et al. 2020 AHA/ACC Guideline for the diagnosis and treatment of patients with hypertrophic cardiomyopathy: a report of the American College of Cardiology/American Heart Association Joint Committee on Clinical Practice Guidelines. *Circulation.* (2020) 142:e533–57. doi: 10.1161/CIR.0000000000000938
5. Watkins H, MacRae C, Thierfelder L, Chou YH, Frenneaux M, McKenna W, et al. A disease locus for familial hypertrophic cardiomyopathy maps to chromosome 1q3. *Nat Genet.* (1993) 3:333–7. doi: 10.1038/ng0493-333
6. Watkins H, Conner D, Thierfelder L, Jarcho JA, MacRae C, McKenna WJ, et al. Mutations in the cardiac myosin binding protein-C gene on chromosome 11 cause familial hypertrophic cardiomyopathy. *Nat Genet.* (1995) 11:434–7. doi: 10.1038/ng1295-434
7. Bonne G, Carrier L, Bercovici J, Cruaud C, Richard P, Hainque B, et al. Cardiac myosin binding protein-C gene splice acceptor site mutation is associated with familial hypertrophic cardiomyopathy. *Nat Genet.* (1995) 11:438–40. doi: 10.1038/ng1295-438
8. Carrier L, Bonne G, Schwartz K. Cardiac Myosin-binding protein C and hypertrophic cardiomyopathy. *Trends Cardiovasc Med.* (1998) 8:151–7. doi: 10.1016/S1050-1738(97)00144-8
9. Spirito P, Seidman CE, McKenna WJ, Maron BJ. The management of hypertrophic cardiomyopathy. *N Engl J Med.* (1997) 336:775–85. doi: 10.1056/NEJM199703133361107
10. Harris SP, Lyons RG, Bezold KL. In the thick of it: HCM-causing mutations in myosin binding proteins of the thick filament. *Circ Res.* (2011) 108:751–64. doi: 10.1161/CIRCRESAHA.110.231670
11. Gersh BJ, Maron BJ, Bonow RO, Dearani JA, Fifer MA, Link MS, et al. 2011 ACCF/AHA guideline for the diagnosis and treatment of hypertrophic cardiomyopathy: executive summary: a report of the American College of Cardiology Foundation/American Heart Association Task Force on Practice Guidelines. *Circulation.* (2011) 124:2761–96. doi: 10.1161/CIR.0b013e318223e230
12. Barefield D, Kumar M, de Tombe PP, Sadayappan S. Contractile dysfunction in a mouse model expressing a heterozygous MYBPC3 mutation associated with hypertrophic cardiomyopathy. *Am J Physiol Heart Circ Physiol.* (2014) 306:H807–15. doi: 10.1152/ajpheart.00913.2013
13. Kuster DW, Sadayappan S. MYBPC3's alternate ending: consequences and therapeutic implications of a highly prevalent 25 bp deletion mutation. *Pflugers Arch.* (2014) 466:207–13. doi: 10.1007/s00424-013-1417-7
14. Previs MJ, Beck Previs S, Gulick J, Robbins J, Warshaw DM. Molecular mechanics of cardiac myosin-binding protein C in native thick filaments. *Science.* (2012) 337:1215–8. doi: 10.1126/science.1223602
15. Morita H, Rehm HL, Menesses A, McDonough B, Roberts AE, Kucherlapati R, et al. Shared genetic causes of cardiac hypertrophy in children and adults. *N Engl J Med.* (2008) 358:1899–908. doi: 10.1056/NEJMoa075463
16. Niimura H, Bachinski LL, Sangwatanaroj S, Watkins H, Chudley AE, McKenna W, et al. Mutations in the gene for cardiac myosin-binding protein C and late-onset familial hypertrophic cardiomyopathy. *N Engl J Med.* (1998) 338:1248–57. doi: 10.1056/NEJM199804303381802
17. Moolman JA, Reith S, Uhl K, Bailey S, Gautel M, Jeschke B, et al. A newly created splice donor site in exon 25 of the MyBP-C gene is responsible for inherited hypertrophic cardiomyopathy with incomplete disease penetrance. *Circulation.* (2000) 101:1396–402. doi: 10.1161/01.CIR.101.12.1396
18. Adalsteinsdottir B, Teekakirikul P, Maron BJ, Burke MA, Gudbjartsson DF, Holm H, et al. Nationwide study on hypertrophic cardiomyopathy in Iceland: evidence of a MYBPC3 founder mutation. *Circulation.* (2014) 130:1158–67. doi: 10.1161/CIRCULATIONAHA.114.011207
19. Helms AS, Davis FM, Coleman D, Bartolone SN, Glazier AA, Pagani F, et al. Sarcomere mutation-specific expression patterns in human

hypertrophic cardiomyopathy. *Circ Cardiovasc Genet.* (2014) 7:434–43. doi: 10.1161/CIRCGENETICS.113.000448
20. Michels M, Soliman OI, Phefferkorn J, Hoedemaekers YM, Kofflard MJ, Dooijes D, et al. Disease penetrance and risk stratification for sudden cardiac death in asymptomatic hypertrophic cardiomyopathy mutation carriers. *Eur Heart J.* (2009) 30:2593–8. doi: 10.1093/eurheartj/ehp306
21. Page SP, Kounas S, Syrris P, Christiansen M, Frank-Hansen R, Andersen PS, et al. Cardiac myosin binding protein-C mutations in families with hypertrophic cardiomyopathy: disease expression in relation to age, gender, and long term outcome. *Circ Cardiovasc Genet.* (2012) 5:156–66. doi: 10.1161/CIRCGENETICS.111.960831
22. Niimura H, Patton KK, McKenna WJ, Soults J, Maron BJ, Seidman JG, et al. Sarcomere protein gene mutations in hypertrophic cardiomyopathy of the elderly. *Circulation.* (2002) 105:446–51. doi: 10.1161/hc0402.102990
23. Maron BJ, Shirani J, Poliac LC, Mathenge R, Roberts WC, Mueller FO. Sudden death in young competitive athletes. Clinical, demographic, and pathological profiles. *JAMA.* (1996) 276:199–204. doi: 10.1001/jama.1996.03540030033028
24. Klues HG, Schiffers A, Maron BJ. Phenotypic spectrum and patterns of left ventricular hypertrophy in hypertrophic cardiomyopathy: morphologic observations and significance as assessed by two-dimensional echocardiography in 600 patients. *J Am Coll Cardiol.* (1995) 26:1699–708. doi: 10.1016/0735-1097(95)00390-8
25. Maron BJ. Hypertrophic cardiomyopathy: an important global disease. *Am J Med.* (2004) 116:63–5. doi: 10.1016/j.amjmed.2003.10.012
26. Dhandapany PS, Sadayappan S, Xue Y, Powell GT, Rani DS, Nallari P, et al. A common MYBPC3 (cardiac myosin binding protein C) variant associated with cardiomyopathies in South Asia. *Nat Genet.* (2009) 41:187–91. doi: 10.1038/ng.309
27. Viswanathan SK, Puckelwartz MJ, Mehta A, Ramachandra CJA, Jagadeesan A, Fritsche-Danielson R, et al. Association of cardiomyopathy with MYBPC3 D389V and MYBPC3Delta25bpIntronic deletion in South Asian Descendants. *JAMA Cardiol.* (2018) 3:481–8. doi: 10.1001/jamacardio.2018.0618
28. Arif M, Nabavizadeh P, Song T, Desai D, Singh R, Bazrafshan S, et al. Genetic, clinical, molecular, and pathogenic aspects of the South Asian-specific polymorphic MYBPC3(Delta25bp) variant. *Biophys Rev.* (2020) 12:1065–84. doi: 10.1007/s12551-020-00725-1
29. Waldmuller S, Sakthivel S, Saadi AV, Selignow C, Rakesh PG, Golubenko M, et al. Novel deletions in MYH7 and MYBPC3 identified in Indian families with familial hypertrophic cardiomyopathy. *J Mol Cell Cardiol.* (2003) 35:623–36. doi: 10.1016/S0022-2828(03)00050-6
30. Sadayappan S, Puckelwartz MJ, McNally EM. South Asian-specific MYBPC3(Delta25bp) intronic deletion and its role in cardiomyopathies and heart failure. *Circ Genom Precis Med.* (2020) 13:e002986. doi: 10.1161/CIRCGEN.120.002986
31. Harper AR, Bowman M, Hayesmoore JBG, Sage H, Salatino S, Blair E, et al. Reevaluation of the South Asian MYBPC3(Delta25bp) intronic deletion in hypertrophic cardiomyopathy. *Circ Genom Precis Med.* (2020) 13:e002783. doi: 10.1161/CIRCGEN.119.002783
32. Puckelwartz MJ, Pesce LL, Nelakuditi V, Dellefave-Castillo L, Golbus JR, Day SM, et al. Supercomputing for the parallelization of whole genome analysis. *Bioinformatics.* (2014) 30:1508–13. doi: 10.1093/bioinformatics/btu071
33. Richards S, Aziz N, Bale S, Bick D, Das S, Gastier-Foster J, et al. ACMG laboratory quality assurance committee. standards and guidelines for the interpretation of sequence variants: a joint consensus recommendation of the American College of Medical Genetics and Genomics and the Association for Molecular Pathology. *Genet Med.* (2015) 5:405–24. doi: 10.1038/gim.2015.30
34. Ho CY, Carlsen C, Thune JJ, Havndrup O, Bundgaard H, Farrohi F, et al. Echocardiographic strain imaging to assess early and late consequences of sarcomere mutations in hypertrophic cardiomyopathy. *Circ Cardiovasc Genet.* (2009) 2:314–21. doi: 10.1161/CIRCGENETICS.109.862128
35. Michels M, Soliman OI, Kofflard MJ, Hoedemaekers YM, Dooijes D, Majoor-Krakauer D, et al. Diastolic abnormalities as the first feature of hypertrophic cardiomyopathy in Dutch myosin-binding protein C founder mutations. *JACC Cardiovasc Imaging.* (2009) 2:58–64. doi: 10.1016/j.jcmg.2008.08.003
36. Olivotto I, Cecchi F, Poggesi C, Yacoub MH. Patterns of disease progression in hypertrophic cardiomyopathy: an individualized approach to clinical staging. *Circ Heart Fail.* (2012) 5:535–46. doi: 10.1161/CIRCHEARTFAILURE.112.967026
37. Bashyam MD, Purushotham G, Chaudhary AK, Rao KM, Acharya V, Mohammad TA, et al. A low prevalence of MYH7/MYBPC3 mutations among familial hypertrophic cardiomyopathy patients in India. *Mol Cell Biochem.* (2012) 360:373–82. doi: 10.1007/s11010-011-1077-x
38. Simonson TS, Zhang Y, Huff CD, Xing J, Watkins WS, Witherspoon DJ, et al. Limited distribution of a cardiomyopathy-associated variant in India. *Ann Hum Genet.* (2010) 74:184–8. doi: 10.1111/j.1469-1809.2010.00561.x
39. Srivastava A, Garg N, Mittal T, Khanna R, Gupta S, Seth PK, et al. Association of 25 bp deletion in MYBPC3 gene with left ventricle dysfunction in coronary artery disease patients. *PLoS ONE.* (2011) 6:e24123. doi: 10.1371/journal.pone.0024123
40. Sorensen LL, Liang HY, Pinheiro A, Hilser A, Dimaano V, Olsen NT, et al. Safety profile and utility of treadmill exercise in patients with high-gradient hypertrophic cardiomyopathy. *Am Heart J.* (2017) 184:47–54. doi: 10.1016/j.ahj.2016.10.010
41. Desai MY, Bhonsale A, Patel P, Naji P, Smedira NG, Thamilarasan M, et al. Exercise echocardiography in asymptomatic HCM: exercise capacity, and not LV outflow tract gradient predicts long-term outcomes. *JACC Cardiovasc Imaging.* (2014) 7:26–36. doi: 10.1016/j.jcmg.2013.08.010
42. Mora S, Redberg RF, Cui Y, Whiteman MK, Flaws JA, Sharrett AR, et al. Ability of exercise testing to predict cardiovascular and all-cause death in asymptomatic women: a 20-year follow-up of the lipid research clinics prevalence study. *JAMA.* (2003) 290:1600–7. doi: 10.1001/jama.290.12.1600
43. Myers J, Prakash M, Froelicher V, Do D, Partington S, Atwood JE. Exercise capacity and mortality among men referred for exercise testing. *N Engl J Med.* (2002) 346:793–801. doi: 10.1056/NEJMoa011858
44. Kumar S, Mishra A, Srivastava A, Bhatt M, Garg N, Agarwal SK, et al. Role of common sarcomeric gene polymorphisms in genetic susceptibility to left ventricular dysfunction. *J Genet.* (2016) 95:263–72. doi: 10.1007/s12041-016-0623-4
45. Yogeswaran A, Troidl C, McNamara JW, Wilhelm J, Truschel T, Widmann L, et al. The C0-C1f region of cardiac myosin binding protein-C induces pro-inflammatory responses in fibroblasts via TLR4 signaling. *Cells.* (2021) 10:1326. doi: 10.3390/cells10061326
46. Kuster DW, Govindan S, Springer TI, Martin JL, Finley NL, Sadayappan S. A hypertrophic cardiomyopathy-associated MYBPC3 mutation common in populations of South Asian descent causes contractile dysfunction. *J Biol Chem.* (2015) 290:5855–67. doi: 10.1074/jbc.M114.607911
47. Chen XJ, Zhang W, Bian ZP, Wang ZM, Zhang J, Wu HF, et al. Cardiac myosin-binding protein c release profile after cardiac surgery in intensive care unit. *Ann Thorac Surg.* (2019) 108:1195–201. doi: 10.1016/j.athoracsur.2019.03.072
48. Glazier AA, Thompson A, Day SM. Allelic imbalance and haploinsufficiency in MYBPC3-linked hypertrophic cardiomyopathy. *Pflugers Arch.* (2019) 471:781–93. doi: 10.1007/s00424-018-2226-9
49. Kuster DWD, Lynch TL, Barefield DY, Sivaguru M, Kuffel G, Zilliox MJ, et al. Altered C10 domain in cardiac myosin binding protein-C results in hypertrophic cardiomyopathy. *Cardiovasc Res.* (2019) 115:1986–97. doi: 10.1093/cvr/cvz111
50. Moolman-Smook J, Flashman E, de Lange W, Li Z, Corfield V, Redwood C, et al. Identification of novel interactions between domains of Myosin binding protein-C that are modulated by hypertrophic cardiomyopathy missense mutations. *Circ Res.* (2002) 91:704–11. doi: 10.1161/01.RES.0000036750.81083.83
51. McConnell BK, Jones KA, Fatkin D, Arroyo LH, Lee RT, Aristizabal O, et al. Dilated cardiomyopathy in homozygous myosin-binding protein-C mutant mice. *J Clin Invest.* (1999) 104:1235–44. doi: 10.1172/JCI7377
52. Hossain MB, Elbeck Z, Siga H, Knoll R. Myosin binding protein-C and hypertrophic cardiomyopathy: role of altered C10 domain. *Cardiovasc Res.* (2019) 115:1943–5. doi: 10.1093/cvr/cvz167
53. McNamara JW, Li A, Lal S, Bos JM, Harris SP, van der Velden J, et al. MYBPC3 mutations are associated with a reduced super-relaxed state in patients with hypertrophic cardiomyopathy. *PLoS ONE.* (2017) 12:e0180064. doi: 10.1371/journal.pone.0180064
54. Toepfer CN, Wakimoto H, Garfinkel AC, McDonough B, Liao D, Jiang J, et al. (2019). Hypertrophic cardiomyopathy mutations in MYBPC3 dysregulate myosin. *Sci. Transl. Med.* 11:eaat1199. doi: 10.1126/scitranslmed.aat1199

55. McNamara JW, Schwanekamp JA, Patel PN, Viswanathan SK, Bohlooly M, Madeyski-Bengtson K, et al. The highly prevalent 25bp intronic deletion of MYBPC3 is benign under baseline conditions. *Circ Res.* (2019) 125:772. doi: 10.1161/res.125.suppl_1.772
56. Olivotto I, Maron MS, Adabag AS, Casey SA, Vargiu D, Link MS, et al. Gender-related differences in the clinical presentation and outcome of hypertrophic cardiomyopathy. *J Am Coll Cardiol.* (2005) 46:480–7. doi: 10.1016/j.jacc.2005.04.043

Conflict of Interest: SS provides consulting and collaborative research studies to the Leducq Foundation (CURE-PLAN), Red Saree Inc., Greater Cincinnati Tamil Sangam, Pfizer, Novo Nordisk, AstraZeneca, MyoKardia, Merck, and Amgen. EM serves as a consultant to AstraZeneca, Amgen, Pfizer, Tenaya Therapeutics, and Invitae. RB serves on scientific advisory boards for Janssen and Basking Biosciences and DSMB Committees for Ionis Pharmaceuticals, Akcea Therapeutics, and Novartis. These activities are unrelated to the content of this work. RRS has been a postdoctoral fellow of Amgen, starting from June 2019, and performs research at the University of Cincinnati.

The remaining authors declare that the research was conducted in the absence of any commercial or financial relationships that could be construed as a potential conflict of interest.

Publisher's Note: All claims expressed in this article are solely those of the authors and do not necessarily represent those of their affiliated organizations, or those of the publisher, the editors and the reviewers. Any product that may be evaluated in this article, or claim that may be made by its manufacturer, is not guaranteed or endorsed by the publisher.

frontiers in Cardiovascular Medicine

ORIGINAL RESEARCH
published: 22 March 2022
doi: 10.3389/fcvm.2022.824657

Ginsenoside Rg2 Ameliorates Myocardial Ischemia/Reperfusion Injury by Regulating TAK1 to Inhibit Necroptosis

Yao Li[1], Hao Hao[2], Haozhen Yu[3], Lu Yu[4], Heng Ma[2]* and Haitao Zhang[1,5]**

[1] Clinical Medical College of Air Force, Anhui Medical University, Hefei, China, [2] Department of Pathology and Pathophysiology, School of Basic Medical Sciences, Fourth Military Medical University, Xi'an, China, [3] School of Basic Medical Sciences, Shaanxi University of Chinese Medicine, Xianyang, China, [4] Department of Pathology, Xijing Hospital, Fourth Military Medical University, Xi'an, China, [5] Department of Cardiology, PLA Air Force Medical Center, Beijing, China

OPEN ACCESS

Edited by:
Anindita Das, Virginia Commonwealth University, United States

Reviewed by:
Abhinav Diwan, Washington University in St. Louis, United States
Jun Ren, University of Washington, United States

***Correspondence:**
Haitao Zhang
kjzht@sina.com
Heng Ma
hengma@fmmu.edu.cn
Lu Yu
yulu@fmmu.edu.cn

Specialty section:
This article was submitted to General Cardiovascular Medicine, a section of the journal Frontiers in Cardiovascular Medicine

Received: *29 November 2021*
Accepted: *11 February 2022*
Published: *22 March 2022*

Citation:
Li Y, Hao H, Yu H, Yu L, Ma H and Zhang H (2022) Ginsenoside Rg2 Ameliorates Myocardial Ischemia/Reperfusion Injury by Regulating TAK1 to Inhibit Necroptosis. Front. Cardiovasc. Med. 9:824657. doi: 10.3389/fcvm.2022.824657

Necroptosis contribute to the pathogenesis of myocardial ischemia/reperfusion (MI/R) injury. Ginsenoside Rg2 has been reported to have cardioprotective effects against MI/R injury; however, the underlying mechanism remains unclear. This work aimed to investigate the effect of ginsenoside Rg2 on necroptosis induced by MI/R and to explore the mechanism. In this study, hypoxia/reoxygenation (H/R) injury model was established in H9c2 cells. *In vivo*, male C57/BL6 mice were subjected to myocardial ischemia 30 min/reperfusion 4 h. Rg2 (50 mg/kg) or vehicle was intravenously infused 5 min before reperfusion. Cardiac function and the signaling pathway involved in necroptosis were investigated. Compared with H/R group, Rg2 significantly inhibited H/R-induced cardiomyocyte death. Rg2 treatment effectively inhibited the phosphorylation of RIP1, RIP3, and MLKL in H/R cardiomyocytes, and inhibited RIP1/RIP3 complex (necrosome) formation. In mice, Rg2 treatment manifested significantly lower ischemia/reperfusion (I/R)-induced myocardial necroptosis, as evidenced by decrease in phosphorylation of RIP1, RIP3, and MLKL, inhibited lactate dehydrogenase (LDH) release and Evans blue dye (EBD) penetration. Mechanically, an increased level of tumor necrosis factor α (TNFα), interleukin (IL)-1β, IL-6, and MCP-1 were found in MI/R hearts, and Rg2 treatment significantly inhibit the expression of these factors. We found that TNFα-induced phosphorylation of RIP1, RIP3, and MLKL was negatively correlated with transforming growth factor-activated kinase 1 (TAK1) phosphorylation, and inhibition of TAK1 phosphorylation led to necroptosis enhancement. More importantly, Rg2 treatment significantly increased TAK1 phosphorylation, enhanced TAK1 binding to RIP1 while inhibiting RIP1/RIP3 complex, ultimately reducing MI/R-induced necroptosis. These findings highlight a new mechanism of Rg2-induced cardioprotection: reducing the formation of RIP1/RIP3 necrosome by regulating TAK1 phosphorylation to block necroptosis induced by MI/R.

Keywords: myocardial ischemia/reperfusion, necroptosis, ginsenoside Rg2, transforming growth factor β activated kinase 1, cardioprotection and ischemia-reperfusion injury

INTRODUCTION

As terminally differentiated cells, cardiomyocytes have highly limited ability to regenerate. Excessive death of cardiomyocytes induced by injury stress and their pathological effects leads to a variety of cardiovascular diseases, such as myocardial infarction (MI), malignant arrhythmia, heart failure (HF), and sudden cardiac death (1). Ischemic heart disease (IHD) is the leading cause of death and disability worldwide (2). The best way to prevent myocardial ischemic injury is to restore myocardial blood flow, i.e., reperfusion. However, reperfusion elicits further damage to the heart, which is called myocardial ischemia/reperfusion (MI/R) injury. Therefore, elucidating the mechanism of cardiomyocyte death and determining the intervention measures are of great significance for the prevention and treatment of IHD.

In the past, most of the studies on cardiomyocyte death focused on apoptosis, which is usually considered as programmed cell death. Necrosis is initial considered to be an unregulated process. In 1988, studies pointed out that tumor necrosis factor α (TNFα) can trigger a kind of cell death with necrotic morphological features (3). With the discovery of necroptosis by Degterev et al. (4), death receptor stimulation under the condition of apoptosis defect (i.e., caspase inhibition) can still trigger cell death with morphological features of necrosis in some cell types, which supported the existence of programmed cell death and provided a new mechanism for the intervention of cell death. Necroptosis, a regulated form of necrosis, is mediated by death receptors such as tumor necrosis factor receptor 1(TNFR1), and is executed through the induction of the RIP1–RIP3 necroptotic complex (5). As a death receptor-mediated caspase-independent cell death model, necroptosis has further completed cell death mechanism theory. Meanwhile, necroptosis inhibitors showed significant preventive and therapeutic effects in a variety of stress injury models, indicating that blocking necroptosis may become a new strategy for the prevention and treatment of stress-related injuries. Necroptosis plays an important role in IHD. It has been reported that RIP3 knockout or the use of Necrostatin-1 (RIP1 inhibitor) can significantly improve MI/R injury, which confirmed that inhibition of necroptosis is an effective cardioprotection against MI/R injury (6, 7).

Ginsenosides are the main components of ginseng, which exert a variety of pharmacological effects, such as vasodilation, anti-tumor, anti-diabetes, anti-inflammation, anti-oxidation, and so on. Ginsenoside Rg2 is one of the compounds in the protopanaxatriol group (8). Studies have shown that Rg2 can significantly improve myocardial ischemia injury and reduce MI area by increasing myocardial oxygen utilization, enhancing superoxide dismutase (SOD), scavenging free radicals, and so on. Rg2 can increase the mRNA expression of endothelial nitric oxide synthase gene (eNOS), which is also studied in ginsenoside Rb1 and Re (9) protect cardiomyocytes, reduce the content of malondialdehyde (MDA), the metabolite of lipid peroxidation, and reduce MI (10). Previous studies have reported that ginsenoside Rg2 has a protective effect on hydrogen peroxide-induced cardiomyocyte injury and apoptosis in rats (11, 12). Rg2 with a variety of biological activities and pharmacological effects, has the potential value for the treatment of cardiovascular diseases. However, whether Rg2 can inhibit myocardial necroptosis during MI/R and the underlying mechanism remains unknown.

Transforming growth factor-activated kinase 1 (TAK1, also known as map3k7), as a node regulator of apoptosis and necrosis, plays an important role in regulating the formation of RIP1–FADD–Caspase8 and RIP1–RIP3 necrotic complex (13). Studies have shown that TAK1 phosphorylation is essential to the interaction of RIP1 and TAK1. At the same time, TAK1 phosphorylation can also block the formation of RIP1–FADD–Caspase8 cell death complex induced by TNF receptor (14). There is a potential regulatory relationship between TAK1 and RIP1, and RIP3 is involved in the necroptosis-related pathway. The relationship between Rg2, TAK1, and necroptosis in MI/R settings has never been determined *in vivo*.

Here, we demonstrated that Rg2 treatment promotes the phosphorylation of TAK1 and enhances its binding to RIP1, thereby inhibiting the RIP1/RIP3 complex formation, and ultimately preventing MI/R-induced necroptosis.

MATERIALS AND METHODS

Animals

All animal experiments were approved by the Animal Ethical Experimentation Committee of the Fourth Military Medical University. Male C57BL/6 mice at age of 12 weeks weighting 22–25 g were used. All animals were breed with regular pellet diets *ad libitum* in conventional facility on conditions of 12:12-h light/dark cycle.

Materials

Evans blue was purchased from Sigma-Aldrich (St. Louis, MO, United States). The antibody against RIP1 (3493), RIP3 (95702), MLKL (37705), phosphor-MLKL (91689), phosphor-RIP1 (31122), phosphor-TAK1 (9339S), TAK1 (5206S), and β-tubulin (15115) were obtained from Cell Signaling Technology (Beverly, MA, United States), phosphor-RIP3 (AF7443) were obtained from Affinity. TNF-α was purchased from Novoprotein and caveolin 3 (CaV3) (ab2912) was obtained from Abcam (Cambridge, MA, United States). The level of serum lactate dehydrogenase (LDH) was detected by the kit purchased from Genesource.

Cells Culture and Treatment

The H9c2 cells were cultured in Dulbecco's modified Eagle's medium (DMEM) with 10% fetal bovine serum and 1% Penicillin–Streptomycin Solution. To establish the hypoxia-reoxygenation cell model *in vitro*, the cells were added DMEM without sugar and serum upon reaching 70–80% confluence, and then were placed in an anoxic box, and replaced the air in the anoxic chamber with 95% N_2, 5% CO_2 mixed gas until the oxygen concentration was less than 1%, and cultured in the incubator at 37°C for 9 h (15). After the hypoxia, time was reached; the cells were replaced with high glucose DMEM medium (complete

medium) and treated with Rg2. Finally, the cells were cultured and incubate at 37°C 5% CO_2, respectively, for 2 h.

Cell Counting Kit-8 Assay

Cell viability was detected using a Cell Counting Kit-8 (CCK8) assay. H9c2 cells were cultured in 96-well plates at about 2×10^4/well. After incubating in 5% CO_2 incubator at 37°C for 1 h, CCK8 assay solution (10 μl) contained water-soluble tetrazolium salt (WST8) was then added to each well and the cells were incubated for 1 h. The optical density of each well was measured using a microplate reader at 450 nm.

Detection of Lactate Dehydrogenase

Lactate dehydrogenase determination kit (rate method) produced by Shanghai Kean Science and Technology Company uses continuous monitoring method to determine the activity of LDH, liquid A and liquid B are mixed into working reagent according to the ratio of 1:5. *In vitro*, the supernatant culture medium 40 μl after H/R added with 200 μl working reagent was ready to detect relative LDH release. *In vivo*, blood samples were collected from control and MI/R (30 min ischemia/4 h reperfusion) mice subjected to vehicle or Rg2 and centrifuged for 10 min at 3,000 r.p.m. to obtain serum. The serum 2 μl plus 38 μl double distilled water and then the working reagent of 200 μl was added to detect.

Establishment of Myocardial Ischemia/Reperfusion Model in Mice

The procedure of MI/R injury model was built as previously described (15). In short, animals were anesthetized with pentobarbital (65 mg/kg, i.p.). After tracheostomy, ventilation was sustained on the Harvard rodent respirator. A left thoracic incision was performed, and the left anterior descending coronary artery was blocked by placing a 7-0 silk suture slipknot. The slipknot was released after 30 min. Reperfusion was sustained for 4 h in acute ischemia/reperfusion (I/R) injury (for western blot analysis, immunohistochemistry). Electrocardiogram was connected to monitor ST-segment changes during ischemia period. Rg2 (50 mg/kg) or vehicle was administered to mice randomly *via* caudal tail injection 5 min before reperfusion (16), then obtained the heart and picked up the white infarct zone for western blotting.

Myocardial Necroptosis Measurement

Mice were injected intraperitoneally Evans blue dye (EBD) dissolved in saline (10 mg/ml) 12 h before MI/R operation. The heart was excised to separate the ventricular myocardium, then embedded it in optimal cutting temperature (OCT) compound, and immediately froze it in liquid nitrogen, finally cut into 5 μm cryosections. The Cav-3 antibody was performed to label viable cardiomyocytes while EBD-labeled necroptosis as previously described (15). The image was pictured by a fluorescence microscope.

Immunohistochemistry Analysis of TNFα

The heart was obtained in control, MI/R (30 min ischemia/2 h reperfusion) group and MI/R + Rg2 group, fixed in 4% paraformaldehyde for 24 h and embedded in paraffin. The tissue was cut into 5 μm slices, and incubated with TNF-α antibody overnight at 4°C, then the second antibody was incubated at 37°C for 1 h, finally observed under microscope.

Echocardiographic Measurement and Infarct Size

Ejection fraction (EF) and fractional shortening (FS) were measured as previously described (15). To evaluate the extent of myocardial necrosis hearts were excised and stained 3 days after MI/R induction. Hearts were sectioned into 1-mm slices and imaged using a Leica microscope. Viable cardiac tissue in the ischemic area was red-stained with 2,3,5-triphenyltetrazolium (TTC) and myocardium in non-ischemic area was blue-stained with the Evan's blue, and infarcted tissues were white or light yellow. The infarct size was calculated as infarct area divided by area at risk (IF/AAR) (17).

Enzyme-Linked Immunosorbent Assay

Serum levels of TNFα were measured in control and MI/R (30 min ischemia/2 h reperfusion) mice subjected to vehicle or Rg2 according to instructions (Beyotime.PT512).

Western Blot

Total protein was extracted quantitatively, and separated by 10% sodium dodecyl sulfate polyacrylamide gel electrophoresis (SDS-PAGE) (30 g/lane), then transferred to PVDF membrane. The membranes were blocked with 5% slim milk with TBST and incubated with the primary antibody at 4°C overnight, then washed with TBST and incubated with second antibody for 1 h at room temperature. β-tubulin was used as the loading control.

Statistical Analysis

Quantitative data were analyzed by Prism 8.0, and were expressed as mean ± SEM. double-tailed unpaired Student's *t*-test and one-way ANOVA with Turkey's test correction were applied to analyze significance between two groups, statistical significance was considered at $p < 0.05$.

RESULTS

Rg2 Inhibits Hypoxia/Reoxygenation-Induced Cardiomyocytes Death

By observing the effect of Rg2 concentration on cell survival rate by CCK8 assay, the results showed that Rg2 at a concentration of 1–10 μM has no effect on survival rate of H9c2, although an excessively high concentration of Rg2 (20–100 μM) will inhibit cell survival (**Figure 1A**). Next, to determine cell viability after H/R treatment, after hypoxia for 9 h, H9c2 cell viability was determined after various exposure times to reoxygenation time (1, 2, 3, 4, 5, and 6 h). The results showed that the cell survival rate decreased significantly at 3 h of reoxygenation (50.6 ± 2.5%) (**Figure 1B**). Therefore, a direct effect of Rg2 on H/R cardiomyocytes was assessed. H9c2 cardiomyocytes were

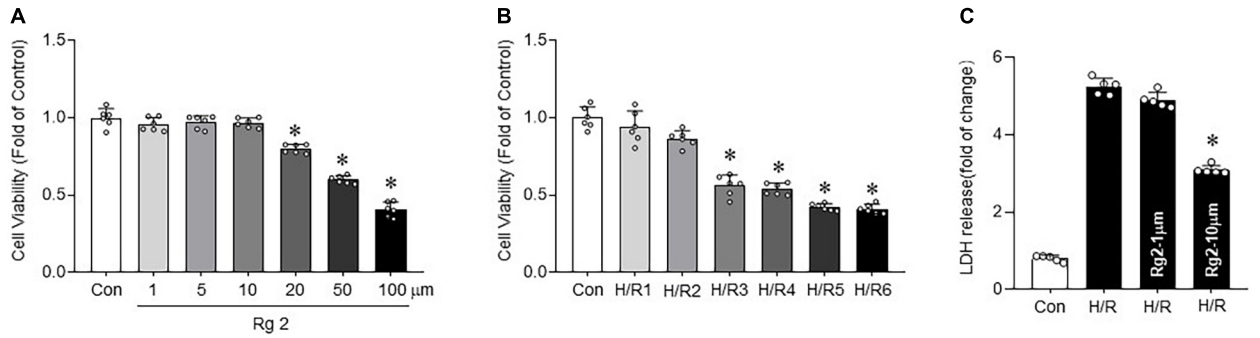

FIGURE 1 | The Rg2 inhibits hypoxia/reoxygenation (H/R)-induced cardiomyocytes death. **(A)** The effect of gradient concentration of Rg2 (1, 5, 10, 20, 50, and 100 μM) on the viability of cardiomyocytes was detected by cell counting kit-8 (CCK8). **(B)** The effect of 1, 2, 3, 4, 5, and 6 h reoxygenation time after hypoxia 9 h on the viability of H9C2 cells was detected by CCK8. **(C)** Cell injury as assessed by LDH release after H/R (hypoxia 9 h and reoxygenation 3 h) with Rg2 treatment (1 and 10 μM). The values are the means ± SEM, $n = 6$ per group, $^*p < 0.05$ vs. the control group.

treated with 1 and 10 μM Rg2 under hypoxia 9 h followed by reoxygenation 3 h. The results revealed that H/R treatment significantly increased H9c2 cell death evidenced by LDH release, while Rg2 administration significantly inhibited H/R-induced cardiomyocytes death in a dose-dependent manner (**Figure 1C**). In subsequent H/R experiments, hypoxia 9 h followed by reoxygenation 3 h is used. The results showed that Rg2 inhibits H/R-induced cardiomyocytes death.

Rg2 Inhibits Hypoxia/Reoxygenation-Induced Cardiomyocytes Necroptosis

To determine whether there is a relationship between Rg2 and H/R-induced necroptosis in cardiomyocytes, RIP1, RIP3, and MLKL phosphorylation was determined. Compared with the control group, H/R significantly increased the RIP1, RIP3, and MLKL phosphorylation (**Figures 2A–D**) combined with increased LDH release (**Figure 2E**), suggesting activation of necroptotic pathway. Treatment with 10 μM Rg2 effectively inhibited H/R-induced necroptosis, as evidenced by reduced RIP1, RIP3, and MLKL phosphorylation and LDH release. Co-immunoprecipitation assays revealed that H/R-induced cardiac RIP1–RIP3 interaction was suppressed by Rg2 treatment (**Figure 2F**), which was similar to the effect of Nec-1 (a pharmacological inhibitor of RIP1 that blocks the RIP1–RIP3 interaction and inhibits necroptosis (18)). The above results confirmed that ginsenoside Rg2 can effectively inhibit H/R-induced cardiomyocytes necroptosis.

Rg2 Attenuates Myocardial Ischemia/Reperfusion-Induced Necroptosis

To further explore the effect of Rg2 on MI/R injury *in vivo*, mice were subjected to 30 min ischemia followed by 4 h or 4 weeks reperfusion *in vivo* with vehicle or Rg2 treatment. The results demonstrated that Rg2 markedly reduced the I/R-induced myocardial infarct size to the area at risk, although the groups had comparable areas at risk (**Supplementary Figure 1A**). Furthermore, MI/R-induced (30 min ischemia/4 week reperfusion) cardiac contractile dysfunction (as indicated by decreases in EF) was rescued by Rg2 treatment (**Figure 3A**). We found that MI/R-induced (30 min ischemia/4 h reperfusion) cardiac necroptosis was markedly suppressed by Rg2 treatment, as evidenced by reductions in EBD penetration (**Figure 3B**) and LDH release (**Figure 3C**) in hearts. Accordingly, MI/R-induced myocardial RIP1, RIP3, and MLKL phosphorylation were effectively inhibited by Rg2 (**Figures 3D–G**). Thus, the *in vivo* data indicated that Rg2 attenuates MI/R-induced necroptosis.

Rg2 Reduces TNFα and Ameliorates Myocardial Inflammation

Evidence shows that TNFα-induced necroptosis was involved in MI/R injury, myocardial TNFα level, and associated inflammatory factors were detected in MI/R (30 min ischemia/2 h reperfusion) myocardium. Myocardial TNFα level was markedly increased by MI/R injury, which was effectively mitigated by Rg2, as evidenced by enhanced TNFα IHC staining (**Figure 4A**), which is collaborated with plasma TNFα level (**Figure 4B**). Furthermore, Rg2 treatment significantly inhibited the MI/R induced increase in TNFα, IL-1 β, IL-6, and MCP-1 mRNA levels (**Figure 4C**), indicating that ginsenoside Rg2 can inhibit the activation of myocardial inflammation-related pathways induced by MI/R.

Inhibition of Transforming Growth Factor-Activated Kinase 1 Phosphorylation Aggravates TNFα-Induced Necroptosis

In order to further clarify how Rg2 regulates TNFα-induced necroptosis, H9c2 cardiomyocytes were stimulated by TNFα (10 ng/ml) to induce necroptosis. The results showed that 2 h after TNFα exposure, the RIP1 and RIP3 phosphorylation levels increased significantly (**Figure 5A**) associated with increased cell death (**Figure 5F**), while the phosphorylation of TAK1 decreased (**Figure 5A**), suggesting a negative relationship between the two. Furthermore, pre-treatment with 5Z-7-OX (2 μM, 1 h), a TAK1 phosphorylation inhibitor (19, 20), followed by TNFα exposure 2 h further enhanced the TNFα-induced RIP1, RIP3, and MLKL

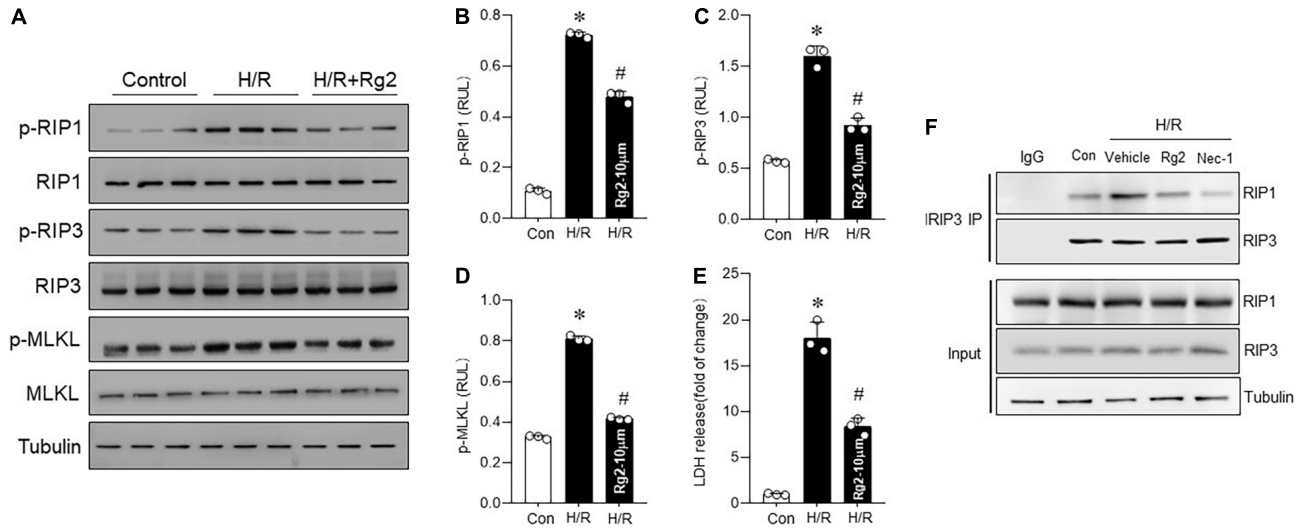

FIGURE 2 | The Rg2 inhibits H/R-induced cardiomyocytes necroptosis. **(A)** Representative western blots in control, H/R group, and H/R + Rg2 group. **(B)** The averaged data for p-RIP1 level. **(C)** The averaged data for p-RIP3 level. **(D)** The averaged data for p-MLKL level. **(E)** Lactate dehydrogenase (LDH) release was detected to assess cardiomyocytes injury. **(F)** The Co-IP was conducted to detect the formation of RIP1/RIP3 necrosome. The values are the means ± SEM, $n = 3$ per group, $^*p < 0.05$ vs. the control group, $\#p < 0.05$ vs. the H/R group.

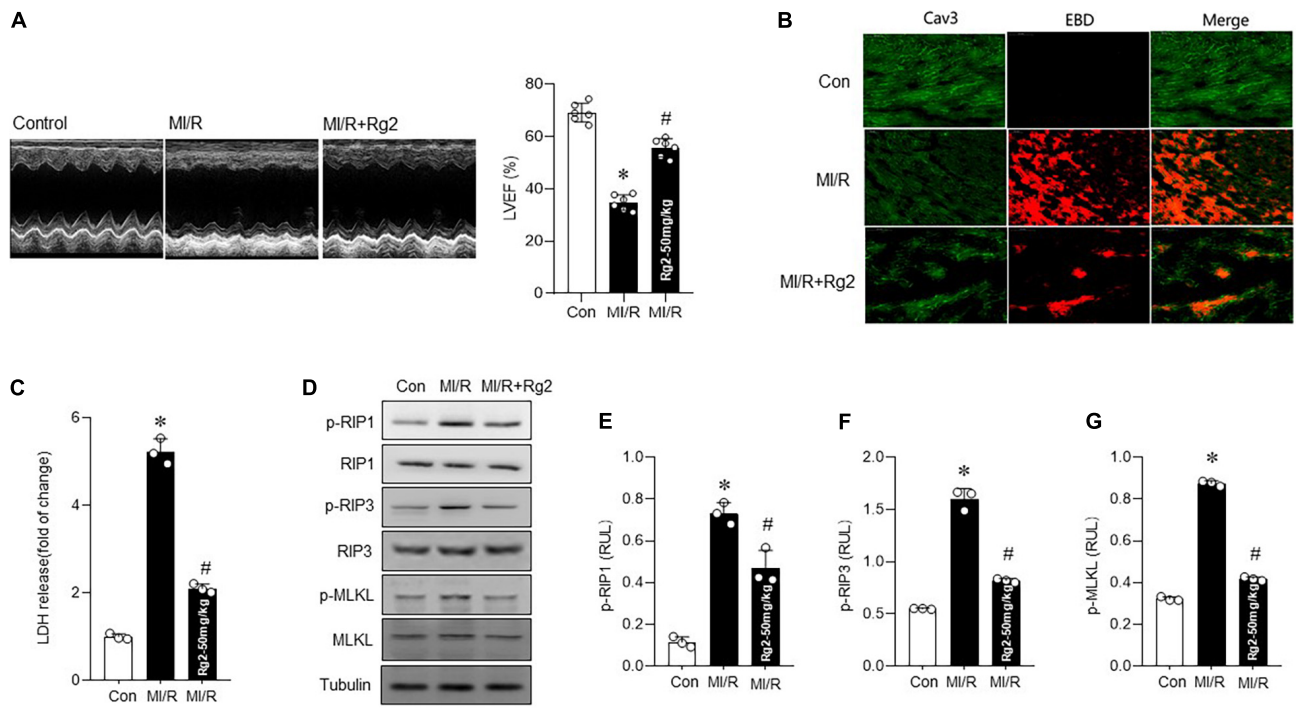

FIGURE 3 | The Rg2 attenuates myocardial ischemia/reperfusion (MI/R) *in vivo* induced necroptosis. **(A)** Representative echocardiographic images in control and MI/R (30 min ischemia/4 weeks reperfusion) subjected to vehicle or Rg2. Left ventricular ejection fraction (EF) (LVEF)% was measured. **(B)** Representative photomicrographs from myocardial EBD uptake and viable cardiomyocytes labeled by caveolin 3 (CaV3) antibody in control, MI/R (30 min ischemia/4 h reperfusion), and MI/R + Rg2 group. **(C)** Myocardial injury as assessed by LDH release (30 min ischemia/4 h reperfusion). **(D–G)** Representative western blots in control, MI/R (30 min ischemia/4 h reperfusion) group and MI/R + Rg2 group and averaged data for p-RIP1, p-RIP3, and p-MLKL level. The values are the means ± SEM, $n = 6$ per group, $^*p < 0.05$ vs. the control group, $\#p < 0.05$ vs. the MI/R group.

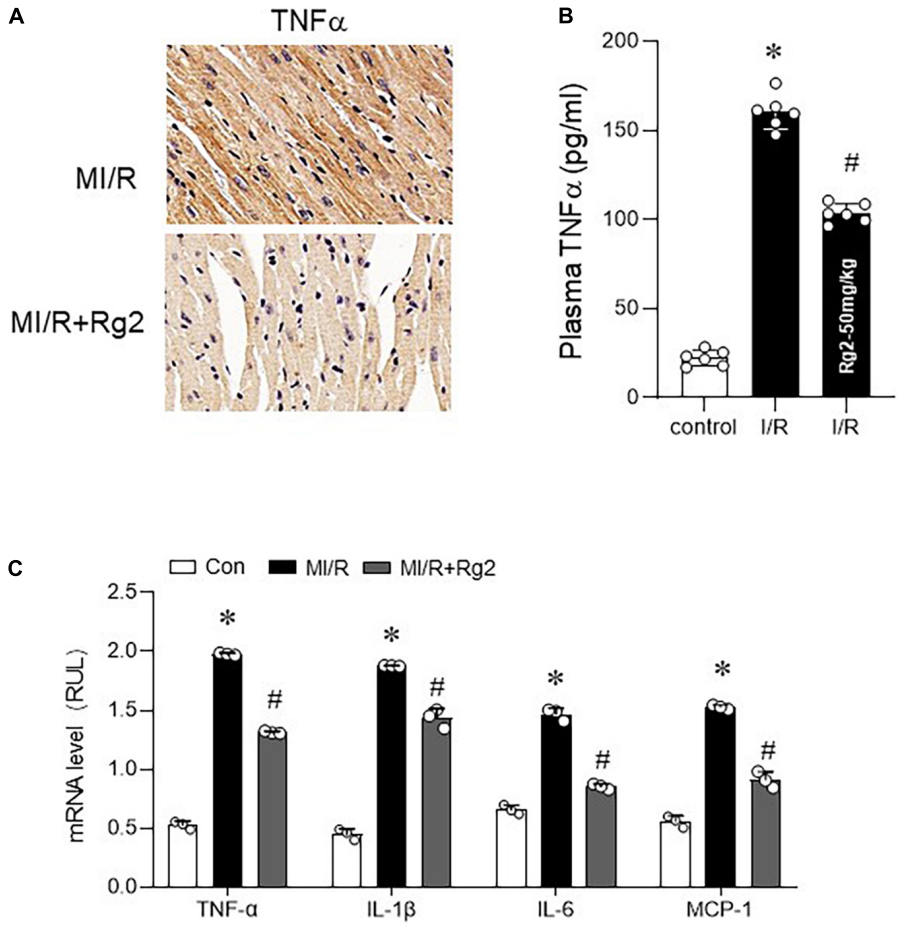

FIGURE 4 | The Rg2 reduces tumor necrosis factor α (TNFα) and ameliorates myocardial inflammation. **(A)** Representative photomicrographs of myocardial TNFα (30 min ischemia/2 h reperfusion) demonstrated by IHC. **(B)** Plasma TNF-α concentration was evaluated after reperfusion for 2 h by ELISA assay. **(C)** The mRNA levels of TNFα, interleukin (IL)-1β, IL-6, and MCP-1 among control, MI/R, and MI/R + Rg2 group (30 min ischemia/2 h reperfusion). The values are the means ± SEM, $n = 3$ per group, $*p < 0.05$ vs. the control group, $\#p < 0.05$ vs. the MI/R group.

phosphorylation (**Figures 5B–E**) and cell death (**Figure 5F**). The above results confirm that inhibition of TAK1 phosphorylation further enhances TNF-induced necroptosis.

Rg2 Enhances Transforming Growth Factor-Activated Kinase 1 Phosphorylation to Inhibit Necroptosis

Based on the above *in vitro* experiments, we further clarify whether Rg2 can regulate myocardial necroptosis through phosphorylation of TAK1. Indeed, TAK1 phosphorylation was markedly decreased in H/R injury H9c2 cells. However, compared with the H/R group, Rg2 effectively enhanced TAK1 phosphorylation (**Figure 6A**). In line with this notion, we also found that, in the TNFα-induced H9c2 necroptosis model, the protective effect of Rg2 can be blocked by 5Z-7-OX, as evidenced by enhanced RIP1, RIP3, MLKL phosphorylation and cell death (**Figures 6B–D**). More importantly, corresponding to the enhancement of TAK1 phosphorylation by Rg2, Co-IP results directly show that Rg2 treatment can enhance the binding ability of TAK with RIP1, and competitively inhibit the RIP1 and RIP3 binding to combine to form Necrosome (**Figure 6E**). The above data confirm that Rg2 inhibits myocardial Necroptosis by enhancing the phosphorylation of TAK1 (**Figure 6F**).

DISCUSSION

Our findings delineate that Rg2 treatment repressed myocardial necroptosis against MI/R injury both *in vitro* and *in vivo*. We have also identified Rg2 treatment effectively inhibited the inflammatory factors production in MI/R hearts, among which TNFα is an important factor in inducing necroptosis. The results of this study indicate that TAK1 phosphorylation leads to necroptosis inhibition. Rg2 enhanced TAK1 phosphorylation inhibits the RIP1 and RIP3 combination, and also inhibits myocardial necroptosis signal activation, and ultimately reduces MI/R injury. Our research provides new insights into the cardioprotective mechanism of Rg2.

In the past, most studies have focused on cardiomyocyte apoptosis, and it is believed that apoptosis is the only regulated form of cell death. However, necrosis, as the main

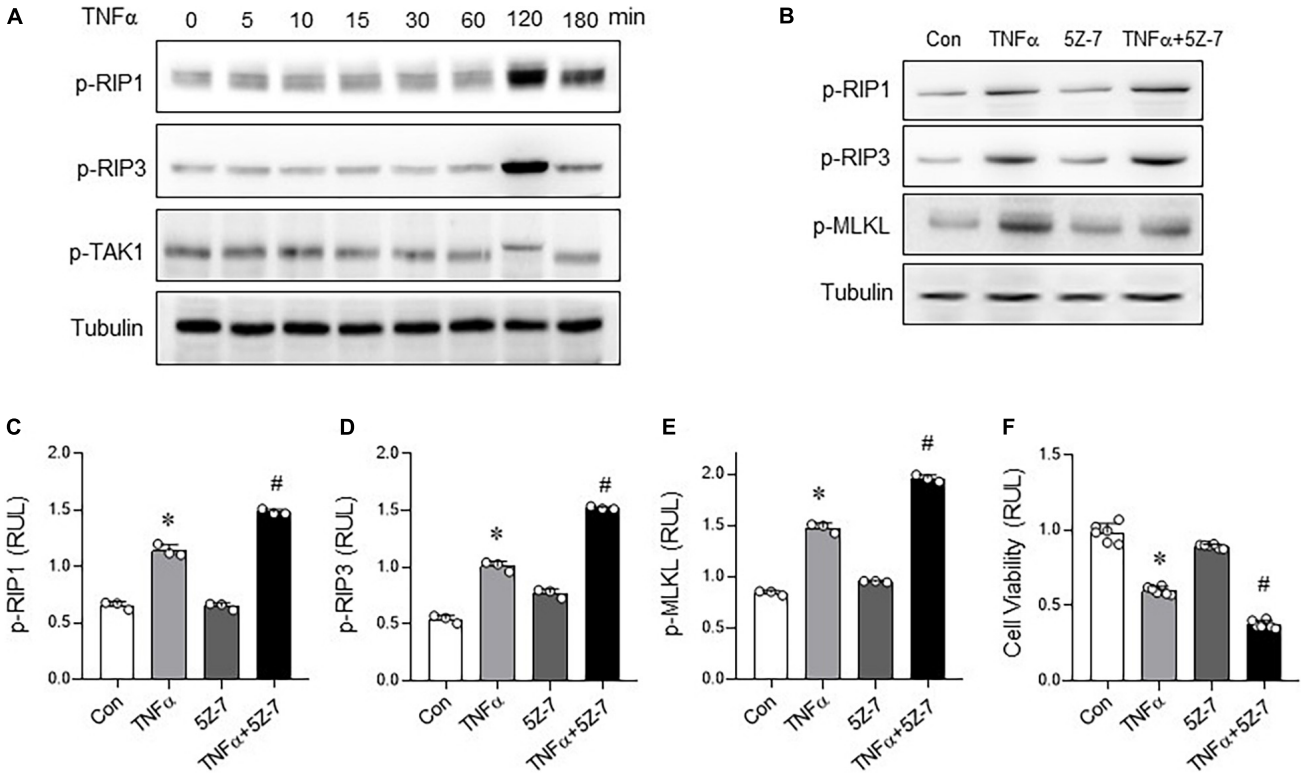

FIGURE 5 | Inhibition of transforming growth factor activated kinase 1 (TAK1) phosphorylation aggravates TNFα-induced necroptosis. **(A)** Levels of p-RIP1, p-RIP3, and p-TAK1 in H9C2 cells with different treatment time of TNFα (10 ng/ml). **(B)** Levels of p-RIP1, p-RIP3, and p-MLKL in H9c2 cells treated with TNF-α (10 ng/ml, 2 h) with or without 5Z-7-OX (TAK1 inhibitor, 2 μM, pre-treatment 1 h) were detected by western blots. **(C–E)** p-RIP1, p-RIP3 and p-MLKL relative levels in H9c2 cells treated with TNF-α with or without 5Z-7-OX. **(F)** Cell viability was assessed by CCK8. The values are the means ± SEM, $n = 3$ or 6 per group, $^{*}p < 0.05$ vs. the control group, $\#p < 0.05$ vs. the TNFα group.

pathological feature of various cardiac pathological conditions, has been completely ignored. Necrosis is considered to be an uncontrollable and passive mode of death. However, this view has since been challenged (21, 22). According to genetic and biochemical analysis, depending on the death initiating stimulus, necrosis is orchestrated and executed by appropriate mechanisms, rather than simply representing a disorganized breakdown of the cell. Nowadays, many studies have proved that necrosis also occurs in a regulated way and is closely related to the physiology and pathology in many organs, including the heart. As a regulated cell death form, necroptosis usually shows necrotic morphological characteristics depending on the interaction of RIP1, RIP3, and MLKL. Myocardial necroptosis can be activated by myocardial I/R, and the goal of treating myocardial I/R injury is to save ischemic myocardium, that is, to reduce myocardial cell death and reduce infarct size. Therefore, it is of important clinical and basic research significance to further clarify the potential mechanism of myocardial necroptosis in myocardial I/R injury and to find effective prevention and treatment strategies. Death receptor ligands such as TNF receptors can trigger a variety of cell responses, such as cell survival, apoptosis, and necrosis, depending on the type of cell stimulation (13). TNFR1 ligand binding leads to plasma membrane binding signal complex, called complex I, which consists of TNF receptor associated with death domain protein (TRADD), TNF receptor associated protein 2 (TRAF2), RIP1 and apoptosis inhibitor protein 1 and 2 (cIAP1 and cIAP2). Complex I recruits and activates the complex of TAK1 and I-receptor kinase (IKK), which leads to the activation of NFκB, which drives the transcription of pro-survival genes. Under certain conditions, complex I was disassociated from the membrane and transformed into an apoptosis-inducing complex, called complex II, and further recruited FADD (Fas-related protein and death domain) and caspase8. In addition, a complex composed of RIP1 and RIP3 (called necrosome) can be induced, which is very important for the initiation of necroptosis (23). Although some progress has been made recently, the precise molecular mechanisms that determine different cellular biological modes responding to TNFR1 have not been fully elucidated. In this study, it was found that Rg2 could inhibit myocardial necroptosis induced by TNF-α in myocardium subjected to I/R injury, promote the TAK1 phosphorylation and alleviate myocardial I/R injury.

Ginsenosides are the main components of Panax ginseng. Previous studies have shown that ginsenosides have myocardial protective effects. However, the potential mechanism of different types of ginsenosides on myocardial I/R injury remains unclear, which limits its clinical application. Ginsenoside Rg2 belongs to protopanaxatriol compounds. It has the effects of anti-tumor,

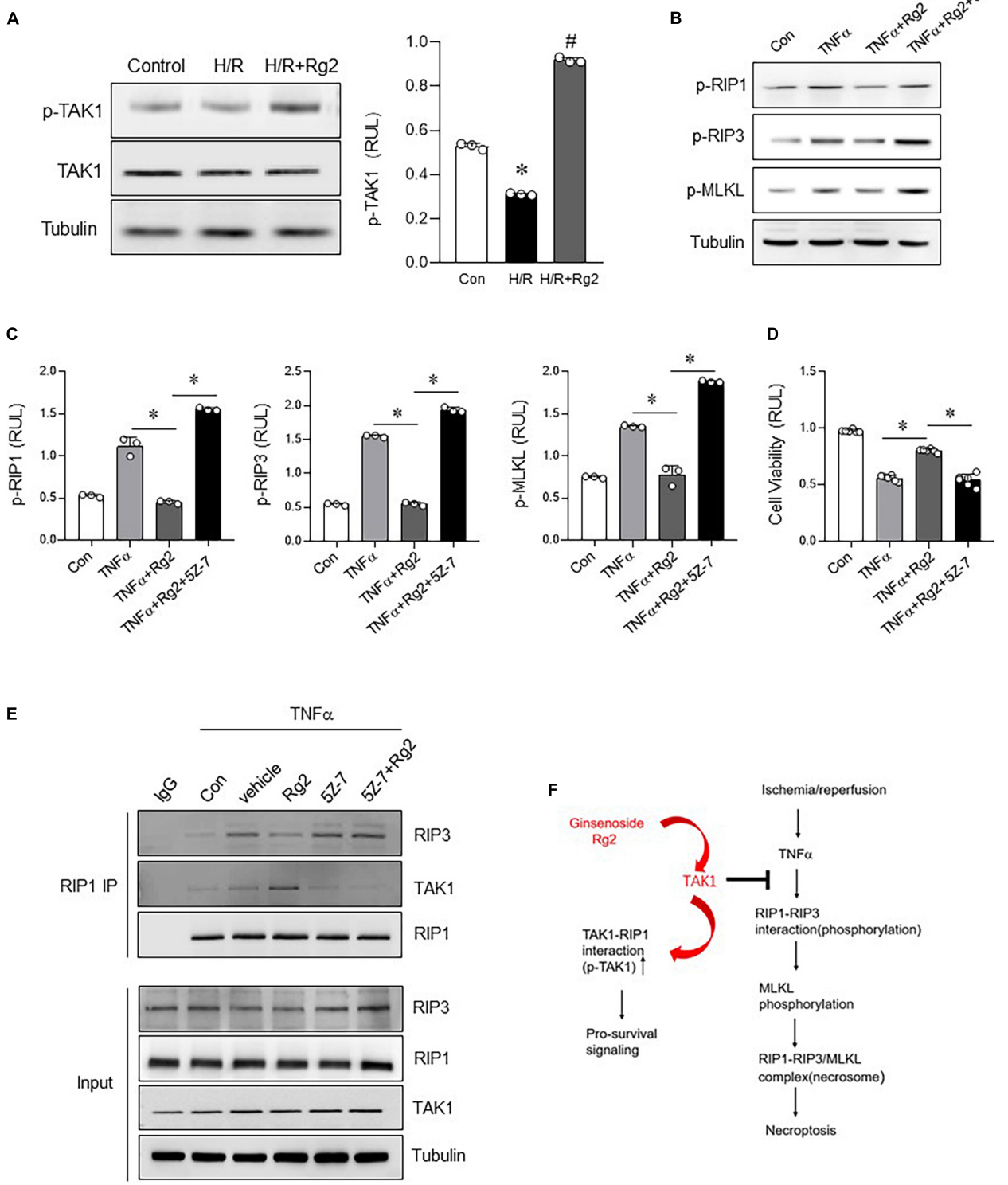

FIGURE 6 | The Rg2 enhances TAK1 phosphorylation to inhibit necroptosis. **(A)** Levels of p-TAK1 and TAK1 in H/R with or without Rg2-treated H9c2 cells was detected by western blots. **(B)** Levels of p-RIP1, p-RIP3, and p-MLKL in H9c2 cells treated with TNF-α with or without Rg2 and 5Z-7-OX were detected by western blots. **(C)** Relative levels of p-RIP1, p-RIP3, and p-MLKL. **(D)** Cell viability was assessed by CCK8. **(E)** Co-IP was performed to detect the interaction between RIP1 and RIP3 or TAK1 in H9c2 cells treated with TNF-α with or without Rg2 and 5Z-7-OX. **(F)** Summary of this study. The values are the means ± SEM, $n = 3$ or 6 per group, $^*p < 0.05$ vs. the TNFα or TNFα + Rg2 group.

anti-diabetes, anti-inflammation, anti-oxidation, and so on. Related studies have shown that Rg2 can inhibit cell apoptosis by activating SIRT1 and activating PI3K/AKT pathway, and has a protective effect on myocardial I/R injury in rats (11). However, about 70% of the cardiomyocytes death induced by H/R cannot be inhibited by zVAD (pan-caspase inhibitor), indicating that the cell death induced by H/R is mainly mediated by necrosis, and this kind of necrosis can be regulated (15, 24). However, it has not been reported whether ginsenoside Rg2 has regulatory effect on necroptosis, the dominant cell death in myocardium subjected to I/R. The study confirmed that ginsenoside Rg2 had obvious inhibitory effect on MI/R-induced necroptosis both *in vivo* and *in vitro*, and could attenuate myocardial inflammation, which further clarified the myocardial protective mechanism of Rg2 and provided a theoretical basis for the clinical application of Rg2.

Transforming growth factor activated kinase 1 is essential for regulating many important biological processes, such as immune cell activation, inflammation, cell differentiation, and cardiac hypertrophy. Previous studies have reported the role of TAK1 in regulating cardiomyocyte apoptosis and necroptosis (25). TAK1 regulates and maintains myocardial homeostasis and prevents cardiac remodeling by controlling cardiac programmed cell death (26, 27). Cardiac specific knockout of TAK1 induces spontaneous apoptosis and necroptosis of cardiomyocytes, followed by poor remodeling and heart failure (13). The related studies have reported that TAK1 plays a role in cardiotoxicity induced by DOX. The expression of TAK1 is decreased in cardiotoxicity induced by DOX *in vivo* and *in vitro*, and TAK1 inhibition by TAK1 phosphorylation inhibitor 5Z-7-OX would further aggravate cardiomyocyte apoptosis and necroptosis induced by DOX (28). TAK1 phosphorylation is very important for its catalytic activity (29). Previous studies have shown that the inactivation of TAK1 in cardiomyocytes eliminates the phosphorylation of c-Jun-N-terminal kinase (JNK) induced by TNFα and the degradation of IKκB, thus inhibiting the activation of JNK and NFκB pathway, indicating that TAK1 phosphorylation is essential for the activation of pro-survival pathway induced by TNFα (13). And the study initially targeting TAK1 phosphorylation was performed on non-alcoholic fatty liver disease (NAFLD) (30). At present, related studies have revealed the biological role of TAK1 in regulating myocardial survival/death and cardiac homeostasis. However, the protective mechanism of TAK1 has not been determined yet. In this study, it confirmed that there was an antagonistic relationship between TNFα-induced necroptosis and TAK1 phosphorylation. Rg2 could play a cardioprotective role *via* enhancing the phosphorylation of TAK1, and promote the interaction between TAK1 and RIP1. Thus, Rg2 prevents the formation of RIP1/RIP3 necrosome inhibiting necroptosis. This study suggests a new mechanism of cardioprotection for Rg2 and further reveals the role of TAK1 phosphorylation in regulating TNFα-induced myocardial necroptosis. However, whether Rg2 promotes TAK1 phosphorylation directly or indirectly to inhibit necroptosis needs to be further studied. In addition to TAK1 phosphorylation, whether it is related to other modifications, such as ubiquitin, TAK1 as a molecular switch of programmed cell death, whether the activation time of TAK1 phosphorylation will alter its inhibitory effect on necroptosis, such as whether hyperphosphorylation will reverse the inhibitory effect of necroptosis. These problems need to be further discussed. Some studies have shown that regulator of G protein signaling 5 (RGS5) can directly interact with TAK1 to inhibit its hyperphosphorylation and thus inhibit c-JNK/P38 signaling pathway, thus effectively alleviating the progression of NAFLD (31). Meanwhile, RGS5 can inhibit cardiomyocyte apoptosis in myocardial I/R injury (30). However, whether the protective mechanism of Rg2 in I/R myocardial necroptosis induced by TNFα *via* regulating TAK1 is related to the activation of RGS5 and the interaction between RIP1-TAK1-RGS5 remains to be further elucidated. In addition, due to the limitations of the H9c2 cell line, more *in vitro* experiments are needed to determine the generality of our findings, such as using the human-induced Pluripotent Stem Cell derived cardiomyocytes (hiPSC-CMs).

CONCLUSION

In conclusion, based on *in vivo* and *in vitro* experiments, the study demonstrates that TAK1 phosphorylation plays an important role in regulating myocardial necroptosis induced by TNFα. Rg2 enhances TAK1 phosphorylation to inhibit necroptosis. This research is important in furthering our understanding of Ginsenoside-induced cardioprotection.

DATA AVAILABILITY STATEMENT

The original contributions presented in the study are included in the article/**Supplementary Material**, further inquiries can be directed to the corresponding authors.

ETHICS STATEMENT

The animal study was reviewed and approved by the Animal Ethical Experimentation Committee of the Fourth Military Medical University. Written informed consent was obtained from the owners for the participation of their animals in this study.

AUTHOR CONTRIBUTIONS

YL, HY, and HH performed the material preparation, data collection, and analysis. LY, HM, and HZ wrote the first draft of the manuscript. All authors commented on previous versions of the manuscript, contributed to the study conception and design, and read and approved the final manuscript.

FUNDING

This work was supported by the following grants: National Natural Science Foundation of China Nos.

82070261, 82170251, and 91749108, the Science and Technology Research and Development Program of Shaanxi Province, China (2018SF-270, 2015KW-050, and 2018SF-101), the Youth Innovation Team of Shaanxi Universities, and "The Thirteenth Five-Year Plan" Momentous Project of PLA (No. AKJ15J003).

SUPPLEMENTARY MATERIAL

The Supplementary Material for this article can be found online at: https://www.frontiersin.org/articles/10.3389/fcvm.2022.824657/full#supplementary-material

REFERENCES

1. Whelan RS, Kaplinskiy V, Kitsis RN. Cell death in the pathogenesis of heart disease: mechanisms and significance. *Annu Rev Physiol.* (2010) 72:19–44. doi: 10.1146/annurev.physiol.010908.163111
2. Orogo AM, Gustafsson AB. Cell death in the myocardium: my heart won't go on. *IUBMB Life.* (2013) 65:651–6. doi: 10.1002/iub.1180
3. Laster SM. Tumor necrosis factor can induce both apoptic and necrotic forms of cell lysis. *J Immunol.* (1988) 141:2629–34.
4. Degterev A, Huang Z, Boyce M, Li Y, Jagtap P, Mizushima N, et al. Chemical inhibitor of nonapoptotic cell death with therapeutic potential for ischemic brain injury. *Nat Chem Biol.* (2005) 1:112–9. doi: 10.1038/nchembio711
5. Nikoletopoulou V, Markaki M, Palikaras K, Tavernarakis N. Crosstalk between apoptosis, necrosis and autophagy. *Biochim Biophys Acta.* (2013) 1833:3448–59. doi: 10.1016/j.bbamcr.2013.06.001
6. Smith CC, Davidson SM, Lim SY, Simpkin JC, Hothersall JS, Yellon DM. Necrostatin: a potentially novel cardioprotective agent? *Cardiovasc Drugs Ther.* (2007) 21:227–33. doi: 10.1007/s10557-007-6035-1
7. Lim SY, Davidson SM, Mocanu MM, Yellon DM, Smith CCT. The cardioprotective effect of necrostatin requires the cyclophilin-D component of the mitochondrial permeability transition pore. *Cardiovasc Drugs Ther.* (2007) 21:467–9. doi: 10.1007/s10557-007-6067-6
8. Li Y, Wang H, Wang R, Lu X, Wang Y, Duan M, et al. Pharmacokinetics, tissue distribution and excretion of saponins after intravenous administration of ShenMai Injection in rats. *J Chromatogr B Analyt Technol Biomed Life Sci.* (2019) 1128:121777. doi: 10.1016/j.jchromb.2019.121777
9. Scott G, Colligan PB, Ren BH, Ren J. Ginsenosides Rb1 and Re decrease cardiac contraction in adult rat ventricular myocytes: role of nitric oxide. *Br J Pharmacol.* (2001) 134:1159–65. doi: 10.1038/sj.bjp.0704377
10. Li X, Xiang N, Wang Z. Ginsenoside Rg2 attenuates myocardial fibrosis and improves cardiac function after myocardial infarction via AKT signaling pathway. *Biosci Biotechnol Biochem.* (2020) 84:2199–206. doi: 10.1080/09168451.2020.1793292
11. Fu W, Sui D, Yu X, Gou D, Zhou Y, Xu H. Protective effects of ginsenoside Rg2 against H2O2-induced injury and apoptosis in H9c2 cells. *Int J Clin Exp Med.* (2015) 8:19938–47.
12. Feng R, Liu J, Wang Z, Zhang J, Cates C, Rousselle T, et al. The structure-activity relationship of ginsenosides on hypoxia-reoxygenation induced apoptosis of cardiomyocytes. *Biochem Biophys Res Commun.* (2017) 494:556–68. doi: 10.1016/j.bbrc.2017.10.056
13. Morioka S, Broglie P, Omori E, Ikeda Y, Takaesu G, Matsumoto K, et al. TAK1 kinase switches cell fate from apoptosis to necrosis following TNF stimulation. *J Cell Biol.* (2014) 204:607–23. doi: 10.1083/jcb.201305070
14. Li L, Chen Y, Doan J, Murray J, Molkentin JD, Liu Q. Transforming growth factor beta-activated kinase 1 signaling pathway critically regulates myocardial survival and remodeling. *Circulation.* (2014) 130:2162–72. doi: 10.1161/CIRCULATIONAHA.114.011195
15. Zhang T, Zhang Y, Cui M, Jin L, Wang Y, Lv F, et al. CaMKII is a RIP3 substrate mediating ischemia- and oxidative stress-induced myocardial necroptosis. *Nat Med.* (2016) 22:175–82. doi: 10.1038/nm.4017
16. Jiang L, Yin X, Chen Y, Chen Y, Jiang W, Zheng H, et al. Proteomic analysis reveals ginsenoside Rb1 attenuates myocardial ischemia/reperfusion injury through inhibiting ROS production from mitochondrial complex I. *Theranostics.* (2021) 11:1703–20. doi: 10.7150/thno.43895
17. Xua H, Yua W, Suna S, Li C, Ren J, Zhang Y, et al. TAX1BP1 protects against myocardial infarction associated cardiac anomalies through inhibition of inflammasomes in a RNF34/MAVS/NLRP3-dependent manner. *Sci Bull.* (2021) 66:1669–83. doi: 10.1016/j.scib.2021.01.030
18. Cao L, Mu W. Necrostatin-1 and necroptosis inhibition: pathophysiology and therapeutic implications. *Pharmacol Res.* (2021) 163:105297. doi: 10.1016/j.phrs.2020.105297
19. Ninomiya-Tsuji J, Kajino T, Ono K, Ohtomo T, Matsumoto M, Shiina M, et al. A resorcylic acid lactone, 5Z-7-oxozeaenol, prevents inflammation by inhibiting the catalytic activity of TAK1 MAPK kinase kinase. *J Biol Chem.* (2003) 278:18485–90. doi: 10.1074/jbc.M207453200
20. Fan Y, Cheng J, Vasudevan SA, Patel RH, Liang L, Xu X, et al. TAK1 inhibitor 5Z-7-oxozeaenol sensitizes neuroblastoma to chemotherapy. *Apoptosis.* (2013) 18:1224–34. doi: 10.1007/s10495-013-0864-0
21. Holler N, Thome M, Zaru R. Fas triggers an alternative, caspase-8-independent cell death pathway using the kinase RIP as effector molecule. *Nat Immunol.* (2000) 1:489–95. doi: 10.1038/82732
22. Tavernarakis KXN, Driscoll M. Necrotic cell death in C. elegans requires the function of calreticulin and regulators of Ca2+ release from the endoplasmic reticulum. *Neuron.* (2001) 31:957–71. doi: 10.1016/s0896-6273(01)00432-9
23. Vandenabeele P, Declercq W, Herreweghe FV. The role of the kinases RIP1 and RIP3 in TNF-induced necrosis. *Cell Death Differ.* (2010) 3:1–8. doi: 10.1126/scisignal.3115re4
24. Kung G, Konstantinidis K, Kitsis RN. Programmed necrosis, not apoptosis, in the heart. *Circ Res.* (2011) 108:1017–36. doi: 10.1161/CIRCRESAHA.110.225730
25. Mihaly SR, Ninomiya-Tsuji J, Morioka S. TAK1 control of cell death. *Cell Death Differ.* (2014) 21:1667–76. doi: 10.1038/cdd.2014.123
26. Zhang D-W, Shao J, Lin J. RIP3, an energy metabolism regulator that switches TNF-induced cell death from apoptosis to necrosis. *Science.* (2009) 325:332–6. doi: 10.11126/science.1172308
27. Liu Q, Busby JC, Molkentin JD. Novel interaction between the TAK1-TAB1-TAB2 and the RCAN1-calcineurin regulatory pathways defines a signaling nodal control point. *Nat Cell Biol.* (2009) 11:154–61.
28. Wang C, Hu L, Guo S, Yao Q, Liu X, Zhang B, et al. Phosphocreatine attenuates doxorubicin-induced cardiotoxicity by inhibiting oxidative stress and activating TAK1 to promote myocardial survival in vivo and in vitro. *Toxicology.* (2021) 460:1–11. doi: 10.1016/j.tox.2021.152881
29. Kishimoto K, Matsumoto K, Ninomiya-Tsuji J. TAK1 mitogen-activated protein kinase kinase kinase is activated by autophosphorylation within its activation loop. *J Biol Chem.* (2000) 275:7359–64. doi: 10.1074/jbc.275.10.7359
30. Wang Z, Huang H, He W, Kong B, Hu H, Fan Y, et al. Regulator of G-protein signaling 5 protects cardiomyocytes against apoptosis during in vitro cardiac ischemia-reperfusion in mice by inhibiting both JNK1/2 and P38 signaling pathways. *Biochem Biophys Res Commun.* (2016) 473:551–7. doi: 10.1016/j.bbrc.2016.03.114
31. Wang J, Ma J, Nie H. Hepatic regulator of G protein signaling 5 ameliorates NAFLD by suppressing TAK1JNK/p38 signaling. *Hepatology.* (2021) 73:104–25. doi: 10.1002/hep.31242

Conflict of Interest: The authors declare that the research was conducted in the absence of any commercial or financial relationships that could be construed as a potential conflict of interest.

Publisher's Note: All claims expressed in this article are solely those of the authors and do not necessarily represent those of their affiliated organizations, or those of the publisher, the editors and the reviewers. Any product that may be evaluated in this article, or claim that may be made by its manufacturer, is not guaranteed or endorsed by the publisher.

frontiers | Frontiers in Cardiovascular Medicine

ORIGINAL RESEARCH
published: 25 May 2022
doi: 10.3389/fcvm.2022.888982

Genetically Predicted Obesity Causally Increased the Risk of Hypertension Disorders in Pregnancy

Wenting Wang[1,2†], Jiang-Shan Tan[3†], Lu Hua[3], Shengsong Zhu[3], Hongyun Lin[2], Yan Wu[3] and Jinping Liu[1*]*

[1] Department of Cardiopulmonary Bypass, State Key Laboratory of Cardiovascular Disease, Fuwai Hospital, National Center for Cardiovascular Diseases, Chinese Academy of Medical Sciences and Peking Union Medical College, Beijing, China, [2] Department of Anaesthesiology, Second Affiliated Hospital, Hainan Medical College, Haikou, Hainan, China, [3] Center for Respiratory and Pulmonary Vascular Diseases, Department of Cardiology, Key Laboratory of Pulmonary Vascular Medicine, National Clinical Research Center of Cardiovascular Diseases, Fuwai Hospital, Chinese Academy of Medical Sciences and Peking Union Medical College, Beijing, China

OPEN ACCESS

Edited by:
Laura Arbour,
University of British Columbia, Canada

Reviewed by:
Ya-Li Chen,
Second Hospital of Hebei Medical University, China
Jian Cao,
Chinese PLA General Hospital, China

***Correspondence:**
Yan Wu
yanr222@sina.cn
Jinping Liu
liujinping@fuwai.com

[†]These authors have contributed equally to this work and share first authorship

Specialty section:
This article was submitted to Cardiovascular Genetics and Systems Medicine, a section of the journal Frontiers in Cardiovascular Medicine

Received: 03 March 2022
Accepted: 20 April 2022
Published: 25 May 2022

Citation:
Wang W, Tan J-S, Hua L, Zhu S, Lin H, Wu Y and Liu J (2022) Genetically Predicted Obesity Causally Increased the Risk of Hypertension Disorders in Pregnancy. Front. Cardiovasc. Med. 9:888982. doi: 10.3389/fcvm.2022.888982

Aims: This study aimed to evaluate the causal association between obesity and hypertension disorders in pregnancy.

Methods: Two-sample Mendelian randomization (MR) study was conducted based on the data obtained from the GIANT (n = 98,697 participants) consortium and FinnGen (n = 96,449 participants) consortium to determine the causal effect of obesity on the risk of hypertension disorders in pregnancy. Based on a genome-wide significance, 14 single-nucleotide polymorphisms (SNPs) associated with obesity-related databases were used as instrumental variables. The random-effects inverse-variance weighted (IVW) method was adopted as the main analysis with a supplemented sensitive analysis of the MR-Egger and weighted median approaches.

Results: All three MR methods showed that genetically predicted obesity causally increased the risk of hypertension disorders in pregnancy. IVW analysis provided obesity as a risk factor for hypertension disorders in pregnancy with an odds ratio (OR) of 1.39 [95% confidence interval (CI) 1.21–1.59; $P = 2.46 \times 10^{-6}$]. Weighted median and MR Egger regression also showed directionally similar results [weighted median OR = 1.49 (95% CI, 1.24–1.79), $P = 2.45 \times 10^{-5}$; MR-Egger OR = 1.95 (95% CI, 1.35–2.82), $P = 3.84 \times 10^{-3}$]. No directional pleiotropic effects were found between obesity and hypertension disorders in pregnancy with both MR-Egger intercepts and funnel plots.

Conclusions: Our findings provided directed evidence that obesity was causally associated with a higher risk of hypertension disorders in pregnancy. Taking measures to reduce the proportion of obesity may help reduce the incidence of hypertension disorders in pregnancy.

Keywords: genetic susceptibility, obesity, hypertension disorders in pregnancy, two-sample, Mendelian randomization

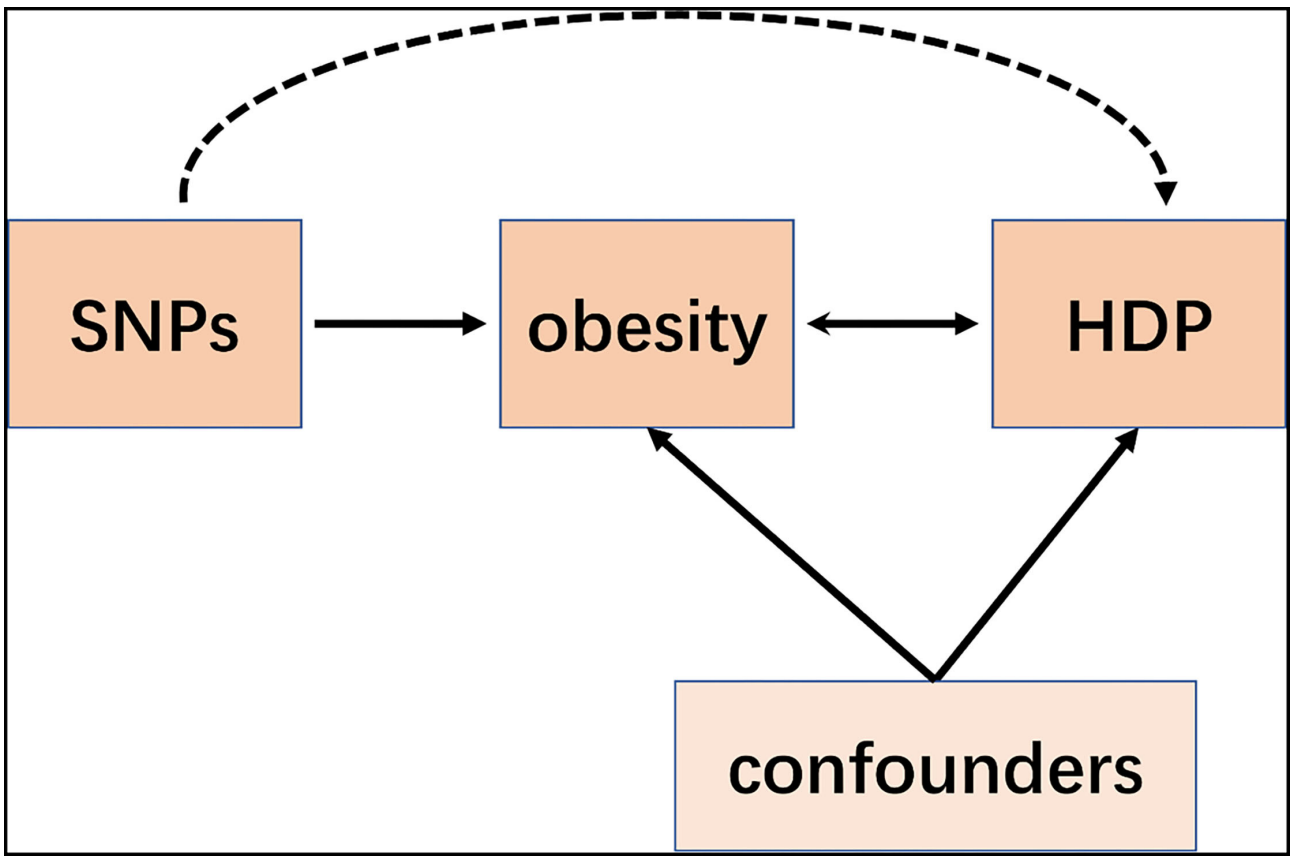

FIGURE 1 | Schematic representation of an MR analysis. We selected SNPs which associated with obesity and the corresponding effect for these SNPs was estimated based on the risk of HDP obtained from a large cohort of the European population.

INTRODUCTION

Hypertension disorders in pregnancy (HDP) are defined as elevated office blood pressure ≥140/90 mmHg during the pregnancy (1), which is the most common complication of gestation, affecting up to 10% of pregnant women all over the world (2). HDP is also the major cause of morbidity and mortality in maternal, fetal, and neonatal and is associated with an increased risk of multiple organ failure, placental disruption, disseminated intravascular coagulation, major cardiovascular events, and death for the mother, and a higher risk of the fetus and newborn in intrauterine growth retardation, intrauterine death, stillborn, premature delivery, neonatal death (3, 4). Therefore, it is of practical significance to explore modifiable risk factors of HDP and make early predictions such that interventions can be carried out in advance to reduce the adverse effect brought by HDP. Many studies have shown that there is an observational correlation between obesity and the risk of HDP (5, 6). Since previous studies have only described that obesity can increase the risk of HDP, but how much risk can be increased, there is no relevant research data. Meanwhile, these observational studies were susceptible to reverse causality and confounding risk factors. As a consequence, whether the observed associations between obesity and HDP are causal is unclear.

Mendelian Randomization (MR) is a recent emerging technique that applies single-nucleotide polymorphisms (SNPs) associated with risk factors as instrumental variables (IVs) to determine whether the observational association between a risk factor and a specific disease is causal (7–9). Although a MR study was performed retrospectively, it is similar to prospective randomized controlled trials (RCT) conceptually (**Figure 1**). Since all the germline hereditary genetic variants start with the formation of a zygote as a result of the fertilization of an oocyte, which occurs before the disease onset. Therefore, the potential bias of confounding or non-differential measurement error can be avoided in a MR study (10).

In this study, we aimed to explore the causal association between obesity and the risk of HDP from published genome-wide association studies (GWAS) correlation data by using two-sample MR analysis.

MATERIALS AND METHODS

Study Design

In this study, we performed a two-sample MR (11, 12) to investigate the causal association between obesity with increased risk of HDP. Thus, our study does not require further sanction since the published studies were used for

the data extraction, which has been approved by their respective institutional review committee and the informed consent of the participants has been obtained in their original research.

Data Sources

Study Exposure: Obesity

Summary-level genetics were acquired from published GWAS, the Genetic Investigation of Anthropometric Traits (GIANT)

TABLE 1 | List of genetic instruments for obesity and log odds ratios of hypertension disorders in pregnancy risk by each instrumental SNP (GWAS significance with $P < 5\times 10^{-8}$ and linkage disequilibrium threshold with $R^2 < 0.001$).

No	SNP	Gene	Chr	EA	OA	EAF.obesity	EAF.HDP	Obesity β(SE)	HDP β(SE)
1	rs987237	*TFAP2B*	6	A	G	0.10	0.79	0.13	−0.06
2	rs13393304	_	2	G	A	0.89	0.84	0.18	0.06
3	rs13130484	_	4	C	T	0.42	0.52	0.11	−0.03
4	rs7138803	_	12	A	G	0.44	0.38	0.08	0.04
5	rs527248	_	1	A	G	0.26	0.82	0.11	−0.06
6	rs887912	_	2	T	C	0.62	0.25	−0.08	−0.01
7	rs10182181	_	2	A	G	0.50	0.58	0.07	0.03
8	rs9816226	_	3	T	A	0.85	0.85	0.11	0.06
9	rs2307111	*POC5*	5	T	C	0.43	0.58	−0.07	−0.02
10	rs4929923	*TRIM66*	11	T	C	0.73	0.34	0.08	−0.04
11	rs8028313	*MAP2K5*	15	G	C	0.78	0.22	−0.10	−0.06
12	rs11075989	*FTO*	16	C	T	0.44	0.41	0.21	−0.09
13	rs523288	_	18	T	A	0.62	0.29	0.13	0.03
14	rs29939	_	19	A	G	0.22	0.67	0.07	0.01

Chr. indicates chromosome; EA, effect allele; OA, other allele; EAF, effect allele frequency. A total of 14 genetic instruments were included in the present MR analysis, located in four genes (POC5, TRIM66, MAP2K5, and FTO) and 12 chromosomes (1, 2, 3, 4, 5, 6, 11, 12, 15, 16, 18, and 19) with an effect allele frequency (EAF) of 0.1–0.9 in SNPs of obesity and 0.2–0.9 in SNPs of hypertension disorders in pregnancy.

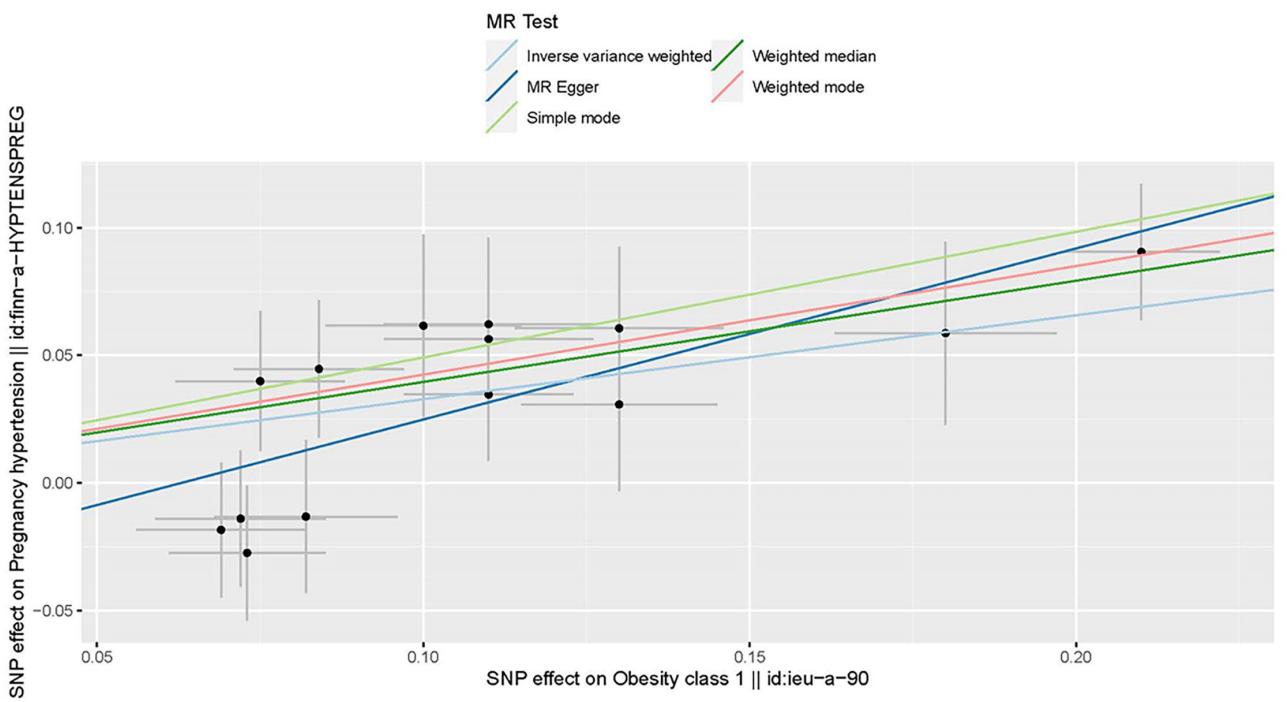

FIGURE 2 | Scatter plot to visualize the causal effect of obesity on the risk of hypertension disorders in pregnancy (HDP). Each black point representing an SNP is plotted in relation to the effect size of the SNP on obesity (x-axis) and on the risk of HDP (y-axis) with corresponding standard error bars. The slope of each line corresponds to the causal estimate using different MR methods. IVW indicates inverse-variance weighted; and MR, Mendelian randomization.

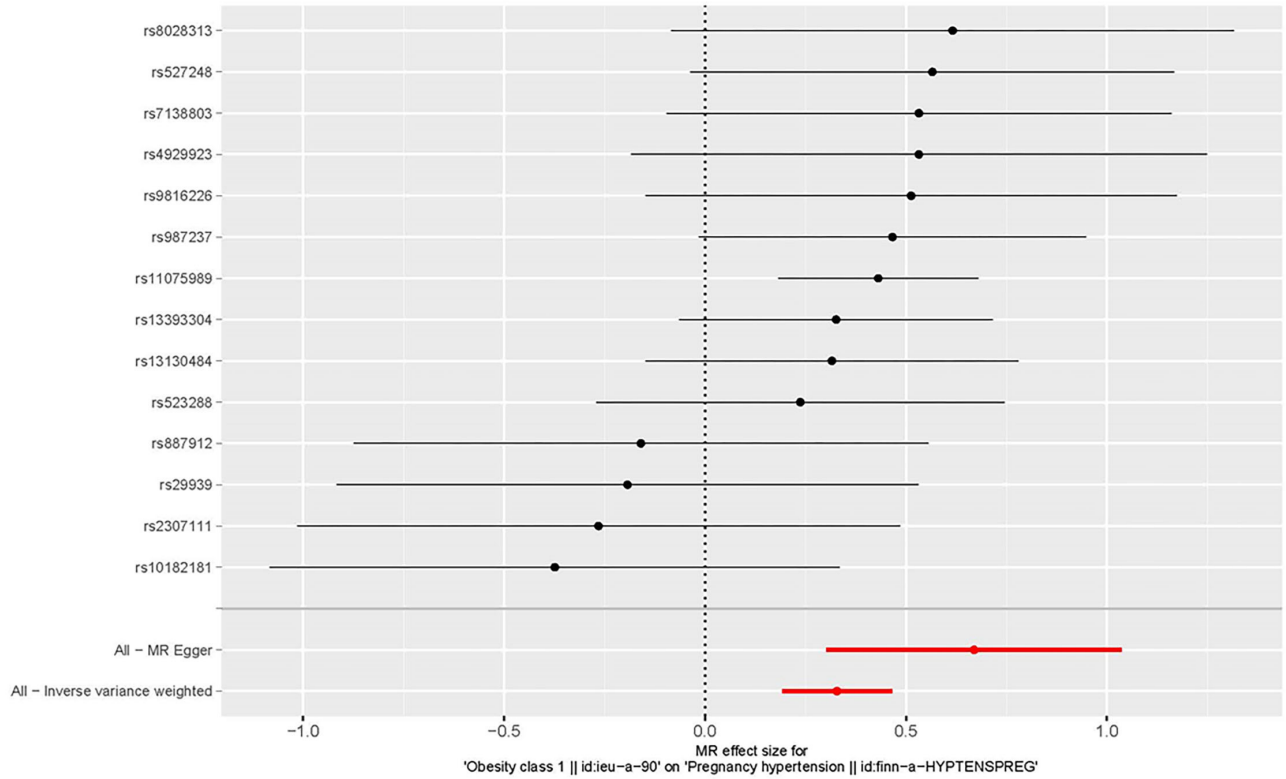

FIGURE 3 | Forest plot to visualize the causal effect of every single SNP on the risk of hypertension disorders in pregnancy.

consortium, which included 32,858 obesity patients and 65,839 controls from Europe. The IVs we selected satisfy the following criteria: (1) The obesity-associated SNPs with a genome-wide significance ($P < 5 \times 10^{-8}$). (2) For avoiding bias caused by strong linkage disequilibrium among SNPs, the linkage disequilibrium of obesity-associated SNPs must satisfy the $r^2 < 0.001$ and window size = 10,000 kb. (3) We selected the SNPs with F statistic >10 to avoid the effect of weak IVs. F statistic = $(\beta/SE)^2$. Totally, 14 obesity-associated SNPs were obtained as IVs, and the details of IVs were presented in **Table 1** (13, 14).

Study Outcome: Pregnancy Hypertension

We obtained the GWAS summary data of HDP from the FinnGen project, which was acquirable at https://gwas.mrcieu.ac.uk/datasets/finn-a-HYPTENSPREG/. Our project contained 3,363 pregnancy hypertension cases and 93,136 controls. Totally, 14 SNPs were correspondingly found in the database. Consequently, the final MR analysis was finished based on all the SNPs found in the exposure.

Statistical Analysis

Due to no individual-level GWAS data available in our study, we leveraged two-sample MR analyses, as mentioned previously (15, 16), to assess the causal association between obesity and HDP. Horizontal pleiotropy is that the outcome may be exposed by other pathways but not only the exposure, which violates the assumption of MR and can bias causal estimates. To prevent this, we use three different analysis methods in the present MR analysis. Each statistical approach conducted is based on different horizontal pleiotropy models. To make our results more reliable, we compared the consistency of all results in three different statistical approaches (17), including inverse-variance weighted (IVW) method, MR-Egger and weighted median MR methods. The "mRnd" tool was used to calculate the power of the present MR analysis. All of the statistical analysis was finished based on the MR software packages version 0.5.6 and R version 4.1.2 (2021-11-15) (18).

RESULTS

Genetic Instruments of Obesity

All genetic instrumental variables related to obesity and HDP were shown in **Table 1**. Totally, 14 genetic instruments, which located in four genes (POC5, TRIM66, MAP2K5, and FTO) and 12 chromosomes (1, 2, 3, 4, 5, 6, 11, 12, 15, 16, 18, and 19), were included in the present MR analysis. The effect allele frequency (EAF) of SNPs in obesity ranged from 0.1 to 0.9 and the EAF of SNPs in HDP ranged from 0.2 to 0.9. The risk of each genetic variant associations with obesity and HDP is presented in **Figures 2**, **3**.

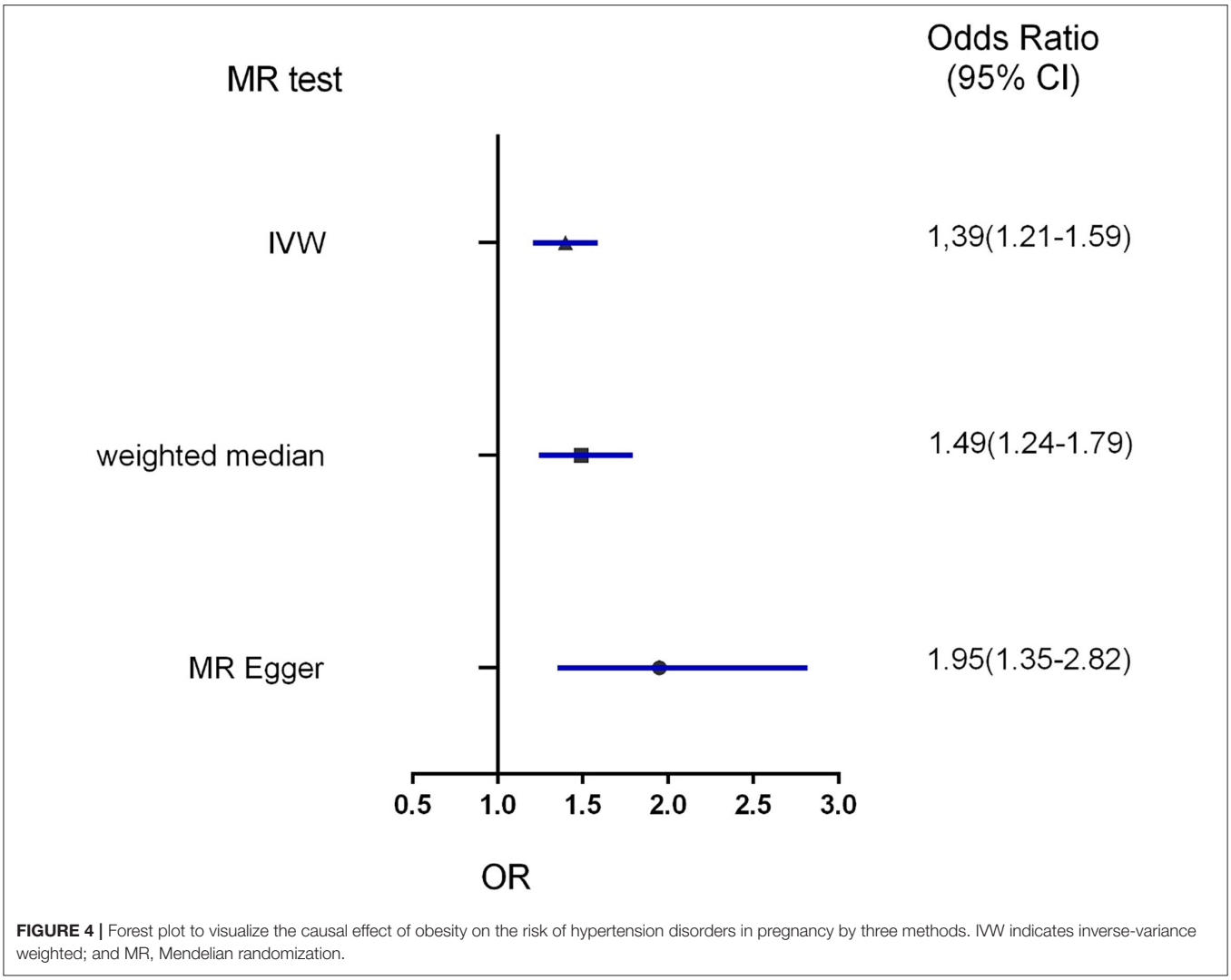

FIGURE 4 | Forest plot to visualize the causal effect of obesity on the risk of hypertension disorders in pregnancy by three methods. IVW indicates inverse-variance weighted; and MR, Mendelian randomization.

MR for HDP

Three MR methods including IVW, MR-Egger, and weighted median regression, were used to investigate the causal effects of obesity on the risk of HDP (**Figures 2**, **4**). IVW method showed that genetically predicted obesity was causally associated with a higher risk of HDP [IVW odds ratio (OR) = 1.39; 95%CI, 1.21–1.59); $P = 2.46 \times 10^{-6}$]. Besides, the MR power is 88% in the present study by using the "mRnd" tool. Weighted median and MR Egger regression also presented similar directed estimates [weighted median OR = 1.49 (95% CI, 1.24–1.79), $P = 2.45 \times 10^{-5}$; MR-Egger OR = 1.95 (95% CI, 1.35–2.82), $P = 3.84 \times 10^{-3}$]. The consistency in the results of all three MR approaches suggested that genetically predicted obesity causally reliably increased the risk of HDP.

Horizontal Pleiotropy Analysis

The asymmetry of funnel plots with individual Wald ratios of each SNP that plotted according to its precision represents directional horizontal pleiotropy. However, it is difficult to investigate the symmetry of a funnel plot when using a small number of IVs (**Figure 5**). Therefore, the MR-Egger intercept was used to further explore the directional horizontal pleiotropy. And no evidence of directional pleiotropy was shown between obesity and HDP in the present MR analysis ($P = 0.07$).

The Effects of Individual Genetic Instruments Correlated With HDP

The leave-one-out approach was selected for a sensitivity analysis to confirm the effect of each SNP on the overall causal estimate. When individual SNP was systematically removed and MR analyses were repeated. No substantial difference was observed in estimated causality and the findings have important credibility (**Figure 6**). Consequently, the estimated effects couldn't be interpreted by any single genetic instrument.

DISCUSSION

In this two-sample MR study, we firstly assessed the causal association between obesity and HDP based on the European

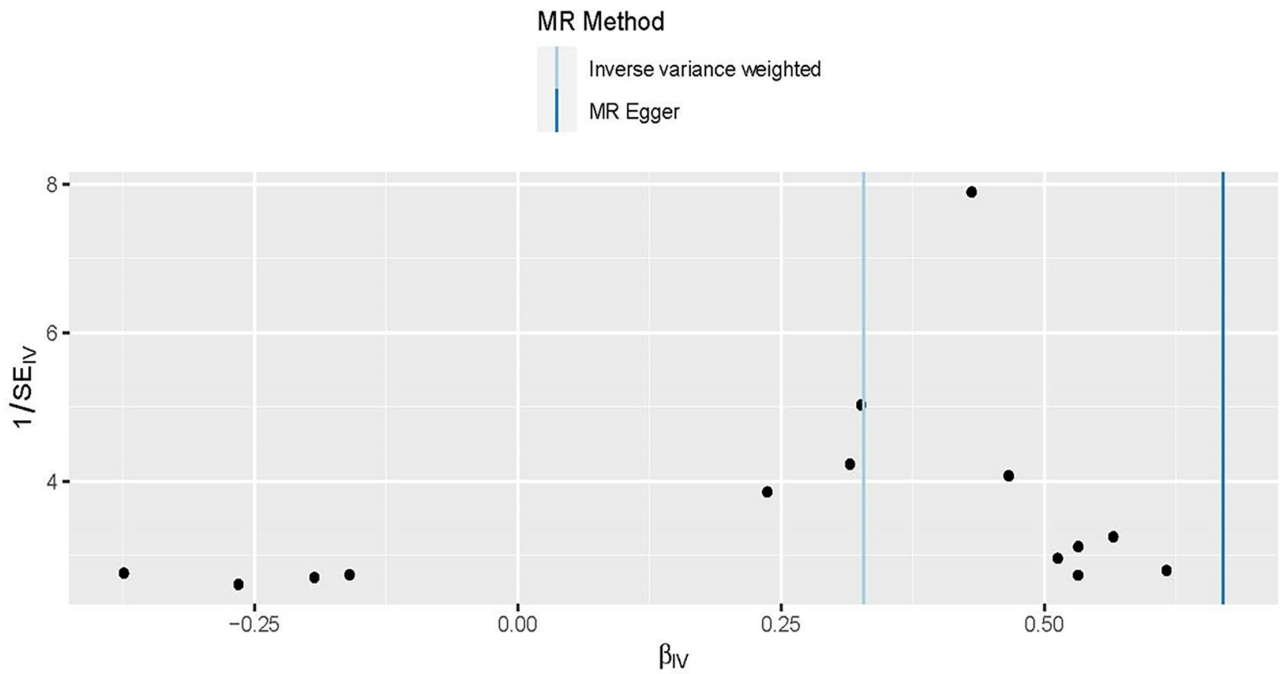

FIGURE 5 | Funnel plots to visualize overall heterogeneity of Mendelian randomization (MR) estimates for the effect of obesity on the risk of HDP. The black point representing an SNP is plotted in relation to the effect size of the SNP on hypertension disorders in pregnancy (x-axis) and reciprocal of the standard errors (y-axis) in the inverse-variance weighted Mendelian randomization. The asymmetry of funnel plots represents directional horizontal pleiotropy, with individual Wald ratios of each SNP that plotted according to its precision.

ancestry population. Our findings suggested a causal association between genetically determined obesity and the increased risk of HDP, with an increase in obesity by 1 SD resulting in a 39% increased risk of HDP, which was consistent with previous observational studies (5, 6).

Compared with MR analysis, reverse causation or confounding factors are more susceptible to bias the results of traditionally observational epidemiological studies. MR study relies on a natural random allocation of genetic variation during meiosis, resulting in a random distribution of genetic variation in populations. Since obesity-associated genetic variants are randomly assigned at birth, which occurred before the onset of HDP. Therefore, MR analysis may provide the best evidence for assessing the causal association between obesity and HDP. Our result suggests that obesity itself can causally increase the risk of HDP, which can be interpreted from the genetic perspective in our MR analysis. The result of this MR was consistent with the findings of previous studies, supporting obesity as a risk predictor for HDP (5, 6). We used three different methods to estimate the causal association to minimize potential pleiotropy in the current sensitivity analysis, including IVW, MR-Egger, and weighted median regression. IVW analysis provided obesity as a risk factor for HDP with an OR of 1.39 (95% CI, 1.21–1.59; $P = 2.46 \times 10^{-6}$). Weighted median and MR Egger regression also showed directionally similar results [weighted median OR = 1.49 (95% CI, 1.24–1.79), $P = 2.45 \times 10^{-5}$; MR-Egger OR = 1.95 (95% CI, 1.35–2.82), $P = 3.84 \times 10^{-3}$]. In our MR analysis, all three methods give similar statistically significant results to confirm the reliability of our causal association between obesity and HDP. Previous observational studies have shown obesity is correlated with an increased risk of gestational hypertension, cesarean section rates, and the risk of anesthesia. These emphasize the potential benefit of weight loss among obese women of childbearing age (6). Hence, our results highlight the importance of weight control in pregnant women and provide genetic evidence for future elucidating the pathogenesis of hypertension formation during pregnancy. Gene analyses of lifestyle and environment interaction have suggested that our increasingly obesogenic environment may increase the genetic risk of obesity, but those risks could be reduced by increasing physical activity and avoiding specific dietary components. Exploring a causal association of obesity with HDP, which could be preventable through weight-loss interventions has clinical significance. In other words, verifying the causal detrimental impact between obesity and HDP risk has a great social significance and clinical value.

It has been reported that several genes significantly associated with the increase of obesity risk, which also played an important role in the appetite regulation of hypothalamus (19). rs987237 located in the chromosome 6 transcription factor AP-2 beta gene (*TFAP2B*) has been related to obesity defined by body mass index (BMI), and waist circumference (20), and has been shown interaction with the dietary fat-to-carbohydrate ratio, which has an impact on weight loss. The transcription factor encoded

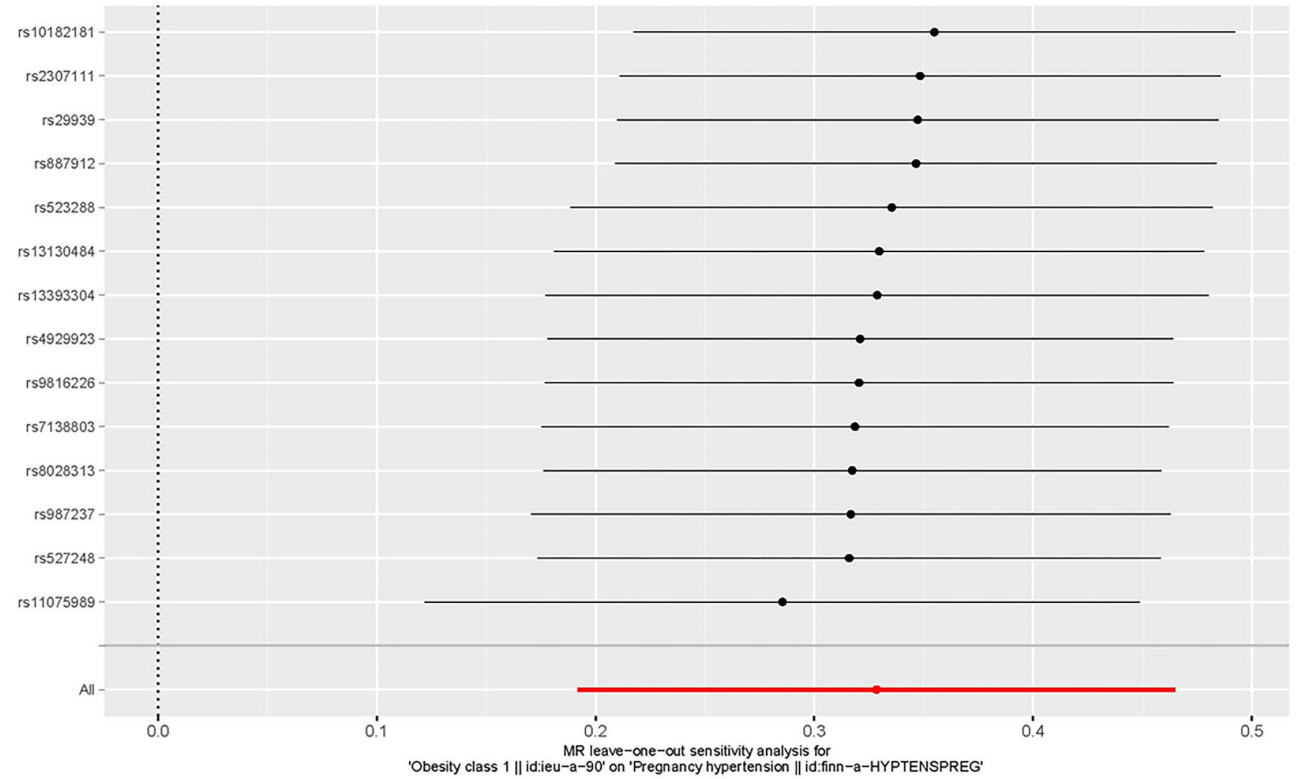

FIGURE 6 | The leave-one-out plot to visualize the causal effect of obesity on the risk of hypertension disorders in pregnancy when leaving one SNP out.

by *TFAP2B* is mainly expressed in adipose tissue, where its regulation of adipocyte function and expression of adipokine is considered to be the functional link to obesity (21, 22), to provide a mechanistic basis for the genetic correlation of *TFAP2B* and obesity. HDP is influenced by environmental factors and a variety of genetics which is a complex disease (23). Epidemiological research has recently examined the correlation between a history of HDP and future risks of other diseases. These studies have reported associations between HDP history and risk of stroke, coronary heart disease, diabetes, heart failure, hypertension, and dysrhythmia. Therefore, reducing the risk of HDP contributes to reducing the risk of diseases for pregnant women. Observational studies have shown a correlation between obesity and HDP, but it is unclear whether the observed associations are causal or caused by confounding bias or reverse causation. Besides, no genetic variants correlated with obesity were reported in HDP, suggesting that the causal correlation between obesity and HDP is independent of the known genetic variants. The most important implication is through public health interventions to reduce the incidence of obesity in pregnant women can make the incidence of high blood pressure in pregnant women during pregnancy lower.

This study has many advantages. We used a two-sample MR design, which minimized confounding and reverse causal bias, to assess the causal association between obesity and increased risk of HDP. To the best of our knowledge, this study is the first MR analysis to investigate the causal association between obesity and the risk of HDP. Besides, several key measures were implemented to meet the basic assumptions of two-sample MR analysis: (1) We only included the SNPs which were correlated with obesity at a GWAS significant level to guarantee an effective correlation between SNPs and risk factors (obesity) in the present MR; (2) All the included GWAS data was finished in the ancestral populations of Europe to reduce the impact of race/ethnicity. Thus, the potential confounding factor is small in this study; (3) MR Egger and weighted median were conducted for the sensitive analysis to guarantee the reliability of our analysis. This study has important clinical implications for predicting HDP risk in clinical practice, which will help rationalize weight-loss strategies to reduce the risk of HDP.

However, the study still had some limitations. First, these data adopted to infer the correlation between obesity and HDP risk factors came mainly from European ancestry, therefore, subsequent studies need to test other regions and races to determine whether the correlation is consistent in other populations (24). Second, we are not able to further explore subgroup analysis on the interest covariates because we just adopted the summary data rather than individual patient data (25).

CONCLUSION

In summary, after adopting a two-sample MR analysis, we found a causal correlation between obesity and hypertension disorders

in pregnancy. Taking measures to reduce the proportion of obesity may help reduce the incidence of hypertension disorders in pregnancy.

DATA AVAILABILITY STATEMENT

The original contributions presented in the study are included in the article, further inquiries can be directed to the corresponding authors.

AUTHOR CONTRIBUTIONS

WW and J-ST designed the study and wrote the manuscript. WW, J-ST, LH, SZ, and HL contributed to the data analysis and data interpretation. YW and JL contributed to the revision of the manuscript. All authors contributed to the article and approved the submitted version.

FUNDING

This work was supported by the National Natural Science Foundation of China Grant Awards (Grant No. 81960669), CAMS Innovation Fund for Medical Sciences (CIFMS) (Grant Nos. 2020-12M-C&T-B-063), Hainan Province Clinical Medical Center, the National Clinical Research Center for Cardiovascular Diseases, Fuwai Hospital, Chinese Academy of Medical Sciences (NCRC2020007), and the Research Project of Clinical Toxicology from the Chinese Society of Toxicology (CST2020CT303).

REFERENCES

1. Brown MA, Magee LA, Kenny LC, Karumanchi SA, McCarthy FP, Saito S, et al. Hypertensive disorders of pregnancy: ISSHP classification, diagnosis, and management recommendations for international practice. *Hypertension.* (2018) 72:24–43. doi: 10.1161/HYPERTENSIONAHA.117.10803
2. Regitz-Zagrosek V, Roos-Hesselink JW, Bauersachs J, Blomström-Lundqvist C, Cífková R, De Bonis M, et al. 2018 ESC Guidelines for the management of cardiovascular diseases during pregnancy. *Eur Heart J.* (2018) 39:3165–241. doi: 10.1093/eurheartj/ehy478
3. Duffy JM, van 't Hooft J, Gale C, Brown M, Grobman W, Fitzpatrick R, et al. A protocol for developing, disseminating, and implementing a core outcome set for pre-eclampsia. *Pregnancy Hypertens.* (2016) 6:274–8. doi: 10.1016/j.preghy.2016.04.008
4. von Dadelszen P, Payne B, Li J, Ansermino JM, Broughton Pipkin F, Côté AM, et al. Prediction of adverse maternal outcomes in pre-eclampsia: development and validation of the fullPIERS model. *Lancet.* (2011) 377:219–27. doi: 10.1016/S0140-6736(10)61351-7
5. Coroyannakis C, Khalil A. Management of hypertension in the obese pregnant patient. *Curr Hypertens Rep.* (2019) 21:24. doi: 10.1007/s11906-019-0927-x
6. Poston L, Harthoorn LF, Van Der Beek EM, Contributors to the ILSI Europe Workshop. Obesity in pregnancy: implications for the mother and lifelong health of the child. A consensus statement. *Pediatr Res.* (2011) 69:175–80. doi: 10.1203/PDR.0b013e3182055ede
7. Smith GD, Ebrahim S. 'Mendelian randomization': can genetic epidemiology contribute to understanding environmental determinants of disease?. *Int J Epidemiol.* (2003) 32:1–22. doi: 10.1093/ije/dyg070
8. Davies NM, Holmes MV, Davey Smith G. Reading Mendelian randomisation studies: a guide, glossary, and checklist for clinicians. *BMJ.* (2018) 362:k601. doi: 10.1136/bmj.k601
9. Emdin CA, Khera AV, Kathiresan S. Mendelian randomization. *JAMA.* (2017) 318:1925–6. doi: 10.1001/jama.2017.17219
10. Bowden J, Holmes MV. Meta-analysis and Mendelian randomization: a review. *Res Synth Methods.* (2019) 10:486–96. doi: 10.1002/jrsm.1346
11. Lawlor DA. Commentary: two-sample Mendelian randomization: opportunities and challenges. *Int J Epidemiol.* (2016) 45:908–15. doi: 10.1093/ije/dyw127
12. Richmond RC, Hemani G, Tilling K, Davey Smith G, Relton CL. Challenges and novel approaches for investigating molecular mediation. *Hum Mol Genet.* (2016) 25:R149–R156. doi: 10.1093/hmg/ddw197
13. Berndt SI, Gustafsson S, Mägi R, Ganna A, Wheeler E, Feitosa MF, et al. Genome-wide meta-analysis identifies 11 new loci for anthropometric traits and provides insights into genetic architecture. *Nat Genet.* (2013) 45:501–12. doi: 10.1038/ng.2606
14. Locke AE, Kahali B, Berndt SI, Justice AE, Pers TH, Day FR, et al. Genetic studies of body mass index yield new insights for obesity biology. *Nature.* (2015) 518:197–206. doi: 10.1038/nature14177
15. Tan JS, Liu NN, Guo TT, Hu S, Hua L. Genetically predicted obesity and risk of deep vein thrombosis. *Thromb Res.* (2021) 207:16–24. doi: 10.1016/j.thromres.2021.08.026
16. Tan JS, Liu NN, Guo TT, Hu S, Hua L. Genetic predisposition to COVID-19 may increase the risk of hypertension disorders in pregnancy: a two-sample Mendelian randomization study. *Pregnancy Hypertens.* (2021) 26:17–23. doi: 10.1016/j.preghy.2021.08.112
17. Xu L, Borges MC, Hemani G, Lawlor DA. The role of glycaemic and lipid risk factors in mediating the effect of BMI on coronary heart disease: a two-step, two-sample Mendelian randomisation study. *Diabetologia.* (2017) 60:2210–20. doi: 10.1007/s00125-017-4396-y
18. Tan JS, Liu N, Guo TT, Hu S, Hua L, Qian Q. Genetic predispositions between COVID-19 and three cardio-cerebrovascular diseases. *Front Genet.* (2022) 13:743905. doi: 10.3389/fgene.2022.743905
19. Speliotes EK, Willer CJ, Berndt SI, Monda KL, Thorleifsson G, Jackson AU, et al. Association analyses of 249,796 individuals reveal 18 new loci associated with body mass index. *Nat Genet.* (2010) 42:937–48. doi: 10.1038/ng.686
20. Paternoster L, Evans DM, Nohr EA, Holst C, Gaborieau V, Brennan P, et al. Genome-wide population-based association study of extremely overweight young adults–the GOYA study. *PloS ONE.* (2011) 6:e24303. doi: 10.1371/journal.pone.0024303
21. Lindgren CM, Heid IM, Randall JC, Lamina C, Steinthorsdottir V, Qi L, et al. Genome-wide association scan meta-analysis identifies three Loci influencing adiposity and fat distribution. *PLoS Genet.* (2009) 5:e1000508. doi: 10.1371/annotation/b6e8f9f6-2496-4a40-b0e3-e1d1390c1928
22. Ugi S, Nishio Y, Yamamoto H, Ikeda K, Kobayashi M, Tsukada S, et al. Relation of the expression of transcriptional factor TFAP2B to that of adipokines in subcutaneous and omental adipose tissues. *Obesity.* (2010) 18:1277–82. doi: 10.1038/oby.2009.442
23. Kosicka K, Siemiatkowska A, Pekal A, Majchrzak-Celińska A, Breborowicz G, Krzyścin M, et al. Variants of HSD11B2 gene in hypertensive disorders of pregnancy. *J Matern Fetal Neonatal Med.* (2017) 30:1360–5. doi: 10.1080/14767058.2016.1214125
24. Tan JS, Yan XX, Wu Y, Gao X, Xu XQ, Jiang X, et al. Rare variants in MTHFR predispose to occurrence and recurrence of pulmonary embolism. *Int J Cardiol.* (2021) 331:236–42. doi: 10.1016/j.ijcard.2021.01.073
25. Tan JS, Hu MJ, Yang YM, Yang YJ. Genetic predisposition to low-density lipoprotein cholesterol may increase risks of both individual and Familial Alzheimer's Disease. *Front Med.* (2022) 8:798334. doi: 10.3389/fmed.2021.798334

Conflict of Interest: The authors declare that the research was conducted in the absence of any commercial or financial relationships that could be construed as a potential conflict of interest.

Publisher's Note: All claims expressed in this article are solely those of the authors and do not necessarily represent those of their affiliated organizations, or those of the publisher, the editors and the reviewers. Any product that may be evaluated in this article, or claim that may be made by its manufacturer, is not guaranteed or endorsed by the publisher.

frontiers | Frontiers in Cardiovascular Medicine

REVIEW
published: 11 July 2022
doi: 10.3389/fcvm.2022.954780

Is Location Everything? Regulation of the Endothelial CCM Signaling Complex

*Harsha Swamy and Angela J. Glading**

Department of Pharmacology and Physiology, University of Rochester, Rochester, NY, United States

Recent advances have steadily increased the number of proteins and pathways known to be involved in the development of cerebral cavernous malformation (CCM). Our ability to synthesize this information into a cohesive and accurate signaling model is limited, however, by significant gaps in our knowledge of how the core CCM proteins, whose loss of function drives development of CCM, are regulated. Here, we review what is known about the regulation of the three core CCM proteins, the scaffolds KRIT1, CCM2, and CCM3, with an emphasis on binding interactions and subcellular location, which frequently control scaffolding protein function. We highlight recent work that challenges the current model of CCM complex signaling and provide recommendations for future studies needed to address the large number of outstanding questions.

Keywords: CCM, vascular malformations, scaffolding protein, subcellular localization, signaling

OPEN ACCESS

Edited by:
Anindita Das,
Virginia Commonwealth University,
United States

Reviewed by:
Axel Pagenstecher,
Uniklinikum Giessen und
Marburg, Germany
Cinzia Antognelli,
University of Perugia, Italy

***Correspondence:**
Angela J. Glading
angela_glading@urmc.rochester.edu

Specialty section:
This article was submitted to Cardiovascular Genetics and Systems Medicine, a section of the journal Frontiers in Cardiovascular Medicine

Received: *27 May 2022*
Accepted: *17 June 2022*
Published: *11 July 2022*

Citation:
Swamy H and Glading AJ (2022) Is Location Everything? Regulation of the Endothelial CCM Signaling Complex. Front. Cardiovasc. Med. 9:954780. doi: 10.3389/fcvm.2022.954780

INTRODUCTION

Cerebral cavernous malformation (CCM) is a disease characterized by the formation of microvascular lesions primarily in the brain. These lesions derive from highly proliferative endothelial cells with poor barrier function (1–3). A consequence of this perturbed endothelial behavior is the formation of large vascular "caverns" lacking surrounding mural cells and astrocytes, as well as altered extracellular matrices surrounding the endothelial cells (2, 4). CCM occurs in the general population at a rate of ∼0.5% (5), and may be hereditary (familial CCM) or occur sporadically. A genetic component for the development of CCM was first described in 1995 (6, 7). Further study revealed this gene to encode the protein Krev-Interaction Trapped 1 [KRIT1, also called CCM1; (8–10)], which had been previously identified as a binding partner of the small GTPase Rap1 (11), making KRIT1 the first protein linked to CCM pathogenesis. In 1998 two other genetic components were found (12), and by the mid 2000s these proteins were identified: CCM2/malcavernin (13) and the apoptosis-related protein, CCM3/PDCD10 (14, 15). Loss of function mutations in any of these three genes is sufficient to induce CCM lesion development, and have also been found in some sporadic CCMs (16). Recent studies have discovered other genes involved in CCM development, i.e., PIK3CA (17) and Cdc42 (18), but mutations in KRIT1, CCM2, or CCM3 remain the most commonly identified genetic basis for CCM.

The three core CCM proteins (i.e., KRIT1, CCM2 and CCM3) can bind directly to each other under normal physiological conditions (19–21) forming what is referred to as the CCM signaling complex. All three CCM proteins are scaffolding proteins, and each member of this complex has a unique set of binding partners that allow it to affect a wide range of cellular functions. Based on studies in human tissues, cell culture, and animal models, the CCM complex appears to promote endothelial quiescence by stabilizing cell-cell contact, limiting inflammatory and

angiogenic signaling, and constraining proliferation (2, 4, 22–25). These abilities have been strongly linked to the regulation of mitogen activated protein kinase kinase kinase 3 (MEKK3), which binds to CCM2 (26, 27). However, how CCM2 curbs the activation of MEKK3 and its downstream signaling has not been established, nor has it been shown how loss of KRIT1 or CCM3 lead to activation of MEKK3 in cells that still maintain CCM2 expression. Moreover, studies using KRIT1 or CCM2 deficient cell or animal models have shown highly similar phenotypes (28), but loss of CCM3 causes more severe and acute CCM development both in animal models and human patients (29, 30), suggesting that the pathophysiology and progression of CCM lesion development is a complex process that is influenced by the specific gene affected.

These questions lay bare a significant gap in our current knowledge, that is, what mechanisms regulate the function of the CCM proteins and the CCM complex? Scaffolding proteins, such as the CCM proteins, are a functionally defined set of proteins which are able to bring together (at a minimum) two proteins in a relatively stable conformation and promote signaling between these target proteins. Scaffolding proteins function to organize cellular signaling, making possible the specific and temporal regulation of the vast array of signaling information that cells must continuously process. Regulation of scaffolding proteins depends, to some extent, on their domain composition and on the pathways in which they operate. Notably, scaffolding proteins must be localized to the same subcellular compartment as their target proteins, and relatedly, can promote the localization of their targets to specific cellular locations. Thus, protein expression and alternative splicing and control of location are common features in the regulation of scaffolding proteins. In addition, the interaction of scaffolding proteins with their targets can be regulated by post-translational modification (phosphorylation, ubiquitination, etc.) as well as autoinhibitory interactions between domains of the scaffolding protein itself. Indeed, the ERM family of scaffolding proteins, to which KRIT1 is structurally similar, are regulated by a well-characterized mechanism involving the interaction of the N-terminal ERM associate domain with sequences in the C-terminal ERM associate domain (31). In order to fully understand CCM pathogenesis, we need to know how the CCM proteins individually, and CCM complex formation as a whole, are regulated. In this review, we will examine what is currently known about how KRIT1, CCM2, and CCM3 are regulated, with an emphasis on binding interactions and sub-cellular localization, and discuss how that regulation may affect the function of the CCM complex.

DOMAIN STRUCTURE AND BINDING INTERACTIONS OF CCM PROTEINS

Krev-Interaction Trapped 1, KRIT1

KRIT1 is an 84kDa protein containing multiple protein-interacting domains (**Figure 1**). At the N-terminus (residues 1–170), Liu et al. identified a Nudix-like fold by structural homology (32). Nudix hydrolases are a superfamily of hydrolytic enzymes capable of cleaving nucleoside diphosphates, but the homologous domain in KRIT1 lacks catalytic activity. The remainder of the N-terminal half of KRIT1 is relatively unstructured, but contains three NPXY/F motifs (19, 32, 33) which are recognition sites for phospho-tyrosine binding (PTB) domains. The integrin regulatory protein ICAP1α binds to the first NPXY/F motif [NPAY, residues 192–195, (32)], while CCM2 is thought to bind to the second or third NPXY motifs (19, 34). The cytoplasmic sorting nexin adaptor protein sorting nexin 17 (SNX17) binds to the second NPXY motif (NPLF, residues 231–234). In the center of the protein are four ankyrin repeats [residues 259–422, (11, 35)] that putatively promote association with lipid membranes. The C-terminal half of KRIT1 is folded into a triple-lobed Band 4.1, ezrin, radixin, moesin (FERM) domain, which contains 3 subdomains (F1, F2, and F3) featuring a ubiquitin-like fold, a four-helix bundle, and a phospho-tyrosine binding domain, respectively (35–38). Co-crystallization of KRIT1 with the small GTPase Rap1 demonstrated that Rap1 binds to KRIT1 *via* an interaction with both the F1 and F2 subdomains (36), whereas the transmembrane orphan receptor Heart of Glass (HEG1) binds to an interface involving the FERM F1 and F3 subdomains (39). The C-terminal PTB domain (F3) of KRIT1 could theoretically interact with several NPXY-containing proteins, however the only defined interaction of this domain is an intermolecular interaction with a NPXY motif of KRIT1 itself. This interaction, between the C-terminal PTB domain and the first NPXY motif (40) is highly similar to the autoinhibitory self-interaction seen in other ERM family proteins (31). In addition, KRIT1 contains a nuclear localization sequence [NLS, residues 46–51, (41–44)], which may also be important for binding of KRIT1 to microtubules. Finally, while KRIT1 contains several predicted nuclear export sequences (43, 44), none have been confirmed to regulate subcellular trafficking of KRIT1.

CCM2

CCM2 is a 49 kDa protein that contains a N-terminal PTB domain (13), which binds to KRIT1 (19, 44) and the cell death receptor TrkA (45) (**Figure 1**). A single point mutation in the CCM2 PTB, F217A, blocks the interaction of KRIT1 and CCM2 and is sufficient to cause CCM (21). CCM2 also contains a leucine-rich aspartate (LD)-like domain (residues 223–238), which binds to CCM3, and a C-terminal harmonin-homology domain (HHD) (residues 283–379), which is structurally similar to the N-terminal domain of the Usher syndrome protein harmonin (46). Interestingly, harmonin binds directly to the cell adhesion protein cadherin 23, expressed specifically in neurosensory epithelial cells, via two domains: its N-terminal domain and a PDZ domain (47). However, direct interaction of CCM2 with cadherins has not been reported. CCM2 also binds to the respective upstream kinases mitogen-activated protein kinase kinase 3 (MKK3) and MEKK3 (26, 48). One of the first studies of CCM2 identified it as an osmo-sensing scaffold for the MAP kinase MKK3 (48), a key mediator of p38 inflammatory signaling (49). Later studies demonstrated that CCM2 was a regulator of MEKK3, an upstream activator of big mitogen-activated protein kinase/extracellular signal regulated kinase 5 (BMK1/ERK5). Destabilization of the complex with MEKK3

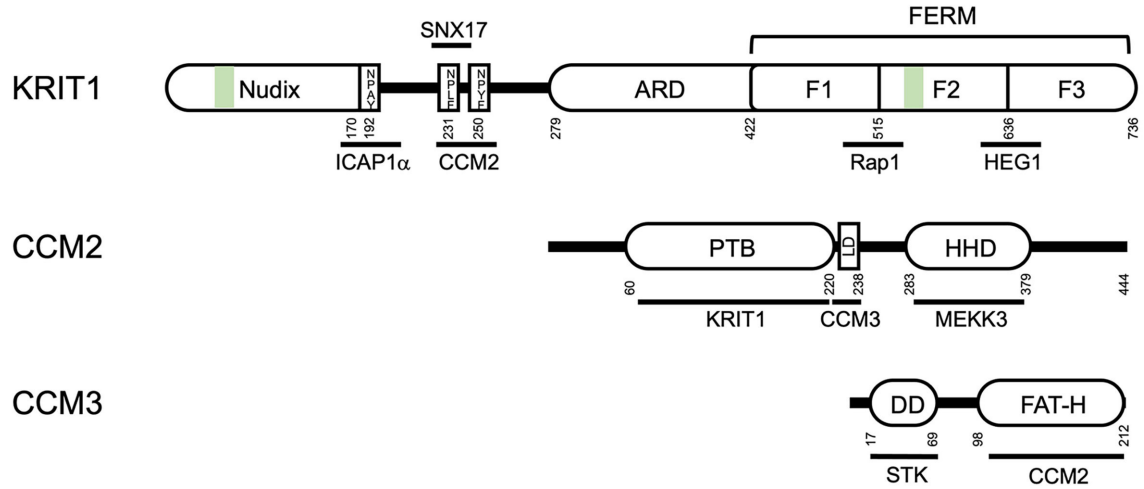

FIGURE 1 | Domain structure of the CCM proteins KRIT1, CCM2 and CCM3. ARD- ankyrin repeat domain; FERM- Band 4.1, ezrin, radixin, moesin domain; F1, F2, and F3, globular subdomains of the FERM domain; PTB, protein tyrosine binding domain; LD, leucine-rich aspartate domain; HHD, harmonin homology domain; DD, dimerization domain; FAT-H, focal adhesion targeting domain; STK, sterile kinase. Green bars indicate nuclear localization sequences/microtubule binding sites. Residue numbers (from human proteins) are noted below the domain diagram.

through loss of any of the CCM proteins is a potent driver of CCM through perturbations of several pathways (26).

CCM3

CCM3 (25kDa) is the most recently identified member of the CCM complex, and binds directly to CCM2 (**Figure 1**). CCM3 contains an N-terminal dimerization domain (50) which mediates interactions with the germinal center kinase III group of protein kinases, including sterile-kinases 24 and 25, forming part of the striatin interacting phosphatase and kinase (STRIPAK) signaling complex (51). CCM3 also contains a C-terminal focal adhesion targeting-homology (FAT-H) domain (50). Sequences within the FAT-H domain bind to the LD-like domain of CCM2 (21, 52), and also mediate interaction with the focal adhesion protein paxillin (50, 53).

REGULATION OF CCM PROTEIN LOCALIZATION

All three CCM proteins have been shown to localize to the plasma membrane (particularly at cell-cell contacts), the cytoplasm, and the nucleus (**Figure 2**). While several studies have investigated the formation of the tripartite complex using co-immunoprecipitation, few have examined complex formation at the subcellular level. However, what evidence there is suggests that KRIT1●CCM2 and CCM2●CCM3 interactions can occur at or near the plasma membrane (50, 54). Alternatively, it is possible that some or all of the CCM proteins could function individually in unique locations. For example, CCM3, which associates with the STRIPAK complex at the Golgi (55) (**Figure 2**), also has been found at the apical epithelial membrane during excretory canal development in C. elegans (56), and in focal adhesions in cancer associated fibroblasts, where it regulates integrin-dependent adhesion and mechano-transduction (53). The relevance of these interactions to CCM pathogenesis or, more specifically, endothelial/epithelial barrier function is unknown. Indeed, only the KRIT1●CCM2 association has been directly implicated in the stabilization of endothelial barrier function, as a point mutation of the PTB domain of CCM2 (F217A) results in a primarily cytoplasmic distribution of both proteins and loss of barrier function (54). Immunofluorescence imaging has also shown that KRIT1 and CCM2 colocalize at cell peripheries in COS-7 cells after osmotic shock (34), suggesting that the localization of this complex could be regulated by external signals. Consequently, subcellular localization is expected to play a key role in the regulation of CCM proteins and the function of the CCM complex, thus it is critical that we understand the mechanisms involved. In the next sections, we will review what is known about how the localization of CCM proteins are regulated and how that relates to the function of the CCM complex.

CCM Complex Localization to Cell-Cell Contacts

Several studies have associated the localization of the CCM complex to sites of cell-cell contact with the ability of this complex to stabilize endothelial barrier function, suggesting that subcellular localization is critical to the functional consequence of active CCM complex signaling. Indeed, several mechanisms have been suggested to regulate localization of the CCM complex to the plasma membrane in general, and to adherens junctions specifically.

In vitro binding assays have shown that KRIT1, CCM2, and CCM3 can directly interact with cellular membranes. KRIT1 can bind phosphatidylinositol (4,5) bisphosphate (PIP2) *via* its FERM domain [residues 208–736, (40)], CCM2 preferentially interacts with phosphatidylinositol monophosphates (52), and

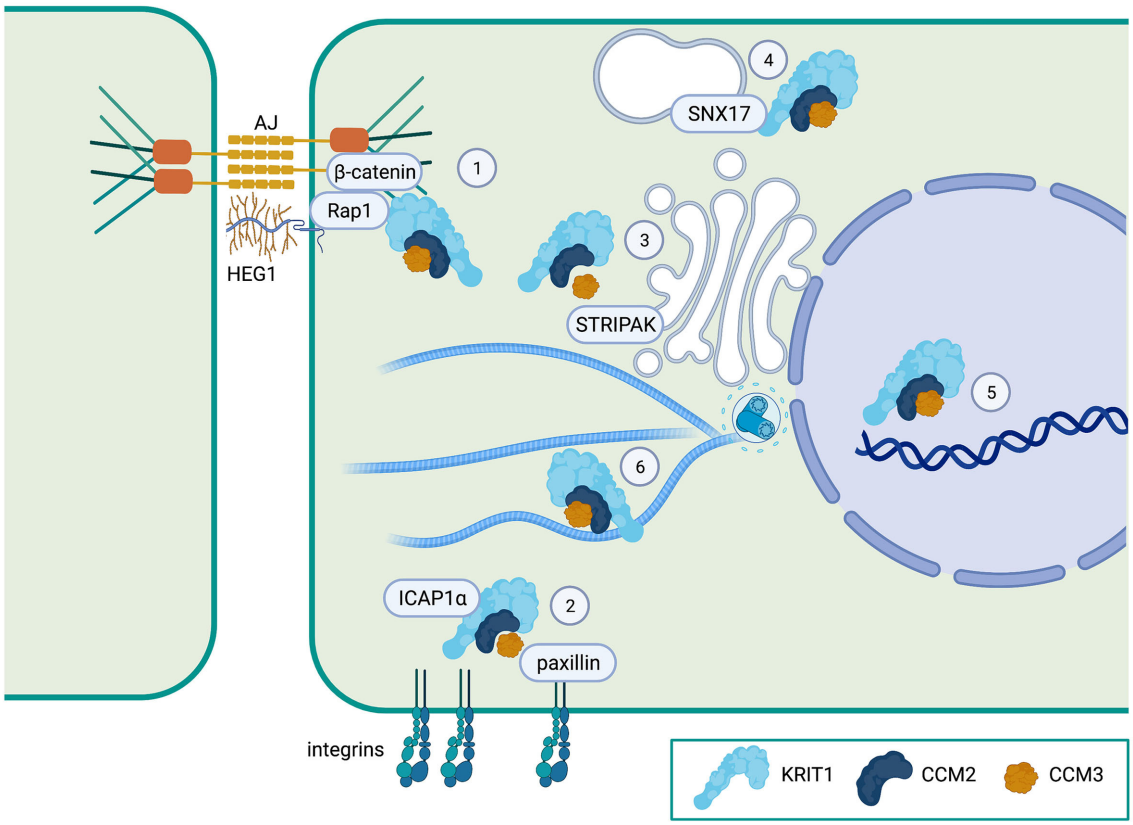

FIGURE 2 | Proposed localization of the CCM complex. (1) The CCM complex is known to co-localize with β-catenin at adherens junctions (AJ) and to associate with the Heart of Glass (HEG1) orphan transmembrane receptor at the plasma membrane. (2) The CCM complex (at least KRIT1), regulates ICAP1α interactions with integrins. CCM3 can also bind to paxillin, a focal adhesion protein. (3) CCM3 is a member of the STRIPAK signaling complex which regulates cell polarity and Golgi assembly. (4) KRIT1 can bind to the endosomal trafficking protein sorting nexin-17 (SNX17). (5) All three CCM proteins can localize to the nucleus, but whether they have a nuclear function is unknown. (6) The CCM complex is also distributed in the cytoplasm, where KRIT1 can bind to microtubules. Created with Biorender.com.

CCM3 binds phosphatidylinositol (3,4,5) triphosphate [PIP3, (57)], potentially indicating that all CCM proteins can associate directly with membranes. While these direct interactions support the ability of the CCM complex to localize with membranes enriched in specific phospholipids, it has not been determined whether these interactions are sufficient for membrane localization of the complex.

In contrast, the ability of specific protein-protein interactions to regulate membrane localization of the CCM proteins, particularly KRIT1, has been more extensively studied. KRIT1 was first identified as an interacting partner of the small GTPase Rap1 in a yeast two-hybrid screen (11). Subsequent studies validated KRIT1 as a Rap1 effector that preferentially binds active (GTP-bound) Rap1 (24, 36, 37, 40). Binding of active Rap1 promotes the localization of KRIT1 to points of cell-cell contact where it associates with adherens junction proteins (24, 37), while co-expression of KRIT1 and RapGAP reduces the association of KRIT1 with β-catenin (24) (**Figure 2**). Binding of Rap1 to KRIT1 blocks the co-sedimentation of KRIT1 with microtubules, and reduces co-localization of KRIT1 with tubulin in baby hamster kidney (BHK) cells (40), suggesting that Rap1 activation could promote trafficking of KRIT1 from the cytoplasm to the plasma membrane. *In vitro* binding assays using KRIT1 peptide fragments initially revealed that Rap1 binds to the C-terminal FERM domain (24, 40, 42). One such study suggested a role for the F3 lobe of the FERM domain using yeast two-hybrid analysis (42). However, X-ray crystallography studies have definitively demonstrated that Rap1 binds KRIT1 at the interface of the F1 and F2 lobes (36). This supports prior reports that the KRIT1 FERM domain fragment could localize to adherens junctions, but mutation or deletion of the F1 lobe ablates this effect (24, 37). Furthermore, a charge switch mutation in this binding interface (R452E) results in a significant reduction in Rap1-binding affinity (37). As a result, KRIT1-R452E is unable to localize to adherens junctions. However, we recently reported that Rap1 binding, though a key regulator of KRIT1 junctional localization, was not absolutely required for the ability of KRIT1 to stabilize barrier function (58). In this study, we expressed various mutated forms of KRIT1 at replacement levels in KRIT1 shRNA expressing human pulmonary artery endothelial cells. Compared to wildtype KRIT1, KRIT1 containing a mutated Rap1 binding site (KRIT1-R452E) is unable to localize to adherens

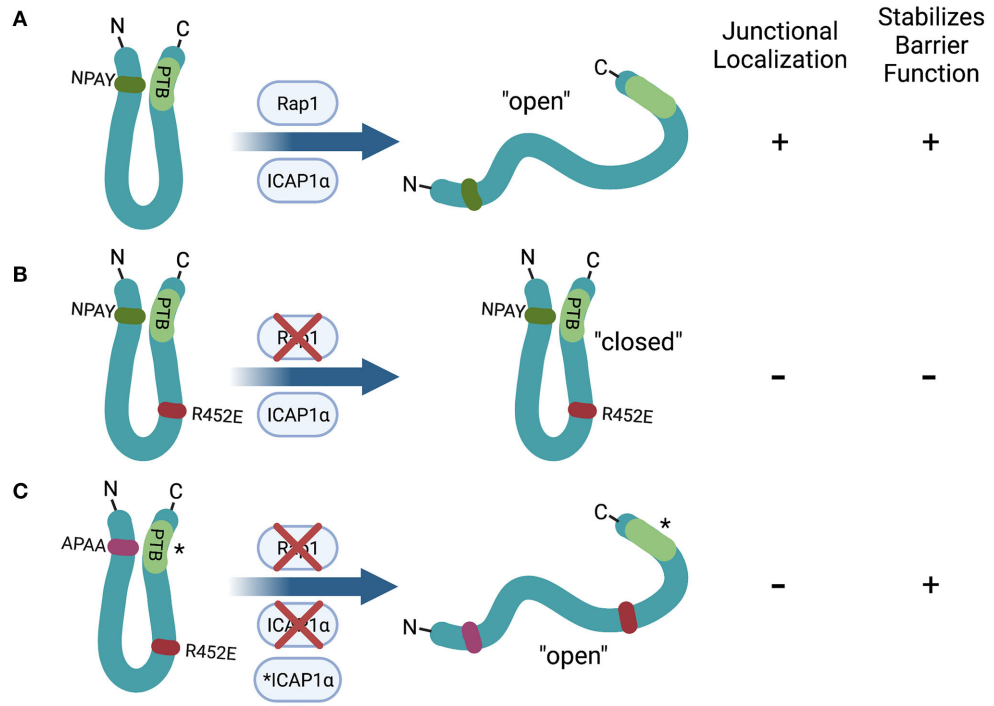

FIGURE 3 | Hypothetical role of the N- to C- terminal self-interaction of KRIT1 in the regulation of barrier function. **(A)** Rap1 or ICAP1α binding to wildtype KRIT1 inhibits the N- to C-terminal interaction, leading to enhanced junctional localization (due to Rap1 binding) and stabilization of endothelial cell-cell contacts. **(B)** Mutation of the Rap1 binding interface (R452E) ablates junctional localization and barrier stabilization, likely due to a reduction in the proportion of the "open" conformation. **(C)** KRIT1 containing mutations in both the Rap1 binding interface (R452E) and the first NPXY motif (APAA) stabilizes cell junctions even though it remains cytoplasmic. Mutation of the PTB domain (*) has the same effect as mutating the NPXY motif, indicating that ICAP1α binding is not required for this effect. Created with Biorender.com.

junctions and does not rescue barrier function of KRIT1 deficient cells. However, when we added an additional mutation of the first NPXY motif (APAA), which would block binding of ICAP1α or the N- to C-terminal self-interaction, we restored barrier function but not junctional localization. Furthermore, mutation of the KRIT1 PTB, which blocked the self-interaction but not ICAP1α association, also restored barrier function in the absence of junctional localization (58) (**Figure 3**). These data suggest that Rap1 binding may regulate KRIT1 in two distinct ways, first, it promotes junctional localization through an as yet undefined mechanism, and second, it negatively regulates the N- to C-terminal interaction, the latter of which appears critical for the function of KRIT1 and the CCM complex. This novel finding, while possibly controversial, may explain why the transmembrane protein HEG1 is not a necessary component of the CCM complex, despite the fact that it binds to KRIT1. HEG1 binds to KRIT1 at the interface of the F1 and F3 lobes of the KRIT1 FERM domain. Ablation of this interaction by mutation of KRIT1 (L717A,721A) disrupts localization of KRIT1 to endothelial junctions (39), suggesting that HEG1 may be important for anchoring KRIT1 at junctions (**Figure 2**). However, knockout of HEG1 *in vivo* failed to lead to the formation of CCM (59), suggesting that this binding interaction is dispensable for normal vascular development. Clearly, much remains to be understood about how the localization of the CCM complex to the plasma membrane, or more specifically cell-cell contacts, is regulated, which is critical to our ability to understand how this localization affects the functional outcome of CCM complex signaling.

Cytoplasmic Localization of the CCM Complex

As mentioned above, the CCM proteins are often observed in the cytoplasm. KRIT1 can bind to microtubules, as demonstrated by co-sedimentation with tubulin in BHK fibroblast lysates. *In vitro* binding assays indicated that this interaction is mediated by regions in both the N- (residues 46–51) and C-termini (residues 569–572) of KRIT1. Binding of Rap1 or ICAP1α to KRIT1 inhibits KRIT1 binding to microtubules. Activation of Rap1 with non-hydrolysable GTPγS reduces co-sedimentation with tubulin. Similarly, over-expression of constitutively active Rap1 (RapV12) prevents co-localization of YFP-KRIT1 with fluorescently-tagged tubulin in cell culture (40). That Rap1 may regulate the interaction of KRIT1 with microtubules in some contexts was also supported by Liu et al. who showed that the KRIT1-R452E mutation reduces co-sedimentation with tubulin in human osteosarcoma epithelial cells [U2OS, (37)]. However, others have not observed co-localization of KRIT1 with the microtubule cytoskeleton in confluent human or bovine aortic endothelial cells (24, 58), which calls into

question the ubiquity of this interaction. In addition, the microtubule binding domain in the N-terminus of KRIT1 overlaps with the reported nuclear localization sequence, thus studies to determine the relevance of the microtubule binding to KRIT1 function would be complicated by possible alteration of nucleocytoplasmic trafficking.

Another possible mediator of cytoplasmic localization of the CCM complex is the protein sorting nexin 17 (SNX17, **Figure 2**). Yeast two-hybrid screens as well as GST-trapping assays previously identified KRIT1 as an interacting partner of SNX17 and defined an interaction between the N-terminus of KRIT1 and the SNX17 FERM domain (60). Crystallography studies further confirmed this interaction, and pointed to the particular importance of KRIT1's second NPXY motif in this interaction (33) (**Figure 1**). Sorting nexins are involved in a variety of endocytic and endosomal processes, with SNX17 playing a role in endosomal recycling, particularly of integrins (61). Thus, it is possible that the presence of SNX17 on endosomal membranes could recruit the CCM complex away from the plasma membrane. Furthermore, based on the fact that both CCM2 and SNX17 bind to the second NPXY sequence on KRIT1, SNX17 could compete with CCM2 for binding to KRIT1, thus altering the composition of the signaling complex in a location specific manner. The implications of the interaction of KRIT1 with SNX17 are intriguing, and should be investigated further.

The interaction of KRIT1 with CCM2 has also been reported to promote cytoplasmic localization of both proteins. Zawistowski et al. first reported that co-expression of KRIT1 and CCM2 led to the cytoplasmic localization of both proteins in sub-confluent COS-7 cells. This paper also reported that ICAP1α can form a tertiary complex with KRIT1 and CCM2 (34). As is discussed in depth in the next section, ICAP1α expression promotes the nuclear localization of KRIT1. Thus together, these data suggest that the relative binding of ICAP1α and CCM2 to KRIT1 may control the distribution of the CCM complex. Indeed, Francalanci et al. found that the nuclear accumulation of ICAP1α and KRIT1 was lost in the presence of CCM2 (42), which could suggest that CCM2 binding retains KRIT1 in the cytoplasm or promotes nuclear export. CCM2 may also promote the cytoplasmic localization of CCM3, as over-expressed CCM3 exhibits more nuclear localization when the FAT domain is mutated and it no longer binds to CCM2 (50).

The cytoplasmic localization of KRIT1 could also be regulated by post-translational modification, such as phosphorylation. To this point, we recently demonstrated that activation of PKC, particularly PKCα, led to a predominantly cytoplasmic distribution of KRIT1 and blocked localization of KRIT1 to the nucleus in both sub-confluent and confluent endothelial cells. Pre-treatment with the antioxidant N-acetyl-cysteine reversed the ability of PKC activation to promote localization of KRIT1 to the cytoplasm, but did not go so far as to promote nuclear localization (62). Work is ongoing to determine the target(s) of PKCα which regulate KRIT1 nuclear-cytoplasmic shuttling, but these data raise the question of why the shuttling of KRIT1 (and potentially the CCM complex) between the cytoplasm and nucleus is so highly regulated, and what effect it might have on complex function or CCM pathogenesis.

Nuclear Localization of the CCM Complex

Finally, the CCM proteins have been consistently observed in the nucleus (**Figure 2**). While CCM2 and CCM3 lack established nuclear localization or export sequences, KRIT1 has been reported to have both (41). Full-length KRIT1 partially localizes to the nucleus, as does the KRIT1 FERM domain [residues 409–736, (24)]. Truncating the FERM domain to eliminate the F1 subdomain eliminates this nuclear localization (24), as does mutating/deleting the F3 subdomain (42). Interestingly, compared to full-length KRIT1, a truncated KRIT1 construct containing the ankyrin repeats and the FERM domain (residues 207–736) is retained in the nucleus and is insensitive to PKC activation (62). These observations have led to the conjecture that KRIT1 contains two nuclear localization sequences, one in its N-terminus (residues 46-KKKRKK-51); and one in the C-terminus (residues 569-KKHK-572). Several studies have shown that mutation of the N-terminal KRIT1 NLS is sufficient to decrease localization of KRIT1 to the nucleus (42, 43), while mutation of the second NLS in full-length KRIT1 is insufficient (43), suggesting that the N-terminal NLS is functionally dominant and that the nuclear localization of the FERM domain may be driven by some other mechanism. Complicating matters, an N-terminal fragment (residues 1–207), though it contains the NLS, was shown to have a cytoplasmic distribution in transfected HeLa cells (42).

Recently, Draheim et al. reported that KRIT1 nuclear localization can be driven by its interaction with ICAP1α, even in the absence of the KRIT1 NLS. Mutation of either ICAP1α's NLS or KRIT1's ICAP1α binding site significantly inhibited KRIT1 nuclear localization (43). This agrees with early reports that demonstrated that co-expression of exogenous KRIT1 and ICAP1α in COS-7 cells induced the complete nuclear localization of both proteins (41). ICAP1α binding to KRIT1's first NPXY motif also sterically hinders KRIT1's association with microtubules, similar to what has been suggested of the KRIT1●Rap1 interaction (40). Interestingly, the sequence through which KRIT1 likely binds to microtubules is the same stretch of lysines that form the KRIT1 NLS. Thus, changes in the accessibility of this sequence, whether through ICAP1α binding or through Rap1 binding, could cause dissociation from microtubules and also allow for nuclear localization.

While the mechanism(s) governing trafficking of KRIT1 into the nucleus appear clear, the shuttling of KRIT1 out of the nucleus is much less well understood. Sequence prediction has led to several papers proposing that KRIT1 has a nuclear export sequence in the C-terminal FERM domain [residues 551–559, (42, 44)]. However, when this sequence was mutated in a recent study, it failed to lead to enrichment of KRIT1 in the nucleus (43), suggesting that it is not a functional NES. Our recent study suggests that export could be regulated by PKC activity (62), but additional work will be necessary to fully characterize the mechanism. Intriguingly, Zhang et al. reported in 2007 that treatment with leptomycin B, an inhibitor of exportin 1, led to accumulation of KRIT1 and CCM2 in the nucleus (44), leaving

the possibility open that, if KRIT1 does not contain a functional NES, perhaps CCM2 does.

In sum, it is clear that localization of the CCM proteins is dynamically regulated by several potential mechanisms. The current models of CCM signaling in the literature alternatively obfuscate where in the cell the CCM complex is active (though they restrict the possibilities to cytoplasm or membrane) or point to membrane localization as being important- and imply that cytoplasmic localization of the CCM complex acts to sequester the complex away from the plasma membrane. The available evidence supports both models, as we lack the direct evidence needed to resolve these possibilities. However, in order to fully understand the link between loss of function mutations in the CCM proteins and CCM pathogenesis, future work will need to address this gap in knowledge and illuminate how these key binding interactions are segregated in time and place, and how they collectively determine the location and function of the CCM complex.

ROLE OF SUBCELLULAR LOCALIZATION IN REGULATING THE SIGNALING DOWNSTREAM OF THE CCM COMPLEX

At the Membrane: Adherens Junctions, Tight Junctions, and Integrins

The early finding that KRIT1 localizes to points of cell-cell contact (24) led to the development of a broadly accepted working model in which junctional localization of the CCM signaling complex is required to maintain endothelial and vascular homeostasis. Conversely, loss of junctional localization of KRIT1, such as after treatment with thrombin, correlated with down-regulation of VE-cadherin adhesion and loss of barrier function (24). Conspicuously, most of the studies supporting this concept have focused on KRIT1, though CCM2 and CCM3 are assumed to co-localize with KRIT1 in order to form a functional signaling complex. In confluent endothelial cells, KRIT1 co-immunoprecipitates with the integral adherens junction proteins β-catenin and p120-catenin (24), and stabilizes the interaction of β-catenin with VE-cadherin (63), a classical indication of mature adherens junctions (64). Additionally, CCM lesions from both human patients and mouse models exhibit a reduction in TJ protein expression (4, 65, 66). In particular, claudin-5, the major claudin isoform in endothelial cells, is downregulated after loss of KRIT1 (65, 66). While the mechanism by which loss of CCM protein expression leads to reduced barrier function remains undefined, KRIT1 appears to affect cell-cell contacts by stabilizing β-catenin association with adherens junction complexes. Accordingly, loss of KRIT1 expression induces phosphorylation of β-catenin at Y654, a key residue regulating the cadherin●β-catenin interaction (67), leading to translocation of β-catenin to the nucleus and changes in β-catenin mediated TCF/LEF transcriptional activity, including increased expression of cyclinD1 and *Vegf-a (63)*. Claudin-5 transcription is also under the control of a β-catenin●FoxO1●Tcf4 repressor complex, thus increased β-catenin signaling in the nucleus negatively regulates claudin-5 gene transcription (68). Though the total effect of increased β-catenin transcriptional activity on CCM pathogenesis has not been examined, Distefano et al. demonstrated that increased expression of VEGF in KRIT1 deficient endothelial cells formed a feed-forward mechanism that promoted several CCM-related changes in endothelial phenotype (63). Furthermore, blocking the activation of the VEGF receptor VEGFR2 limited lesion formation and bleeding in a mouse model of CCM (69), suggesting that down-regulation of the β-catenin●VE-cadherin complex may be a critical signal in CCM pathogenesis.

Another potential mechanism reliant on the localization of CCM proteins to cell-cell contacts lies downstream of HEG. Mutating the binding sites for HEG1 or Rap1 on KRIT1 inhibits KRIT1 localization to endothelial junctions and disrupts junctional VE-cadherin (39). Additionally, *in vitro* binding and immunofluorescence data indicate that the Rap1 effector Rasip1 also appears to be anchored at cell-cell contacts by HEG1 (70), suggesting that HEG1 is an important focus for Rap1 signaling. The Rap1●Rasip1 interaction appears to inhibit Rho signaling through activation of the RhoGAP ArhGAP29 (71). Though HEG1 does not regulate the Rap1●Rasip1 or Rasip1●ArhGAP29 interactions, because KRIT1 and Rasip1 both bind HEG1 at cell-cell contacts (70), HEG1 may be an important center point for regulation of a balance between Rap1 and RhoA signaling necessary for junctional homeostasis. Interestingly, Castro et al. reported that postnatal deletion of Cdc42, a downstream target of Rap1 signaling, also leads to formation of CCM-like lesions (18). This further suggests that CCM pathogenesis may be linked to activation/inactivation of specific signals downstream of Rap1 signaling.

KRIT1 also plays a role in regulating β1-integrin activity through its interaction with ICAP1α (**Figure 2**). KRIT1 competes with the β1-integrin cytoplasmic domain to bind ICAP1α, and can promote β1-integrin activation (32, 43). However, recent examination of these signaling mechanisms by Lisowska et al. suggests that KRIT1 or CCM2 depletion triggers enhanced development of centrally localized β1-integrin-dependent focal adhesions (72), which runs contrary to expectations based on a competitive mechanism. This study also found that activation of β1-integrin correlated with increased RhoA signaling and remodeling of fibronectin ECM structure after loss of either KRIT1 or CCM2 (72). The finding that loss of KRIT1 or CCM2 upregulates β1 integrin activity corroborates previous work by Faurobert and colleagues, who proposed that KRIT1 depletion in HUVEC destabilized the ICAP1α protein leading to ICAP1α degradation and subsequent increased β1-integrin activation (73). The contradictory results may be explained by the observation that the EA.hy926 cell line used in the studies which demonstrated competitive inhibition of the ICAP1α●integrin interaction by KRIT1 express more ICAP1α and KRIT1, but significantly less β1-integrin compared to HUVECs (32, 73).

Another potential explanation for increased β1-integrin activation after KRIT1 depletion may lie in changes in Rap1 signaling. Studies have established that Rap1 is major regulator of integrin activation, particularly β1-integrin (74), likely *via* interaction with the integrin-activating protein talin

(75–77). Following this line of thought, it is possible that depletion of KRIT1 would free Rap1 to bind to other effectors. Excess free Rap1 could then promote talin-mediated activation of β1-integrin, leading to the development of focal adhesions, stress fibers, and other phenotypes associated with β1-integrin activation.

As described earlier in this review, our recent study challenges the idea that the physical localization of KRIT1 at the plasma membrane is required for cell contact stability. Mutant KRIT1 in which the Rap1 binding domain is disrupted and in which the N- to C-terminal interaction is blocked by mutation of the first NPXY motif or the PTB domain rescues β-catenin localization and restores barrier function of KRIT1-depleted endothelial cells. Notably, these mutants have a predominantly cytoplasmic localization, and are not present at cell-cell contacts nor at the basal membrane. Thus, membrane localization appears dispensable for the ability of KRIT1 to stabilize endothelial cell-cell contacts (**Figure 3**). Interestingly, we found that stabilization of cell-cell contacts does correlate with the capacity of KRIT1 to regulate integrin signaling, and specifically to limit β1 integrin activation. As previously reported, we observed that loss of KRIT1 increased β1 integrin activity. This increase could be rescued by expression of wildtype KRIT1 or KRIT1 in which the N- to C-terminal self-interaction was ablated by mutation of either the first NPXY motif or the PTB domain. However, KRIT1 containing the R452E mutation failed to reverse the activation of β1 integrin and cells expressing this construct exhibited large centralized β1-dependent focal adhesions similar to KRIT1 shRNA alone (58). Thus, these data suggest a potential connection between the regulation of cell-cell contact and cell-matrix contact by the CCM complex that should be explored further.

In the Cytoplasm: Kinase Cascades

The effect of cytoplasmic localization on the function of the CCM complex has not yet been extensively tested. However, the CCM proteins, particularly CCM2 and CCM3, bind to several protein partners with a presumed cytoplasmic distribution. CCM2 binds to MKK3 and MEKK3, which regulate activation of p38 MAPK in response to stress and inhibit BMK1/ERK5 activation respectively (26, 48). CCM3 binds to the STRIPAK complex, which is found in the cytoplasm and at the membrane and has several functions, including regulation of cell polarity and Golgi assembly (51) (**Figure 2**). While the interaction of CCM2 and CCM3 with these larger complexes has been well documented, it is unknown whether the organization or function of these complexes is affected by specific subcellular localization of the CCM proteins. Precedent for such regulation exists, as there are many examples of scaffolding proteins regulating MAPK signaling cascades, including the classic scaffolds Ste5 and KSR which control MAPK pathway localization (i.e., membrane anchoring) and signaling efficiency (78). In this manner, the CCM complex could target or anchor these signaling complexes to the appropriate cellular location to receive incoming signals, and/or control the flow of signaling information to specific downstream processes.

In the Nucleus: A Blank Page

Lastly, despite the widespread presence of KRIT1, CCM2 and CCM3 in the nucleus, only one publication has investigated a possible function for the CCM proteins in the nucleus. Using ultrastructural immunocytochemistry, Marzo et al. showed that KRIT1 localized to perichromatin fibrils, which are markers of transcriptional activity (79), as well as to the dense fibrillar component of the nucleolus which contains pre-ribosomal RNA (80), which hints at a possible role in transcriptional regulation. This, combined with the presence of a Nudix domain in KRIT1, makes it tempting to hypothesize that KRIT1 could bind directly to nucleic acids and regulate transcription or RNA stability, as do several of members of the Nudix protein superfamily (81). This could provide another mechanistic link between expression of the CCM proteins and changes in gene expression, which have been widely reported (22, 82). In addition, it has been proposed that KRIT1 and ICAP1α regulate each other by sequestering the other partner inside the nucleus, thus preventing interaction with cytoplasmic or membrane proteins. This idea is supported by the positive influence that the KRIT1 NLS exerts on ICAP1α nuclear localization (43), which would theoretically diminish the ability of ICAP1α to suppress β1 integrin activation. Accordingly, one could propose several mechanisms by which the localization of the CCM proteins in the nucleus could regulate CCM complex function, however it is still unclear whether, and how, this would occur.

DISCUSSION

Loss of function mutations in KRIT1, CCM2 or CCM3 lead to the development of CCM, a process that has been shown to involve major changes in endothelial function and behavior. The CCM proteins suppress cell division and inflammatory signaling by regulating the p38-MEKK3-KLF2/4 signaling axis (26, 83–85) while also regulating oxidative stress responses (22, 86–89), autophagy (23), apoptosis (87) and cell contractility (54, 72) (in addition to stabilizing cell-cell contacts). However, most of these disease-mediating mechanisms have only been tied to the expression of the CCM proteins, not to their localization or function. Thus, how CCM protein localization fits in the context of CCM pathology is unclear. What's more, many, if not the majority, of the CCM-causing mutations described in the literature are nonsense mutations which lead to premature termination of translation (90, 91). CCM may develop as the result of nonsense-mediated mRNA decay of CCM protein transcripts (91–93) or due to degradation of the truncated protein products *via* the unfolded protein response. This implies that CCM develops due to the complete lack of expression of one CCM protein, rather than the presence of non-functional, truncated proteins. However, as the three CCM proteins form a tripartite complex (52, 94), loss of one CCM protein could result in perturbation of the localization and function of the remaining complex members, which is indeed the case. This could eventually explain why, for example, patients with CCM3 mutations display earlier and more severe disease (30). By continuing to advance our knowledge of the mechanisms

regulating the individual CCM proteins and the CCM signaling complex, we can not only discover more about the mechanisms that underlie CCM pathogenesis, but potentially identify new therapeutic targets and perhaps expand our understanding of other endothelial pathologies.

At the risk of sounding like a broken record, it is clear that much work remains to be done in order to fully understand how the CCM complex is regulated, whether by binding interactions, subcellular localization, or other mechanisms. Current knowledge is not only incomplete, but complicated by differences in cell type, cell density, and expression level between studies, making it difficult to form solid conclusions. This is a critical need, as only by being able to fully understand and manipulate the components and interactions of the CCM complex will we be able to answer such questions as: what is the function of the CCM complex in the nucleus, does the CCM complex generate differential downstream signals depending on its location, and how does loss of just one CCM complex protein lead to the development of CCM? This will require both a fuller understanding of the CCM interactome as well as cutting-edge approaches to track protein location and binding (potentially in real time). To make these future studies the most effective, it will be important to consider effects of the level of protein expression (i.e., over-expression vs. replacement studies), as well as issues caused by differences in cell type (i.e., epithelial vs. endothelial) and cell culture conditions (i.e., sub-confluent vs. confluent). The recent interest in structure-function relationships, particularly in regard to KRIT1, is encouraging, but we still know relatively little about these relationships in CCM2 and CCM3. These gaps in knowledge will need to be filled if we are to someday understand how disrupting the balance of protein-protein interactions in the greater CCM complex (either by mutation, manipulating expression, or post-translational modification) contribute to endothelial dysfunction and CCM pathology.

AUTHOR CONTRIBUTIONS

HS and AG both contributed to the conceptual development and writing of this manuscript. All authors contributed to the article and approved the submitted version.

FUNDING

This work was supported by grants from the National Institutes of Health (HL117885 and HL141131 to AG) and the State of New York (FuzeHub New York State Technology & Innovation Grant to AG).

REFERENCES

1. Fischer A, Zalvide J, Faurobert E, Albiges-Rizo C, Tournier-Lasserve E. Cerebral cavernous malformations: from ccm genes to endothelial cell homeostasis. *Trends Mol Med.* (2013) 19:302–8. doi: 10.1016/j.molmed.2013.02.004
2. Clatterbuck R, Eberhart C, Crain B, Rigamonti D. Ultrastructural and immunocytochemical evidence that an incompetent blood-brain barrier is related to the pathophysiology of cavernous malformations. *J Neurol Neurosurg Psychiatr.* (2001) 71:188–92. doi: 10.1136/jnnp.71.2.188
3. Robinson JR, Awad IA, Little JR. Natural history of the cavernous angioma. *J Neurosurg.* (1991) 75:709–14.
4. Schneider H, Errede M, Ulrich NH, Virgintino D, Frei K, Bertalanffy H. Impairment of tight junctions and glucose transport in endothelial cells of human cerebral cavernous malformations. *J Neuropathol Exp Neurol.* (2011) 70:417–29. doi: 10.1097/NEN.0b013e31821bc40e
5. Al-Shahi R, Bhattacharya JJ, Currie DG, Papanastassiou V, Ritchie V, Roberts RC, et al. Prospective, population-based detection of intracranial vascular malformations in adults: the scottish intracranial vascular malformation study (Sivms). *Stroke.* (2003) 34:1163–9. doi: 10.1161/01.STR.0000069018.90456.C9
6. Dubovsky J, Zabramski J, Kurth J, Spetzler R, Rich S, Orr H, et al. A gene responsible for cavernous malformations of the brain maps to chromosome 7q. *Hum Mol Genet.* (1995) 4:453–8. doi: 10.1093/hmg/4.3.453
7. Johnson E, Iyer L, Rich S, Orr H, Gil-Nagel A, Kurth J, et al. Refined localization of the cerebral cavernous malformation gene (Ccm1) to a 4-cm interval of chromosome 7q contained in a welldefined yac contig. *Genome Res.* (1995) 5:368–80. doi: 10.1101/gr.5.4.368
8. Laberge-le Couteulx S, Jung H, Labauge P, Houtteville J, Lescoat C, Cecillon M, et al. Truncating Mutations in Ccm1, Encoding Krit1, cause hereditary cavernous angiomas. *Nat Genet.* (1999) 23:189–93. doi: 10.1038/13815
9. Sahoo T, Johnson EW, Thomas JW, Kuehl PM, Jones TL, Dokken CG, et al. Mutations in the gene encoding krit1, a Krev-1/Rap1a binding protein, cause cerebral cavernous Malformations (Ccm1). *Hum Mol Genet.* (1999) 8:2325–33. doi: 10.1093/hmg/8.12.2325
10. Eerola I, Plate K, Spiegel R, Boon L, Mulliken J, Vikkula M. Krit1 is mutated in hyperkeratotic cutaneous capillary-venous malformation associated with cerebral capillary malformation. *Hum Mol Genet.* (2000) 9:1351–5. doi: 10.1093/hmg/9.9.1351
11. Serebriiskii I, Estojak J, Sonoda G, Testa JR, Golemis EA. Association of Krev-1/Rap1a with Krit1, a novel ankyrin repeat-containing protein encoded by a gene mapping to 7q21-22. *Oncogene.* (1997) 15:1043–9. doi: 10.1038/sj.onc.1201268
12. Craig H, Gunel M, Cepeda O, Johnson E, Ptacek L, Steinberg G, et al. Multilocus linkage identifies two new loci for a mendelian form of stroke, cerebral cavernous malformation, at 7p15-13 and 3q252-27. *Hum Mol Genet.* (1998) 7:1851–8. doi: 10.1093/hmg/7.12.1851
13. Liquori C, Berg M, Siegel A, Huang E, Zawistowski J, Stoffer T, et al. Mutations in a gene encoding a novel protein containing a phosphotyrosine-binding domain cause type 2 cerebral cavernous malformations. *Am J Hum Genet.* (2003) 73:1459–64. doi: 10.1086/380314
14. Bergametti F, Denier C, Labauge P, Arnoult M, Boetto S, Clanet M, et al. Mutations within the programmed cell death 10 gene cause cerebral cavernous malformations. *Am J Hum Genet.* (2005) 76:42–51. doi: 10.1086/426952
15. Guclu B, Ozturk AK, Pricola KL, Bilguvar K, Shin D, O'Roak BJ, et al. Mutations in apoptosis-related gene, pdcd10, cause cerebral cavernous malformation 3. *Neurosurgery.* (2005) 57:1008–13. doi: 10.1227/01.neu.0000180811.56157.e1
16. McDonald DA, Shi C, Shenkar R, Gallione CJ, Akers AL Li S, et al. Lesions from patients with sporadic cerebral cavernous malformations harbor somatic mutations in the ccm genes: evidence for a common biochemical pathway for ccm pathogenesis. *Hum Mol Genet.* (2014) 23:4357–70.
17. Ren AA, Snellings DA, Su YS, Hong CC, Castro M, Tang AT, et al. Pik3ca and Ccm mutations fuel cavernomas through a cancer-like mechanism. *Nature.* (2021) 594:271–6. doi: 10.1093/hmg/ddu153
18. Castro M, Lavina B, Ando K, Alvarez-Aznar A, Abu Taha A, Brakebusch C, et al. Cdc42 deletion elicits cerebral vascular malformations *via* increased mekk3-dependent Klf4 expression. *Circ Res.* (2019) 124:1240–52. doi: 10.1161/CIRCRESAHA.118.314300
19. Fisher OS, Liu W, Zhang R, Stiegler AL, Ghedia S, Weber JL, et al. Structural basis for the disruption of the cerebral cavernous malformations 2 (Ccm2) interaction with krev interaction trapped 1 (Krit1) by disease-associated mutations. *J Biol Chem.* (2015) 290:2842–53. doi: 10.1074/jbc.M114.616433

20. Draheim KM Li X, Zhang R, Fisher OS, Villari G, Boggon TJ, et al. Ccm2-Ccm3 interaction stabilizes their protein expression and permits endothelial network formation. *J Cell Biol.* (2015) 208:987–1001. doi: 10.1083/jcb.201407129
21. Voss K, Stahl S, Schleider E, Ullrich S, Nickel J, Mueller TD, et al. Ccm3 interacts with ccm2 indicating common pathogenesis for cerebral cavernous malformations. *Neurogenetics.* (2007) 8:249–56. doi: 10.1007/s10048-007-0098-9
22. Goitre L, Balzac F, Degani S, Degan P, Marchi S, Pinton P, et al. Krit1 Regulates the homeostasis of intracellular reactive oxygen species. *PLoS One.* (2010) 5:e11786. doi: 10.1371/journal.pone.0011786
23. Marchi S, Corricelli M, Trapani E, Bravi L, Pittaro A, Delle Monache S, et al. Defective autophagy is a key feature of cerebral cavernous malformations. *EMBO Mol Med.* (2015) 7:1403–17. doi: 10.15252/emmm.201505316
24. Glading A, Han J, Stockton RA, Ginsberg MH. Krit-1/Ccm1 is a rap1 effector that regulates endothelial cell cell junctions. *J Cell Biol.* (2007) 179:247–54. doi: 10.1083/jcb.200705175
25. Detter MR, Snellings DA, Marchuk DA. Cerebral cavernous malformations develop through clonal expansion of mutant endothelial cells. *Circ Res.* (2018) 123:1143–51. doi: 10.1161/CIRCRESAHA.118.313970
26. Zhou Z, Tang AT, Wong WY, Bamezai S, Goddard LM, Shenkar R, et al. Cerebral cavernous malformations arise from endothelial gain of Mekk3-Klf2/4 signalling. *Nature.* (2016) 532:122–6. doi: 10.1038/nature17178
27. Choi JP, Wang R, Yang X, Wang X, Wang L, Ting KK, et al. Ponatinib (Ap24534) inhibits mekk3-klf signaling and prevents formation and progression of cerebral cavernous malformations. *Sci Adv.* (2018) 4:eaau0731. doi: 10.1126/sciadv.aau0731
28. Chan AC, Drakos SG, Ruiz OE, Smith AC, Gibson CC, Ling J, et al. Mutations in 2 distinct genetic pathways result in cerebral cavernous malformations in mice. *J Clin Invest.* (2011) 121:1871–81. doi: 10.1172/JCI44393
29. Yoruk B, Gillers BS, Chi NC, Scott IC. Ccm3 functions in a manner distinct from ccm1 and ccm2 in a zebrafish model of ccm vascular disease. *Dev Biol.* (2012) 362:121–31. doi: 10.1016/j.ydbio.2011.12.006
30. Shenkar R, Shi C, Rebeiz T, Stockton RA, McDonald DA, Mikati AG, et al. Exceptional aggressiveness of cerebral cavernous malformation disease associated with Pdcd10 mutations. *Genet Med.* (2015) 17:188–96. doi: 10.1038/gim.2014.97
31. Pufall MA, Graves BJ. Autoinhibitory domains: modular effectors of cellular regulation. *Annu Rev Cell Dev Biol.* (2002) 18:421–62. doi: 10.1146/annurev.cellbio.18.031502.133614
32. Liu W, Draheim KM, Zhang R, Calderwood DA, Boggon TJ. Mechanism for Krit1 release of icap1-mediated suppression of integrin activation. *Mol Cell.* (2013) 13:5. doi: 10.1016/j.molcel.2012.12.005
33. Stiegler AL, Zhang R, Liu W, Boggon TJ. Structural determinants for binding of sorting nexin 17 (Snx17) to the cytoplasmic adaptor protein krev interaction trapped 1 (Krit1). *J Biol Chem.* (2014) 289:25362–73. doi: 10.1074/jbc.M114.584011
34. Zawistowski J, Stalheim L, Uhlik M, Abell A, Ancrile B, Johnson G, et al. Ccm1 and Ccm2 protein interactions in cell signaling: implications for cerebral cavernous malformations pathogenesis. *Hum Mol Genet.* (2005) 14:2521–31. doi: 10.1093/hmg/ddi256
35. Zhang R, Li X, Boggon TJ. Structural analysis of the Krit1 ankyrin repeat and ferm domains reveals a conformationally stable ard-ferm interface. *J Struct Biol.* (2015) 192:449–56. doi: 10.1016/j.jsb.2015.10.006
36. Li X, Zhang R, Draheim KM, Liu W, Calderwood DA, Boggon TJ. Structural basis for the small g-protein-effector interaction of ras-related protein 1 (Rap1) and the adaptor protein krev interaction trapped 1 (Krit1). *J Biol Chem.* (2012) 12:3615. doi: 10.1074/jbc.M112.361295
37. Liu JJ, Stockton RA, Gingras AR, Ablooglu AJ, Han J, Bobkov AA, et al. A mechanism of rap1-induced stabilization of endothelial cell–cell junctions. *Mol Biol Cell.* (2011) 22:2509–19. doi: 10.1091/mbc.E11-02-0157
38. Gingras AR, Puzon-McLaughlin W, Ginsberg MH. The Structure of the ternary complex of krev interaction trapped 1 (Krit1) bound to both the rap1 gtpase and the heart of glass (Heg1) cytoplasmic tail. *J Biol Chem.* (2013) 288:23639–49. doi: 10.1074/jbc.M113.462911
39. Gingras AR, Liu JJ, Ginsberg MH. Structural basis of the junctional anchorage of the cerebral cavernous malformations complex. *J Cell Biol.* (2012) 199:39–48. doi: 10.1083/jcb.201205109
40. Beraud-Dufour S, Gautier R, Albiges-Rizo C, Chardin P, Faurobert E. Krit 1 Interactions with microtubules and membranes are regulated by rap1 and integrin cytoplasmic domain associated Protein-1. *FEBS J.* (2007) 274:5518–32. doi: 10.1111/j.1742-4658.2007.06068.x
41. Zawistowski J, Serebriiskii I, Lee M, Golemis E, Marchuk D. Krit1 Association with the integrin-binding protein icap-1: a new direction in the elucidation of cerebral cavernous malformations (ccm1) pathogenesis. *Hum Mol Genet.* (2002) 11:389–96. doi: 10.1093/hmg/11.4.389
42. Retta S, Avolio M, Francalanci F, Procida S, Balzac F, Degani S, et al. Identification of krit1b: a novel alternative splicing isoform of cerebral cavernous malformation gene-1. *Gene.* (2004) 325:63–78. doi: 10.1016/j.gene.2003.09.046
43. Draheim KM, Huet-Calderwood C, Simon B, Calderwood DA. Nuclear localization of integrin cytoplasmic domain-associated protein-1 (Icap1) influences beta1 integrin activation and recruits krev/interaction trapped-1 (Krit1) to the nucleus. *J Biol Chem.* (2017) 292:1884–98. doi: 10.1074/jbc.M116.762393
44. Zhang J, Rigamonti D, Dietz H, Clatterbuck R. Interaction between Krit1 and malcavernin: implications for the pathogenesis of cerebral cavernous malformations. *Neurosurgery.* (2007) 60:353–9. doi: 10.1227/01.NEU.0000249268.11074.83
45. Harel L, Costa B, Tcherpakov M, Zapatka M, Oberthuer A, Hansford LM, et al. Ccm2 mediates death signaling by the trka receptor tyrosine kinase. *Neuron.* (2009) 63:585–91. doi: 10.1016/j.neuron.2009.08.020
46. Fisher OS, Zhang R, Li X, Murphy JW, Demeler B, Boggon TJ. Structural studies of cerebral cavernous malformations 2 (Ccm2) reveal a folded helical domain at its C-terminus. *FEBS Lett.* (2013) 587:272–7. doi: 10.1016/j.febslet.2012.12.011
47. Pan L, Yan J, Wu L, Zhang M. Assembling stable hair cell tip link complex *via* multidentate interactions between harmonin and cadherin 23. *Proc Natl Acad Sci U S A.* (2009) 106:5575–80. doi: 10.1073/pnas.0901819106
48. Uhlik M, Abell A, Johnson N, Sun W, Cuevas B, Lobel-Rice K, et al. Rac-Mekk3-Mkk3 scaffolding for P38 mapk activation during hyperosmotic shock. *Nat Cell Biol.* (2003) 5:1104–10. doi: 10.1038/ncb1071
49. Deacon K, Blank JL. Mek Kinase 3 Directly activates Mkk6 and Mkk7, specific activators of the P38 and C-Jun Nh2-terminal kinases. *J Biol Chem.* (1999) 274:16604–10.
50. Li X, Zhang R, Zhang H, He Y, Ji W, Min W, et al. Crystal Structure of Ccm3, a cerebral cavernous malformation protein critical for vascular integrity. *J Biol Chem.* (2010) 285:24099–107. doi: 10.1074/jbc.M110.128470
51. Hwang J, Pallas DC. Stripak complexes: structure, biological function, and involvement in human diseases. *Int J Biochem Cell Biol.* (2014) 47:118–48. doi: 10.1016/j.biocel.2013.11.021
52. Hilder TL, Malone MH, Bencharit S, Colicelli J, Haystead TA, Johnson GL, et al. Proteomic identification of the cerebral cavernous malformation signaling complex. *J Proteome Res.* (2007) 6:4343–55. doi: 10.1021/pr0704276
53. Wang S, Englund E, Kjellman P, Li Z, Ahnlide JK, Rodriguez-Cupello C, et al. Ccm3 Is a gatekeeper in focal adhesions regulating mechanotransduction and Yap/Taz signalling. *Nat Cell Biol.* (2021) 23:758–70. doi: 10.1038/s41556-021-00702-0
54. Stockton RA, Shenkar R, Awad IA, Ginsberg MH. Cerebral cavernous malformations proteins inhibit rho kinase to stabilize vascular integrity. *J Exp Med.* (2010) 207:881–96. doi: 10.1084/jem.20091258
55. Fidalgo M, Fraile M, Pires A, Force T, Pombo C, Zalvide J. Ccm3/Pdcd10 stabilizes gckiii proteins to promote golgi assembly and cell orientation. *J Cell Sci.* (2010) 123:1274–84. doi: 10.1242/jcs.061341
56. Lant B, Yu B, Goudreault M, Holmyard D, Knight JD, Xu P, et al. Ccm-3/Stripak promotes seamless tube extension through endocytic recycling. *Nat Commun.* (2015) 6:6449. doi: 10.1038/ncomms7449
57. Goudreault M, D'Ambrosio LM, Kean MJ, Mullin MJ, Larsen BG, Sanchez A, et al. A Pp2a phosphatase high density interaction network identifies a novel striatin-interacting phosphatase and kinase complex linked to the cerebral cavernous malformation 3 (Ccm3) protein. *Mol Cell Proteomics.* (2009) 8:157–71. doi: 10.1074/mcp.M800266-MCP200
58. Swamy H, Glading AJ. Contribution of protein-protein interactions to the endothelial-barrier-stabilizing function of Krit1. *J Cell Sci.* (2022) 135:25816. doi: 10.1242/jcs.258816

59. Zheng X, Riant F, Bergametti F, Myers CD, Tang AT, Kleaveland B, et al. Cerebral cavernous malformations arise independent of the heart of glass receptor. *Stroke.* (2014) 45:1505–9. doi: 10.1161/STROKEAHA.114.004809
60. Czubayko M, Knauth P, Schluter T, Florian V, Bohnensack R. Sorting Nexin 17, a Non-self-assembling and a ptdins(3)P high class affinity protein, interacts with the cerebral cavernous malformation related protein Krit1. *Biochem Biophys Res Commun.* (2006) 345:1264–72. doi: 10.1016/j.bbrc.2006.04.129
61. Cullen PJ. Endosomal sorting and signalling: an emerging role for sorting nexins. *Nat Rev Mol Cell Biol.* (2008) 9:574–82. doi: 10.1038/nrm2427
62. De Luca E, Perrelli A, Swamy H, Nitti M, Passalacqua M, Furfaro AL, et al. Protein kinase calpha regulates the nucleocytoplasmic shuttling of Krit1. *J Cell Sci.* (2021) 134:217. doi: 10.1242/jcs.250217
63. DiStefano PV, Kuebel JM, Sarelius IH, Glading AJ. Krit1 protein depletion modifies endothelial cell behavior *via* increased vascular endothelial growth factor (Vegf) Signaling. *J Biol Chem.* (2014) 289:33054–65. doi: 10.1074/jbc.M114.582304
64. Oas RG, Xiao K, Summers S, Wittich KB, Chiasson CM, Martin WD, et al. P120-catenin is required for mouse vascular development. *Circ Res.* (2010) 106:941–51. doi: 10.1161/CIRCRESAHA.109.207753
65. Lopez-Ramirez MA, Fonseca G, Zeineddine HA, Girard R, Moore T, Pham A, et al. Thrombospondin1 (Tsp1) replacement prevents cerebral cavernous malformations. *J Exp Med.* (2017) 214:3331–46. doi: 10.1084/jem.20171178
66. Maddaluno L, Rudini N, Cuttano R, Bravi L, Giampietro C, Corada M, et al. Endmt contributes to the onset and progression of cerebral cavernous malformations. *Nature.* (2013) 498:492–6. doi: 10.1038/nature12207
67. Roura S, Miravet S, Piedra J, Garcia de. Herreros A, Dunach M. Regulation of E-cadherin/catenin association by tyrosine phosphorylation. *J Biol Chem.* (1999) 274:36734–40.
68. Taddei A, Giampietro C, Conti A, Orsenigo F, Breviario F, Pirazzoli V, et al. Endothelial adherens junctions control tight junctions by ve-cadherin-mediated upregulation of claudin-5. *Nat Cell Biol.* (2008) 10:923–34. doi: 10.1038/ncb1752
69. DiStefano PV, Glading AJ. Vegf signalling enhances lesion burden in krit1 deficient mice. *J Cell Mol Med.* (2020) 24:632–9. doi: 10.1111/jcmm.14773
70. de Kreuk BJ, Gingras AR, Knight JD, Liu JJ, Gingras AC, Ginsberg MH. Heart of glass anchors rasip1 at endothelial cell-cell junctions to support vascular integrity. *Elife.* (2016) 5:e11394. doi: 10.7554/eLife.11394
71. Post A, Pannekoek WJ, Ross SH, Verlaan I, Brouwer PM, Bos JL. Rasip1 mediates rap1 regulation of rho in endothelial barrier function through arhgap29. *Proc Natl Acad Sci U S A.* (2013) 110:11427–32. doi: 10.1073/pnas.1306595110
72. Lisowska J, Rodel CJ, Manet S, Miroshnikova YA, Boyault C, Planus E, et al. The Ccm1-Ccm2 complex controls complementary functions of rock1 and rock2 that are required for endothelial integrity. *J Cell Sci.* (2018) 131, 15. doi: 10.1242/jcs.216093
73. Faurobert E, Rome C, Lisowska J, Manet-Dupe S, Boulday G, Malbouyres M, et al. Ccm1-Icap-1 complex controls beta1 integrin-dependent endothelial contractility and fibronectin remodeling. *J Cell Biol.* (2013) 202:545–61. doi: 10.1083/jcb.201303044
74. Carmona G, Gottig S, Orlandi A, Scheele J, Bauerle T, Jugold M, et al. Role of the small gtpase rap1 for integrin activity regulation in endothelial cells and angiogenesis. *Blood.* (2009) 113:488–97. doi: 10.1182/blood-2008-02-138438
75. Gingras AR, Lagarrigue F, Cuevas MN, Valadez AJ, Zorovich M, McLaughlin W, et al. Rap1 binding and a lipid-dependent helix in talin f1 domain promote integrin activation in tandem. *J Cell Biol.* (2019) 218:1799–809. doi: 10.1083/jcb.201810061
76. Camp D, Haage A, Solianova V, Castle WM, Xu QA, Lostchuck E, et al. Direct binding of talin to rap1 is required for cell-ecm adhesion in drosophila. *J Cell Sci.* (2018) 131, 24. doi: 10.1242/jcs.225144
77. Bromberger T, Zhu L, Klapproth S, Qin J, Moser M. Rap1 and membrane lipids cooperatively recruit talin to trigger integrin activation. *J Cell Sci.* (2019) 132, 21. doi: 10.1242/jcs.235531
78. Good MC, Zalatan JG, Lim WA. Scaffold proteins: hubs for controlling the flow of cellular information. *Science.* (2011) 332:680–6. doi: 10.1126/science.1198701
79. Biggiogera M, Cisterna B, Spedito A, Vecchio L, Malatesta M. Perichromatin fibrils as early markers of transcriptional alterations. *Differentiation.* (2008) 76:57–65. doi: 10.1111/j.1432-0436.2007.00211.x
80. Marzo S, Galimberti V, Biggiogera M. Unexpected distribution of krit1 inside the nucleus: new insight in a complex molecular pathway. *Eur J Histochem.* (2014) 58:2358. doi: 10.4081/ejh.2014.2358
81. Ray A, Frick DN. Fluorescent probe displacement assays reveal unique nucleic acid binding properties of human nudix enzymes. *Anal Biochem.* (2020) 595:113622. doi: 10.1016/j.ab.2020.113622
82. Glading AJ, Ginsberg MH. Rap1 and Its Effector Krit1/Ccm1 regulate beta-catenin signaling. *Dis Model Mech.* (2010) 3:73–83. doi: 10.1242/dmm.003293
83. Zhou Z, Rawnsley DR, Goddard LM, Pan W, Cao XJ, Jakus Z, et al. The cerebral cavernous malformation pathway controls cardiac development *via* regulation of endocardial Mekk3 signaling and klf expression. *Dev Cell.* (2015) 32:168–80. doi: 10.1016/j.devcel.2014.12.009
84. Hong CC, Tang AT, Detter MR, Choi JP, Wang R, Yang X, et al. Cerebral cavernous malformations are driven by adamts5 proteolysis of versican. *J Exp Med.* (2020) 217, 10. doi: 10.1084/jem.20200140
85. Cuttano R, Rudini N, Bravi L, Corada M, Giampietro C, Papa E, et al. Klf4 is a key determinant in the development and progression of cerebral cavernous malformations. *EMBO Mol Med.* (2016) 8:6–24. doi: 10.15252/emmm.201505433
86. Goitre L, DiStefano PV, Moglia A, Nobiletti N, Baldini E, Trabalzini L, et al. Up-regulation of nadph oxidase-mediated redox signaling contributes to the loss of barrier function in krit1 deficient endothelium. *Sci Rep.* (2017) 7:8296. doi: 10.1038/s41598-017-08373-4
87. Antognelli C, Trapani E, Delle Monache S, Perrelli A, Daga M, Pizzimenti S, et al. Krit1 loss-of-function induces a chronic nrf2-mediated adaptive homeostasis that sensitizes cells to oxidative stress: implication for cerebral cavernous malformation disease. *Free Radic Biol Med.* (2018) 115:202–18. doi: 10.1016/j.freeradbiomed.2017.11.014
88. Goitre L, De Luca E, Braggion S, Trapani E, Guglielmotto M, Biasi F, et al. Krit1 Loss of function causes a ros-dependent upregulation of C-Jun. *Free Radic Biol Med.* (2014) 68:134–47. doi: 10.1016/j.freeradbiomed.2013.11.020
89. Antognelli C, Trapani E, Delle Monache S, Perrelli A, Fornelli C, Retta F, et al. Data in support of sustained upregulation of adaptive redox homeostasis mechanisms caused by krit1 loss-of-function. *Data Brief.* (2018) 16:929–38. doi: 10.1016/j.dib.2017.12.026
90. Laberge S, Labauge P, Marechal E, Maciazek J, Tournier-Lasserve E. Genetic heterogeneity and absence of founder effect in a series of 36 french cerebral cavernous angiomas families. *Eur J Hum Genet.* (1999) 7:499–504. doi: 10.1038/sj.ejhg.5200324
91. Cave-Riant F, Denier C, Labauge P, Cecillon M, Maciazek J, Joutel A, et al. Spectrum and expression analysis of krit1 mutations in 121 consecutive and unrelated patients with cerebral cavernous malformations. *Eur J Hum Genet.* (2002) 10:733–40. doi: 10.1038/sj.ejhg.5200870
92. Frischmeyer PA, Dietz HC. Nonsense-mediated mrna decay in health and disease. *Hum Mol Genet.* (1999) 8:1893–900.
93. Khajavi M, Inoue K, Lupski JR. Nonsense-mediated mrna decay modulates clinical outcome of genetic disease. *Eur J Hum Genet.* (2006) 14:1074–81.
94. Cullere X, Plovie E, Bennett PM, MacRae CA, Mayadas TN. The cerebral cavernous malformation proteins Ccm2l and Ccm2 prevent the activation of the map kinase Mekk3. *Proc Natl Acad Sci U S A.* (2015) 112:14284–9. doi: 10.1073/pnas.1510495112

Conflict of Interest: The authors declare that the research was conducted in the absence of any commercial or financial relationships that could be construed as a potential conflict of interest.

frontiers | Frontiers in Cardiovascular Medicine

TYPE Original Research
PUBLISHED 14 July 2022
DOI 10.3389/fcvm.2022.952114

OPEN ACCESS

EDITED BY
Anindita Das,
Virginia Commonwealth University,
United States

REVIEWED BY
Martin Young,
University of Alabama at Birmingham,
United States
Jürgen A. Ripperger,
Université de Fribourg, Switzerland

*CORRESPONDENCE
Zheng Sun
zheng.sun@bcm.edu
Lilei Zhang
lileiz@bcm.edu

†These authors have contributed equally to this work

SPECIALTY SECTION
This article was submitted to Cardiovascular Genetics and Systems Medicine,
a section of the journal
Frontiers in Cardiovascular Medicine

RECEIVED 24 May 2022
ACCEPTED 28 June 2022
PUBLISHED 14 July 2022

CITATION
Li H, Song S, Tien C-l, Qi L, Graves A, Nasiotis E, Burris TP, Zhao Y, Sun Z and Zhang L (2022) SR9009 improves heart function after pressure overload independent of cardiac REV-ERB. *Front. Cardiovasc. Med.* 9:952114. doi: 10.3389/fcvm.2022.952114

SR9009 improves heart function after pressure overload independent of cardiac REV-ERB

Hui Li[1†], Shiyang Song[2†], Chih-liang Tien[1], Lei Qi[1], Andrea Graves[1], Eleni Nasiotis[1], Thomas P. Burris[3], Yuanbiao Zhao[1], Zheng Sun[2,4*] and Lilei Zhang[1*]

[1]Department of Molecular and Human Genetics, Baylor College of Medicine, Houston, TX, United States, [2]Division of Diabetes, Department of Medicine, Endocrinology and Metabolism, Baylor College of Medicine, Houston, TX, United States, [3]Genetics Institute, University of Florida, Gainesville, FL, United States, [4]Department of Molecular and Cellular Biology, Baylor College of Medicine, Houston, TX, United States

The core clock component REV-ERB is essential for heart function. Previous studies show that REV-ERB agonist SR9009 ameliorates heart remodeling in the pressure overload model with transverse aortic constriction (TAC). However, it is unknown whether SR9009 indeed works through cardiac REV-ERB, given that SR9009 might target other proteins and that REV-ERB in non-cardiac tissues might regulate cardiac functions indirectly. To address this question, we generated the REV-ERBα/β cardiac-specific double knockout mice (cDKO). We found that REV-ERB cardiac deficiency leads to profound dilated cardiac myopathy after TAC compared to wild-type (WT) control mice, confirming the critical role of REV-ERB in protecting against pressure overload. Interestingly, the cardioprotective effect of SR9009 against TAC retains in cDKO mice. In addition, SR9009 administered at the time points corresponding to the peak or trough of REV-ERB expression showed similar cardioprotective effects, suggesting the REV-ERB-independent mechanisms in SR9009-mediated post-TAC cardioprotection. These findings highlight that genetic deletion of REV-ERB in cardiomyocytes accelerates adverse cardiac remodeling in response to pressure overload and demonstrated the REV-ERB-independent cardioprotective effect of SR9009 upon pressure overload.

KEYWORDS

circadian clock, REV-ERB, SR9009, TAC, heart disease

Introduction

Most living organisms' behavior and physiological processes oscillate in day/night cycles. Disruption of the circadian rhythm has been well associated with cardiovascular disease, as exemplified by studies of shift workers (1, 2). In mammalian systems, the central clock exists in the suprachiasmatic nucleus (SCN) of the brain, while peripheral

clocks outside the SCN exist and function in almost all cell types throughout the body. The function of the peripheral clocks, including those in the heart, has been increasingly appreciated from murine studies using tissue-specific peripheral clock deletion models (3–5).

The molecular clock is comprised of a transcriptional-translational feedback loop with the conserved core clock factors, including the transcription activators BMAL1/CLOCK and transcription repressor CRY/PER. REV-ERBα/REV-ERBβ are nuclear receptors with heme as the physiological ligand (6, 7), which stabilize and enhance the core clock. They are thought to act primarily as transcriptional repressors due to their lack of an activation domain, although recent work has shown that they may "tether" with other transcription factors for target recognition (8, 9).

The function of REV-ERB in the heart was initially established by a series of works using a pharmacological tool drug, SR9009. REV-ERB agonist was shown to protect cardiac function after pressure overload and myocardial infarction (10–12). Recently, we and others have demonstrated the physiological function of cardiac REV-ERB by constructing REV-ERBα/β double cardiac knockout mice (cDKO) that present progressive dilated cardiomyopathy (13, 14). In addition, we have shown that an abnormal temporal pattern of clock gene expression correlates with the severity of cardiac dilation in patients with idiopathic dilated cardiomyopathy (14).

It remains undetermined to what degree the cardioprotective effect of SR9009 is dependent on cardiac REV-ERB, considering that SR9009, like many small molecules, has off-target effects (15). The relative functional importance of REV-ERBα vs. REV-ERBβ in the heart is also unclear. REV-ERBα and REV-ERBβ are encoded by two different genes with a high homology (16, 17). Previous literature suggests that in most systems *Nr1d1* is dominant with some overlapping functions between the two (17–19).

Here we show that mice with REV-ERBα/β cardiac-specific double deletion (cDKO) are exquisitely sensitive to pressure overload and display a rapid onset of lethal dilated cardiomyopathy upon TAC as compared to the wild-type (WT) control. In comparison, REV-ERBβ single KO mice show a very mild phenotype, suggesting that REV-ERBα is dominant or there is significant functional redundancy between REV-ERBα and REV-ERBβ. We have found that SR9009 remains cardioprotective in cDKO mice compared to WT mice, indicating that cardiomyocyte REV-ERB is not required for the cardioprotection effect of SR9009. We also show that anti-phasic administration of SR9009 has similar effects to phasic administration, suggesting its effect is unlikely through REV-ERB in other cell types in the heart.

Materials and methods

Animals

Wild-type C57BL/6J mice were purchased from the Jackson Laboratory at the age of 7 weeks and allowed to acclimate in the Baylor College of Medicine for 2 weeks prior to the experiments described below. REV-ERBα and β floxed mice were previously described (Rev-erbα^{loxP} (*Nr1d1*$^{TM1.2Rev}$, MGI ID 5426700) and Rev-erbβ^{loxP} (*Nr1d2*$^{TM1.1Rev}$, MGI ID 5426699) (14). They were crossed to generate the double floxed mouse line (*Nr1d1/2*$^{fl/fl}$). Exons 3 and 4 of *Nr1d1* were floxed, which leads to an in-frame deletion of the DNA binding domain upon Cre recombinase cleavage (20). Exon 4 of *Nr1d2* was floxed,[1] which led to a frameshift deletion and nonsense-mediated decay of the transcript upon Cre recombinase cleavage (20). All the animal procedures were approved by the Institutional Animal Care and Use Committee at Baylor College of Medicine.

Preparation and administration of SR9009

SR9009 was synthesized and purified in the laboratory of Thomas Burris (Department of Pharmacology and Physiology, St. Louis University, St. Louis, MO, United States) as previously published (13). For *in vivo* experiments, SR9009 was dissolved in 5% DMSO/10% Cremophor EL (Sigma-Aldrich, C5135)/85% PBS in a working solution at 10 mg/ml. Mice were injected at a dose of 100 mg/kg/day given i.p. once daily at zeitgeber time 6 or 18 (ZT6 and ZT18) as indicated. The diluent without SR9009 of the same volume was used as the control.

Pressure overload (TAC)

All mice were C57BL/6J littermate males aged 9 weeks at the start of the experiment. Mice were anesthetized with 1% inhalational isoflurane, mechanically ventilated (Harvard apparatus), and subjected to thoracotomy. The aortic arch was constricted between the left and right carotid arteries using a 7.0 silk suture and a 27 gauge needle as previously described (20). Pre-surgical and post-surgical analgesics with buprenorphine (0.05 mg/kg, Sigma-Aldrich) and meloxicam (5 mg/kg, Sigma-Aldrich)were administered.

Echocardiography

For transthoracic echocardiography, mice were anesthetized with 1% inhalational isoflurane and imaged using the Vevo

1 http://www.informatics.jax.org/allele/MGI:5426699

2100 High-Resolution Imaging System (Visual Sonics Inc.) with the MS-550 40 MHz probe. Measurements were obtained from M-mode sampling, and integrated EKV images were taken in the LV short axis at the mid-papillary level.

Histological analysis

Short-axis heart sections from the mid ventricle were fixed in PBS/4% paraformaldehyde and embedded in paraffin. Fibrosis was visualized using Gomori's Trichrome staining kit (Sigma-Aldrich) with quantification of the fibrotic area using ImagePro software. The cardiomyocyte cross-sectional area was determined by staining with WGA Alexa 488 (Invitrogen W11261) and analyzed using ImageJ (National Institutes of Health).

Cell isolation from mice heart

Mouse cardiomyocytes isolation was performed by langendorff perfusion method, which was described in details previously (21). Cardiac fibroblast and endothelial cell isolation was performed using MACS cell separation (Miltenyi Biotech) following the manufacturer's instructions. Briefly, the mouse heart was dissected and minced into small pieces. Collagenase type I (Worthington LS004196) was used for digestion in 37°C for 1 h. After 1 h incubation, a strainer was used to remove large particle and undigested tissues. RBC lysis buffer (ab204733) was used to remove red blood cells. Next, CD45 microbeads (Miltenyi Biotec, 130-052-301) and MS column (Miltenyi Biotec, 130-042-201) were used to remove leukocytes. To isolate cardiac fibroblast, CD90.2 microbeads (Miltenyi Biotec, 130-049-101) and MS were used. CD90.2 positive cells were collected from MACS column. CD31 microbeads (Miltenyi Biotec, 130-097-418) and MS column were used to isolate endothelial cells from flow through samples. The enrichment of the target cells was validated by qRT-PCR.

Reverse transcription and quantitative real-time PCR

Total RNA was extracted using RNeasy Mini Kit (Qiagen 74106) according to the manufacturer's protocol. The concentration was measured by a microplate reader (FLUOstar Omega, BMG LABTECH, Ortenberg, Germany). cDNA was synthesized using a reverse transcription supermix (iScript, BIO-RAD 1708841, CA, United States). Quantitative real-time PCR was performed on QuantStudio 5 Dx Real-Time PCR Systems (Applied Biosystems, Thermo Fisher Scientific, Inc.) with 2× qPCRBIO Probe Blue Mix Lo-ROX (PCR Biosystems Inc.) and TaqMan universal probes (Roche). All primers used in this manuscript are listed in **Supplementary Table 1**. *Ppib* was used as a reference for normalization. The relative mRNA expression was calculated by the $\Delta\Delta$Ct method.

Statistical analysis

Data were shown as means ± *SEM*. Comparisons were analyzed by Student's *t*-test, one-way or two-way analysis of variance (ANOVA). Multiple comparisons were taken into account when necessary. All statistical analysis was performed on IBM SPSS Statistics 22.0 (Armonk, NY, United States) or GraphPad Prism (San Diego, CA, United States). $P < 0.05$ was considered statistically significant.

Results

Double deletion of REV-ERBα/β in cardiomyocytes led to severe cardiac dysfunction and ventricular dilation after pressure overload

We generated cardiomyocyte-specific REV-ERBα/β double knockout mice, referred to as cDKO, by crossbreeding *Nr1d1/2*$^{fl/fl}$ mice (*Nr1d1*$^{TM1.2Rev}$, MGI ID 5426700 and *Nr1d2*$^{TM1.1Rev}$, MGI ID 5426699) with the αMHC-Cre line (22). Cre negative *Nr1d1/2*$^{fl/fl}$ littermates were used as WT controls. cDKO mice develop age-dependent dilated cardiomyopathy, as we recently reported. However, the cardiac stress response and pathological remodeling after pressure overload have not been studied in these mice (13, 14). cDKO mice did not show significant ventricular dilation or contractile dysfunction before the age of 20 weeks. Therefore, we performed the transverse aortic constriction (TAC) from 9 to 13 weeks of age when the cardiac structure and function were indistinguishable to the controls (**Supplementary Figures 1A–I**). We show that the cDKO mice were highly sensitive to pressure overload and had a significant drop in ejection fraction (EF) as early as 2 weeks after the surgery, with an average EF of 20.9 vs. 53.5% in WT controls (**Figure 1A**); this is accompanied by a significant left ventricle dilation at 5.02 vs. 3.33 mm in the controls (**Figure 1B**). The left ventricular (LV) dimension (LVID;d) was also increased in cDKO mice compared to WT controls, with no change for LV wall thickness (**Figure 1C**). We had to terminate the experiment at 4 weeks after surgery, as the cDKO mice showed a significant drop in body weight (21.0 g in cDKO vs. 28.6 g in WT controls) and reached the humane endpoint (**Figure 1D**). Histology with trichrome staining showed significantly increased fibrosis in cDKO compared to the WT mice (**Figures 1E,F**). WGA staining analysis of the cross-section area of muscle fiber did not reveal obvious changes in cDKO vs. WT mice, which supports

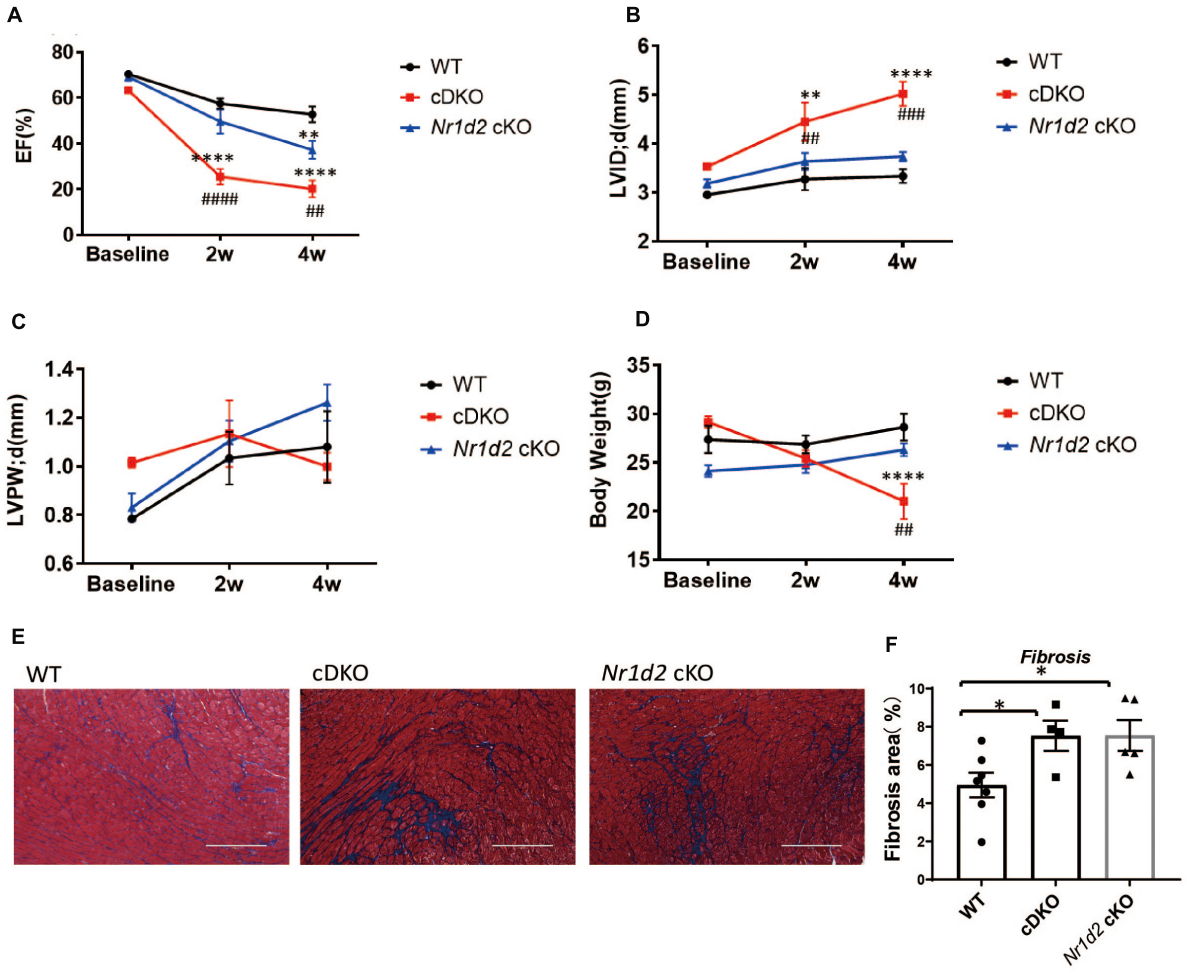

FIGURE 1
Deficiency of REV-ERBα/β or REV-ERBβ in cardiomyocytes exacerbates heart failure upon pressure overload. **(A–C)** Echocardiography analysis of ejection fraction (EF), LVID;d (left ventricle internal diameter; end-diastole), and LVPW;d (left ventricle posterior wall thickness; end-diastole) at __ weeks after TAC. **(D)** Body weight in WT, cDKO, and *Nr1d2* cKO mice. **(E,F)** Representative images and quantification of fibrosis area by Masson's trichrome staining at 4 weeks after TAC. WT $n = 10$, cDKO $n = 6$, *Nr1d2* cKO $n = 5$. Data are shown as mean ± S.E.M. $^{\#\#}p < 0.01$, $^{\#\#\#}P < 0.001$, $^{\#\#\#\#}P < 0.0001$, $^{**}p < 0.01$, $^{***}P < 0.0001$ by two-way ANOVA, *indicates comparison to WT, $^{\#}$indicates comparison to cDKO. Tukey's test was used for multiple comparison corrections.

eccentric hypertrophy or dilated cardiomyopathy as opposed to concentric hypertrophy (**Supplementary Figures 1N,O**). Thus, cardiac REV-ERB is essential for cardiac stress response and remodeling upon pressure overload since cDKO mice are highly susceptible to dilated cardiomyopathy in response to pressure overload.

Single deletion of REV-ERBβ in cardiomyocytes showed mild cardiac dysfunction after pressure overload

To distinguish the functional significance between REV-ERBα and REV-ERBβ, we used a similar strategy to generate REV-ERBβ single cardiac deletion (*Nr1d2*$^{f/f}$: α-*MHC-cre*), referred to as *Nr1d2* cKO. In contrast to cDKO, *Nr1d2* cKO showed a modest reduction in EF (36.2% in cKO vs. 20.9% in cDKO) at 4 week after TAC (**Figure 1B**). cKO mice did not show significant chamber dilation or LV wall thinning compared to WT mice (**Figures 1C,D**). Consistent with echocardiography analysis, *Nr1d2* cKO mice were able to maintain their body weight and normal activities on physical exams during the entire experiment (**Figure 1A**). However, trichrome staining showed significantly increased fibrosis in cKO heart compared to WT (**Figures 1E,F**), indicating that REV-ERBβ has an indispensable role on its own during pressure overload. The mild phenotypic changes in *Nr1d2* cKO mice suggest that REV-ERBα and REV-ERBβ could have largely redundant roles or REV-ERBα is the dominant isoform in the heart.

SR9009 alleviates pressure overload-induced heart failure in the absence of cardiac REV-ERBs

SR9009 is a widely used REV-ERB agonist that targets both REV-ERBα and REV-ERBβ. We have shown that SR9009 is cardioprotective in WT mice after pressure overload when administered at Zeitgeber time 6 (ZT6), a time point immediately before REV-ERB peak expression in the heart (10). To test if the SR9009 effects are through REV-ERB, we administered SR9009 to cDKO mice one day after TAC at ZT6. SR9009 still protected the cDKO mice from cardiac dysfunction, just as in the WT mice (**Figures 2A–C** and **Supplementary Figures 2A–D**). EF was normalized from 20.9% in the vehicle-treated group to 53.8% in the SR9009 ZT6 group at 4 weeks after TAC (**Figure 2A**). SR9009 also prevented the dilation of the left ventricle in cDKO hearts (LVID; d 5.06 mm with SR9009 vs. 3.74 mm with a vehicle in cDKO) (**Figure 2B**). The LV wall thickness also improved (LVPW;d 0.98 mm with SR9009 vs. 0.62 mm with a vehicle in cDKO) (**Figure 2C**). Trichrome staining revealed a reduction in cardiac fibrosis after SR9009 in cDKO mice (**Figures 2D,E**). Thus, SR9009 retains the full cardioprotective capacity in cDKO mice after TAC, demonstrating that the cardioprotective effect of SR9009 against pressure overload is not dependent on REV-ERB in cardiomyocytes.

SR9009 alleviates pressure overload-induced heart failure similarly at different times of the day

As a core component of the circadian clock, REV-ERBα expression in the heart oscillates robustly, this was validated by our RNA sequencing result in the mouse heart (14) as well as an independent previously published microarray study (GSE36407) (**Supplementary Figures 3A–D**). REV-ERBβ has a similar phase to REV-ERBα with a smaller amplitude of oscillation (**Supplementary Figures 3A–D**). We examined the expression of REV-ERBα and β in each of the main cell types in the adult mouse heart, including cardiomyocytes, cardiac fibroblasts, and cardiac endothelial cells at baseline and TAC conditions. The robust oscillatory pattern of REV-ERB was retained in all cell types tested, with ZT6 close to the expression peak and ZT18 close to the expression trough (**Figure 3**). While TAC does not change REV-ERB expression in the heart globally, when we examined each individual cell types, REV-ERBα expression is reduced by about 50% in cardiac fibroblasts and endothelial cells but not the cardiomyocytes (**Figures 3A–C** and **Supplementary Figures 3A,B**). So, the bulk RNA expression in the heart primarily reflects gene expression in the cardiomyocytes. At ZT18, REV-ERBα expression is at 1–2% compared to ZT6 for cardiac fibroblasts or cardiac endothelial cells and about 20% compared to ZT6 for cardiomyocytes (**Figures 3A–C**), which is comparable to what can be achieved

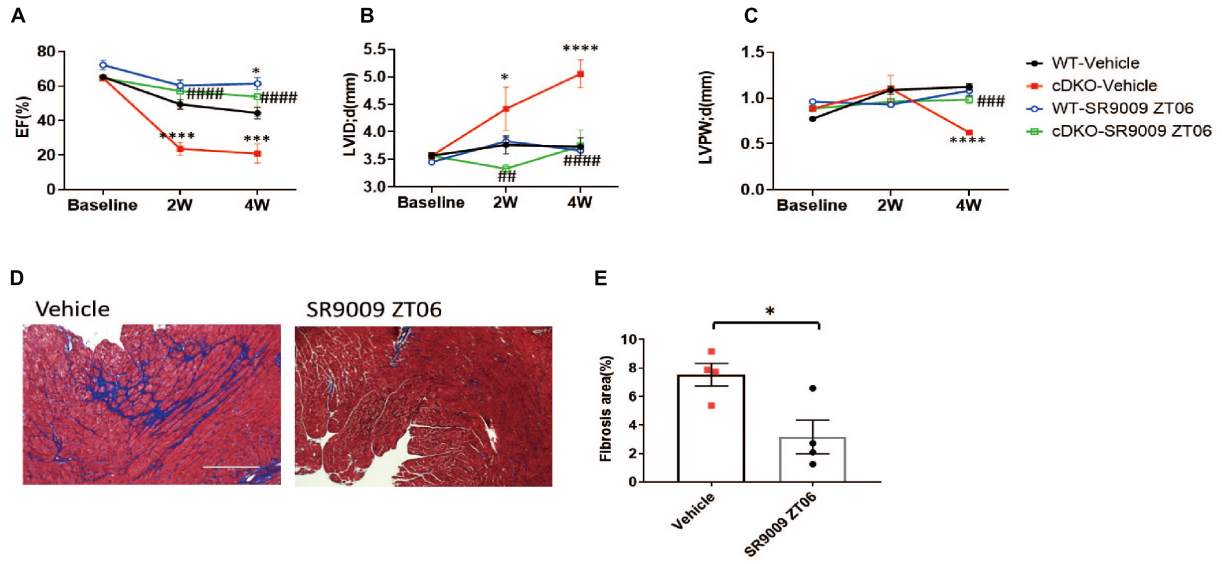

FIGURE 2
SR9009 rescues post-TAC cardiac dysfunction in REV-ERB deficient mice. **(A–C)** Echocardiography of WT and cDKO after vehicle or SR9009 treatment at ZT06. WT-vehicle n = 10, cDKO-vehicle n = 5, WT-SR9009 n = 5, and cDKO-SR9009 n = 6. **(D,E)** Representative images and quantification of fibrosis area by Masson's trichrome staining at 4 weeks after TAC for cDKO mice treated with SR9009 at ZT06. Data are shown as mean ± S.E.M. $^{\#\#}p < 0.01$, $^{\#\#\#}P < 0.001$, $^{\#\#\#\#}P < 0.0001$, $^{*}p < 0.05$, $^{***}p < 0.001$, $^{****}P < 0.0001$ by two-way ANOVA, *indicates comparison to WT-vehicle, $^{\#}$indicates comparison to cDKO-vehicle. Tukey's test was used for multiple comparison corrections.

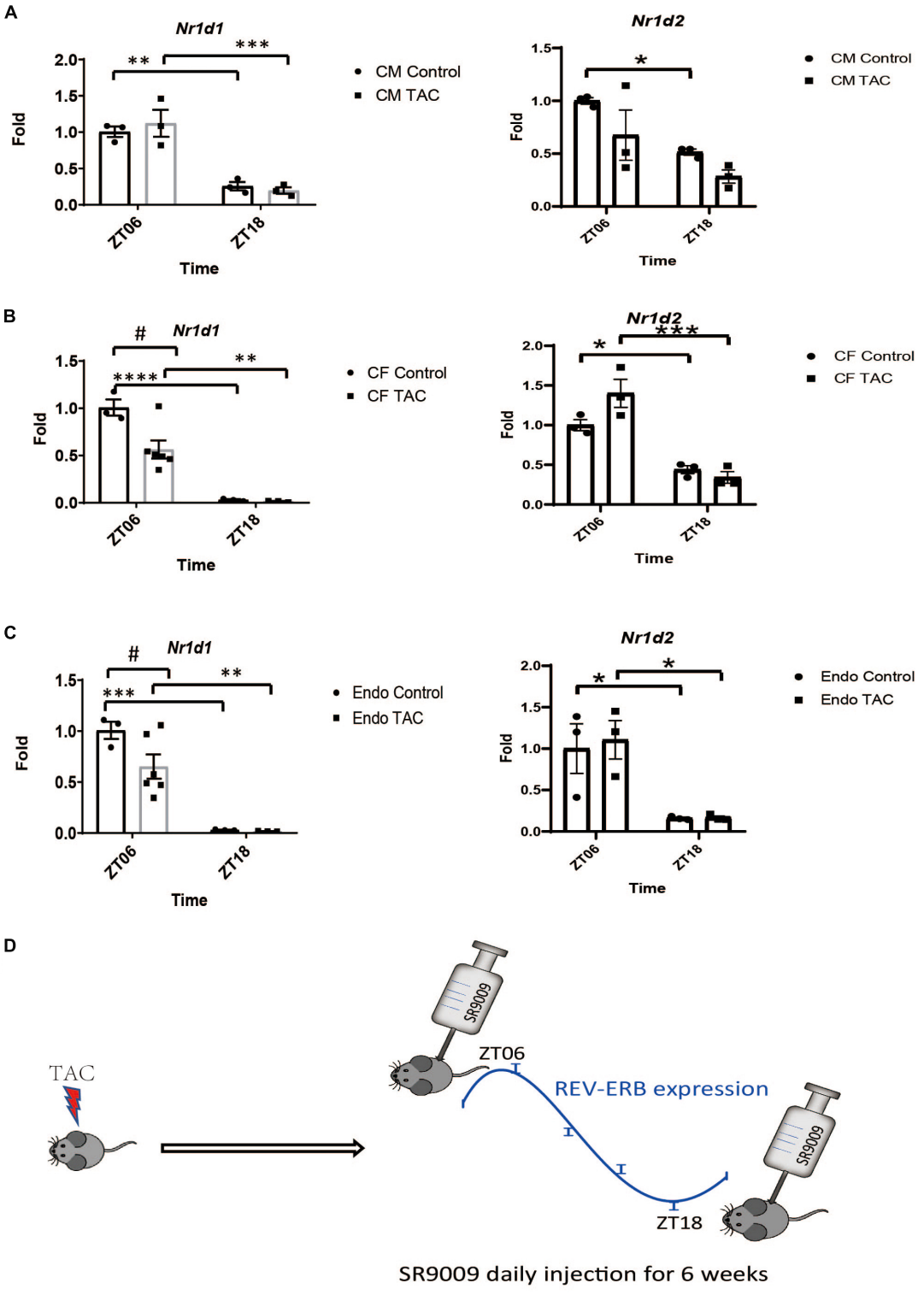

FIGURE 3
The rhythmic expression of REV-ERB in the major cell types of the heart. **(A–C)** Relative mRNA expression levels of *Nr1d1* and *Nr1d2* in major cell types in the heart (CM-cardiomyocytes, CF-cardiac fibroblasts and Endo-endothelial cells) isolated from mouse hearts at 6 weeks after TAC or sham surgery at ZT6 or ZT18. $^{\#}p < 0.05$, $^{*}P < 0.05$, $^{**}p < 0.01$, $^{***}P < 0.001$ by two-way ANOVA. Tukey's test was used for multiple comparison corrections. $n = 3$. **(D)** Diagram of the SR9009 treatment schemes. Mice receive daily SR9009 injection post-TAC at ZT06 or ZT18 for 6 weeks. $^{****}P < 0.0001$.

by Cre deletion or siRNA knockdown. REV-ERBβ also shows a significant reduction pattern in the baseline condition of all cell types detected at ZT18 (**Figures 3A–C**). Thus, ZT18 is a time point when REV-ERB expression is sufficiently low in all major cardiac cell types that it creates a transient *de facto* KO or knockdown condition in the entire heart. Given the short half-life of SR9009 (2 h), we hypothesized that if SR9009 has a major effect on other non-myocyte cell types in the heart, its effects may be diminished when administered at a different time point (ZT18). In fact, a previous report showed the cardioprotective effect of SR9009 upon myocardial infarction was only evident at ZT6 and not evident at ZT18, which supports this notion (11).

We then performed TAC surgery in WT mice and treated them with daily SR9009 at ZT18 (**Figure 3D**), when REV-ERB expression is very low in all cardiac cell types. Surprisingly, the effects of SR9009 at ZT18 were comparable to those at ZT6 as we had previously published (10). SR9009 given at ZT18 rescued TAC-induced cardiac dysfunction to a similar degree as SR9009 given at ZT6 (**Figure 4A**). Both showed EF in the normal range after 6 weeks of TAC (52.0 and 60.6% individually), significantly higher than the vehicle-treated group at 38% (**Figure 4A**). SR9009 did not seem to alter the chamber size or wall thickness of left ventricle (**Figures 4B,C** and **Supplementary Figures 4A–D**), but ameliorated fibrosis drastically (**Figures 4D,E**). The similar cardioprotective effects of SR9009 administrated at the peak and trough of REV-ERB expression suggest a REV-ERB-independent mechanism of SR9009 in counteracting pressure overload-mediated contractile dysfunction.

Discussion

The cardioprotective function of REV-ERB was first established using the pharmacological tool drug SR9009 (10, 11). Although SR9009 can have non-specific targets (15), the essential role of REV-ERB in the heart was confirmed by more recent reports using two independent REV-ERB cardiac-specific knockout murine models (13, 14). To specifically investigate the role of REV-ERB in cardiac disease remodeling processes, we challenged REV-ERB cardiac-specific knockout mice (cDKO) with pressure overload. Our results from the genetic model demonstrated the key protective role of REV-ERB in cardiac pressure overload in addition to maintaining normal physiological homeostasis.

Nr1d1 and *Nr1d2* genes that encode REV-ERBα and REV-ERBβ, respectively, share a high degree of homology (16, 17). *Nr1d1* has been demonstrated to be the dominant isoform in most systems studied to date, with partially redundant functions between the two (17–19). To investigate the contribution of REV-ERBα and REV-ERBβ in the heart, we studied the *Nr1d2* single cardiac cKO and compared it to cDKO. We found that *Nr1d2* cKO mice only show mild dysfunction when compared to the cDKO mice under TAC stress, indicating that *Nr1d2* alone is dispensable for cardiac protection upon pressure overload. Therefore, *Nr1d1* is the dominant isoform in the heart, or the two isoforms have largely redundant roles.

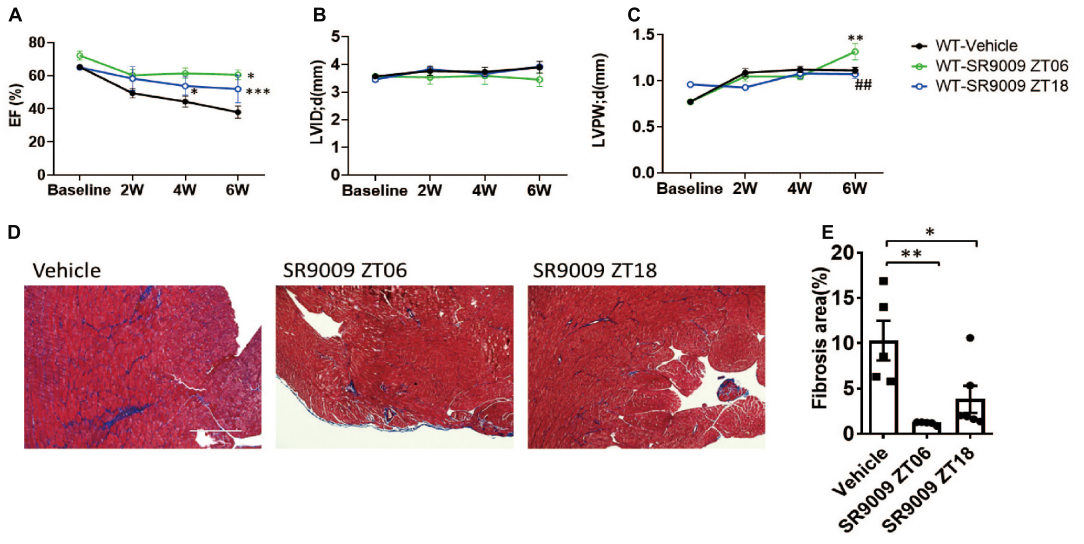

FIGURE 4
Post-TAC SR9009 treatment at ZT6 or ZT18 is equally cardioprotective. **(A–C)** Echocardiography analysis of time-dependent effect of SR9009 on cardiac functions in WT TAC mice. WT-vehicle n = 10, WT-SR9009 ZT06 n = 6, WT-SR9009 ZT18 n = 5. Data are shown as mean ± S.E.M. $^{\#\#}p < 0.01$ by two-way ANOVA comparing to the WT-SR9009 ZT18 group, $^{*}P < 0.05$, $^{**}p < 0.01$, $^{***}P < 0.001$ by two-way ANOVA comparing to the WT vehicle group. Tukey's test was used for multiple comparison corrections. **(D,E)** Representative images and quantification of fibrosis area by Masson's trichrome staining at 6 weeks after TAC. $^{*}P < 0.05$, $^{**}p < 0.01$ by one-way ANOVA. Tukey's test was used for multiple comparison corrections.

Considering the potential off-target effects of SR9009, we set out to evaluate its target specificity in the heart. We used the same regime we previously treated WT mice with, and found, SR9009 retains the full cardioprotective capacity in cDKO mice. The *Nr1d1* deletion allele results in an in-frame deletion of the DNA binding domain and a mutant protein, which may be able to "tether" to other transcription factors for target recognition (9). The *Nr1d2* deletion allele is a complete loss of function frameshift allele where no protein is expressed. One could argue that the truncated REV-ERBα might mediate the SR9009 effects. However, another cardiac REV-ERBα/β double KO mouse line with a frameshift *Nr1d1* deletion and a complete loss-of-function allele has an almost identical phenotype to the cDKO mice used in this study (13, 14), suggesting that the truncated REV-ERBα unlikely has a cardiac function.

As SR9009 is systemically administered, the effect of SR9009 may depend on REV-ERB in other cell types, as cardiomyocytes account for 30–50% of the number of cells in a healthy heart (23) and probably even lower proportion in a heart with fibrosis or inflammation. By carefully isolating various major cell types in the heart, we found that all cell types tested have the same phase for the oscillatory REV-ERB expression. This allowed us to administer SR9009 at a time when REV-ERB expression nadirs in all cell types. As our previous experiments were designed to administer SR9009 to match the peak of REV-ERB and capture the maximum target availability, we chose to also administer SR9009 at ZT18 when minimum REV-ERB is expressed. We found that SR9009 is equally effective at ZT6 or ZT18 despite the huge difference of REV-ERB expression levels between these two time-points in all major cell types in the heart. Therefore, SR9009 can have cardioprotective effects independent of REV-ERB. We realized that we have only examined 2 time points (the peak and the nadir of REV-ERB), additional time points in a 24-h day and increased number of animals may allow detection of more subtle differences in the timing of SR9009 treatment. Given its robust cardioprotective effects in multiple disease models, it will be interesting to explore the genuine targets of SR9009 in the future.

In conclusion, we demonstrate the cardioprotective role of the core circadian clock component REV-ERB in the pressure overload disease model. REV-ERVβ is largely dispensable in this process. SR9009 likely protects the heart through REV-ERB independent mechanisms, which warrants further investigations.

Data availability statement

Publicly available datasets were analyzed in this study. This data can be found here: https://www.ncbi.nlm.nih.gov/geo/, GSE152372 and GSE36407.

Ethics statement

The animal study was reviewed and approved by the Institutional Animal Care and Use Committee at Baylor College of Medicine.

Author contributions

LZ, ZS, and TB conceived the project. HL, SS, C-lT, LQ, AG, EN, and YZ performed the experiment and analyzed the data. HL, YZ, ZS, and LZ wrote the manuscript with contributions from others. All authors contributed to the article and approved the submitted version.

Funding

This work was supported by the NIH grant HL143067 (LZ). We are also thankful for HL153320, DK111436, AG069966, AG070687, RF1AG060769, and ES027544, Cardiovascular Research Institute at BCM, the DLDCCC, the Specialized Programs of Research Excellence (SPORE) program (P50CA126752), the Gulf Coast Center for Precision Environmental Health (P30ES030285), and the Texas Medical Center Digestive Diseases Center (P30 DK056338).

Conflict of interest

The authors declare that the research was conducted in the absence of any commercial or financial relationships that could be construed as a potential conflict of interest.

Publisher's note

Supplementary material

The Supplementary Material for this article can be found online at: https://www.frontiersin.org/articles/10.3389/fcvm.2022.952114/full#supplementary-material

SUPPLEMENTARY FIGURE 1
Echocardiography parameters and histology analysis in WT, cDKO, and Nr1d2 cKO mice in Sham and TAC groups. **(A–H)** Echocardiography analysis of EF, FS (fractional shortening), LVID;s (left ventricular internal dimension end-systole), LVID;d (left ventricle internal diameter; end-diastole), LVPW;s (left ventricle posterior wall thickness; end systole), LVPW;d (left ventricle posterior wall thickness; end-diastole), LV Mass AW (corrected) (corrected left ventricular mass) and Body weight in WT. **(I)** Representative images and quantification of fibrosis area by Masson's trichrome staining of Sham animal hearts at 13 weeks. WT $n = 3$, cDKO $n = 3$. **(J–M)** Echocardiography analysis of FS (fractional shortening), LVID;s (left ventricular internal dimension end-systole), LV Mass AW (corrected) (corrected left ventricular mass), and LVPW;s (left ventricle posterior wall thickness; end systole) in WT, cDKO and *Nr1d2* cKO mice after TAC. WT $n = 10$, cDKO $n = 6$, *Nr1d2* cKO $n = 5$. Data are shown as mean ± S.E.M. $^{\#}p < 0.05$, $^{\#\#}p < 0.01$, $^{\#\#\#\#}P < 0.0001$, $^{**}p < 0.01$, $^{****}P < 0.0001$ by two-way ANOVA, *indicates comparison to WT, $^{\#}$indicates comparison to cDKO. Tukey's test was used for multiple comparison corrections. **(N,O)** Representative images and quantification of cross-section area by WGA (Wheat Germ Agglutinin) staining $n = 4$.

SUPPLEMENTARY FIGURE 2
Echocardiography analysis of post-TAC cardiac protective effect of SR9009 in WT TAC and cDKO mice. **(A–D)** Echocardiography analysis of cardiac protective effect of SR9009 in WT and cDKO mice before and after TAC. FS, LVID;s, LV Mass AW (corrected) and LVPW;s were shown. WT-vehicle $n = 10$, cDKO-vehicle $n = 5$, WT-SR9009 ZT06 $n = 5$, and cDKO-SR9009 ZT06 $n = 6$. Data are shown as mean ± S.E.M. $^{***}p < 0.001$, $^{****}P < 0.0001$, $^{\#\#}p < 0.01$, $^{\#\#\#}P < 0.001$, $^{\#\#\#\#}P < 0.0001$, $^{**}p < 0.01$, $^{***}p < 0.001$, $^{****}P < 0.0001$ by two-way ANOVA, *indicates comparison to WT-vehicle, # indicates comparison to cDKO-vehicle. Tukey's test was used for multiple comparison corrections.

SUPPLEMENTARY FIGURE 3
Nr1d1 expression from GSE36407. **(A,B)** Relative mRNA expression levels of *Nr1d1* and *Nr1d2* in mouse hearts at multiple Zeitgeber times (ZTs) in Sham (Curve shows in Black) and TAC (Curve shows in Red) conditions. Raw data is from GSE36407 in GEO (Gene Expression Omnibus) $^{*}P < 0.05$, $^{***}P < 0.001$, by two-way ANOVA, *indicates comparison to sham group. **(C,D)** Relative mRNA expression levels of *Nr1d1* and *Nr1d2* in mouse hearts at multiple Zeitgeber times (ZTs) with data from previous RNAseq study (14). **(E)** Relative mRNA expression levels of cardiomyocytes (*Myh6*), cardiac fibroblasts (*Col1a1*), and cardiac endothelial (*CDH5*) marker genes in the isolated cells from mice hearts. $^{*}P < 0.05$, $^{**}p < 0.01$, $^{***}P < 0.001$, $^{****}P < 0.0001$, by one-way ANOVA, *indicates comparison between cell types.

SUPPLEMENTARY FIGURE 4
Echocardiography analysis of the role of SR9009 on post-TAC cardiac protection when administered at different time points. **(A–D)** Echocardiography analysis. FS, LVID;s, LV Mass AW (corrected), and LVPW;s after TAC were shown. WT-vehicle $n = 10$, WT-SR9009 ZT06 $n = 6$, WT-SR9009 ZT18 $n = 5$. Data are mean ± S.E.M. $^{*}P < 0.05$, $^{**}p < 0.01$, $^{***}P < 0.001$ by two-way ANOVA, *indicates comparison to WT vehicle group. Tukey's test was used for multiple comparison corrections.

References

1. Knutsson A, Akerstedt T, Jonsson BG, Orth-Gomer K. Increased risk of ischaemic heart disease in shift workers. *Lancet.* (1986) 2:89–92.

2. Cohen MC, Rohtla KM, Lavery CE, Muller JE, Mittleman MA. Meta-analysis of the morning excess of acute myocardial infarction and sudden cardiac death. *Am J Cardiol.* (1997) 79:1512–6. doi: 10.1016/s0002-9149(97)00181-1

3. Ingle KA, Kain V, Goel M, Prabhu SD, Young ME, Halade GV. Cardiomyocyte-specific bmal1 deletion in mice triggers diastolic dysfunction, extracellular matrix response, and impaired resolution of inflammation. *Am J Physiol Heart Circ Physiol.* (2015) 309:H1827–36. doi: 10.1152/ajpheart.00608.2015

4. Lefta M, Campbell KS, Feng HZ, Jin JP, Esser KA. Development of dilated cardiomyopathy in bmal1-deficient mice. *Am J Physiol Heart Circ Physiol.* (2012) 303:H475–85.

5. Young ME, Brewer RA, Peliciari-Garcia RA, Collins HE, He L, Birky TL, et al. Cardiomyocyte-specific BMAL1 plays critical roles in metabolism, signaling, and maintenance of contractile function of the heart. *J Biol Rhythms.* (2014) 29:257–76. doi: 10.1177/0748730414543141

6. Yin L, Wu N, Curtin JC, Qatanani M, Szwergold NR, Reid RA, et al. Rev-erbalpha, a heme sensor that coordinates metabolic and circadian pathways. *Science.* (2007) 318:1786–9.

7. Raghuram S, Stayrook KR, Huang P, Rogers PM, Nosie AK, McClure DB, et al. Identification of heme as the ligand for the orphan nuclear receptors REV-ERBalpha and REV-ERBbeta. *Nat Struct Mol Biol.* (2007) 14:1207–13. doi: 10.1038/nsmb1344

8. Zhu B, Gates LA, Stashi E, Dasgupta S, Gonzales N, Dean A, et al. Coactivator-dependent oscillation of chromatin accessibility dictates circadian gene amplitude via REV-ERB loading. *Mol Cell.* (2015) 60:769–83. doi: 10.1016/j.molcel.2015.10.024

9. Zhang Y, Fang B, Emmett MJ, Damle M, Sun Z, Feng D, et al. GENE REGULATION. Discrete functions of nuclear receptor Rev-ERBα couple metabolism to the clock. *Science.* (2015) 348:1488–92. doi: 10.1126/science.aab3021

10. Zhang L, Zhang R, Tien CL, Chan RE, Sugi K, Fu C, et al. REV-ERB α ameliorates heart failure through transcription repression. *JCI Insight.* (2017) 2:e95177. doi: 10.1172/jci.insight.95177

11. Reitz CJ, Alibhai FJ, Khatua TN, Rasouli M, Bridle BW, Burris TP, et al. SR9009 administered for one day after myocardial ischemia-reperfusion prevents heart failure in mice by targeting the cardiac inflammasome. *Commun Biol.* (2019) 2:353. doi: 10.1038/s42003-019-0595-z

12. Stujanna EN, Murakoshi N, Tajiri K, Xu D, Kimura T, Qin R, et al. Rev-ERB agonist improves adverse cardiac remodeling and survival in myocardial infarction through an anti-inflammatory mechanism. *PLoS One.* (2017) 12:e0189330. doi: 10.1371/journal.pone.0189330

13. Dierickx P, Zhu K, Carpenter BJ, Jiang C, Vermunt MW, Xiao Y, et al. Circadian REV-ERBs repress E4bp4 to activate NAMPT-dependent NAD^{+} biosynthesis and sustain cardiac function. *Nat Cardiovasc Res.* (2022) 1:45–58. doi: 10.1038/s44161-021-00001-9

14. Song S, Tien CL, Cui H, Basil P, Zhu N, Gong Y, et al. Myocardial Rev-ERB-mediated diurnal metabolic rhythm and obesity paradox. *Circulation.* (2022) 145:448–64. doi: 10.1161/CIRCULATIONAHA.121.056076

15. Dierickx P, Emmett MJ, Jiang C, Uehara K, Liu M, Adlanmerini M, et al. SR9009 has REV-ERB-independent effects on cell proliferation and metabolism. *Proc Natl Acad Sci USA.* (2019) 116:12147–52. doi: 10.1073/pnas.1904226116

16. Zhao Q, Khorasanizadeh S, Miyoshi Y, Lazar MA, Rastinejad F. Structural elements of an orphan nuclear receptor-DNA complex. *Mol Cell.* (1998) 1:849–61. doi: 10.1016/s1097-2765(00)80084-2

17. Kojetin DJ, Burris TP. REV-ERB and ROR nuclear receptors as drug targets. *Nat Rev Drug Discov.* (2014) 13:197–216.

18. Pariollaud M, Gibbs JE, Hopwood TW, Brown S, Begley N, Vonslow R, et al. Circadian clock component REV-ERBα controls homeostatic regulation of pulmonary inflammation. *J Clin Invest.* (2018) 128:2281–96. doi: 10.1172/JCI93910

19. Hunter AL, Pelekanou CE, Barron NJ, Northeast RC, Grudzien M, Adamson AD, et al. Adipocyte NR1D1 dictates adipose tissue expansion during obesity. *Elife.* (2021) 10:e63324. doi: 10.7554/eLife.63324

20. Cho H, Zhao X, Hatori M, Yu RT, Barish GD, Lam MT, et al. Regulation of circadian behaviour and metabolism by REV-ERB-alpha and REV-ERB-beta. *Nature.* (2012) 485:123–7.

21. Chelu MG, Sarma S, Sood S, Wang S, van Oort RJ, Skapura DG, et al. Calmodulin kinase II-mediated sarcoplasmic reticulum $Ca2^{+}$ leak promotes atrial fibrillation in mice. *J Clin Invest.* (2009) 119:1940–51.

22. Agah R, Frenkel PA, French BA, Michael LH, Overbeek PA, Schneider MD. Gene recombination in postmitotic cells. *J Clin Invest.* (1997) 100:169–79.

23. Litviňuková M, Talavera-López C, Maatz H, Reichart D, Worth CL, Lindberg EL, et al. Cells of the adult human heart. *Nature.* (2020) 588:466–72.

frontiers | Frontiers in Cardiovascular Medicine

TYPE Review
PUBLISHED 04 August 2022
DOI 10.3389/fcvm.2022.964675

OPEN ACCESS

EDITED BY
Joanne E. Curran,
The University of Texas Rio Grande Valley, United States

REVIEWED BY
Chantal Josephina Maria Van Opbergen,
Grossman School of Medicine, New York University, United States
Jinzhu Hu,
Nanchang University, China

*CORRESPONDENCE
Laura T. Arbour
larbour@uvic.ca
Leigh Anne Swayne
lswayne@uvic.ca

SPECIALTY SECTION
This article was submitted to Cardiovascular Genetics and Systems Medicine,
a section of the journal Frontiers in Cardiovascular Medicine

RECEIVED 08 June 2022
ACCEPTED 11 July 2022
PUBLISHED 04 August 2022

CITATION
York NS, Sanchez-Arias JC, McAdam ACH, Rivera JE, Arbour LT and Swayne LA (2022) Mechanisms underlying the role of ankyrin-B in cardiac and neurological health and disease.
Front. Cardiovasc. Med. 9:964675.
doi: 10.3389/fcvm.2022.964675

Mechanisms underlying the role of ankyrin-B in cardiac and neurological health and disease

Nicole S. York[1], Juan C. Sanchez-Arias[1], Alexa C. H. McAdam[2], Joel E. Rivera[1], Laura T. Arbour[1,2]* and Leigh Anne Swayne[1,3]*

[1]Division of Medical Sciences, University of Victoria, Victoria, BC, Canada, [2]Department of Medical Genetics, University of British Columbia, Victoria, BC, Canada, [3]Department of Cellular and Physiological Sciences and Djavad Mowafaghian Centre for Brain Health, University of British Columbia, Vancouver, BC, Canada

The *ANK2* gene encodes for ankyrin-B (ANKB), one of 3 members of the ankyrin family of proteins, whose name is derived from the Greek word for anchor. ANKB was originally identified in the brain (B denotes "brain") but has become most widely known for its role in cardiomyocytes as a scaffolding protein for ion channels and transporters, as well as an interacting protein for structural and signaling proteins. Certain loss-of-function *ANK2* variants are associated with a primarily cardiac-presenting autosomal-dominant condition with incomplete penetrance and variable expressivity characterized by a predisposition to supraventricular and ventricular arrhythmias, arrhythmogenic cardiomyopathy, congenital and adult-onset structural heart disease, and sudden death. Another independent group of *ANK2* variants are associated with increased risk for distinct neurological phenotypes, including epilepsy and autism spectrum disorders. The mechanisms underlying ANKB's roles in cells in health and disease are not fully understood; however, several clues from a range of molecular and cell biological studies have emerged. Notably, ANKB exhibits several isoforms that have different cell-type–, tissue–, and developmental stage– expression profiles. Given the conservation within ankyrins across evolution, model organism studies have enabled the discovery of several ankyrin roles that could shed important light on ANKB protein-protein interactions in heart and brain cells related to the regulation of cellular polarity, organization, calcium homeostasis, and glucose and fat metabolism. Along with this accumulation of evidence suggesting a diversity of important ANKB cellular functions, there is an on-going debate on the role of ANKB in disease. We currently have limited understanding of how these cellular functions link to disease risk. To this end, this review will examine evidence for the cellular roles of ANKB and the potential contribution of ANKB functional variants to disease risk and presentation. This contribution will highlight the impact of ANKB dysfunction on cardiac and neuronal cells and the significance of understanding the role of ANKB variants in disease.

KEYWORDS

scaffolding protein, cellular morphology, calcium homeostasis, excitation-contraction coupling, arrhythmia, sudden cardiac death, seizure, autism spectrum disorders

Introduction

Loss-of-function variants in the *ANK2* gene are associated with a wide range of electrical and structural heart disease. Reported cardiac phenotypes include arrhythmia, corrected QT interval prolongation (sometimes referred to as long QT type 4), and sudden cardiac death. A prolonged QT interval on an electrocardiogram corrected for heart rate (QTc) is a predictor of ventricular arrythmias and sudden cardiac death (1, 2). At least 15 congenital long QT syndromes (LQTS) have been described, associated with genes encoding for ion channels, ion channel modulatory subunits, signaling proteins, and cytoskeleton-associated proteins (3). One of the first identified *ANK2* variants, p.E1458G, was associated with prolonged QTc, and this QTc prolongation has since been associated with other *ANK2* variants (4–7). Notably, a prolonged QTc is not observed in all patients harboring cardiac phenotype- associated *ANK2* variants. In fact, there is minimal evidence of a prolonged QTc in individuals under the age of 25 (7). Additional reported cardiac manifestations include bradycardia, sinus arrhythmia, idiopathic ventricular fibrillation, and catecholaminergic polymorphic ventricular tachycardia (5, 8). Separately, *ANK2* is also emerging as a gene of interest in neurological disorders. *ANK2* has been identified as a key risk gene for autism spectrum disorders (ASD) (9, 10) and as a candidate gene for epilepsy (11).

The protein produced from the *ANK2* gene, ankyrin-B (ANKB), is a large scaffolding protein that has become known as a key regulator of cardiac physiology (4, 12). There are three mammalian ankyrin protein family members, including ANKB, ankyrin-R (ANKR, *ANK1* gene), and ankyrin-G (ANKG, *ANK3* gene). ANKR is primarily expressed in erythrocytes (13) while ANKB and ANKG are co-expressed in a variety of cell types and tissues (14–16). Ankyrins, including ANKB, are composed of four domains: a membrane binding domain comprised of 24 *ANK* repeats that interacts with membrane proteins such as ion channels and transporters, a spectrin binding domain responsible for interacting with βII spectrin, a death domain of which the function has not yet been identified but in other proteins is key for signal transduction cascades resulting in apoptosis and inflammation (17), and a C-terminal domain. The death domain and C-terminal domain comprise the regulatory domain which is named due to its ability to directly bind the membrane binding domain and play a role in inhibition (15). As this review is focused on ANKB, the following information is specific to ANKB, except where information about other ankyrin family members provides key insight.

ANK2 has critical roles for cardiac and neuronal physiology as indicated by loss-of-function variants and studies using model organisms. ANKB's structure and different isoforms allow for a diverse array of protein-protein interactions within a variety of different cell types. As such, dysfunction in ANKB can lead to a wide range of cellular impacts. There are different groups of variants associated with different phenotypes; one group of *ANK2* variants is primarily associated with a broad cardiac phenotype, another is associated with neurological diseases including ASD and epilepsy, and others are linked to metabolic perturbations. The *ANK2* variant-associated clinical phenotypes inform investigation of ANKB cellular roles, including key potential protein-protein interactions and cellular processes that could, in turn, help to develop new therapeutic strategies. To this end, we first highlight certain *ANK2* variants associated with disease and then discuss the potential underlying mechanisms garnered from cell biological studies using a variety of model organisms. These studies have revealed key cellular roles for ANKB in the localization and spatial organization of ion channels and transporters, signaling molecules, and structural proteins involved in variety of cellular processes, including development of cellular morphology, calcium homeostasis, and glucose and fat metabolism. By linking ANKB's emergent cellular roles with phenotypes associated with *ANK2* variants, a picture of ANKB's many contributions to cardiac, neurological, and metabolic health and disease begins to emerge. Making these links is key to translating this knowledge into the clinical setting and helps understand disease risk and presentation.

Tissue- and cell-type-specific expression of ANKB isoforms across development

There are several ANKB isoforms which exhibit cell-type–, tissue–, and developmental stage–specific expression patterns. While the 220 kDa ANKB isoform is the primary isoform in both the heart and brain [as well as other cells and tissues, such as skeletal muscle, thymus, pancreas, and adipose tissue (18, 19) certain isoforms exhibit tissue-specific expression. The initial discovery of *ANK2* (and its product ANKB) resulted from a series of studies characterizing ankyrin cDNA enriched in non-erythroid cells (20, 21). After the identification of a 440 kDa isoform, consisting of a large insertion (exon 40) between the regions encoding for the spectrin binding domain and death domain (20, 22), transcript and protein level characterization showed that 440 kDa ANKB was detectable at birth, with expression levels peaking at postnatal day 10 and decreasing progressively in the adult rat brain (down to 30% of peak levels) (22). Meanwhile, the 220 kDa ANKB transcript and protein levels were found to increase progressively through development into adulthood (20, 23). In addition to the 220 kDa isoform, additional ANKB isoforms have been detected in the heart: a 188 kDa isoform that, similarly to 220 kDa ANKB isoform, when knocked down results in altered expression and localization of the sodium calcium exchanger, a 212 kDa isoform which is localized to striated muscle and the cardiac M-line (24), and a 160 kDa isoform that is highly expressed in mouse hearts along with the 220 kDa isoform (25).

TABLE 1 Spectrum of cardiac features associated with *ANK2* variants in humans.

		E1458G[a] N = 25	**R990Q N = 2**	**V3634D[b] N = 4**	**S646F N = 15**	**E1813K[c] N = 3**	**Q1283H N = 1**	**T1404I N = 1**	**M1988T N = 5**	**T3744N[d] N = 10**	**R3906W[e] N = 2**	**I3437T N = 1**	**W1535R N = 6**	**46,XX,t (4;9) (q25;q31.1) N = 5**
Variant type		Missense	Missense	Missense	Missense	Missense	Missense	Missense	Missense	Missense	Missense	Missense	Missense	LOF
Location		SBD	SBD	DD	MBD	CTD	SBD	SBD	CTD	CTD	CTD	Disordered	DD	n/a
Arrhythmia	LQTS	X	X		X					X	X		X	
	Drug-induced LQTS			X		X		X					X	
	CPVT			X								X		
	Atrial Fibrillation	X				X		X						
	Cardiac arrest		X	X								X		
	SCD	X			X				X	X				
	Bradycardia			X	X	X		X					X	X
	VT			X			X		X		X			
	Other arrhythmia		Recurrent VF	Type 1 brugada pattern	SVT				Late potential on SAECG		Torsades de pointes		Torsades de pointes, VF, BrS	
Conduction abnormalities	WPW				X									
	SND	X												X
	Other					Heart block								
Symptoms	Syncope	X	X	X	X	X	X		X	X	X		X	X
	Palpitations						X							
Structural	HCM	X	X									X		
	DCM				X									
	ARVC	X							X					
	Other structural													LV dysfunction, cardiomegaly
	Congenital Heart Defect				X									X
Other	Seizures				X								X	

(Continued)

10.3389/fcvm.2022.964675

TABLE 1 Continued

	E1458G[a]	R990Q	V3634D[b]	S646F	E1813K[c]	Q1283H	T1404I	M1988T	T3744N[d]	R3906W[e]	I3437T	W1535R	46,XX,t
	N = 25	*N* = 2	*N* = 4	*N* = 15	*N* = 3	*N* = 1	*N* = 1	*N* = 5	*N* = 10	*N* = 2	*N* = 1	*N* = 6	(4;9) (q25;q31.1) *N* = 5
GnomAD	0.0005346	0.00001971	0.002051	Not observed	0.002286	Not observed	Not observed	Not observed	0.0007363	0.0009337	Not observed	0.00001314	N/a
Clinvar Classification	LP (3)	VUS (3)	VUS (2)	P (1)	VUS (1)			VUS (1)	VUS (4)	VUS (1)		LP (1)	
(# labs)	VUS (4)		LB (5)		LB (5)				LB (7)	LB (6)		VUS (1)	
	LB (2)		B (1)		B (5)					B (1)			
ClinVar ID	VCV0000	VCV000	VCV0000	VCV000	VCV0000			VCV00	VCV0000	VCV0000		VCV0000	
	18056.18	190560.9	67599.12	190552.2	18060.14			1341732.1	18057.26	18059.23		67596.4	
Reference	(4, 44)	(6, 43)	(8)	(7)	(130)	(95)	(8)	(44)	(5)	(5)	(40)	(46)	(39)

SBD, Spectrin Binding Domain; DD, Death Domain; MBD, Membrane Binding Domain; CTD, C-Terminal Domain; LQTS, Long QT Syndrome; CPVT, Catecholaminergic Polymorphic Ventricular Tachycardia; SCD, Sudden Cardiac Death; VT, Ventricular Tachycardia; VF, Ventricular Fibrillation; SVT, Supraventricular Tachycardia; SAECG, Signal Averaged ECG; BrS, Brugada Syndrome; WPW, Wolff Parkinson White; SND, Sinus Node Dysfunction; HCM, Hypertrophic Cardiomyopathy; DCM, Dilated Cardiomyopathy; ARVC, Arrhythmogenic Right Ventricular Cardiomyopathy; P, Pathogenic; LP, Likely pathogenic; VUS, Variant of Uncertain Significance; LB, Likely benign; B, Benign. [a]Previously E1425G; [b]Previously V1516D; [c]Proband also carried variant in KCNH2-H562R, only the phenotype in those carrying the *ANK2* E1813K variant alone described in table. See text for description of the combined KCNH2 and *ANK2* phenotype; [d]Previously T1626N; e Previously R1788W.

Newer transcriptomics studies and databases of the developing human heart show that *ANK2* is differentially expressed in human embryonic ventricular and atrial cardiomyocytes, with high transcript levels also detected in fibroblast-like cells associated with vascular development and cardiac neural crest cells (https://spatialtranscriptomics3d.shinyapps.io/Developmental_heart_explorer/) (26). *ANK2* transcript levels peak during early mid-fetal human development (and mouse *Ank2* transcript levels peak during late embryonic development) to eventually plateau during later developmental stages (https://hbatlas.org/mouseNCXtranscriptome/, https://hbatlas.org/pages/hbtd) (26–29). In the 1-week-old mouse brain, *Ank2* transcript levels are enriched in astrocytes, neurons, and oligodendrocyte progenitors (https://www.brainrnaseq.org/) (30). At the single RNA-seq level, *ANK2* transcript levels are slightly enriched in inhibitory and excitatory neuron populations [Allen Cell Type Database – "M1 - 10X GENOMICS (2020)"; https://portal.brain-map.org/atlases-and-data/rnaseq] (31). Consideration of this ANKB enrichment in select cell types, tissues, and developmental stages could help provide important clues to the clinical impacts of *ANK2* variants. In the next section, we will highlight several *ANK2* variants and associated phenotypes that provide important areas of focus for investigation of ANKB's cellular roles.

ANK2 variants and risk for disease

Consistent with enriched ANKB expression in heart and brain, a number of *ANK2* variants have been associated with a range of cardiac phenotypes while others are associated with neurological or metabolic phenotypes.

ANK2 variants associated with (primarily) cardiac phenotypes

Certain *ANK2* loss-of-function variants are associated with a broad spectrum of cardiac phenotypes including arrhythmia, conduction abnormalities, and cardiomyopathy (Table 1) (4, 8, 32). Amino acid changes produced by these variants are present in all four domains of ANKB and are associated with autosomal dominant inheritance, reduced penetrance, and variable expressivity (Figure 1) (32). Initially described as LQTS type 4, QTc prolongation is commonly linked with cardiac-phenotype associated *ANK2* variants, although the role in QT prolongation has been since debated (33) (Table 1). ANKB p.E1458G (previously p.E1425G), the result of an amino acid substitution in the spectrin binding domain, was among the first *ANK2* variants identified. It was found in a French kindred with LQTS associated with atrial fibrillation and sinus node dysfunction (4). There was a family history of sudden

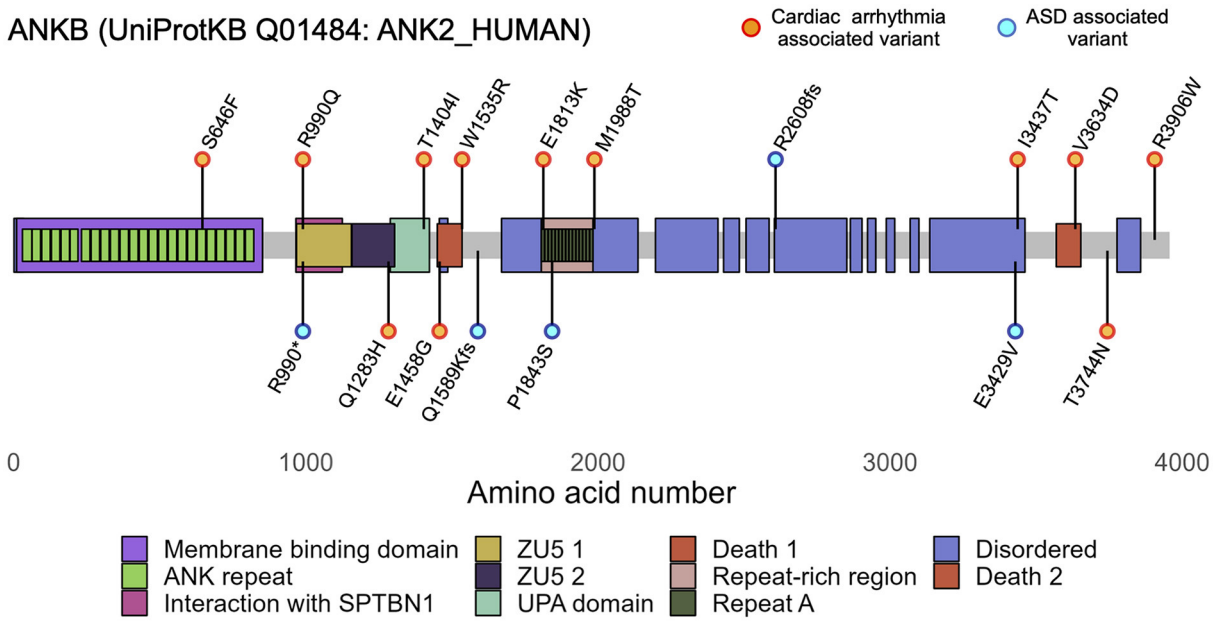

FIGURE 1
ANK2 variants are associated to cardiac arrhythmias and autism spectrum disorders (ASD). Diagram of canonical human ANKB (UniProtKB Q01484-4, 3,957 aa) showing ANKB regions and domains. Canonically, ANKB can be divided into 4 main domains: an initial membrane binding domain, a spectrin binding domain, a death domain, and a C-terminus domain. The ANKB membrane binding domain contains 24 consecutive ankyrin (ANK) repeats and associates with ion channels and transporters; the spectrin binding domain contains highly conserved ZU5-ZU5-UPA domains and associates with βII-spectrin and the B56α subunit of PP2A; and the regulatory domain comprised of the death domain and C-terminus domain comprised is unstructured and highly variable between species. Orange and cyan dots represent the main cardiac and ASD variants discussed in the main text. Functional variants have been identified in each of ANKB's domains.

death, including an 18 and 12 y.o. The variant demonstrated incomplete penetrance in one out of 23 carriers. Age related effects were also observed, affected children had sinus node abnormalities (diagnosed *in utero*) whereas atrial fibrillation was present only in adults (4). Of note, the p.E1458G variant has also been identified in a healthy Danish exome cohort without evidence of QTc prolongation and has a frequency of 0.11% (41/35360) in the Latino population according to the Genome Aggregation Database (gnomAD) (34, 35). Similarly, while two *ANK2* variants p.E1458G and p.V3634D (initially reported as p.V1516D) were over-represented in a private cohort from an inherited heart rhythm clinic, most patients carrying *ANK2* variants that were referred to this clinic showed no symptoms or had electrocardiographic findings of unknown significance; however, their genetic ancestry composition and clinical and epidemiological information is not publicly available (36). Another variant associated with prolonged QTc and ventricular tachyarrhythmias is the *ANK2* p.L1622I variant, found with higher frequency in individuals of African ancestry (minor allele frequency: 0.03, 850/24964, gnomAD) (5, 37).

ANKB p.S646F, the first identified variant located in the membrane binding domain, also came to attention due to LQTS. This variant was found in two large multigenerational Gitxsan families identified because of LQTS in the context of a known high community prevalence of *KCNQ1*-mediated LQTS. The probands in each family did not carry the known *KCNQ1* variant (38), but instead, carried the p.S646F variant (7). As with the p.E1458G variant, QTc prolongation was not the only associated feature. The variant was identified in one individual who died suddenly due to dilated cardiomyopathy, another carrier had a history of Wolf-Parkinson-White (WPW) syndrome, and this individual's daughter was born with a congenital heart defect (total anomalous pulmonary venous return). Age related effects were observed, with limited evidence of QTc prolongation in those under 25 years (7). Congenital heart defects were also reported in a fetus carrying a duplication of 4q25-ter and 9pter-q31.1 with breakpoints in chromosome four transecting *ANK2*; the fetus was born with multiple cardiac malformations including a large atrioventricular septal defect (39). However, it is unclear whether the congenital heart defects may be related to the duplications or whether *ANK2* haploinsufficiency played a role. Carriers of the balanced translocation, which includes breakpoints transecting *ANK2*, did not have congenital heart defects but other cardiac features including bradycardia, ventricular ectopy, sinus node dysfunction, and mild left ventricular dysfunction (Table 1).

LQTS is not the only phenotype associated with loss of ANKB function. Over time, several other arrhythmias and conduction anomalies have been associated with *ANK2* variants including catecholaminergic polymorphic ventricular tachycardia (CPVT), bradycardia, and WPW. An occurrence of CPVT in carriers of an *ANK2* variant has been reported in a small number of cases, with a recent report by Song et al. (40) of a 20 y.o. man with diagnosis of CPVT and non-ischemic cardiomyopathy who was found to carry the p.I3437T variant located in the disordered domain of ANKB (8, 41). WPW has been suggested to be another feature of Ankyrin-B syndrome. In addition to the one individual with WPW carrying the p.S646F variant previously mentioned, two rare de novo and one inherited variant in *ANK2* were identified in a cohort of patients with WPW (7, 42).

Beyond inherited arrhythmias, loss-of-function variants in *ANK2* have also been associated with cardiomyopathy, such as hypertrophic cardiomyopathy, dilated cardiomyopathy, and LV dysfunction (7, 39, 43). In a cohort of patients with HCM, rare variants in *ANK2* showed a statistically significant association with greater maximal mean left ventricular wall thickness, contributing to more severe LV hypertrophy (43). Recently, the role of *ANK2* in arrhythmogenic right ventricular cardiomyopathy (ARVC), a condition characterized by fibrofatty replacement of the myocardium, ventricular arrhythmias, and sudden cardiac death has come to attention. The previously reported p.E1458G variant was identified in an individual who died suddenly while running and was found to have ARVC on autopsy. A second *ANK2* variant was identified in a family where the proband died suddenly during exercise and was also found to have ARVC on autopsy. Post-mortem genetic testing was carried out and identified a novel p. M1988T variant, which is located in the C-terminal domain. Additional family members were identified through cascade screening to have definite or borderline diagnoses of ARVC (44).

With the emergence of a broad spectrum of features linked to *ANK2* variants came the term "Ankyrin-B syndrome," which at the time more fully captured the complexity of the range of associated phenotypes (8, 32). Although the origin of Ankyrin-B syndrome is associated solely with cardiac phenotypes (8, 45), through the investigation and identification of new variants, it has become apparent that ANKB dysfunction is not exclusive to cardiac phenotypes but underlies neurological ones as well. Thus the term, Ankyrin-B syndrome, does not fully capture the broad spectrum of ANKB dysfunction across all cell types and variants. The pleiotropic nature of *ANK2* is highlighted by individuals that experience seizures in combination to the cardiac manifestations (7, 46), as well as unique *ANK2* variants associated with ASD (47–49) of which we will discuss in the next section.

ANK2 variants associated with neurological phenotypes

Beyond the heart, *ANK2* is emerging as an important gene in neurological conditions, including ASD and epilepsy. It is important to note that the variants associated with Ankyrin-B syndrome (cardiac-phenotype associated ANKB variants) are distinct from those reported in association with ASD, and a combination of cardiac and ASD phenotypes has not been reported. Rare variants in *ANK2* including missense, frameshift, non-sense, and copy number variants have been identified in individuals with ASD (Table 2) (10, 47–50). *ANK2* is classified as a high-confidence gene clearly implicated in ASD by the Simons Foundation Autism Research initiative due to the reports of at least three de-*novo* loss-of-function variants in the literature and meeting the threshold false discovery rate of <0.1 (https://gene.sfari.org/database/human-gene/ANK2). ASD-associated *ANK2* variants are largely non-syndromic and typically not associated with intellectual disability (Table 2) (51). While some variants are present within both the 220-kDa and 440 kDa ANKB proteins, certain variants are unique to the 440-kDa giant ANKB isoform. For instance, a knock-in mouse model carrying ANKB p.P2580fs (analogous to the human p.R2608fs), which expresses a truncated giant ANKB polypeptide, demonstrated ASD-like behaviors including repetitive behavior, decreased ultrasonic vocalization, reduced territory marking, and superior executive functioning. Of note, mice homozygous and heterozygous for the p.P2580fs variant exhibited the same behaviors, supporting that haploinsufficiency of *ANK2* could contribute to risk for ASD (51). Using a multiplex network that characterized modules of epilepsy and ASD genes sharing similar phenotypes and protein-protein interactions, *ANK2* has also been identified as a novel candidate gene for epilepsy (11). Similarly, in a workflow using the random walk with restart algorithm in addition to permutation and functional association tests *ANK2* was also predicted as a novel gene for epilepsy (52).

Notably, independent of the connection between *ANK2* variants and risk for epilepsy, seizures were reported in association with cardiac-phenotype associated *ANK2* variants. A history of seizures was reported in eight of eighteen carriers of the ANKB p.S646F variant, and in two out of six patients carrying the ANKB p.W1535R variant (7, 46). In a study which sequenced cases of epilepsy-related sudden unexpected death for inherited heart disease related genes, one individual was found to carry two variants in *ANK2* (p.Ser105Thr, p.Glu1934Val). Of note, this death occurred by drowning, and the individual was reported to have mildly prolonged QTc (53). Given that seizures can be linked to cardiac arrhythmias (54) and the fact that some cardiac-associated *ANK2* variants are linked with seizures (7, 46) it would be worth investigation to determine if the seizures are a result of the arrhythmia or independent and owed to dysfunction in the brain. Furthermore, with the

TABLE 2 ANK2 variants associated with autism spectrum disorder.

Variant	Type	Location	ASD	Intellectual disability	Other	gnomAD	Clinvar ID	Reference
Affect only giant ANKB *(440 kDa)* isoform								
P1843S	Missense	Disordered	X			0.000003979		(134)
E3429V	Missense	Disordered	X			Absent		(48)
R2608fs	Frameshift	Disordered			Pervasive developmental disorder	Absent		(135)
Affect giant ANKB *(440 kDa)* and *220 kDa* isoform								
R990*	Nonsense	ZU5-1			Asperger's disorder	Absent	VCV000450028.2	(10)
Q1589Kfs	Frameshift		X	X	Sensorimotor neuropathy, facial dysmorphism	Absent	VCV000235896.1	(50)
4:113593803_113967887dup	Duplication		X			n/a	VCV000236353.1	(47)
4:114077690_118094709dup	Duplication		X			n/a	VCV000236354.1	(47)
4: 114225715-114429181del	Deletion		X			n/a	VCV000236355.1	(47)

Table adapted from Yang et al. (51); ASD, Autism Spectrum Disorder.

link to epilepsy in neurological-associated *ANK2* variants (11) it raises the question of how ANKB dysfunction is impacting neuronal mechanisms.

ANK2 variants associated with metabolic phenotypes

ANK2 variants have also been implicated in the regulation of fat and glucose metabolism. In particular, the *ANK2* p.R1788W variant, which is associated to cardiac phenotypes (Table 1), was enriched in individuals of white and Hispanic descent diagnosed with type 2 diabetes in the American Diabetes Association GENNID cohort. Moreover, the *ANK2* p.L1622I variant, associated with a less severe cardiac phenotype, is the most frequent *ANK2* variant (7.5%) in African Americans who carry up to a 2-fold increased risk for type 2 diabetes (19, 55, 56). Whether other primarily cardiac or neuronal *ANK2* variants also result in global or local metabolic disturbances remains to be investigated.

Fundamental research studies revealing the many roles of ANKB within cells have provided insights into possible mechanisms behind the various phenotypes associated with *ANK2* variants. ANKB is implicated in different pathways, as it is a scaffolding protein for ion channels and transporters as well as a link for structural and signaling proteins, some of which are outlined below and summarized in Table 3.

Insights on the cellular role(s) of ANKB from model organism studies

Given their sequence similarity, it is possible to understand the biological role of *ANK2* (and its homologs) through studying model organisms. Mouse *Ank2* is comprised of exons exhibiting considerable homology to those found in human *ANK2* and exhibits similar tissue-specific isoform expression patterns (24, 25). In mice, global *Ank2* knockout causes neonatal death (57), while conditional *Ank2* knockout in the heart and brain results in significant electrical and structural impairments and death (44, 51, 58, 59). Heterozygous *Ank2* knockout ($Ank2^{+/-}$) mice model haploinsufficiency (i.e., expression of a single wildtype *Ank2* allele fails to produce a wildtype phenotype), are relatively viable, and therefore used in many preclinical studies. $Ank2^{+/-}$ mice display increased susceptibility to atrial and catecholamine-induced ventricular arrhythmias and sudden death, as well as, premature senescence and reduced lifespan (4, 8, 45). These cardiac manifestations have been associated with decreased presence of the sodium calcium exchanger, the sodium potassium ATPase subunits 1 and 2, and the inositol 1,4,5-trisphosphate receptor at the T-tubules of cultured primary cardiomyocytes (4, 60) (Figure 2). Mice with complete global loss of *Ank2* ($Ank2^{-/-}$) display severe structural brain defects, such as hypoplasia of white matter tracts, dilated ventricles, and degeneration of the optic nerve (57). As several developmental signaling pathways are strongly intertwined with the homeostasis of ions, such as calcium (61–63), the severe structural phenotypes observed in the context of ANKB

TABLE 3 ANKB interacting partners.

Domain	Classification	Interacting partner	Cell type interaction confirmed in	References
MBD	Ion channels/ Transporters	Inositol 1,4,5-trisphosphate receptor	Cardiac and Neuronal	(4, 5, 14, 60, 103, 136)
		$Ca_V1.3$	Cardiac	(136, 137)
		$Ca_V2.1$	Neuronal	(101, 102)
		$Ca_V2.2$	Neuronal	(101)
		$Ca_V3.1$	Neuronal	(138)
		$Ca_V3.2$	Neuronal	(138)
		Kir6.2	Cardiac	(139, 140)
		Sodium Calcium Exchanger	Cardiac and Neuronal	(4, 5, 24, 60, 103, 137)
		Sodium Potassium ATPase (a1 and a2)	Cardiac and Neuronal	(4, 5, 60, 103, 137, 140, 141)
		Erythrocyte anion channel	Neuronal	(12)
	Structural	EHD1-4	Cardiac	(142)
	Structural/ Signaling	Beta-catenin	Cardiac	(44)
	Cell adhesion	L1CAM	Neuronal	(51, 120, 143)
		Dystrophin	Cardiac	(144, 145)
SBD	Motor movement	Dynactin-4	Cardiac and Neuronal	(144–146)
	Structural	βII-spectrin	Cardiac and Neuronal	(6, 59, 103, 147)
	Signaling	Phosphatidylinositol 3-phosphate	Neuronal and Fibroblast	(146, 148)
		PP2A B56α	Cardiac	(95, 149, 150)
Giant insertion	Enzyme	Ndel1	Neuronal	(151)
DD	Signaling	RABGAP1L	Fibroblast	(148)
CTD	Chaperone	HSP40	Cardiac	(69)
	Signaling	Obscurin	Cardiac	(24, 152)
	Regulatory	Ankyrin-B MBD	Cardiac	(15)
Unknown	Signaling	SadA/SadB	Neuronal	(153)
	Chaperone	UNC-119	Neuronal	(80)

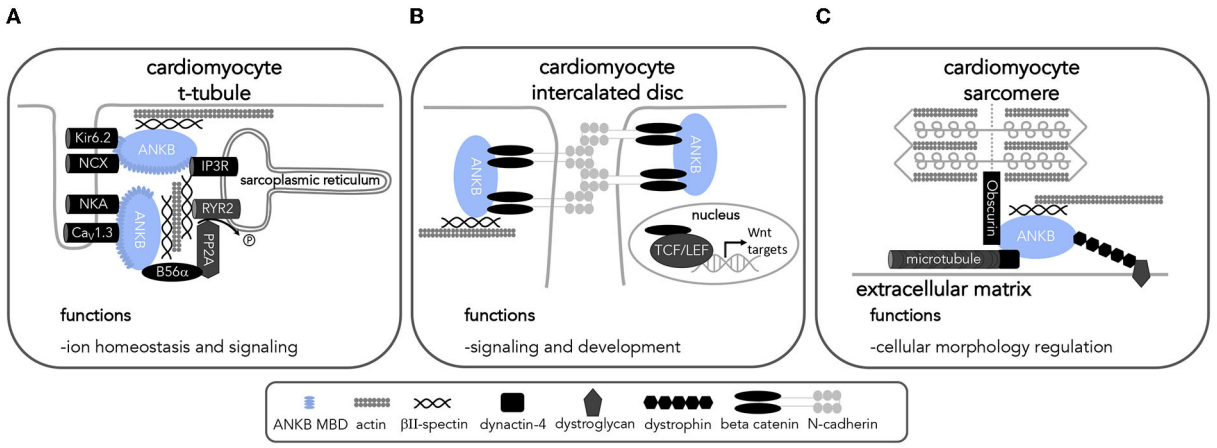

FIGURE 2
ANKB interactions in cardiomyocytes implicates ANKB in a variety of cellular processes. Diagram of ANKB interacting partners and their localization allowing for proper cardiac function. ANKB interactions at the **(A)** t-tubule **(B)** intercalated disc and **(C)** sarcomere allow for proper cell functions. Kir6.2, inward rectifier potassium channel; NCX, sodium calcium exchanger; NKA, sodium potassium ATPase; CaV1.3, voltage-gated calcium channel; IP3R, Inositol 1,4,5-trisphosphate receptor; PP2A, protein phosphatase 2A; RYR2, ryanodine receptor 2; L1CAM, L1 cell adhesion molecule; PI3P, phosphatidylinositol 3-phosphate; CaV1.3, voltage-gated calcium channel; TCF/LEF, T cell factor/lymphoid enhancer factor transcription factors.

dysfunction (or haploinsufficiency) may be related to ANKB regulatory roles in ion homeostasis and cytoskeletal proteins.

Analysis of the molecular evolution of ankyrins has revealed a single *ankyrin* gene in *Caenorhabditis elegans* (*unc-44*), two *ankyrin* genes in *Drosophila melanogaster* (*Dank1, Dank2*), and three mammalian *ankyrin* genes (*ANK1, ANK2, ANK3*) that likely originated from a single *ankyrin* ancestor gene in *Ciona intestinalis* (64, 65). Moreover, these analyses have also demonstrated a closer evolutionary relationship between *ANK2* and *ANK3*, which despite their high sequence and structural similarity localize to different cellular compartments and associate with different proteins (66, 67). In most cases, ankyrins do not have the ability to compensate for each other (68, 69). However, previous studies from the Rasband lab have shown that in the central nervous system ANKB can partially compensate for loss of paranodal ANKG and ANKR can compensate ANKG's role in sodium channel clustering at nodes of Ranvier (70, 71). While each ankyrin protein appears to have different roles they share some protein-protein interactions and can provide insight into each other's roles in cells.

The use of model organisms can help unravel the mechanisms behind the clinical phenotypes associated with *ANK2* variants. Insights from model organisms have elucidated ANKB's essential roles in regulating cellular morphology, polarization, calcium homeostasis, and glucose and fat metabolism, as outlined below and summarized in Tables 3–5 and Figures 2, 3.

ANKB regulates cellular morphology and polarization

As cells develop, migrate, and mature, cytoskeletal rearrangements lead to the specification of a directionality axis resulting in well-organized regions that support motility, cell-to-cell contacts, and surfaces for secretion or absorption (72). This spatiotemporal phenomenon is known as cell polarity and it is what influences the shape, motility, and trafficking and signaling domains in cells, as well as their ability to respond and adapt to extracellular and intracellular signals (72, 73). In the mouse heart, for example, cell polarization allows round embryonic ventricular cardiomyocytes to postnatally adopt the shape of a rod and direct their junctional proteins to the ends of the now elongated cells to form the intercalated disc, a specialization for cell-to-cell communication (74, 75). In other cell types, such as neurons, cell polarization defines specialized compartments for receiving (dendrites) and sending (axons) electrochemical signals (76). Insights from studies using model organisms have shown ANKB's essential role in neuronal development which raises the question of how ANKB may play a role in cardiomyocyte development as well.

Although it is yet unclear whether ANKB plays a role in the morphological development of cardiomyocytes and other cardiac cell-types in which it is expressed, there is evidence of ANKB's roles in neuronal development. Studies using the model organism *C. elegans* have demonstrated that *ANK2*'s ortholog *unc-44*/ankyrin is a known master regulator cell polarization and axonal neurite outgrowth in this roundworm's sensory neurons (77–80). Mutations affecting *unc-44*/ankyrin function result in abnormal neural development, locomotor defects, and microtubule networks with mixed polarity in axons and dendrites leading to abnormal protein sorting and trafficking into these compartments (77–79, 81–83). *Unc-44*/ankyrin, along with *unc-33*/crmp (an actin and microtubule associating protein) and *unc-116*/kinesin-1 (a motor protein) help establish neuronal polarity by regulating the organization of dendritic and axonal microtubule networks (79, 81). Furthermore, *unc-44*/ankyrin acts upstream of *unc-33*/crmp and *vab-8*/kinesin-like protein to regulate the removal of gap junction channels (84) which allow for the direct electrical communication between cells and play a key role in development (85, 86). In *Drosophila melanogaster*, *Dmel\ank2*, which has a short and long/ giant isoform localized to different sub-cellular compartments (cell body and axon, respectively) supports the stabilization and remodeling of the synaptic microtubule network (87, 88). Loss of *Dmel\ank2* results in retraction of synaptic boutons, collapse of the pre-synaptic active zones, reduction of the terminal size, and altered neuromuscular junction morphology (88, 89). While the role of *ANK2* in cardiomyocyte polarization during heart development remains to be investigated, some of the *ANK2* variants listed above have been associated with cardiac malformations suggesting that ANKB dysfunction results in an impact to the structural development of these cells (7, 39).

Recent organ-specific *ANK2* conditional knockouts further underscore the important role of *ANK2* in the structural development of cardiomyocytes and neurons. Specifically, the beta-catenin/Wnt signaling pathway is important in both cardiac and neuronal cell fate determination, axis patterning and polarity, and proliferation (90–92). This pathway is initiated by the accumulation of beta-catenin in the nucleus leading to the transcription of Wnt responsive genes (92). Evidence underlying ANKB's role in cell proliferation and survival has been highlighted by the p.S646F variant. In H9c2 cells, a cell model with similar traits of primary cardiomyocytes (93), expression of the p.S646F variant resulted in decreased cellular viability and proliferation (94). Using a cardiac-specific conditional knockout model, Roberts *et al.* found that loss of *Ank2* in the heart leads to severe cardiac remodeling resulting in ventricular dilation, fibrosis, bradycardia, QTc prolongation, and increased susceptibility to catecholamine-induced ventricular arrythmias (44). Associated with decreased protein expression and altered localization of beta-catenin away from the intercalated disk, this cardiac-specific *ANK2* knockout phenotype recapitulates what has been observed

TABLE 4 Summary of ANKB's cellular roles identified using model organisms.

Model organism		Biological process	Elucidated roles and implications	Reference
Mus musculus	*Ank2*$^{-/-}$ (*Ank2* null)	N/a	Global knockout is deadly	(57)
	Ank2$^{+/-}$ (Models haploinsufficiency)	Cardiomyocyte structural development	Cardiac malformations imply role in structural development	(4, 8, 45)
		Calcium homeostasis and signaling	Localization and expression of the sodium/calcium exchanger, inositol trisphosphate receptor, and voltage-gated calcium channels L-type channels; $Ca_v1.3$ expression (SAN isolated cells and atrial cardiomyocytes) P/Q-type channels; $Ca_v2.1$ and $Ca_v2.2$ expression (cortex, cerebellum, and brainstem)	(4, 60, 101, 136, 137)
			Regulation of RYR2-mediated sarcoplasmic reticulum calcium leak *via* PP2A (cardiomyocytes)	(104)
			Regulation of calcium homeostasis affects calcium cycling dynamics (calcium transients, sparks) and delayed afterdepolarizations	(4, 5, 95, 104)
		Glucose and fat metabolism	Downstream effects on oral glucose tolerance	(114)
	shAnkB knockdown	Calcium homeostasis and signaling	Localization and expression of T-type channels $Ca_v3.2$ expression (hippocampal neurons)	(138)
	Cardiac-specific conditional knockout	Cardiomyocyte structural development	Cardiac remodeling implies structural role Involved in Beta-catenin localization and expression; possible implications on beta-catenin/Wnt signaling	(44)
	Brain-specific knockout (brain-specific ANKB 440-kDa isoform not expressed)	Neuronal structural development	Synaptic signaling and synapse excitability Axon branching and connectivity (linked to *Ank2* involvement in microtubule bundle formation) Abnormal social behavior. Impaired communicative behavior. Enhanced executive function.	(51)
	Excitatory neuron-specific knockout (ANKB 220-kDa and 440-kDa are not expressed in excitatory neurons)	Calcium homeostasis and signaling	Regulation of Cav2.1 expression (decreased Cav2.1 expression in whole cortex homogenates)	(102)
	Adipose tissue-specific conditional knockout	Glucose and fat metabolism	Adiposity Pancreatic islet size Insulin resistance	(117)
	ANK2 p.R1788W knock-in	Glucose and fat metabolism	Abnormal insulin secretion. Insulin resistance Increased peripheral glucose uptake (increased cell surface GLUT4) Adiposity	(19)
Caenorhabditis elegans: unc-44		Neuronal development and polarization	Regulating organization/ polarization neurite microtubule networks	(79, 81)
Drosophila melanogaster: Dank2 (Dmel\ank2)		Neuronal development and polarization	Supporting stabilization and remodeling of synaptic microtubule network	(87, 88)

TABLE 5 Summary of primary biological functions affected by ANKB dysfunction/loss-of-function.

Biological function	Level	Heart	Brain
Structural development and cell polarization	Cellular	Trafficking and distribution of ion channels and exchangers along T-tubules and beta-catenin at the intercalated disc	Definition of axonal and dendritic compartments in neurons Trafficking of proteins to axonal and dendritic compartments
	Tissue/Organ	Dilated cardiomyopathy Ventricular wall fibrosis	White matter tract defects Increased axonal connectivity
Calcium homeostasis and signaling	Cellular	Increased calcium transient amplitude (putatively, increased intracellular calcium concentration) Increased calcium sparks (calcium release events from the sarcoplasmic reticulum) Decreased calcium transient frequency Decreased spontaneous contraction rate	Increased miniature excitatory postsynaptic potentials Decreased excitability Decreased action potential firing rate
	Tissue/Organ	Increased contractility Increased rate of delayed afterdepolarizations	Decreased expression of calcium voltage gated channels ($Ca_V2.1$ and $Ca_V2.2$)

in arrhythmogenic cardiomyopathy phenotypes as well as in patients carrying predicted loss-of-function *ANK2* variants and their respective knock-in mouse models (Figure 2) (4, 37, 95). It is worth noting that cardiomyocytes with *Ank2* loss do not show altered expression nor mislocalization of intercalated disc proteins such as plakoglobin, plakophilin 2, connexin 43, N-cadherin, desmoplakin, and desmoglein 2 (44). Further insights regarding the involvement of ankyrin proteins in this context may be drawn from ANKG, which also interacts with beta-catenin. Loss of ANKG results in a comparable decrease in beta-catenin localization at the membrane and increased nuclear levels leading to an increase in neural progenitor proliferation in mice *via* Wnt signaling (96). Given ANKB also plays a role in organizing beta-catenin localization and expression, it is worth future investigations to determine if ANKB leads to any effects on Wnt signaling. In parallel, another ANKB interacting partner, protein phosphatase 2A (PP2A), is also a regulator of Wnt signaling (97). With ANKB's potential involvement at two stages of the Wnt signaling pathway, future studies should explore the implications of ANKB dysfunction on the latter as well as concomitant developmental processes.

In the case of loss of brain-specific giant ANKB 440-kDa, which primarily localizes to axons, mice display ectopic axon branching and connectivity, transient increase in excitatory synapses, and neurodevelopmental disorder-like behaviors such as stereotype movements and impaired social behavior (51). The impairment on axonal connectivity has been linked to *ANK2's* role in regulating the formation of microtubule bundles in the axon and reducing branching points enriched with F-actin by promoting growth cone collapse in response to semaphorin 3A signaling (58, 98) (Figure 3). While brain specific *Ank2* knockout mice do not exhibit impairments in memory and learning (51), the identified structural and connectivity changes recapitulate some of the morphological features observed in neurodevelopmental disorders, such as ASD (51, 99, 100). The identification of giant ANKB-specific roles in critical aspects of neuronal structural development warrants further exploration in the heart and its intrinsic nervous system. Furthermore, given that ANKB is associated with several critical steps in the development of cells and the establishment of their polarity, studies aiming to elucidate the role that *ANK2* plays during early heart and cardiac conduction system development will be crucial to understand the various phenotypes associated with *ANK2* variants.

ANKB regulates calcium homeostasis

With its role in proper localization of the calcium the sodium/calcium exchanger, the inositol trisphosphate receptor, and calcium voltage-gated channels, ANKB is a key hub for regulation of calcium homeostasis in excitable cells (14, 101–103). In mouse cardiomyocytes, complete and partial loss of *Ank2* leads to abnormal calcium dynamics as summarized in Tables 4, 5 (4, 5, 104). Using global and partial loss of *Ank2* knockout mouse models, it has been demonstrated that *ANK2* variants identified in cardiogenetic studies have differential effects on cardiomyocyte calcium dynamics *in vitro*, with some variants (namely: p.G1406C, p.R1450W, p.L1503V) rescuing calcium transient amplitude defects, while others (namely: p.E1425G, p.L1622I, p.T1626N, p.R1788W, p.T1404I, p.V1516D, p.T1552N, p.V1777M, and p.E1813K) fail to rescue calcium and spontaneous activity abnormalities (8). These *in vitro* experimental findings are in line the variable expressivity and penetrance observed in individuals carrying *ANK2* variants (4, 7).

ANK2 regulates calcium homeostasis in excitable cells through various potential mechanisms, some of which still

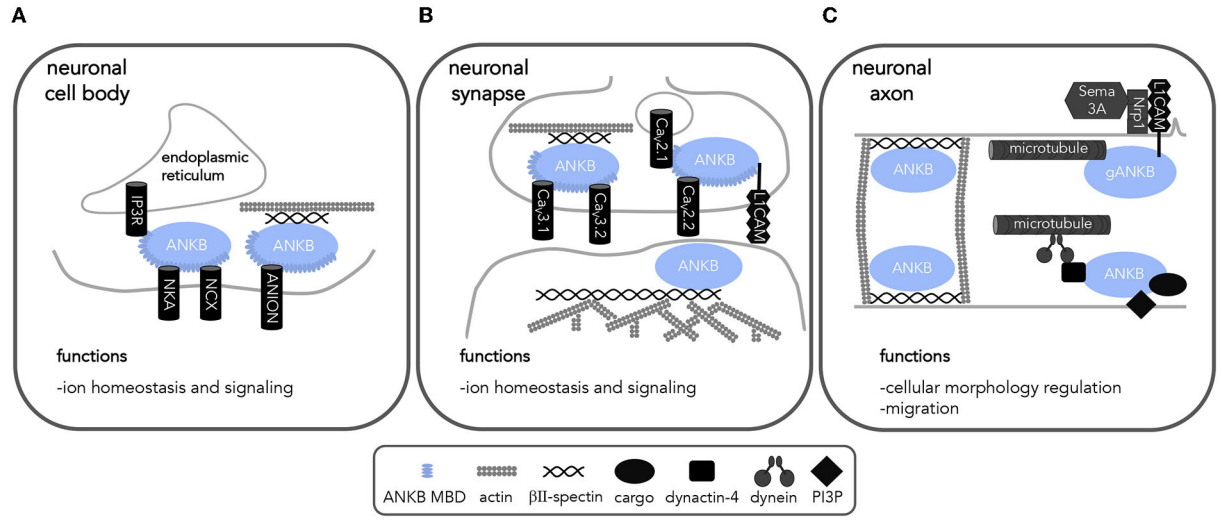

FIGURE 3
ANKB interactions in neurons implicates ANKB in a variety of cellular processes. Diagram of ANKB interacting partners and their localization allowing for proper neuronal function. **(A)** cell body **(B)** synapse and **(C)** axon allow for proper cell functions. NCX, sodium calcium exchanger; NKA, sodium potassium ATPase; IP3R, Inositol 1,4,5-trisphosphate receptor; Ca_V, voltage-gated calcium channels; PP2A, protein phosphatase 2A; RYR2, ryanodine receptor 2; L1CAM, L1 cell adhesion molecule; PI3P, phosphatidylinositol 3-phospate; Sema 3A, semaphorin 3A; Nrp1, semaphorin 3A receptor neuropilin 1.

require additional in-depth characterization. Loss of *ANK2* or *ANK2* dysfunction (as in the case of pathogenic *ANK2* variants) leads to the mis-localization of channels and transporters involved in calcium handling (sodium/calcium exchanger, inositol trisphosphate receptor, and calcium voltage-gated channels) (4, 7, 95, 105). Furthermore, lack of *ANK2* (and in some cases, *ANK2* dysfunction) leads to decreased protein expression of the sodium/calcium exchanger and L-type, T-type, and P/Q-type voltage gated calcium channels in cardiomyocytes and neurons (7, 101, 102, 104). Specifically, two clinically relevant ANKB variants, p.E1458G and p.S646F, differentially modulate levels of $Ca_V2.1$, the pore forming subunit of P/Q-type voltage gated calcium channels, in HEK293T cells (102). The p.E1458G variant was found to decrease surface $Ca_V2.1$ levels while the p.S646F variant increased intracellular $Ca_V2.1$ levels. Another variant, p.Q879R, which to our knowledge has not yet been associated with disease, is located at the linker region required for proper ANKB localization. Expression of p.Q879R increased the surface level expression of $Ca_V2.1$ in the presence of the Ca_V accessory subunits (102). Additionally, ANKB may also regulate the key intracellular calcium release channel, ryanodine receptor 2 (RYR2). RYR2 hyperphosphorylation in the mouse *Ank2* knock-in model harboring the p.Q1283H variant suggests ANKB's interaction with the regulatory subunit, B56α, of the protein phosphatase PP2A, of the protein phosphatase PP2A (*PPP2R5A*) is necessary for PP2A activity on RYR2 (Figure 2) (95). Abnormal calcium handling associated with ANKB variant expression is a plausible pathophysiological mechanism underlying the increase in frequency of delayed afterdepolarizations and susceptibility for cardiac arrhythmias observed with *ANK2* cardiac variants (104, 106), as well as a possible mechanism for the increased susceptibility to epileptic seizures associated with some *ANK2* variants.

PP2A is a key regulator in most signal transduction pathways and cellular processes (107, 108). Other targets of PP2A and the resulting impact of ANKB dysfunction has not yet been investigated and should be an area of research in the future. Of the many PP2A targets some include other ANKB interactors such as the inositol trisphosphate receptor (109) and the sodium potassium ATPase (110) of whose phosphorylation and therefore function may also be altered as a result of ANKB dysfunction. In neuronal cells PP2A is one of the major enzymes associated with regulating microtubules, neurofilaments, and the actin cytoskeleton (111–113). While ANKB's interaction with PP2A in neurons has not yet been confirmed, this likely regulation of signaling events has key implications to the functioning and development of neuronal cells as well.

ANKB functions in glucose and fat metabolism regulation

ANKB has also been linked to regulating glucose and fat metabolism. An earlier study by Healy et al. (114) described that mice with partial global loss of *Ank2* ($Ank2^{+/-}$) exhibit impaired oral glucose tolerance likely secondary to

decreased expression of the inositol trisphosphate receptor in pancreatic islets, which mediates the signaling for augmented glucose-induced insulin secretion after parasympathetic stimulation (115, 116). Knock-in mice harboring the type-2 diabetes-associated *ANK2* p.R1788W variant exhibit decreased insulin secretion following parasympathetic stimulation and increased peripheral glucose uptake (coupled with increased plasma membrane density of the glucose co-transporter 4 in skeletal muscle and adipose tissue) (19). Notably, older *ANK2* R1788W mice had increased adiposity and showed insulin resistance (19). The increase in adiposity is also observed in adipose tissue-specific *Ank2* knockout mice, which develop progressive pancreatic islet dysfunction, accumulation of fat with age or high fat diet, and insulin resistance associated with impaired glucose co-transporter clathrin-mediated endocytosis (117). Importantly, a subset of *ANK2* variants associated with cardiac arrhythmias failed to rescue the metabolic defects in $Ank2^{-/-}$ adipocytes (117), calling to attention additional cardiovascular risk considerations for individuals with known *ANK2* cardiac arrhythmia variants. A knock in *ANK2* p.L1622I model exhibited a measurable and distinct cardiac phenotype, reduced ANKB expression, and even developed insulin resistance and age-dependent increases in adiposity (19).

Discussion

Variants in *ANK2* are associated primarily to complex cardiac phenotypes; however, some functional *ANK2* variants also have neurological or metabolic manifestations. Cardiac phenotypes associated with *ANK2* functional variants are characterized by a predisposition to arrhythmias, conduction anomalies, and congenital and adult-onset structural heart disease, and in some cases, seizure (Table 1). Other *ANK2* variants may contribute to risk for ASD and epilepsy (Table 2). With type 2 diabetes also linked to specific *ANK2* antecedents, the putative compounding effects of metabolic perturbation on cardiac and neurological phenotypes may pose additional risk to individuals carrying *ANK2* variants. The diversity of manifestations associated with *ANK2* variants could result, in part, from complex ANKB protein interaction networks involving critical proteins that regulate cellular structure and function (Table 3). Overall, improved knowledge of ANKB cellular roles and regulation is now needed to advance understanding of clinical phenotypes associated with *ANK2* variants and, ultimately to develop improved, targeted therapeutic approaches.

As there is such diversity in features reported across *ANK2* variants with cardiac phenotypes, further studies are required to better understand which features are truly linked to Ankyrin-B syndrome. For example, congenital heart defects have been described in association with only one variant to date, p.S464F (7), and a structural chromosomal re-arrangement involving breakpoints in *ANK2* (39). Whether congenital heart defects are part of the ANKB spectrum of manifestations or just isolated events remains to be determined. In favor of the notion that *ANK2* functional variants can also contribute to structural heart disease, a British study on hypertrophic cardiomyopathy reported that the proportion of patients with a maximum left ventricular wall thickness >30 mm (i.e., extreme wall thickness) was higher in carriers of *ANK2* variants (43). This effect was still present when restraining the analysis to patients carrying sarcomeric protein variants (43), suggesting that *ANK2* might play a role of a disease modifier in cases of hypertrophic cardiomyopathy (43, 118, 119). Further population and laboratory studies are required to fully elucidate the connection between *ANK2* variants and hypertrophic cardiomyopathy, which could involve ANKB interactions with structural/cytoskeletal elements within cardiac cells.

Given the cases of structural malformations it is also important to investigate the potential role of ANKB in cardiac cell development. Of note, the p.S6464F variant is less stable and experiences reduced expression only in undifferentiated H9c2 cells suggesting this variant's impact to cells occurs during their development (94) and provides some additional rationale behind investigating ANKB's roles during cardiac development. As seen in patients with both the p.S646F (7) and p.E1458G (4) variants there appears to be an age-related effect. This implies that not only is ANKB function important in early development but also over a lifespan. Some possible mechanisms behind ANKB's role in cardiac development include its interactions with beta-catenin, PP2A, and ion channels. Understanding the developmental expression of ANKB and the impact of variants may provide insight into the cardiac dysfunction observed in patients over their lifetime.

While ANKB's link to neuronal development has been better pieced together through studies with model organisms, we have highlighted key knowledge gaps and areas of future investigations. Early observations revealed neuroanatomical defects in the global *Ank2* knockout mouse (57) and model organisms have highlighted homologous ankyrin roles in neuronal polarization (79). Other mainly *in vitro* studies point to a role for ANKB in GABAergic synaptic development (120), axonal branching (51, 58, 98), and voltage-gated calcium channel trafficking (101, 102) (Figure 3). These studies suggest ANKB regulates neurodevelopmental processes and could help explain its putative role in risk for ASD, as well as its association with epilepsy and seizure. Given the important roles of giant ANKB in the development of the nervous system, future studies aiming to elucidate the roles of giant ANKB in the development of the heart and conduction system are warranted. Moreover, recent single cell transcriptomics surveys identifying several non-myocyte cells that contribute to heart development, such as cardiac neural crest cells, neuronal cells, and glial-like cells (all with detectable *ANK2* transcripts levels) (26, 121–123) open the door to novel lines of research investigating

ANK2's functions within these cells and their impact in shaping heart development. Notably, many studies in the brain have focused primarily on the giant isoform of ANKB, the putative central nervous system-specific, neonatal isoform (51, 58, 98); however, the roles of the smaller, more prominent 220 kDa isoform are vastly understudied. ANKB's roles at the mammalian synapse are yet to be studied even though ANKB is not only enriched at synapses, but also seems to associate with multiple postsynaptic scaffolding proteins (124, 125). Given ANKB's interactions with ion channels, βII-spectrin, and components of the cytoskeleton (126), it is possible that ANKB plays important roles in regulating the shape of postsynaptic structures and protein sorting therein contributing to maturation of synapses and establishment of neuronal circuits.

Recently, disease associations of *ANK2* variants and LQTS and CPVT have been debated in part due to the population frequency of certain previously reported variants (34–36, 127). Although the minor allele frequency is certainly a useful predictive tool (128), an elevated minor allele frequency may not completely eliminate a role for the variants in disease. For example, while the *ANK2* p.L1622I variant is associated with prolonged QTc and ventricular tachyarrhythmias, which is modeled in a knock-in homozygous mouse, the study was limited by the use of juvenile homozygous mice. This cardiac phenotype likely exceeds that of the carriers in the general population, who are most likely heterozygous for the *ANK2* p.L1622I variant (37). It is possible that *ANK2* variants are part of an oligogenic/polygenic disease (129). Such a possibility is seen with the p.E1813K variant which has been shown to aggravate the cardiac phenotype of an individual carrying KCNH2 p.H562R variant (130). In isolation, the p.E1813K variant was associated with age-related conduction disease, and the individual carrying only the KCNH2 p.H562R variant was asymptomatic. *ANK2* is a gene that appears to tolerate mutations well as seen by the allele frequencies of many variants. This variant toleration may be a result of a compensatory mechanism to protect the overall function of the protein given its apparent importance in cellular biology. Overall, this evidence highlights the importance of integrating allele frequency, genetic ancestry, and environmental and genetic factors in the analysis and determination of cardiovascular gene-disease associations of *ANK2* variants.

Insights from model organism studies have highlighted the significance of ANKB's many roles within cells. *ANK2* variants are linked with cardiac, neurological, or metabolomic phenotypes consisting of electrical, structural, and signaling impacts. The mechanisms behind *ANK2* variant dysfunction can be explained in part due to ANKB's protein interactions and cellular partners outlined within the review. With many interactions in both signaling and cytoskeletal components, ANKB can easily be implicated in a variety of cellular events and basic functions. Furthermore, interactions identified and studied within one cell type could hold relevance across multiple cell types in which ANKB is expressed. With the large number of ANKB protein-protein interactions the phenotype associated with one particular variant could be anticipated to be vastly different from another depending on the amino acid location and the degree of conservation (chemical similarity). A variant located within the membrane binding domain is likely to have a different phenotype than a variant located within the spectrin binding domain as an ion channel disruption will result in altered signaling compared to losing a structural interaction.

Improved understanding of ANKB cellular roles and the effects of variant expression at a mechanistic level is needed to advance the identification possible therapeutic targets and biomarkers for individuals with *ANK2* variants. Comprehensive characterization of ANKB's interacting and signaling partners would facilitate the design of small molecule modulators or repurposing of compounds to mitigate cellular pathology associated with ANKB variants. For example, inhibition of CamKII with KN-93 was able to mitigate RYR2 hyperphosphorylation and subsequent excessive calcium release in $Ank2^{+/-}$ pro-arrhythmogenic mouse hearts, resulting in a net reduction of RYR2 phosphorylation, calcium spark frequency, and delayed afterdepolarizations (95, 131, 132). More recently, inhibition of the GSK-3β pathway with SB-216763 (resulting in a net activation of the Wnt/beta-catenin signaling cascade) was effective in ameliorating cardiac remodeling in mice presenting with arrhythmogenic cardiomyopathy associated with cardiac specific loss of ANKB (44). However, given ANKB expression in other excitable tissues and the important roles linked to signaling pathways in which ANKB directly or indirectly participates, it is paramount to continue advancing the understanding of ANKB's role in cells and molecular pathways before defining and launching ANKB-targeting therapeutic programs. This is particularly important given the limited mechanistic appreciation of neurological phenotypes associated with *ANK2* variants, such as seizure and white matter abnormalities. By exploiting the relatively conserved amino acid sequence and biological functions of ANKB and the availability of experimental model organisms, high-throughput cellular and molecular characterization of variants can bridge the gap to improved clinical understanding and development of targeted, specific therapeutic interventions.

The variability of clinical phenotypes associated with *ANK2* variants poses challenges for treatment. At present, the understanding of the source of this variability is incomplete but could be partly due to the pleiotropic effects of ANKB, as well as surreptitious layering of variants in related pathways and/or environmental factors. The complexity and incomplete mechanistic understanding of ANKB cellular roles and regulation pose significant challenges for development of precise therapeutic interventions. As technological advances in personalized and precision medicine continue to expand, successful therapeutic strategies will arise from testing and modeling *ANK2* variants directly on induced pluripotent

stem cells derived from affected individuals themselves (133). A combination of experimental approaches, including personalized and precision medicine methods such as *in vitro* studies using patient-derived induced pluripotent stem cells, and model organism approaches will help to bridge the gaps to the identification of key pathways and therapeutics that target them safely and effectively. Current clinical efforts should therefore focus on monitoring carriers of *ANK2* functional variants for arrhythmia and cardiomyopathy, along with symptomatic and treatment and control of co-morbidities (106).

Highlighted within this review are a variety of *ANK2* variants and the different disease-linked phenotypes that arise as a result of their expression. Bringing together studies from model organisms and laboratory findings this review identifies potential mechanisms underlying ANKB dysfunction and possible contributions to disease. Investigating mechanisms underlying this link to disease will not only aid in our understanding of cellular pathways and ANKB's roles within them but will provide insight into disease risk and presentation. Understanding ANKB's roles in health and disease will advance the ability to translate this information into clinic and provide insights into developing treatments and therapies.

Author contributions

Conceived by NY, LAS, and LTA. All authors wrote and revised the manuscript, contributed to the article, and approved the submitted version.

Funding

This work was supported by a Canadian Institutes for Health Research Project Grant (CIHR; PJT-169064) awarded to LTA and LAS. NY was supported by a CIHR Graduate Scholarship-Master's Program scholarship and University of Victoria Donor Awards. JCSA was supported by a Michael Smith Health Research BC Trainee Award (RT-2021-1735). LTA was supported by a BC Children's Hospital Research Institute Investigator award.

Acknowledgments

We acknowledge the Indigenous traditional territory of the W̱SÁNEĆ, Lekwungen, and Wyomilth peoples of the Coast Salish Nation and appreciate the continued partnership with the Gitxsan peoples and the Gitxsan Health Society as we address their research priorities together.

Conflict of interest

The authors declare that the research was conducted in the absence of any commercial or financial relationships that could be construed as a potential conflict of interest.

Publisher's note

References

1. Roden DM. Keep the QT interval: it is a reliable predictor of ventricular arrhythmias. *Heart Rhythm.* (2008) 5:1213–5. doi: 10.1016/j.hrthm.2008.05.008

2. O'Neal WT, Singleton MJ, Roberts JD, Tereshchenko LG, Sotoodehnia N, Chen LY, et al. The Association between QT interval components and sudden cardiac death: the atherosclerosis risk in communities study. *Circ Arrhythm Electrophysiol.* (2017) 10:e005485. doi: 10.1161/CIRCEP.117.005485

3. Bohnen MS, Peng G, Robey SH, Terrenoire C, Iyer V, Sampson KJ, et al. Molecular pathophysiology of congenital long QT syndrome. *Physiol Rev.* (2017) 97:89–134. doi: 10.1152/physrev.00008.2016

4. Mohler PJ, Schott J-J, Gramolini AO, Dilly KW, Guatimosim S, duBell WH, et al. Ankyrin-B mutation causes type 4 long-QT cardiac arrhythmia and sudden cardiac death. *Nature.* (2003) 421:634–9. doi: 10.1038/nature01335

5. Mohler PJ, Splawski I, Napolitano C, Bottelli G, Sharpe L, Timothy K, et al. cardiac arrhythmia syndrome caused by loss of ankyrin-B function. *Proc Natl Acad Sci U A.* (2004) 101:9137–42. doi: 10.1073/pnas.0402546101

6. Smith SA, Sturm AC, Curran J, Kline CF, Little SC, Bonilla IM, et al. Dysfunction in the βII Spectrin-dependent cytoskeleton underlies human arrhythmia. *Circulation.* (2015) 131:695–708. doi: 10.1161/CIRCULATIONAHA.114.013708

7. Swayne LA, Murphy NP, Asuri S, Chen L, Xu X, McIntosh S, et al. A novel variant in the ANK2 membrane-binding domain is associated with Ankyrin-B syndrome and structural heart disease in a first nations population with a high rate of long QT syndrome. *Circ Cardiovasc Genet.* (2017) 10:e001537. doi: 10.1161/CIRCGENETICS.116.001537

8. Mohler PJ, Le Scouarnec S, Denjoy I, Lowe JS, Guicheney P, Caron L, et al. Defining the cellular phenotype of "Ankyrin-B Syndrome" variants. *Circulation.* (2007) 115:432–41. doi: 10.1161/CIRCULATIONAHA.106.656512

9. Satterstrom FK, Kosmicki JA, Wang J, Breen MS, De Rubeis S, An J-Y, et al. Large-scale exome sequencing study implicates both developmental and functional changes in the neurobiology of autism. *Cell.* (2020) 180:568–84.e23. doi: 10.1016/j.cell.2019.12.036

10. Willsey AJ, Sanders SJ, Li M, Dong S, Tebbenkamp AT, Muhle RA, et al. Coexpression networks implicate human midfetal deep cortical

projection neurons in the pathogenesis of autism. *Cell.* (2013) 155:997–1007. doi: 10.1016/j.cell.2013.10.020

11. Peng J, Zhou Y, Wang K. Multiplex gene and phenotype network to characterize shared genetic pathways of epilepsy and autism. *Sci Rep.* (2021) 11:952. doi: 10.1038/s41598-020-78654-y

12. Davis JQ, Bennett V. Brain ankyrin. a membrane-associated protein with binding sites for spectrin, tubulin, and the cytoplasmic domain of the erythrocyte anion channel. *J Biol Chem.* (1984) 259:13550–9. doi: 10.1016/S0021-9258(18)90728-3

13. Bennett V, Stenbuck PJ. The membrane attachment protein for spectrin is associated with band 3 in human erythrocyte membranes. *Nature.* (1979) 280:468–73. doi: 10.1038/280468a0

14. Mohler PJ, Gramolini AO, Bennett V. The Ankyrin-B C-terminal domain determines activity of Ankyrin-B/G chimeras in rescue of abnormal inositol 1,4,5-Trisphosphate and ryanodine receptor distribution in Ankyrin-B (–/–) Neonatal Cardiomyocytes*. *J Biol Chem.* (2002) 277:10599–607. doi: 10.1074/jbc.M110958200

15. Abdi KM, Mohler PJ, Davis JQ, Bennett V. Isoform specificity of ankyrin-b: a site in the divergent C-TERMINAL domain is required for intramolecular association*. *J Biol Chem.* (2006) 281:5741–9. doi: 10.1074/jbc.M506697200

16. Galiano MR, Jha S, Ho TS, Zhang C, Ogawa Y, Chang K-J, et al. distal axonal cytoskeleton forms an intra-axonal boundary that controls axon initial segment assembly. *Cell.* (2012) 149:1125–39. doi: 10.1016/j.cell.2012.03.039

17. Park HH, Lo Y-C, Lin S-C, Wang L, Yang JK, Wu H. The death domain superfamily in intracellular signaling of apoptosis and inflammation. *Annu Rev Immunol.* (2007) 25:561–86. doi: 10.1146/annurev.immunol.25.022106.141656

18. Tuvia S, Buhusi M, Davis L, Reedy M, Bennett V. Ankyrin-B is required for intracellular sorting of structurally diverse Ca2+ homeostasis proteins. *J Cell Biol.* (1999) 147:995–1008. doi: 10.1083/jcb.147.5.995

19. Lorenzo DN, Healy JA, Hostettler J, Davis J, Yang J, Wang C, et al. Ankyrin-B metabolic syndrome combines age-dependent adiposity with pancreatic β cell insufficiency. *J Clin Invest.* (2015) 125:3087–102. doi: 10.1172/JCI81317

20. Otto E, Kunimoto M, McLaughlin T, Bennett V. Isolation and characterization of cDNAs encoding human brain ankyrins reveal a family of alternatively spliced genes. *J Cell Biol.* (1991) 114:241–53. doi: 10.1083/jcb.114.2.241

21. Tse WT, Menninger JC, Yang-Feng TL, Francke U, Sahr KE, Lux SE, et al. Isolation and chromosomal localization of a novel nonerythroid ankyrin gene. *Genomics.* (1991) 10:858–66. doi: 10.1016/0888-7543(91)90173-C

22. Kunimoto M, Otto E, Bennett V. A new 440-kD isoform is the major ankyrin in neonatal rat brain. *J Cell.* (1991) 115:1319–31. doi: 10.1083/jcb.115.5.1319

23. Kunimoto M, Adachi T, Ishido M. Expression and localization of brain ankyrin isoforms and related proteins during early developmental stages of rat nervous system. *J Neurochem.* (1998) 71:2585–92. doi: 10.1046/j.1471-4159.1998.71062585.x

24. Wu HC, Yamankurt G, Luo J, Subramaniam J, Hashmi SS, Hu H, et al. Identification and characterization of two ankyrin-B isoforms in mammalian heart. *Cardiovasc Res.* (2015) 107:466–77. doi: 10.1093/cvr/cvv184

25. Cunha SR, Le Scouarnec S, Schott J-J, Mohler PJ. Exon organization and novel alternative splicing of the human ANK2 gene: implications for cardiac function and human cardiac disease. *J Mol Cell Cardiol.* (2008) 45:724–34. doi: 10.1016/j.yjmcc.2008.08.005

26. Asp M, Giacomello S, Larsson L, Wu C, Fürth D, Qian X, et al. A spatiotemporal organ-wide gene expression and cell atlas of the developing human heart. *Cell.* (2019) 179:1647–60.e19. doi: 10.1016/j.cell.2019.11.025

27. Kang HJ, Kawasawa YI, Cheng F, Zhu Y, Xu X, Li M, et al. Spatiotemporal transcriptome of the human brain. *Nature.* (2011) 478:483–9. doi: 10.1038/nature10523

28. Fertuzinhos S, Li M, Kawasawa YI, Ivic V, Franjic D, Singh D, et al. Laminar and temporal expression dynamics of coding and noncoding RNAs in the mouse neocortex. *Cell Rep.* (2014) 6:938–50. doi: 10.1016/j.celrep.2014.01.036

29. Kawano S, Baba M, Fukushima H, Miura D, Hashimoto H, Nakazawa T. Autism-associated ANK2 regulates embryonic neurodevelopment. *Biochem Biophys Res Commun.* (2022) 605:45–50. doi: 10.1016/j.bbrc.2022.03.058

30. Zhang Y, Chen K, Sloan SA, Bennett ML, Scholze AR, O'Keeffe S, et al. An RNA-sequencing transcriptome and splicing database of glia, neurons, and vascular cells of the cerebral cortex. *J Neurosci.* (2014) 34:11929–47. doi: 10.1523/JNEUROSCI.1860-14.2014

31. Bakken TE, Jorstad NL, Hu Q, Lake BB, Tian W, Kalmbach BE, et al. Comparative cellular analysis of motor cortex in human, marmoset and mouse. *Nature.* (2021) 598:111–9. doi: 10.1038/s41586-021-03465-8

32. Koenig SN, Mohler PJ. The evolving role of Ankyrin-B in cardiovascular disease. *Heart Rhythm.* (2017) 14:1884–9. doi: 10.1016/j.hrthm.2017.07.032

33. Giudicessi JR, Wilde AAM, Ackerman MJ. The genetic architecture of long QT syndrome: a critical reappraisal. *Trends Cardiovasc Med.* (2018) 28:453–64. doi: 10.1016/j.tcm.2018.03.003

34. Ghouse J, Have CT, Weeke P, Bille Nielsen J, Ahlberg G, Balslev-Harder M, et al. Rare genetic variants previously associated with congenital forms of long QT syndrome have little or no effect on the QT interval. *Eur Heart J.* (2015) 36:2523–9. doi: 10.1093/eurheartj/ehv297

35. Adler A, Novelli V, Amin AS, Abiusi E, Care M, Nannenberg EA, et al. An international, multicentered, evidence-based reappraisal of genes reported to cause congenital long QT syndrome. *Circulation.* (2020) 141:418–28. doi: 10.1161/CIRCULATIONAHA.119.043132

36. Giudicessi JR, Ackerman MJ. Established loss-of-function variants in ANK2-Encoded Ankyrin-B rarely cause a concerning cardiac phenotype in humans. *Circ Genomic Precis Med.* (2020) 13:80–2. doi: 10.1161/CIRCGEN.119.002851

37. Musa H, Murphy NP, Curran J, Higgins JD, Webb TR, Makara MA, et al. Common human ANK2 variant confers in vivo arrhythmia phenotypes. *Heart Rhythm.* (2016) 13:1932–40. doi: 10.1016/j.hrthm.2016.06.012

38. Arbour L, Rezazadeh S, Eldstrom J, Weget-Simms G, Rupps R, Dyer Z, et al. A KCNQ1 V205M missense mutation causes a high rate of long QT syndrome in a first nations community of northern British Columbia: a community-based approach to understanding the impact. *Genet Med Off J Am Coll Med Genet.* (2008) 10:545–50. doi: 10.1097/GIM.0b013e31817c6b19

39. Huq A, Pertile M, Davis A, Landon H, James P, Kline C, et al. Novel mechanism for human cardiac Ankyrin-B syndrome due to reciprocal chromosomal translocation. *Heart Lung Circ.* (2017) 26:612–8. doi: 10.1016/j.hlc.2016.09.013

40. Song J, Sasmita BR, Deng G. Ankyrin-2 genetic variants: a case of Ankyrin-B syndrome. *Ann Noninvasive Electrocardiol.* (2022). doi: 10.1111/anec.12933

41. Sumitomo N. Current topics in catecholaminergic polymorphic ventricular tachycardia. *J Arrhythmia.* (2016) 32:344–51. doi: 10.1016/j.joa.2015.09.008

42. Coban-Akdemir ZH, Charng W-L, Azamian M, Paine IS, Punetha J, Grochowski CM, et al. Wolff-parkinson-white syndrome: de novo variants and evidence for mutational burden in genes associated with atrial fibrillation. *Am J Med Genet A.* (2020) 182:1387–99. doi: 10.1002/ajmg.a.61571

43. Lopes LR, Syrris P, Guttmann OP, O'Mahony C, Tang HC, Dalageorgou C, et al. Novel genotype–phenotype associations demonstrated by high-throughput sequencing in patients with hypertrophic cardiomyopathy. *Heart.* (2015) 101:294–301. doi: 10.1136/heartjnl-2014-306387

44. Roberts JD, Murphy NP, Hamilton RM, Lubbers ER, James CA, Kline CF, et al. Ankyrin-B dysfunction predisposes to arrhythmogenic cardiomyopathy and is amenable to therapy. *J Clin Invest.* (2019) 129:3171–84. doi: 10.1172/JCI125538

45. Mohler PJ, Healy JA, Xue H, Puca AA, Kline CF, Rand Allingham R, et al. Ankyrin-B syndrome: enhanced cardiac function balanced by risk of cardiac death and premature senescence. *PLoS ONE.* (2007) 2:e1051. doi: 10.1371/journal.pone.0001051

46. Ichikawa M, Aiba T, Ohno S, Shigemizu D, Ozawa J, Sonoda K, et al. Phenotypic variability of ANK2 mutations in patients with inherited primary arrhythmia syndromes. *Circ J.* (2016) 80:2435–42. doi: 10.1253/circj.CJ-16-0486

47. Leppa VM, Kravitz SN, Martin CL, Andrieux J, Le Caignec C, Martin-Coignard D, et al. Rare inherited and de novo CNVs reveal complex contributions to ASD risk in multiplex families. *Am J Hum Genet.* (2016) 99:540–54. doi: 10.1016/j.ajhg.2016.06.036

48. Yuen RK, Thiruvahindrapuram B, Merico D, Walker S, Tammimies K, Hoang N, et al. Whole-genome sequencing of quartet families with autism spectrum disorder. *Nat Med.* (2015) 21:185–91. doi: 10.1038/nm.3792

49. Iossifov I, Ronemus M, Levy D, Wang Z, Hakker I, Rosenbaum J, et al. De novo gene disruptions in children on the autistic spectrum. *Neuron.* (2012) 74:285–99. doi: 10.1016/j.neuron.2012.04.009

50. Bowling KM, Thompson ML, Amaral MD, Finnila CR, Hiatt SM, Engel KL, et al. Genomic diagnosis for children with intellectual disability and/or developmental delay. *Genome Med.* (2017) 9:43. doi: 10.1186/s13073-017-0433-1

51. Yang R, Walder-Christensen KK, Kim N, Wu D, Lorenzo DN, Badea A, et al. ANK2 autism mutation targeting giant ankyrin-B promotes axon branching and ectopic connectivity. *Proc Natl Acad Sci U S A.* (2019) 116:15262–71. doi: 10.1073/pnas.1904348116

52. Guo W, Shang D-M, Cao J-H, Feng K, He Y-C, Jiang Y, et al. Identifying and analyzing novel epilepsy-related genes using random walk with restart algorithm. *BioMed Res Int.* (2017) 2017:1–13. doi: 10.1155/2017/6132436

53. Hata Y, Yoshida K, Kinoshita K, Nishida N. Epilepsy-related sudden unexpected death: targeted molecular analysis of inherited heart disease genes using next-generation DNA sequencing. *Brain Pathol.* (2017) 27:292–304. doi: 10.1111/bpa.12390

54. Costagliola G, Orsini A, Coll M, Brugada R, Parisi P, Striano P. The brain–heart interaction in epilepsy: implications for diagnosis, therapy, and SUDEP prevention. *Ann Clin Transl Neurol.* (2021) 8:1557–68. doi: 10.1002/acn3.51382

55. Cheng CY, Reich D, Haiman CA, Tandon A, Patterson N, Elizabeth S, et al. African Ancestry and its correlation to type 2 diabetes in African Americans: a genetic admixture analysis in three US population cohorts. *PLoS ONE.* (2012) 7:e32840. doi: 10.1371/journal.pone.0032840

56. Ng MC. Genetics of Type 2 diabetes in African Americans. *Curr Diab Rep.* (2015) 15:74. doi: 10.1007/s11892-015-0651-0

57. Scotland P, Zhou D, Benveniste H, Bennett V. Nervous system defects of AnkyrinB (–/–) Mice suggest functional overlap between the cell adhesion molecule L1 and 440-kD AnkyrinB in premyelinated axons. *J Cell Biol.* (1998) 143:1305–15. doi: 10.1083/jcb.143.5.1305

58. Creighton BA, Afriyie S, Ajit D, Casingal CR, Voos KM, Reger J, et al. Giant ankyrin-B mediates transduction of axon guidance and collateral branch pruning factor sema 3A. *Elife.* (2021) 10:e69815. doi: 10.7554/eLife.69815

59. Lorenzo DN, Badea A, Zhou R, Mohler PJ, Zhuang X, Bennett V. βII-spectrin promotes mouse brain connectivity through stabilizing axonal plasma membranes and enabling axonal organelle transport. *Proc Natl Acad Sci U S A.* (2019) 116:15686–95. doi: 10.1073/pnas.1820649116

60. Mohler PJ, Davis JQ, Bennett V. Ankyrin-B coordinates the Na/K ATPase, Na/Ca exchanger, and InsP3 receptor in a cardiac T-tubule/SR microdomain. *PLoS Biol.* (2005) 3:e423. doi: 10.1371/journal.pbio.0030423

61. Smith RS, Walsh CA. Ion channel functions in early brain development. *Trends Neurosci.* (2020) 43:103–14. doi: 10.1016/j.tins.2019.12.004

62. Porter GA Jr, Makuck RF, Rivkees SA. Intracellular calcium plays an essential role in cardiac development. *Dev Dyn.* (2003) 227:280–90. doi: 10.1002/dvdy.10307

63. Rosenberg SS, Spitzer NC. Calcium signaling in neuronal development. *Cold Spring Harb Perspect Biol.* (2011) 3:a004259. doi: 10.1101/cshperspect.a004259

64. Cai X, Zhang Y. Molecular evolution of the ankyrin gene family. *Mol Biol Evol.* (2006) 23:550–8. doi: 10.1093/molbev/msj056

65. Hopitzan AA, Baines AJ, Kordeli E. Molecular evolution of Ankyrin: gain of function in vertebrates by acquisition of an Obscurin/Titin-Binding–related domain. *Mol Biol Evol.* (2006) 23:46–55. doi: 10.1093/molbev/msj004

66. Bennett V, Baines AJ. Spectrin and ankyrin-based pathways: metazoan inventions for integrating cells into tissues. *Physiol Rev.* (2001) 81:1353–92. doi: 10.1152/physrev.2001.81.3.1353

67. He M, Tseng W-C, Bennett V. A single divergent exon inhibits Ankyrin-B association with the plasma membrane. *J Biol Chem.* (2013) 288:14769–79. doi: 10.1074/jbc.M113.465328

68. Kordeli E, Lambert S, Bennett V. AnkyrinG: a new ankyrin gene with neural-specific isoforms localized at the axonal initial segment and node of Ranvier (∗). *J Biol Chem.* (1995) 270:2352–9. doi: 10.1074/jbc.270.5.2352

69. Mohler PJ, Hoffman JA, Davis JQ, Abdi KM, Kim C-R, Jones SK, et al. Isoform specificity among ankyrins: an amphipathic α-helix in the divergent regulatory domain of ankyrin-b interacts with the molecular co-chaperone Hdj1/Hsp40*. *J Biol Chem.* (2004) 279:25798–804. doi: 10.1074/jbc.M401296200

70. Chang KJ, Zollinger DR, Susuki K, Sherman DL, Makara MA, Brophy PJ, et al. Glial ankyrins facilitate paranodal axoglial junction assembly. *Nat Neurosci.* (2014) 17:1673–81. doi: 10.1038/nn.3858

71. Ho TS, Zollinger DR, Chang K-J, Xu M, Cooper EC, Stankewich MC, et al. Hierarchy of ankyrin-spectrin complexes clusters sodium channels at nodes of Ranvier. *Nat Neurosci.* (2014) 17:1664–72. doi: 10.1038/nn.3859

72. Rappel W-J, Edelstein-Keshet L. Mechanisms of cell polarization. *Curr Opin Syst Biol.* (2017) 3:43–53. doi: 10.1016/j.coisb.2017.03.005

73. Vicente-Manzanares M, Sánchez-Madrid F. Cell polarization: a comparative cell biology and immunological view. *Dev Immunol.* (2000) 7:51–65. doi: 10.1155/2000/70801

74. Hirschy A, Schatzmann F, Ehler E, Perriard J-C. Establishment of cardiac cytoarchitecture in the developing mouse heart. *Dev Biol.* (2006) 289:430–41. doi: 10.1016/j.ydbio.2005.10.046

75. Henderson DJ, Anderson RH. The development and structure of the ventricles in the human heart. *Pediatr Cardiol.* (2009) 30:588–96. doi: 10.1007/s00246-009-9390-9

76. Takano T, Xu C, Funahashi Y, Namba T, Kaibuchi K. Neuronal polarization. *Development.* (2015) 142:2088–93. doi: 10.1242/dev.114454

77. Boontrakulpoontawee P, Otsuka A. Mutational analysis of the Caenorhabditis elegans ankyrin gene unc-44 demonstrates that the large spliceoform is critical for neural development. *Mol Genet Genomics.* (2002) 267:291–302. doi: 10.1007/s00438-002-0661-x

78. Otsuka AJ, Franco R, Yang B, Shim KH, Tang LZ, Zhang YY, et al. An ankyrin-related gene (unc-44) is necessary for proper axonal guidance in Caenorhabditis elegans. *J Cell Biol.* (1995) 129:1081–92. doi: 10.1083/jcb.129.4.1081

79. Maniar TA, Kaplan M, Wang GJ, Shen K, Wei L, Shaw JE, et al. UNC-33 (CRMP) and ankyrin organize microtubules and localize kinesin to polarize axon-dendrite sorting. *Nat Neurosci.* (2011) 15:48–56. doi: 10.1038/nn.2970

80. He L, Kooistra R, Das R, Oudejans E, van Leen E, Ziegler J, et al. Cortical anchoring of the microtubule cytoskeleton is essential for neuron polarity. *Elife.* (2020) 9:e55111. doi: 10.7554/eLife.55111

81. Harterink M, Edwards SL, de Haan B, Yau KW, van den Heuvel S, Kapitein LC, et al. Local microtubule organization promotes cargo transport in C. elegans dendrites. *J Cell Sci.* (2018) 131:jcs223107. doi: 10.1242/jcs.223107

82. McIntire SL, Garriga G, White J, Jacobson D, Robert Horvitz H. Genes necessary for directed axonal elongation or fasciculation in C. elegans. *Neuron.* (1992) 8:307–22. doi: 10.1016/0896-6273(92)90297-Q

83. Desai C, Garriga G, Mclntire SL, Horvitz HR. A genetic pathway for the development of the Caenorhabditis elegans HSN motor neurons. *Nature.* (1988) 336:638–46. doi: 10.1038/336638a0

84. Meng L, Chen C, Yan D. Regulation of gap junction dynamics by UNC-44/ankyrin and UNC-33/CRMP through VAB-8 in C. elegans neurons. *PLoS Genet.* (2016) 12:e1005948. doi: 10.1371/journal.pgen.1005948

85. Montoro RJ, Yuste R. Gap junctions in developing neocortex: a review. *Brain Res Rev.* (2004) 47:216–26. doi: 10.1016/j.brainresrev.2004.06.009

86. Belousov AB, Fontes JD. Neuronal gap junctions: making and breaking connections during development and injury. *Trends Neurosci.* (2013) 36:227–36. doi: 10.1016/j.tins.2012.11.001

87. Hortsch M, Paisley KL, Tian M-Z, Qian M, Bouley M, Chandler R. The axonal localization of large drosophila Ankyrin2 protein isoforms is essential for neuronal functionality. *Mol Cell Neurosci.* (2002) 20:43–55. doi: 10.1006/mcne.2002.1113

88. Koch I, Schwarz H, Beuchle D, Goellner B, Langegger M, Aberle H. Drosophila Ankyrin 2 is required for synaptic stability. *Neuron.* (2008) 58:210–22. doi: 10.1016/j.neuron.2008.03.019

89. Pielage J, Cheng L, Fetter RD, Carlton PM, Sedat JW, Davis GW, et al. Presynaptic giant ankyrin stabilizes the NMJ through regulation of presynaptic microtubules and transsynaptic cell adhesion. *Neuron.* (2008) 58:195–209. doi: 10.1016/j.neuron.2008.02.017

90. Fan Y, Ho BX, Pang JKS, Pek NMQ, Hor JH, Ng S-Y, et al. Wnt/β-catenin-mediated signaling re-activates proliferation of matured cardiomyocytes. *Stem Cell Res Ther.* (2018) 9:338. doi: 10.1186/s13287-018-1086-8

91. Komiya Y, Habas R. Wnt signal transduction pathways. *Organogenesis.* (2008) 4:68–75. doi: 10.4161/org.4.2.5851

92. Pahnke A, Conant G, Huyer LD, Zhao Y, Feric N, Radisic M. The role of Wnt regulation in heart development, cardiac repair and disease: a tissue engineering perspective. *Biochem Biophys Res Commun.* (2016) 473:698–703. doi: 10.1016/j.bbrc.2015.11.060

93. Ménard C, Pupier S, Mornet D, Kitzmann M, Nargeot J, Lory P. Modulation of L-type calcium channel expression during retinoic acid-induced differentiation of H9C2 cardiac cells. *J Biol Chem.* (1999) 274:29063–70. doi: 10.1074/jbc.274.41.29063

94. Chen L, Choi CSW, Sanchez-Arias JC, Arbour LT, Swayne LA. Ankyrin-B pS646F undergoes increased proteasome degradation and reduces cell viability in the H9c2 rat ventricular cardiomyoblast cell line. *Biochem Cell Biol.* (2020) 98:299–306. doi: 10.1139/bcb-2019-0082

95. Zhu W, Wang C, Hu J, Wan R, Yu J, Xie J, et al. Ankyrin-B Q1283H variant linked to arrhythmias *via* loss of local protein phosphatase 2A activity causes ryanodine receptor hyperphosphorylation. *Circulation.* (2018) 138:2682–97. doi: 10.1161/CIRCULATIONAHA.118.034541

96. Durak O, de Anda FC, Singh KK, Leussis MP, Petryshen TL, Sklar P, et al. Ankyrin-G regulates neurogenesis and Wnt signaling by altering the subcellular localization of β-catenin. *Mol Psychiatry.* (2015) 20:388–97. doi: 10.1038/mp.2014.42

97. Thompson JJ, Williams CS. Protein phosphatase 2A in the regulation of Wnt signaling, stem cells, and cancer. *Genes.* (2018) 9:121. doi: 10.3390/genes9030121

98. Chen K, Yang R, Li Y, Zhou JC, Zhang M. Giant ankyrin-B suppresses stochastic collateral axon branching through direct interaction with microtubules. *J Cell Biol.* (2020) 219:e201910053. doi: 10.1083/jcb.201910053

99. Benkarim O, Paquola C, Park B, Hong S-J, Royer J, Vos de Wael R, et al. Connectivity alterations in autism reflect functional idiosyncrasy. *Commun Biol.* (2021) 4:1–15. doi: 10.1038/s42003-021-02572-6

100. Nomi JS, Uddin LQ. Developmental changes in large-scale network connectivity in autism. *NeuroImage Clin.* (2015) 7:732–41. doi: 10.1016/j.nicl.2015.02.024

101. Kline CF, Scott J, Curran J, Hund TJ, Mohler PJ. Ankyrin-B regulates Cav21 and Cav22 channel expression and targeting*. *J Biol Chem.* (2014) 289:5285–95. doi: 10.1074/jbc.M113.523639

102. Choi CSW, Souza IA, Sanchez-Arias JC, Zamponi GW, Arbour LT. Swayne LA. Ankyrin B and Ankyrin B variants differentially modulate intracellular and surface Cav21 levels. *Mol Brain.* (2019) 12:75. doi: 10.1186/s13041-019-0494-8

103. Lencesova L, O'Neill A, Resneck WG, Bloch RJ, Blaustein MP. Plasma membrane-cytoskeleton-endoplasmic reticulum complexes in neurons and astrocytes. *J Biol Chem.* (2004) 279:2885–93. doi: 10.1074/jbc.M310365200

104. Camors E, Mohler PJ, Bers DM, Despa S. Ankyrin-B reduction enhances Ca spark-mediated SR Ca release promoting cardiac myocyte arrhythmic activity. *J Mol Cell Cardiol.* (2012) 52:1240–8. doi: 10.1016/j.yjmcc.2012.02.010

105. Cunha SR, Bhasin N, Mohler PJ. Targeting and stability of Na/Ca Exchanger 1 in cardiomyocytes requires direct interaction with the membrane adaptor Ankyrin-B*. *J Biol Chem.* (2007) 282:4875–83. doi: 10.1074/jbc.M607096200

106. Sucharski HC, Dudley EK, Keith CBR, El Refaey M, Koenig SN, Mohler PJ. Mechanisms and alterations of cardiac ion channels leading to disease: role of Ankyrin-B in cardiac function. *Biomolecules.* (2020) 10:211. doi: 10.3390/biom10020211

107. Schuhmacher D, Sontag J-M, Sontag E. Protein phosphatase 2A: more than a passenger in the regulation of epithelial cell–cell junctions. *Front Cell Dev Biol.* (2019) 7:30. doi: 10.3389/fcell.2019.00030

108. Wlodarchak N, Xing Y. PP2A as a master regulator of the cell cycle. *Crit Rev Biochem Mol Biol.* (2016) 51:162–84. doi: 10.3109/10409238.2016.1143913

109. Kirchhefer U, Heinick A, König S, Kristensen T, Müller FU, Seidl MD, et al. Protein phosphatase 2A is regulated by protein kinase Cα (PKCα)-dependent phosphorylation of its targeting subunit B56α at Ser41*. *J Biol Chem.* (2014) 289:163–76. doi: 10.1074/jbc.M113.507996

110. Lecuona E, Dada LA, Sun H, Butti ML, Zhou G, Chew T-L, et al. Na,K-ATPase alpha1-subunit dephosphorylation by protein phosphatase 2A is necessary for its recruitment to the plasma membrane. *FASEB J.* (2006) 20:2618–20. doi: 10.1096/fj.06-6503fje

111. Hoffman A, Taleski G, Sontag E. The protein serine/threonine phosphatases PP2A, PP1 and calcineurin: a triple threat in the regulation of the neuronal cytoskeleton. *Mol Cell Neurosci.* (2017) 84:119–31. doi: 10.1016/j.mcn.2017.01.005

112. Yeh P-A, Chang C-J. A novel function of twins, B subunit of protein phosphatase 2A, in regulating actin polymerization. *PLoS ONE.* (2017) 12:e0186037. doi: 10.1371/journal.pone.0186037

113. Westphal RS, Colbran RJ. Ebner FF, Wadzinski BE. Protein serine/threonine phosphatase 1 and 2A associate with and dephosphorylate neurofilaments. *Brain Res Mol Brain Res.* (1997) 49:15–28. doi: 10.1016/s0169-328x(97)00117-4

114. Healy JA, Nilsson KR, Hohmeier HE, Berglund J, Davis J, Hoffman J, et al. Cholinergic augmentation of insulin release requires Ankyrin-B. *Sci Signal.* (2010) 3:ra19–ra19. doi: 10.1126/scisignal.2000771

115. Komatsu M, Takei M, Ishii H, Sato Y. Glucose-stimulated insulin secretion: a newer perspective. *J Diabetes Investig.* (2013) 4:511–6. doi: 10.1111/jdi.12094

116. Ahrén B. Autonomic regulation of islet hormone secretion–implications for health and disease. *Diabetologia.* (2000) 43:393–410. doi: 10.1007/s001250051322

117. Lorenzo DN, Bennett V. Cell-autonomous adiposity through increased cell surface GLUT4 due to ankyrin-B deficiency. *Proc Natl Acad Sci U S A.* (2017) 114:12743–8. doi: 10.1073/pnas.1708865114

118. Lopes LR, Zekavati A, Syrris P, Hubank M, Giambartolomei C, Dalageorgou C, et al. Uk10k Consortium, Plagnol V, et al. Genetic complexity in hypertrophic cardiomyopathy revealed by high-throughput sequencing. *J Med Genet.* (2013) 50:228–39. doi: 10.1136/jmedgenet-2012-101270

119. Sabater-Molina M, Pérez-Sánchez I, Hernández Del Rincón JP, Gimeno JR. Genetics of hypertrophic cardiomyopathy: a review of current state. *Clin Genet.* (2018) 93:3–14. doi: 10.1111/cge.13027

120. Guan H, Maness PF. Perisomatic GABAergic innervation in prefrontal cortex is regulated by ankyrin interaction with the L1 cell adhesion molecule. *Cereb Cortex N Y NY.* (2010) 20:2684–93. doi: 10.1093/cercor/bhq016

121. Litvinuková M, Talavera-López C, Maatz H, Reichart D, Worth CL, Lindberg EL, et al. Cells of the adult human heart. *Nature.* (2020) 588:466–72. doi: 10.1038/s41586-020-2797-4

122. Tucker NR, Chaffin M, Fleming SJ, Hall AW, Parsons VA, Bedi KC, et al. Transcriptional and cellular diversity of the human heart. *Circulation.* (2020) 142:466–82. doi: 10.1161/CIRCULATIONAHA.119.045401

123. Kikel-Coury NL, Brandt JP, Correia IA, O'Dea MR, DeSantis DF, Sterling F, et al. Identification of astroglia-like cardiac nexus glia that are critical regulators of cardiac development and function. *PLoS Biol.* (2021) 19:e3001444. doi: 10.1371/journal.pbio.3001444

124. Smith KR, Penzes P. Ankyrins: roles in synaptic biology and pathology. *Mol Cell Neurosci.* (2018) 91:131–9. doi: 10.1016/j.mcn.2018.04.010

125. Li J, Zhang W, Yang H, Howrigan DP, Wilkinson B, Souaiaia T, et al. Spatiotemporal profile of postsynaptic interactomes integrates components of complex brain disorders. *Nat Neurosci.* (2017) 20:1150–61. doi: 10.1038/nn.4594

126. Lorenzo DN. Cargo hold and delivery: ankyrins, spectrins, and their functional patterning of neurons. *Cytoskeleton.* (2020) 77:129–48. doi: 10.1002/cm.21602

127. Walsh R, Adler A, Amin AS, Abiusi E, Care M, Bikker H, et al. Evaluation of gene validity for CPVT and short QT syndrome in sudden arrhythmic death. *Eur Heart J.* (2022) 43:1500–10. doi: 10.1093/eurheartj/ehab687

128. Kido T, Sikora-Wohlfeld W, Kawashima M, Kikuchi S, Kamatani N, Patwardhan A, et al. Are minor alleles more likely to be risk alleles? *BMC Med Genomics.* (2018) 11:3. doi: 10.1186/s12920-018-0322-5

129. Cerrone M, Remme CA, Tadros R, Bezzina CR, Delmar M. Beyond the one gene-one disease paradigm: complex genetics and pleiotropy in inheritable cardiac disorders. *Circulation.* (2019) 140:595–610. doi: 10.1161/CIRCULATIONAHA.118.035954

130. Gessner G, Runge S, Koenen M, Heinemann SH, Koenen M, Haas J, et al. ANK2 functionally interacts with KCNH2 aggravating long QT syndrome in a double mutation carrier. *Biochem Biophys Res Commun.* (2019) 512:845–51. doi: 10.1016/j.bbrc.2019.03.162

131. DeGrande S, Nixon D, Koval O, Curran JW, Wright P, Wang Q, et al. CaMKII inhibition rescues proarrhythmic phenotypes in the model of human ankyrin-B syndrome. *Heart Rhythm.* (2012) 9:2034–41. doi: 10.1016/j.hrthm.2012.08.026

132. Popescu I, Galice S, Mohler PJ, Despa S. Elevated local [Ca 2+] and CaMKII promote spontaneous Ca 2+ release in ankyrin-B-deficient hearts. *Cardiovasc Res.* (2016) 111:287–94. doi: 10.1093/cvr/cvw093

133. Matsa E, Ahrens JH, Wu JC. Human induced pluripotent stem cells as a platform for personalized and precision cardiovascular medicine. *Physiol Rev.* (2016) 96:1093–126. doi: 10.1152/physrev.00036.2015

134. Krumm N, Turner TN, Baker C, Vives L, Mohajeri K, Witherspoon K, et al. Excess of rare, inherited truncating mutations in autism. *Nat Genet.* (2015) 47:582–8. doi: 10.1038/ng.3303

135. Iossifov I, O'Roak BJ, Sanders SJ, Ronemus M, Krumm N, Levy D, et al. The contribution of de novo coding mutations to autism spectrum disorder. *Nature.* (2014) 515:216–21. doi: 10.1038/nature13908

136. Le Scouarnec S, Bhasin N, Vieyres C, Hund TJ, Cunha SR, Koval O, et al. Dysfunction in ankyrin-B-dependent ion channel and transporter targeting causes human sinus node disease. *Proc Natl Acad Sci U S A.* (2008) 105:15617–22. doi: 10.1073/pnas.0805500105

137. Cunha SR, Hund TJ, Hashemi S, Voigt N, Li N, Wright P, et al. Defects in ankyrin-based membrane protein targeting pathways underlie atrial fibrillation. *Circulation.* (2011) 124:1212–22. doi: 10.1161/CIRCULATIONAHA.111.023986

138. Garcia-Caballero A, Zhang F-X, Hodgkinson V, Huang J, Chen L, Souza IA, et al. T-type calcium channels functionally interact with spectrin (α/β) and ankyrin B. *Mol Brain.* (2018) 11:24. doi: 10.1186/s13041-018-0368-5

139. Kline CF, Kurata HT, Hund TJ, Cunha SR, Koval OM, Wright PJ, et al. Dual role of K ATP channel C-terminal motif in membrane targeting and metabolic regulation. *Proc Natl Acad Sci U S A.* (2009) 106:16669–74. doi: 10.1073/pnas.0907138106

140. Li J, Kline CF, Hund TJ, Anderson ME, Mohler PJ. Ankyrin-B regulates Kir62 membrane expression and function in heart*. *J Biol Chem.* (2010) 285:28723–30. doi: 10.1074/jbc.M110.147868

141. Liu X, Spicarová Z, Rydholm S, Li J, Brismar H, Aperia A. Ankyrin B modulates the function of Na,K-ATPase/inositol 1,4,5-trisphosphate receptor signaling microdomain. *J Biol Chem.* (2008) 283:11461–8. doi: 10.1074/jbc.M706942200

142. Gudmundsson H, Hund TJ, Wright PJ, Kline CF, Snyder JS, Qian L, et al. EH domain proteins regulate cardiac membrane protein targeting. *Circ Res.* (2010) 107:84–95. doi: 10.1161/CIRCRESAHA.110.216713

143. Gil OD, Sakurai T, Bradley AE, Fink MY, Cassella MR, Kuo JA, et al. Ankyrin binding mediates L1CAM interactions with static components of the cytoskeleton and inhibits retrograde movement of L1CAM on the cell surface. *J Cell Biol.* (2003) 162:719–30. doi: 10.1083/jcb.200211011

144. Ayalon G, Hostettler JD, Hoffman J, Kizhatil K, Davis JQ, Bennett V. Ankyrin-B Interactions with Spectrin and Dynactin-4 Are Required for Dystrophin-based protection of skeletal muscle from exercise injury. *J Biol Chem.* (2011) 286:7370–8. doi: 10.1074/jbc.M110.187831

145. Ayalon G, Davis JQ, Scotland PB, Bennett V. An ankyrin-based mechanism for functional organization of dystrophin and dystroglycan. *Cell.* (2008) 135:1189–200. doi: 10.1016/j.cell.2008.10.018

146. Lorenzo DN, Badea A, Davis J, Hostettler J, He J, Zhong G, et al. PIK3C3–Ankyrin-B–Dynactin pathway promotes axonal growth and multiorganelle transport. *J Cell Biol.* (2014) 207:735–52. doi: 10.1083/jcb.201407063

147. Mohler PJ, Yoon W, Bennett V. Ankyrin-B Targets β2-Spectrin to an intracellular compartment in neonatal cardiomyocytes*. *J Biol Chem.* (2004) 279:40185–93. doi: 10.1074/jbc.M406018200

148. Qu F, Lorenzo DN, King SJ, Brooks R, Bear JE, Bennett V. Ankyrin-B is a PI3P effector that promotes polarized α5β1-integrin recycling *via* recruiting RabGAP1L to early endosomes. *Elife.* (2016) 5:e20417. doi: 10.7554/eLife.20417

149. Bhasin N, Cunha SR, Mudannayak M, Gigena MS, Rogers TB, Mohler PJ. Molecular basis for PP2A regulatory subunit B56α targeting in cardiomyocytes. *Am J Heart Circ Physiol.* (2007) 293:H109–19. doi: 10.1152/ajpheart.00059.2007

150. Little SC, Curran J, Makara MA, Kline CF, Ho H-T, Xu Z, et al. Protein phosphatase 2A regulatory subunit B56α limits phosphatase activity in the heart. *Sci Signal.* (2015) 8:ra72. doi: 10.1126/scisignal.aaa5876

151. Ye J, Li J, Ye F, Zhang Y, Zhang M, Wang C. Mechanistic insights into the interactions of dynein regulator Ndel1 with neuronal ankyrins and implications in polarity maintenance. *Proc Natl Acad Sci U S A.* (2020) 117:1207–15. doi: 10.1073/pnas.1916987117

152. Cunha SR, Mohler PJ. Obscurin targets Ankyrin-B and protein phosphatase 2A to the Cardiac M-line. *J Biol Chem.* (2008) 283:31968–80. doi: 10.1074/jbc.M806050200

153. Di Meo D, Ravindran P, Sadhanasatish T, Dhumale P, Püschel AW. The balance of mitochondrial fission and fusion in cortical axons depends on the kinases SadA and SadB. *Cell Rep.* (2021) 37:110141. doi: 10.1016/j.celrep.2021.110141

frontiers | Frontiers in Cardiovascular Medicine

TYPE Review
PUBLISHED 24 November 2022
DOI 10.3389/fcvm.2022.964743

OPEN ACCESS

EDITED BY
Mete Civelek,
University of Virginia, United States

REVIEWED BY
Sander W. van der Laan,
University Medical Center Utrecht, Netherlands
Michael C. Mahaney,
The University of Texas Rio Grande Valley, United States

*CORRESPONDENCE
Marie Pigeyre
pigeyrem@mcmaster.ca

SPECIALTY SECTION
This article was submitted to Cardiovascular Genetics and Systems Medicine, a section of the journal Frontiers in Cardiovascular Medicine

RECEIVED 08 June 2022
ACCEPTED 21 October 2022
PUBLISHED 24 November 2022

CITATION
Lamri A, De Paoli M, De Souza R, Werstuck G, Anand S and Pigeyre M (2022) Insight into genetic, biological, and environmental determinants of sexual-dimorphism in type 2 diabetes and glucose-related traits. *Front. Cardiovasc. Med.* 9:964743. doi: 10.3389/fcvm.2022.964743

Insight into genetic, biological, and environmental determinants of sexual-dimorphism in type 2 diabetes and glucose-related traits

Amel Lamri[1,2], Monica De Paoli[1,3], Russell De Souza[2,4], Geoff Werstuck[1,3], Sonia Anand[1,2,4] and Marie Pigeyre[1,2]*

[1]Department of Medicine, McMaster University, Hamilton, ON, Canada, [2]Population Health Research Institute (PHRI), Hamilton, ON, Canada, [3]Thrombosis and Atherosclerosis Research Institute (TaARI), Hamilton, ON, Canada, [4]Department of Health Research Methods, Evidence, and Impact, McMaster University, Hamilton, ON, Canada

There is growing evidence that sex and gender differences play an important role in risk and pathophysiology of type 2 diabetes (T2D). Men develop T2D earlier than women, even though there is more obesity in young women than men. This difference in T2D prevalence is attenuated after the menopause. However, not all women are equally protected against T2D before the menopause, and gestational diabetes represents an important risk factor for future T2D. Biological mechanisms underlying sex and gender differences on T2D physiopathology are not yet fully understood. Sex hormones affect behavior and biological changes, and can have implications on lifestyle; thus, both sex-specific environmental and biological risk factors interact within a complex network to explain the differences in T2D risk and physiopathology in men and women. In addition, lifetime hormone fluctuations and body changes due to reproductive factors are generally more dramatic in women than men (ovarian cycle, pregnancy, and menopause). Progress in genetic studies and rodent models have significantly advanced our understanding of the biological pathways involved in the physiopathology of T2D. However, evidence of the sex-specific effects on genetic factors involved in T2D is still limited, and this gap of knowledge is even more important when investigating sex-specific differences during the life course. In this narrative review, we will focus on the current state of knowledge on the sex-specific effects of genetic factors associated with T2D over a lifetime, as well as the biological effects of these different hormonal stages on T2D risk. We will also discuss how biological insights from rodent models complement the genetic insights into the sex-dimorphism effects on T2D. Finally, we will suggest future directions to cover the knowledge gaps.

KEYWORDS

genetics, type 2 diabetes, sex-specific effect, sex-dimorphism, gestational diabetes, genome wide association studies, animal models

Introduction

Type 2 diabetes (T2D) is a metabolic disorder characterized by a combination of insulin resistance, (especially in adipose tissue, skeletal muscles and the liver), and relative insulin secretion deficiency (1). A wide variety of lifestyle factors, including excess body weight, smoking, and a sedentary lifestyle increase the risk of developing T2D (2). Globally, over 422 million individuals are affected by T2D worldwide and over 1.5 million deaths are annually attributed to T2D, ranking it among the top ten leading causes of mortality (3). Notably, epidemiological studies show that men develop insulin resistance and T2D earlier than women and at a lower BMI (4, 5). Premenopausal women have a reduced risk of developing T2D, compared to men or postmenopausal women (4, 6), but when women reach menopause, the risk becomes similar to that of men (7, 8).

Sex and gender differences play an important role in pathophysiology of T2D (4). Sex differences refer to biological differences, which are caused by differences in sex chromosomes, sex-specific gene expression, sex hormones, and their effects on organ systems. Gender differences refer to the effect of identities, expressions and societal roles and their implications on lifestyles. Both sex- and gender-specific biological and behavioral risk factors interact within a complex network to explain the differences in T2D risk and physiopathology in men and women. Polycystic ovary syndrome, gestational diabetes mellitus (GDM), and the age of menopause are three major woman-specific risk factors of T2D. For instance, women diagnosed with polycystic ovary syndrome typically have significant insulin resistance, regardless of body weight (9). Of women who had a history of GDM and were not given metformin or provided lifestyle interventions, almost 50% developed T2D within 10 years (10). T2D risk increases for women entering menopause before the age of 40, with a 30% increase in risk of T2D vs. women entering menopause from 50 to 54 years old (11). Moreover, women with T2D face an increased risk for cardiovascular disease that is at least two to four fold higher than the increase in cardiovascular disease risk seen in men with T2D (12). Premenopausal women without T2D are at a lower risk for cardiovascular disease than men without T2D of the same age, and much of this protection from cardiometabolic risk is thought to be due to the effects of estrogen, including estrogen receptor-mediated effects on lipid and glucose metabolism, endothelial function, and fat deposition (13). Estrogen appears to be cardioprotective unless T2D is present, but after the menopause, the protective effects are lost as estrogen deficiency develops (12).

From a biological perspective, T2D pathophysiology is partially driven by genetic factors (14). Thereby, progress in genetic studies have facilitated the identification of more than 300 loci associated with glucose-related variables and T2D. These studies have led to a better understanding of the biological pathways involved, as well as the common underlying biological mechanisms linking polycystic ovary syndrome and T2D (15), or GDM and T2D (16). Several rodent models of diabetes exhibiting an exaggerated form of sexual dimorphism have also been useful to delineate the mechanisms underlying the protection against T2D conferred by estrogens.

In this narrative review, we will focus on the current state of knowledge on the sex-specific effects of genetic factors associated with glucose-related traits, insulin resistance and T2D during the life course. Given that sex hormones dramatically change during a women's lifetime (e.g., ovarian cycle, pregnancy, and menopause), we will discuss the biological effects of these different hormonal stages on type 2 diabetes risk. We will further discuss how rodent models provide evidence on the effects of sex-dimorphism on type 2 diabetes risk. We will finally suggest future directions to cover the current knowledge gaps.

Genetic evidence for sexual dimorphism in type 2 diabetes

Regulatory differences in blood glucose and insulin levels are both heritable traits. When estimated separately, the single nucleotide polymorphism (SNP)-based heritability (17) for T2D is significantly higher in men than in women (18), which suggests differences in the underlying genetic determinants of T2D risk due to sex-dimorphic effects in specific genes (or loci).

Given the complex nature of T2D related traits, Genome wide association studies (GWAS) have been one of the most powerful approaches used to identify new loci. While the methodology has essentially remained unchanged since the publication of the first T2D GWAS (19), the list of associated genes has considerably expanded due to the increase in sample size, and the inclusion of samples of multiple ancestries (20, 21). However, the proportion of variance in glucose related traits is still not fully explained by the currently known loci, and gene × gene and gene × environment interactions are thought to contribute to this missing heritability, with gene × sex interactions being one of these modulators. Three main statistical approaches have been used to date to investigate sex-dimorphic effects. The first approach involves performing sex-stratified analysis, followed by a heterogeneity test of effect between the two sexes at each genetic locus. The second approach consists in performing a single analysis with sex and SNP × sex interaction terms in the statistical model tested (22). The third, referred to as a sex-differentiated test, combines data for both sexes in a single analysis, includes the number of X-chromosome copies (1 or 2) as an independent variable in the model and allows for testing heterogeneity of allelic effects between males and females at the cost of one degree

of freedom (22). Each one of these approaches have their own limitations as to the ability and power to detect sex-dimorphic effects (19, 20). However, one major advantage of the first approach is the possibility of testing for sex-related heterogeneity using summary statistics of publicly available sex-stratified data, while the other two methods require individual level data.

The spectrum of sex-dimorphic effects varies from (i) different (significant) direction of effects between males and females, (ii) similar (significant) direction of effects with differences in magnitude of the effect between sexes (e.g., larger effect sizes in one of the two sexes), to (iii) sex-specific effects whereby the association is significantly observed in one of the sexes only; this last case scenario being an extreme example of the second. It is important to note that the distinction between these three cases heavily relies on the statistical method, power, and parameters used to determine the significance of a SNP-T2D association in each sex. Hence, intermediary/inconclusive scenarios that do not clearly fit in the above-mentioned categories can often be observed (e.g., a SNP with a GWAS significant association ($p\text{-value} < 5 \times 10^{-8}$) in one sex and suggestive association only ($p\text{-value} < 1 \times 10^{-6}$) in the other. Therefore, balanced sample sizes in the two sex groups (and hence a comparable statistical power) is a crucial component for sex-comparison analyses.

Human genes/loci with sex-dimorphic effects on glucose related-traits

Primary evidence of sex-specific effects in glucose metabolism-related genes/loci are rare, and replication attempts are even more sparse, due to the lack of power concomitant to the sex-stratified or the sex-interaction analyses. A large proportion of genes contributing to sex-dimorphic effects on FG and FI were described in a recent study lead by Lagou et al. (23). The authors conducted genome wide association studies (GWAS) in over 140,000 (for FG) and 98,000 (for FI) adult normoglycemic men and women (separately) of European ancestry from the Meta-Analyses of Glucose and Insulin-related traits Consortium (MAGIC). GWAS results were subsequently meta-analyzed and the heterogeneity of allelic effects between the two sexes was estimated (23). A targeted analysis for 36 and 19 previously established FG and FI loci that aimed to detect sex-dimorphic effects in these loci, was also conducted. To date, this study is largest one to investigate the modulating effect of sex on the genetic determinants of glucose-related traits on a genome wide level, complemented with genetic correlations and gene expression analysis. The absence of replication data represents the main limitations of this study.

Given the lack of replication studies and the weak significance of the associations in most studies, we investigated the sex-dimorphic effects of the autosomal genes/loci described in the literature with glucose-related traits [e.g., fasting glucose (FG), fasting insulin (FI), T2D], other correlated anthropometric traits including body mass index (BMI), waist to hip ratio (WHR), and GDM, using publicly available data from large genetic consortia, in order to identify the candidate genes with the most robust evidence of sex-dimorphic effect (spanning across multiple phenotypes). The list and description of genes/loci with the strongest evidence of sexual dimorphism across multiple traits is presented in Table 1. Results of an assessment of the sex-specific effects for each gene/locus on anthropometric and glucose-related traits is presented in Tables 1, 2.

Genes identified in childbearing women

Autosomal genes

COBLL1/GRB14 locus

The locus which includes *growth factor receptor bound protein 14* (*GRB14*) and *cordon-bleu WH2 repeat protein like 1* (*COBLL1*) genes, has the strongest evidence of sexual dimorphism across multiple traits. *GRB14* encodes for a protein that binds to insulin, inhibiting its signaling activity (24). The biological function of *COBLL1*'s protein is unclear beyond its possible involvement in the Wnt/PCP pathway regulation in mammals (that regulates crucial aspects of cell fate determination, cell migration, cell polarity, neural patterning and organogenesis during embryonic development) (25), and its association to multiple metabolic traits and tumor types. SNPs in this gene displayed nominal evidence of sex-differences, with an association with FI observed in females only (23). The FI increasing allele of the lead SNP described by Lagou et al. (23) (*rs10195252*) was also significantly associated with a lower BMI and WHR in women only (effect of the same SNP in men was weaker and nominal) (Table 1). The same FI increasing allele (T) was associated with an increased risk of T2D in a female-specific manner (Table 1). Sex-differences influencing WHR (23–25), triglycerides (26) and T2D (27) at this locus have also been described in the literature. Finally, gene expression of *COBLL1* was higher in women's gluteal fat, abdominal fat and whole blood, while men had a higher expression than women in the liver (23). Levels of *GRB14* were nominally higher in women's gluteal fat. Levels of *GRB14* in abdominal fat were similar between men and women (23). Given all these results, it is possible that an effect of variants within/near to *COBLL1* and *GRB14* could influence glucose metabolism *via* adipose tissue and body fat distribution differences between men and women. More studies are needed in order to establish this link.

TABLE 1 Associations of sex dimorphic effects of most important genes identified to date on type 2 diabetes and related phenotypes.

Gene/locus	Reported lead SNP with sex-dimorphism	Effect /other allele	Primary phenotype	Direction of association for primary phenotype	Secondary phenotypes tested	Direction for secondary phenotype	# other SNPs with nominal sex heterogeneity	r^2 range with reported lead SNP
COBLL1/GRB14	*rs10195252*	T/C	FI	**Association with FI in women only** Women: Beta = 0.02, SE = 0.004, $P = 1.23 \times 10^{-6}$ Men: Beta = 0.007, SE = 0.004, $P = 0.07$ Sex heterogeneity (Cochran's Q-test) $P = 0.03$	BMI	**T allele associated with lower BMI in women** Women: Beta = −0.01, SE = 0.002, $P = 9.58 \times 10^{-10}$ Men: Beta = 0.006, SE = 0.002, $P = 0.01$ Sex heterogeneity (Cochran's Q-test) $P = 0.02$	32	0–1.00
					T2D	**T allele associated with higher T2D in women** Women: Beta = 0.08, SE = 0.01, $P = 4.20 \times 10^{-15}$ Men: Beta = 0.05, SE = 0.009, $P = 4 \times 10^{-8}$ Sex heterogeneity (Cochran's Q-test) $P = 0.02$	77	0–1.00
					WHR	**T allele associated with higher WHR in women** Women: Beta = 0.06, SE = 0.002, $P = 6.35 \times 10^{-149}$ Men: Beta = −0.005, SE = 0.003, $P = 0.05$ Sex heterogeneity (Cochran's Q-test) $P = 1.81 \times 10^{-78}$	120	0.4–1
					FG	NS-Cochran's Q-test $P = 0.59$	7	0–0.28
ADCY5	*rs11708067*	A/G	FG	**Stronger effect on FG in women** Women: Beta = 0.03, SE = 0.003, $P = 5.01 \times 10^{-16}$ Men: Beta = 0.02, SE = 0.004, $P = 2.19 \times 10^{-6}$ Sex heterogeneity (Cochran's Q-test) $P = 0.04$	BMI	NS-Cochran's Q-test $P = 0.18$	0	NA
					T2D	NS-Cochran's Q-test $P = 0.28$	21	0.17–0.21
					WHR	NS-Cochran's Q-test $P = 0.69$	14	0.04–0.27
					FI	NS-Cochran's Q-test $P = 0.52$	25	0.17–0.18

(Continued)

10.3389/fcvm.2022.964743

TABLE 1 (Continued)

Gene/locus	Reported lead SNP with sex-dimorphism	Effect /other allele	Primary phenotype	Direction of association for primary phenotype	Secondary phenotypes tested	Direction for secondary phenotype	# other SNPs with nominal sex heterogeneity	r^2 range with reported lead SNP
PROX1	*rs340874*	C/T	FG	**Stronger effect on FG in women** Women: Beta = 0.02, SE = 0.003, $P = 1.69 \times 10^{-13}$ Men: Beta = 0.01, SE = 0.003, $P = 4.81 \times 10^{-4}$ Sex heterogeneity (Cochran's Q-test) $P = 0.01$	BMI	NS-Cochran's Q-test $P = 0.36$	2	0.03–0.11
					T2D	NS-Cochran's Q-test $P = 0.28$	9	0.02–0.04
					WHR	**C allele associated with higher WHR in women** Women: Beta = 0.009, SE = 0.002, $P = 0.0001$ Men: Beta = −0.0001, SE = 0.002, $P = 0.97$ Sex heterogeneity (Cochran's Q-test) $P = 0.009$	9	0.09–0.65
					FI	NS-Cochran's Q-test $P = 0.63$	1	0.1
RGS17	*rs1281962*	C/G	FG	**Stronger effect on FG in women** Women: Beta = 0.01, SE = 0.003, $P = 2.60 \times 10^{-7}$ Men: Beta = 0.006, SE = 0.003, $P = 0.04$ Sex heterogeneity (Cochran's Q-test) $P = 0.04$	BMI	NS-Cochran's Q-test $P = 0.33$	7	0.00–0.11
					T2D	NS-Cochran's Q-test $P = 0.12$	103	0.00–0.37
					WHR	NS-Cochran's Q-test $P = 0.85$	19	0.05–0.42
					FI	NS-Cochran's Q-test $P = 0.71$	0	NA

Beta, mean change in primary phenotype per risk allele; SE, standard error for Beta; P, p-value of association between primary phenotype and risk allele; NA, not applicable; NS, not significant; #, number; r^2, Linkage disequilibrium between SNPs.

10.3389/fcvm.2022.964743

TABLE 2 Summary of cross-phenotype sex-heterogeneity tests in BMI, WHR, T2D, FG, and FI consortium data at genetic loci with previously known sex-dimorphism.

Gene/locus	Phenotype with known sex-dimorphism	New phenotype tested for heterogeneity	# SNPs tested in gene/locus	# SNPs with $P < 5 \times 10^{-6*}$	# SNPs with $P < 5 \times 10^{-6*}$ and $P_{Het<0.05}$	# SNPs with $P < 5 \times 10^{-6*}$ and $P_{Het} < P_{Het\ Bonferroni}$
ADCY5	Fasting glucose	Type 2 Diabetes	750	60	3	0
		WHR	98	9	9	4
		Fasting insulin	92	0	-	-
		BMI	92	0	-	-
COBLL1/GRB14	Fasting insulin	BMI	168	30	22	0
		Fasting glucose	103	0	-	-
		Type 2 Diabetes	922	51	41	0
		WHR	154	105	105	98
RGS17	Fasting glucose	Fasting insulin	109	0	-	-
		Type 2 Diabetes	631	124	88	0
		WHR	145	3	2	2
		BMI	154	0	-	-
DSCAM	Fasting glucose	BMI	980	13	1	0
		WHR	863	0	-	-
		Fasting insulin	440	0	-	-
		Type 2 Diabetes	5,542	0	-	-
PROX1	Fasting glucose	BMI	30	0	-	-
		WHR	17	6	6	2
		Fasting insulin	6	0	-	-
		Type 2 Diabetes	218	0	-	-

*#, number of SNPs with a suggestive association ($P < 5 \times 10^{-6}$) with the phenotypes in males only, females only, or both. A total of 22 autosomal loci (Table 3) were tested for association in 5 different consortia, for a phenotype other than the one for which the sex-dimorphism was originally described. This table only includes only loci with at least 1 SNP with $P < 5 \times 10^{-6*}$ and $P_{Het} < 0.05$ in at least one of the test consortia (BMI, WHR, FG, FI or T2D).

ADCY5 gene

In sex-combined studies, SNPs in the *adenylate cyclase 5 (ADCY5)* gene are associated with multiple T2D-related traits including FG (23, 28–32), FI (21), glycated hemoglobin (33), HOMA-B (i.e., index of insulin secretion) and T2D (34–43), anthropometric and body fat distribution traits, such as WHR (44, 45), body fat percentage (46), BMI (47), inflammation phenotypes such as C-reactive protein (48), early life factors including gestation duration (49), birth weight (50–56), blood lipid levels, including total cholesterol (57, 58), HDL-cholesterol, apolipoprotein A1 (59), and blood pressure measures (60). SNPs in the vicinity of *ADCY5* showed sex-dimorphic effects in association to FG. The lead SNP associated with FG described by Lagou et al. (23) (*rs11708067*) did not show evidence for sexual dimorphism when tested for FI, T2D, WHR or BMI (Table 1). Nevertheless, another variant in this gene likely independent from the aforementioned SNP (*rs3934729*), shows nominal sex-dimorphic effect with a stronger effect in women (Table 1). The sex-dimorphic effect of *rs11708067* on T2D risk was also previously described in the literature (27). In a gene expression analysis, *ADCY5* SNPs were associated with levels of sex hormone binding protein (SHBG) (61), which provides a possible clue as to the mechanisms and pathways involved in *ADCY5's* sex-specific effects.

PROX1 gene

The *prospero homeobox 1* (*PROX1*), which encodes for the Prospero homeobox protein 1 transcription factor plays a key role in embryonic cellular development and differentiation in multiple organs of complex organisms including *Drosophila*, mice and humans (62, 63). On a molecular level, *PROX1* was mostly studied for its prominent role in lymphatic endothelial cell fate determination of which it is generally considered as the master regulator (64). Mutations in *PROX1* have been associated with multiple forms of cancer. In human adult GWASs, *PROX1* genetic variants have been overwhelmingly associated with glycemic traits overall (65), blood glucose levels (23, 30, 31, 66, 67), glycated hemoglobin levels, HOMA-B, T2D (32, 34–37, 39, 43), and to a lesser extent to birth weight (51), and

other cardiometabolic traits such as triglycerides (68) or WHR (suggestive association only) (45). As an established FG locus, Lagou et al. (23) tested and observed nominal evidence for sex heterogeneity in multiple *PROX1* genetic variants on FG, where the associations were stronger in women. This potentially sex-dimorphic FG SNP described by Lagou et al. (23) (*rs340874*) did not show evidence for association with BMI but nominal association with FI in both sexes, with no significant sex-related heterogeneity. However, the FG increasing allele (T) was associated with higher WHR in women only, with a significant heterogeneity. Multiple other SNPs located next to this locus showed nominal sex-dimorphic effects on WHR (Table 1). Possible clues as to how *PROX1* could influence glycemic traits in a heterogenous manner between men and women come from other GWASs. Indeed, SNPs in the vicinity of *PROX1* and its neighboring non-protein coding *PROX1 Antisense RNA 1 (PROX1-AS1)* genes have been shown to be associated with SHBG levels in both men and women (61, 69). However, the sex-dimorphic SNP in *PROX1* (*rs1281962*) described by Lagou et al. (23) was not associated with SHBG levels and more investigations are required in order to establish a connection between sexual dimorphism for SNPs near *PROX1*, SHBG, and FG. *PROX1* SNPs were also associated with testosterone levels at a GWAS-significance level in men, but not in women, which could suggest a sex-dimorphic effect (61). Whether the *PROX1* plays a differential role in glucose related traits through its regulation of SHBG and testosterone levels remains to be determined.

RGS17 gene

The *regulator of G protein signaling 17 (RGS17)* gene and its corresponding RGS17 protein are involved in the regulation of multiple G protein-coupled receptor signaling cascades (70). SNPs in *RGS17* displayed strong associations with HDL-cholesterol (32, 57–59), triglycerides, apolipoprotein A1, FG (21, 23, 31), glycated hemoglobin, T2D (34), WHR (45), BMI (39, 44, 47, 71, 72), diastolic blood pressure (60), and C-reactive protein. Multiple SNPs in the *RGS17* gene revealed larger effects on FG in women at nominal significance (23). The FG-increasing allele in the lead SNP was associated with higher BMI in a GWAS meta-analysis with larger effects in women (45). The lead SNP (*rs1281962*) did not show evidence for sexual dimorphism on BMI, T2D, FI or WHR (Table 1). However, two other SNPs in *RGS17* gene (*rs3910736*, *rs514784*) showed a weak association with WHR in women only (Table 1). However, these sex-dimorphic effects were not significant after correction for multiple hypothesis testing. No significant interaction was detected at this locus (72). A nominally significant heterogeneity effect was observed against T2D (Table 3). Given its pleiotropic role on cardio-metabolic traits, the mechanisms by which *RGS17* might differentially affect phenotypes remains unclear.

Genes on chromosome X

Only few GWASs of glucose- and T2D-related traits have analyzed and identified chromosome X genetic variants (32, 34, 43, 81–83). This is partially due to the difference in the number of copies of sex chromosomes between men and women, which requires them to be analyzed separately from the autosomes. However, given the male heterogamety nature of sex determination in humans, and that the genes coding for some major regulators of sex steroids levels are located on this chromosome [e.g., *sex hormone binding globulin (SHBG) and androgen receptor (AR)*], loci on Chr X are candidates for gene × sex interactions. Among the studies that identified and validated the largest number of chromosome X variants directly associated with T2D, there was an analysis lead by Vujkovic et al. (34). This study included participants from multiple ancestries and identified a total of ten T2D loci on chromosome X (34). Among these, SNPs at the *AR/OPHN1* locus which displayed male-specific effects (non-significant in females) on T2D risk (Table 3). *AR* is an interesting biological candidate since this codes for the steroid hormone and transcription factor androgen receptor implicated in the expression of multiple male sexual development and differentiation genes under the control of testosterone (84). SNPs in *AR* have been associated with fasting insulin levels, and with baldness in males (34). The mechanism by which the *AR* gene indirectly influences results in sex-dimorphic phenotypes in relation to glucose metabolism still needs to be investigated.

Genes identified during pregnancy

Given the female-specific aspect of pregnancies, genes associated with GDM during the unique physiological state of pregnancy can be considered as sex-dimorphic. GDM is thought to be closely related to T2D from a genetic perspective. T2D polygenic risk score has been strongly associated with risk of GDM, although only a few GDM GWASs have been performed (16, 78, 85). The following genes have been identified.

HKDC1 gene

Although the majority of GDM associated genetic loci were previously known for their association with T2D or glycemic traits (86, 87), two GWASs reported *hexokinase domain containing 1 (HKDC1)* SNPs to be associated with GDM (78), and 2h-post load glucose test (16). *HKDC1* also appears to influence other early life factors, including maternal genetic effect on birth weight (51). This locus was not known for association with glycemic traits or T2D in non-gravid populations except for glycated hemoglobin (31). However, SNPs in *HKDC1* were significantly associated with SHBG levels in sex-combined and women only groups, but not in

TABLE 3 Genes/loci with suggestive evidence of sexual dimorphism on type 2 diabetes and related phenotypes.

Gene/locus	Chr	Phenotype with evidence of sex-dimorphism	Stronger sex-specific effect	Other evidence of sex-dimorphism
European populations				
IRS1	2	FI (23)	Men	WHR (72), body fat percentage
COBLL1/GRB14	2	FI (23, 72)	Women	WHR (72), TG (26, 73–75)
PROX1	1	FG (23)	Women	
ADCY5	3	FG (23)	Women	
PCK1	20	FG (23)	Women	
SLC30A8	8	FG (23)	Women	
COL26A1 (EMID2)	7	FG (76)	Women	
ZNF12	7	FI (23)	Women	
RGS17	6	FG (23)	Women	BMI (45)
HKDC1	10	GDM (16)	Women	
MC4R	18	T2D (77)	Women	
DGKB	7	T2D (27)	Men	
BCAR1	16	T2D (27)	Men	
KCNQ1	11	T2D (27)	Men	
CCND2	12	T2D (27)	Men	
MTNR1B	11	GDM (16), 2-h plasma glucose (78)	Women	
BCL11A	2	T2D (27)	Men	
BCLAF3/MAP7D2	X	T2D (34)	Men	
SPIN2A/FAAH2	X	T2D (34)	Men	
AR/OPHN1	X	T2D (34)	Men	
CCNQ/DUSP9	X	T2D (34)	Men	
BACE2	21	fasting C-peptide (pregnancy) (78)	Women	
NKX2-6	8	FI, FG (72)	Women	WHR (72)
LY86	6	FG (72)	Women	WHR (72)
EYA1	8	T2D, FG (72)	Women	WHR (72)
KLF14	7	T2D (27), FI (72)	Women	WHR (72)
NMU	4	FI (72)	Women	WHR (72)
PIGU	20	HOMA-B, HOMA-IR (72)	Women	WHR (72)
IQGAP2	5	FI (72)	Men	WHR (72)
Non- European populations				
DSCAM	21	FG (79)	Women (Koreans)	
SIRT1	10	T2D (80)	Women (Pima Indians)	

males (61). Other traits associated with *HKDC1* are mostly related to multiple blood cell count phenotypes (32, 88–91) and liver function [e.g., alanine aminotransferase (31, 92, 93), and aspartate aminotransferase].

MTNR1B gene

The *melatonin receptor 1B* (*MTNR1B*) gene is a well-established T2D locus with significant associations with multiple glucose-related traits including FG (21, 23, 28–30, 67, 94–101), glycated hemoglobin (31–33, 102, 103), insulin levels, insulin disposition index and insulin secretion rates (104, 105), acute insulin response, HOMA-B (21), and T2D (27, 34, 35, 37–40, 42, 43, 106, 107). The gene is also associated with various sleep and circadian rhythm-related phenotypes (108, 109). Given the strong association with T2D, it is not surprising that this gene has also been associated with GDM in several GWASs (16, 110). Despite the absence of evidence of sex-dimorphic effects in *MTNR1B*, this locus is of particular interest given that the effect size of *MTNR1B* SNPs are higher in GDM than T2D (16), which suggests a female-specific effect of this locus during pregnancy.

Insights from genetic studies in rodents

The use of rodent models in the study of human disease is an important component of translational knowledge. It has the dual function of either confirming what was observed in human genetic studies or provide more information on the mechanisms by which specific genes can be associated with the development of T2D. Although wild type rodent models do not spontaneously develop diabetes, the condition can be induced genetically or chemically. Examples of human genes whose functional implication in T2D has been validated in mice are numerous. For instance, a human GWAS analysis showed that *SLC30A8's* SNPs are associated with susceptibility to T2D. Subsequent studies showed that the deletion its mouse homolog *Slc30a8* induced defects in insulin secretion and an overall impairment in glucose homeostasis (111).

The implication of genetics factors in diabetes-related sex-dimorphic effects in rodents is evidenced by the fact that different strains, with different genetic backgrounds, display different sex-dimorphic phenotypes in otherwise similar environments. The characteristics of the different models that display sex-dimorphism phenotypes are provided in Table 4. Models with monogenic forms of diabetes provide direct evidence of the involvement of a gene in these sex-dimorphic outcomes. A clear illustration of this is the Zucker Diabetic Fatty (ZDF) rats, a widely used model of obesity caused by the mutation of the *leptin receptor* gene (*Lepr*, also known as *Fa*) (123). Male ZDF develop hyperglycemia, hyperinsulinemia, impaired glucose tolerance, while females are normoglycemic (124) (Table 4). This highlights the differential involvement of the *Lepr* gene and the Leptin/Melanocortin pathway in the development of diabetes between males and females. Another interesting rodent model is the aromatase-knockout (Arko) mice, which result from a targeted disruption of *Cyp19A1,* a gene that encodes for the aromatase, an enzyme involved in the production of endogenous estrogen (113). *Cyp19A1* knock down mice display a range of sex-dimorphic phenotypes as a result. Among these, male ArKO mice show signs of insulin resistance and impaired glucose homeostasis, whereas females develop glucose intolerance, but not insulin resistance (113). The importance of estrogen and all actors involved in its metabolism will be discussed below.

Rodent models of polygenic forms of diabetes also exist, with some models displaying more sex-dimorphic traits than others (Table 4). However, like human studies, the identification of the genes involved in sex-dimorphic phenotypes in these polygenic and more complex forms of diabetes is more difficult and has been poorly studied in rodents. However, given the recent advances in gene editing and other functional genomic tools, several new models have been specifically developed for the study the genetic causes of sex-dimorphic traits (124, 125). Among the most interesting candidates is a mouse for which the sex determining region of Chr Y (*Sry* locus) involved in male sex determination is transferred from chromosome Y to chromosome 3 in a male mouse, therefore detaching gonadal development from sex chromosomes (126). Male mice with this manipulation are then crossed with female mice carrying two X chromosomes. The resulting offspring can be an XY or XX carrying *Sry* in chromosome 3 (corresponding to a model where the effects of sex hormones are independent from the gonadal status), or XY and XX without this manipulation (126). In a recent study, these mice underwent gonadectomy and were subsequently supplemented with either estrogen, testosterone, or a blank control (126). It was observed that in these mice, estrogen and testosterone decrease the gonadal regulation of gene expression in the liver, whereas they enhance it in the adipose tissue. Furthermore, the effect of estrogen is more prominent than that of testosterone. It was also observed that sex chromosomes seem to regulate the expression of the *Hccs* gene, which is involved in the regulation of multiple metabolic pathways. Additionally, the study showed that genes affected by sex hormones in the adipose tissue are highly enriched with variants associated with cardiometabolic diseases and traits (126).

The study just described is an example of how rodent models can be used to decipher the mechanisms by which various sex-related components can individually affect gene expression at the basis of sexual dimorphism observed in glucose-related traits.

Effects of sex hormones on glucose and T2D-related traits

In humans

Although there is no study conducted in humans to investigate the interaction of circulating sex hormone levels with genetic factors on T2D risk, overall evidence shows that circulating levels of sex-hormones directly or indirectly modulate the effects of the genetic susceptibility for T2D, through different pathways and mechanisms. First, estrogen regulates body composition and fat distribution. In women, high estrogen level is usually associated with less ectopic fat deposition, more favorable lipid profile, and less insulin resistance than in men (6). Premenopausal women store fat primarily in gluteofemoral depots, which are considered benign or metabolically beneficial, whereas men tend to store fat in abdominal depots (6). In addition, estradiol has a beneficial impact to decrease visceral adipose tissue and increase brown adipose tissue (127). During female-specific age-related transitions, estrogen loss leads to decreased physical activity, increased adiposity with redistribution of fat to abdominal depots (128), and decreased muscle mass, whereas estrogen

TABLE 4 Genetically and chemically induced rodent models of T2D showing sexual dimorphism in glucose homeostasis.

Rodent model	Methods to induce diabetes	Phenotype	Genetic background
Zucker Diabetic Fatty (ZDF) rats	Genetically induced, monogenic	Males develop hyperglycemia, hyperinsulinemia, impaired glucose tolerance Females are normoglycemic	Mutation (*fa/fa*) in the leptin hormone receptor (112)
ArKO mice	Genetically induced, monogenic	Males are insulin resistant and have impaired glucose homeostasis. Females are glucose intolerant, but not insulin resistant	Mice lack the *Cyp19A1* gene which encodes aromatase, an enzyme involved in producing endogenous estrogen (113)
Otsuka Long-Evans Tokushima Fatty (OLETF) rats	Genetically induced, polygenic	Males develop late onset diabetes Females are normoglycemic	Development of hyperglycemia is associated with three loci (*Dmo1, Dmo2, Dmo3*) situated in Chromosomes 1, 7, 14, respectively (114). Additionally, another gene (*ODB-1*) associated with the development of hyperglycemia is located in the X-chromosome (115)
TALLYHO/JngJ mice	Genetically induced, polygenic	Males are obese and develop insulin resistance and hyperglycemia Females are obese and normoglycemic	Hyperglycemia in the *TALLYHO/JngJ* mice is associated with a recessive non-insulin dependent diabetes mellitus locus, *Tanidd1*, situated in chromosome 19. This locus can interact with other loci such as *Tanidd2* (chromosome 13), Tanidd3 (chromosome 15), TallyHo-associated fat pad, *Tafat* (chromosome 6), TallyHo-associated body weight, *Tabw1* (chromosome 7) (116–118)
New Zealand Obese (NZO) mice	Genetically induced, polygenic	Both males and females are obese and present with impaired glucose tolerance, however only males develop overt T2D	*Zfp69* is likely the gene involved in the susceptibility locus *Nidd/SJL* on Chromosome 4 and is associated with the development of severe hyperglycemia, hypoinsulinemia, as well as beta cell degeneration. Other genes involved in the development of the diabetic phenotype are *Pctp, Nob3* (119)
Streptozotocin-injected rodent (STZ), Alloxan-injected rodent	Chemically induced (STZ and alloxan have selective toxicity to pancreatic beta cells)	Female rodents require higher doses and/or more frequent injections of these chemicals to induce diabetes, compared to males (120–122)	Diabetes can be induced by STZ and alloxan on any rodent model

replacement reverses these changes (6). Second, excess of androgens and lower levels of SHBG have a direct effect on insulin resistance and T2D (129). Interestingly, sex hormones differentially modulate glycemic status and risk of T2D in men and women. High testosterone levels are associated with higher risk of T2D in women but with lower risk in men; the inverse association of SHBG with risk seems to be stronger in women than in men (130). Moreover, in women, low SHBG levels predict higher T2D risk, regardless of BMI and age (130). However, the causal relationships between low SHBG levels and T2D risk have been reported similarly in both sexes (131), though an effect on insulin resistance (132). Interestingly, lower estradiol level in men predicts lower risk of T2D (133).

Evidence on the effects of sex hormones on overall genetic susceptibility for T2D also comes from the usage of hormone replacing therapies (HRT) administered to prevent consequences of menopause including vasomotor/genitourinary symptoms and osteoporosis (134). Several clinical studies have demonstrated that HRT is beneficial for glucose homeostasis (135–138). Evidence provided by the North American Menopause Society/American College of Cardiology/American Heart Association, suggest that in women of <60 y-old, within 10 years after menopause onset, menopausal hormone therapy

with estrogens (combined or not with progestogen) may be beneficial for the prevention of coronary disease and may also reduce the incidence of T2D (139). In post-menopausal women with T2D, menopausal hormone therapy improves glycemic control, and insulin sensitivity (139), by improving β-cell insulin secretion and insulin sensitivity (137).

The study of transgender individuals also provides a unique opportunity to determine which metabolic functions are modulated by the prevailing milieu of sex steroids, because the chromosomal configuration remains unchanged (140). Usage of estrogen therapy in transgender women, as a feminizing hormonal therapy for individuals assigned male sex at birth, showed a significant effect on body composition within 12 months and these changes persist over the time, such as transgender women on estrogen lost lean mass and gained fat mass (141). Estrogen and antiandrogen therapy seemed to be associated with an increase in the absolute amount of visceral fat and subcutaneous fat, but a reduction in the ratio of visceral to subcutaneous fat (142). Effects on insulin sensitivity are controversial. Although transfeminine people may be at higher risk for T2D compared with cisgender women, the corresponding difference relative to cisgender men was not discernable in the STRONG cohort (143). There was little evidence that T2D occurrence in either transgender women or transgender men was attributable to gender-affirming hormone therapy use (143). Data from another large gender identity study suggested that both transgender men and women exhibited higher incidence of T2D than the general population (144), with a higher CV mortality rate among transwomen but not among transgender men. Despite receiving similar estrogen therapy, transgender women who elected orchiectomy had improved metabolic health compared with transgender women who retained their testes. Furthermore, data suggest that suppression of endogenous testosterone in transgender women appears to improve insulin sensitivity and reduce hepatic steatosis (145). Thus, the implications for long-term T2D incidence or cardiovascular health are still unclear, due to a paucity of long term prospective controlled studies. It should also be noted that most of the participants in these studies are of white European ethnicity, which limits the generalizability of the findings to transgender individuals of other ethnic groups.

In rodents

A wide variety of interventions have been used to study the impact of hormonal changes on sex differences in the presence of T2D in rats and mice, with overall results that validate and strengthen the observations made from human studies. Both chemical and surgical approaches can be used to mimic menopause in any rodent model of choice (146). Chemically induced menopause can be attained by exposing rodents to the chemical 4-vinylcyclohexene diepoxide (VCD), which gradually depletes ovarian follicles and therefore mimics the perimenopausal and menopausal stages (147). It has been shown that the loss of ovarian function is associated with an increase in insulin resistance, the development of metabolic syndrome, and T2D (148). Interestingly, another study in VCD mice showed that hyperglycemia was significantly more severe in VCD female mice post-ovarian failure, compared to cycling females (149). Surgical menopause through ovariectomy, which induces immediate estrogen depletion, is the most used models to induce menopause in rodents. The detrimental effects of ovariectomy on glucose homeostasis have been analyzed in several mouse models of diabetes. For instance, female normoglycemic ZDF rats, showed impaired glucose homeostasis after ovariectomy (123). Ovariectomized female New Zealand obese (NZO) mice, who otherwise rarely develop diabetes (150), display severe hyperglycemia with a significantly higher prevalence compared to sham operated controls (151). Similar observations can be made in Wistar rats and C57BL/6J mice, two other rodent models that are typically normoglycemic, but where ovariectomy can impair their glucose homeostasis.

Estrogen supplementation, another commonly used chemical procedure in rodents, has been shown to restore glucose homoeostasis in ovariectomized female ZDF rats (123), and improve glucose tolerance and fasting blood glucose levels in males (152). Estrogen replacement reversed insulin resistance and visceral fat accumulation, and improved insulin sensitivity in the skeletal muscle (when combined with high fat diet) in ovariectomized female Wistar rats (153, 154). Estrogen supplementation in ovariectomized female C57BL/6J mice significantly improved blood glucose levels, glucose-stimulated insulin secretion as well as insulin content in pancreatic beta cells (155) and improved insulin sensitivity in the hepatic tissue (156). Finally, in the ArKO mice, estrogen replacement also significantly improved glucose tolerance and insulin sensitivity in both males and females, further indicating the protective role of estrogen in glucose homeostasis (113).

Of note, rodent studies show that the impact of sex hormones, combined to the exposure to environmental risk factors can lead to sexual dimorphic phenotypes as early as *in utero*. For example, in Sprague-Dawley rats, a multipurpose rodent model typically used in studies of metabolism and diabetes, male offspring born to mothers with diet-induced GDM had altered expression of genes associated with pancreatic growth, reduced beta cell expansion and differentiation, and impaired insulin secretion (157). Sex differences in glucose homeostasis of offspring born to C57BL/6J mice with diet-induced GDM have also been observed (158). Specifically, male offspring were more insulin resistant, had higher plasma insulin levels, and had smaller pancreatic islets compared to female offspring. Additionally, the expression of *PDX-1* which is involved in pancreatic

beta cell maturation was significantly reduced in males, compared to female offspring. These data show that estradiol might exert protective effects in the metabolic homeostasis of female offspring.

Taken together, these studies illustrate how rodent models can help to recapitulate and pinpoint the mechanistic effects at the basis of sexual dimorphism as well as how they can be a valuable and complemental tool to inform genetic analysis on this specific area of research.

Gender-specific genetic determinants for T2D risk

Gender-specific lifestyle behaviors including unhealthy diet, low physical activity and smoking are well-recognized risk factors for T2D that differ between gender (4), yet studies on interaction between gender-specific lifestyle behaviors and genetic determinants on T2D risk are still lacking, for the main reason that such studies need a very large sample size to reach the power required to detect significant effects. It has been shown that men are more likely to smoke than women (159, 160); women are more likely to consume a healthy diet (161, 162), but are less active than men [global average 32% for inactive women vs. 23% for inactive men (163, 164)]. Diets enriched in ultra-processed foods and sugar-sweetened beverages are associated with an increased risk of developing T2D (165), while diets enriched in fruits, whole grains, and dairy products are associated with a decreased risk of T2D (166). Moreover, the influence of lifestyle factors may exert their effects differently along the life stages.

Knowledge gaps and conclusions

Most of GWASs studying the sex-dimorphic effects of genes on T2D risk have been conducted on populations of European ancestry. To date, the list of genes displaying sex dimorphic effects in non-European populations is extremely limited and includes *SIRT1*, identified in a population of Pima Indians (80), and *DSCAM* in Koreans (Table 3). However, the replication of sex-dimorphic effects at these loci is still needed, and larger, more diverse studies are still needed in order to identify more sex-dimorphic loci and increase our understanding on the interplay between genes, sex and the risk of diabetes.

Sex and gender consideration in research studies has improved over the last 20 years, but preclinical research is still primarily done using male rodent models and male-derived cells, with the result that many conclusions are made based on incomplete and sex-biased data (167). Although sex-specific data can improve disease prevention, diagnosis, and treatment as well as reduce inequities, research to address the important

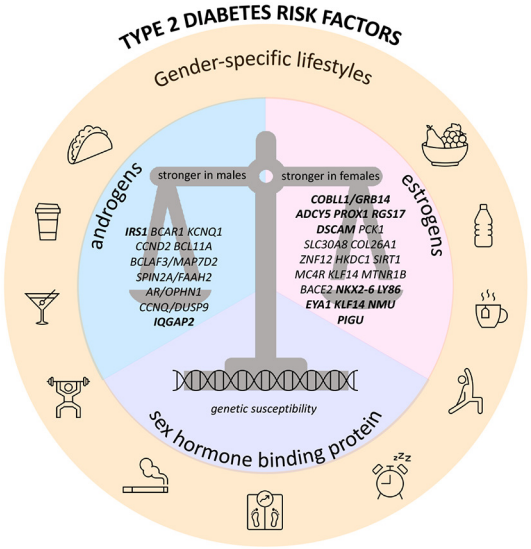

FIGURE 1
Recap figure depicting sex-specific genetic determinants of type 2 diabetes and glucose-related traits, and their interaction with endogenous/exogenous sex hormones, sex hormone binding protein, and gender-specific lifestyle factors. Hereby are presented the genes with sex-dimorphic effect on risk of T2D and/or GDM and/or FG and/or FI; genes in bold also have sex-dimorphic effect on BMI or WHR.

goal of understanding key sex differences in cardiometabolic disease across the lifetime is still lacking. More studies are required to identify the mechanisms responsible for the sex-specific increase in cardiometabolic risk and to develop therapies that are safe and effective in women. Such research should take into account biological and behavioral factors that differ between women and men, including unique exposures in women, such as hormonal fluctuations across the life time from conception through aging (167) (Figure 1). Critical gaps and research priorities should include elucidation of the mechanisms whereby sex hormones regulate body composition, fat distribution and how they interact with diet and age, how are sex differences and race/ethnicity interrelated with T2D what are the mechanisms underlying the apparent paradox of effects of sex hormones in premenopausal women vs. postmenopausal women vs. men, what are the sex differences in therapeutic treatments and effects of T2D drugs, cardiovascular disease outcomes, and what are the metabolic impacts of hormonal replacement therapy, and of androgen and estrogen use in the context of biologically different sex. Previously published reviews on T2D genetics did not address the sex-specific differences on T2D genetic susceptibility. Our review is the first to synthesize the data on sex differences in relation to its effects with genetic variants on T2D and related traits. These offer a solid basis for future research in this field. Ultimately, expanding our understanding on why risk of T2D differs between men and women during life course could

lead to the identification of new therapeutic targets to prevent T2D more effectively in both women and men.

Author contributions

AL, MD, and MP wrote the manuscript. RD, GW, and SA provided guidance and edited the manuscript. All authors have approved the manuscript submission.

Conflict of interest

The authors declare that the research was conducted in the absence of any commercial or financial relationships that could be construed as a potential conflict of interest.

Publisher's note

References

1. DeFronzo RA, Ferrannini E, Groop L, Henry RR, Herman WH, Holst JJ, et al. Type 2 diabetes mellitus. *Nat Rev Dis Primer.* (2015) 1:1–22. doi: 10.1038/nrdp.2015.19

2. Bellou V, Belbasis L, Tzoulaki I, Evangelou E. Risk factors for type 2 diabetes mellitus: an exposure-wide umbrella review of meta-analyses. *PLoS ONE.* (2018) 13:e0194127. doi: 10.1371/journal.pone.0194127

3. *Diabetes.* Available online at: https://www.who.int/health-topics/diabetes (accessed April 28, 2022).

4. Kautzky-Willer A, Harreiter J, Pacini G. Sex and gender differences in risk, pathophysiology and complications of type 2 diabetes mellitus. *Endocr Rev.* (2016) 37:278–316. doi: 10.1210/er.2015-1137

5. Logue J, Walker JJ, Colhoun HM, Leese GP, Lindsay RS, McKnight JA, et al. Do men develop type 2 diabetes at lower body mass indices than women? *Diabetologia.* (2011) 54:3003–6. doi: 10.1007/s00125-011-2313-3

6. Tramunt B, Smati S, Grandgeorge N, Lenfant F, Arnal J-F, Montagner A, et al. Sex differences in metabolic regulation and diabetes susceptibility. *Diabetologia.* (2020) 63:453–61. doi: 10.1007/s00125-019-05040-3

7. Asllanaj E, Bano A, Glisic M, Jaspers L, Ikram M, Laven J, et al. Age at natural menopause and life expectancy with and without type 2 diabetes. *Menopause.* (2019) 26:387–94. doi: 10.1097/GME.0000000000001246

8. Ren Y, Zhang M, Liu Y, Sun X, Wang B, Zhao Y, et al. Association of menopause and type 2 diabetes mellitus. *Menopause.* (2019) 26:325–30. doi: 10.1097/GME.0000000000001200

9. Visser JA. The importance of metabolic dysfunction in polycystic ovary syndrome. *Nat Rev Endocrinol.* (2021) 17:77–8. doi: 10.1038/s41574-020-00456-z

10. Aroda VR, Christophi CA, Edelstein SL, Zhang P, Herman WH, Barrett-Connor E, et al. The effect of lifestyle intervention and metformin on preventing or delaying diabetes among women with and without gestational diabetes: the diabetes prevention program outcomes study 10-year follow-up. *J Clin Endocrinol Metab.* (2015) 100:1646–53. doi: 10.1210/jc.2014-3761

11. Brand JS, van der Schouw YT, Onland-Moret NC, Sharp SJ, Ong KK, Khaw K-T, et al. Age at menopause, reproductive life span, and type 2 diabetes risk: results from the EPIC-InterAct study. *Diabetes Care.* (2013) 36:1012–9. doi: 10.2337/dc12-1020

12. Regensteiner JG, Golden S, Huebschmann AG, Barrett-Connor E, Chang AY, Chyun D, et al. Sex differences in the cardiovascular consequences of diabetes mellitus: a scientific statement from the American heart association. *Circulation.* (2015) 132:2424–47. doi: 10.1161/CIR.0000000000000343

13. Iorga A, Cunningham CM, Moazeni S, Ruffenach G, Umar S, Eghbali M. The protective role of estrogen and estrogen receptors in cardiovascular disease and the controversial use of estrogen therapy. *Biol Sex Differ.* (2017) 8:33. doi: 10.1186/s13293-017-0152-8

14. Fuchsberger C, Flannick J, Teslovich TM, Mahajan A, Agarwala V, Gaulton KJ, et al. The genetic architecture of type 2 diabetes. *Nature.* (2016) 536:41–7. doi: 10.1038/nature18642

15. Tian Y. PCOS-GWAS susceptibility variants in THADA, INSR, TOX3, and DENND1A are associated with metabolic syndrome or insulin resistance in women with PCOS. *Front Endocrinol Lausanne.* (2020) 11:274. doi: 10.3389/fendo.2020.00274

16. Pervjakova N. Multi-ancestry genome-wide association study of gestational diabetes mellitus highlights genetic links with type 2 diabetes. *Hum Mol Genet.* (2022) 31:3377–91. doi: 10.1093/hmg/ddac050

17. Yang J, Zeng J, Goddard ME, Wray NR, Visscher PM. Concepts, estimation and interpretation of SNP-based heritability. *Nat Genet.* (2017) 49:1304–10. doi: 10.1038/ng.3941

18. Bernabeu E. Sex differences in genetic architecture in the UK Biobank. *Nat Genet.* (2021) 53:1283–9. doi: 10.1038/s41588-021-00912-0

19. Scott LJ, Mohlke KL, Bonnycastle LL, Willer CJ Li Y, Duren WL, Erdos MR, et al. A genome-wide association study of type 2 diabetes in Finns detects multiple susceptibility variants. *Science.* (2007) 316:1341–5. doi: 10.1126/science.1142382

20. Mahajan A, Spracklen CN, Zhang W, Ng MCY, Petty LE, Kitajima H, et al. Multi-ancestry genetic study of type 2 diabetes highlights the power of diverse populations for discovery and translation. *Nat Genet.* (2022) 54:560–72. doi: 10.1038/s41588-022-01058-3

21. Chen J. The trans-ancestral genomic architecture of glycemic traits. *Nat Genet.* (2021) 53:840–60. doi: 10.1038/s41588-021-00852-9

22. Magi R, Lindgren CM, Morris AP. Meta-analysis of sex-specific genome-wide association studies. *Genet Epidemiol.* (2010) 34:846–53. doi: 10.1002/gepi.20540

23. Lagou V. Sex-dimorphic genetic effects and novel loci for fasting glucose and insulin variability. *Nat Commun.* (2021) 12:24. doi: 10.1038/s41467-020-19366-9

24. Goenaga D, Hampe C, Carré N, Cailliau K, Browaeys-Poly E, Perdereau D, et al. Molecular determinants of Grb14-mediated inhibition of insulin signaling. *Mol Endocrinol Baltim Md.* (2009) 23:1043–51. doi: 10.1210/me.2008-0360

25. Plešingerová H, Janovská P, Mishra A, Smyčková L, Poppová L, Libra A, et al. Expression of COBLL1 encoding novel ROR1 binding partner is robust predictor of survival in chronic lymphocytic leukemia. *Haematologica.* (2018) 103:313–24. doi: 10.3324/haematol.2017.178699

26. Teslovich TM. Biological, clinical and population relevance of 95 loci for blood lipids. *Nature.* (2010) 466:707–13. doi: 10.1038/nature09270

27. Morris AP. Large-scale association analysis provides insights into the genetic architecture and pathophysiology of type 2 diabetes. *Nat Genet.* (2012) 44:981–90. doi: 10.1038/ng.2383

28. Downie CG. Multi-ethnic GWAS and fine-mapping of glycaemic traits identify novel loci in the PAGE Study. *Diabetologia.* (2022) 65:477–89. doi: 10.1007/s00125-021-05635-9

29. Wessel J. Low-frequency and rare exome chip variants associate with fasting glucose and type 2 diabetes susceptibility. *Nat Commun.* (2015) 6:5897. doi: 10.1038/ncomms6897

30. Dupuis J. New genetic loci implicated in fasting glucose homeostasis and their impact on type 2 diabetes risk. *Nat Genet.* (2010) 42:105–16. doi: 10.1038/ng.520

31. Sinnott-Armstrong N. Genetics of 35 blood and urine biomarkers in the UK Biobank. *Nat Genet.* (2021) 53:185–94. doi: 10.1038/s41588-020-00757-z

32. Sakaue S. A cross-population atlas of genetic associations for 220 human phenotypes. *Nat Genet.* (2021) 53:1415–24. doi: 10.1038/s41588-021-00931-x

33. Wheeler E. Impact of common genetic determinants of Hemoglobin A1c on type 2 diabetes risk and diagnosis in ancestrally diverse populations: A transethnic genome-wide meta-analysis. *PLoS Med.* (2017) 14:1002383. doi: 10.1371/journal.pmed.1002383

34. Vujkovic M. Discovery of 318 new risk loci for type 2 diabetes and related vascular outcomes among 1.4 million participants in a multi-ancestry meta-analysis. *Nat Genet.* (2020) 52:680–91. doi: 10.1101/19012690

35. Xue A. Genome-wide association analyses identify 143 risk variants and putative regulatory mechanisms for type 2 diabetes. *Nat Commun.* (2018) 9:2941. doi: 10.1038/s41467-018-04951-w

36. Mahajan A. Fine-mapping type 2 diabetes loci to single-variant resolution using high-density imputation and islet-specific epigenome maps. *Nat Genet.* (2018) 50:1505–13. doi: 10.1038/s41588-018-0241-6

37. Zhao W. Identification of new susceptibility loci for type 2 diabetes and shared etiological pathways with coronary heart disease. *Nat Genet.* (2017) 49:1450–7. doi: 10.1038/ng.3943

38. Replication DIG. Genome-wide trans-ancestry meta-analysis provides insight into the genetic architecture of type 2 diabetes susceptibility. *Nat Genet.* (2014) 46:234–44. doi: 10.1038/ng.2897

39. Kichaev G. Leveraging polygenic functional enrichment to improve GWAS power. *Am J Hum Genet.* (2019) 104:65–75. doi: 10.1016/j.ajhg.2018.11.008

40. Spracklen CN. Identification of type 2 diabetes loci in 433,540 East Asian individuals. *Nature.* (2020) 582:240–5. doi: 10.1038/s41586-020-2263-3

41. Imamura M. Genome-wide association studies in the Japanese population identify seven novel loci for type 2 diabetes. *Nat Commun.* (2016) 7:10531. doi: 10.1038/ncomms10531

42. Qi Q. Genetics of type 2 diabetes in U.S. hispanic/latino individuals: results from the hispanic community health study/study of latinos (HCHS/SOL. *Diabetes.* (2017) 66:1419–25. doi: 10.2337/db16-1150

43. Bonas-Guarch S. Re-analysis of public genetic data reveals a rare X-chromosomal variant associated with type 2 diabetes. *Nat Commun.* (2018) 9:321. doi: 10.1038/s41467-017-02380-9

44. Christakoudi S, Evangelou E, Riboli E, Tsilidis KK. GWAS of allometric body-shape indices in UK Biobank identifies loci suggesting associations with morphogenesis, organogenesis, adrenal cell renewal and cancer. *Sci Rep.* (2021) 11:10688. doi: 10.1038/s41598-021-89176-6

45. Pulit SL. Meta-analysis of genome-wide association studies for body fat distribution in 694 649 individuals of European ancestry. *Hum Mol Genet.* (2019) 28:166–74. doi: 10.1093/hmg/ddy327

46. Martin S. Genetic evidence for different adiposity phenotypes and their opposing influences on ectopic fat and risk of cardiometabolic disease. *Diabetes.* (2021) 70:1843–56. doi: 10.2337/db21-0129

47. Zhu Z. Shared genetic and experimental links between obesity-related traits and asthma subtypes in UK Biobank. *J Allergy Clin Immunol.* (2020) 145:537–49. doi: 10.1016/j.jaci.2019.09.035

48. Han X. Using Mendelian randomization to evaluate the causal relationship between serum C-reactive protein levels and age-related macular degeneration. *Eur J Epidemiol.* (2020) 35:139–46. doi: 10.1007/s10654-019-00598-z

49. Zhang G. Genetic associations with gestational duration and spontaneous preterm birth. *N Engl J Med.* (2017) 377:1156–67. doi: 10.1056/NEJMc1713902

50. Yang XL. Three novel loci for infant head circumference identified by a joint association analysis. *Front Genet.* (2019) 10:947. doi: 10.3389/fgene.2019.00947

51. Warrington NM. Maternal and fetal genetic effects on birth weight and their relevance to cardio-metabolic risk factors. *Nat Genet.* (2019) 51:804–14. doi: 10.1038/s41588-019-0403-1

52. Freathy RM. Variants in ADCY5 and near CCNL1 are associated with fetal growth and birth weight. *Nat Genet.* (2010) 42:430–5. doi: 10.1038/ng.567

53. Plotnikov D, Williams C, Guggenheim JA. Association between birth weight and refractive error in adulthood: a mendelian randomisation study. *Br J Ophthalmol.* (2020) 104:214–9. doi: 10.1136/bjophthalmol-2018-313640

54. Horikoshi M. Genome-wide associations for birth weight and correlations with adult disease. *Nature.* (2016) 538:248–52. doi: 10.1038/nature19806

55. Horikoshi M. Discovery and fine-mapping of glycaemic and obesity-related trait loci using high-density imputation. *PLoS Genet.* (2015) 11:e1005230. doi: 10.1371/journal.pgen.1005230

56. Beck JJ. Genetic meta-analysis of twin birth weight shows high genetic correlation with singleton birth weight. *Hum Mol Genet.* (2021) 30:1894–905. doi: 10.1093/hmg/ddab121

57. Liu DJ. Exome-wide association study of plasma lipids in >300,000 individuals. *Nat Genet.* (2017) 49:1758–66. doi: 10.1038/ng.3977

58. Hoffmann TJ. A large electronic-health-record-based genome-wide study of serum lipids. *Nat Genet.* (2018) 50:401–13. doi: 10.1038/s41588-018-0064-5

59. Richardson TG. Evaluating the relationship between circulating lipoprotein lipids and apolipoproteins with risk of coronary heart disease: a multivariable Mendelian randomisation analysis. *PLoS Med.* (2020) 17:e1003062. doi: 10.1371/journal.pmed.1003062

60. Evangelou E. Genetic analysis of over 1 million people identifies 535 new loci associated with blood pressure traits. *Nat Genet.* (2018) 50:1412–25. doi: 10.1038/s41588-018-0205-x

61. Ruth KS. Using human genetics to understand the disease impacts of testosterone in men and women. *Nat Med.* (2020) 26:252–8. doi: 10.1038/s41591-020-0751-5

62. Elsir T, Smits A, Lindstrom MS, Nister M. Transcription factor PROX1: its role in development and cancer. *Cancer Metastasis Rev.* (2012) 31:793–805. doi: 10.1007/s10555-012-9390-8

63. Mansour Aly D. Genome-wide association analyses highlight etiological differences underlying newly defined subtypes of diabetes. *Nat Genet.* (2021) 53:1534–42. doi: 10.1038/s41588-021-00948-2

64. Ducoli L, Detmar M. Beyond PROX1: transcriptional, epigenetic, and noncoding RNA regulation of lymphatic identity and function. *Dev Cell.* (2021) 56:406–26. doi: 10.1016/j.devcel.2021.01.018

65. Masotti M, Guo B, Wu B. Pleiotropy informed adaptive association test of multiple traits using genome-wide association study summary data. *Biometrics.* (2019) 75:1076–85. doi: 10.1111/biom.13076

66. Lind L. Genetic determinants of clustering of cardiometabolic risk factors in U.K. *Biobank Metab Syndr Relat Disord.* (2020) 18:121–7. doi: 10.1089/met.2019.0096

67. Manning AK. A genome-wide approach accounting for body mass index identifies genetic variants influencing fasting glycemic traits and insulin resistance. *Nat Genet.* (2012) 44:659–69. doi: 10.1038/ng.2274

68. Surakka I. The impact of low-frequency and rare variants on lipid levels. *Nat Genet.* (2015) 47:589–97. doi: 10.1038/ng.3300

69. Barton AR, Sherman MA, Mukamel RE, Loh PR. Whole-exome imputation within UK biobank powers rare coding variant association and fine-mapping analyses. *Nat Genet.* (2021) 53:1260–9. doi: 10.1038/s41588-021-00892-1

70. Mao H. RGS17/RGSZ2, a novel regulator of Gi/o, Gz, and Gq signaling. *J Biol Chem.* (2004) 279:26314–22. doi: 10.1074/jbc.M401800200

71. Akiyama M. Genome-wide association study identifies 112 new loci for body mass index in the Japanese population. *Nat Genet.* (2017) 49:1458–67. doi: 10.1038/ng.3951

72. Winkler TW. The influence of age and sex on genetic associations with adult body size and shape: a large-scale genome-wide interaction study. *PLoS Genet.* (2015) 11:e1005378. doi: 10.1371/journal.pgen.1005378

73. Randall JC. Sex-stratified genome-wide association studies including 270,000 individuals show sexual dimorphism in genetic loci for anthropometric traits. *PLoS Genet.* (2013) 9:e1003500. doi: 10.1371/journal.pgen.1003500

74. Heid IM. Meta-analysis identifies 13 new loci associated with waist-hip ratio and reveals sexual dimorphism in the genetic basis of fat distribution. *Nat Genet.* (2010) 42:949–60. doi: 10.1038/ng.685

75. Shungin D. New genetic loci link adipose and insulin biology to body fat distribution. *Nature.* (2015) 518:187–96. doi: 10.1038/nature14132

76. Kilpelainen TO. Genetic variation near IRS1 associates with reduced adiposity and an impaired metabolic profile. *Nat Genet.* (2011) 43:753–60. doi: 10.1038/ng.866

77. Vazquez-Moreno M. Sex/gender modifies the association between the MC4R p.Ile269Asn mutation and type 2 diabetes in the Mexican population. *J Clin Endocrinol Metab.* (2021) 106:112–7. doi: 10.1210/clinem/dgaa726

78. Hayes MG. Identification of HKDC1 and BACE2 as genes influencing glycemic traits during pregnancy through genome-wide association studies. *Diabetes.* (2013) 62:3282–91. doi: 10.2337/db12-1692

79. Kong S, Cho YS. Identification of female-specific genetic variants for metabolic syndrome and its component traits to improve the prediction of metabolic syndrome in females. *BMC Med Genet.* (2019) 20:99. doi: 10.1186/s12881-019-0830-y

80. Dong Y. SIRT1 is associated with a decrease in acute insulin secretion and a sex specific increase in risk for type 2 diabetes in Pima Indians. *Mol Genet Metab.* (2011) 104:661–5. doi: 10.1016/j.ymgme.2011.08.001

81. Dominguez-Cruz MG. Pilot genome-wide association study identifying novel risk loci for type 2 diabetes in a Maya population. *Gene.* (2018) 677:324–31. doi: 10.1016/j.gene.2018.08.041

82. Hara K. Genome-wide association study identifies three novel loci for type 2 diabetes. *Hum Mol Genet.* (2014) 23:239–46. doi: 10.1093/hmg/ddt399

83. Bloomer LD. Male-specific region of the Y chromosome and cardiovascular risk: phylogenetic analysis and gene expression studies. *Arter Thromb Vasc Biol.* (2013) 33:1722–7. doi: 10.1161/ATVBAHA.113.301608

84. Tan MHE, Li J, Xu E, Melcher K, Yong E-l. Androgen receptor: structure, role in prostate cancer and drug discovery. *Acta Pharmacol Sin.* (2015).

85. Wu NN. A genome-wide association study of gestational diabetes mellitus in Chinese women. *J Matern Fetal Neonatal Med.* (2021) 34:1557–64. doi: 10.1080/14767058.2019.1640205

86. Powe CE, Kwak SH. Genetic studies of gestational diabetes and glucose metabolism in pregnancy. *Curr Diab Rep.* (2020) 20:69. doi: 10.1007/s11892-020-01355-3

87. Wei W. Gestational diabetes mellitus: the genetic susceptibility behind the disease. *Horm Metab Res.* (2021) 53:489–98. doi: 10.1055/a-1546-1652

88. Vuckovic D. The polygenic and monogenic basis of blood traits and diseases. *Cell.* (2020) 182:1214–31. doi: 10.1016/j.cell.2020.08.008

89. Chen MH. Trans-ethnic and ancestry-specific blood-cell genetics in 746,667 individuals from 5 global populations. *Cell.* (2020) 182:1198–213. doi: 10.1016/j.cell.2020.06.045

90. Astle WJ. The allelic landscape of human blood cell trait variation and links to common complex disease. *Cell.* (2016) 167:1415–29. doi: 10.1016/j.cell.2016.10.042

91. Kachuri L. Genetic determinants of blood-cell traits influence susceptibility to childhood acute lymphoblastic leukemia. *Am J Hum Genet.* (2021) 108:1823–35. doi: 10.1016/j.ajhg.2021.08.004

92. Ward LD. GWAS of serum ALT and AST reveals an association of SLC30A10 Thr95Ile with hypermanganesemia symptoms. *Nat Commun.* (2021) 12:4571. doi: 10.1101/2020.05.19.104570

93. Chen VL. Genome-wide association study of serum liver enzymes implicates diverse metabolic and liver pathology. *Nat Commun.* (2021) 12:816. doi: 10.1038/s41467-020-20870-1

94. Wojcik GL. Genetic analyses of diverse populations improves discovery for complex traits. *Nature.* (2019) 570:514–8. doi: 10.1038/s41586-019-1310-4

95. Loomis SJ. Genome-wide association study of serum fructosamine and glycated albumin in adults without diagnosed diabetes: results from the atherosclerosis risk in communities study. *Diabetes.* (2018) 67:1684–96. doi: 10.2337/db17-1362

96. Chung RH. Multi-omics analysis identifies CpGs near G6PC2 mediating the effects of genetic variants on fasting glucose. *Diabetologia.* (2021) 64:1613–25. doi: 10.1007/s00125-021-05449-9

97. Li-Gao R. Genetic studies of metabolomics change after a liquid meal illuminate novel pathways for glucose and lipid metabolism. *Diabetes.* (2021) 70:2932–46. doi: 10.2337/db21-0397

98. Rasmussen-Torvik LJ. Fasting glucose GWAS candidate region analysis across ethnic groups in the multiethnic study of atherosclerosis (MESA. *Genet Epidemiol.* (2012) 36:384–91. doi: 10.1002/gepi.21632

99. Prokopenko I. Variants in MTNR1B influence fasting glucose levels. *Nat Genet.* (2009) 41:77–81. doi: 10.1038/ng.290

100. Chambers JC. Common genetic variation near melatonin receptor MTNR1B contributes to raised plasma glucose and increased risk of type 2 diabetes among Indian Asians and European Caucasians. *Diabetes.* (2009) 58:2703–8. doi: 10.2337/db08-1805

101. Bouatia-Naji N. A variant near MTNR1B is associated with increased fasting plasma glucose levels and type 2 diabetes risk. *Nat Genet.* (2009) 41:89–94. doi: 10.1038/ng.277

102. Soranzo N. Common variants at 10 genomic loci influence hemoglobin A(1)(C) levels via glycemic and nonglycemic pathways. *Diabetes.* (2010) 59:3229–39. doi: 10.2337/db10-0502

103. Kanai M. Genetic analysis of quantitative traits in the Japanese population links cell types to complex human diseases. *Nat Genet.* (2018) 50:390–400. doi: 10.1038/s41588-018-0047-6

104. Wood AR. A genome-wide association study of IVGTT-based measures of first-phase insulin secretion refines the underlying physiology of type 2 diabetes variants. *Diabetes.* (2017) 66:2296–309. doi: 10.2337/db16-1452

105. Prokopenko I. A central role for GRB10 in regulation of islet function in man. *PLoS Genet.* (2014) 10:1004235. doi: 10.1371/journal.pgen.1004235

106. Voight BF. Twelve type 2 diabetes susceptibility loci identified through large-scale association analysis. *Nat Genet.* (2010) 42:579–89. doi: 10.1038/ng.609

107. Keaton JM. Genome-wide interaction with the insulin secretion locus MTNR1B reveals CMIP as a novel type 2 diabetes susceptibility gene in African Americans. *Genet Epidemiol.* (2018) 42:559–70. doi: 10.1002/gepi.22126

108. Jones SE. Genome-wide association analyses of chronotype in 697,828 individuals provides insights into circadian rhythms. *Nat Commun.* (2019) 10:343. doi: 10.1038/s41467-018-08259-7

109. Dashti HS. Genetic determinants of daytime napping and effects on cardiometabolic health. *Nat Commun.* (2021) 12:900. doi: 10.1038/s41467-020-20585-3

110. Kwak SH. A genome-wide association study of gestational diabetes mellitus in Korean women. *Diabetes.* (2012) 61:531–41. doi: 10.2337/db11-1034

111. Cox RD, Church CD. Mouse models and the interpretation of human GWAS in type 2 diabetes and obesity. *Dis Model Mech.* (2011) 4:155–64. doi: 10.1242/dmm.000414

112. Pugsley MK, Brooks MB, Fishman CE, Katavolos P, Chiang AY, Parish ST, et al. Use of the ZDF rat to model dietary fat induced hypercoagulability is limited by progressive and fatal nephropathy. *J Pharmacol Toxicol Methods.* (2021) 107:106933. doi: 10.1016/j.vascn.2020.106933

113. Van Sinderen M, Steinberg G, Jorgensen SB, Honeyman J, Chow JDY, Simpson ER, et al. Sexual dimorphism in the glucose homeostasis phenotype of the aromatase knockout (ArKO) mice. *J Steroid Biochem Mol Biol.* (2017) 170:39–48. doi: 10.1016/j.jsbmb.2016.05.013

114. Kanemoto N, Hishigaki H, Miyakita A, Oga K, Okuno S, Tsuji A, et al. Genetic dissection of "OLETF", a rat model for non-insulin-dependent diabetes mellitus. *Mamm Genome.* (1998) 9:419–25. doi: 10.1007/s003359900789

115. Hirashima T, Kawano K, Mori S, Matsumoto K, Natori T. A diabetogenic gene (ODB-1) assigned to the X-chromosome in OLETF rats. *Diabetes Res Clin Pract.* (1995) 27:91–6. doi: 10.1016/0168-8227(95)01028-C

116. Kim JH, Stewart TP, Soltani-Bejnood M, Wang L, Fortuna JM, Mostafa OA, et al. Phenotypic characterization of polygenic type 2 diabetes in TALLYHO/JngJ mice. *J Endocrinol.* (2006) 191:437–46. doi: 10.1677/joe.1.06647

117. Leiter EH, Strobel M, O'Neill A, Schultz D, Schile A, Reifsnyder PC. Comparison of two new mouse models of polygenic type 2 diabetes at the jackson laboratory, NONcNZO10Lt/J and TALLYHO/JngJ. *J Diabetes Res.* (2013) 2013:165327. doi: 10.1155/2013/165327

118. Kim JH, Sen S, Avery CS, Simpson E, Chandler P, Nishina PM, et al. Genetic analysis of a new mouse model for non-insulin-dependent diabetes. *Genomics.* (2001) 74:273–86. doi: 10.1006/geno.2001.6569

119. Kluge R, Scherneck S, Schürmann A, Joost H-G. Pathophysiology and genetics of obesity and diabetes in the New Zealand obese mouse: a model of the human metabolic syndrome. *Methods Mol Biol Clifton NJ.* (2012) 933:59–73. doi: 10.1007/978-1-62703-068-7_5

120. Lenzen S. The mechanisms of alloxan- and streptozotocin-induced diabetes. *Diabetologia.* (2008) 51:216–26. doi: 10.1007/s00125-007-0886-7

121. Paik SG, Michelis MA, Kim YT, Shin S. Induction of insulin-dependent diabetes by streptozotocin. inhibition by estrogens and potentiation by androgens. *Diabetes.* (1982) 31:724–9. doi: 10.2337/diabetes.31.8.724

122. Li Y, Huang J, Yan Y, Liang J, Liang Q, Lu Y, et al. Preventative effects of resveratrol and estradiol on streptozotocin-induced diabetes in ovariectomized mice and the related mechanisms. *PLoS ONE.* (2018) 13:e0204499. doi: 10.1371/journal.pone.0204499

123. Weigt C, Hertrampf T, Flenker U, Hülsemann F, Kurnaz P, Fritzemeier KH, et al. Effects of estradiol, estrogen receptor subtype-selective agonists and genistein on glucose metabolism in leptin resistant female Zucker diabetic fatty (ZDF) rats. *J Steroid Biochem Mol Biol.* (2015) 154:12–22. doi: 10.1016/j.jsbmb.2015.06.002

124. Burgoyne PS, Arnold AP. A primer on the use of mouse models for identifying direct sex chromosome effects that cause sex differences in non-gonadal tissues. *Biol Sex Differ.* (2016) 7:68. doi: 10.1186/s13293-016-0115-5

125. De Vries GJ, Rissman EF, Simerly RB, Yang L-Y, Scordalakes EM, Auger CJ, et al. model system for study of sex chromosome effects on sexually dimorphic neural and behavioral traits. *J Neurosci Off J Soc Neurosci.* (2002) 22:9005–14. doi: 10.1523/JNEUROSCI.22-20-09005.2002

126. Blencowe M, Chen X, Zhao Y, Itoh Y, McQuillen CN, Han Y, et al. Relative contributions of sex hormones, sex chromosomes, and gonads to sex differences in tissue gene regulation. *Genome Res.* (2022) 32:807–24. doi: 10.1101/gr.275965.121

127. Martínez de Morentin PB, González-García I, Martins L, Lage R, Fernández-Mallo D, Martínez-Sánchez N, et al. Estradiol regulates brown adipose tissue thermogenesis via hypothalamic AMPK. *Cell Metab.* (2014) 20:41–53. doi: 10.1016/j.cmet.2014.03.031

128. Moreira-Pais A, Ferreira R, Neves JS, Vitorino R, Moreira-Gonçalves D, Nogueira-Ferreira R. Sex differences on adipose tissue remodeling: from molecular mechanisms to therapeutic interventions. *J Mol Med Berl Ger.* (2020) 98:483–93. doi: 10.1007/s00109-020-01890-2

129. Ding EL, Song Y, Manson JE, Hunter DJ, Lee CC, Rifai N, et al. Sex hormone-binding globulin and risk of type 2 diabetes in women and men. *N Engl J Med.* (2009) 361:1152–63. doi: 10.1056/NEJMoa0804381

130. Ding EL, Song Y, Malik VS, Liu S. Sex differences of endogenous sex hormones and risk of type 2 diabetes: a systematic review and meta-analysis. *JAMA.* (2006) 295:1288–99. doi: 10.1001/jama.295.11.1288

131. Perry JRB, Weedon MN, Langenberg C, Jackson AU, Lyssenko V, Sparsø T, et al. Genetic evidence that raised sex hormone binding globulin (SHBG) levels reduce the risk of type 2 diabetes. *Hum Mol Genet.* (2010) 19:535–44. doi: 10.1093/hmg/ddp522

132. Wallace IR, McKinley MC, Bell PM, Hunter SJ. Sex hormone binding globulin and insulin resistance. *Clin Endocrinol.* (2013) 78:321–9. doi: 10.1111/cen.12086

133. Li J, Lai H, Chen S, Zhu H, Lai S. Interaction of sex steroid hormones and obesity on insulin resistance and type 2 diabetes in men: the third national health and nutrition examination survey. *J Diabetes Complications.* (2017) 31:318–27. doi: 10.1016/j.jdiacomp.2016.10.022

134. Harper-Harrison G, Shanahan MM. *"Hormone Replacement Therapy" StatPearls*. Treasure Island, FL: StatPearls Publishing (2022). Available online at: http://www.ncbi.nlm.nih.gov/books/NBK493191/ (accessed March 15, 2022).

135. Bitoska I, Krstevska B, Milenkovic T, Subeska-Stratrova S, Petrovski G, Mishevska SJ, et al. Effects of hormone replacement therapy on insulin resistance in postmenopausal diabetic women. *Open Access Maced J Med Sci.* (2016) 4:83–8. doi: 10.3889/oamjms.2016.024

136. Kanaya AM, Herrington D, Vittinghoff E, Lin F, Grady D, Bittner V, et al. Glycemic effects of postmenopausal hormone therapy: the heart and estrogen/progestin replacement study: a randomized, double-blind, placebo-controlled trial. *Ann Intern Med.* (2003) 138:1–9. doi: 10.7326/0003-4819-138-1-200301070-00005

137. Salpeter SR, Walsh JME, Ormiston TM, Greyber E, Buckley NS, Salpeter EE. Meta-analysis: effect of hormone-replacement therapy on components of the metabolic syndrome in postmenopausal women. *Diabetes Obes Metab.* (2006) 8:538–54. doi: 10.1111/j.1463-1326.2005.00545.x

138. Mauvais-Jarvis F, Manson JE, Stevenson JC, Fonseca VA. Menopausal hormone therapy and type 2 diabetes prevention: evidence, mechanisms, and clinical implications. *Endocr Rev.* (2017) 38:173–88. doi: 10.1210/er.2016-1146

139. Manson JE, Chlebowski RT, Stefanick ML, Aragaki AK, Rossouw JE, Prentice RL, et al. Menopausal hormone therapy and health outcomes during the intervention and extended poststopping phases of the Women's Health Initiative randomized trials. *JAMA.* (2013) 310:1353–68. doi: 10.1001/jama.2013.278040

140. Gooren LJ, Kreukels B, Lapauw B, Giltay EJ. (Patho)physiology of cross-sex hormone administration to transsexual people: the potential impact of male-female genetic differences. *Andrologia.* (2015) 47:5–19. doi: 10.1111/and.12389

141. Spanos C, Bretherton I, Zajac JD, Cheung AS. Effects of gender-affirming hormone therapy on insulin resistance and body composition in transgender individuals: a systematic review. *World J Diabetes.* (2020) 11:66–77. doi: 10.4239/wjd.v11.i3.66

142. Elbers JMH, Giltay EJ, Teerlink T, Scheffer PG, Asscheman H, Seidell JC, et al. Effects of sex steroids on components of the insulin resistance syndrome in transsexual subjects. *Clin Endocrinol.* (2003) 58:562–71. doi: 10.1046/j.1365-2265.2003.01753.x

143. Islam N, Nash R, Zhang Q, Panagiotakopoulos L, Daley T, Bhasin S, et al. Is There a link between hormone use and diabetes incidence in transgender people? data from the STRONG cohort. *J Clin Endocrinol Metab.* (2022) 107:e1549–57. doi: 10.1210/clinem/dgab832

144. Wierckx K, Elaut E, Declercq E, Heylens G, De Cuypere G, Taes Y, et al. Prevalence of cardiovascular disease and cancer during cross-sex hormone therapy in a large cohort of trans persons: a case-control study. *Eur J Endocrinol.* (2013) 169:471–8. doi: 10.1530/EJE-13-0493

145. Morselli E, Santos RS, Criollo A, Nelson MD, Palmer BF, Clegg DJ. The effects of oestrogens and their receptors on cardiometabolic health. *Nat Rev Endocrinol.* (2017) 13:352–64. doi: 10.1038/nrendo.2017.12

146. Rettberg JR, Yao J, Brinton RD. Estrogen: a master regulator of bioenergetic systems in the brain and body. *Front Neuroendocrinol.* (2014) 35:8–30. doi: 10.1016/j.yfrne.2013.08.001

147. Brooks HL, Pollow DP, Hoyer PB. The VCD mouse model of menopause and perimenopause for the study of sex differences in cardiovascular disease and the metabolic syndrome. *Physiology.* (2016) 31:250–7. doi: 10.1152/physiol.00057.2014

148. Romero-Aleshire MJ, Diamond-Stanic MK, Hasty AH, Hoyer PB, Brooks HL. Loss of ovarian function in the VCD mouse-model of menopause leads to insulin resistance and a rapid progression into the metabolic syndrome. *Am J Physiol Regul Integr Comp Physiol.* (2009) 297:R587–92. doi: 10.1152/ajpregu.90762.2008

149. Keck M, Romero-Aleshire MJ, Cai Q, Hoyer PB, Brooks HL. Hormonal status affects the progression of STZ-induced diabetes and diabetic renal damage in the VCD mouse model of menopause. *Am J Physiol-Ren Physiol.* (2007) 293:F193–9. doi: 10.1152/ajprenal.00022.2007

150. Veroni MC, Proietto J, Larkins RG. Evolution of insulin resistance in New Zealand obese mice. *Diabetes.* (1991) 40:1480–7. doi: 10.2337/diabetes.40.11.1480

151. Vogel H, Mirhashemi F, Liehl B, Taugner F, Kluth O, Kluge R, et al. Estrogen deficiency aggravates insulin resistance and induces β-cell loss and diabetes in female New Zealand obese mice. *Horm Metab Res.* (2013) 45:430–5. doi: 10.1055/s-0032-1331700

152. Tiano JP, Delghingaro-Augusto V, Le May C, Liu S, Kaw MK, Khuder SS, et al. Estrogen receptor activation reduces lipid synthesis in pancreatic islets and prevents β cell failure in rodent models of type 2 diabetes. *J Clin Invest.* (2011) 121:3331–42. doi: 10.1172/JCI44564

153. Kawakami M, Yokota-Nakagi N, Uji M, Yoshida K, Tazumi S, Takamata A, et al. Estrogen replacement enhances insulin-induced AS160 activation and improves insulin sensitivity in ovariectomized rats. *Am J Physiol-Endocrinol Metab.* (2018) 315:E1296–304. doi: 10.1152/ajpendo.00131.2018

154. Yokota-Nakagi N, Omoto S, Tazumi S, Kawakami M, Takamata A, Morimoto K. Estradiol replacement improves high-fat diet-induced insulin resistance in ovariectomized rats. *Physiol Rep.* (2022) 10:e15193. doi: 10.14814/phy2.15193

155. Santos RS, Batista TM, Camargo RL, Morato PN, Borck PC, Leite NC, et al. Lacking of estradiol reduces insulin exocytosis from pancreatic β-cells and increases hepatic insulin degradation. *Steroids.* (2016) 114:16–24. doi: 10.1016/j.steroids.2016.05.002

156. Zhu L, Brown WC, Cai Q, Krust A, Chambon P, McGuinness OP, et al. Estrogen treatment after ovariectomy protects against fatty liver and may improve pathway-selective insulin resistance. *Diabetes.* (2013) 62:424–34. doi: 10.2337/db11-1718

157. Agarwal P, Brar N, Morriseau TS, Kereliuk SM, Fonseca MA, Cole LK, et al. Gestational diabetes adversely affects pancreatic islet architecture and function in the male rat offspring. *Endocrinology.* (2019) 160:1907–25. doi: 10.1210/en.2019-00232

158. Yokomizo H, Inoguchi T, Sonoda N, Sakaki Y, Maeda Y, Inoue T, et al. Maternal high-fat diet induces insulin resistance and deterioration of pancreatic β-cell function in adult offspring with sex differences in mice. *Am J Physiol-Endocrinol Metab.* (2014) 306:E1163–75. doi: 10.1152/ajpendo.00688.2013

159. *Who Smokes More, Men or Women? Our World Data.* Available online at: https://ourworldindata.org/who-smokes-more-men-or-women (accessed June 8, 2022).

160. Reitsma MB, Kendrick PJ, Ababneh E, Abbafati C, Abbasi-Kangevari M, Abdoli A, et al. Spatial, temporal, and demographic patterns in prevalence of smoking tobacco use and attributable disease burden in 204 countries and territories, 1990–2019: a systematic analysis from the global burden of disease study 2019. *Lancet.* (2021) 397:2337–60. doi: 10.1016/S0140-6736(21)01169-7

161. Imamura F, Micha R, Khatibzadeh S, Fahimi S, Shi P, Powles J, et al. Dietary quality among men and women in 187 countries in 1990 and 2010: a systematic assessment. *Lancet Glob Health.* (2015) 3:e132–42. doi: 10.1016/S2214-109X(14)70381-X

162. Wardle J, Haase AM, Steptoe A, Nillapun M, Jonwutiwes K, Bellisle F. Gender differences in food choice: the contribution of health beliefs and dieting. *Ann Behav Med Publ Soc Behav Med.* (2004) 27:107–16. doi: 10.1207/s15324796abm2702_5

163. Guthold R, Stevens GA, Riley LM, Bull FC. Worldwide trends in insufficient physical activity from 2001 to 2016: a pooled analysis of 358 population-based surveys with 1·9 million participants. *Lancet Glob Health.* (2018) 6:e1077–86. doi: 10.1016/S2214-109X(18)30357-7

164. Gerovasili V, Agaku IT, Vardavas CI, Filippidis FT. Levels of physical activity among adults 18-64 years old in 28 European countries. *Prev Med.* (2015) 81:87–91. doi: 10.1016/j.ypmed.2015.08.005

165. Levy RB, Rauber F, Chang K, Louzada ML da C, Monteiro CA, Millett C, et al. Ultra-processed food consumption and type 2 diabetes incidence: a prospective cohort study. *Clin Nutr Edinb Scotl.* (2021) 40:3608–14. doi: 10.1016/j.clnu.2020.12.018

166. Gao M, Jebb SA, Aveyard P, Ambrosini GL, Perez-Cornago A, Papier K, et al. Associations between dietary patterns and incident type 2 diabetes: prospective cohort study of 120,343 UK biobank participants. *Diabetes Care.* (2022) 45:1315–25. doi: 10.2337/figshare.19209750

167. Reusch JEB, Kumar TR, Regensteiner JG, Zeitler PS. Conference Participants. Identifying the critical gaps in research on sex differences in metabolism across the life span. *Endocrinology.* (2018) 159:9–19. doi: 10.1210/en.2017-03019

frontiers | Frontiers in Cardiovascular Medicine

TYPE Original Research
PUBLISHED 01 December 2022
DOI 10.3389/fcvm.2022.940894

OPEN ACCESS

EDITED BY
Laura Arbour,
The University of British Columbia,
Canada

REVIEWED BY
Malik Bisserier,
New York Medical College,
United States
Ayham Daher,
University Hospital RWTH Aachen,
Germany

*CORRESPONDENCE
Zhe Cheng
chengzhezzu@outlook.com

†These authors have contributed equally to this work

SPECIALTY SECTION
This article was submitted to Cardiovascular Genetics and Systems Medicine,
a section of the journal
Frontiers in Cardiovascular Medicine

RECEIVED 10 May 2022
ACCEPTED 16 November 2022
PUBLISHED 01 December 2022

CITATION
Duo M, Liu Z, Zhang Y, Li P, Weng S, Xu H, Wang Y, Jiang T, Wu R and Cheng Z (2022) Construction of a diagnostic signature and immune landscape of pulmonary arterial hypertension.
Front. Cardiovasc. Med. 9:940894.
doi: 10.3389/fcvm.2022.940894

Construction of a diagnostic signature and immune landscape of pulmonary arterial hypertension

Mengjie Duo[1†], Zaoqu Liu[2,3,4†], Yuyuan Zhang[2,3,4], Pengfei Li[1], Siyuan Weng[2,3,4], Hui Xu[2,3,4], Yu Wang[1], Tianci Jiang[1], Ruhao Wu[1] and Zhe Cheng[1*]

[1]Department of Respiratory and Critical Care Medicine, The First Affiliated Hospital of Zhengzhou University, Zhengzhou, Henan, China, [2]Department of Interventional Radiology, The First Affiliated Hospital of Zhengzhou University, Zhengzhou, Henan, China, [3]Interventional Institute of Zhengzhou University, Zhengzhou, Henan, China, [4]Interventional Treatment and Clinical Research Center of Henan Province, Zhengzhou, Henan, China

Background: Molecular biomarkers are widely used for disease diagnosis and exploration of pathogenesis. Pulmonary arterial hypertension (PAH) is a rapidly progressive cardiopulmonary disease with delayed diagnosis. Studies were limited regarding molecular biomarkers correlated with PAH from a broad perspective.

Methods: Two independent microarray cohorts comprising 73 PAH samples and 36 normal samples were enrolled in this study. The weighted gene co-expression network analysis (WGCNA) was performed to identify the key modules associated with PAH. The LASSO algorithm was employed to fit a diagnostic model. The latent biology mechanisms and immune landscape were further revealed *via* bioinformatics tools.

Results: The WGCNA approach ultimately identified two key modules significantly associated with PAH. For genes within the two models, differential expression analysis between PAH and normal samples further determined nine key genes. With the expression profiles of these nine genes, we initially developed a PAH diagnostic signature (PDS) consisting of LRRN4, PI15, BICC1, PDE1A, TSHZ2, HMCN1, COL14A1, CCDC80, and ABCB1 in GSE117261 and then validated this signature in GSE113439. The ROC analysis demonstrated outstanding AUCs with 0.948 and 0.945 in two cohorts, respectively. Besides, patients with high PDS scores enriched plenty of Th17 cells and neutrophils,

while patients with low PDS scores were dramatically related to mast cells and B cells.

Conclusion: Our study established a robust and promising signature PDS for diagnosing PAH, with key genes, novel pathways, and immune landscape offering new perspectives for exploring the molecular mechanisms and potential therapeutic targets of PAH.

KEYWORDS

pulmonary arterial hypertension, weighted gene co-expression network analysis, functional analysis, machine learning, diagnostic model, immune infiltration

Introduction

Pulmonary arterial hypertension (PAH) is a rapidly progressive and fatal cardiopulmonary disease, and its incidence is about one–two in a million per year (1, 2). The development and progression of PAH are closely associated with structural and functional abnormalities of the pulmonary vasculature. Pulmonary vascular remolding involves intimal injury, middle hypertrophy, adventitia proliferation and fibrosis, and perivascular inflammatory cell infiltration, leading to progressive stenosis and occlusion of the pulmonary artery lumen. Consequently, increased pulmonary vascular pressure results in right heart failure and even death, ultimately, and PAH is characterized by high mortality (3). The gold-standard test for diagnosing PAH is the right heart catheterization (RHC), but the severe complication rate was 1% (4). Although echocardiography is recommended in current guidelines (5), a meta-analysis had elucidated that the pooled sensitivity was 88% (84–92), and specificity was 56% (46–66) for the diagnosis of PAH (6). Besides, the mechanisms of PAH are not understood, especially at the molecular level. Therefore, it is necessary to explore a novel perspective for diagnosing patients with PAH and gaining deeper insights for understanding the biological mechanisms of PAH.

Recently, the rapid development in bioinformatics facilitated the detection of potential biomarkers and the exploration of latent disease mechanisms in PAH. Large-scale research confirmed that the mutations in BMPR2, ACVRL1, ENG, SMAD9, TBX4, KCNK3, and EIF2AK4 in adult-onset patients were related to specific PAH (7). Mutations of multiple genes and aberrant gene expression are involved in the pathogenesis of PAH *via* promoting the proliferation and reducing apoptosis of pulmonary vascular cells. Nevertheless, based on the available discovery, existing biomarkers lack sufficient sensitivity and specificity on account of heterogeneity and confounding factors of samples and the simplicity of the analytical method. Overall, the previous studies are insufficient to interpret the mechanistic pathways of PAH susceptibility and disease progression, and thus, it is essential to detect biomarkers by integrative and insightful analysis between patients with PAH and normal.

In our study, two independent microarray cohorts were generated from the Gene Expression Omnibus (GEO).[1] In addition, the weighted gene co-expression network analysis (WGCNA), the functional enrichment analysis, and the differentially expressed gene (DEG) analysis were performed to screen the hub genes. Subsequently, the LASSO algorithm was employed to construct a reliable and individualized PAH diagnostic signature (PDS) for diagnosing PAH and evaluating the immune landscape. In addition, the results might shed light on the clinical application and molecular mechanism of PAH.

Materials and methods

Data generation and preprocessing

The keyword "pulmonary hypertension" in GEO's gene expression profile was searched. Two datasets met the inclusion criteria: (i) the datasets contained complete transcriptome data of PAH and normal lung tissues and (ii) the number of samples was more than ten in each group. The GSE117261 dataset contained total RNA gene expression microarray data from 58 PAH and 25 normal lung tissues (**Supplementary Table 1**). GSE113439 contains total RNA gene expression microarray data from 15 PAH and 11 normal lung tissues (**Supplementary Table 2**). They were based on the same platform, GPL6244. The data processing procedure of the research was illustrated in the workflow (**Figure 1**).

Co-expression network analysis

The weighted gene co-expression network analysis (WGCNA) was conducted to screen potential modules of high

1 http://www.ncbi.nlm.nih.gov/geo/

relationship with PAH based on the gene expression profiles *via* the "WGCNA" R package. The expression of genes was ranked *via* standard deviation. Then the top 5,000 genes were picked for the next step of analysis. Next, the hierarchical cluster analysis was used to exclude outlier samples. We calculated the Pearson correlation value between each gene pair to obtain a gene similarity matrix. Then, the formula, aij (adjacency matrix between gene i and j) = | Sij (similarity matrix of all gene pairs)| × β (the soft threshold), was used to construct the adjacency matrix. The optimal β was picked by the "pickSoftThreshold" function in the "WGCNA" R package to meet the scale-free distribution. The adjacency matrix was transformed into a topological overlap matrix (TOM) and a 1-TOM, reflecting the similarity and dissimilarity between genes, separately. Ultimately, the genes were divided into different modules using hierarchical clustering methods. The module eigengene (ME) was calculated, representing the gene expression profile of each module. Therefore, modules highly correlated with PAH were selected as key modules for further analysis. The soft threshold was β = 7, minModuleSize = 50, deep Split = 2, and MEDissThres = 0.3.

Functional enrichment analysis

The "clusterProfiler" R package was used to further describe potential biological functions and obtain pathways of genes in the WGCNA key gene modules *via* Gene Ontology (GO) enrichment analysis and Kyoto Encyclopedia of Genes and Genomes (KEGG) pathway enrichment analysis. The false discovery rate (FDR) was further computed according to the Benjamini–Hochberg procedure (Benjamini and Hochberg, (8). The FDR < 0.05 was considered as statistically significant.

Construction of protein–protein interaction (PPI)

To identify the hub genes and PPI network in the key modules, genes within the key modules were further uploaded to the Search Tool for the Retrieval of Interacting Genes (STRING)[2] for constructing PPI network. The medium confidence score of the PPI network was 0.400. Then the "MCODE" algorithm with default parameters was implemented in the Cytoscape software (version: 3.8.2).

Differentially expressed gene analysis

The differentially expressed genes (DEGs) between PAH and normal lung tissue were identified through the "limma" R package. *P*-adjusted value < 0.05 and |log2 fold change (FC)| > 2/3 were set as the threshold of DEGs.

Identification of key regulatory genes

The intersection of the most positive correlation module in the WGCNA and upregulated genes significantly in the two datasets is known as upregulated key genes of PAH. Similarly, the intersection of the most negative correlation module in the WGCNA and downregulated genes significantly in the two datasets is known as downregulated key genes of PAH.

Machine learning

The least absolute shrinkage and selection operator (LASSO) is a machine-learning algorithm to obtain a robust predictive performance model and is applied to select the best predictive gene for the diagnosis of PAH. This process was achieved through the "glmnet" R package. The performance of PDS was assessed by the area under the receiver operator characteristic (ROC) curve.

Gene set enrichment analysis

The normalized enrichment score (NES) was calculated for PAH on GO and KEGG pathways in the Molecular Signature Database (MSigDB) *via* all GO gene sets (c5.go.v7.4.symbols.gmt) and KEGG gene sets as gene symbols (c2.cp.kegg.v7.4.symbols.gmt), respectively. | NES| > 1.50, FDR < 0.01, and adjusted *P*-value < 0.01 were set as cutoff criteria.

Evaluation of immune cell infiltration

To describe the differences in immune cell infiltration between the high-score and low-score groups, we used single-sample gene set enrichment analysis (ssGSEA), which is an extension of GSEA that generates enrichment scores for individual samples. The abundance of infiltrating immune cells was calculated and visualized through the "GSVA" R package (v1.42.0). Furthermore, we evaluated correlation coefficients between PDS scores of samples and immune cell abundance to investigate the main immune cells engaged in the PAH.

Statistical analysis

The data processing, statistical analysis, and plotting were conducted in R 4.1.0 software. Pearson's correlation

2 https://string-db.org/

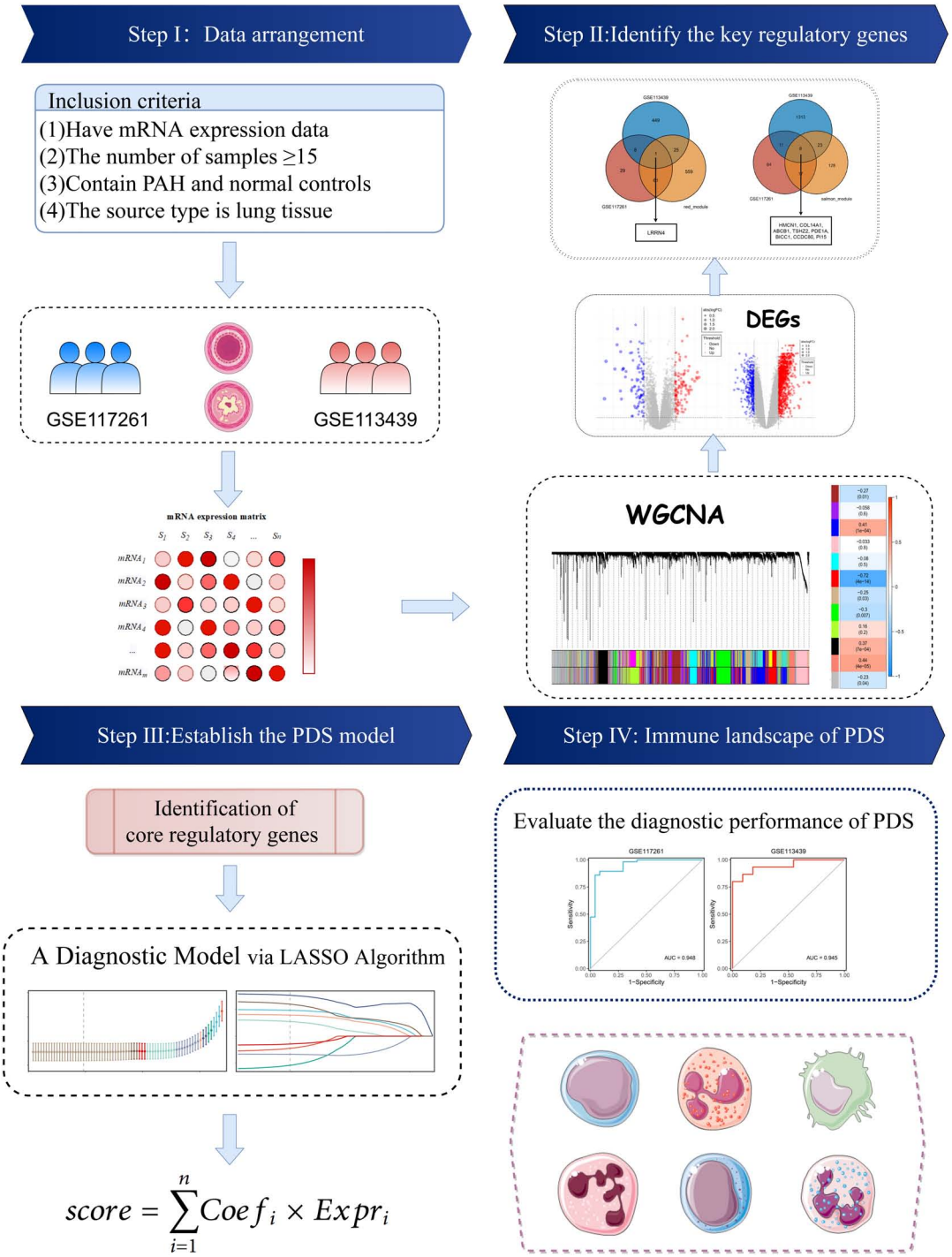

FIGURE 1
Flowchart of this study.

coefficient was assessed for correlations between two continuous variables. The chi-square tests were used to compare categorical variables, while the Wilcoxon rank sum test or *t*-test was used to compare continuous variables. The "survminer" R package was fitted to determine the optimal cutoff value. The LASSO was fitted by "glmnet" R package. The "pROC" R package utilized ROC and the area under the ROC curve (AUC). $P < 0.05$ was determined using the "pROC" R package. It was determined that $P < 0.05$ was statistically significant.

Results

Identification of key modules in pulmonary arterial hypertension *via* weighted gene co-expression network analysis

The GSE117261 dataset was used as a training dataset to recognize the key genes associated with PAH. First, two outlier samples were removed, and the 81 samples and the top 5,000 genes were used to obtain the gene similarity matrix. Then, the gene similarity matrix was constructed as an adjacency matrix according to the formula. Second, the soft-thresholding power was set to seven by the "pickSoftThreshold" function for the analysis of a scale-free network (**Figures 2A,B**). Third, the adjacency matrix was converted to the TOM. We clustered MEs based on calculating the dissimilarity of MEs and using the "mergeCloseModules" function and then 14 MEs were identified (**Figures 2C,D**). Ultimately, data were visualized in regard to the module–trait relationships based on the Pearson correlation coefficient between the MEs and the disease (**Figure 2E**). Among these, the salmon module was the top positive module ($r = 0.441$, $P < 0.0001$) with PAH including 646 genes (**Figure 2F**), and the red module was the top negative module ($r = -0.718$, $P < 0.0001$) including 176 genes (**Figure 2G**).

Enrichment analyses and protein–protein interaction construction of key modules

To acquire a deep understanding of the function of genes in positively and negatively related modules, salmon and red module genes were analyzed through enrichGO and enrichKEGG function in the "clusterProfiler" R package, respectively. Genes of the red module were significantly enriched in "neutrophil activation," "neutrophil activation involved in immune response," "neutrophil degranulation," and "neutrophil mediated immunity," all of which were terms about neutrophil, as shown in **Figure 3A**. The KEGG pathway terms were related to "Osteoclast differentiation," "Neutrophil extracellular trap formation," and "B cell receptor signaling pathway," which might play essential roles in PAH (**Figure 3B**). Meanwhile, the top three GO terms were enriched by genes of the salmon module, including "Extracellular structure organization," "Extracellular matrix organization," and "External encapsulating structure organization," which were mainly associated with the extracellular organization (**Figure 3C**). The KEGG pathways suggested that the "ECM–receptor interaction" and "protein digestion and absorption" might be potential pathways of PAH (**Figure 3D**). The lists of genes involved in the GO and KEGG enrichment analysis in red and salmon modules can be found in **Supplementary Tables 3–6**. These results indicated that inflammation and immune cells played a significant role in the process of PAH.

To screen the hub gene of positive and negative correlation modules with PAH, the PPI network was established through the STRING database, including 852 nodes and 5,841 edges. Then the network was processed in the Cytoscape software, and the possible 38 essential genes ranked by node degree were visualized using the MCODE plugin. The top 10 highest degrees of genes were screened, including ITGAM, CYBB, SPL1, FCGR3A, CD86, ITGB2, LILRB2, CCR1, 1L10RA, and CSF1R (**Figure 3E**).

Identification of differentially expressed genes in two pulmonary arterial hypertension datasets

The DEGs in lung tissue between the patients with PAH and normal controls were excavated by the "limma" R package. Consequently, in the GSE113439 dataset, 1,355 significantly upregulated genes and 483 significantly downregulated genes were defined. Similarly, in the GSE117261 dataset, we identified 120 significantly upregulated genes and 99 significantly downregulated genes. These DEGs are shown as a volcano plot and heatmap in **Figures 4A–D**.

Determination of the key genes

The core downregulated gene was screened through the intersection of the genes in the red module of WGCNA and the significantly downregulated genes in two datasets, including LRRN4 (**Figure 5A**). Likewise, the key upregulated gene was screened through the intersection of the genes in the salmon module of WGCNA and the significantly upregulated genes in the two datasets, including PI15, BICC1, PDE1A, TSHZ2, HMCN1, COL14A1, CCDC80, and ABCB1 (**Figure 5B**). The expression levels of nine key genes are verified in the two datasets shown in **Figures 5C,D**.

Construction of a diagnosis model *via* least absolute shrinkage and selection operator algorithm

The nine key genes were developed as a reliable and individualized PAH diagnostic signature (PDS) by applying the LASSO algorithm to diagnose patients with PAH. The optimal lambda was 0.002116 when the LASSO regression partial likelihood deviation was minimized (**Figure 6A**). Consequently, nine key genes with non-zero LASSO coefficients were regarded as the diagnostic model's main variables (**Figure 6B**). The nine

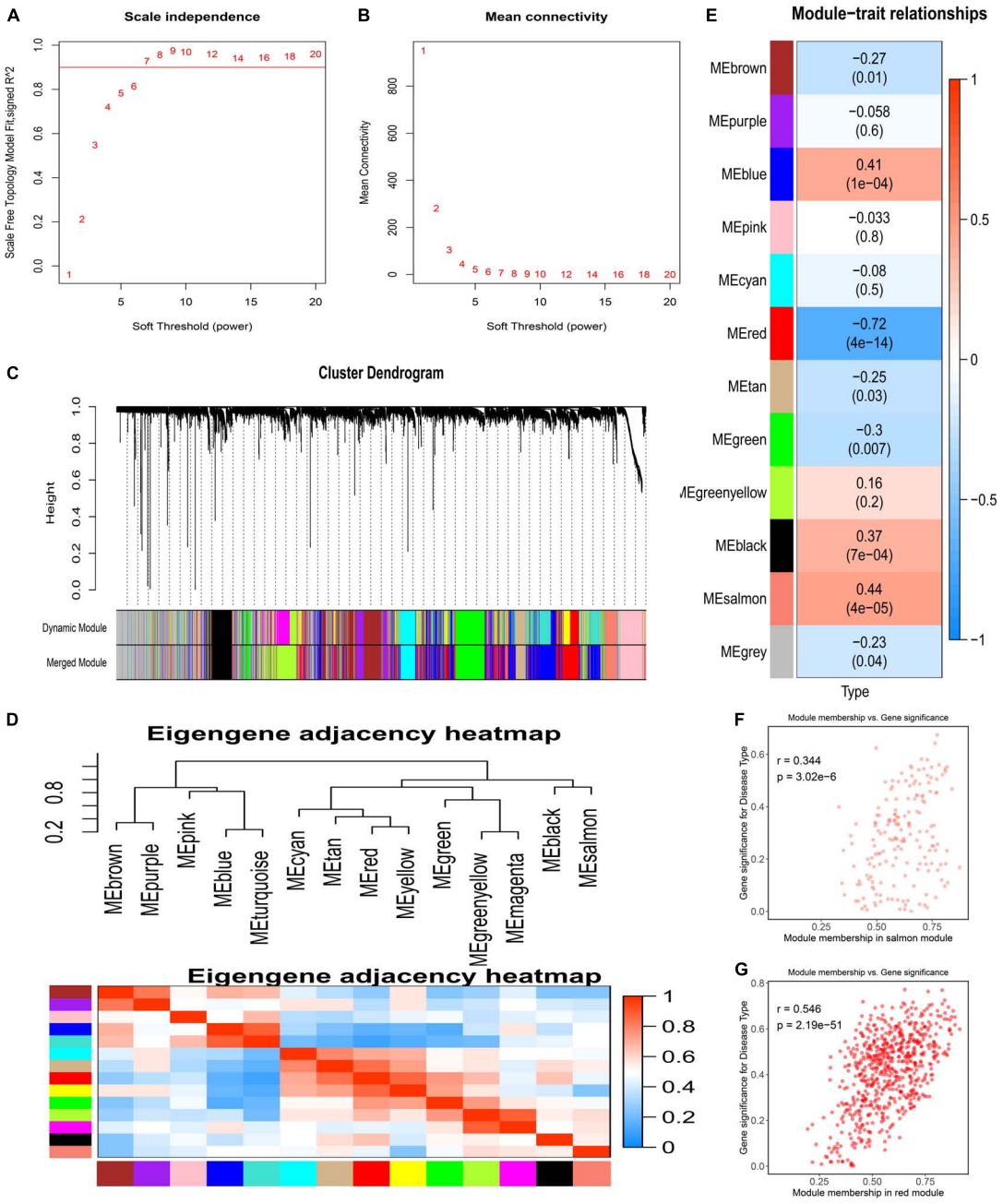

FIGURE 2
Detection of weighted gene co-expression network and modules. **(A)** Scale-free topological indices at various soft-thresholding powers. **(B)** The correlation analysis between the soft-thresholding powers and mean connectivity of the network. **(C)** Gene clustering diagram based on hierarchical clustering under optimal soft-thresholding power. **(D)** The heatmap of the eigengene adjacency. **(E)** Correlations between gene modules and PAH. **(F)** The correlation between the salmon module memberships and the gene significance. **(G)** The correlation between the red module memberships and the gene significance.

genes were COL14A1, TSHZ2, CCDC80, BICC1, HMCN1, LRRN4, PDE1A, ABCB1, and PI15, and their coefficients were 0.1522, 0.1191, −0.1084, −0.0963, 0.0785, −0.0676, −0.0545, −0.0452, and −0.0292, respectively. The ROC analysis demonstrated outstanding AUCs with 0.948 and 0.945 in two cohorts for evaluating the power of the PDS to differentiate the PAH (Figures 6C,D). Therefore, we established an optimal diagnostic signature PDS with the formula: PDS score = 0.1522 × Exp COL14A1 + 0.1191 × Exp TSHZ2 - 0.1084 × Exp CCDC80 - 0.0963 × Exp BICC1 + 0.0785 × Exp HMCN1 - 0.0676 × Exp LRRN4 - 0.0545 × Exp PDE1A – 0.0452 × Exp ABCB1 - 0.0292 × Exp PI15 + 0.7037.

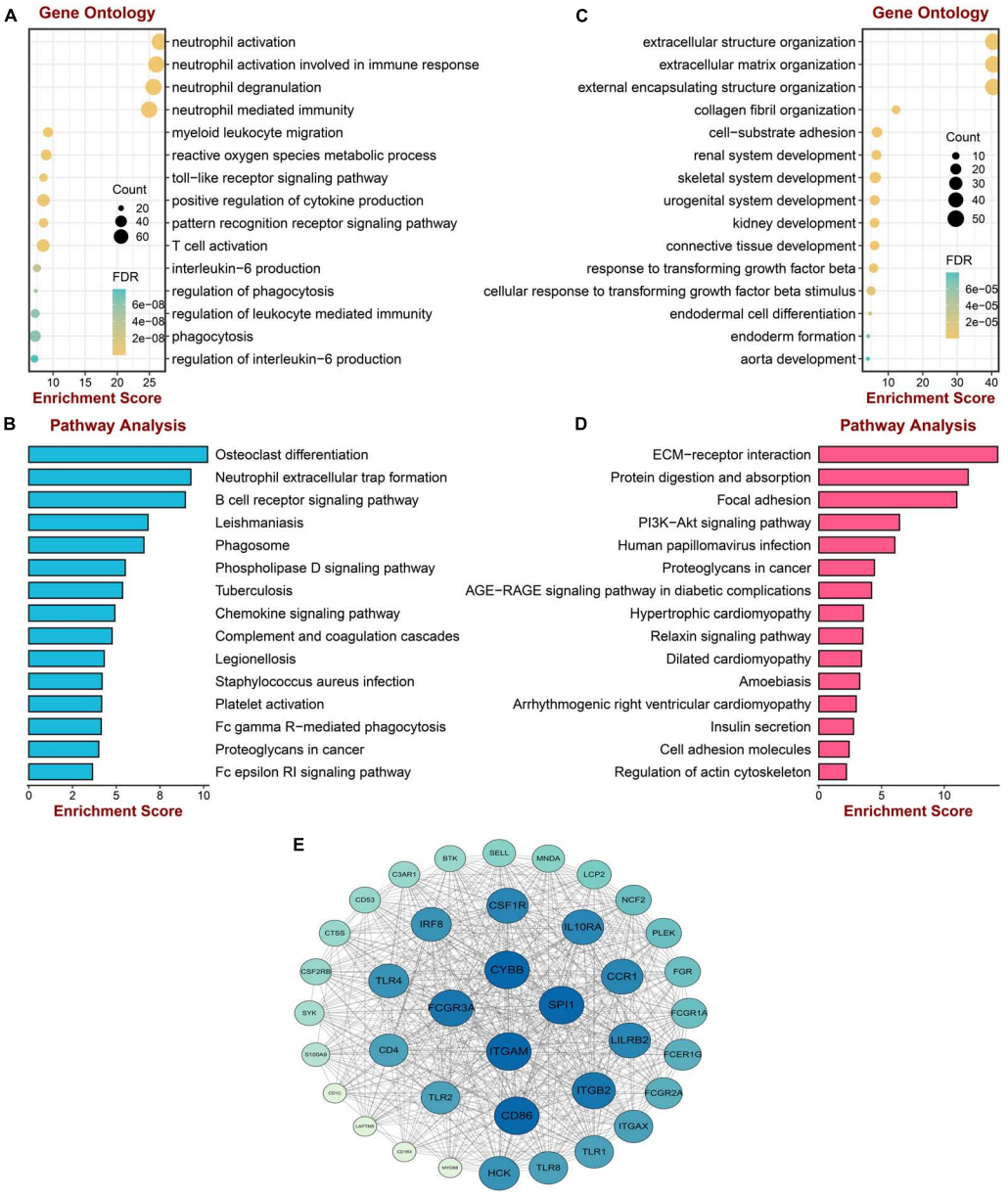

FIGURE 3
Enrichment analysis and protein−protein interaction construction of key modules. **(A)** GO enrichment analysis of genes in the red module. **(B)** KEGG pathway analysis of genes in the red module. **(C)** GO enrichment analysis of genes in the salmon module. **(D)** KEGG pathway analysis of genes in the salmon module. **(E)** The protein−protein network of two modules.

Exploration of biological mechanisms *via* gene set enrichment analysis (GSEA)

First, we calculated the PDS scores and gene expression correlations for gene sequencing. Subsequently, GSEA was performed to detect potential mechanisms for PAH. Figures 7A,B illustrate the most important GO terms and the KEGG pathways. Among these, Figure 7C depicts the top five positively relevant GO terms, including "Regulation of cholesterol metabolic process," "Sterol biosynthetic process," "Sterol metabolic process," "Odorant binding," and "Oxidoreductase activity acting on CH-OH group." Figure 7D depicts the top five negatively relevant GO terms, comprising "Collagen fibril organization," "Basement membrane," "Collagen binding," "Extracellular matrix structural constituent," and "Extracellular matrix structural constituent conferring." On the contrary, Figure 7E describes the top five positively correlated the KEGG pathways, consisting of "Glutathione metabolism,"

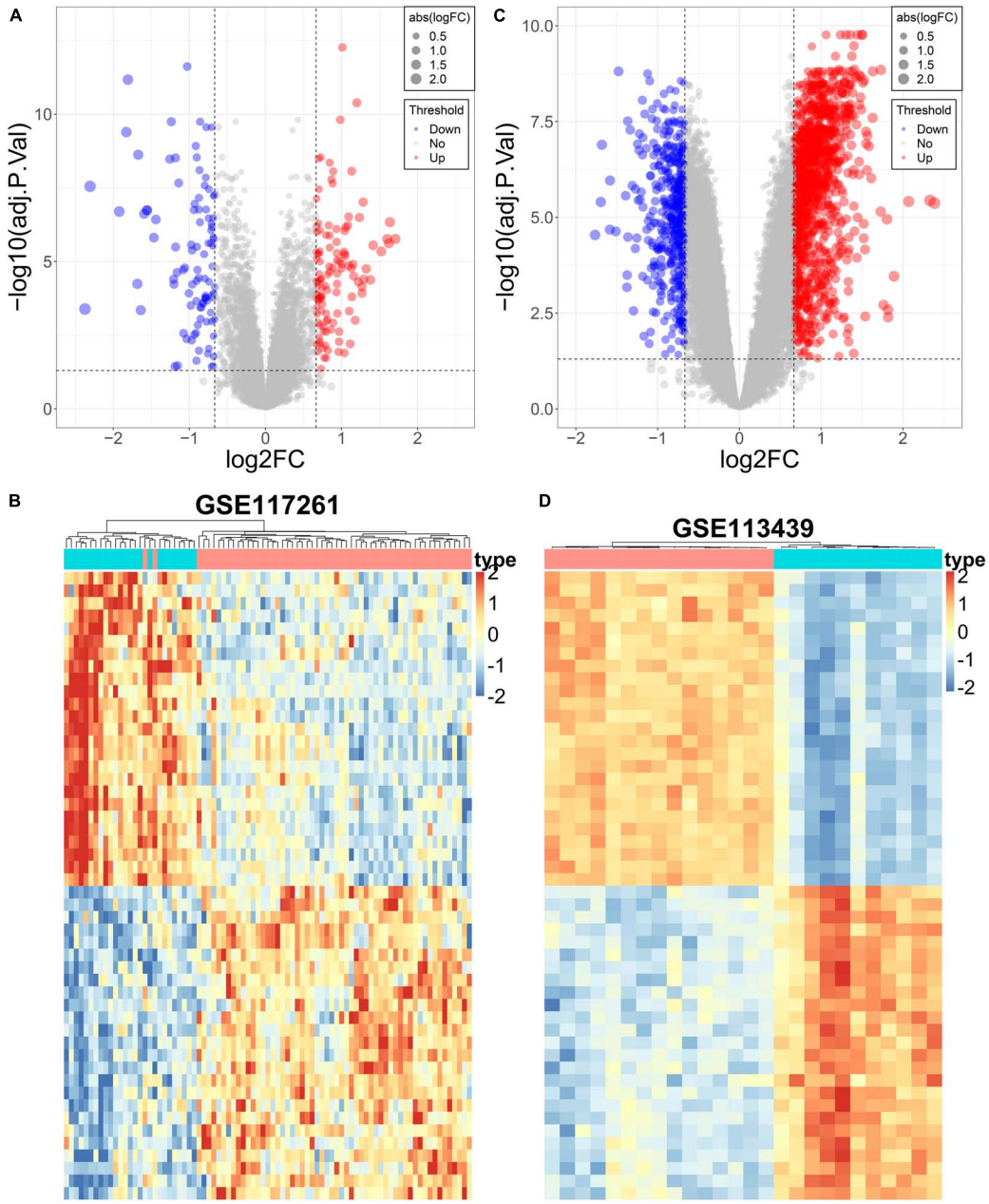

FIGURE 4
Differential expression analysis of the PAH datasets. **(A)** The volcano plot of DEGs in GSE117261. **(B)** The heatmap of DEGs in GSE117261. **(C)** The volcano plot of DEGs in GSE113439. **(D)** The heatmap of DEGs in GSE113439.

"Pathogenic *Escherichia coli* infection," "Pyruvate metabolism," "Steroid biosynthesis," and "Terpenoid backbone biosynthesis." Likewise, **Figure 7F** describes the top five negatively correlated KEGG pathways, consisting of "Arrhythmogenic right ventricular cardiomyopathy ARVC," "ECM-receptor interaction," "Intestinal immune network for IgA production," and "Systemic lupus erythematosus." Notably, "ECM–receptor interaction" was enriched once again which was enriched in the salmon KEGG pathway. It can be concluded that the "extracellular matrix organization" may play an essential role in PAH.

Immune landscape of PAH diagnostic signature

We assumed that the two PDS score groups had different immunological characteristics since inflammation and immune

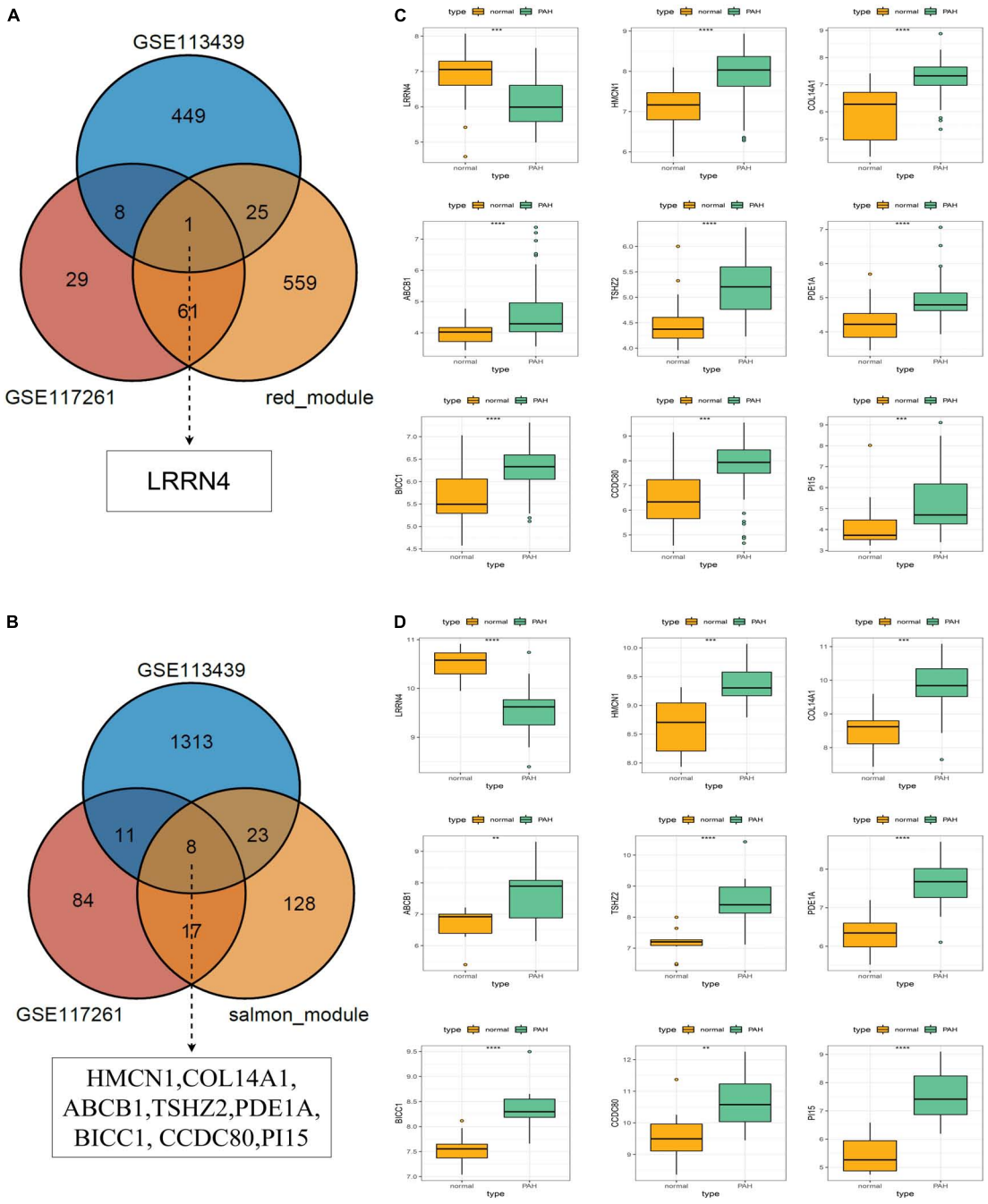

FIGURE 5
Selection and validation of key regulatory genes. **(A)** Venn diagram to indicate one downregulatory gene from the red module and DEGs. **(B)** Venn diagram to indicate eight upregulatory genes from the salmon module and DEGs. **(C)** Validation of key regulatory genes in the dataset GSE117261. **(D)** Validation of key regulatory gene in the dataset GSE113439.

cells are essential in the PAH process. To probe the discriminating immune landscape of patients with PAH, the ssGSEA algorithm was used to estimate the infiltration abundance of 24 types of immune cells among the GSE117261 dataset. The fraction of 24 types of immune cells in GSE117261 samples is depicted as a heatmap in Figure 8A. The relative expression is portrayed as a boxplot in Figure 8B. We can see that a superior abundance of Th17 cells, neutrophils, effective memory T cell (tem), and eosinophils was the immune feature of the high-score group, whereas high infiltration of mast cells, B cells, Th2 cells, interdigitating cell (iDC), Th1 cells, and T cells was the immune feature in the low-score group. Figure 8C

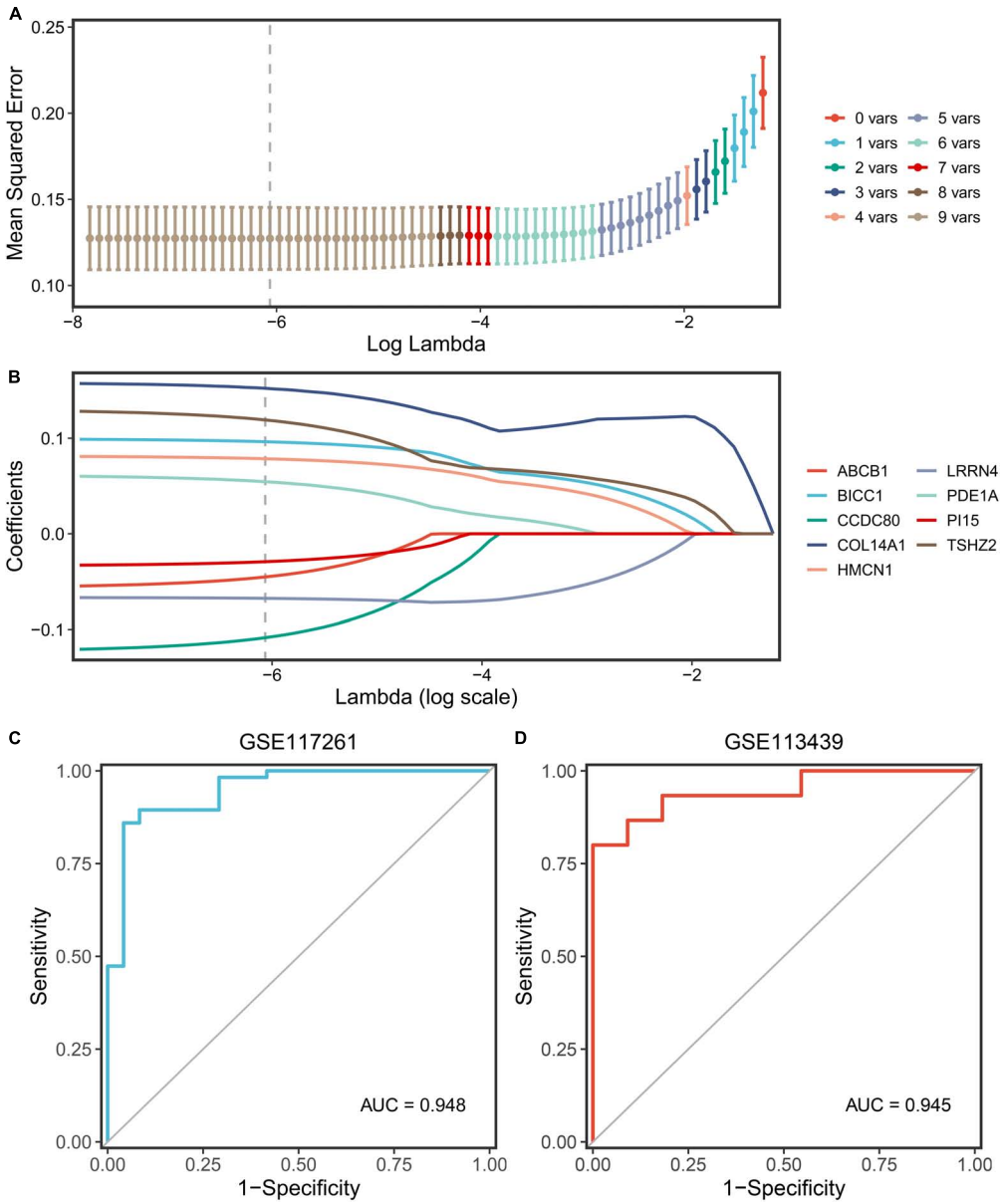

FIGURE 6
Screening and validation of the genes. **(A)** Determination of the optimal lambda was obtained when the partial likelihood deviance reached the minimum value and further generated the key gene with non-zero coefficients. **(B)** LASSO coefficient profiles of the candidate gene for PDS construction. **(C)** The ROC curve of the modeling dataset (GSE117261). **(D)** The ROC curves of validation datasets (GSE113439).

shows the heatmap of correlations between immune cells. The T cells and B cells showed the strongest positive correlation, and the neutrophils and T helper cells showed the strongest negative correlation. Subsequently, we probed the correlation between the PDS score and immune infiltration. As shown in **Figure 8D**, the infiltration level of Th17 cells ($r = 0.467$, $P < 0.0001$), neutrophils ($r = 0.394$, $P = 0.0003$), tem ($r = 0.335$, $P = 0.0023$), and eosinophils ($r = 0.250$, $P = 0.0249$) was positively correlated with the PDS score; the infiltration level of mast cells ($r = -0.470$, $P < 0.0001$), B cells ($r = -0.381$, $P = 0.0005$), Th2 cells ($r = -0.376$, $P = 0.0006$), iDC ($r = -0.355$, $P = 0.0012$), Th1 cells ($r = -0.354$, $P = 0.0012$), and T cells ($r = -0.284$, $P = 0.0103$) was negatively associated with the PDS score.

Discussion

Pulmonary arterial hypertension is a disorder characterized by a progressive increase in pulmonary vascular stress and significant pulmonary vascular remodeling, resulting in

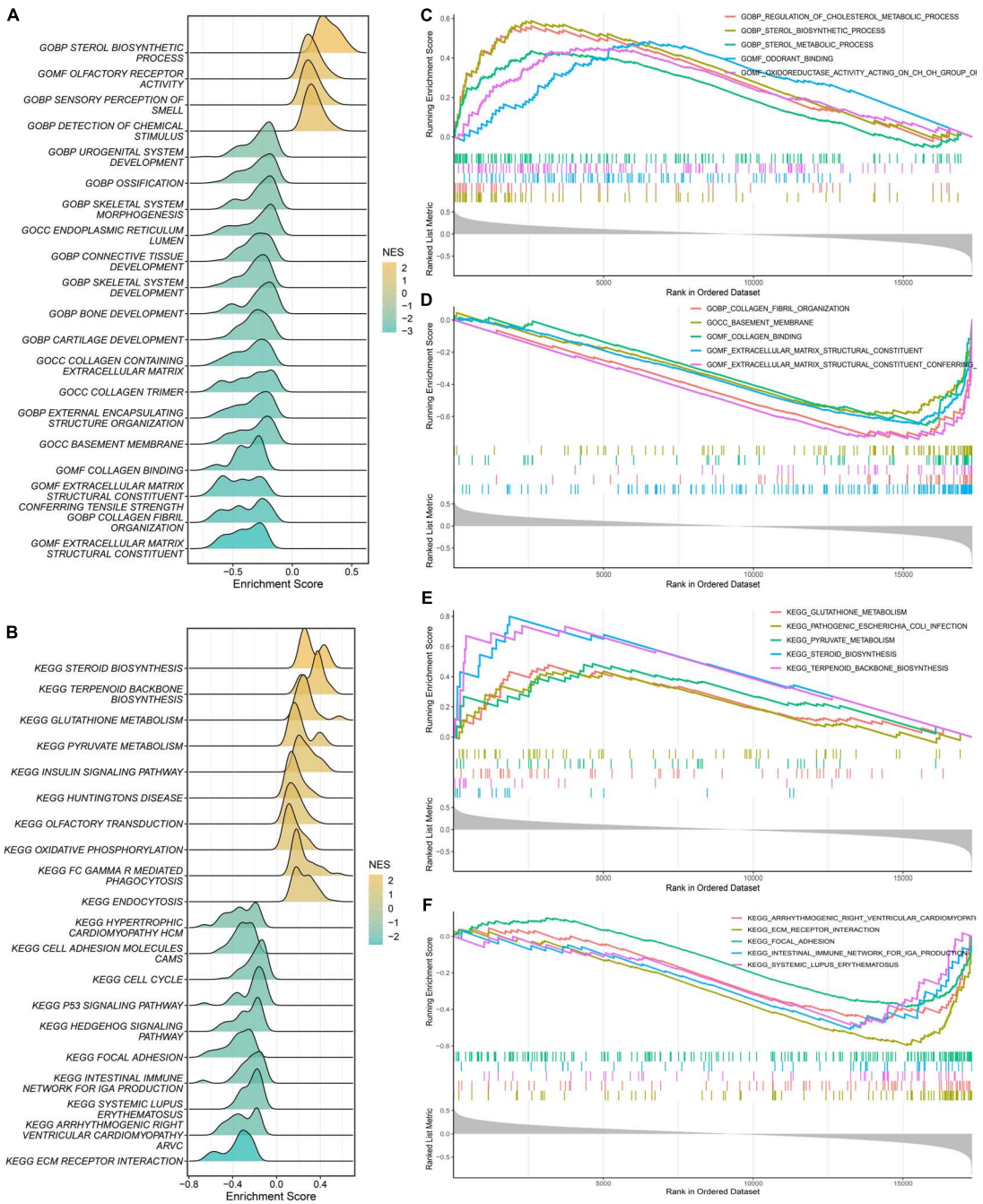

FIGURE 7
Gene Set Enrichment Analysis (GSEA). **(A)** The ridge plot of the top 20 GO terms with ranked genes of the modeling dataset. **(B)** The ridge plot of the top 20 KEGG pathways with ranked genes of the modeling dataset. **(C,D)** The positive and negative top five GO terms with ranked genes of the modeling dataset. **(E,F)** The positive and negative top five KEGG pathways with ranked genes of the modeling dataset.

hypertrophy and remodeling of the right ventricle (9–11). If a patient with pulmonary hypertension is not diagnosed promptly, the probability of death due to right ventricular failure is drastically increased (9). As a rapidly evolving approach, molecular analysis is utilized to comprehend the latent pathways in the context of human disease. The notion is recognized that PAH is actuated by a comprehensive network of molecular processes (12–15). Measurement of RNA expression is one of the high-throughput unbiased techniques in the Omics approach, which provides a snapshot of the transcriptome aspect (13). These insights provide new perspectives for predicting potential pathogenesis and therapeutic aspects. Therefore, it is of great

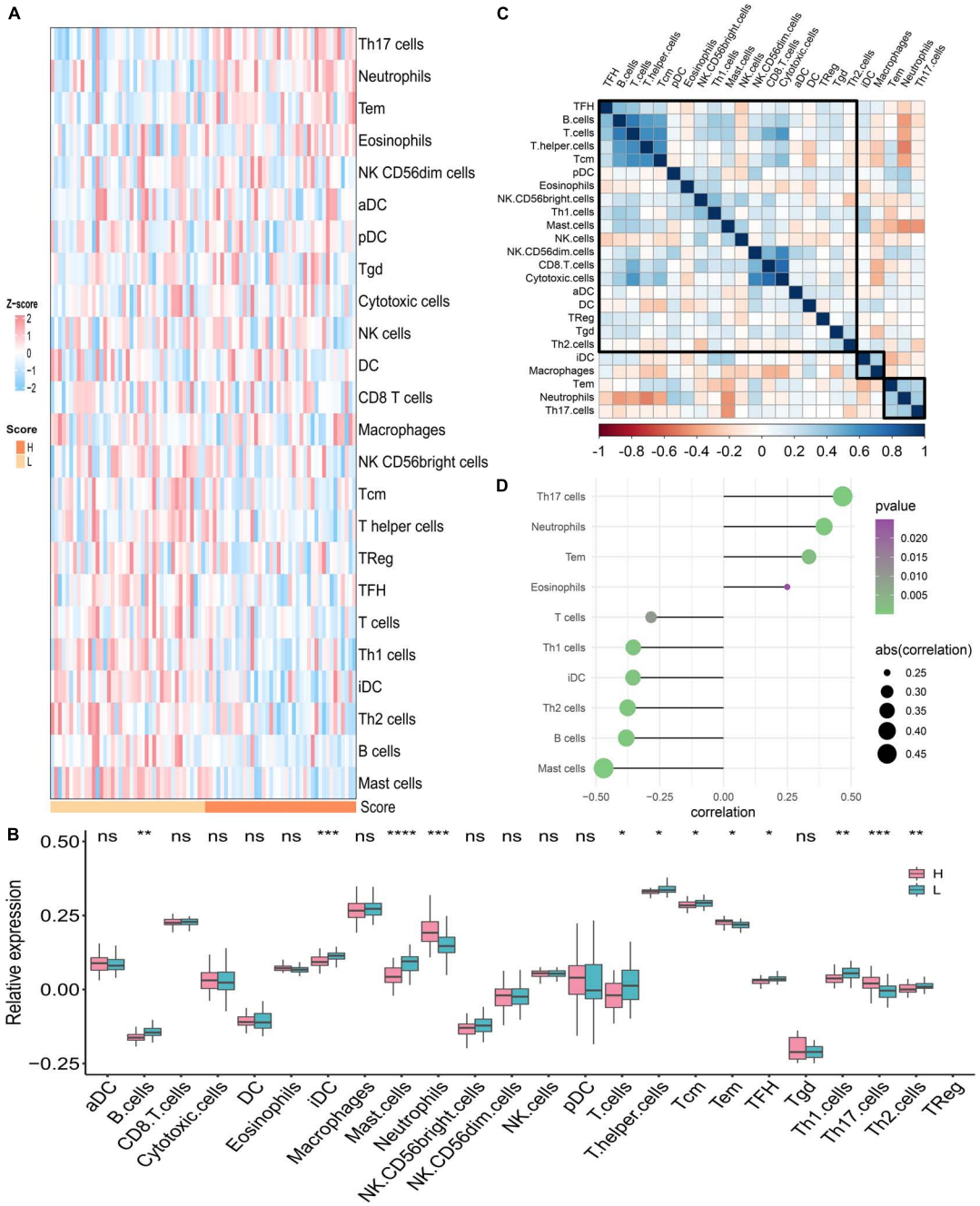

FIGURE 8
Analysis of immune landscape associated with PAH. **(A)** The heatmap of the immune infiltration in high- and low-score groups. **(B)** The boxplot of the 24-type immune infiltration in high- and low-score groups. *$P < 0.05$, **$P < 0.01$, and ***$P < 0.001$. **(C)** The heatmap of the correlations between different immune cells. **(D)** Relationship between the PDS score and immune infiltration. H: high score; L: low score. aDC: activated dendritic cell; DC: dendritic cell; iDC: interdigitating cell; NK cells: natural killer cells; pDC: plasmacytoid dendritic cells; Tcm: central memory T cell; Tem: effector memory T cell; TFH: T follicular helper cell; Tgd: gamma delta T cells; TReg: T regulatory cells.

significance to explore molecular biomarkers and to construct a diagnostic model for the diagnosis of PAH.

The WGCNA, as a bioinformatics approach, explicitly exploits the relationship between gene co-expression modules and disease to further explore the pathogenesis of diseases. Our study screened out 11 modules associated with PAH *via* WGCNA. Among the 11 modules screened, the genes in the salmon module are the most positively correlated with PAH and those in the red modules are the most negatively correlated with PAH. In the salmon modules, genes were mainly concentrated

in extracellular structure organization, extracellular matrix (ECM) organization, and external encapsulating structure organization in GO terms and gathered in the KEGG pathway of ECM–receptor interaction and PI3K–Akt signaling pathway. As mentioned in the literature review, ECM remodeling triggers pulmonary arterial smooth muscle proliferation and pro-inflammatory response in the endothelial cells resulting in increased stiffness of the proximal and distal pulmonary arteries in PAH (16, 17). Meanwhile, the PI3K–Akt signaling pathway is an essential nexus of pulmonary artery smooth muscle cell (PASMC) proliferation and hypoxia-induced pulmonary vascular remodeling (18, 19). Conversely, in the red modules, genes were mainly concentrated in GO terms related to neutrophil and immune response. Besides, genes were gathered in the B-cell receptor signaling pathway and neutrophil extracellular trap (NET) formation in the KEGG pathway. The release of neutrophil elastase is part of neutrophil activity. NE, which is found in PASMCs and neointimal lesions of PAH, is thought to cause vascular remodeling by causing the release of growth factors, aggregation and activation of their receptors, and subsequent migration and proliferation of smooth muscle cells and fibroblasts through extracellular matrix degradation (20–22). NETs, formed from chromatin decondensation provoked by reactive oxygen species (ROC), can trigger the inflammatory activation of lung endothelial cells and stimulate endothelial angiogenesis through myeloperoxidase/H2O2/NFkB/TLR4-dependent signaling. These results confirm the findings of extensive previous work demonstrating the potential pathological relevance between NETs and inflammatory angiogenesis, a disturbance of vascular homeostasis in PAH (23). In summary, the comprehensive bioinformatics analysis perceived that neutrophil activation and immune response played a considerable role in disease pathogenesis and the process of PAH. On the contrary, the complexity of cytokine, cellular immunity, and autoantibody changes indicated that PAH might be an autoimmune and inflammatory disease, which was consistent with previous reports (11, 24–26).

From a broad perspective, the development of PDS for clinical application is of great significance. Previous studies have examined key genes by DEG analysis between PAH lung specimens and normal lung specimens solely based on the public database in the GEO (27–29). The presence of heterogeneity of the disease and confounding factors reduces the sensitivity and specificity of DEGs as biomarkers for PAH. In addition, redundant key genes limited the clinical practice of the clinical application. In our study, the essential biomarkers relevant to the PAH were filtrated by combining the results of the WGCNA and the DEGs. Further analysis identified nine robust PDS by the application of the LASSO algorithm, including COL14A1, TSHZ2, CCDC80, BICC1, HMCN1, LRRN4, PDE1A, ABCB1, and PI15. The PDS demonstrated high discriminatory power with outstanding AUCs in the two cohorts separately. Phosphodiesterase 1 (PDE1), encoded by three genes, namely PDE1A, 1B, and 1C, is a sub-family of enzymes. Some animal studies have shown that the inhibition of PDE1A treats pulmonary arterial hypertension by reversing pulmonary vascular remodeling and right heart hypertrophy (30, 31). The basement membrane collagen COL4A5 was significantly upregulated in the intima and media of the IPAH patient cohort, indicating improved vascular stiffness *via* stabilizing existing collagen fibers (32). PI15 belongs to the CAP superfamily of proteins and is a trypsin inhibitor (33). Against extracellular matrix proteins, trypsin has high protease activity. PI15 has been hypothesized to perform a protective role in elastic tissues against proteolytic damage and a role in controlling extracellular matrix changes (34). LRRN4, also known as leucine-rich repeat neuron protein-4, is a member of the LRRN family and linked to a range of pathological events, including cardiac remodeling (35, 36). BICC family RNA-binding protein 1 (BICC1) is an RNA-binding protein that modulates protein translation to control gene expression. BICC1 can influence biological processes including proliferation and apoptosis. Furthermore, abnormal BICC1 expression has been linked to immune cell infiltration during disease progression (37). Hemicentin-1 (HMCN1) is an ECM fibulin protein that is thought to be required for stable cell-to-cell interactions and ECM structure stability and may interact with receptors on the cell surface, either directly or indirectly, providing a mechanism for cell behavior modulation (38, 39). Taken together, exploring the underlying mechanisms in PAH of key genes contained in PDS might facilitate the clinical translation and application of the diagnostic model.

The PDS score-based GSEA indicated that immune-related pathways were enriched between high and low groups. Hence, deciphering the exact mechanisms of immune cells in pulmonary vessels might lead to a wide range of potential attractive therapeutic targets for PAH therapy. We further estimated the fraction of 24 immune cells between the two groups *via* the ssGSEA algorithm. We discovered that the Th17 cells, neutrophils, tem, and eosinophils were at high expression in the high-score subgroup compared to the low-score subgroup, while mast cells, B cells, Th2 cells, iDC, Th1 cells, and T cells presented low infiltration levels in the low-score group. Th17 cells, a subpopulation of effector T cells that produce IL-17, are highly pro-inflammatory and are widely involved in inflammatory diseases (40). It has been shown that IL-17 is of significance in chronic inflammation-associated pulmonary hypertension, where it correlates with disease severity in SSc-associated pulmonary hypertension. Neutrophils release NE, present in PASMCs of PAH, which can lead to vascular remodeling through aggregation and activation of growth factors and their receptors, and degradation of the smooth muscle cell and fibroblast migration and proliferation (21). In addition, there is growing evidence that eosinophil infiltration of the pulmonary vasculature is an important,

influential factor in the pathological changes of all types of PAH (41). Eosinophils stimulate pulmonary vascular remodeling by releasing granular content and stimulating intravascular PASMC proliferation. Combined with previous studies, we further confirmed that abnormal immune cell expression was critical in the pathogenesis of vascular remodeling and might be potential targets for PAH treatment.

Although advanced bioinformatics techniques and machine-learning algorithms are combined to identify candidate genes and construct diagnostic models for PAH, several limitations should be noticed. First, the relevant genes and pathways screened are not experimentally validated. Fundamental study validation is required for better clinical application in further studies. Second, the PDS needs to be validated with a larger sample size. Last, the dataset lacked comprehensive information on clinical aspects.

In summary, our study constructed a nine-gene diagnostic model of PAH and PDS, through comprehensive bioinformatics analysis. Two modules significantly associated with PAH were identified, and key genes and novel mechanistic pathways were identified. In addition, the inflammatory and immune landscapes of patients with PAH were depicted. Overall, the key genes, novel pathways, and immune landscape may shed light on exploring the molecular mechanisms and potential therapeutic targets of PAH.

Data availability statement

The datasets presented in this study can be found in online repositories. The names of the repository/repositories and accession number(s) can be found in the article/**Supplementary material**.

Author contributions

MD, ZL, and ZC designed the research. MD, ZL, YZ, and SW performed the data acquisition and data analysis. HX assisted with data analysis. MD and PL wrote the manuscript. YW, TJ, and RW edited and revised the manuscript. All authors read and approved the manuscript.

Funding

This study was supported by the National Natural Science Foundation of China (U1904142 and 82170037) and the Medical Science and Technology Research Project of Henan Province (SBGJ202002043).

Acknowledgments

Throughout the writing of this article, I have received a great deal of support and assistance. I would particularly like to acknowledge my supervisor and teammates for their wonderful collaboration and patient support.

Conflict of interest

The authors declare that the research was conducted in the absence of any commercial or financial relationships that could be construed as a potential conflict of interest.

Publisher's note

Supplementary material

The Supplementary Material for this article can be found online at: https://www.frontiersin.org/articles/10.3389/fcvm.2022.940894/full#supplementary-material

References

1. Peacock A, Murphy N, McMurray J, Caballero L, Stewart S. An epidemiological study of pulmonary arterial hypertension. *Eur Respir J.* (2007) 30:104–9. doi: 10.1183/09031936.00092306

2. Dannewitz Prosseda S, Tian X, Kuramoto K, Boehm M, Sudheendra D, Miyagawa K, et al. Fhit, a novel modifier gene in pulmonary arterial hypertension. *Am J Respir Crit Care Med.* (2019) 199:83–98. doi: 10.1164/rccm.201712-2553OC

3. Kiely D, Elliot C, Sabroe I, Condliffe R. Pulmonary hypertension: diagnosis and management. *BMJ.* (2013) 346:f2028. doi: 10.1136/bmj.f2028

4. Hoeper M, Lee S, Voswinckel R, Palazzini M, Jais X, Marinelli A, et al. Complications of right heart catheterization procedures in patients with pulmonary hypertension in experienced centers. *J Am Coll Cardiol.* (2006) 48:2546–52. doi: 10.1016/j.jacc.2006.07.061

5. Galiè N, Humbert M, Vachiery J, Gibbs S, Lang I, Torbicki A, et al. 2015 ESC/ERS guidelines for the diagnosis and treatment of pulmonary hypertension: the joint task force for the diagnosis and treatment of pulmonary hypertension of the European society of cardiology (ESC) and the European respiratory society (ERS): endorsed by: association for European paediatric and congenital cardiology (AEPC), international society for heart and lung transplantation (ISHLT). *Eur Heart J.* (2016) 37:67–119. doi: 10.1093/eurheartj/ehv317

6. Taleb M, Khuder S, Tinkel J, Khouri S. The diagnostic accuracy of doppler echocardiography in assessment of pulmonary artery systolic pressure: a meta-analysis. *Echocardiography.* (2013) 30:258–65. doi: 10.1111/echo.12061

7. Gräf S, Haimel M, Bleda M, Hadinnapola C, Southgate L, Li W, et al. Identification of rare sequence variation underlying heritable pulmonary arterial hypertension. *Nat Commun.* (2018) 9:1416. doi: 10.1038/s41467-018-03672-4

8. Benjamini Y, Hochberg Y. Controlling the false discovery rate: a practical and powerful approach to multiple testing. *J R Stat Soc Series B Stat Methodol.* (1995) 57:289–300. doi: 10.1111/j.2517-6161.1995.tb02031.x

9. Hassoun P. Pulmonary arterial hypertension. *N Eng J Med.* (2021) 385:2361–76. doi: 10.1056/NEJMra2000348

10. McLaughlin V, Archer S, Badesch D, Barst R, Farber H, Lindner J, et al. ACCF/AHA 2009 expert consensus document on pulmonary hypertension: a report of the American college of cardiology foundation task force on expert consensus documents and the American heart association: developed in collaboration with the American college of chest physicians, American thoracic society, inc., and the pulmonary hypertension association. *Circulation.* (2009) 119:2250–94. doi: 10.1161/circulationaha.109.192230

11. Thenappan T, Ormiston M, Ryan J, Archer S. Pulmonary arterial hypertension: pathogenesis and clinical management. *BMJ.* (2018) 360:j5492. doi: 10.1136/bmj.j5492

12. Bertero T, Lu Y, Annis S, Hale A, Bhat B, Saggar R, et al. Systems-level regulation of microrna networks by miR-130/301 promotes pulmonary hypertension. *J Clin Invest.* (2014) 124:3514–28. doi: 10.1172/jci74773

13. Kan M, Shumyatcher M, Himes B. Using omics approaches to understand pulmonary diseases. *Respir Res.* (2017) 18:149. doi: 10.1186/s12931-017-0631-9

14. Mura M, Cecchini M, Joseph M, Granton J. Osteopontin lung gene expression is a marker of disease severity in pulmonary arterial hypertension. *Respirology.* (2019) 24:1104–10. doi: 10.1111/resp.13557

15. Stearman R, Bui Q, Speyer G, Handen A, Cornelius A, Graham B, et al. Systems analysis of the human pulmonary arterial hypertension lung transcriptome. *Am J Respir Cell Mol Biol.* (2019) 60:637–49. doi: 10.1165/rcmb.2018-0368OC

16. Thenappan T, Chan S, Weir E. Role of extracellular matrix in the pathogenesis of pulmonary arterial hypertension. *Am J Physiol Heart Circ Physiol.* (2018) 315:H1322–31. doi: 10.1152/ajpheart.00136.2018

17. Ambade A, Hassoun P, Damico R. Basement membrane extracellular matrix proteins in pulmonary vascular and right ventricular remodeling in pulmonary hypertension. *Am J Respir Cell Mol Biol.* (2021) 65:245–58. doi: 10.1165/rcmb.2021-0091TR

18. Huang X, Wu P, Huang F, Xu M, Chen M, Huang K, et al. Baicalin attenuates chronic hypoxia-induced pulmonary hypertension via adenosine A(2A) receptor-induced SDF-1/CXCR4/PI3K/AKT signaling. *J Biomed Sci.* (2017) 24:52. doi: 10.1186/s12929-017-0359-3

19. Zhang Q, Cao Y, Luo Q, Wang P, Shi P, Song C, et al. The transient receptor potential vanilloid-3 regulates hypoxia-mediated pulmonary artery smooth muscle cells proliferation via PI3K/AKT signaling pathway. *Cell Prolif.* (2018) 51:e12436. doi: 10.1111/cpr.12436

20. Kim Y, Haghighat L, Spiekerkoetter E, Sawada H, Alvira C, Wang L, et al. Neutrophil elastase is produced by pulmonary artery smooth muscle cells and is linked to neointimal lesions. *Am J Pathol.* (2011) 179:1560–72. doi: 10.1016/j.ajpath.2011.05.051

21. Sweatt A, Miyagawa K, Rhodes C, Taylor S, Del Rosario P, Hsi A, et al. Severe pulmonary arterial hypertension is characterized by increased neutrophil elastase and relative elafin deficiency. *Chest.* (2021) 160:1442–58. doi: 10.1016/j.chest.2021.06.028

22. Taylor S, Dirir O, Zamanian R, Rabinovitch M, Thompson A. The role of neutrophils and neutrophil elastase in pulmonary arterial hypertension. *Front Med.* (2018) 5:217. doi: 10.3389/fmed.2018.00217

23. Aldabbous L, Abdul-Salam V, McKinnon T, Duluc L, Pepke-Zaba J, Southwood M, et al. Neutrophil extracellular traps promote angiogenesis: evidence from vascular pathology in pulmonary hypertension. *Arterioscler Thromb Vasc Biol.* (2016) 36:2078–87. doi: 10.1161/atvbaha.116.307634

24. Li C, Liu P, Song R, Zhang Y, Lei S, Wu S. Immune cells and autoantibodies in pulmonary arterial hypertension. *Acta Biochim Biophys Sin.* (2017) 49:1047–57. doi: 10.1093/abbs/gmx095

25. Klouda T, Yuan K. Inflammation in pulmonary arterial hypertension. *Adv Exp Med Biol.* (2021) 1303:351–72. doi: 10.1007/978-3-030-63046-1_19

26. Racanelli A, Kikkers S, Choi A, Cloonan S. Autophagy and inflammation in chronic respiratory disease. *Autophagy.* (2018) 14:221–32. doi: 10.1080/15548627.2017.1389823

27. Zeng H, Liu X, Zhang Y. Identification of potential biomarkers and immune infiltration characteristics in idiopathic pulmonary arterial hypertension using bioinformatics analysis. *Front Cardiovasc Med.* (2021) 8:624714. doi: 10.3389/fcvm.2021.624714

28. Zeng Y, Li N, Zheng Z, Chen R, Liu W, Cheng J, et al. Screening of key biomarkers and immune infiltration in pulmonary arterial hypertension via integrated bioinformatics analysis. *Bioengineered.* (2021) 12:2576–91. doi: 10.1080/21655979.2021.1936816

29. Xu J, Yang Y, Yang Y, Xiong C. Identification of potential risk genes and the immune landscape of idiopathic pulmonary arterial hypertension via microarray gene expression dataset reanalysis. *Genes.* (2021) 12:125. doi: 10.3390/genes12010125

30. Samidurai A, Xi L, Das A, Iness A, Vigneshwar N, Li P, et al. Role of phosphodiesterase 1 in the pathophysiology of diseases and potential therapeutic opportunities. *Pharmacol Ther.* (2021) 226:107858. doi: 10.1016/j.pharmthera.2021.107858

31. Schermuly R, Pullamsetti S, Kwapiszewska G, Dumitrascu R, Tian X, Weissmann N, et al. Phosphodiesterase 1 upregulation in pulmonary arterial hypertension: target for reverse-remodeling therapy. *Circulation.* (2007) 115:2331–9. doi: 10.1161/circulationaha.106.676809

32. Hoffmann J, Marsh L, Pieper M, Stacher E, Ghanim B, Kovacs G, et al. Compartment-specific expression of collagens and their processing enzymes in intrapulmonary arteries of IPAH patients. *Am J Physiol Lung Cell Mol Physiol.* (2015) 308:L1002–13. doi: 10.1152/ajplung.00383.2014

33. Gibbs G, Roelants K, O'Bryan M. The Cap superfamily: cysteine-rich secretory proteins, antigen 5, and pathogenesis-related 1 proteins – roles in reproduction, cancer, and immune defense. *Endocr Rev.* (2008) 29:865–97. doi: 10.1210/er.2008-0032

34. Falak S, Schafer S, Baud A, Hummel O, Schulz H, Gauguier D, et al. Protease inhibitor 15, a candidate gene for abdominal aortic internal elastic lamina ruptures in the Rat. *Physiol Genom.* (2014) 46:418–28. doi: 10.1152/physiolgenomics.00004.2014

35. Brody M, Lee Y. The role of leucine-rich repeat containing protein 10 (LRRC10) in dilated cardiomyopathy. *Front Physiol.* (2016) 7:337. doi: 10.3389/fphys.2016.00337

36. Moc C, Taylor A, Chesini G, Zambrano C, Barlow M, Zhang X, et al. Physiological activation of Akt by PHLPP1 deletion protects against pathological hypertrophy. *Cardiovasc Res.* (2015) 105:160–70. doi: 10.1093/cvr/cvu243

37. Zhao R, Peng C, Song C, Zhao Q, Rong J, Wang H, et al. BICC1 as a novel prognostic biomarker in gastric cancer correlating with immune infiltrates. *Int Immunopharmacol.* (2020) 87:106828. doi: 10.1016/j.intimp.2020.106828

38. Sisto M, D'Amore M, Lofrumento D, Scagliusi P, D'Amore S, Mitolo V, et al. Fibulin-6 expression and anoikis in human salivary gland epithelial cells: implications in sjogren's syndrome. *Int Immunol.* (2009) 21:303–11. doi: 10.1093/intimm/dxp001

39. Welcker D, Stein C, Feitosa N, Armistead J, Zhang J, Lütke S, et al. Hemicentin-1 is an essential extracellular matrix component of the dermal-epidermal and myotendinous junctions. *Sci Rep.* (2021) 11:17926. doi: 10.1038/s41598-021-96824-4

40. Maddur M, Miossec P, Kaveri S, Bayry J. Th17 cells: biology, pathogenesis of autoimmune and inflammatory diseases, and therapeutic strategies. *Am J Pathol.* (2012) 181:8–18. doi: 10.1016/j.ajpath.2012.03.044

41. Weng M, Baron D, Bloch K, Luster A, Lee J, Medoff B. Eosinophils are necessary for pulmonary arterial remodeling in a mouse model of eosinophilic inflammation-induced pulmonary hypertension. *Am J Physiol Lung Cell Mol Physiol.* (2011) 301:L927–36. doi: 10.1152/ajplung.00049.2011

frontiers | Frontiers in Cardiovascular Medicine

TYPE Original Research
PUBLISHED 15 May 2023
DOI 10.3389/fcvm.2023.955060

OPEN ACCESS

EDITED BY
Anindita Das,
Virginia Commonwealth University, United States

REVIEWED BY
Cynthia James,
Johns Hopkins University, United States
Erwin Birnie,
Erasmus University Rotterdam, Netherlands
Birgitte Diness,
University of Copenhagen, Denmark

*CORRESPONDENCE
Brianna Davies
✉ davies7@mail.ubc.ca

†These authors share senior authorship

SPECIALTY SECTION
This article was submitted to Cardiovascular Genetics and Systems Medicine, a section of the journal Frontiers in Cardiovascular Medicine

RECEIVED 28 May 2022
ACCEPTED 10 March 2023
PUBLISHED 15 May 2023

CITATION
Davies B, Allan KS, Carroll SL, Gibbs K, Roberts JD, MacIntyre C, Steinberg C, Tadros R, Dorian P, Healey JS, Gardner M, Laksman ZWM, Krahn AD, Fournier A, Seifer C and Lauck SB (2023) Perceived self-efficacy and empowerment in patients at increased risk of sudden cardiac arrest.
Front. Cardiovasc. Med. 10:955060.
doi: 10.3389/fcvm.2023.955060

Perceived self-efficacy and empowerment in patients at increased risk of sudden cardiac arrest

Brianna Davies[1]*, Katherine S. Allan[2], Sandra L. Carroll[3], Karen Gibbs[1], Jason D. Roberts[4], Ciorsti MacIntyre[5], Christian Steinberg[6], Rafik Tadros[7], Paul Dorian[2], Jeff S. Healey[3], Martin Gardner[5], Zachary W. M. Laksman[1], Andrew D. Krahn[1], Anne Fournier[8], Colette Seifer[9†] and Sandra B. Lauck[1†]

[1]Centre for Cardiovascular Innovation, St. Paul's and Vancouver General Hospitals, University of British Columbia, Vancouver, BC, Canada, [2]Division of Cardiology, St. Michael's Hospital, University of Toronto, Toronto, ON, Canada, [3]School of Nursing, Faculty of Health Science, Population Health Research Institute, McMaster University, Hamilton, ON, Canada, [4]Section of Cardiac Electrophysiology, Division of Cardiology, Department of Medicine, Western University, London, ON, Canada, [5]QEII Health Sciences Center, Halifax, NS, Canada, [6]Institut Universitaire de Cardiologie et Pneumologie de Québec, Laval University, Quebec City, QC, Canada, [7]Department of Medicine, Cardiovascular Genetics Center, Montreal Heart Institute, Université de Montréal, Montreal, QC, Canada, [8]Division of Pediatric Cardiology, CHU Sainte-Justine, Université de Montréal, Montreal, QC, Canada, [9]Department of Internal Medicine, St Boniface Hospital, University of Manitoba, Winnipeg, MB, Canada

Background: The role of multidisciplinary clinics for psychosocial care is increasingly recognized for those living with inherited cardiac conditions (ICC). In Canada, access to healthcare providers differ between clinics. Little is known about the relationship between access to specialty care and a patient's ability to cope with, and manage their condition.

Methods: We leveraged the Hearts in Rhythm Organization (HiRO) to conduct a cross-sectional, community-based survey of individuals with ICC and their family members. We aimed to describe access to services, and explore the relationships between participants' characteristics, cardiac history and self-reported health status and self-efficacy (GSE: General Self-Efficacy Scale) and empowerment (GCOS-24: Genetic Counseling Outcome Scale).

Results: We collected 235 responses from Canadian participants in 10 provinces and territories. Overall, 63% of participants reported involvement of a genetic counsellor in their care. Access to genetic testing was associated with greater empowerment [mean GCOS-24: 121.14 (SD = 20.53) vs. 105.68 (SD = 21.69); $p = 0.004$]. Uncertain genetic test results were associated with lower perceived self-efficacy (mean GSE: uncertain = 28.85 vs. positive = 33.16, negative = 34.13; $p = 0.01$). Low global mental health scores correlated with both lower perceived self-efficacy and empowerment scores, with only 11% of affected participants reporting involvement of psychology services in their care.

Conclusion: Differences in resource accessibility, clinical history and self-reported health status impact the perceived self-efficacy and empowerment of patients with ICC. Future research evaluating interventions to improve patient outcomes is recommended.

KEYWORDS

cardiogenetics, genetic counselling, self efficacy, empowerment, patient engagement

Abbreviations

LQTS, long QT syndrome; ARVC, arrhythmogenic right ventricular cardiomyopathy; ACM, arrhythmogenic cardiomyopathy; CPVT, catecholaminergic polymorphic ventricular tachycardia; BrS, Brugada syndrome; HCM, hypertrophic cardiomyopathy; UCA, unexplained cardiac arrest; ICC, inherited cardiac condition; HiRO, hearts in rhythm organization; GSE, general self efficacy; GCOS, genetic counselling outcome scale.

Introduction

Inherited cardiac conditions (ICC) include, long QT syndrome (LQTS), short QT syndrome (SQTS) arrhythmogenic cardiomyopathies (ARVC/ACM), catecholaminergic polymorphic ventricular tachycardia (CPVT), early repolarization syndromes (ERS) and Brugada syndrome (BrS). These conditions can result in sudden unexpected death, typically in a seemingly healthy child or young adult before the condition can be recognized and treated (1–3). In recent years, advances in genomic technologies have markedly improved the ability to identify those at risk for premature sudden cardiac death due to an arrhythmia, and facilitated the implementation of preventive strategies.

The psychological impact of undergoing screening and/or living with an ICC is also increasingly recognized, with past research demonstrating high levels of patient anxiety, depression and poor adjustment to their diagnosis (4–8). Identifying those struggling to adapt and cope with their ICC is important, particularly given that low self-efficacy and low empowerment are known barriers to engage in risk prevention strategies, such as medication adherence or screening recommendations, critical for reducing risk of sudden cardiac death (9, 10). Further, a positive correlation between empowerment and uptake of cardiac screening in first-degree relatives has been reported (11). Together, this growing evidence underlines the importance of implementing strategies to improve patient self-efficacy and empowerment in cardiogenetic care delivery.

Expert consensus guidelines for the management of families with ICC have highlighted the importance of multidisciplinary clinics, including access to genetic counsellors and psychology resources, to support families cope with and manage the psychological impacts of ICCs (12–15).

In contrast to these recent recommendations, families report differences in both delivery of cardiogenetics care and access to providers across Canada. While access to specialty ICC clinics is covered under the public health system, these clinics are typically located within major urban centres, and the logistics and/or cost of travel for families in rural areas can be a significant barrier to accessing care providers. Further, not all specialty ICC clinics in Canada have a genetic counsellor embedded within the cardiology department, with some requiring patients to be referred to different clinics for a separate genetic counselling appointment, which can often have long waitlists.

Little is known regarding the relationship between access to care services and a patient's ability to cope and manage their ICC. We conducted a cross-sectional survey to explore relationships between patient characteristics, health status and access to care services with perceived self-efficacy and empowerment of ICC patients and their family members in Canada. The main objectives of this study were to (1) understand the current state of care provider access for patients with ICC in Canada and (2) explore relationships between access to certain care providers and perceived self-efficacy and empowerment. Secondary objectives included establishing baseline measures of self-efficacy and empowerment in the ICC population and exploring sub-populations with lower self-efficacy and empowerment to aid in the design of future interventions to improve patient-reported outcomes for ICC patients and their relatives.

Methods

This study was approved by the UBC Providence Health Care research ethics board (H17-01894).

Recruitment and community engagement

The National Hearts in Rhythm Organization (HiRO) is a group of clinicians, researchers, patients and families working together to improve detection and treatment of inherited arrhythmia and cardiomyopathy disorders in Canada (16). In addition to leading a national research registry, HiRO has numerous working groups dedicated to improving clinical care and supporting patient advocacy efforts. We leveraged this national network to form the HiRO Patient-Oriented Research Working Group, bringing together members interested in working alongside patient partners to conduct research to contribute novel evidence and improve psychosocial outcomes for patients living with ICC in Canada. Patient partners co-led framework development, study design and funding applications of this first working group project.

Patients with an ICC or unexplained cardiac arrest, their first-degree family members and their caregivers over the age of 18, were invited to complete an anonymous survey administered electronically through a university-affiliated online survey tool. Participants were recruited from families followed at nine HiRO clinics in five provinces across Canada. We provided clinical teams with business cards to distribute to families containing the online survey link at the time of their clinic visit. Additionally, families who were already participating in the National HiRO Registry [including Cardiac Arrest Survivors with Preserved Ejection Fraction Registry (CASPER), National ARVC registry and National Long QT Syndrome registry] at these centers who had previously consented to be re-contacted for research purposes received a letter of invitation. The online survey link was also available from the HiRO website (www.heartsinrhythm.org) and social media accounts (@heartsinrhythm). Additionally, the Canadian Sudden Arrhythmogenic Death Syndrome (SADS) Foundation partnered with the HiRO research team to promote survey recruitment on their online platforms, and increase the awareness of the survey outside of major care centers.

Study framework and survey design

This study was grounded in a framework developed by the HiRO Patient-Oriented Research Group based on current evidence, clinician expertise and the input of people with lived experience. We hypothesized four domains (personal demographics, cardiac history and risk profile, self-reported health status, and resource accessibility) that drive patients' capacity for self-efficacy and empowerment (**Figure 1**).

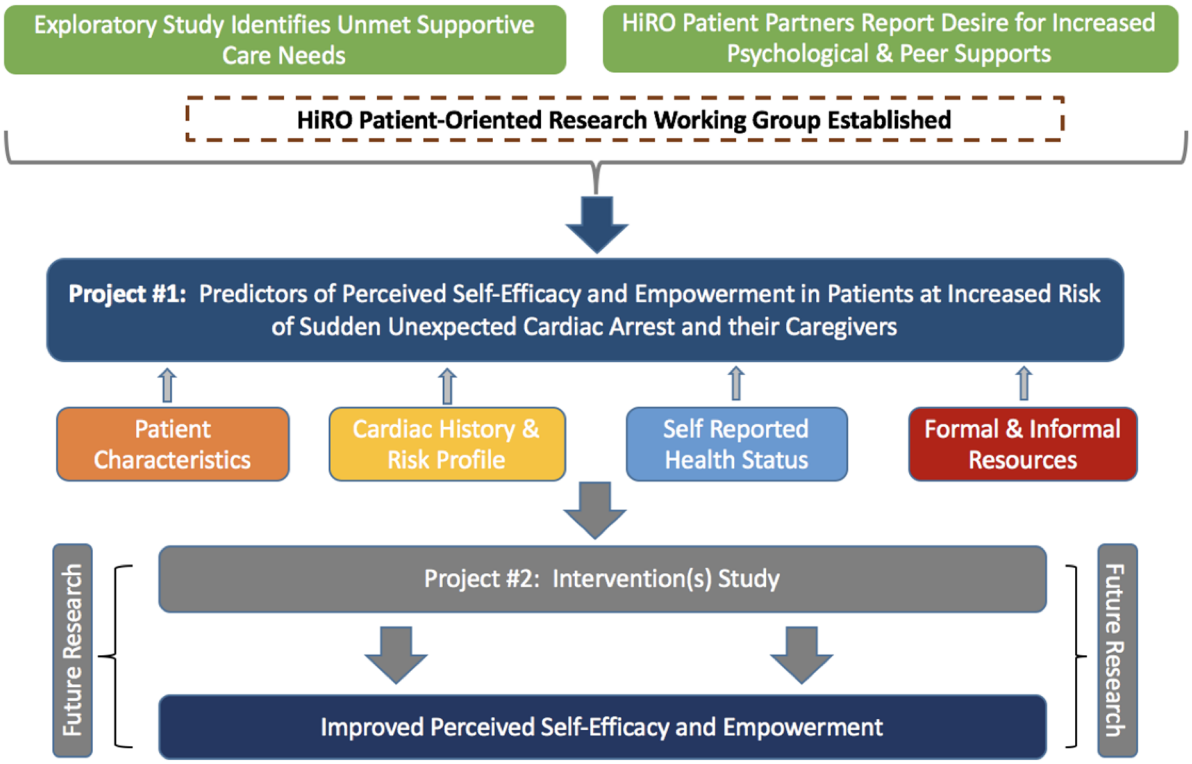

FIGURE 1
Framework of the HiRO patient-oriented research working group.

The constructs of general self-efficacy and empowerment were selected as key patient-reported outcome measures for the psychological well-being of ICC patients and their relatives. Both have previously been associated with health-related quality of life and adherence to risk-prevention measures, making these outcomes well-suited to measure impact of future interventions (9–11, 17–21). Self-efficacy is defined as the belief that one can perform a novel or difficult task, or cope with adversity (22). Self-efficacy is considered a key component of patient self-management of their disease, and has been found to positively correlate with self-esteem and optimism and negatively correlate with anxiety (22). While there have been differing definitions of patient empowerment in the literature, most agree that it relates to a patient's ability to take control of their wellbeing, play an active role in their healthcare and integrate their diagnosis within their self-identity (23, 24). Measures of patient empowerment have been found to correlate positively with constructs of perceived personal control, and decisional conflict and negatively with depression (25). While some have previously described an empowered patient as one who has "mastered" self-efficacy, there is general consensus that measures of self-efficacy fail to capture the broader psychosocial components of patient empowerment, particularly the emotional and cognitive domains (23, 24, 26). In 2018, a study by Kohler at el evaluated both patient empowerment and general self-efficacy in patients with coronary heart disease, and found the relationship between the two variables to be weak ($r = 0.38$) (27). The study concluded that patient empowerment and general self-efficacy are not interchangeable and should both be taken into consideration with designing healthcare to maximize health-related quality of life (27).

Survey design

An electronic survey (**Supplementary Appendix S1**) was designed to collect candidate variables in each of these four predicted domains, and was available in both English and French. Patient demographics, cardiac history and risk profile (including history of cardiac arrest & ICD shocks), and access to resources were captured by a survey designed by the research team. Self-reported health status was collected from three validated measures: 10-item Global Health PROMIS scale, 4-item Anxiety PROMIS 4a Scale, and 12-item Multidimensional Scale of Perceived Social Support (MSPSS). The Global Health PROMIS Scale is a measure of overall health-related quality of life which generates a physical and emotional health score with high internal reliability scores ($r = 0.81$ and 0.86) (28–31). Participants' emotional distress was captured with the Anxiety PROMIS 4a Scale, the short form version that is well correlated ($r = 0.90$) to the extensively validated PROMIS Anxiety 8a ($\alpha = 0.93$; $r = 0.79$) (32). Lastly, the domain of social health status was measured with the Multidimensional Scale of Perceived Social Support (MSPSS), designed to assess global perceived support from family, friends and significant others. This validated measure has good internal reliability ($\alpha = 0.85$–0.91) and factor analysis

10.3389/fcvm.2023.955060

between each sub-group has been shown to correlate with different sources of support (33–35). Each of the PROMIS and MSPSS scales have been validated in both English and French.

Participants' level of confidence in managing their condition was measured using the General Self-Efficacy Scale (GSE), which has strong internal reliability and concurrent validity with numerous positive emotions and optimism and has been validated in both English and French (17, 36). Lastly, the Genetic Counselling Outcome Scale (GCOS-24) was used to measure patient empowerment (25). In this study, empowerment was defined based on the contributions of McAllister et al. as the belief that one can make important life decisions (decisional control), has sufficient information about their family's condition (cognitive control), can manage one's feelings (behavioural control), can make effective use of the healthcare system (emotional regulation), and has hope for the future (hope) (25). The scale has been shown to have high internal consistency, test-retest reliability and construct validity with the measurement of health locus of control, satisfaction with life and depression. While this scale has yet to be validated in French, the feasibility of translation and cultural consistency has been demonstrated by recent validation of the scale in both Danish and Spanish populations (37, 38). The English version of this survey was professionally translated to French and reviewed by a bilingual study team member for use in this study.

Statistical analysis

Categorical variables are reported as total responses and percentages. Continuous variables are listed as means and standard deviations. Each of the validated instruments were scored according to the reference scoring guides to provide an overall score (15–18).

Part 1: Demographic variables are reported as total response and percentages (**Table 1**). Single variable analysis was performed to identify the relationship between each predictor variable and general self-efficacy and empowerment. Unpaired t-tests were used to compare mean outcome scores between those who reported access to each care provider versus those who did not (**Table 2**). Analysis of variance (ANOVA) tests were performed to test the interaction between cardiac history variables with more than two groups with mean outcome scores reported. Tukey HSD tests were performed if ANOVA was significant (**Supplementary Tables S1–S6**). Bivariable linear regression was performed to identify the relationship between self-reported health status scores and outcome variables (**Table 3** and **Supplementary Table S7**). For all statistical tests, level of significance was considered 0.05 and *t*-tests were one-tailed.

Part 2: Predictor variables identified to have a *p*-value less than or equal 0.2 on single variable analysis for each outcome variable were then entered into a multiple linear regression model for each general self-efficacy and patient empowerment. Separate models were calculated for (1) affected patients (**Tables 4, 5**) and (2) unaffected relatives and/or caregivers (**Supplementary Tables S8, S9**). For each model, coefficients and 95% confidence intervals were reported.

All statistical tests were performed in R-statistic (Version 1.2.1335). Survey participants who selected "no answer" or did not provide a response were excluded from analysis utilizing those variables. Only participants who provided answers to each of the applicable predictor variables were included in the multivariable analyses.

Results

In total, 235 survey responses were completed between January 2018 and March 2021 (**Table 1**). Incomplete data for one of GSE or

TABLE 1 Demographics of HiRO survey participants.

Demographics	*n* (%)
Responses	235
Survey language	
English	226 (96%)
French	9 (4%)
Sex	
Female	156 (66%)
Male	75 (32%)
Other	1 (0%)
No answer	3 (1%)
Age	
18–34	37 (16%)
35–54	96 (41%)
55 and up	72 (31%)
No Answer	30 (12%)
Province/Territory	
Western Canada	115 (49%)
Prairies	29 (12%)
Ontario	56 (24%)
Quebec	19 (8%)
Eastern Canada	14 (6%)
No answer	1 (0%)
Primary language	
English	202 (86%)
Another language	25 (11%)
No answer	8 (3%)
Highest education	
High school	25 (11%)
Some post-secondary	83 (35%)
Undergraduate degree or more	122 (52%)
Other	1 (0%)
No answer	4 (2%)
Main activity	
Employed	158 (67%)
Not employed	68 (29%)
Other	7 (3%)
No answer	2 (1%)
Annual household income	
Less than $69,999	65 (28%)
More than $70,000	143 (61%)
No answer	27 (11%)
Relationship status	
In a relationship	178 (76%)
Not in a relationship	48 (20%)
No answer	9 (4%)

TABLE 2 Self-efficacy and empowerment scores by health care provider (HCP) accessed for ICC care.

HCP Accessed for ICC care:	Affected ($n = 160$)							Unaffected relative/partner ($n = 51$)						
	n (%)	Mean GSE score (SD)			Mean GCOS score (SD)			*n* (%)	Mean GSE score (SD)			Mean GCOS score (SD)		
		YES	NO	*p*	YES	NO	*p*		YES	NO	*p*	YES	NO	*p*
Heart rhythm specialist	152 (95%)	32.87 (5.36)	29.25 (5.70)	0.12	118.71 (20.52)	111.89 (30.68)	0.53	30 (59%)	30.89 (6.05)	34.41 (3.61)	0.02*	114.33 (9.81)	120.00 (24.22)	0.46
Genetic counsellor	100 (63%)	32.96 (5.17)	32.18 (5.85)	0.42	120.46 (20.47)	114.35 (22.29)	0.12	19 (37%)	30.22 (6.63)	33.56 (4.21)	0.07	114.76 (19.87)	117.33 (22.59)	0.70
Psychologist	17 (11%)	30.92 (7.55)	32.86 (5.15)	0.37	114.92 (18.86)	118.61 (21.56)	0.52	4 (8%)	22.67 (13.01)	32.90 (4.12)	0.31	94.67 (18.61)	117.97 (20.74)	0.15
Family doctor	116 (73%)	32.41 (5.71)	33.39 (4.51)	0.29	117.82 (22.16)	119.36 (18.96)	0.69	22 (43%)	30.45 (6.59)	33.64 (4.03)	0.07	116.25 (18.44)	116.29 (24.15)	0.99
Pharmacist	45 (28%)	32.52 (5.38)	32.73 (5.47)	0.83	119.26 (17.87)	117.82 (22.62)	0.70	3 (6%)	23.50 (19.09)	32.63 (4.38)	0.62	123.00 (36.77)	115.92 (20.95)	0.83
Social worker	11 (7%)	32.40 (7.21)	32.69 (5.30)	0.90	111.80 (14.39)	118.77 (21.70)	0.18	5 (10%)	26.75 (3.60)	32.76 (5.38)	0.03*	100.25 (17.84)	118.00 (21.10)	0.14
Physical therapist	10 (6%)	29.00 (6.24)	32.94 (5.29)	0.08	110.50 (19.50)	118.88 (21.36)	0.22	0 (0%)	NA	32.22 (5.49)	NA	NA	116.27 (21.29)	NA
Pediatrician	3 (2%)	29.33 (5.13)	32.74 (5.43)	0.37	103.67 (12.22)	118.58 (21.35)	0.16	5 (10%)	33.00 (4.08)	32.15 (5.65)	0.72	120.75 (19.47)	115.78 (21.67)	0.66
Trauma counsellor	6 (4%)	35.33 (4.13)	32.56 (5.46)	0.17	113.17 (9.97)	118.48 (21.66)	0.27	1 (2%)	31.00 (NA)	32.25 (5.55)	NA	144.00 (NA)	115.58 (21.08)	NA
Research coordinator	41 (26%)	32.23 (5.50)	32.84 (5.41)	0.55	120.53 (21.16)	117.32 (21.36)	0.43	10 (20%)	31.00 (3.81)	32.53 (5.84)	0.35	114.22 (11.38)	116.84 (3.45)	0.64

HCP, healthcare provider; ICC, inherited cardiogenetic condition; GSE, general self-efficacy score; GCOS, genetic counselling outcome score. Six affected participants did not answer which HCPs they accessed for ICC care and were excluded from this analysis.
*Denotes statistical significance ($p < 0.05$).

GCOS scores was reported in 59 cases (25.1%). Overall, 66% of respondents identified as female, 41% were between the ages of 34–54 years, and 86% of participants reported English as their primary language.

166 (71%) respondents had a personal diagnosis of an ICC or experienced an unexplained cardiac arrest, 44 (19%) were unaffected first-degree relatives, 7 (3%) identified as a spouse/partner or close friend, and 18 (7%) declined to answer this question (**Supplementary Table S1**).

Part 1

Participant's education, main activity, relationship status and income were associated with statistically significant differences for both general self-efficacy (GSE) and patient empowerment (GCOS-24).

Overall, unaffected first-degree relatives and partner/spouses of someone with an ICC had similar mean perceived self-efficacy (GSE) and empowerment (GCOS-24) compared to those living with a diagnosis [GSE: 28.51 (SD = 3.58) (unaffected relative) vs. 29.17 (SD = 1.17) (partner/spouse) vs. 28.52 (SD = 2.62) (affected proband) vs. 28.93 (SD = 2.46) (affected relatives); $p = 0.80$]; [GCOS: 115.53 (SD = 20.98) (unaffected relative) vs. 121.60 (SD = 25.32) (partner/spouse) vs. 117.91 (SD = 21.09) (affected proband) vs. 118.71 (SD = 21.71) (affected relative); $p = 0.81$] (**Supplementary Table S1**). There were no statistically significant differences in general self-efficacy or patient empowerment in those with a different ICC diagnoses (**Supplementary Table S2**).

Access to healthcare providers

Among participants with a personal diagnosis of an ICC, 95% ($n = 152$) reported access to a heart rhythm specialist and 63% ($n = 100$) had access to a genetic counsellor (**Table 2**). The majority of participants had access to both these care providers (59%; $n = 98$), whereas 36% ($n = 59$) had access to a heart rhythm specialist only; 2 participants (1%) had access to a genetic counsellor only and 4% ($n = 7$) reported access to neither. A lower proportion of unaffected first-degree relatives or partners reported access to a heart rhythm specialist (59%; $n = 30$) or genetic counsellor

TABLE 3 Self-efficacy and empowerment scores by self-reported health status in affected patients.

Self-reported health status:	General self-efficacy (GSE)					Patient empowerment (GCOS-24)				
	B	95% CI		*F*-Statistic	*p*	*B*	95% CI		*F*-Statistic	*p*
Global health—physical	−0.78	−2.50	0.95	0.788	0.38	−4.51	−11.59	2.57	1.59	0.21
Global health—mental	4.69	3.32	6.07	45.45	<0.001*	14.57	8.38	20.75	21.73	<0.001*
Perceived social support	1.20	0.63	1.76	17.36	<0.001*	4.69	2.16	7.22	13.43	<0.001*

*Denotes statistical significance ($p < 0.05$).

TABLE 4 Multiple linear regression model for general self-efficacy (gse): affected patients.

Affected patients ($n = 125$):		*B*	95% CI	
Highest education: (*High School*)	Some post-secondary education	1.68	−1.17	4.52
	Bachelor's degree or higher	2.26	−0.57	5.09
Main activity (*Employed or Student*)	Not currently employed	−0.78	−2.53	0.98
Relationship (*Not in a relationship*)	In a relationship	1.39	−1.07	3.84
Income (*No Answer*)	Under $69,000 per year	2.26	−1.19	5.72
	More than $70,000 per year	2.83	−0.59	6.25
Healthcare providers	Heart rhythm speciality	3.16	−0.19	6.51
	Physical therapist	−3.24	−6.34	−0.13
	Trauma counsellor	2.66	−1.24	6.56
GT result: (*Not applicable*)	Positive	−0.58	−2.56	1.41
	Negative	−0.13	−2.63	2.38
	The results were unclear	−3.52	−6.60	−0.44
Exercise restrictions: (*No restrictions*)	Yes—Worried about cardiac risk	−3.95	−6.32	−1.58
	Yes—Physical limitations	1.31	−2.66	5.27
	Yes—Healthcare provider recommendations	−1.33	−5.30	2.64
	Yes—Other	1.20	−0.90	3.30
ICD Shock	Yes (No)	−1.32	−3.88	1.23
Hx anxiety or depression	Yes (No)	−0.22	−2.04	1.60
Global health—mental		2.44	0.74	4.15
MSPSS		−0.01	−0.66	0.65

Variables in brackets denotes the variable used as reference. GT, genetic testing; MSPSS, multidimensional scale of perceived social support. 41 of 166 affected participants did not provide an answer for at least one of the predictor variables are were excluded from this analysis ($n = 125$).

TABLE 5 Multiple linear regression model for patient empowerment (GCOS-24): affected patients.

Affected patients ($n = 115$)		*B*	95% CI	
Highest education: *(High School)*	Some post-secondary education	5.66	−6.78	18.10
	Bachelor's degree or higher	10.37	−2.07	22.81
Main activity (Employed or Student)	Not currently employed	−4.32	−12.73	4.09
Relationship *(Not in a relationship)*	In a relationship	5.82	−4.18	15.83
Income *(No answer)*	Under $69,000 per year	−0.49	−23.27	22.30
	More than $70,000 per year	−0.13	−22.76	22.50
Healthcare providers	Genetic counsellor	−2.88	−12.67	6.92
	Social worker	6.92	−7.60	21.43
	Pediatrician	−7.74	−34.66	19.18
Genetic testing	Yes (No)	16.41	5.99	26.82
Exercise restrictions: *(No restrictions)*	Yes—Worried about cardiac risk	−25.25	−34.85	−15.64
	Yes—Physical limitations	−1.47	−19.77	16.83
	Yes—Healthcare provider recommendations	−3.58	−18.24	11.08
	Yes—Other	1.32	−8.70	11.33
Sudden cardiac arrest	Yes (No)	−4.94	−15.13	5.26
ICD	Yes (No)	4.67	−4.61	13.94
Shocks	Yes (No)	−8.51	−20.65	3.64
Hx anxiety or depression	Yes (No)	−1.46	−9.58	6.66
Global health—mental		11.37	3.90	18.85
MSPSS		0.53	−2.45	3.52

Variables in brackets denotes the variable used as reference. MSPSS, multidimensional scale of perceived social support. 51 of 166 affected participants did not provide an answer for at least one of the predictor variables are were excluded from this analysis ($n = 115$).

(37%; $n = 19$). Access to psychologists was low amongst both affected patients and their relatives/partners [affected:11% ($n = 17$); relatives: 8% ($n = 4$)].

Overall, affected participants whose ICC team included a heart rhythm specialist reported greater self-efficacy scores (GSE) [32.87 (SD = 5.36) vs. 29.25 (SD = 5.70); $p = 0.12$] whereas those who reported access to a genetic counsellor had greater empowerment scores [120.46 (SD = 20.47) vs. 114.35 (SD = 22.29); $p = 0.12$], however neither of these findings were statistically significant (Table 2). In unaffected relatives, those who reported access to a heart rhythm specialist had significantly lower self-efficacy scores [heart rhythm specialist: mean GSE: 30.89 (SD = 6.05) vs. 34.41 (SD = 3.61); $p = 0.02$].

Clinical history

Affected participants who had genetic testing performed reported significantly higher empowerment (GCOS-24), regardless of the findings, compared to those who were not tested [121.14 (SD = 20.53) vs. 105.68 (SD = 21.69); $p = 0.004$] (Supplementary Table S3). However, participants with an unclear genetic test result (i.e., variant of uncertain significance) had lower self-efficacy scores compared to those with either a positive [28.85 (SD = 5.32) (VUS) vs. 33.16 (SD = 5.31) (positive); $p = 0.04$] or negative genetic test result [28.85 (SD = 5.32) (VUS) vs. 34.13 (SD = 4.40) (negative); $p = 0.02$] (Supplementary Table S4). In unaffected relatives/spouses, those whose family members had genetic testing performed also had higher empowerment scores, however this was not statistically significant [118.22 (SD = 22.08) vs. 103.71 (SD = 18.27); $p = 0.22$] (Supplementary Table S6).

Affected participants who restricted exercise based on their ICC diagnosis had significantly lower empowerment (GCOS-24) scores compared to those whose exercise habits were not changed [112.03 (SD = 21.22) vs. 123.76 (SD = 19.90) $p = 0.001$] (Supplementary Table S3). Participants who reported self-restricting exercise due to worry it may increase risk of cardiac arrest or ICD shock had significantly lower empowerment (GCOS-24) scores compared to those who reduce exercise due to physical limitations [95.71 (SD = 15.07) vs. 117.86 (SD = 17.86); $p = 0.03$], healthcare provided advice [95.71 (SD = 15.07) vs. 124.75 (SD = 14.11); $p = <0.001$] or other reasons [95.71 (SD = 15.07) vs. 121.32 (SD = 20.95); $p = <0.001$] (Supplementary Table S5). Affected participants with a prior history of anxiety or depression prior to receiving a diagnosis of an ICC had both lower perceived self-efficacy [31.20 (SD = 6.06) vs. 33.58 (SD = 4.92); $p = 0.01$] and empowerment scores [114.30 (SD = 22.59) vs. 120.54 (SD = 20.39); $p = 0.05$] (Supplementary Table S3). Additionally, unaffected relatives/partners whose family member experienced a sudden cardiac death reported lower empowerment scores [109.21 (SD = 20.33) vs. 123.65 (SD = 21.00); $p = 0.04$] (Supplementary Table S6).

Self-reported health status

Lower scores on both the mental health component of the PROMIS Scale v1.2—Global Health survey and the Multidimensional Scale of Perceived Social Support (MSPSS) were associated with lower perceived self-efficacy (GSE) (Global Health—Mental: $B = 4.69$, $p = <0.001$; MSPSS: $B = 1.20$, $p = <0.001$) and empowerment (GCOS-24) (Global Health—Mental: $B = 14.57$, $p = <0.001$; MSPSS: $B = 4.69$; $p = <0.001$) in affected participants (**Table 3**). In unaffected relatives/partners, higher scores on the mental health component of the PROMIS Scale v1.2—Global Health survey was associated with higher self-efficacy ($B = 5.32$; $p = <0.001$), whereas higher scores on the Multidimensional Scale of Perceived Social Support (MSPSS) were associated with higher empowerment ($B = 5.64$; $p = 0.01$) (**Supplementary Table S7**).

Part 2

All variables identified in Part 1 to correlate with general self-efficacy (GSE) or patient empowerment (GCOS-24) at a significance level of 0.2 or less were then entered to multivariable linear regression models for both affected patients (**Tables 4**, **5**) and unaffected relatives/partners (**Supplementary Tables S8, S9**).

Affected patients

In the multiple linear regression model, uncertain genetic test results (VUS) ($B = -3.52$), exercise restrictions due to worry about cardiac risk ($B = -3.95$) and PROMIS Global Health—Mental Health scores ($B = 2.44$) were correlated with general self-efficacy (**Table 4**). Access to genetic testing ($B = 16.41$), exercise restrictions due to worry about cardiac risk ($B = -25.25$) and PROMIS Global Health—Mental Health scores ($B = 11.37$) were correlated with patient empowerment (**Table 5**).

Unaffected relatives and partners

PROMIS Global Health—Mental Health scores ($B = 5.69$) correlated with general self-efficacy in unaffected relatives or partners (**Supplementary Table S8**).

Discussion

This study makes novel contributions to better understand the needs of individuals and families affected by ICC. Our unique focus on exploring the complex drivers of living well with ICC provide innovative insights to strengthen patient-oriented research. We identified clinical history and self-reported health status variables associated with general self-efficacy and empowerment in a cohort of patients at increased risk of sudden death. In partnership with people with lived experience and community partners, we sought to capture diverse perspectives. Access to specialized care, including availability of genetic testing was associated with higher patient empowerment, whereas receiving uncertain genetic test results was associated with lower general self-efficacy. Lower self-reported mental health scores were associated with lower perceived self-efficacy and empowerment. Despite lower cardiac risk profiles, no significant differences in self-efficacy and empowerment scores were found between affected patients and their unaffected relatives.

Access to speciality care

Overall, 95% of ICC patients reported access to a heart rhythm specialist and 63% reported access to a genetic counsellor, with 59% reporting access to both healthcare professionals. Genetic counselling for inherited cardiac disorders has previously been associated with greater patient empowerment (39). Our study identified a similar trend, with mean patient empowerment scores being greater in affected patients who reported access to a genetic counsellor, although this was not statistically significant ($p = 0.12$). The benefits of receiving multidisciplinary care in specialized cardiogenetics clinics is also becoming increasingly recognized, including improved access to genetic testing, identified to be a predictor of greater patient empowerment in this study (13, 39–41). In this model of health service delivery, genetic counsellors may also be involved in the care of patients over time, allowing for the development of a therapeutic relationship and greater involvement in psychosocial care after initial diagnosis. Recently, a study by Murray et al. reported an association between strength of genetic counsellor-patient relationship and patient empowerment, further supporting the added value of this model of care (42). Continued efforts should be made to improve access to both genetic counselling and genetic testing for ICC patients in Canada *via* the establishment of multidisciplinary clinics. Barriers to creating multidisciplinary clinics in Canada include identifying funding to support genetic counsellor salary, in addition to recruitment challenges given the small genetic counsellor workforce.

Clinical history and risk profiles

Multiple studies have previously explored patients' motivations to pursue genetic testing in the cardiac context, with a common theme being the desire to reduce uncertainty surrounding their diagnosis (43, 44). However, for those whose result includes a variant of uncertain significance (VUS), the finding may instead add to the burden of uncertainty. A study by Predham et al., evaluated patients' perspective of receiving inconclusive genetic test results in LQTS, and highlighted that some patients were disappointed by the lack of conclusive findings. In some cases, this led to patients questioning their clinical diagnosis (45). A similar finding was reported by Burns et al. in 2017 who identified patients with hypertrophic cardiomyopathy (HCM) who received a VUS often questioned the validity of their diagnosis and struggled to effectively communicate the familial implications of uncertain genetic test results (46). Further, genetic variants may be re-classified over time, which can also add to the burden of uncertainty for patients (47, 48). Our study

adds to this evidence by demonstrating that patients with an uncertain genetic test result have lower perceived self-efficacy compared to those with either positive or negative results. Genetic counsellors are well-suited to support patients' ability to cope with the complexity and uncertainty of genetic testing results, but are often limited to only one post-test session with patients. The opportunity to meet with a genetic counsellor during follow-up appointments to review their genetic testing results over time may also serve as an intervention to improve self-efficacy. Further research on additional interventions to mitigate the impact of receiving uncertain results on perceived self-efficacy is warranted.

The psychological impact of exercise restrictions has previously been well-described for patients living with inherited cardiac conditions and was further supported by this study (49, 50). ICC clinics should be proactive in identifying those self-limiting exercise due to fear of cardiac symptoms and facilitate access to additional support when needed. Further, care teams are encouraged to use a share-decision making model when discussing exercise restrictions, incorporating the patient's perceived value of exercise to their physical, emotional and social well-being when developing a safe-exercise plan (10, 51).

Self-reported health-status

In this study, self-reported, mental health scores were associated with perceived self-efficacy and empowerment. Given general self-efficacy and empowerment have previously been correlated with constructs such as anxiety, depression, optimism and shyness, these findings are not particularly surprising, but support the importance of identifying patients with low health status score(s) in order to assess whether any interventions to improve perceived self-efficacy and empowerment are available (17, 25). Systematic psychosocial screening *via* pre-appointment questionnaires have previously been implemented in other out-patient cardiology settings, and may be a useful tool to identify ICC patients and family members with low mental health scores (52). This provides an opportunity to address low score(s) with the families during their appointment, and identify willingness and appropriateness of available interventions, such as referral to psychology services. In this study, only 11% of affected participants and 8% of unaffected relatives reported involvement of a psychologist as part of their care. Improving pathways for patients and their relatives to access these services is recommended for ICC clinics, either by embedding psychology services within a multidisciplinary model or establishing referral process to a psychologist familiar with issues faced by ICC families (53). In Canada, additional barriers to accessing counselling services include financial burden and excessive wait-times, and avenues to reduce these barriers should be considered for ICC patients (52). In addition to psychology services, past research has demonstrated informal peer support opportunities to be desired by cardiology patients, with some evidence supporting this as an effective intervention to improve both self-efficacy and empowerment (54, 55).

Unaffected relatives and partners

This study found no significant differences in self-efficacy and empowerment scores between affected patients and their unaffected relatives or partners, suggesting family members of those with an ICC may also experience negative psychosocial impacts. Interestingly, access to a heart rhythm specialist was associated with significantly lower self-efficacy scores in unaffected relatives. This finding suggests the act of undergoing cardiac screening and/or being evaluated in an ICC may in of itself reduce general self-efficacy in relatives, even when the results are reassuring. Interestingly, a recent study by Fusco et al. found more than half of ICC relatives (54%) of who tested negative for a familial variant continued to undergo longitudinal cardiac surveillance, which may extend the negative psychological impact of cardiac evaluation (56). Future research evaluating longitudinal psychosocial outcomes in unaffected relatives and interventions to mitigate undue distress is warranted.

Study limitations

The conduct of community-based research presents significant challenges. Despite best efforts to engage patients and families across Canada, participants from select provinces were over-represented. Therefore, these exploratory results may not be generalizable across all Canadian ICC patients. Participants' clinical and risk profiles, including genetic test results, were self-reported and not confirmed with clinical records. Survey participants were primarily female (68%), and well-educated, with over 70% reporting post-secondary education, suggesting a potential response bias and a failure to capture important social determinants. Additionally, it's possible participants with greater self-efficacy and empowerment were more likely to respond to the survey, which may have resulted in biased estimates of self-efficacy and empowerment. Importantly, given the cross-sectional design of this project, we're unable to determine directionality of the relationship between candidate variables and outcome measures. Lastly, associations between time since diagnosis or last follow-up visit and perceived self-efficacy and empowerment are unknown and were not evaluated as part of this study.

Conclusion

This study identified differences in resource availability, clinical history and self-reported health status impact the perceived self-efficacy and empowerment of patients with ICC and their unaffected relatives. Based on a developed conceptual framework, this HiRO Patient-Oriented Research project was strengthened by utilizing a community-based approach with support from patient partners and advocacy groups. Further efforts to increase access to genetic testing *via* multidisciplinary clinics should be made, given the association with patient empowerment. Development of interventions to mitigate the negative impact of uncertain genetic

test results on perceived self-efficacy is warranted. Finally, we recommend ICC clinics develop processes to identify patients and their family members at risk of low self-efficacy and empowerment in order to offer interventions, including establishing pathways to access psychology services.

Data availability statement

The datasets presented in this article are not readily available because sharing of participant data is restricted to those with research ethics approvals and data transfer agreements. Requests to access the datasets should be directed to akrahn@mail.ubc.ca.

Ethics statement

The studies involving human participants were reviewed and approved by UBC Providence Health Care Research Ethics Board. Written informed consent for participation was not required for this study in accordance with the national legislation and the institutional requirements.

Author contributions

BD, KA, SC, KG, AF, CoS and SL were involved in project development and survey design. JR, CM, ChS, RT, PD, JH, MG, ZL and AK were involved in participant recruitment. BD, CoS and SL lead data analysis and initial manuscript drafting. All authors contributed to the article and approved the submitted version.

Funding

This study was supported by the Cardiac Arrhythmia Network of Canada (CANet) (Principle Investigator: CoS; FIP-SSC-002), the Canadian Institute of Health Research Strategy for Patient-Oriented Research (CIHR-SPOR) (Principle Investigator: SL; PEG-157056), the Fond BoBeauCoeur du Hospital Ste-Justine, and the University of Manitoba.

Conflict of interest

The authors declare that the research was conducted in the absence of any commercial or financial relationships that could be construed as a potential conflict of interest.

Publisher's note

All claims expressed in this article are solely those of the authors and do not necessarily represent those of their affiliated organizations, or those of the publisher, the editors and the reviewers. Any product that may be evaluated in this article, or claim that may be made by its manufacturer, is not guaranteed or endorsed by the publisher.

Supplementary material

The Supplementary Material for this article can be found online at: https://www.frontiersin.org/articles/10.3389/fcvm.2023.955060/full#supplementary-material.

References

1. Perrin MJ, Gollob MH. Genetics of cardiac electrical disease. *Can J Cardiol*. (2013) 29(1):89–99. doi: 10.1016/j.cjca.2012.07.847

2. Sarkozy A, Brugada P. Sudden cardiac death: what is inside our genes? *Can J Cardiol*. (2005) 21(12):1099–110. doi: 10.1111/j.1540-8167.2005.50110.x

3. Theilade J, Kanters J, Henriksen FL, Gilsa-Hansen M, Svendsen JH, Eschen O, et al. Cascade screening in families with inherited cardiac diseases driven by cardiologists: feasibility and nationwide outcome in long QT syndrome. *Cardiology*. (2013) 126(2):131–7. doi: 10.1159/000350825

4. Wilder Schaaf KP, Artman LK, Peberdy MA, Walker WC, Ornato JP, Gossip MR, et al. Anxiety, depression, and PTSD following cardiac arrest: a systematic review of the literature. *Resuscitation*. (2013) 84(7):873–7. doi: 10.1016/j.resuscitation.2012.11.021

5. Hendriks KS, Hendriks MM, Birnie E, Grosfeld FJ, Wilde AA, van den Bout J, et al. Familial disease with a risk of sudden death: a longitudinal study of the psychological consequences of predictive testing for long QT syndrome. *Heart Rhythm*. (2008) 5(5):719–24. doi: 10.1016/j.hrthm.2008.01.032

6. Wesołowska K, Elovainio M, Koponen M, Tuiskula AM, Hintsanen M, Keltikangas-Järvinen L, et al. Is symptomatic long QT syndrome associated with depression in women and men? *J Genet Couns*. (2016) 26(3):1–10. doi: 10.1007/s10897-016-0004-4

7. Czosek RJ, Kaltman JR, Cassedy AE, Shah MJ, Vetter VL, Tanel RE, et al. Quality of life of pediatric patients with long QT syndrome. *Am J Cardiol*. (2016) 117(4):605–10. doi: 10.1016/j.amjcard.2015.11.051

8. Aatre RD, Day SM. Psychological issues in genetic testing for inherited cardiovascular diseases. *Circ Cardiovasc Genet*. (2011) 4(1):81–90. doi: 10.1161/CIRCGENETICS.110.957365

9. O'Donovan CE, Waddell-Smith KE, Skinner JR, Broadbent E. Predictors of β-blocker adherence in cardiac inherited disease. *Open Heart*. (2018) 5(2):e000877. doi: 10.1136/openhrt-2018-000877

10. Kambhampati S, Ashvetiya T, Stone NJ, Blumenthal RS, Martin SS. Shared decision-making and patient empowerment in preventive cardiology. *Curr Cardiol Rep*. (2016) 18(5):1–7. doi: 10.1007/s11886-016-0729-6

11. Hancock B, Miller EM, Parrott A, Weaver KN, Tretter JT, Pilipenko V, et al. Retrospective comparison of parent-reported genetics knowledge, empowerment, and familial uptake of cardiac screening between parents who received genetic counseling by a certified genetic counselor and those who did not: a single US academic medical center study. *J Genet Couns*. (2022) 31(4):965–75. doi: 10.1002/jgc4.1570

12. Priori SG, Wilde AA, Horie M, Cho Y, Behr ER, Berul C, et al. Executive summary: HRS/EHRA/APHRS expert consensus statement on the diagnosis and management of patients with inherited primary arrhythmia syndromes. *Europace*. (2013) 15(10):1389–406. doi: 10.1093/europace/eut272

13. Ahmad F, McNally EM, Ackerman MJ, Baty LC, Day SM, Kullo IJ, et al. Establishment of specialized clinical cardiovascular genetics programs: recognizing the need and meeting standards: a scientific statement from the American heart association. *Circ Genom Precis Med*. (2019) 12(6):e000054. doi: 10.1161/HCG.0000000000000054

14. Stiles MK, Wilde AA, Abrams DJ, Ackerman MJ, Albert CM, Behr ER, et al. 2020 APHRS/HRS expert consensus statement on the investigation of decedents with sudden unexplained death and patients with sudden cardiac arrest, and of their families. *Heart Rhythm*. (2021) 18(1):e1–e50. doi: 10.1016/j.hrthm.2020.10.010

15. Wilde AAM, Semsarian C, Márquez MF, Sepehri Shamloo A, Ackerman MJ, Ashley EA, et al. European Heart Rhythm Association (EHRA)/Heart Rhythm

Society (HRS)/Asia Pacific Heart Rhythm Society (APHRS)/Latin American Heart Rhythm Society (LAHRS) expert consensus statement on the state of genetic testing for cardiac diseases. *J Arrhythm*. (2022) 38(4):491–553. doi: 10.1002/joa3.12717

16. Davies B, Roberts JD, Tadros R, Green MS, Healey JS, Simpson CS, et al. The hearts in rhythm organization: a Canadian national cardiogenetics network. *CJC Open*. (2020) 2(6):652–62. doi: 10.1016/j.cjco.2020.05.006

17. Brink E, Alsén P, Herlitz J, Kjellgren K, Cliffordson C. General self-efficacy and health-related quality of life after myocardial infarction. *Psychol Health Med*. (2012) 17 (3):346–55. doi: 10.1080/13548506.2011.608807

18. Kvarme LG, Haraldstad K, Helseth S, Sørum R, Natvig GK. Associations between general self-efficacy and health-related quality of life among 12-13-year-old school children: a cross-sectional survey. *Health Qual Life Outcomes*. (2009) 7 (1):1–8. doi: 10.1186/1477-7525-7-85

19. Thomet C, Moons P, Schwerzmann M, Apers S, Luyckx K, Oechslin EN, et al. Self-efficacy as a predictor of patient-reported outcomes in adults with congenital heart disease. *Eur J Cardiovasc Nurs*. (2018) 17(7):619–26. doi: 10.1177/1474515118771017

20. Marks R, Allegrante JP. A review and synthesis of research evidence for self-efficacy-enhancing interventions for reducing chronic disability: implications for health education practice (part II). *Health Promot Pract*. (2005) 6(2):148–56. doi: 10.1177/1524839904266792

21. Kaal SEJ, Husson O, van Duivenboden S, Jansen R, Manten-Horst E, Servaes P, et al. Empowerment in adolescents and young adults with cancer: relationship with health-related quality of life. *Cancer*. (2017) 123(20):4039–47. doi: 10.1002/cncr.30827

22. Schwarzer R, Jerusalem M. Generalized self-efficacy scale. In: J Weinman, S Wright, M Johnston, editors. *Measures in health psychology: A user's portfolio. Causal and control beliefs*. Windsor, UK: NFER-NELSON (1995). p. 35–7.

23. McAllister M, Dunn G, Payne K, Davies L, Todd C. Patient empowerment: the need to consider it as a measurable patient-reported outcome for chronic conditions. *BMC Health Serv Res*. (2012) 12(1):1–8. doi: 10.1186/1472-6963-12-157

24. Aujoulat I, Marcolongo R, Bonadiman L, Deccache A. Reconsidering patient empowerment in chronic illness: a critique of models of self-efficacy and bodily control. *Soc Sci Med*. (2008) 66(5):1228–39. doi: 10.1016/j.socscimed.2007.11.034

25. McAllister M, Wood A, Dunn G, Shiloh S, Todd C. The genetic counseling outcome scale: a new patient-reported outcome measure for clinical genetics services. *Clin Genet*. (2011) 79(1):413–24. doi: 10.1111/j.1399-0004.2011.01636.x

26. Krok D, Zarzycka B. Self-efficacy and psychological well-being in cardiac patients: moderated mediation by affect and meaning-making. *J Psychol*. (2020) 154 (6):411–25. doi: 10.1080/00223980.2020.1772702

27. Kärner Köhler A, Tingström P, Jaarsma T, Nilsson S. Patient empowerment and general self-efficacy in patients with coronary heart disease: a cross-sectional study. *BMC Fam Pract*. (2018) 19(1):1–10. doi: 10.1186/s12875-018-0749-y

28. Cella D, Riley W, Stone A, Rothrock N, Reeve B, Yount S, et al. The patient-reported outcomes measurement information system (PROMIS) developed and tested its first wave of adult self-reported health outcome item banks: 2005–2008. *J Clin Epidemiol*. (2010) 63(11):1179–94. doi: 10.1016/j.jclinepi.2010.04.011

29. Hays RD, Bjorner J, Revicki RA, Spritzer KL, Cella D. Development of physical and mental health summary scores from the patient reported outcomes measurement information system (PROMIS) global items. *Qual Life Res*. (2009) 18(7):873–80. doi: 10.1007/s11136-009-9496-9

30. Cella D, Choi SW, Condon DM, Schalet B, Hays RD, Rothrock NE, et al. PROMIS® adult health profiles: efficient short-form measures of seven health domains. *Value Health*. (2019) 22(5):537–44. doi: 10.1016/j.jval.2019.02.004

31. Coste J, Rouquette A, Valderas JM, Rose M, Leplège A. The French PROMIS-29. Psychometric validation and population reference values. *Rev Epidemiol Sante Publique*. (2018) 66(5):317–24. doi: 10.1016/j.respe.2018.05.563

32. Pilkonis PA, Choi SW, Reise SP, Stover AM, Riley WT, Cella D, et al. Item banks for measuring emotional distress from the patient-reported outcomes measurement information system (PROMIS®): depression, anxiety, and anger. *Assessment*. (2011) 18(3):263–83. doi: 10.1177/1073191111411667

33. Zimet GD, Dahlem NW, Zimet SG, Farley GK. The multidimensional scale of perceived social support. *J Pers Assess*. (1988) 52(1):30–41. doi: 10.1207/s15327752jpa5201_2

34. Denis A, Callahan S, Bouvar M. Evaluation of the French version of the multidimensional scale of perceived social support during the postpartum period. *Matern Child Health J*. (2015) 19(6):1245–51. doi: 10.1007/s10995-014-1630-9

35. Osman A, Lamis DA, Freedenthal S, Gutierrez PM, McNaughton-Cassill M. The multidimensional scale of perceived social support: analyses of internal reliability, measurement invariance, and correlates across gender. *J Pers Assess*. (2014) 96 (1):103–12. doi: 10.1080/00223891.2013.838170

36. Aleh D, Romo L, Camart N. Validation de l'échelle du sentiment d'auto-efficacité (GSE: General Self-Efficacy Scale) chez des étudiants universitaires français (2016).

37. Diness BR, Overbeck G, Hjortshøj TD, Hammer TB, Timshel S, Sørensen E, et al. Translation and adaptation of the genetic counselling outcome scale (GCOS-24) for use in Denmark. *J Genet Couns*. (2017) 26(5):1080–9. doi: 10.1007/s10897-017-0086-7

38. Muñoz-Cabello P, García-Miñaúr S, Espinel-Vallejo ME, Fernández-Franco L, Stephens A, Santos-Simarro F, et al. Translation and cross-cultural adaptation with preliminary validation of GCOS-24 for use in Spain. *J Genet Couns*. (2018) 27 (3):732–43. doi: 10.1007/s10897-017-0154-z

39. Ison HE, Ware SM, Schwantes-An TH, Freeze S, Elmore L, Spoonamore KG. The impact of cardiovascular genetic counseling on patient empowerment. *J Genet Couns*. (2019) 28(3):570–7. doi: 10.1002/jgc4.1050

40. Erskine KE, Hidayatallah NZ, Walsh CA, McDonald TV, Cohen L, Marion RW, et al. Motivation to pursue genetic testing in individuals with a personal or family history of cardiac events or sudden cardiac death. *J Genet Couns*. (2014) 23 (5):849–59. doi: 10.1007/s10897-014-9707-6

41. Rhodes A, Rosman L, Cahill J, Ingles J, Murray B, Tichnell C, et al. Minding the genes: a multidisciplinary approach towards genetic assessment of cardiovascular disease. *J Genet Couns*. (2017) 26(2):224–31. doi: 10.1007/s10897-016-0017-z

42. Murray B, Tichnell C, Burch AE, Calkins H, James CA. Strength of the genetic counselor: patient relationship is associated with extent of increased empowerment in patients with arrhythmogenic cardiomyopathy. *J Genet Couns*. (2021) 31(2):388–97. doi: 10.1002/jgc4.1499

43. Charron P, Heron D, Gargiulo M, Richard P, Dubourg O, Desnos M, et al. Genetic testing and genetic counselling in hypertrophic cardiomyopathy: the French experience. *J Med Genet*. (2002) 39:741–6. doi: 10.1136/jmg.39.10.741

44. Smart A. Impediments to DNA testing and cascade screening for hypertrophic cardiomyopathy and long QT syndrome: a qualitative study of patient experiences. *J Genet Couns*. (2010) 19:630–9. doi: 10.1007/s10897-010-9314-0

45. Predham S, Hathaway J, Hulait G, Arbour L, Lehman A. Patient recall, interpretation, and perspective of an inconclusive long QT syndrome genetic test result. *J Genet Couns*. (2017) 26(1):150–8. doi: 10.1007/s10897-016-9991-4

46. Burns C, Yeates L, Spinks C, Semsarian C, Ingles J. Attitudes, knowledge and consequences of uncertain genetic findings in hypertrophic cardiomyopathy. *Eur J Hum Genet*. (2017) 25(7):809–15. doi: 10.1038/ejhg.2017.66

47. Davies B, Bartels K, Hathaway J, Xu F, Roberts JD, Tadros R, et al. Variant re-interpretation in survivors of cardiac arrest with preserved ejection fraction (CASPER registry) by clinicians and clinical commercial laboratories. *Circ Genom Precis Med*. (2021) 14(3):e003235. doi: 10.1161/circgen.120.003235

48. Wong EK, Bartels K, Hathaway J, Burns C, Yeates L, Semsarian C, et al. Perceptions of genetic variant reclassification in patients with inherited cardiac disease. *Eur J Hum Genet*. (2019) 27(7):1134–42. doi: 10.1038/s41431-019-0377-6

49. Berg AE, Meyers LL, Dent KM, Rothwell EW, Everitt MD. Psychological impact of sports restriction in asymptomatic adolescents with hypertrophic cardiomyopathy, dilated cardiomyopathy, and long QT syndrome. *Prog Pediatr Cardiol*. (2018) 49:57–62. doi: 10.1016/j.ppedcard.2018.05.001

50. Luiten RC, Ormond K, Post L, Asif IM, Wheeler MT, Caleshu C. Exercise restrictions trigger psychological difficulty in active and athletic adults with hypertrophic cardiomyopathy. *Open Heart*. (2016) 3(2):e000488. doi: 10.1136/openhrt-2016-000488

51. Etheridge SP, Saarel EV, Martinez MW. Exercise participation and shared decision-making in patients with inherited channelopathies and cardiomyopathies. *Heart Rhythm*. (2018) 15(6):915–20. doi: 10.1016/j.hrthm.2017.12.020

52. Struemph KL, Barhight LR, Thacker D, Sood E. Systematic psychosocial screening in a paediatric cardiology clinic: clinical utility of the pediatric symptom checklist 17. *Cardiol Young*. (2016) 26(6):1130–6. doi: 10.1017/S1047951115001900

53. Caleshu C, Kasparian NA, Edwards KS, Yeates L, Semsarian C, Perez M, et al. Interdisciplinary psychosocial care for families with inherited cardiovascular diseases. *Trends Cardiovasc Med*. (2016) 26(7):647–53. doi: 10.1016/j.tcm.2016.04.010

54. Collopy CM, Cosh SM, Tully PJ. Screening and referral is not enough: a qualitative exploration of barriers to access and uptake of mental health services in patients with cardiovascular diseases. *BMC Health Serv Res*. (2021) 21(1):1–11. doi: 10.1186/s12913-020-06030-7

55. Burke E, Pyle M, Machin K, Varese F, Morrison AP. The effects of peer support on empowerment, self-efficacy, and internalized stigma: a narrative synthesis and meta-analysis. *Stigma Health*. (2019) 4(3):337. doi: 10.1037/sah0000148

56. Fusco KM, Hylind RJ, Cirino AL, Harris SL, Lubitz SA, Abrams DJ, et al. Cascade testing for inherited cardiac conditions: risk perception and screening after a negative genetic test result. *J Genet Couns*. (2022) 31(6):1273–81. doi: 10.1002/jgc4.1602

Frontiers in
Cardiovascular Medicine

Innovations and improvements in cardiovascular treatment and practice

Focuses on research that challenges the status quo of cardiovascular care, or facilitates the translation of advances into new therapies and diagnostic tools.

Discover the latest Research Topics

See more →

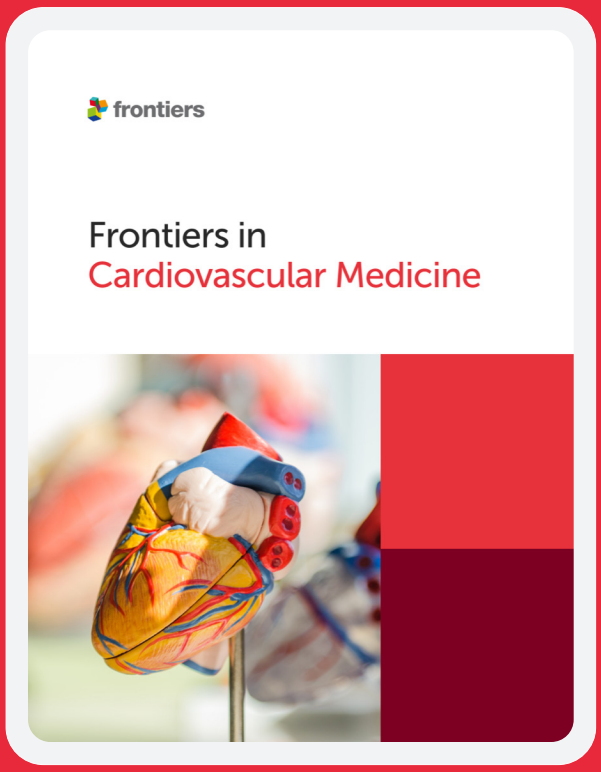

Frontiers

Avenue du Tribunal-Fédéral 34
1005 Lausanne, Switzerland
frontiersin.org

Contact us

+41 (0)21 510 17 00
frontiersin.org/about/contact